NUREG/CR-4829
UCID-20733
Vol. 1

Shipping Container Response to Severe Highway and Railway Accident Conditions

Main Report

Prepared by L. E. Fischer, C. K. Chou, M. A. Gerhard, C. Y. Kimura, R. W. Martin, R. W. Mensing, M. E. Mount, M. C. Witte

Lawrence Livermore National Laboratory

Prepared for
U.S. Nuclear Regulatory Commission

Reprinted October 1988

NUREG/CR-4829
UCID-20733
Vol. 1
RT

Shipping Container Response to Severe Highway and Railway Accident Conditions

Main Report

Manuscript Completed: April 1986
Date Published: February 1987

Prepared by
L. E. Fischer, C. K. Chou, M. A. Gerhard, C. Y. Kimura,
R. W. Martin, R. W. Mensing, M. E. Mount, M. C. Witte

Lawrence Livermore National Laboratory
7000 East Avenue
Livermore, CA 94550

Prepared for
Division of Reactor System Safety
Office of Nuclear Regulatory Research
U.S. Nuclear Regulatory Commission
Washington, DC 20555
NRC FIN A0397

ABSTRACT

This report describes a study performed by the Lawrence Livermore National Laboratory to evaluate the level of safety provided under severe accident conditions during the shipment of spent fuel from nuclear power reactors. The evaluation is performed using data from real accident histories and using representative truck and rail cask models that likely meet 10 CFR 71 regulations. The responses of the representative casks are calculated for structural and thermal loads generated by severe highway and railway accident conditions. The cask responses are compared with those responses calculated for the 10 CFR 71 hypothetical accident conditions. By comparing the responses it is determined that most highway and railway accident conditions fall within the 10 CFR 71 hypothetical accident conditions. For those accidents that have higher responses, the probabilities and potential radiation exposures of the accidents are compared with those identified by the assessments made in the "Final Environmental Statement on the Transportation of Radioactive Material by Air and other Modes," NUREG-0170. Based on this comparison, it is concluded that the radiological risks from spent fuel under severe highway and railway accident conditions as derived in this study are less than risks previously estimated in the NUREG-0170 document.

TABLE OF CONTENTS

TABLE OF CONTENTS (continued)

TABLE OF CONTENTS (continued)

TABLE OF CONTENTS (continued)

TABLE OF CONTENTS (continued)

TABLE OF CONTENTS (continued)

LIST OF FIGURES

LIST OF FIGURES (continued)

LIST OF FIGURES (continued)

LIST OF FIGURES (continued)

LIST OF FIGURES (continued)

LIST OF TABLES

LIST OF TABLES (continued)

PREFACE

This report describes a study conducted to estimate the responses of spent fuel casks to severe highway and railway accident conditions and to assess the level of safety provided to the public during the shipment of spent fuel. The study was performed by the Lawrence Livermore National Laboratory for the U.S. Nuclear Regulatory Commission (NRC), Office of Nuclear Regulatory Research.

This report is divided into two volumes: Volume I, the main report, describes the study, the technical approach, the study results, and conclusions; and Volume II, the Appendixes, provide supporting accident data and engineering calculations. This report has been reviewed by the Denver Research Institute at the University of Denver under a separate contract to the NRC as the peer review. A companion summary report entitled "Transporting Spent Fuel-Protection Provided Against Severe Highway and Railway Accidents" (NUREG/BR-0111) has been prepared by the NRC for wide distribution to federal agencies, local governments, and interested citizens.

Commercial spent fuel shipments are regulated by both the Department of Transportation (DOT) and the NRC. The NRC evaluates and certifies the design, manufacture, operation, and maintenance of spent fuel casks, whereas the DOT regulates the vehicles and drivers which transport the spent fuel.

Current NRC regulations require spent fuel casks to meet certain performance standards. The performance standards include normal and hypothetical accident conditions which a cask must be capable of withstanding without exceeding established acceptance criteria that

(1) limit the release of radioactive material from the cask,
(2) limit the radiation levels external to the cask, and
(3) assure that the spent fuel remains subcritical.

This study evaluates the possible mechanical and thermal loads generated by actual and potential truck and railroad transportation accidents. The magnitudes of the loads from accidents are compared with the loads implied from the hypothetical accident conditions. The frequency of the accidents that can produce defined levels of mechanical and thermal loads are developed from the accident data base. Using this information, it is determined that

for certain broad classes of accidents, spent fuel casks provide essentially complete protection against radiological hazards. For extremely severe accidents--those which could impose loads on the cask greater than those implied by the hypothetical accident conditions--the likelihood and magnitude of any radiological hazards are conservatively estimated. The radiological risk is then estimated and compared with risk estimates previously used by the NRC in judging the adequacy of its regulations.

The results of this study depend primarily on the quality of the cask response models, the radiation release models, and the probability models and distributions used in the analysis. Models for cask responses, radioactive releases, and distributions for the accident parameters are new developments based on current computer codes, limited test data on radioactive releases, and limited historical accident data. The results are derived using representative spent fuel casks which use design principles and materials that have been used in casks currently licensed by the NRC. The representative casks are assumed to have been designed, manufactured, operated, and maintained in accordance with national codes and standards (or equivalent) which have adequate margins of safety embedded in them. The results of this study are limited to spent fuel casks designed and fabricated under current technologies and operated under current regulations. New designs using alternative design principles and materials, or changes to regulations such as the imposition of a 75 mph national speed limit, could affect the results and conclusions of this study.

This study does not consider the effects which human factors can have on the cask design, manufacture, operation, and maintenance. If further study is conducted, human factors should be considered because they can contribute to the overall risk in each phase of transporting spent fuel.

L. E. Fischer

ACKNOWLEDGEMENTS

The authors wish to acknowledge the technical contributions made to this report by R. C. Chun, L. L. George, T. E. McKone, and M. W. Schwartz of Lawrence Livermore National Laboratory. The authors wish to thank G. E. Cummings of Lawrence Livermore National Laboratory for his report review and comments. The authors also wish to thank J. R. Cook, W. R. Lahs, and W. H. Lake of the U.S. Nuclear Regulatory Commission for their support and comments during the research and preparation of this report. Many thanks to N. J. Barnes and E. A. Sturmer for report preparation and D. Bowden for report editing.

In addition, the authors would particularly like to thank the following organizations for providing information and counsel which were used in preparing this report:

Anatech International Corporation
Association of American Railroads
Bureau of Motor Carrier Safety
California Department of Transportation
Central Electricity Generating Board, England
Denver Research Institute
Department of California Highway Patrol
Electric Power Research Institute
Engineering Computer Corporation
Federal Highway Administration
Federal Railroad Administration
Health and Safety Executive, England
Los Alamos National Laboratory
National Fire Protection Association
Oak Ridge National Laboratory
Ridihalgh, Eggers and Associates, Inc.
Sandia National Laboratories
Southern Pacific Transportation Company

1.0 INTRODUCTION

This report addresses the level of safety provided during the shipment of spent fuel from nuclear power reactors. The number of shipments will increase in the near future because of the need to transfer this fuel from the nuclear power reactors to a waste repository. During the shipments the shipping containers (casks) carrying the spent fuel could be exposed to severe highway and railway accident conditions. At the request of the U.S. Nuclear Regulatory Commission (NRC) the Lawrence Livermore National Laboratory (LLNL) has performed studies to evaluate and document the response of spent fuel casks exposed to severe highway and railway accident conditions.

1.1 Background

Nuclear fuel, contained in fuel rods, is used in nuclear power reactors to generate useful heat for electric power generation. The fuel rods used in most nuclear power reactors in the United States are made up of approximately one-half-inch-diameter ceramic pellets of uranium oxide encased within a cylindrical cladding. The fuel rods are approximately 15 feet in length. The cladding is made from metallic materials such as zirconium. After being capped, the cladding provides a contained environment for the uranium oxide fuel pellets. Depending on the type of nuclear power reactor, square arrays of the fuel rods numbering from about 50 to 300 are structurally assembled to form a single fuel bundle.

When nuclear fuel burns or fissions, it not only generates useful heat, but also creates radioactive fission products. Spent fuel is nuclear fuel that has been burned to its specified limits and has served its useful purpose. Spent fuel is highly radioactive when initially removed from a nuclear power reactor. Before being transported to a waste repository, spent fuel is usually stored five or more years in the spent fuel pool at the reactor site to allow the fuel to cool or decay to lower radiation levels.

Because of its radioactive nature, spent fuel is shipped in specially designed shipping containers called casks. These casks are massive, cylindrically shaped objects weighing from 25 to more than 100 tons. The

designs of several currently used casks consist of steel shells enclosing a dense metallic material (lead or depleted uranium) that is used to provide radiation shielding. In the United States, these casks must be certified by the U.S. NRC as being in compliance with the regulations contained in Title 10 of the Code of Federal Regulations, Part 71 (10 CFR 71).[1] These regulations, which are almost identical in substance to internationally accepted standards, have been in effect for nearly 20 years. The regulations are intended to assure that the public will be protected both during normal transportation or in the event that a spent fuel shipment is involved in a transportation accident.

Basically, the regulations state that each spent fuel cask must meet certain containment, radiation control, and criticality control requirements when it is subjected to specified normal transport conditions and also hypothetical accident conditions. The hypothetical accident conditions are of most interest to this discussion. They are specified in terms of regulation defined test conditions that include a free drop (30 feet onto a flat unyielding surface), a puncture (40-inch drop onto a vertical 6-inch-diameter mild steel bar), thermal exposure (30 minutes to a defined 1475^{o}F environment), and immersion under specified depths of water. The test conditions must be sequentially imposed on all casks in a manner that would cause maximum damage. The resulting cask response must then be determined by test or analysis.

The regulations do not define the allowable structural or thermal damage a cask may sustain, but instead use radiological criteria, i.e., radioactivity release (leakage) and radiation levels external to the cask as a measure of the acceptability of the design. The cask response must be such that the cask can (1) meet containment requirements (any radioactive material release must be restricted within extremely small limits), (2) keep radiation levels external to the cask within stated limits, and (3) ensure that a criticality event cannot occur. In more practical terms, these compliance criteria require the cask structural integrity to be effectively unimpaired.

Historically, the few shipments of spent fuel that have been involved in transportation accidents have never created any significant radiological hazard. However, the number of these events has been limited. To quantify the radiological risk to the public from all shipments of radioactive material, including spent fuel, the NRC published, NUREG-0170, in 1977 entitled, "Final Environmental Statement on the Transportation of Radioactive Material by Air and Other Modes."[2] The study was primarily performed using conservative engineering judgments. The analysis performed in that document presumed that, in certain classes of accidents, transportation accident loads could exceed those implied by the hypothetical accident conditions specified in the regulations. The analysis further presumed that for these classes of accident, releases of radioactive material could occur. Even under these presumptions, the analysis indicated that the potential radiological hazards from real transportation accident loadings on a spent fuel cask were most often very small (i.e., limited to minor property contamination which required only cleanup actions). Since no release of spent fuel material has ever occurred, this assessment is consistent with historical events. Even though NUREG-0170 presumed the release of radioactive material under certain severe accident circumstances, the overall resulting radiological risk from transporting spent fuel under current regulations was calculated to be acceptable.

Nevertheless, because of the lack of actual data on the real effects of severe accidents on spent fuel casks, studies were initiated by the NRC prior to this work to define more precisely (1) the variability of mechanical and thermal loads which could be experienced by a cask in recorded severe railway and highway accidents, and (2) the degree to which these loads might exceed those implied by the hypothetical accident conditions.[3] In order to better understand the effectiveness of current regulations, this recorded severe accident information supplemented with other accident data has been used by the LLNL, working under contract to the NRC, to evaluate the responses of spent fuel casks exposed to severe highway and railway accident conditions. This report documents the work performed under this contract.

1.2 Regulations and Past Assessments

1.2.1 Title 10, Code of Federal Regulations, Part 71

To protect the public health and safety, commercial shipments of spent fuel are required to be made in spent fuel casks which are designed, fabricated, and operated in accordance with provisions of 10 CFR 71. The three basic safety requirements addressed by the regulations and which must be met when transporting spent fuel are:

1. Adequate containment of radioactive material
2. Adequate shielding of the radiation emitted by the radioactive contents
3. Prevention of nuclear criticality.

The containment requirements, as they apply to spent fuel shipments, impose a limit on radioactive material releases following the application of certain mechanical and thermal loadings on a spent fuel cask. The loadings are imposed by a series of test conditions called hypothetical accident conditions. The radioactive material release limits include a value for the relatively innocuous inert gas, ^{85}Kr, ($\leq$ 10,000 curies in one week) and a separate limit on other releases over a 1-week period (called an A_2 quantity). These limits on specific radioactive material releases are such that the doses to members of the public can be expected to be less than the allowable annual dose to individuals whose occupation involves potential exposure to radiation.

The shielding requirement following the application of the hypothetical accident condition is stated in terms of an external radiation dose rate at 1 meter from the external surface of the cask. This radiation level must not exceed one rem per hour.

The prevention of criticality under accident conditions is achieved by cask design features which assure subcriticality. This subcriticality must be achieved assuming (1) optimum (most reactive) configurations of the spent fuel consistent with the cask damage imposed by the hypothetical accident conditions and (2) most reactive conditions associated with the presence of water. (Water or other materials which act as neutron moderators or reflectors enhance criticality possibilities when in close contact with spent fuel.)

The safety requirements of 10 CFR 71 play an important role in this study because they provide a benchmark for relating a specific magnitude of mechanical or thermal loading (implied by the hypothetical accident conditions) to a specified level of cask response. For example, in practice, the containment limits are usually met by demonstrating that the cask containment experiences essentially no permanent deformations and the closure seals and penetration remain essentially leak tight (Fig. 1-1). The external dose rate limit is met by demonstrating that essentially no loss of the gamma shield occurs under accident conditions. Finally, the prevention of criticality requirement is typically met by demonstrating that essentially no deformation occurs to the basket, the structure within the cask which holds the spent fuel. These limits serve as benchmarks against which cask responses in real accident conditions can be compared.

One particular cask design feature is especially significant in ensuring that a spent fuel cask will meet the containment, shielding, and subcriticality requirements when the cask is subjected to the 30-foot drop onto the unyielding surface called for by 10 CFR 71. This feature is called an impact limiter (Fig. 1-1). Impact limiters reduce the mechanical loads to the main cask body under accident conditions.

Impact limiters are typically made of crushable material surrounding the extremities of a cask, but designs can also include the use of crushable exterior metal fins. In either case, the impact limiters are designed to absorb most of the energy generated in the regulatory-defined 30-foot drop onto the unyielding surface without causing any significant permanent damage to the cask containment or closure features.

The significant point is that, through the response of this design feature, a load level is defined which translates into no cask containment damage and, therefore, essentially no radiological hazard. For those real accidents which result in mechanical loads less than this limit, the radiological hazard is insignificant.

Similarly, protection against the regulatory-defined thermal loading conditions is typically provided by the use of thermal barriers. Thermal

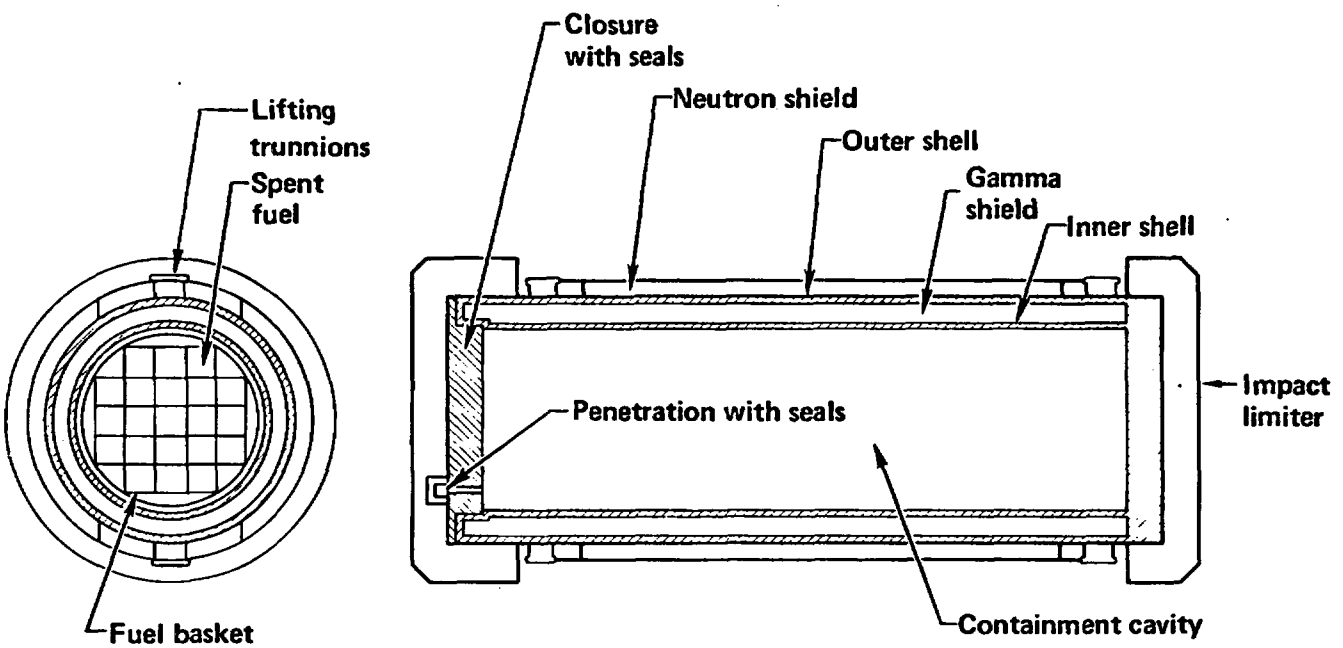

Figure 1-1 Schematic of a typical spent fuel cask.

barriers limit the heat transfer from a fire or thermal source external to the cask, to the cask containment structure, and to the contained spent fuel. Again, real world accidents involving fire can be compared with this defined thermal loading. These types of comparisons form the essence of the first-stage of a screening process used in this study.

1.2.2 Transportation of Radioactive Material - Environmental Statement (NUREG-0170)

In December 1977, the NRC published NUREG-0170, "Final Environmental Statement on the Transportation of Radioactive Material by Air and Other Modes".[2] The report included an assessment of the likelihood and magnitude of the radiological consequences associated with potential transportation accidents for all shipments of radioactive material. Most shipments consisted of medical and industrial isotopes, but spent fuel shipments were specifically addressed. The assessment indicated that the radiological risk involved in all shipments was small. This conclusion provided the technical basis for the Commission's decision that the existing 10 CFR 71 regulations are adequate and not in need of immediate change.

The NUREG-0170 analysis provides an additional benchmark for this study. Specifically, the radiological risk from spent fuel shipments reported in NUREG-0170 can be compared with the risk estimated in this study. In NUREG-0170, accident severities were divided into eight categories. For each category, the radiological hazards were assigned based on conservative engineering judgments. These hazards were measured in terms of the fraction of radioactive material released from the spent fuel and an equivalent fraction caused by shine from any unshielded fuel. For truck and rail accidents, the estimates in NUREG-0170 indicated that 91% of truck accidents and 80% of train accidents would result in no significant radiological hazard. In the remaining accidents, the radiological hazards increased as the accident severity increased. The increase is indicated in Table 1.1. As a point of reference, NUREG-0170 indicated that 0.4% of truck accidents and 0.2% of train accidents could involve a complete release from the cask of certain gaseous and volatile materials. These materials represent the radioactivity

Table 1.1
Correlation of NUREG-0170 Accident Fractional Occurrence and Radiological Hazards as a Function of Accident Severity

Accident Severity Category	Truck Fractional Occurrences	Train Fractional Occurrences	Radiological Hazards	
			Fraction of Radioactive Material Released[a/]	Fraction of Equivalent Unshielded Fuel[b/]
I	0.55	0.50	0	0
II	0.36	0.30	0	0
III	0.07	0.18	0.01	0
IV	0.016	0.018	0.10	0
V	0.0028	0.0018	1	0
VI	0.0011	1.3×10^{-4}	1	3.18×10^{-7}
VII	8.5×10^{-5}	6.0×10^{-5}	1	3.18×10^{-5}
VIII	1.5×10^{-5}	1.0×10^{-5}	1	3.12×10^{-3}

a/ Radioactive gases and vapors

b/ Approximates the reduction in radiation shielding

which typically migrates from the fuel pellets to the fuel rod gap, the void space between the fuel pellets and the surrounding fuel rod. In this small percentage of accidents, all the fuel rods in the shipment were assumed to fail and to release their radioactivity.

Also, for accidents in Category VI and greater, a reduction of shielding was assumed. To provide a consistent measure of the radiological effects with cask damage, the radiological hazard due to the reduction in shielding was presented in terms of an equivalent fraction of unshielded fuel. The equivalent fraction of unshielded fuel is the ratio of that portion of the total spent fuel inventory that, if unshielded, would produce radiation levels equivalent to those being emitted from a damaged cask with reduced shielding.

The results of NUREG-0170 rely in part on the presumption that spent fuel casks have sufficient margins designed into them that major radioactive hazards will not occur even at loading conditions which exceed those specified in regulations. These margins of safety are included in all licensed cask designs through the use of established codes and standards which have margins of safety embedded in them.

The evaluation conducted in this study analyzes the response of representative shipping casks in severe accident environments. This evaluation uses representative cask designs that are likely to be licensed and have margins of safety included in their designs. The responses of the representative casks to all possible accident conditions are analyzed and categorized into cask response regions. For each cask response region, assessments are made of the potential for release of radioactive material and the potential for reducing the radiation shielding capabilities of the cask. This evaluation is the basis for a comparison with NUREG-0170; that is, what accident classes result in radiological hazards and how do those hazards and their likelihoods compare in terms of radiological risk to the public.

1.3 Objective and Approach

The objective of this study, the Shipping Container Response to Severe Highway and Railway Accident Conditions, is to estimate the adequacy of

radiological protection offered the public by the current NRC regulations when highway or railway accidents occur involving spent fuel shipments. The estimates are performed using data from real accident histories of similar types of vehicles and using models of cask designs that have a likelihood of meeting requirements for spent fuel shipments.

A two-stage screening process is used. The screening process is illustrated in Fig. 1-2. The first stage compares cask responses to accident loading conditions with those associated with the accident test conditions specified in 10 CFR 71. As an example of such a comparison, cask loadings from a class of accidents involving impacts exceeding 30 mph (the velocity reached in the 30-foot drop) are examined.

An example of such an accident class is the accident scenario involving a 60-mph collision with a highway sign pole. The cask loading in this scenario is such that no damage occurs to the containment, radiation shielding, or subcriticality assurance features of the cask, even though the accident velocity exceeds the regulatory-implied impact velocity. The reason is that although the accident velocity is twice the regulatory defined velocity, the loading imposed on the cask in the 30-foot drop test far exceeds the loading achieved on impact with the sign pole. The pole failure essentially limits the load to which the cask is exposed.

There are classes of accidents in which the loading can be conceived to approach or exceed the values imposed by the accident test conditions. Examples of these classes are high-speed impacts with massive bridge abutments and falls from great heights onto hard rocks. Sophisticated analysis can be used in many cases to demonstrate that the loadings on a cask are still less than those imposed by the regulation-defined hypothetical accident conditions. However, questions arise involving the specifics of a particular cask design and the orientation of impact (i.e., does the orientation assumed cause maximum damage). On the analysis side, the validity of analytical methods used to predict the cask response can be questioned. A major part of this report is directed toward demonstrating what broad classes of real-world accidents and their associated loadings are enveloped by the loadings implied

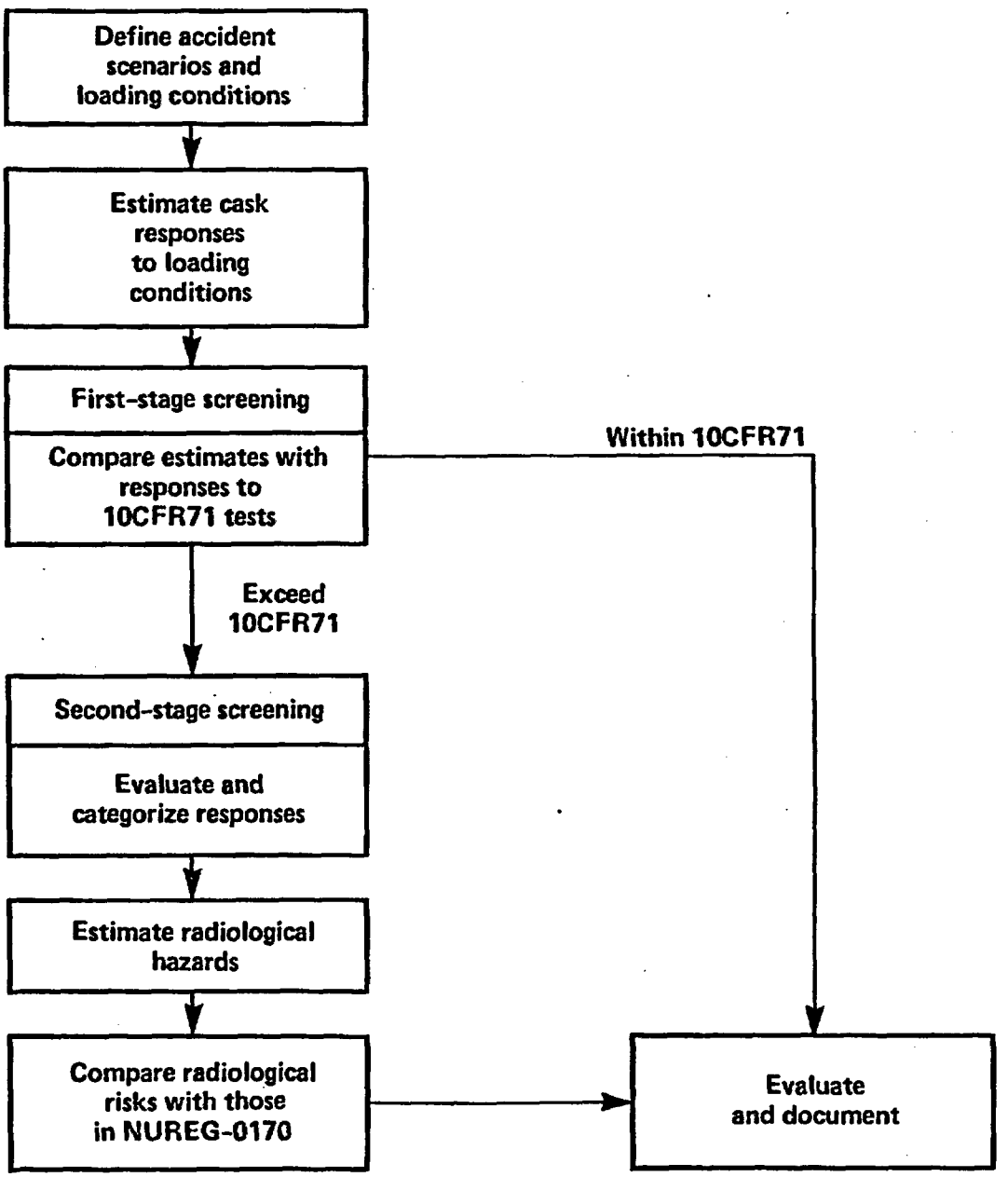

Figure 1-2 Two-stage screening process used in evaluating the regulations.

in the current regulatory standards. The first-stage screening envelopes accident loading conditions whose magnitudes do not exceed those defined by the accident test conditions and, therefore, the potential radiological hazards are less than those implied by regulations.

For those accident scenarios with loads and cask responses greater than those implied by the accident test conditions, a second-stage screening is performed. This screening evaluates the likelihood of the cask responses.

The potential radiological hazards associated with the cask responses are then determined. By summing all accident scenarios, the probability and magnitude of the radiological hazards is estimated and then compared with the risk evaluated in NUREG-0170.

Because of the numerous variables involved in defining cask loading and response, and because of the broad range of possibilities and interrelationships for each of the variables, a systematic scheme is developed to accomplish the two-stage screening process and to assess the effectiveness of 10 CFR 71 in assuring adequate radiological protection to the public. To describe this systematic process, this report is arranged into several sections. Many tasks are performed: model developments, data sources, data development, analysis of models, classification, and comparison of results. Although the tasks are described in the report by sections, the separate tasks are not developed independently, and they cannot be described without considering the interrelationship involved.

Figure 1-3 shows the interrelationship of the various tasks and how they influence the performance of the analysis. The initial tasks in this study involve developing models for casks and accident environments. Methods are also developed for evaluating how the cask models respond to accidents and for classifying their responses into response regions. The screening analyses are performed by subjecting the casks to the accident events identified in the accident scenarios, determining the predicted responses of the casks to these events, and classifying these predicted responses into the response regions. The cask physical responses are then related to any resulting radiological hazards. Because the likelihood or probability associated with an accident

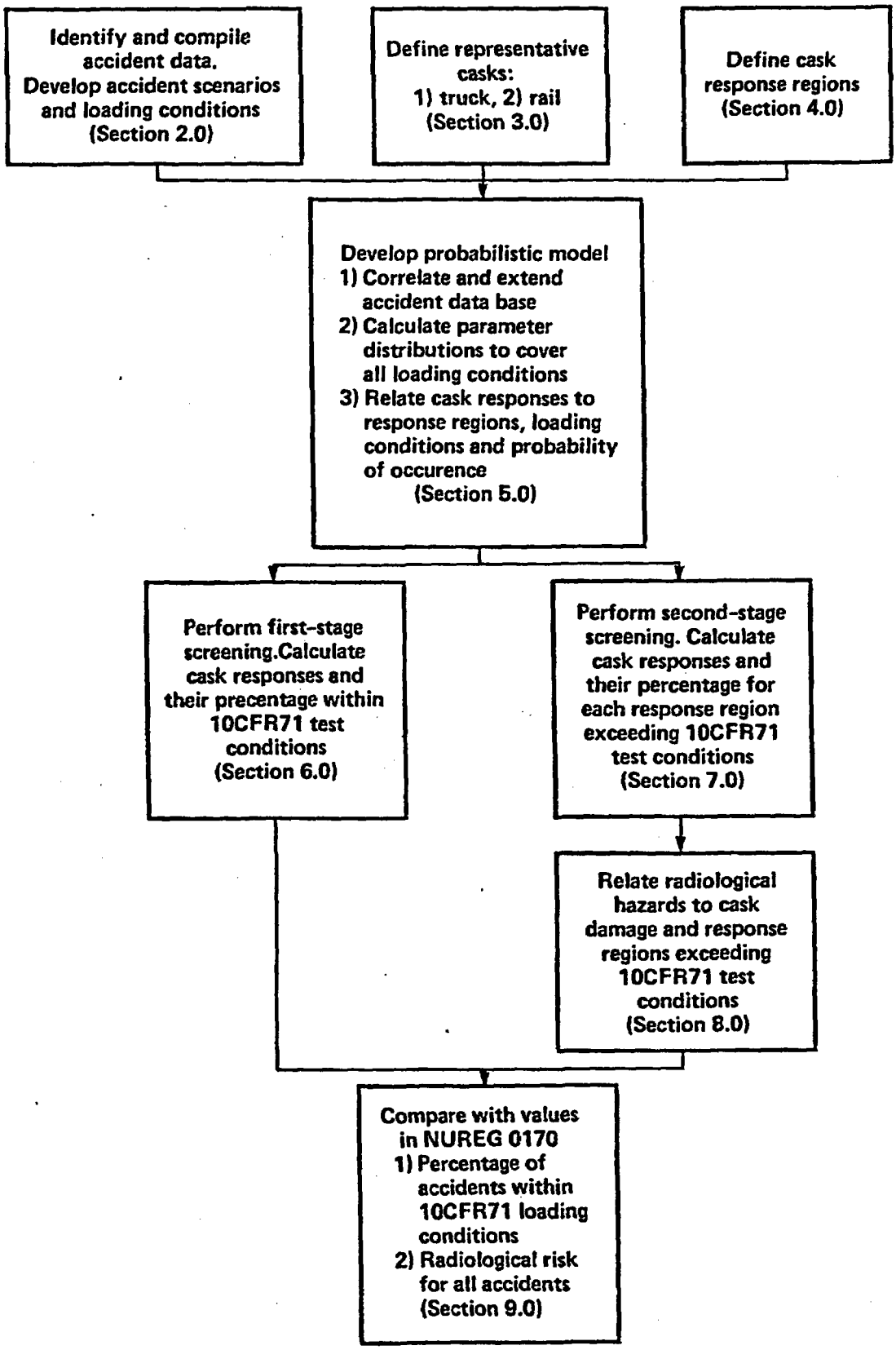

Figure 1-3 Schematic representation of the report.

event can be derived from accident data, the probability associated with the response and radiological hazard can be estimated.

In Section 2.0, the mechanical and thermal loads associated with real accidents are discussed. Also, accidents are classified into accident scenarios to systematize the analysis. Statistical accident data have been used and enhanced where necessary to establish likelihood estimates for the occurrence of those mechanical and thermal accident loads determined to be important to cask response. The mechanical loads are described in terms of parameters such as velocity of the cask, the hardness of the object that the cask hits, and whether the crash is head-on, glancing, or at some intermediate direction. The thermal loads are described in terms of location, temperature, and duration of a fire.

In Section 3.0, two casks are defined as representative of those used for ground transportation of spent fuel, one for highway and one for railway. The details and justification for selecting the representative cask designs are explained. The margins of safety included in their designs are discussed.

Cask response regions are specified in terms of the physical response of the cask to accident events. The response regions are described in Section 4.0; they are represented as strain for mechanical loads, and as temperature for thermal loads. The strains from mechanical loads and temperatures created by thermal loads which define the response regions are related to deformations and degradation of the cask's containment and shielding system. Deformation and degradation of the cask's containment and shielding systems can result in specific radiological hazards for each of the response regions. Details for relating radiological hazards to the response regions are found in Section 8.0.

In Section 5.0, the probabilistic model used in the analysis is described. The formulations used to relate cask responses to loading conditions, response regions, and the probability of occurrence are described. Techniques also are developed for calculating the probability for combined loading conditions for each accident scenario.

In Section 6.0, the first-stage screening process is described. The first step in this process is to subject the casks to each accident scenario identified in Section 2.0 and to estimate the responses. The responses are sorted into the response regions. The appropriate response region for the first-stage screening is the lowest response region since it is defined to encompass 10 CFR 71 accident test conditions. Since the accident rates are known, the fraction of accidents falling into each response region can be determined.

In Section 7.0, the second-stage screening process is described. The accidents not falling into the lowest response region are analyzed and the responses calculated. These responses are then categorized into the other response regions.

In Section 8.0, the radiological hazards associated with each cask response region are estimated. The radioactive material releases are estimated from laboratory test data. The radiation increases caused by lead slump are estimated from structural, thermal, and shielding calculations.

Finally, in Section 9.0, the results of the two-stage screening process are presented with respect to NUREG-0170. The conclusion reached is that at least 99.4% of truck and train accidents involving a spent fuel shipment will result in negligible radiological hazards which are less than those implied by the current 10 CFR 71 regulations. Of the remaining spent fuel shipment accidents, the overall radiological risk is less than the risk estimated in NUREG-0170.

2.0 ACCIDENT RATES, ACCIDENT SCENARIOS, AND LOADING PARAMETER DISTRIBUTIONS

2.1 Introduction

Severe accidents are typically characterized and reported by fatalities, injuries, property damage, transportation equipment damage, or a combination of these consequences. In this study, however, the characterization is in terms of the magnitude and frequency of loads that could be experienced by a spent fuel cask under accident conditions. Normally the higher the load on a cask, the higher the cask response and the greater the potential for radioactive release.

Both mechanical and thermal loads generate response states for a cask which could result in damage to the cask. High mechanical loads caused by impact can cause damage to the cask shielding or cause the cask containment to leak. High thermal loads caused by fires can cause the cask containment seals to deteriorate and leak or the lead shield to melt. In performing the two-stage screening process of accidents discussed in Sections 6.0 and 7.0, all possible accidents have to be included, especially those that could cause high mechanical and thermal loads on a cask.

Mechanical and thermal loads depend on the magnitudes of the accident loading parameters. Two examples of accident loading parameters and their magnitudes are a velocity of 50 mph and a fire duration of one hour. The same accident-caused load on a cask can occur for various combinations of loading parameters and loading magnitudes. For example, the same impact force on the cask can be generated by a low-velocity impact on a hard object or a high-velocity impact on a soft object. Also, the same heat load on a cask can occur for a short duration high-temperature fire or a long duration low-temperature fire. Consequently, specific mechanical and thermal loading conditions on the cask can occur under a variety of accident conditions.

Accident loading conditions must take into account many loading parameters and must include a wide range of values for each loading parameter. Accident scenarios can be derived from historical records. An accident scenario describes a sequence of events as they occur, allowing the

identification of possible loading conditions. For example, an accident scenario can involve a truck running off the highway, going over an embankment, and crashing into a rock. The loading conditions for this scenario primarily depend on the hardness of the rock, the velocity of the truck when it hits the rock, the direction of the truck velocity, and the orientation of the truck with respect to the rock. By varying these four parameters, thousands of loading conditions are possible for one accident scenario.

In order to evaluate all possible accident loading conditions on a cask, the following accident information is derived in this section:

(1) Accident rates for spent fuel shipments are estimated from historical accident records for truck and train accidents for similar vehicles.

(2) Accident loads that dominate the accident loading conditions and the structural and thermal responses of spent fuel casks are identified. The significant loading parameters for the dominant accident loads are identified.

(3) Accident scenarios, to include all possible accident loading conditions for truck and train transport, are identified. Accident data, survey results, and engineering judgment are used to establish accident loading parameter distributions.

The accident information derived in this section is used with the probabilistic computer code called TASP (Transportation Accident Scenario Probabilities) described in Section 5.0 to calculate and screen the expected magnitude and frequency of cask responses to accident conditions.

In Sections 2.2 and 2.3, the expected accident rates for spent fuel shipments by highway and railway are estimated. In Section 2.4, the accident data required to estimate the accident loads on a cask are identified. In Sections 2.5 and 2.6, the accident scenarios and loading parameter distributions are discussed.

2.2 Highway Accident Rates

Highway accident rates depend on many elements including road type, vehicle type, regulations, and driving practices. The accident rate for all vehicles on California highways during 1981 through 1983 ranged from 1×10^{-6} accidents/vehicle-mile for freeways with limited access to 5×10^{-6} accidents/vehicle-mile for conventional four-lane highways.[1] Studies by the U.S. Department of Transportation (DOT) have indicated that accident rates are significantly lower for interstate federal highways (usually freeways) than for other road types. Routes for transport of spent fuel are selected in accordance with the DOT regulations to minimize the radiological risk. In general, the routes follow interstate federal highways.[2]

As discussed in Appendix B, two sources are used for estimating a typical accident rate for spent fuel transportation. An average accident rate of 2.5×10^{-6} accidents/vehicle-mile is derived from the data published by the Bureau of Motor Carrier Safety (BMCS) for all roadways.[3-5] Their data covered all truck and carrier type accidents from 1960 through 1972. The second data source is the American Petroleum Institute (API) for the period of 1968 through 1981 for all roadways.[6-10] The average accident rate is 6.4×10^{-6} accidents/vehicle-mile or approximately 2.5 times higher than that based on the BMCS data. For this study the API accident rate is used as the estimate for spent fuel truck accident rates because the data is judged to be more reliable, and trucks which transport hazardous petroleum materials are similar in size and weight to trucks that transport spent fuel casks. The use of the more conservative API value is not critical to the results of this study.

2.3 Railway Accident Rates

Train accident rates depend on many elements including the type of train, the type of track, and the reporting requirements. Freight trains are used to transport spent fuel over all track types and are subject to Federal Railroad Administration (FRA) reporting requirements. Because over 90% of all train mileage is attributed to freight trains, there is no significant difference in applying data based on all trains to freight trains in order to estimate accident rates, accident velocities, fire frequencies, etc.

Appendix C discusses the train accident rate selected for spent fuel shipments by train. Based on the FRA data for all train and track types, an accident rate of 1.2×10^{-5} accidents/train-mile is assumed for spent fuel rail shipments.[11-17]

2.4 Accident Loading Data Requirements

Historical data bases on transportation accidents exist at all government levels. These data bases range from local accident records to state and national accident statistics. Typically, these records include many accident conditions and consequences that are not pertinent to this study, including weather conditions, fatalities, injuries, and property damage. However, some of the data are pertinent to this study; namely, data pertaining to accident loading conditions which could cause cask damage. Typical of such data are estimations of accident velocities, descriptions of objects impacted, and duration of fires. Most of these data bases are compiled to aid general transportation safety with the main focus on reducing injuries, fatalities, and property damage. They do not always include all the information necessary to define the loading a cask might experience. Therefore, specific data necessary to estimate accident loads on a cask are not always available.

Table 2.1 presents mechanical and thermal loads that can occur in an accident. The accident loading parameters that cause the loads and affect the response of the cask for various load types are also listed.

Mechanical loads include forces on the cask caused by impact with a surface or hard object, puncture by strong objects, and crushing by heavy objects. Based on the evaluation in Appendix E, it is concluded that impact loads are the dominant mechanical loads and have the greatest potential for causing significant structural damage to a spent fuel cask. Therefore, only impact loads and their associated loading parameters are used to perform the two-stage screening of accidents generating mechanical loads.

Mechanical loads from impacts can be analyzed using three loading parameters that affect the cask response and potential damage: impact velocity, orientation of the cask, and the hardness of the object impacted.

Table 2.1
Accident Loads and Loading Parameters

Loading Parameter	Accident Loads					
	Mechanical Load Type			Thermal Load Type		
	Impact	Punch	Crush	Fire	Torch	Decay Heat[a/]
Object Hardness	X	X	X			
Impact Velocity	X	X				
Cask Orientation	X	X	X			
Object Weight	X	X	X			
Object Impact Area		X				
Flame Temperature				X	X	
Fire Duration				X	X	
Fire Location				X	X	
Flame Emissivity				X	X	
Convection Coefficient				X	X	
Surrounding Material						X

a/ Decay heat from spent fuel cargo.

Figure 2-1 defines these three loading parameters. The impact velocity is the cask velocity perpendicular to the surface impacted. The angle of impact, α, represents the angle between the cask velocity vector and the object's surface. When an accident occurs, the cask velocity vector can take any direction. However, it can always be decomposed into two components: one perpendicular to the impacted object surface and one parallel to it. The accident velocity is a function of reported vehicle velocity, braking effects, and fall heights from bridges or embankments. In the cask response calculations, only the velocity component perpendicular to the object surface is considered. The velocity component parallel to the object surface introduces a sliding-friction effect to the cask structure. The sliding-friction effect will not induce any significant structural deformation in the cask. In this study, the angle of impact is combined with the cask velocity to produce the cask impact velocity, i.e., impact velocity equals cask velocity times sine α where α is the angle of impact and the impact velocity is treated as a single loading parameter.

The angle defining the cask orientation, β, is the angle between the cask longitudinal axis and the object's surface. The cask orientation affects the cask response, particularly for endwise impacts ($\beta = 90^{o}$) where lead slump can occur at high impact velocities.

Object hardness needs to be considered because casks can strike objects such as concrete abutments, roadbeds, hard rock, soft rock, hard soil, and water. The hardness of the objects and the associated impact responses vary greatly. The weight of the object impacted can also affect the response of the cask. However, only massive objects can cause significant mechanical loads on a cask, hence the object hardness is the dominant parameter that is considered for objects impacted.

In some accidents, such as rail grade-crossing accidents, the impact limiters on the cask can be bypassed and the side of the cask can be struck directly. Once again the mechanical loads depend on the impact velocity, the orientation of the cask, and the hardness of the object struck. Figure 2-2 defines these three loading parameters for this type of accident. The impact

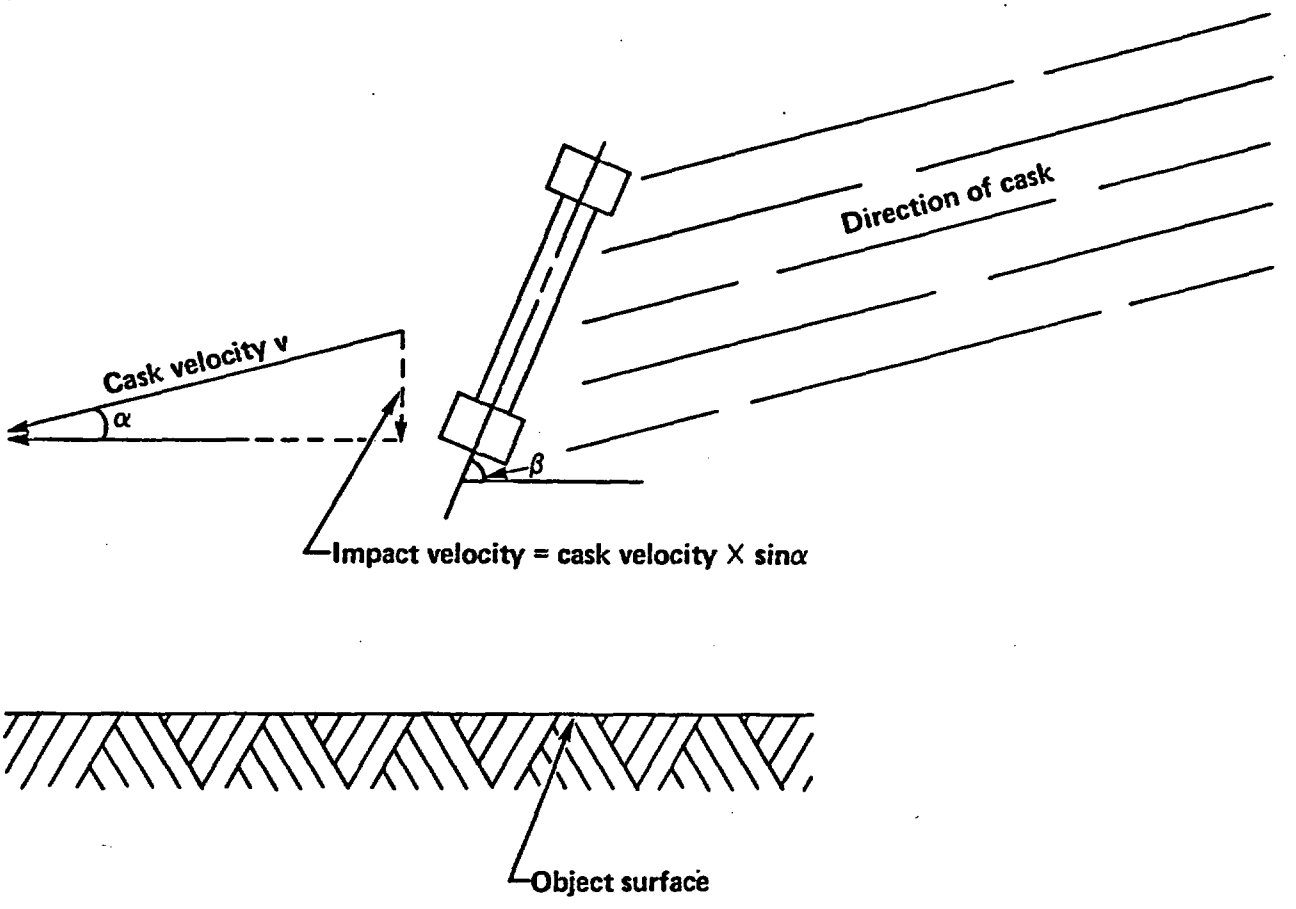

- o Object surface hardness
- o Impact velocity: Cask velocity component perpendicular to the object surface
- o Cask orientation is defined by angle β, the angle between the cask longitudinal axis and the object's surface

Figure 2-1 Three impact loading parameters considered in the response analysis for impacts on surfaces.

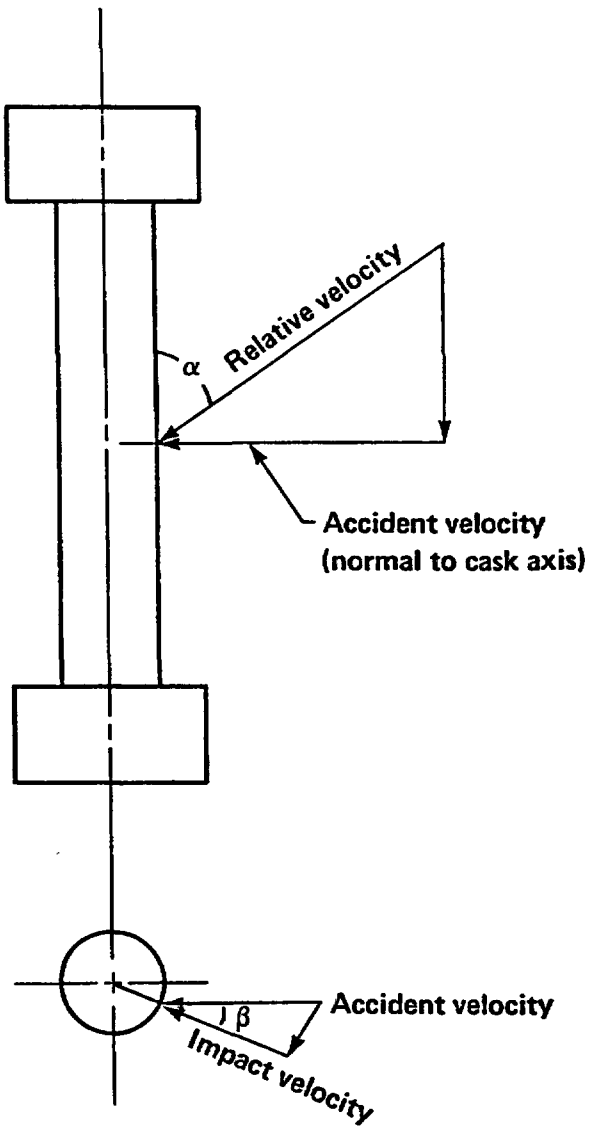

- o Object hardness
- o Impact velocity: Relative velocity component perpendicular to cask surface.
- o Cask orientation angle, β: the angle between the accident velocity and impact velocity.

Figure 2-2 Three impact loading parameters considered in the response analysis for impacts with objects such as train sills.

velocity is the component of the relative velocity of the cask and object that is perpendicular to the cask surface. The angle of impact, α, represents the angle between the relative velocity direction and the cask axis. For the purpose of this study, the impact angle is conservatively assumed to be 90^{o}, that is, perpendicular to the cask axis in all cases. Also, it is assumed that the impact occurs at the mid-plane of the cask to cause the most damage. The cask orientation angle, β, is the angle at which the impact occurs on the cask surface as shown in Fig. 2-2. In the worst case the cask is hit at 0^{o} or head-on. For orientation angles near 90^{o}, the cask is essentially not struck. The object hardness depends on the object hitting the cask, such as a train sill or a small bridge column.

The thermal loads identified in Table 2.1 include the heating of a spent fuel cask by large fires, both engulfing and non-engulfing; torch fires; and decay heat from the spent fuel, particularly when the cask is accidentally buried in debris. Based on the evaluation in Appendix F, it is concluded that heat loads from large fires, both engulfing and non-engulfing, have the greatest potential for causing significant damage to a spent fuel cask. Therefore, only heat loads from large fires and their associated loading parameters are used in the screening of accidents generating thermal loads.

Thermal loads from large fires depend on three loading parameters that affect the cask response and potential damage: fire duration, flame temperature, and fire location. The fire duration affects the amount of heat that is transferred into the cask--the longer the fire burns the greater the amount of heat that is absorbed by the cask. Higher flame temperatures cause greater amounts of heat to be transferred to the cask. As discussed in Appendix F, the flame temperature, assuming a flame emissivity of 0.9, is the single parameter used to characterize both radiation and convection heat transfer over a wide range of conditions. The location of the fire with respect to the cask affects the amount of heat that can be transferred to the cask. An engulfing fire would transfer the most heat to the cask, given the same flame temperature and fire durations, whereas less heat would be transferred from non-engulfing fires.

Accident records typically classify accidents into broad categories or types that describe, in general, the causes of the accidents. Examples are ran-off-the-road, overturn, and derailment. Accident scenarios describe a sequence of events and involve individual accidents that occur at specific velocities, impact specific objects at specific angles, and perhaps include a fire. For the purpose of this study, accident scenarios are specified and typically identified by the object impacted. By interpreting accident data bases in the context of these scenarios, the analysis is made manageable.

2.5 Highway Accident Loading Parameters

2.5.1 Mechanical Loading Parameters

Three mechanical loading parameters have been identified which can affect the structural response of a cask in a severe accident: object hardness, impact velocity, and cask orientation. The distribution functions for these parameters can differ with each specific accident scenario. The object hardness distribution is derived from the truck accident data base. For accident scenarios that could cause high mechanical loads on a cask, impact velocity distributions are estimated from truck and train accident velocity data, bridge height data, and engineering models. No specific data is available to estimate cask orientation on impacts; therefore, distributions are estimated from engineering models.

2.5.1.1 Accident Scenarios and Object Hardness

Data from several sources are collected and combined in Appendix B to estimate the frequency of specific accident scenarios and potential impacts on specific objects of varying hardness. The accident scenarios are primarily based on truck accident data documented in the BMCS annual reports for the years 1973 through 1983.[18-27] The BMCS accident data are for all truck sizes and all roadways including city streets, county roads, state and interstate highways.

Figures 2-3 and 2-4 list the truck collision and non-collision accident scenarios used to categorize the response of spent fuel casks to accident loads. Thirty-one scenarios, each identified with an accident index number, are presented. By combining historical accident records with a survey of highway roadside structures, the probability associated with each accident scenario is estimated in percent. For example, a truck can be involved in a collision accident, hit a bridge railing, run over the bridge, and drop into water below (accident index 7 in Fig. 2-3). This scenario describes a sequence of events involving many different accident features such as collision objects, bridge railings, and water.

An example will be used to illustrate how this probability estimate is made. Figure 2-3 shows that 74.12% of truck accidents are collisions. Of these collision accidents, 11.95% involve hitting a roadside fixed object. The probability that the roadside object is a bridge railing is 5.77%. The probability that the truck, after hitting the bridge railing, breaks through the bridge railing and lands in the water is 20.34%. Therefore, the fractional occurrence for the example scenario is 0.104% given that a truck accident occurs. Multiplying this fractional occurrence by the assumed truck accident rate of 6.4×10^{-6} accidents/vehicle-mile gives the chance of this kind of accident occurring per mile traveled as 6.7×10^{-9}.

2.5.1.1.1 Collision Accident Hardness Data

Figure 2-3 summarizes collision accident scenarios and the frequencies of collisions with moving objects such as trucks, autos, and trains as compiled from the BMCS data. Over 56% of the truck accidents involve collisions with another truck or auto. The BMCS accident data did not classify collisions with fixed objects, even though they ranged from stop signs to bridge columns. To classify fixed objects, highway accident data are obtained from the California Department of Transportation (CALTRANS) reports of stationary objects struck along state and interstate highways for the years 1975 through 1983.[28-36] Those objects in the CALTRANS survey are tabulated and a fraction calculated for each type of fixed object. These fractions are then applied to the fixed object collision accidents in the BMCS data to estimate the number of accidents involving each type of object, such as a bridge rail or column.

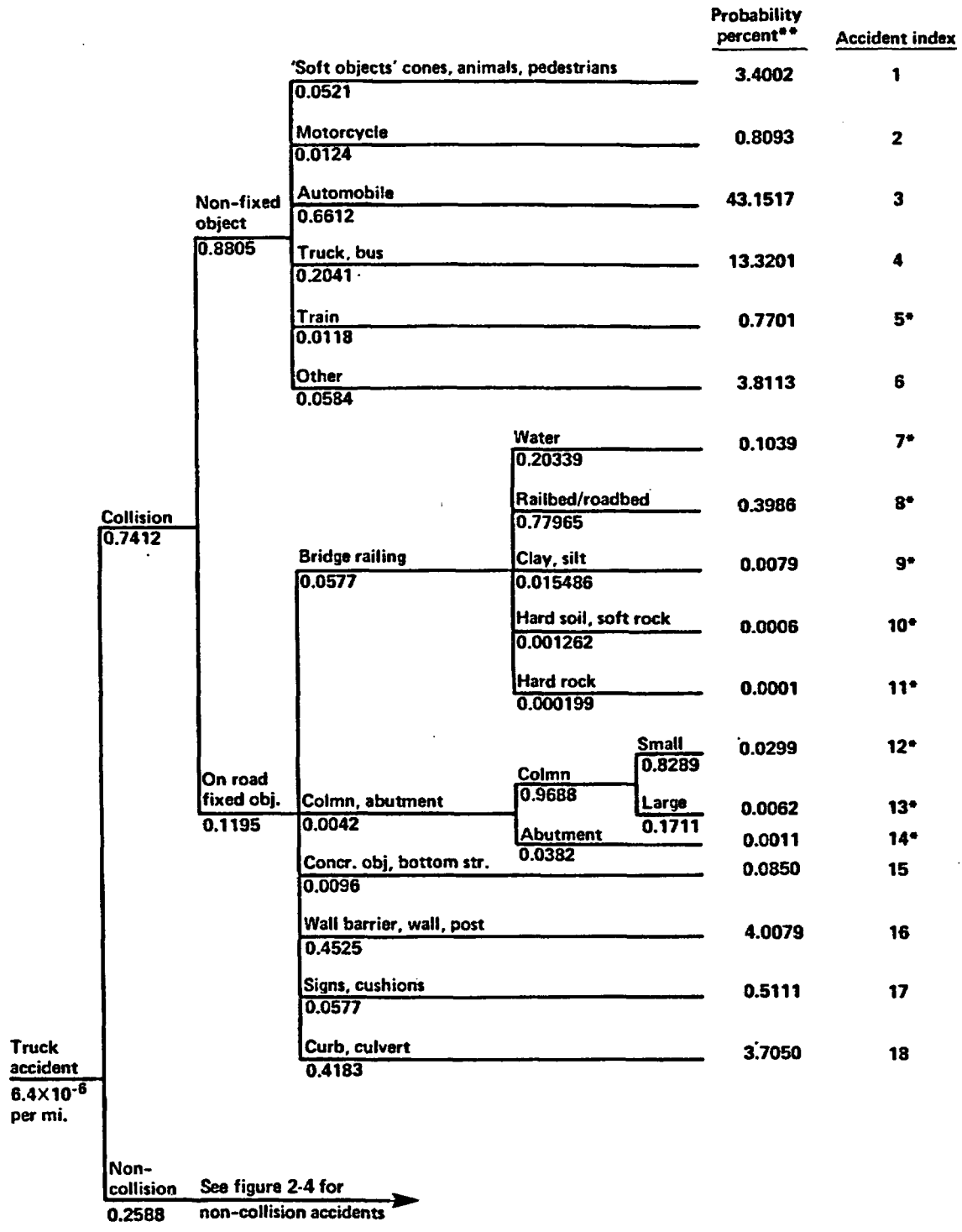

* Potentially significant accident scenarios

** Conditional probability which assumes an accident occurs

Figure 2-3 Truck collision accident scenarios and their percent probabilities.

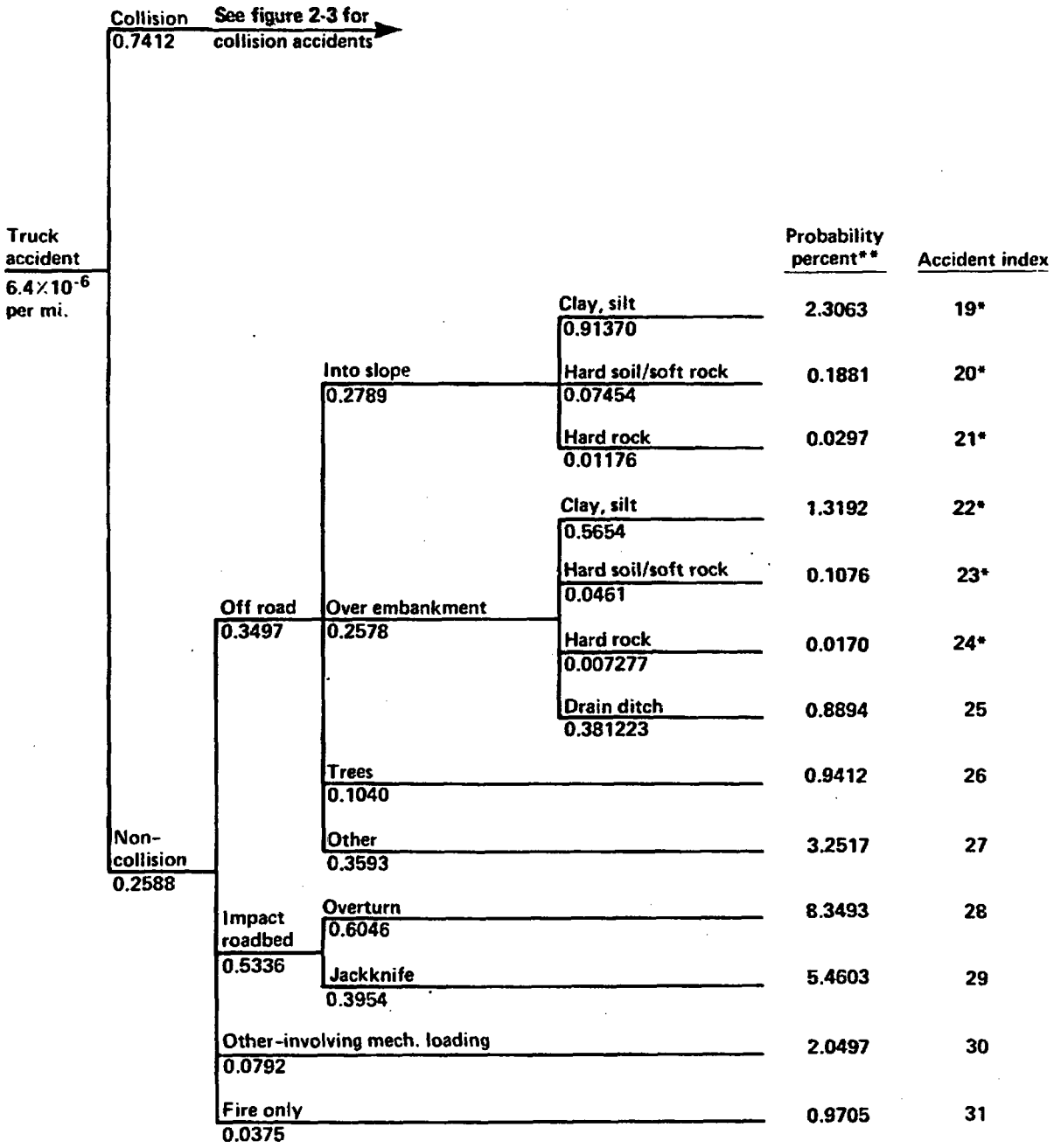

* Potentially significant accident scenarios

** Conditional probability which assumes as accident occurs

Figure 2-4 Truck non-collision accident scenarios and their percent probabilities.

Based on the quasi-static screening analysis in Section 6.0 for mechanical loads and responses of the representative truck cask, only three significant accident scenarios can cause mechanical loads high enough to damage a spent fuel cask: collisions with trains and columns, trucks running off bridges and over embankments, and trucks running into slopes. Therefore, detailed accident loading information is compiled only for these significant scenarios.

Since collision accidents involving piers, columns, and abutments may lead to significant damage to a spent fuel cask, a survey is performed to differentiate among the various sizes of piers, columns, and abutments along state and interstate highways.[37] From the survey data, the fractional occurrence is determined for each pier, column, and abutment size and is used to estimate the probability of collision accidents involving piers, columns, and abutments. For example, the expected probability of collisions with large concrete abutments is estimated to be 0.0011% as given in Fig. 2-3.

In the event a truck runs off a bridge, the magnitude of the resulting impact load depends not only on the bridge height, but also on the surface being impacted below the bridge. A survey along Interstate 80 in California is performed to identify the types and frequency distributions of surfaces that could be impacted below the bridge.[38] These surfaces are classified into four categories: roadbeds, railbeds, water, and earth. The earth category is then subdivided into three sub-categories: soil, soft rock, and hard rock. The earth sub-category distributions are determined by the survey performed for "ran-off-the-road." Table 2.2 is a summary of the impact surface distribution under bridges.

2.5.1.1.2 Non-Collision Accident Hardness Data

Non-collision accident scenarios include rollover, jackknifing, and running off the road. The accident scenarios judged to have greatest damage potential for a spent fuel cask are the ran-off-the-road scenarios. In these accidents, the truck could impact a slope or go over an embankment, with the possibility of hitting a hard rock such as granite.

Table 2.2
Fractional Occurrence of Surface Types below Bridges on Interstate 80 from Davis, California to Nevada Border

Surface Type	Fractional Occurrence
Water	0.2034
Roads/Railways	0.7797
Earth	
Soil	0.0154
Soft Rock	0.0013
Hard Rock	0.0002

The hardness of earth surfaces adjacent to highways can vary over a wide range. This variability can have a significant effect on the loadings that could be imposed on a cask or any other impacting object. The water and land (hard rock, soft rock/hard soil, and tillable soil) distribution along proposed spent fuel shipment routes between the east coast and west coast is initially estimated using agricultural soil survey data and geological highway maps for the United States.[39,40] The initial distributions estimated from these sources are considered to be indicative of the types of surfaces which could be impacted along highways in the various regions of the United States. However, since highway construction and landscaping can greatly affect the adjacent surroundings, the initial distributions are used to select representative portions of Interstates 5 and 80 in California to perform detailed highway surveys and to establish final distributions along highways.

The types of earth adjacent to 133 miles of Interstate 5 through Orange and Los Angeles Counties in California are classified into three groups: tillable soil, non-tillable soil, and hard rock (Appendix D, Table D.2). Only tillable soil (92.8% fractional occurrence) and untillable soil, classified as soft rock (7.2% fractional occurrence), are identified on a total mileage basis. Although this survey included portions of the Santa Susana Mountain, no hard rock is identified in the survey.

A highway survey of soil types adjacent to the roadway is then performed on a section of Interstate 80 from Davis, California, to the Nevada border.[38] This 122 mile section of Interstate 80 crosses the Sierra where numerous outcroppings of granite rock occur. This survey (Appendix D, Table D.3) indicates the following earth distribution : tillable 90.2%, non-tillable 7.3%, hard rock 2.5%.

Based on the results of both highway surveys and the reviews of the agricultural soil surveys, the geological highway maps, and proposed spent fuel shipping routes, the representative earth distribution used in this study is tillable soil 91.4%, soft rock/hard soil 7.4%, hard rock 1.2%.

2.5.1.2 Impact Velocity

The impact velocity depends on the relative velocity of the cask and the angle of impact with respect to the object impacted. The distributions of these two variables are estimated from truck accident records, train accident records, highway surveys, and engineering judgments for the significant accident scenarios.

2.5.1.2.1 Cask Velocity

The distribution of potential cask velocities can vary depending on the specifics of the accident scenario. Each accident scenario may have a different historically based velocity distribution. For example, the distribution of accident velocities experienced in truck-truck collisions differs from the distribution associated with accidents involving falls from bridges. In the truck-truck accidents, the distribution depends on the individual velocities of the trucks at collision. For accidents involving falls from bridges, the accident velocity is determined by the fall height. The accident velocity distribution for accident scenarios involving trucks running over or off embankments could, at worst, be represented by the vector sum of the vehicle velocity and the velocity attained in the resulting fall.

One of the following distributions of cask velocities at impact is considered applicable to a particular truck accident scenario:

V1: A distribution based on truck accident velocities with braking effects included,

V2: A distribution based on fall heights from bridges,

V3: A distribution based on truck accident velocities with braking effects and fall heights from bridges, or

V4: A distribution based on train accident velocities at grade crossings.

Reports record accident velocity data in many different forms. Most reports give the vehicle velocity prior to the accident. Therefore, it is difficult to estimate the actual velocity of impact which a cask can realistically experience.

Distribution V1 is determined by consideration of accident reports involving trucks/semitrailers. Table 2.3 gives the fraction of accidents occurring in the State of California for 1958 through 1967 for trucks/semitrailers as a function of truck velocity prior to the accident.[41-51] This accident data is derived from the California Highway Patrol's (CHP) annual report on fatal and injury motor vehicle traffic accidents. This data represents a sample of truck/semitrailer drivers involved in fatal and injury accidents and their estimated accident velocity without braking effects included. Approximately half of truck accidents occur at velocities greater than 30 mph. This velocity data is conservative because it does not include non-injury accidents, which typically occur at lower velocities.

Accident velocities for the State of California are compared with those in the states of Alabama, Texas, Virginia, and North Carolina.[52-56] The comparison is made for all vehicles because not all of the states had information on trucks. The comparison shows that the California accident velocities are comparable for the same conditions. Therefore, it is concluded that the accident velocities from California are representative of those in the nation and that the truck/semitrailer accident velocities for California provide a reasonable estimate of future accident velocities for spent fuel transport trucks. Accident data from North Carolina is used to estimate the effects of braking on the reduction of impact velocity. The method used to estimate the velocity reduction is described in Subsection 5.2.1.2.

Distribution V2, the velocity attained in falls from bridges is developed directly from a survey of bridge height data presented in Table 2.4.[37] This bridge height data is collected along Interstate 5 during the survey of bridge column sizes and types of soil along the highway. The bridge height distribution is reasonable for representing travel on interstate and state highways.

Table 2.3
Distribution of Velocities for Trucks/Semitrailers
Involved in Fatal and Injury Accidents in California, 1958-1967[a/]

Velocity (mph)	Number of Accidents	Fractional Percent (%)	Cumulative Percent (%)
0	1,774	6.41	6.41
1 - 10	4,143	14.96	21.37
11 - 20	4,122	14.89	36.25
21 - 30	4,248	15.34	51.59
31 - 40	4,733	17.09	68.69
41 - 50	7,264	26.23	94.92
51 - 60	1,173	4.24	99.15
61 - 70	171	0.62	99.77
>70	63	0.23	100.00
Subtotal	27,691	100.00	-
Not stated	2,834	-	-
Total	30,525	-	-

a/. Data derived from the 1958 to 1967 annual reports on fatal and injury motor vehicle traffic accidents, California Highway Patrol

Table 2.4
Distribution of Bridge Heights along Interstate 5
through Orange and Los Angeles Counties, California

Bridge Height (ft)	Number of Bridges	Fractional Percent (%)	Cumulative Percent (%)
0 - 10	5	4.13	4.13
11 - 20	22	18.18	22.31
21 - 30	74	61.16	83.47
31 - 40	14	11.57	95.04
41 - 50	3	2.48	97.57
51 - 60	1	0.83	98.34
61 - 70	1	0.83	99.17
71 - 80			
81 - 90	1	0.83	100.00
Total	121	100.00	-

Distribution V3 is developed for those accident scenarios in which the velocity is considered to be the vector sum of the accident velocity V1 and the fall velocity V2. This distribution is used for accidents that involve running off of embankments and into slopes.

Distribution V4 is used for accident scenarios involving train-truck collisions at grade crossings. The magnitude and frequency of the cask velocity is estimated from rail-highway grade-crossing accident velocity data. This accident data is derived from the FRA annual report on rail-highway grade-crossing accident/incident and inventory for the years 1975 through 1982.[57-64] Table 2.5 gives the fraction of rail-highway grade-crossing accidents as a function of train velocity. Fewer than 30% of the accidents occur at velocities greater than 30 mph.

2.5.1.2.2 Impact Angle

The impact angle is the angle between the cask velocity and the plane of the surface struck. The damage caused in a transportation accident is not controlled solely by the vehicle(s) velocity at impact. A head-on impact is more severe than a sideswiping event, even though both accidents could involve similar accident velocities. The reason is that accident severity is most directly related to the vector component of the accident velocity perpendicular to the object being struck. The orientation of the vehicle, or in this case, cask motion relative to the plane or surface of the object impacted, is established by a parameter called the impact angle, depicted earlier as angle α in Fig. 2-1. A 90^{0}-impact angle defines the accident as head-on; that is, the impact velocity and accident velocity at impact are the same. An impact angle close to 0^{0} defines the accident as a sideswiping impact; that is, the impact velocity is only a small fraction of the accident velocity. In mathematical terms the impact velocity is the accident velocity multiplied by the sine of the impact angle.

The distribution of impact angles can be expected to be a function of the accident scenario being considered. For example, if an accident involves a collision with another vehicle on the road, any impact angle is equally

Table 2.5
Train Velocity Distribution for Rail-Highway Grade-Crossing Accident/Incidents Involving Motor Vehicles, 1975-1982[a]

Velocity (mph)	Number of Accidents	Fractional Percent (%)	Cumulative Percent (%)
0 - 9	27,553	33.79	33.79
10 - 19	16,765	20.56	54.35
20 - 29	14,611	17.92	72.47
30 - 39	10,788	13.23	85.50
40 - 49	7,617	9.34	94.84
50 - 59	2,879	3.53	98.37
60 - 69	824	1.01	99.38
70 - 79	461	0.57	99.94
80 - 89	29	0.04	99.98
>90	17	0.02	100.00
Subtotal	81,544	100.00	-
Unknown	573	-	-
Total	82,117	-	-

a/ Data derived from the 1975 to 1982 annual inventory on rail-highway grade-crossing accidents/incidents, Federal Railroad Administration

likely. Information on impact angle distributions is not readily available; however, three distributions are defined. The distributions include:

VV1: A uniform distribution in which any impact angle is equally likely,

VV2: A distribution which considers all impacts as 90^{o} occurrences, and

VV3: A triangular distribution in which 90^{o} impacts are most likely with other orientations decreasing in likelihood as the impact angle decreases.

2.5.1.3 Cask Orientation

Historical records do not contain significant information on the orientation of the cask with respect to the object impacted. For impacts on a surface 0^{o} cask orientation defines a sidewise impact while a 90^{o} cask orientation defines an endwise impact of the cask. Alternatively for impacts by train sills, a 0^{o} cask orientation defines a head-on impact to the cask side while a 90^{o} cask orientation indicates a near miss. Again, since the cask orientation distribution can be dependent on the accident scenario being considered, three cask orientation distributions are defined. The distributions include:

CT1: A uniform distribution in which all cask impact orientations are equally likely,

CT2: A triangular distribution in which end-on impacts on surfaces or head-on impacts to the side of the cask by train sills are most likely, with other orientations decreasing linearly in likelihood as the orientation angle approaches 0^{o}, and

CT3: A triangular distribution in which impacts at 45^{o} are most likely, with other orientations decreasing linearly in likelihood as the orientation angle approaches either 0^{o} or 90^{o}.

2.5.2 Thermal Loading Parameters

The thermal response of a cask, specifically the temperature reached within the gamma shield, is determined by three major thermal loading parameters: fire duration, flame temperature, and fire location with respect to the cask. The distribution functions for these parameters can be a function of the specific accident scenario being evaluated and can also vary from accident to accident within the same accident scenario (e.g., variations of fire locations with respect to the cask).

The BMCS reports and other sources provide information such as the accident type, the cause of fire property damage, and method of extinguishment.[65] This information is useful for defining actions to improve public safety. The sources, however, do not provide data on thermal loading parameters such as flame temperature and fire duration. Limited data on thermal loading parameters are sometimes included in the National Transportation Safety Board severe accident reports, but the data is not sufficient to adequately define thermal loads and their fractional occurrence.

A truck-fire accident has many variables that affect the fire and thermal loads. The variables include the involvement of the truck's fuel tank and its contents; the possibilities of a collision with an auto, another truck or a tanker truck; and the availability of fire fighting equipment. The many variables and the lack of specific data lead to the use of the Monte Carlo technique[66] and engineering models to determine the distribution functions for the thermal loading parameters.

2.5.2.1 Accident Scenarios and Fire Frequency

The accident scenario in which a truck is involved can affect the thermal loads on the truck and its cargo. Table 2.6 presents the accident type and the frequency of fires.[66] In Subsection 5.3 these accident fire frequencies are correlated with the accident scenarios in Figs. 2-3 and 2-4 to determine the probabilities of fire for each of the scenarios.

Table 2.6
Frequency of Fire for Truck Accident Types

Accident Type	Fire Involved in Accident (%)	No Fire in Accident (%)
Collision with Auto	0.3	99.7
Collision with Truck	0.8	99.2
Collision with Fixed Object	0.4	99.6
Other Collision	0.9	99.1
Ran off Road	1.1	98.9
Overturns	1.2	98.8
Other Noncollision	13.0	87.0

2.5.2.2 Fire Duration

Since the available fire-accident data do not provide specific information on fire duration, the Monte Carlo method is used to derive the fire duration distribution for each accident scenario.[66] This method combines data on accident types, cause of the fire, availability of combustibles, and fire-fighting efforts with statistical engineering models on the burning of combustibles for various types of accidents. A Monte Carlo computer code is used as recommended[66] to analyze the interaction and probabilistic involvement of fuel tanks, tires, cargo, brakes, and electrical systems, as well as the effects of fire fighting efforts.

The Monte Carlo code is also used to predict fire duration distributions for each accident scenario in Figs. 2-3 and 2-4. As might be expected, there is a large variation in the fire duration distributions for the scenarios. In general, the fire durations following high impact loads on hard surfaces are shorter compared to those involving lower impact loads or collisions with other trucks, particularly tanker trucks.

2.5.2.3 Flame Temperature

Flame temperature depends on the burning materials and the amount of oxygen present in the flame. This study uses the flame temperature probability distribution from Sandia.[66] The fire distribution is primarily based on the open burning of hydrocarbon fuels such as diesel and gasoline in the temperature range of 1400 to 2400°F, but also includes other materials which tend to burn at lower temperatures.

The size of a fire affects both the radiation heat transfer capabilities and the duration of the fire. Fires with a flame that is at least four feet high radiate essentially as a blackbody with flame emissivity in the range of 0.9 to 1.0. Smaller fires have much lower emissivities and are usually of short duration, and would have little effect on a cask.

The convection heat transfer from a fire to a truck and its cargo is usually less than 10% of the radiation heat transfer. As discussed in Appendix F, an equivalent flame temperature for specific cask configurations

can be used to estimate the thermal loads for various combinations of flame temperatures, flame emissivities, and convection coefficients. In this study, it is conservatively assumed that all fires will have an emissivity of 0.9.

2.5.2.4 Fire Location

The heat load to a cask varies with the location of the fire with respect to the cask. The heat load to the cask can decrease by a factor of 4 for a fire 20 feet from the cask compared with the heat load for an engulfing fire. As with other fire parameters, insufficient historical accident data exists to develop fire location distributions with respect to the cask. A uniform distribution for cask-to-fire location is assumed for all fire accident scenarios defined by:

L1: A uniform distribution in which any fire location relative to the cask is equally likely, in the interval between 0 and 31.5 feet. The cask is sidewise to the fire in all cases to maximize the heat load to the cask.

2.6 Railway Accident Loading Parameters

2.6.1 Mechanical Loading Parameters

Types of train accidents are identified from FRA data, and supplemented by other sources to define accident scenarios used in this study. For some of the accident scenarios, loading parameter magnitudes and frequencies are estimated from highway data. In other cases, loading parameter data is derived from severe accident reports. In all cases, the selection of the data is justified as being suitably conservative. As with highway accident scenarios, the primary effort in obtaining railway accident data is placed on collecting information on those accident scenarios that could result in high loads to a cask. In this subsection the distribution functions are determined for three mechanical loading parameters: object hardness, impact velocity, and cask orientation.

2.6.1.1 Accident Scenarios and Object Hardness

Data is collated from several sources to derive accident scenarios and to estimate the cask impact frequency with a particular object. The combined data are presented in Fig. 2-4 for derailment, collision, and other accident types. The fraction of train accidents due to each type is estimated from the FRA data in Appendix C.[11-17] Derailment is the most common railway accident, accounting for 77.1%. Derailment involves a section or all of the train leaving the track. The section leaving the track separates from the preceding car as it leaves the track, causing the braking system to activate for all cars in the train. The lead car leaves the track at the highest speed, and the other cars follow at successively slower speeds. The average derailment involves approximately 10% of the cars in the train.

Collision accidents account for 13.4% of train accidents. The damage during a collision is usually limited to the cars near the impact point and involves less than 10% of the cars. For head-on collisions, damage is usually limited to the locomotive and the few cars that follow. For rear-end collisions, only the caboose and the few cars ahead of it are damaged.

Other accidents, including grade-crossing accidents, account for the remaining 9.5% of the accidents. These accidents usually do not cause serious impact forces to the train.

As shown in Fig. 2-5, collision accidents can result in derailments. In 64% of the collisions, the train remains on the tracks. In this case the cars may impact each other, but the forces would be relatively low or else the cars would have left the tracks. In 36% of the collisions, a derailment results and the cars leave the tracks. When considering the percentage of derailments occurring with collisions, the total percentage of train accidents that involve derailment is 82%.

The severe accident data in Appendix A is used in conjunction with the highway data to identify the objects and to estimate impact frequencies for the derailment accidents.[67] Owing to the limited amount of severe accident data and the nature of the reports, there is a high uncertainty in applying the data to the continuous spectrum of accidents.

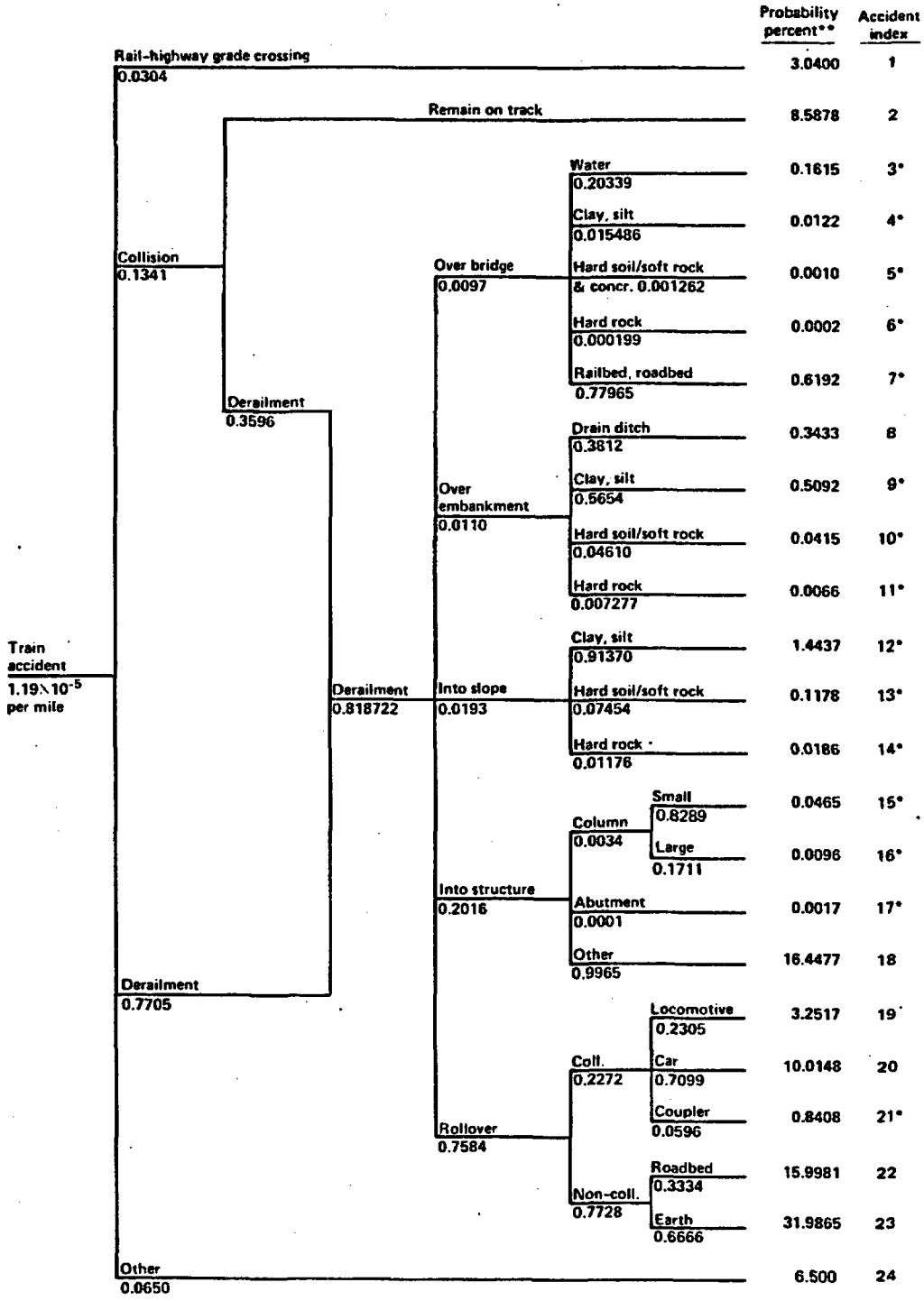

*Potentially significant accident scenarios
**Conditional probability which assumes an accident occurs

Figure 2-5 Train accident scenarios.

If a derailment accident occurs, the train can go off a bridge or an embankment, strike a slope, or rollover onto the adjacent ground. In this study, the percentage of accidents that go off a bridge or an embankment or onto a slope is estimated to be the same as those for highway accidents. For these types of accidents, the frequencies of impacting different soils, roadways, and water are also assumed to be the same as those used for highway accidents. These estimates and assumptions are made because of the lack of data on railway accidents and the fact that railways cross similar terrain as highways for similar routings. The remaining derailment accidents are assumed to be rollover-type accidents.

When a train derails in a rollover type of accident, it can (1) slide along the adjacent railbed or earth with relatively low damage occurring; (2) hit the superstructure of adjacent cars or locomotives; (3) strike couplers from adjacent cars; or (4) impact structures adjacent to the track. The severe accident data from Eggers[67] is used to estimate the frequencies for impact on railbed, earth, car superstructure, locomotive superstructures, car couplers, and adjacent structures. As shown in Fig. 2-5, it is estimated from the Eggers database that 0.8% of the train derailment accidents involve train couplers. The frequency for impacting large structures, such as columns and abutments, is estimated to be the same as the frequencies obtained from the CALTRANS highway data.

2.6.1.2 Impact Velocity

The impact velocity of a cask involved in a train accident depends on the cask velocity and the impact angle. The cask velocity depends on the train velocity prior to collision or derailment and the height of any fall that might occur. The impact velocity distributions for a cask involved in train accidents are estimated from train accident records, surveys, and engineering judgments.

2.6.1.2.1 Cask Velocity

For potential accidents in which the rail cask impacts an object, the magnitude and frequency of the impact velocity are estimated from the train accident velocity provided in Appendix C. This estimate conservatively disregards the fact that a reduction in impact velocity occurs because of energy absorption by the transporting car or the rest of the train. Tables 2.7 and 2.8 give the average frequencies of train collisions and derailments as functions of accident velocities, respectively, for the years 1979 through 1982. This accident data is derived from the FRA reports on train accidents.[13-17] The velocities for other accidents include grade-crossing incidents which are included in the truck data.

In the absence of a statistical data base on distance fallen by trains going off bridges and embankments in actual accidents, the highway survey bridge distribution in Table 2.4 is used to estimate distances fallen in this type of accident. Since specific train and truck routes for transporting spent fuel traverse similar terrain, the use of the highway bridge data for this study is reasonable.

In summary, the cask velocity distributions for each of the potentially significant train accident scenarios are:

TV1: A distribution based on train collision accident velocities without braking,

TV2: A distribution based on train derailment accident velocities without braking,

TV3: A distribution based on fall heights from bridges, and

TV4: A distribution based on the vector sum of train derailment velocities and fall heights from bridges.

Table 2.7
Railroad Accident Velocity Distribution, Collisions, Main Line, 1979-1982[a/]

Velocity (mph)	Number of Accidents	Fractional Percent (%)	Cumulative Percent (%)
1 - 10	392	46.12	46.12
11 - 20	182	21.41	67.53
21 - 30	117	13.76	81.29
31 - 40	92	10.82	92.12
41 - 50	47	5.53	96.65
51 - 60	14	1.65	99.29
61 - 70	3	0.35	99.65
71 - 80	2	0.24	99.88
81 - 90	0	0.00	99.88
>91	1	0.12	100.00
Subtotal	850	100.00	-
Unknown	8	-	-
Total	858	-	-

a/ Data derived from Federal Railroad Administration reports on train accidents, 1979 - 1982.

Table 2.8
Railroad Accident Velocity Distribution, Derailments, Main Line, 1979-1982[a/]

Velocity (mph)	Number of Accidents	Fractional Percent (%)	Cumulative Percent (%)
1 - 10	4,394	40.42	40.42
11 - 20	2,250	20.70	61.12
21 - 30	2,183	20.08	81.21
31 - 40	1,091	10.04	91.24
41 - 50	659	6.02	97.30
51 - 60	239	2.20	99.50
61 - 70	41	0.38	99.88
71 - 80	10	0.09	99.97
81 - 90	3	0.03	100.00
>91	0	0.00	-
Subtotal	10,870	100.00	-
Unknown	76	-	-
Total	10,946	-	-

a/ Data derived from Federal Railroad Administration reports on train accidents, 1979 - 1982.

2.6.1.2.2 Impact Angle

As for highway accidents, there is insufficient historical accident data available to define distribution functions for the impact angle of a spent fuel cask onto an object. Three distribution functions for spent fuel cask impacts are assumed for train accidents, namely: (1) uniform distribution, (2) all impacts at 90^{o}, and (3) triangular distribution in which 90^{o} impacts are most likely.

2.6.1.3 Cask Orientation

Since there is insufficient historical railway accident data available to define distribution functions for the cask orientation at the time of impact, three distribution functions are assumed for train accidents. The distribution functions are (1) uniform distribution, (2) all impacts endwise or head-on to the cask, and (3) triangular distributions in which 45^{o} impacts are most likely.

2.6.2 Thermal Loading Parameters

As with truck accidents, every train accident does not necessarily result in a fire. As indicated in Appendix C, approximately 1% of train collision and derailment accidents involves a fire. As for truck accidents, the train accidents have data on type of accident, frequency of fire, cause of fire, and property damage estimates. However, the accident records do not provide data on thermal loading parameters such as flame temperature and fire duration.

A train-fire accident has a large number of variables that affect the thermal loads. Such variables are (1) type of accident (collision, derailment, grade crossing, etc.), (2) type and amount of cargo (flammable or nonflammable), (3) involvement of locomotive fuel, (4) types of cars involved (box car, tanker, etc.), and (5) the availability of fire fighting equipment.

The same methods used in Subsection 2.5.2 to estimate the truck fire duration distribution are used here to estimate the distribution functions for the three thermal loading parameters: fire duration, flame temperature, and fire location.

2.6.2.1 Accident Scenarios and Fire Frequency

The type of railway accident can affect the thermal load on a train and its cargo. Table 2.9 presents the accident type and the frequency of fires, modified to include grade-crossing accidents which were separately identified beginning in 1978 (see Appendix C).[66] The fire frequency for "other" accidents is judged to be too high, but owing to the lack of consistent data, this conservative estimate is used.[66]

2.6.2.2 Fire Duration

Since the available fire-accident data do not provide specific information on fire duration for each of the railway accidents, the same method used in Subsection 2.5.2.2 to estimate truck fire duration distribution is used to estimate the fire duration distribution for trains. A Monte Carlo scheme is used in analyzing a large number of variables and their interactions.[66] The code can evaluate the interaction and involvement of locomotive fuel tanks, different types of rail cars and their flammability, and different types and amounts of flammable cargo, as well as the effects of fire fighting efforts. The code is used to predict the fire distributions for each of the accident types in Table 2.9 and the accident scenarios in Fig. 2-5.

2.6.2.3 Flame Temperature

The thermal loads on a train and its cargo are affected by the flame temperature of the fire. They are primarily determined by the type of material involved in the fire, the oxygen supply, and geometric configuration. Train fires often include diesel fuel, flammable cargo, and flammable parts of the cars. The flame temperature for train fires are the same as those evaluated for truck fires in Subsection 2.5.2.3. For the purpose of this study, it is assumed that all train fires will have an emissivity of 0.9.

Table 2.9
Train-Fire Accident Types

Accident Type	Fire Involved in Accident (%)	No Fire in Accident (%)
Collision	1	99
Derailment	1	99
Grade Crossing	1	99
Other	90	10

2.6.2.4 Fire Location

As with other fire parameters, insufficient historical accident data exists to develop fire location distributions with respect to a spent fuel cask. As is done for the truck cask accident scenarios, uniform distributions (L1) are assumed for each of the fire accident scenarios for fire locations 0 to 43.0 feet from the cask.

3.0 SELECTION OF REPRESENTATIVE SPENT FUEL CASKS FOR EVALUATION

3.1 Introduction

Casks currently certified for shipment of spent fuel from nuclear power reactors in the United States vary distinctly in design.[1-4] The most obvious difference between these casks is that they are designed to carry differing amounts of spent fuel. Casks weighing under 25 tons carry one or two fuel assemblies and can be transported by truck. Other casks can carry three to seven fuel assemblies and can also be carried by truck if appropriate highway overweight permits are secured. Finally, because railroads can carry greater loads, currently licensed rail casks can carry between 7 and 24 assemblies.

All of these casks must be designed to accomplish certain basic safety functions which are defined by a set of performance-oriented regulatory requirements.[5] In this regulatory approach, the cask design features which accomplish a specific safety function can vary, but the functional result must meet minimum specified requirements. In order to study the adequacy of the regulations to provide radiological protection, representative casks are defined which have design features likely to meet the regulations. Sufficient features must be defined to evaluate the protection provided by spent fuel casks involved in transportation accidents.

In addition, casks designed to meet regulatory requirements are usually designed and manufactured to code and standards which have margins of safety embedded in them. These margins of safety ensure that the spent fuel cask not only will meet the regulatory accident test conditions and radiation hazard limits but will survive loading conditions beyond the regulatory conditions.

The purpose of this section is to define the representative casks which are used in the accident response calculations described in later sections of this report. These representative casks are developed from current cask designs and technology. These representative casks include the necessary design features and safety margins for evaluating their response to accident conditions.

In Section 3.2, general safety functions for the cask are defined. The cask features needed to meet these functions are identified. Specific characteristics are determined for the various design features.

In Section 3.3, each design feature is evaluated from two standpoints: (1) the feature's susceptibility to damage under transportation accident conditions, and (2) the feature's ability to mitigate damage to other important cask features. Some features, e.g., impact limiters, are characteristically sacrificial and highly susceptible to damage, but are effective in mitigating further damage to the rest of the system. At the other extreme are features that are characteristically highly resistant to damage, but transmit damaging forces into other parts of the system with little mitigation.

In Section 3.4, six preliminary cask designs are evaluated on a comparative basis. From this comparison the gamma shielding material for the representative truck and rail cask designs is selected. The six designs include three truck casks and three rail casks which use the candidate shield materials: lead, depleted uranium, and steel.

Section 3.5 describes the two representative cask designs selected--one for truck shipments and the other for rail shipments. The physical and material specifications for the two designs are established. Those design features which are necessary to perform the evaluations in this study are identified. The rationale and the sensitivity studies used to define the required design features are also described.

Section 3.6 describes the typical safety margins that are included in licensed cask designs and the representative cask. These safety margins are embedded in the codes and standards used in designing and manufacturing casks.

3.2 Cask Functions and Design Features

Casks currently certified for shipment of spent fuel are relatively complex engineering structures designed to meet certain functional needs.[1-4] Many of these functional needs are dictated by the characteristics of the spent fuel being shipped. The spent fuel is a source of radioactivity and

heat, both originating within the fuel pellets which are contained within the rods of a fuel assembly. The primary cask functions include (1) containment of radioactive material, (2) shielding against the radiation emanating from the spent fuel, and (3) the assurance that subcriticality is maintained.

Containment is the retention of radioactive material within a closed vessel. Containment is provided to preclude any contact between people and radioactive material. Typically, containment is provided by the integrity of the spent fuel and by a cylindrical steel vessel (Fig. 3-1). The vessel is provided with a bolted end closure to accommodate spent fuel loading and unloading operations. The closure contains a seal to inhibit leakage between the cask containment and the environment. Piping penetrations of this containment are needed for operating purposes, and the associated closure valves are considered a part of the containment system. These penetrations are in the containment vessel for draining, filling, testing, etc. The containment cavity is filled with a non-oxidizing gas for shipments.

A radiation shield is a barrier which absorbs ionizing radiation or subatomic particles emanating from a radioactive source. Two types of radiation shielding are typically included in spent fuel cask design, gamma and neutron. The most important shielding provides protection against the highly penetrating gamma radiation. This protection is achieved through the use of dense materials such as lead, depleted uranium, or steel. These materials surround the containment vessel (Fig. 3-1) and are, in turn, enclosed within an outer steel shell. If steel is the shield material, this shield can be an integral part of the containment vessel. The second type of shielding is used to mitigate radiation caused by spent fuel emission of neutrons. This source of radiation is typically less significant than gamma radiation. Hydrogenous materials provide shielding against neutrons. The neutron shield, usually a water jacket, surrounds the cask on its exterior surfaces. The hazard associated with neutron radiation is such that loss of neutron shielding does not result in radiation levels that exceed regulations for accident situations. The regulations allow for higher external radiation levels following an accident than during normal transport.

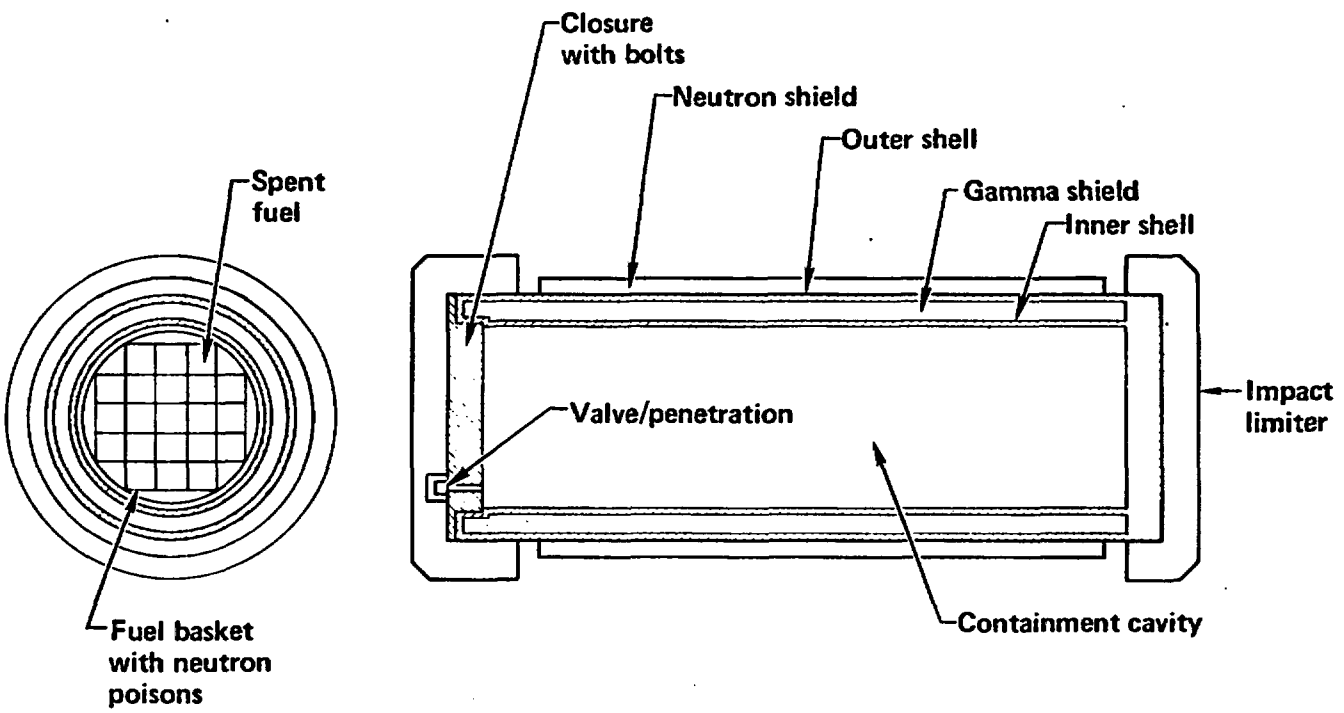

Figure 3-1 Spent fuel cask features important to safety.

Criticality is a self-sustained nuclear chain reaction which might result in high energy production and a radiation burst before self-termination. Spent fuel casks are designed to maintain a condition of subcriticality. The subcriticality assurance function, if not achieved by the physical limitation on the amount of spent fuel being shipped, is assured by maintaining geometric control of the spent fuel during shipment and by including neutron poisons in appropriate cask structural materials. Neutron fission interactions with spent fuel must attain a prescribed level before criticality can occur. The neutron poisons, which are typically included in the basket holding the fuel assemblies, absorb emitted neutrons to a sufficient degree to limit neutron fission interaction and thus assure subcriticality.

As the above discussions of containment, shielding, and subcriticality assurance indicate, two fundamentally different concepts are applied in the regulations: containment and shielding are limiting in nature while subcriticality is absolute.

In all casks, the design features used to meet each of the specific functional needs have many mutual dependencies. The containment shell, for example, must be designed to structurally support the heavy surrounding gamma shielding material. Also the geometry control achieved by internal cask features is dependent on the protection against deformations provided by the overall cask structure. These dependencies between specific design features are further described in Section 3.3 which discusses the performance requirements for the design features important to safety.

3.3 Cask Design Features Important to Safety

3.3.1 Containment

This subsection describes several design features which basically compose the typical cask containment system: (1) the cylindrical steel containment shell, (2) the bolted end-closure, (3) the closure seal, and (4) the piping and valves associated with any containment system penetrations. The containment system must be designed so that when subjected to the hypothetical

accident conditions specified in existing regulations, the regulatory limits for radioactive material releases are met. In practice, the required function of the containment vessel is achieved by a combination of three factors: (1) the structural integrity of the individual containment system features, (2) the provision of external features such as energy-absorbing structures designed to protect the cask and its containment system against external forces, and (3) the integration of the containment features into an overall cask design which maximizes the protection provided against these external forces.

The steel containment is designed as a system and must support itself and the weight of the spent fuel and other internal structure under regulatory-defined normal and accident transport conditions. The steel containment shell provides a substantial resistance to any externally applied forces. To provide ensurance that this shell maintains its integrity under potential transportation accident conditions, casks are designed with impact limiters. Impact limiting devices can take the shape of large end-caps made of a crushable material such as balsa wood or rigid foam, or they can be in the form of bendable metal fins or tubes which protrude from the outer cask body. In all cases, impact limiters are designed to limit, or reduce, the mechanical loads imposed on the cask containment shell. The impact limiters do this by deforming and sacrificially absorbing the energy of the accident. The containment shell is designed for the impact-limited loads which arise from the accident test conditions.

The bolted containment end closure and the closure seal are located within the envelope of protection provided by the impact limiting devices (Fig. 3-2). The bolted closure is typically recessed within the outer cask shell, and the closure seal is located between the end closure and the containment shell wall. These cask features are designed so that if the cask is subjected to accident conditions, the containment function is not compromised.

Piping and valves associated with subsystems that penetrate the containment are also located in protected recessed areas within the outer cask

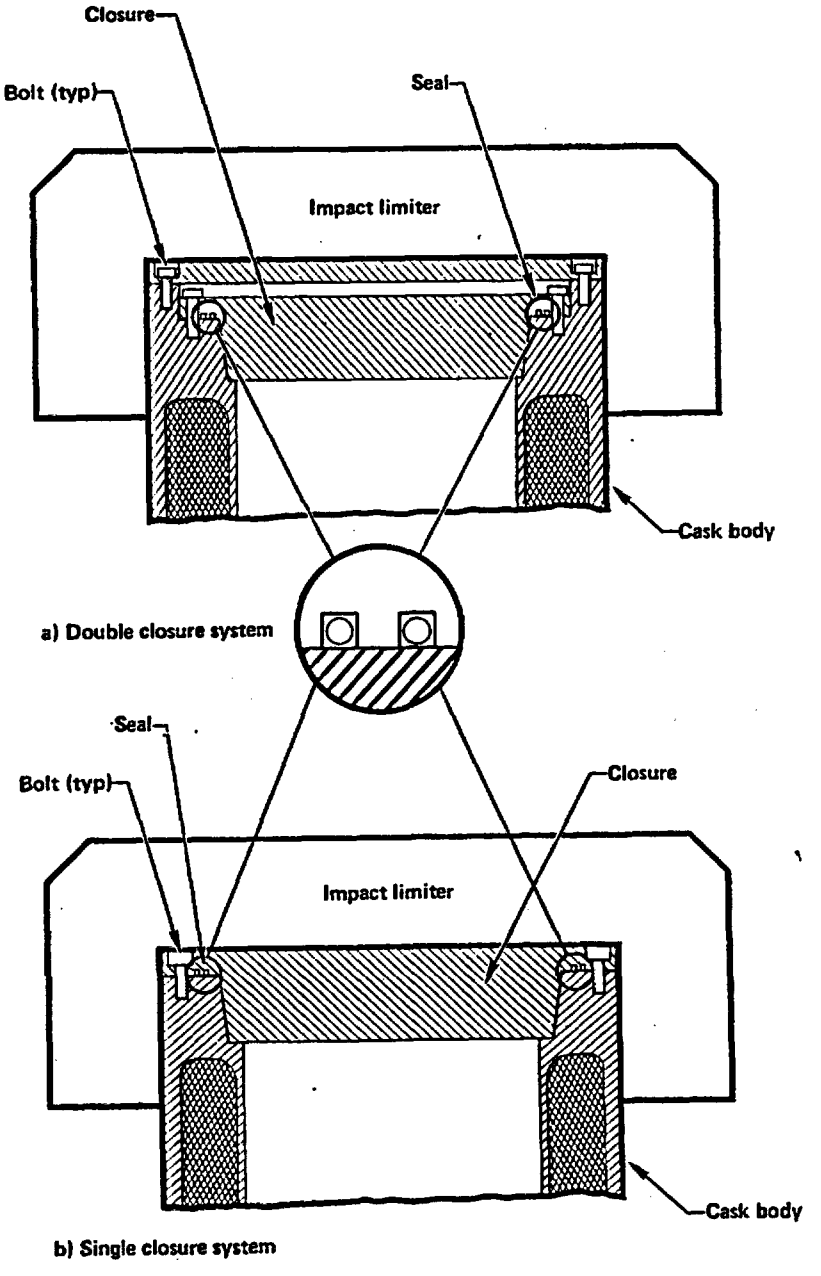

Figure 3-2 Typical closure designs for spent fuel casks.

structure (Fig. 3-3). As a result, this piping system and its related valves are also protected by the impact limiting devices. Again, this system is designed to withstand the accident conditions without compromising containment integrity.

3.3.2 Radiation Shielding

Shielding is provided in all cask designs to limit the gamma and neutron radiation which emanates from the spent fuel. The gamma shield is typically a dense metal, such as lead, depleted uranium, or steel. These materials surround the cask containment vessel and, in the case of lead and depleted uranium, are enclosed within an outer steel shell. The neutron radiation shield typically consists of hydrogenous compounds such as water. The neutron shield is generally located beyond the outer steel shell which encases the gamma shield. When water is used for neutron shielding, it is contained within a water jacket. The thicknesses of these shields are determined to ensure that the radiation levels external to the cask are within regulatory values which are specified for both normal transport and transportation accident conditions, (i.e., $\leq$200 mrem/hr on the external surface and $\leq$1 rem/hr at 1 meter from the external surface, respectively).

In practice, the dose rate of $\leq$1 rem/hr at 1 meter from the external surface can be achieved by maintaining the integrity of the gamma shield. The magnitude of neutron radiation is intrinsically limited to levels that allow the loss of neutron shielding to be presumed in the event of a transportation accident. The gamma shielding is protected by both the outer steel shell of the cask and the cask's impact limiters. If the cask is subjected to the accident test conditions, the cask gamma shield is designed to assure that external radiation levels remain within regulatory limits.

3.3.3 Subcriticality Assurance

Subcriticality for one pressurized water reactor (PWR) assembly or two boiling water reactor (BWR) assembly shipments (typically made by truck) is assured because the amount of fissile material available in the UO_2 fuel form

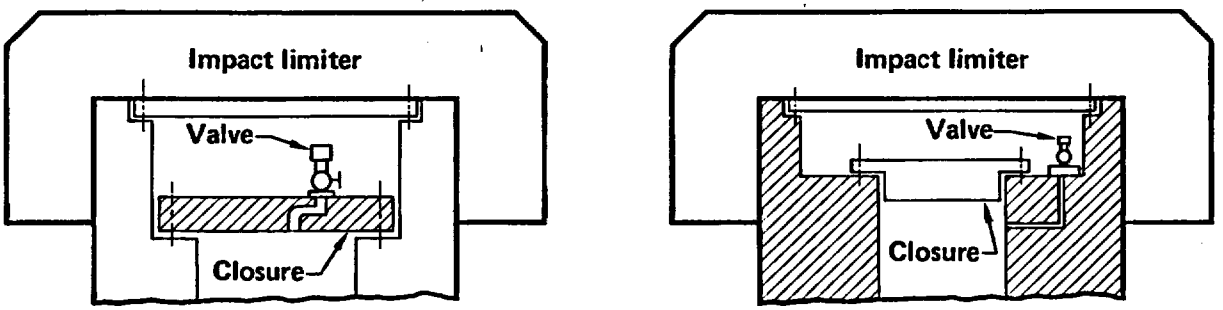

a) Valve through closure

b) Valve through flange

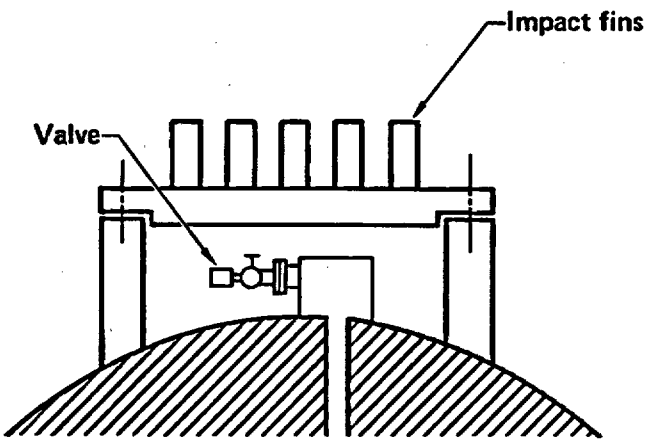

c) Exterior reinforced valve box

Figure 3-3 Typical cask penetration subsystems.

is insufficient to achieve criticality under any credible circumstances. Larger shipments, however, which are generally made by rail, do contain enough fissile material to make criticality a theoretical possibility if: (1) the material can be optimally rearranged geometrically, (2) a neutron reflecting material surrounds the fuel, and (3) a neutron moderating media such as water can be interspersed between fuel rods and assemblies. For these shipments, subcriticality assurance is achieved by geometry control features and the use of neutron poisons, materials which preclude a self-sustaining fission process.

A cask's capability to assure spent fuel subcriticality for these larger shipments is evaluated in an extremely conservative manner. The effectiveness of the geometry control provisions and the neutron poisons must be demonstrated not only under the specified accident test conditions but also under defined conditions which optimize the possibility for criticality. Among these other conditions, the larger shipments must be demonstrated to be subcritical when: (1) two similar casks are assumed to be stacked together in an arrangement which optimizes criticality potential, (2) the stacked casks are closely reflected on all sides by water, and (3) the fuel within each cask is subjected to optimum, interspersed hydrogenous moderation.

The assumed presence of the reflecting and moderating materials increases the possibility of achieving a critical configuration. The use of this conservative approach to assure subcriticality highlights the importance of cask features other than the spent fuel geometry control features and neutron poisons previously described. For example, if containment integrity is maintained, water or other hydrogenous material could not enter the cask containment vessel and the possibility of criticality would be precluded. Similarly, if the overall cask structure prevents gross internal distortions, then spent fuel geometry control and neutron poisons would be sufficient to assure subcriticality even if water or other hydrogenous material entered the cask containment vessel.

3.4 Selection of Cask Shielding Material

Shielding provides protection from both the neutron and gamma radiation emanating from spent fuel. The gamma shielding can be provided by several different materials, each with a distinct capability to withstand the mechanical and thermal loads associated with potential transportation accidents. The selection of the gamma shield material for a representative cask is based on an evaluation of the comparative performance of different preliminary cask designs: three each for truck and rail. The six preliminary designs shown schematically in Figs. 3-4 and 3-5 include consideration of sizing differences typical to truck and rail casks and the use of each of the three candidate gamma shield materials: lead, depleted uranium, and steel.

These six designs are evaluated against two quasi-static mechanical loading conditions, i.e., end-on and side loads. Then the magnitude of loads necessary to initiate yielding of the containment shell is determined. Static loads are applied to the end and side of the casks for this evaluation. The details of these evaluations are described in Appendix E. The results indicate that the lead shielded casks--both the railway and highway configurations--will begin to yield when subjected to a lower external force than the casks with steel or depleted uranium shields. From a structural standpoint, lead is the worst of the three candidate gamma shield materials and is, therefore, the material of choice.

The six preliminary designs also are compared in terms of their capability to absorb thermal energy from potential fire environments. In terms of thermal capacities, the steel-shielded designs are capable of absorbing the most heat; the depleted uranium and lead designs have essentially equal capabilities. Lead has a melting temperature below the other cask shield materials, which is considered another factor significant to safety. The thermal expansion effect is also the most significant for lead shielded casks. From a thermal standpoint, lead is again the worst of the three candidate shield materials and is the material of choice.

Based on these structural and thermal evaluations, lead is selected as the gamma shield material for the representative cask designs.

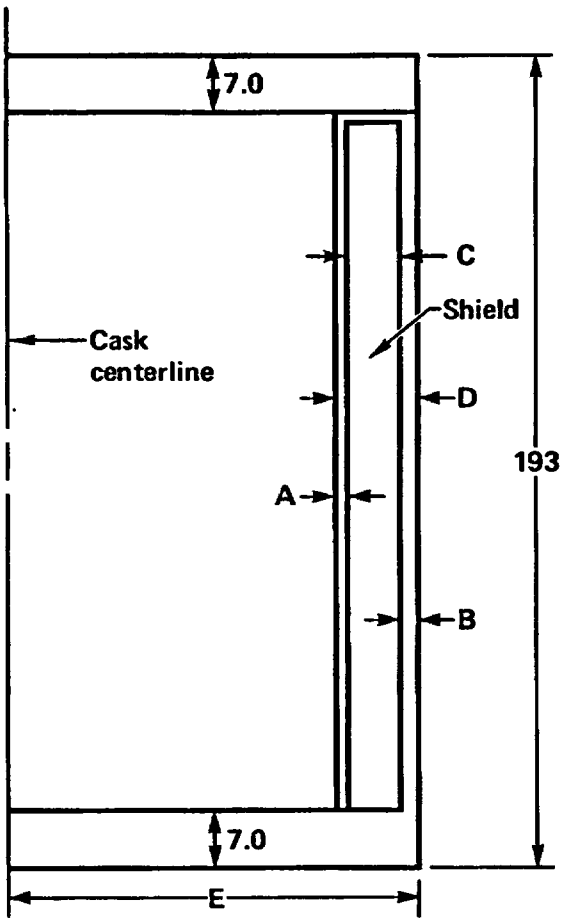

Dim	Thickness (in.)	Material
	Truck Cask 1	
A	0.5	304SS
B	1.25	304SS
C	5.25	Lead
E	13.75	304SS
	Truck Cask 2	
A	0.5	304SS
B	1.25	304SS
C	4.25	Depleted uranium
E	12.75	304SS
	Truck Cask 3	
D	12.25	Steel
E	19.00	Steel

Figure 3-4 Preliminary truck cask designs with three types of gamma shielding, used for quasi-static loading response studies only.

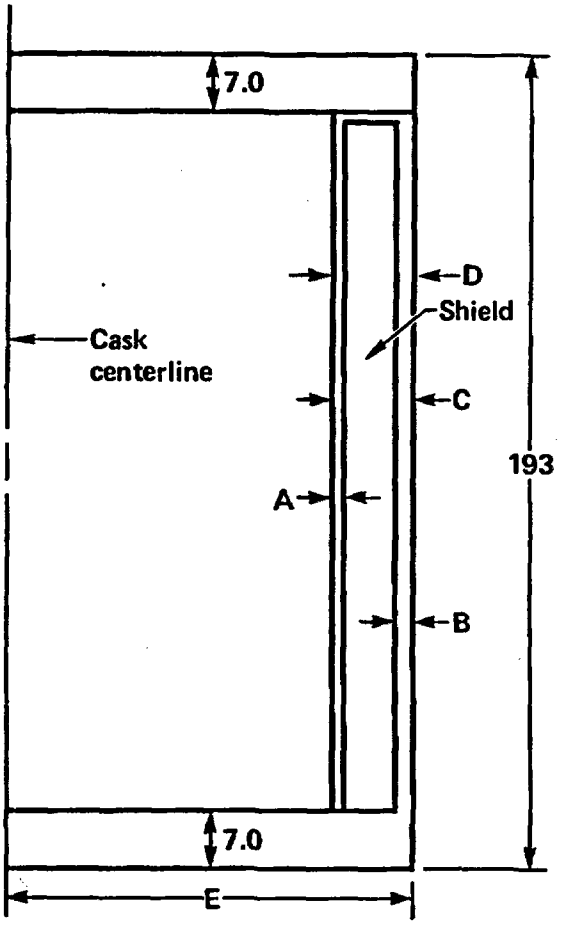

Dim	Thickness (in.)	Material
	Rail Cask 1	
A	0.5	304SS
B	1.5	304SS
C	5.25	Lead
E	26.0	304SS
	Rail Cask 2	
A	0.5	304SS
B	1.5	304SS
C	4.0	Depleted uranium
E	24.8	304SS
	Rail Cask 3	
D	12.25	Steel
E	30.75	Steel

Figure 3-5 Preliminary rail cask designs with three types of gamma shielding, used for quasi-static loading response studies only.

3.5 Definition of Representative Cask Designs

Previous sections discuss the functions of a spent fuel cask which are important to safety in the event of a transportation accident. This section presents the basis for the selection of the representative spent fuel casks used in the response analyses. The response of these casks is evaluated when subjected to the forces of real world accident environments in later sections of this report. The definition of a representative cask involves the accomplishment of two major tasks: (1) a determination of what cask features important to safety require specific design definition, and (2) a selection of a design definition which considers the variety of design features that can accomplish a specific safety function.

The following subsections present the rationale for accomplishing these two tasks. Separate subsections consider features which are important to the containment, shielding, and subcriticality assurance functions of cask designs. An additional subsection considers the definition of those cask features whose principal purpose is to mitigate the damage to the cask caused by accident forces (principally the impact limiters).

3.5.1 Shielding Features

Based on the evaluations in Section 3.4, lead is selected as the gamma shield material for the representative cask designs. Under impact conditions, lead is not self-supporting and can slump. A properly designed cask has adequate thickness in each steel shell as well as a soft impact limiter to prevent any significant lead slump from occurring under the 30-foot drop test conditions. Bonding of the lead to the inner shell of the cask can provide resistance to lead slump, but bonding varies significantly with the cask design and the fabrication process. Lead slump effects and damage to the cask are maximized when there is no bonding between the lead and the inner wall of the cask. Therefore bonding of the lead is not assumed.

The neutron shield design will not be expected to significantly affect cask response to the mechanical loads associated with severe transportation

accident environments. In fact, as indicated previously, the safety evaluations performed on all current casks presume that the capabilities of the neutron shield to reduce external radiation levels is lost as a result of the effects of transportation accident forces. On this basis, specifying the neutron shield design will not be necessary for the representative cask designs. However, this neutron shield, whether lost or maintained, will affect heat transfer. If a water neutron shield is maintained, it will exhibit high heat capacity as well as good heat transfer characteristics. If the water is lost, the empty tank containing air does not have high heat capacity, but provides an effective thermal barrier against heat from a fire. The post-fire effect of a neutron shield tank is to increase resistance to dissipation of internal heat, thereby increasing internal temperatures. Therefore, the volumetric characteristics of the neutron shield design must be considered in the definition of the representative casks.

3.5.2 Containment Features

The containment system includes the steel containment shell, the closure seal, the bolted-end closure, and the piping and valves in the containment-penetrating subsystems.

The steel shell is the containment feature most likely to be subjected to the full brunt of any severe transportation accident forces. The magnitude of any accident damage sustained by the shell provides a broad indication of the possibility and the magnitude of any resulting radiological hazard.

The containment seal can be subjected to damage by mechanical or thermal accident loads transmitted through the cask body to the seal region. However, the radiological hazard resulting from seal damage is limited to the spent fuel material which can escape from the confines of the cask through the damaged or deformed seal region. Rather than attempting to model one of several possible seal designs, a worst-case evaluation of seal performance can be made by presuming a loss of the seal functional capability and the release of radioactive material. Specific levels of damage to the cask must be exceeded as a result of accident forces.

The bolted cask end-closure can be subjected to damage by mechanical loads transmitted through the cask body. Damage can also result from the mechanical loads which can be caused by severe thermal environments associated with certain transportation accidents. The end-closure, however, is a massive structure highly resistant to mechanically imposed loads. Furthermore, the closure bolts are designed with sufficient strength to resist tensile forces from corner or end drops of the cask. The recessed characteristics of all current closure designs provide significant protection against shearing of the many large-diameter bolts typically used to secure the end-closure to the cask body. Forces sufficient to cause significant damage to the cask containment shell could occur in many of the conceived severe accident events without compromising the gross integrity of the bolted end-closure. The converse, that is, significant damage to the end-closure without similar containment shell damage is certainly conceivable, but far from likely. From an evaluation standpoint, the definition of a specific closure in a representative cask design will add considerable complexity to the calculations of cask response to severe accident environments. For the above reasons, although the mass and configuration of the closure requires definition, the details of the closure design are not included in the representative cask design(s). Again, a specific level of damage to the cask containment is used as a surrogate measure to indicate damage to, and the occurrence of radioactive material leakage from, the cask closure region.

The penetration subsystems are typically located within the confines of the cask body with exterior valves situated within heavily protected enclosures. These subsystems are easily protected by design features. Unless accident loads are highly localized, damage done to the cask shell will dominate overall cask damage. Notwithstanding, a highly localized load can violate the containment function by providing an opening from the cask containment to the environment through a failed penetration subsystem. Such a violation of containment will limit the escape of any spent fuel material to that which can migrate or be driven out through the small-diameter, tortuous passageways presented by the damaged penetration system.

As a result of the above considerations, the details of a penetration subsystem are not included in any representative cask design. Damage to the containment shell again is used to indicate the possibility of a failed or damaged penetration subsystem.

3.5.3 Subcriticality Assurance Features

Subcriticality assurance features, are provided in casks used for the shipment of larger numbers of spent fuel assemblies. The spent fuel geometry control features and the neutron poisons can be subjected to transportation-accident-induced mechanical forces transmitted through the cask body. These features form an integral part of the overall cask structure internal to the containment shell. Significant damage to these features requires that significant damage be incurred by the total cask structure including the containment shell. Physical damage, taken alone however, does not affect the cask's subcriticality assurance function. A hydrogenous material, such as water, must surround the cask and be interspersed between the individual fuel rods and fuel assemblies before criticality can become a credible possibility.

For these reasons, the subcriticality features are not specifically modeled in the representative cask designs. Instead, a maximum estimate of the likelihood of a criticality incident is provided in Section 9.0. This estimate considers those transportation accident events in which the structural damage is sufficiently severe to cause gross fuel assembly damage. The estimate then evaluates the likelihood that such an event will involve the intimate presence of hydrogenous material in the accident scenario.

3.5.4 Damage-Mitigating Features

The principal damage-mitigating features provided in cask designs are the impact limiters. These devices are designed to be sacrificial and can be of two general types, hard and soft. In either case, they absorb some of the energy of impact by deforming. The ratio of the energy absorbed by the impact limiter to that transmitted to the cask depends on the accident severity and

the type of impact limiter. The choice of an impact limiter is strongly affected by the choice of gamma shielding. If lead is the gamma shield material, soft impact limiters of balsa wood or rigid foam are typically used in cask designs. Soft impact limiters are designed to ensure that imposition of the accident test condition loads will not produce forces sufficient to cause lead slump.

Hard impact limiters in the form of bendable metal fins have been used in casks using depleted uranium as the gamma shield material. In these designs, the casks are more rigid. As a result, the forces transmitted through the cask body when the cask is subjected to the accident test conditions (specifically, the 30-foot cask drop onto an unyielding surface) are higher than those associated with casks using soft impact limiters. In either case, however, the cask design must meet the regulatory-defined post-test acceptance criteria.

A soft impact limiter is selected for the representative cask design for two major reasons. First, the soft impact limiter is consistent with the selection of the lead gamma shield. Second, and more significant, casks with soft impact limiters, if subjected to transportation accidents resulting in severe mechanical and thermal loads, will be more likely to incur damage.

3.5.5 Representative Cask Design Description

Two representative cask designs are developed: one for truck shipments and one for rail shipments of spent fuel. The representative truck cask design uses the same dimensions as the preliminary lead truck cask design (Fig. 3-4). The truck cask design allows transport of a single PWR fuel assembly. The representative rail cask design dimensions differ from the preliminary lead rail cask design (Fig. 3-5). The capacity of the rail cask is 21 PWR fuel assemblies which reflects the greater capacities of anticipated cask designs. Each design uses helium in the cask cavity.

Both designs include a lead gamma shield sized to meet current regulatory requirements. The truck cask gamma shield of 5.25 inches is thicker than the rail cask gamma shield of 4.00 inches to allow for the possibility of shipping

fuel decayed less than 5 years by truck. The neutron shield dimensions reflect values typical of current cask designs. The cask shell structures, including the containment shell, are sized to support the lead shield. Specifically, the thickness of each cask steel shell is selected based on standard design practice; that is, the cask structure can withstand a force level typically generated from the accident test conditions. The resultant representative cask designs are indicative of current designs.[1-4]

The pertinent materials, weights, and dimensions of the representative truck and rail casks are shown in Figs. 3-6 and 3-7, respectively. The structural shell material is type 304 stainless steel. The lead shield is assumed to be unbonded to the steel shells. This fabrication assumption maximizes the potential for lead slump during transportation accidents involving impacts. Cask resistance to accident forces is thereby minimized, which introduces an element of conservatism to the results of this study. The impact limiters are made from balsa wood or rigid foam. Figure 3-8 shows the force deflection characteristics of the representative limiter design as a function of the presumed angle of impact between a cask and an impact surface. The impact limiter is sized to transmit a force of approximately 40 g if the cask is subjected to the impact environment specified by the accident test conditions.

3.6 Margins of Safety

The representative casks are designed to meet the regulatory accident test conditions. However, before a cask is allowed to transport spent fuel, it must be certified by the U.S. Nuclear Regulatory Commission (NRC). The certification process requires that all activities related to the design, manufacture, use, and maintenance of the cask be documented in a Safety Analysis Report (SAR). The SAR is submitted to the NRC for review and approval. The analyses and evaluations in the SAR must demonstrate that the spent fuel cask meets all 10 CFR 71 requirements and has sufficient margins of safety included to protect the public from undue risk. In general, margins of safety are included by using established practices, codes, and standards such as the American Society of Mechanical Engineers (ASME) Code and the American

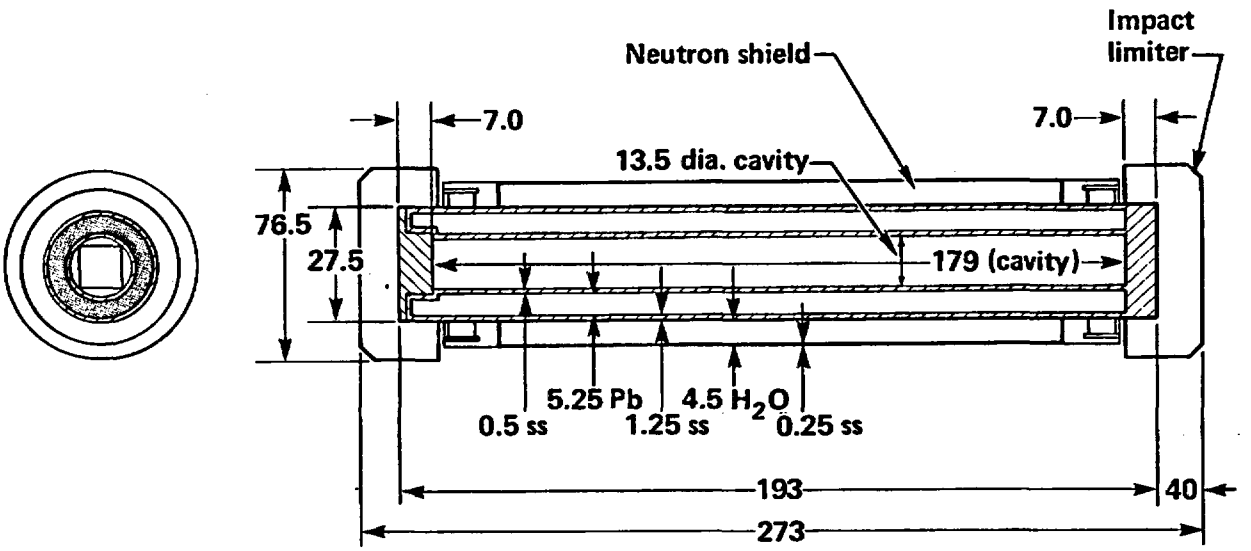

All dimensions in inches

Item	Weight, lbs
Body	32,000
Limiter	4,500
Contents	2,500
	39,000

Figure 3-6 Representative truck cask design used for dynamic structural and thermal response studies.

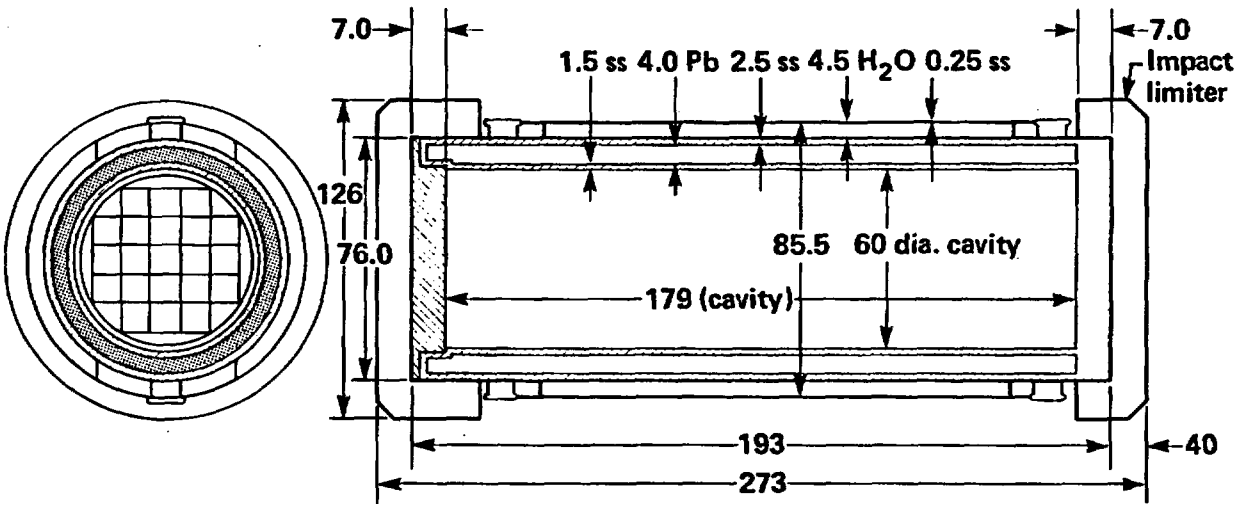

All dimensions in inches

Item	Weight, lbs
Body	122,500
Limiter	22,500
Contents	52,000
	197,000

Figure 3-7 Representative rail cask design used for dynamic structural and thermal response studies.

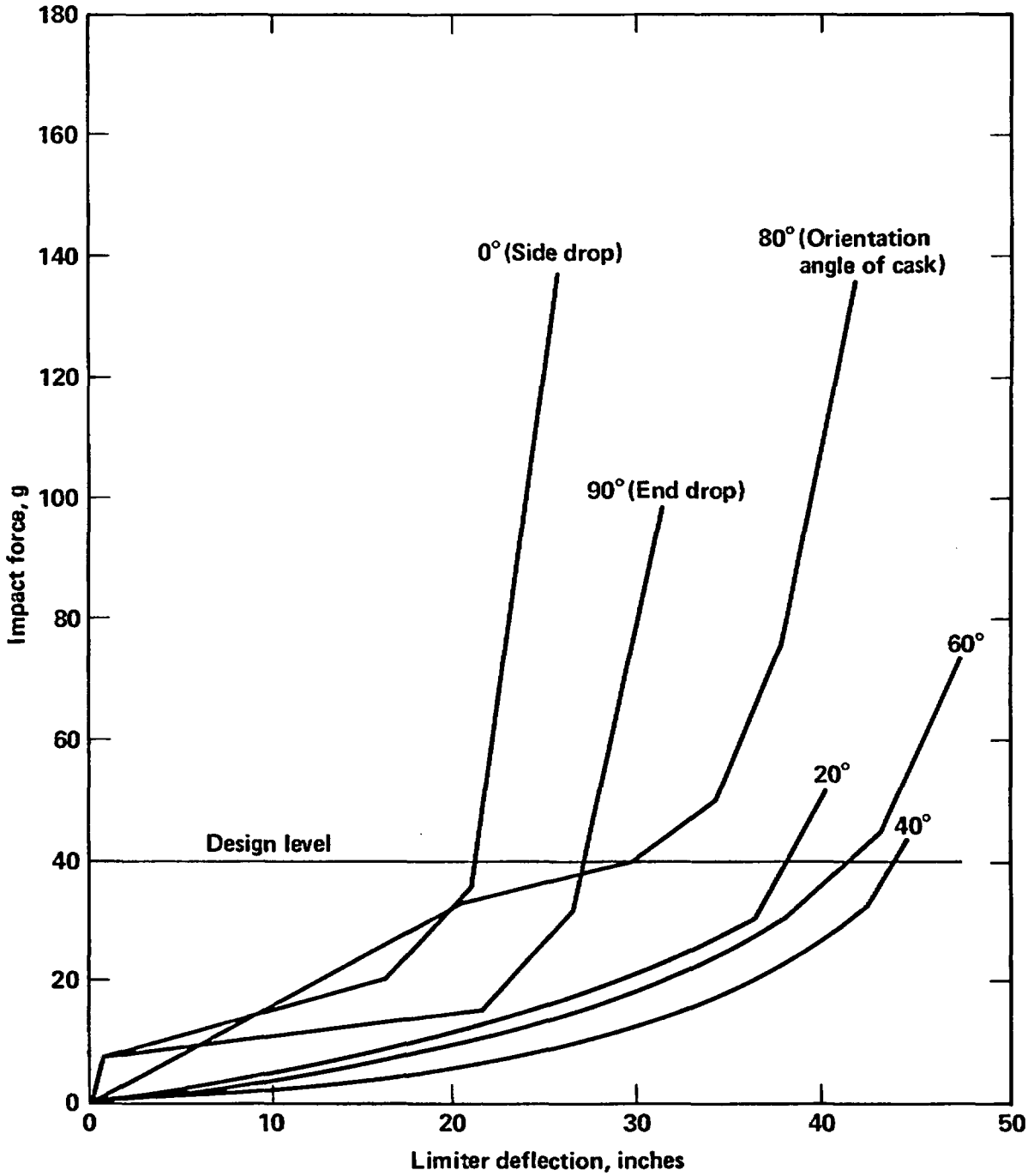

Figure 3-8 Force-deflection characteristics of the limiter design as a function of cask orientation at impact.

National Standards Institute (ANSI) Standards, and Regulatory Guides, all of which must be identified in the SAR.

Regulatory Guides are written by the NRC to provide guidance in many areas of licensing that result in acceptable margins of safety. For example, Regulatory Guide 7.6 adapts portions of the ASME Code, Section III to the design of spent fuel casks and recommends that elastic methods of structural analysis be used in the containment design.[6] Other Regulatory Guides relating to spent fuel casks are 7.4 (Leak Testing), 7.8 (Load Combinations), 7.9 (SAR Format), and 7.10 (Quality Assurance).[7-10]

Although there is no specific section in the ASME Code applicable to spent fuel casks, the ASME Code has been used extensively in designing, manufacturing, using, and maintaining spent fuel casks.[11] In general, materials adopted by the ASME Code provide a large margin of safety against rupture because the materials have high ductility. Also the use of elastic analysis for structural design usually results in a large margin of safety. For example, cask containments using 304 stainless steel are designed for the accident test conditions to ASME stress intensity limits that result only in slight yielding of the cask structure. In most cases, depending on the limiter design, the 304 stainless steel material can experience an off-set strain less than 1% under accident test conditions but rupture of 304 stainless steel occurs at strains greater than 30%. Therefore, large amounts of energy can be absorbed by the cask structure though large deformations under loading conditions exceeding the accident test conditions without catastrophic rupture occurring. To preclude brittle fracture failure from occurring at low temperatures, only materials with adequate toughness can be used in the structural design of spent fuel casks.[12,13,14]

In this study it is assumed that the representative casks have been properly designed and manufactured to appropriate codes and standards.[15,16] The representative cask designs are based on currently licensed cask designs and are likely to be certified if a SAR were prepared and submitted to the NRC. The margins of safety included in the cask design are representative of those included in currently licensed casks.

4.0 REPRESENTATIVE CASK RESPONSE STATES, LEVELS, AND REGIONS

4.1 Introduction

If a shipping container is involved in an accident, a cask response is generated and damage can occur. The response depends on many elements, such as the magnitude of the loadings generated by the accident impact velocity, the object struck, and if a fire is involved, the flame temperature and the duration of the fire. The response can be different at different locations or by various components within a cask. Different cask designs can have different magnitudes and types of responses when subjected to the same accident conditions. The actual response is a result of the combined effect of all these factors. Normally, the higher the response, the greater the damage to the cask and, therefore, the greater the potential for an event with a radiological significance.

In order to determine the response, three methods are commonly used: analytical, experimental, and a combination of the two. In this study, the analytical method is used to estimate responses. Many different computer codes are used to perform the analyses. These computer codes, as pointed out throughout the report, are benchmarked against closed-form solutions and experimental data. Appendix H discusses benchmarking for some of these codes.

In order to calculate response by analysis, a proper selection of computer codes is essential. Every computer code has limitations. The proper selection of a code requires a thorough understanding of its limitations. Sections 6.0 and 7.0 discuss the method of analysis, including the assumptions used in the analysis and the modeling technique by which the cask structures are represented. Individual analyses and their results are also presented.

The purpose of estimating the response is to determine the degree of structural damage. Certain types of damage, such as damage at specific locations or to certain components within the cask structure, can result in radiological hazards. Other types of damage may appear to be large, but result in essentially no radiological hazards. In order to evaluate the consequences resulting from structural damage, it is necessary to relate the

potential radiological hazard to the type of damage and cask response. Sections 4.2 and 4.3 qualitatively discuss the association between the structural and thermal damages and the potential radiation hazard. Section 8.0 provides a detailed discussion that relates the level of response to the level of potential radiological hazard.

Defining a specific response state is a very complex problem because response varies with different cask designs, severity of accidents, and location within the cask structure. In order to evaluate the level of damage between one response state and another, it is essential to establish some kind of measurement scale.

Response can be expressed in terms of many parameters, such as force, moment, displacement, stress, strain, and temperature. To establish a measuring scale with too many different types of response parameters will make any assessment unmanageable. The most effective approach is to identify one response parameter which provides both an adequate indication of cask structural damage and also an easy linkage to a radiological hazard estimate. This section discusses the selection of the parameters to represent the structural and thermal responses for the representative cask designs, the justification of the selections, and the discretized levels of response states used in this study.

4.2 Response States and Levels for Mechanical Loads

Various types of damage can occur to casks subjected to mechanical loads. The most important types of damage to a lead shielded cask are yielding, large dimensional changes, and rupture of the cask structure. Any parameter selected to represent the structural response state of the representative casks should indicate these types of structural damage.

Three engineering response parameters--stress, strain, and displacement--are considered as candidates for the single parameter to represent the response state for mechanical loads.

Stress is commonly used in structural analysis to represent the state of response. Both the American Society of Mechanical Engineers and the American

Institute of Steel Construction use stress as the parameter to define acceptance design limits in terms of yield and ultimate stress.[1,2] It is a good parameter for design within the elastic range of the material. When the response is beyond the elastic range, however, large dimensional changes can occur with only small changes in the stress level. The purpose of this study is to estimate the damage and consequence to the representative casks when subjected to severe accident conditions in which the response could exceed the elastic range. Therefore, stress is not the best parameter to represent the response state for mechanical loads applied to the representative casks.

Displacement is a parameter for measuring the dimensional change of structural elements. It is capable of describing the deformation shape for both small and large loading conditions. The deficiency in using displacement is that it cannot provide direct comparison with the design acceptance limits. Displacement cannot indicate directly when the structure has yielded or ruptured.

Strain is the most appropriate single parameter to represent the response state for mechanical loads. For a given material, dimensional changes occurring with loading conditions are directly related to strain. Strain can also indicate yielding and rupture when responses reach strain limits. Therefore, strain is selected for mechanical load responses of the representative casks.

Strain will most likely vary according to location within the structure. Under one specific accident load, strain at the inner shell is different from that at the outer shell, at the bolts, and at the enclosures. Sensitivity studies are conducted using the representative casks to find out the relationship between the strains at different locations or on different components inside the cask structure. This relationship helps to estimate the total cask damage level when strain at a particular component is identified. The strain on the inner shell of the cask structure is selected as the best single parameter to characterize mechanical load response states for the representative casks.

Although the response of a cask is continuous over a loading range, three discrete response levels are defined to relate ranges of response states and mechanical loads to potential radiological hazards. The response levels are defined as discrete levels of maximum effective strain on the inner shell of the representative cask structure. The maximum effective strain of the representative truck and rail cask impacting an unyielding surface can be significantly different as shown schematically in Fig. 4-1. The three discrete response levels or strain levels that bound the response state ranges are identified on the figure.

4.2.1 Structural Response Level, S_1

The first response level, S_1, is defined to be 0.2% strain at the inner shell. This level of strain is selected for the first response level because the structural material of the representative casks is 304 stainless steel which has a 0.2% offset yield point. For strains within the 0.2% yield strain (S_1), shown as range A in Fig. 4-1, the response of the structure is elastic and there is no permanent dimensional change after the loading is removed. This characteristic assures that little, if any, radiation release occurs when the cask is subjected to accident loads that are within range A because the seal and bolts remain functional. At 0.2% strain (S_1), the representative lead cask designs experience less than 40 g axial force on the lead for all orientations of impact. No lead slump occurs. The fuel basket remains functional. Up to 3% of the fuel rods can release limited amounts of radioactive material into the cask cavity under these loading conditions. Essentially all of the impact loads on the casks are absorbed by their impact limiters. These loads and releases are within the regulatory design conditions and release limits.

4.2.2 Structural Response Level, S_2

The second response level, S_2, is defined to be 2% plastic strain at the inner shell. For strains between 0.2% (S_1) and 2% (S_2), shown as range B in Fig. 4-1, the response of the structure is plastic, and small permanent dimensional changes occur. The dimensional changes can affect the cask

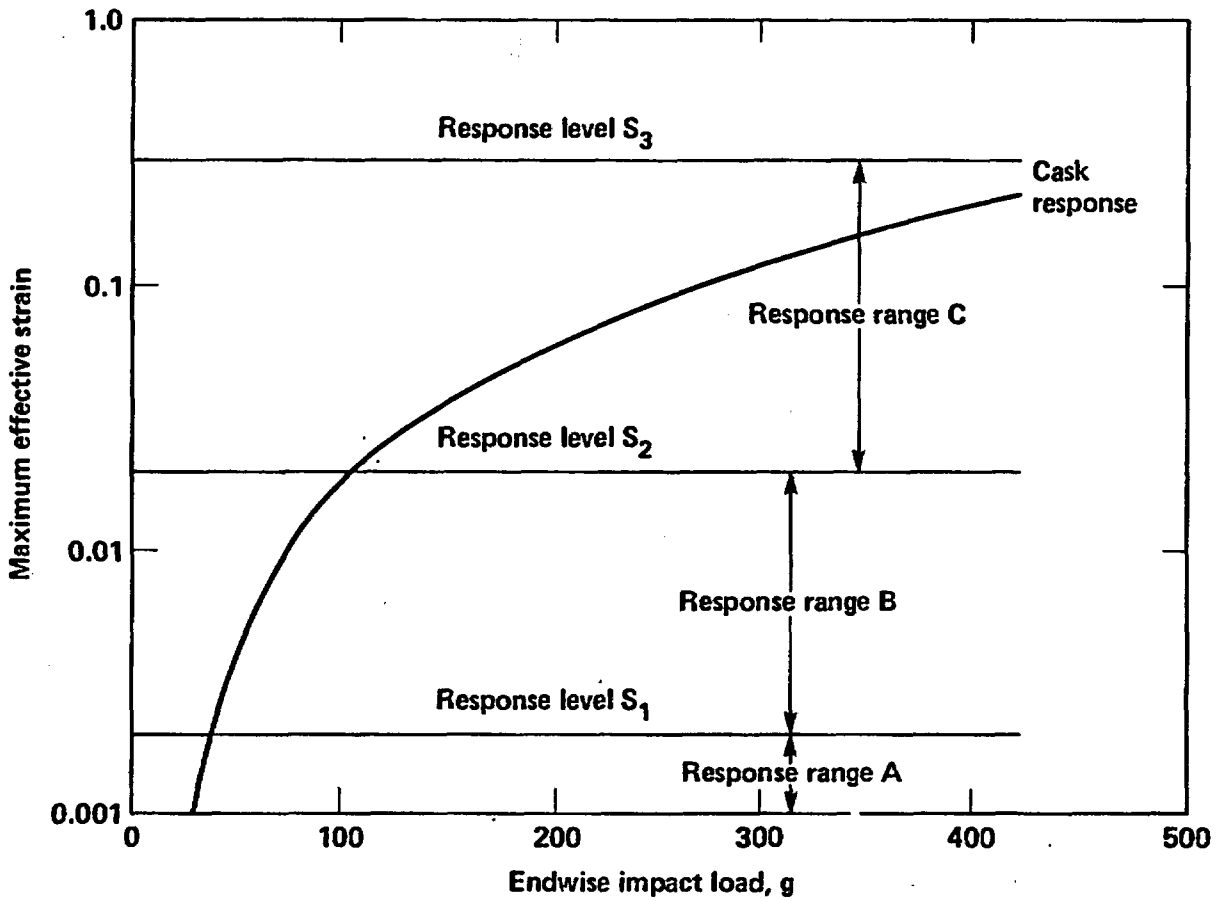

Figure 4-1 Schematic representation of cask response state for mechanical load.

closure seals and result in limited radioactive material releases. Also, a small dimensional change can result from limited lead slump which can result in an increase of radiation emanating from the cask. Up to 10% of the fuel rods can leak into the cask cavity under these loading conditions. The radiation hazards caused by seal leakage and lead slump in range B are near regulatory limits. The loads that produce the second response state are near the loads imposed by the accident test conditions. In this range, the impact loads on the representative casks are absorbed mostly by their impact limiters, but part of the loads are absorbed by the cask structure.

4.2.3 Structural Response Level, S_3

The third response level, S_3, is defined to be 30% plastic strain at the inner shell. The 30% strain (S_3) level is below the fracture strain of 304 stainless steel, but the large distortions occurring with this strain level can cause local cracking in the welded regions. For strains between 2% (S_2) and 30% (S_3), shown as range C in Fig. 4-1, the response is plastic deformation with large dimensional changes occurring, particularly for strain near 30% (S_3). Any large distortions of the cask will likely cause seal leakage in the closure region, lead slump, localized weld cracking, and some crushing of the cask contents. All of the fuel rods are expected to release limited amounts of radioactive material into the cask cavity under these extreme loading conditions. The radiological hazards associated with this response can be outside of regulatory limits; however, there will not be any failure that will result in release of solids from fuel rods, except very small particles that may escape to the environment. In this response range, an increasing amount of the impact force is absorbed by the cask compared to the force absorbed by the limiter. In fact, at the 30% strain (S_3) level, the energy absorption by the representative casks may be eight times higher than the energy absorbed by the limiter.

4.2.4 Application of Response States and Levels

Each response state implies a force on the cask as a result of impacts upon various objects. The force is primarily determined by the impact

velocity and the hardness of the object, but various combinations of velocity and object hardness can result in the same force. Consequently, the force associated with each structural response state can be related to various accident scenarios. Furthermore, the potential radiation hazard associated with these response states can be related to these same accident conditions.

Figure 4-2 shows schematically the structural response state of a representative cask in terms of strain as a function of both impact velocity and surface hardness for endwise impacts. The combination of impact velocity and surface hardness for the strain levels 0.2% (S_1), 2% (S_2), and 30% (S_3) are also shown on the plot. For example, the impact velocities required to reach the 0.2% strain (S_1) level, will be 30 mph for an unyielding object, 60 mph for an object of medium hardness, and 90 mph for a soft object. For very soft objects, the 0.2% strain (S_1) level can never be attained. Limiting the velocities impacting various objects can similarly be obtained corresponding to the 2% (S_2) and 30% (S_3) strain levels.

4.3 Response States and Levels for Thermal Loads

Various types of damage can occur to the representative casks subjected to thermal loads. The most important types of damage are degradation of the closure seal material, melting of the lead shield, dimensional changes to the structure, and alloying of the lead with the nickel in the 304 stainless steel structural material. Any parameter selected to represent the thermal response state of the cask should indicate the various types of thermal damage that can occur.

Two engineering response parameters, strain (thermally-induced) and temperature, are considered as candidates for the single parameter to represent the response state for thermal loads.

In Section 4.2, mechanical strain is selected as the single parameter to represent the response state for mechanical loads. Thermally induced strain provides a good indication of dimensional changes to the cask structure, but does not provide any indication of seal deterioration, melting of lead, or alloying of lead with the nickel in stainless steel. Therefore strain is

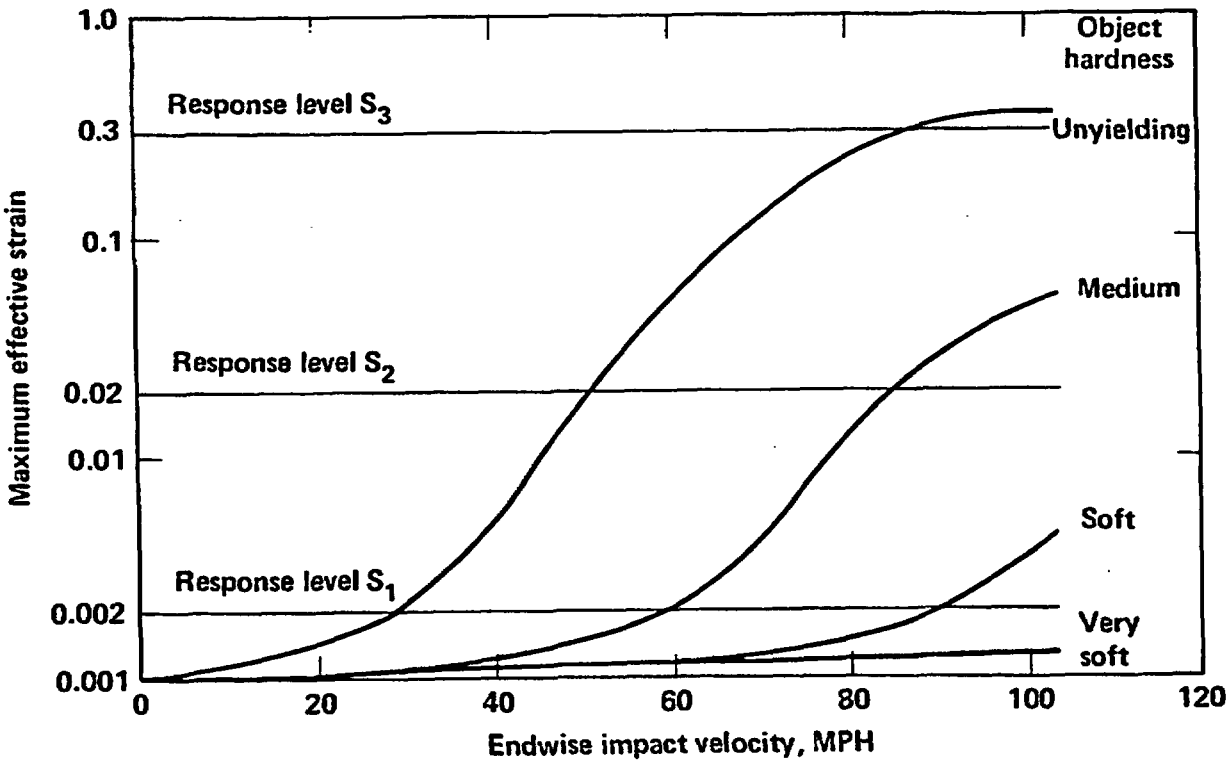

Figure 4-2 Schematic representation of cask structural response for various surface hardness and impact velocities.

determined not to be the best parameter to represent the response state for thermal loads.

Temperature is the best single parameter to represent the response state for thermal loads. Temperature provides an indication of seal deterioration, melting of lead, and alloying of lead with the nickel in stainless steel. It also provides an indirect measure of dimensional changes with lead melt. Therefore, temperature is selected for thermal load responses.

Temperature varies from location to location within the cask. For any specific fire-accident, the temperature at the inner shell is different from that at the outer shell, at the bolts, and at the enclosures. Sensitivity studies are conducted to find out the relationship between the temperatures at different locations and on different components inside the cask structure. This relationship provides a means to estimate the total cask damage level when the temperature at a particular component is identified. The temperature at the middle of the lead shield thickness is selected as the appropriate single parameter to characterize thermal load response states.

Although the response of a cask is continuous over a loading range, four discrete response levels are defined to relate ranges of response states and thermal loads to radiological hazard. The response levels are defined in terms of the temperature at the middle of the lead shield thickness. As an illustration of a cask exposed to a regulatory fire, Fig. 4-3 shows schematically the lead mid-thickness temperatures as a function of the thermal loads to the cask. The four discrete response levels, or lead mid-thickness temperatures, that bound the response state ranges are identified on the figure.

4.3.1 Thermal Response Level, T_1

The first response level, T_1, is defined as a temperature of 500°F at the middle of the lead shield thickness. This temperature is selected because the cask seals are below temperatures that can cause degradation of properties to such materials as silicon and fluorocarbons. Also, there is a significant margin between 500°F (T_1) and the melting point of lead at 621°F. For

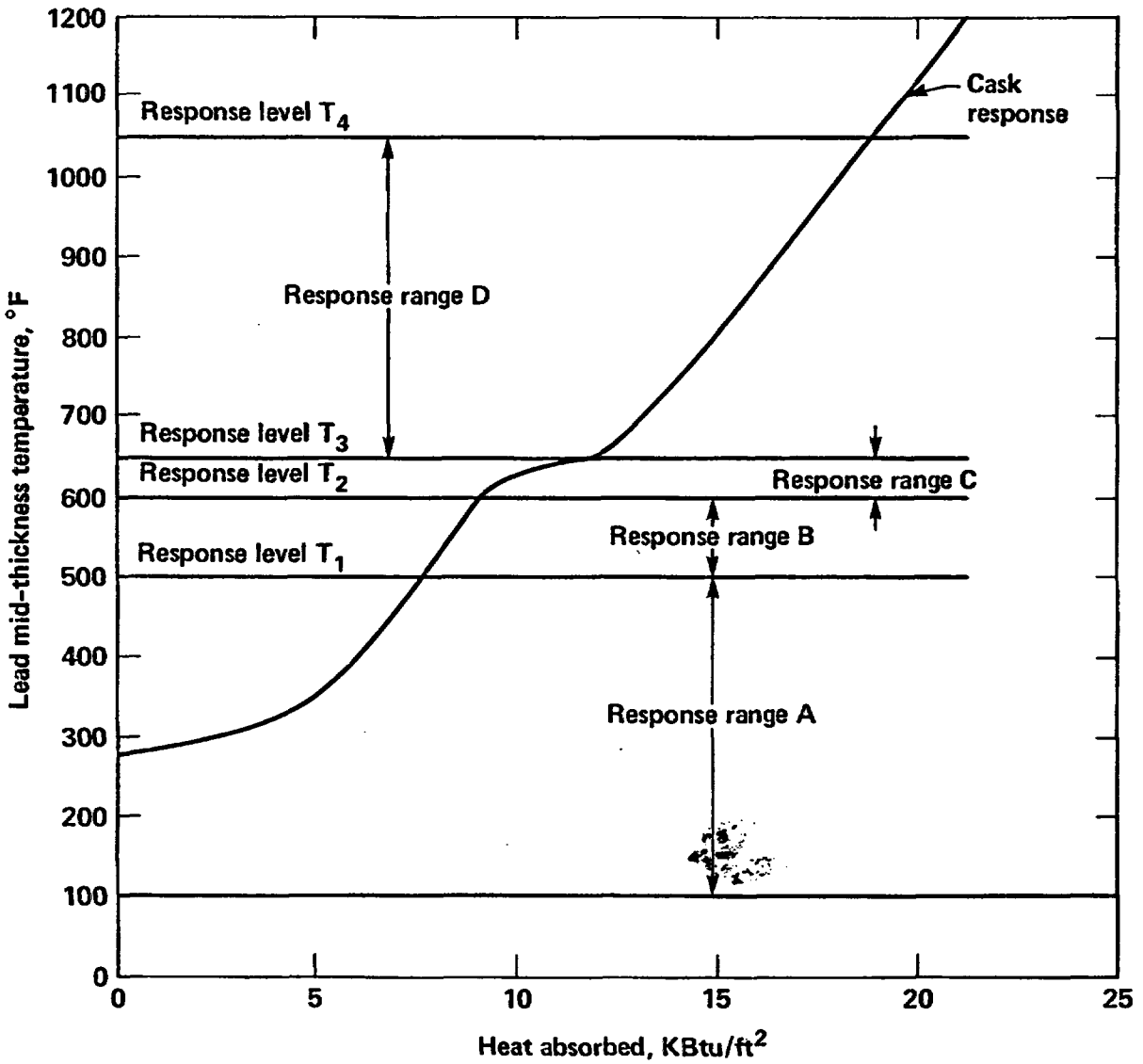

Figure 4-3 Schematic representation of cask response state for thermal load.

temperatures less than 500°F (T_1), shown as range A in Fig. 4-3, there is no significant damage to the cask due to thermal loads. However, it is assumed that the water in the neutron shield is released before the 500°F temperature (T_1) is reached. The release of the water forms a thermal barrier between the neutron shield wall and the cask outer wall which protects the cask from any fire. The release of the water also increases the neutron radiation surrounding the cask; however, all radiological hazards are within regulatory limits below this first level thermal response.

4.3.2 Thermal Response Level, T_2

The second response level, T_2, is defined as a temperature of 600°F at the middle of the lead shield thickness. Temperatures between 500°F (T_1) and 600°F (T_2) are shown to be in range B in Fig. 4-3. In this temperature range, the lead at the outer stainless steel wall of the cask is still below 621°F, the melting point of lead. Even though the lead does not melt, the cask closure seals can degrade and potentially release limited radioactive material. Any radiological hazards caused by seal leakage and the loss of the neutron shield are likely to be within regulatory limits.

4.3.3 Thermal Response Level, T_3

The third response level, T_3, is defined as a lead mid-thickness temperature of 650°F. For temperatures between 600°F (T_2) and 650°F (T_3), shown as range C in Fig. 4-3, melting of the lead shield occurs. Lead melt results in a phase change with a lead density decrease of approximately 10%. The density change results in an increase in the lead volume and significant plastic straining of the inner cask wall. After the cask cools, the lead returns to its original density, and voids can occur in the lead shield owing to the increased volume from the plastic strain of the inner cask wall. The cask closure seals are assumed to leak. The increase in radiation level from the lead shield reduction and any radioactive material releases will likely be outside of regulatory limits.

4.3.4 Thermal Response Level, T_4

The fourth response level, T_4, is defined as a lead mid-thickness temperature of 1050°F. For temperatures in the range of 650°F (T_3) to 1050°F (T_4), shown as range D in Fig. 4-3, the lead shield thickness is reduced further due to differential thermal expansion between the liquid lead and stainless steel structural material. The fuel rods can also increase in temperature and begin to burst. For temperatures above 1050°F (T_4), the alloying of the lead with the nickel in the stainless steel structure can become significant and result in stress corrosion cracking.[3-5] In this response range, the further reduction in shielding and possible bursting of fuel rods increases the radiological hazards.

4.3.5 Application of Response States and Levels

Each response state implies a thermal load applied to the cask as a result of various fire conditions. The thermal load is determined by the fire characteristics. However, various fire characteristics can result in the same thermal load. Consequently, the thermal load associated with each thermal response state can be related to various accident conditions involving fires. Furthermore, the potential radioactive hazards associated with these response states can also be related to the same accident conditions.

Figure 4-4 schematically presents the thermal response of a cask in terms of the lead mid-thickness temperature as a function of both fire duration and fire location. The combination of fire duration and location for the temperature levels 500°F (T_1), 600°F (T_2), 650°F (T_3), and 1050°F (T_4) is also shown on the plot. For example, for a fire with a flame temperature of 1700°F, the time duration to reach the 500°F temperature (T_1) level, will be 1.3 hours for an engulfing fire, 2.3 hours for a fire tangent to the cask, and 3.6 hours for a fire 20 feet from the cask. For fires greater than 50 feet away, the 500°F temperature (T_1) level can never be attained. Fire durations for the various fire locations can similarly be estimated corresponding to the 600°F (T_2), 650°F (T_3), and 1050°F (T_4) temperature levels.

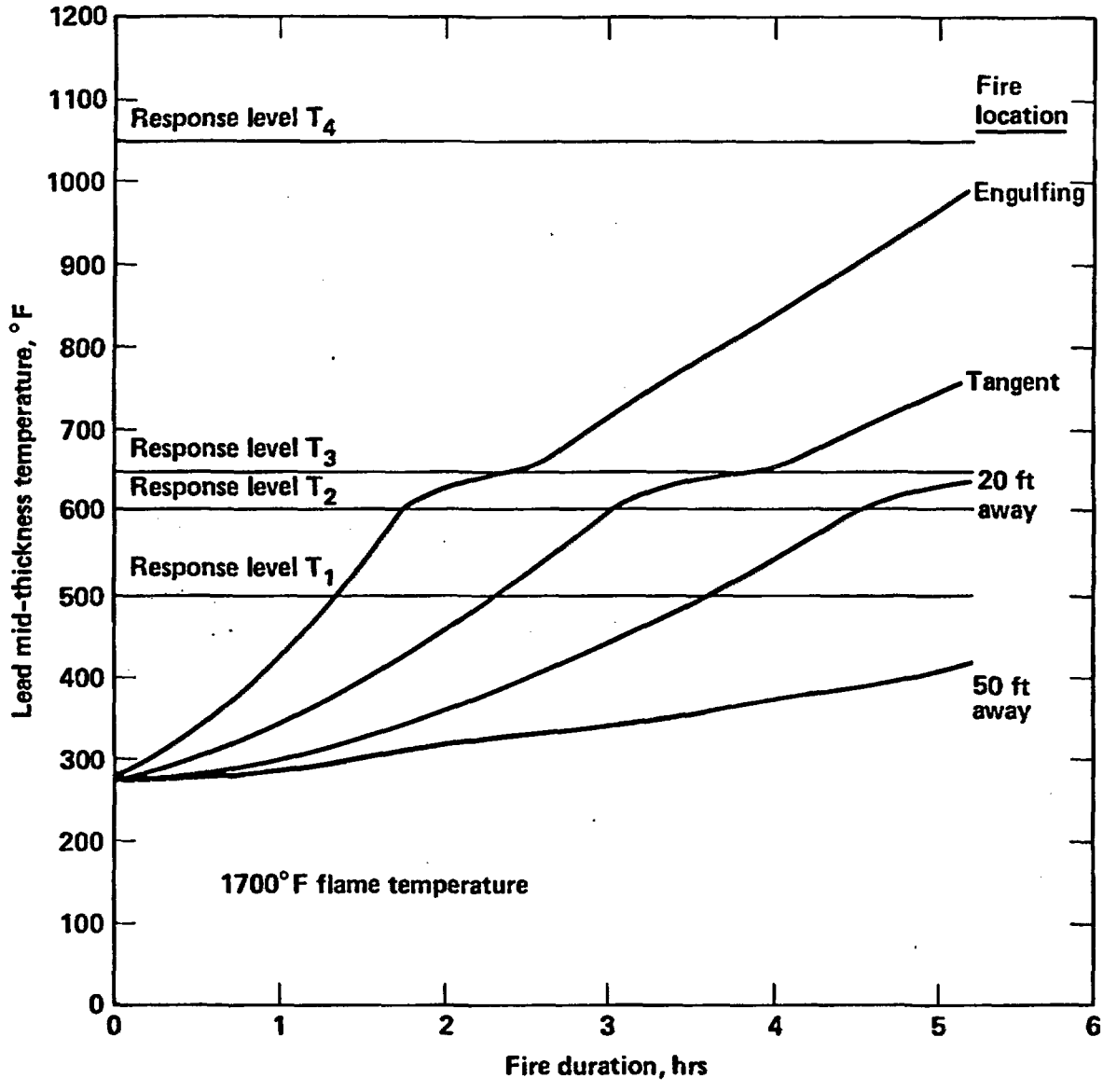

Figure 4-4 Schematic representation of cask response for various fire locations and fire durations.

4.4 Cask Response Regions

In some cases, a cask will be exposed to both mechanical and thermal loads. A range of combined structural and thermal responses for a cask can be represented by the response matrix shown in Fig. 4-5. The ordinate of the response matrix represents the structural response states; the abscissa represents the thermal response states; and the boundaries of the response regions are defined by the structural and thermal response levels.

There are 20 response regions denoted by $R(S_i,T_j)$ where S_i is the structural response level and T_j is the thermal response level. Although only three discrete structural response levels are defined, a fourth unbounded level exists that consists of cask strain responses greater than 30% (S_3). Similarly, a fifth unbounded thermal response level exists which consists of cask temperature responses greater than 1050°F (T_4). The first region, R(1,1), represents the cask response to combined mechanical and thermal loads within the 0.2% strain (S_1) and 500°F temperature (T_1) levels. Radioactive releases, if any, for cask responses in R(1,1) will be within regulatory limits. The twentieth region, R(4,5), represents the most extreme combined response state in which the potential radiological hazards will be a maximum. In general, the probability of occurrence of a particular combination of mechanical and thermal loadings decreases with the severity of these loads. The probabilities associated with each region of the load matrix are discussed in more detail in Section 5.0.

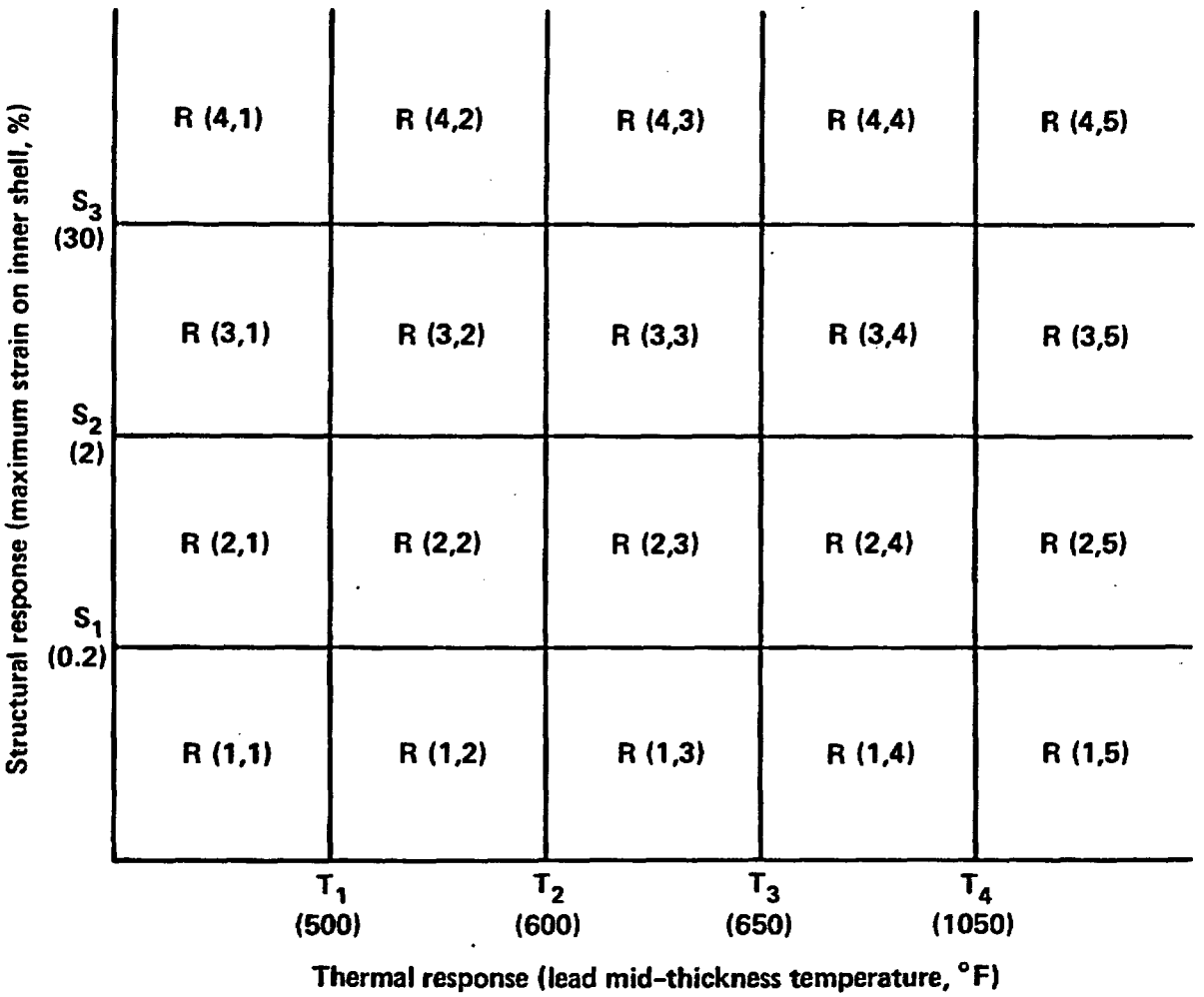

Figure 4-5 Matrix of cask response regions for combined mechanical and thermal loads.

5.0 PROBABILITY ANALYSIS

5.1 Introduction

The emphasis of the discussion in Sections 6.0 and 7.0 is on the physical loads, both mechanical and thermal, which a spent fuel cask can experience in a transportation accident. Specifically, cask response states, evaluated in terms of containment vessel strains and lead shield temperatures, are related to basic accident parameters such as impact velocities and fire duration.

The relationships between cask responses to mechanical loads and the impact velocity of the cask are derived for several cask impact orientations involving interactions with objects of differing hardness. The effect of cask orientation on the strain-impact velocity relationship for an unyielding object is shown in Fig. 5-1 for the truck cask. The impact velocity, defined as the cask velocity in the direction perpendicular to the object impacted, is determined by the velocity of the cask due to the accident and the impact angle.

The thermal loading to a cask depends on the flame temperature and fire location as well as the duration of a fire. Thus, the relationship between cask response to thermal loads and the duration of a fire is affected by the flame temperature and location of the fire with respect to the cask. The effects of these parameters are illustrated in Fig. 5-2.

In summary, the following accident parameters, which affect the cask response to mechanical and thermal loads, are identified and are considered in the probability analysis:

- Mechanical loads
  - impact velocity
    - cask velocity
    - impact angle
  - cask orientation
  - hardness of the impacted object

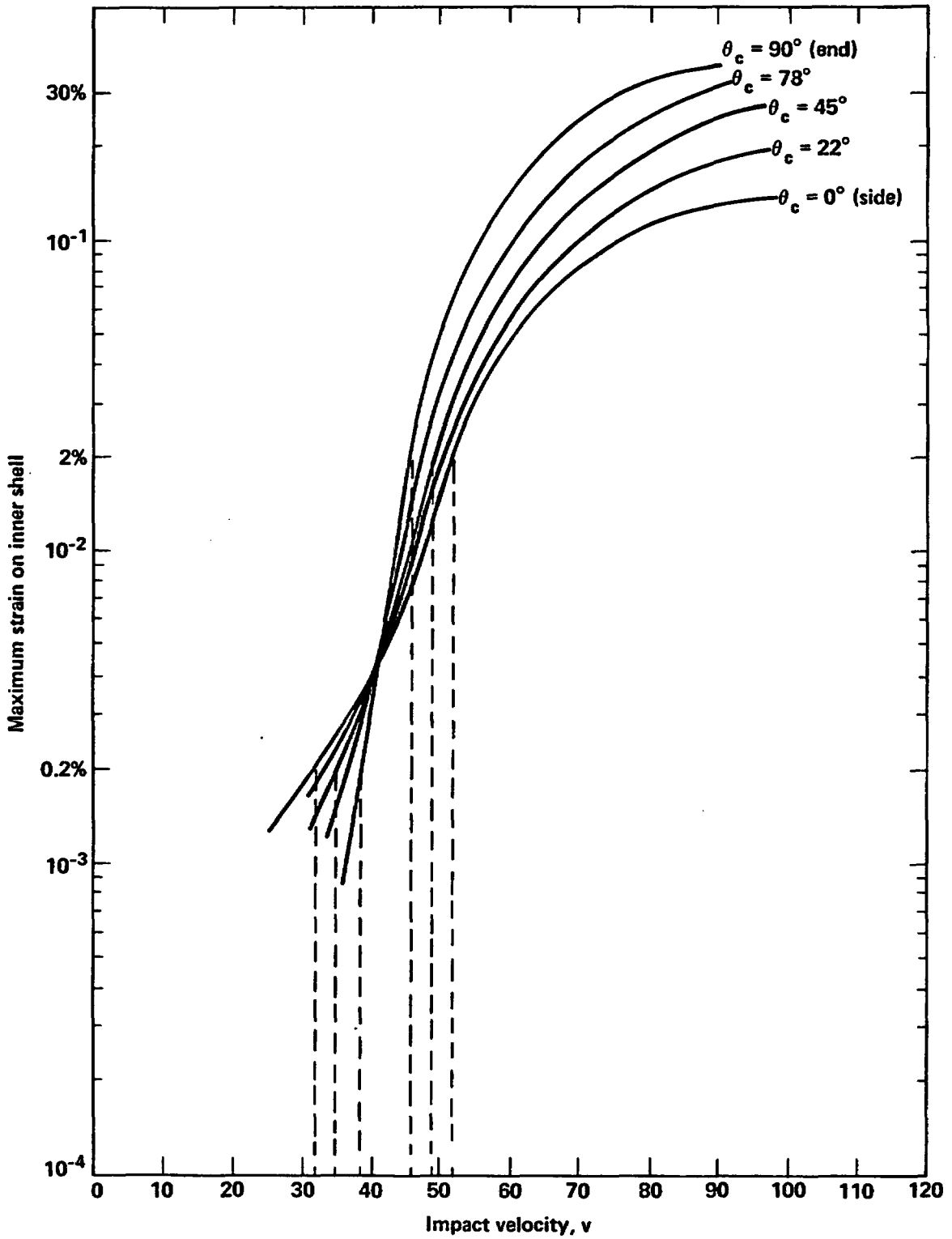

Figure 5-1 Effect of cask orientation on the strain-impact velocity relationship for a truck cask impacting an unyielding object.

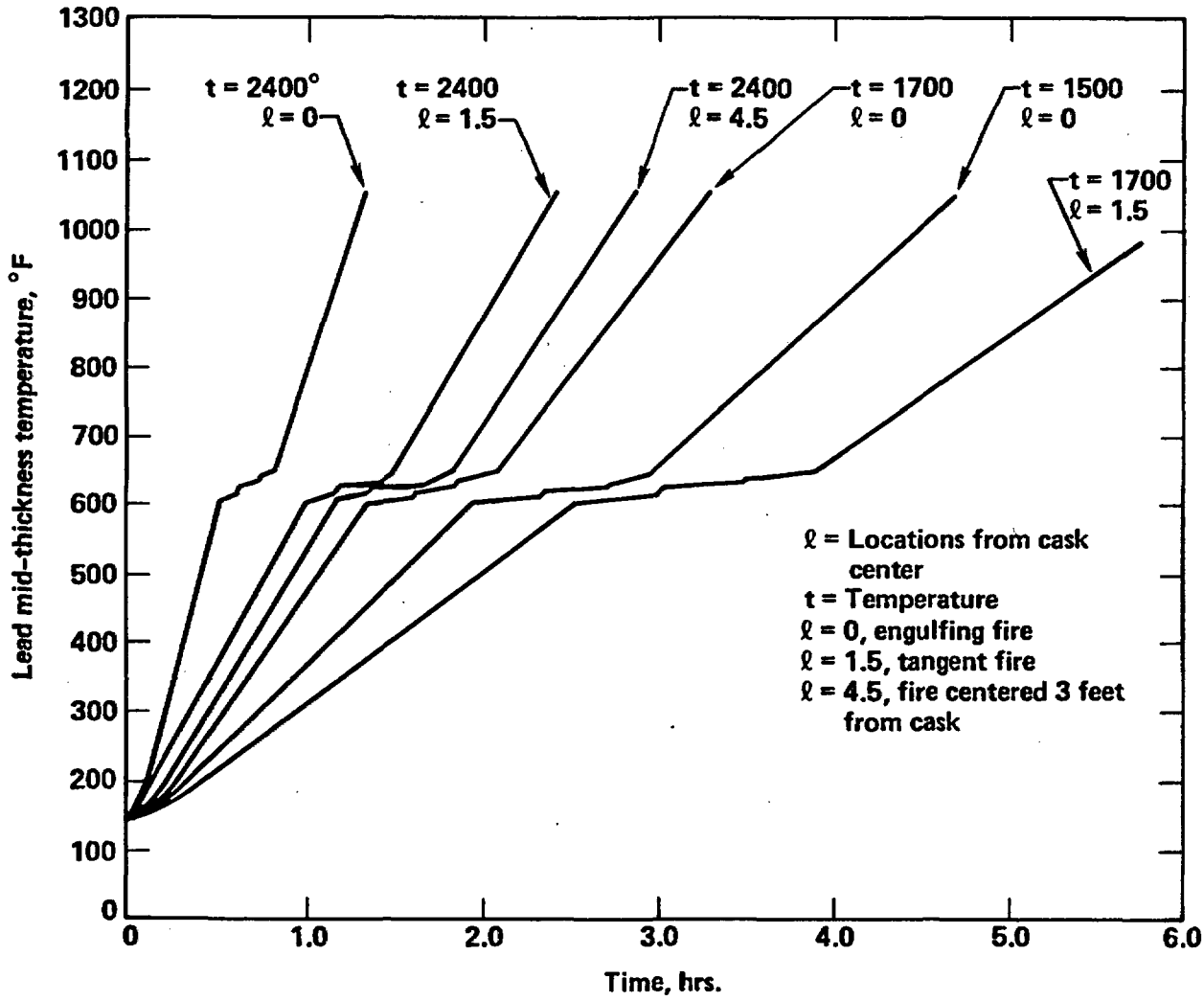

Figure 5-2 Effect of flame temperature and fire location on lead-temperature-time relationship for a truck cask.

- o Thermal loads
  - fire duration
  - flame temperature
  - fire location with respect to the cask.

Because future accident conditions are unpredictable, i.e., random, the response state of a spent fuel cask cannot be predicted deterministically. Assessment of the response states and the subsequent damage and release of radioactive materials due to transportation accidents can only be expressed probabilistically.

The purpose of this section is to describe the probability analysis developed to estimate the likelihood that a spent fuel cask will attain various response states during a transportation accident. Section 5.2 catalogs the probability distributions used to describe the random variation associated with the accident parameters. The probability calculations are outlined in Section 5.3.

5.2 Probabilistic Inputs

Estimation of the likelihood of various cask response states, represented by the containment vessel strain and the lead mid-thickness temperature, is based on estimates of the distributions of the accident parameters which affect the response of the cask during a transportation accident. The distributions of the accident parameters are described in terms of a cumulative distribution function, $F(x)$, if the parameter is quantitative, or a probability function, $h(\theta)$, if the parameter is qualitative, e.g., the object impacted. The cumulative distribution function describes the likelihood that the parameter value is less than or equal to x, the argument of $F(.)$, i.e.,

$$F(x) = P_r(X \leq x) \tag{5.1}$$

where X denotes the accident parameter. The probability function describes the likelihood of each θ or object, i.e.,

$$h(\theta) = P_r(\theta) \quad (5.2)$$

where θ denotes the qualitative object.

The distributions of the accident parameters used to estimate the likelihood of cask response states are presented in this section. Development of these distributions was discussed in Section 2.0. The data used to estimate accident rates and velocity distributions is summarized in Appendixes B and C. The method of estimation is discussed in Appendix G.

5.2.1 Mechanical Loading Parameter Distributions

Object hardness, impact velocity, and cask orientation are three mechanical loading parameters which have a significant influence on a cask's structural response in a transportation accident.

5.2.1.1 Object Hardness Distributions

Each of the accident scenarios, described in Section 2.0 and shown in Figs. 2-3, 2-4, and 2-5, identifies a type of accident, e.g., a collision, and the object or surface which a cask could impact, e.g., a truck, bridge abutment, or embankment. From these descriptions, object hardness is estimated. Thus, the distribution of hardness of the impacted object is described in terms of the probabilities of the accident scenarios. These are included in Figs. 2-3, 2-4 and 2-5 for highway and railway accidents.

5.2.1.2 Impact Velocity Distributions

5.2.1.2.1 Cask Velocity

The distribution of cask velocity during a transportation accident varies between accident scenarios. For example, the distribution of cask velocity experienced in truck-truck collisions is expected to differ from the distribution associated with accidents involving falls from bridges. In truck-truck accidents, the distribution depends on the speeds of the individual trucks at the time of the collision. For accidents involving falls from bridges, the cask impact velocity is determined by the fall height.

The following distributions of cask velocities are applicable to highway accidents:

V1: The truck velocity, adjusted for braking, prior to an accident
V2: The velocity due to bridge heights
V3: The vector sum of truck velocity, adjusted for braking, and velocity due to bridge heights
V4: The train velocities at grade crossing accidents.

As discussed in Subsection 2.5.1.2.1, the primary source of truck velocities is based on accident reports that estimate velocities prior to an accident. The observed data does not account for any reduction in velocity at impact due to braking efforts by the drivers. However, a North Carolina study provides data which allow for braking effects.[1] These results are used to adjust the basic cumulative distribution function of truck velocities as shown in Fig. 5-3. The adjustment is based on the identity

$$F_{V1}(s) = F_I[s/\delta(s)] \tag{5.3}$$

where

$$\delta(s) = \begin{cases} 0.65 + \frac{0.35}{78}\, s & 0 \le s \le 78 \\ 1.0 & s \ge 78 \end{cases} \tag{5.4}$$

and $F_{V1}(.)$ and $F_I(.)$ denote the adjusted and initial truck velocity cumulative distribution functions, respectively. At velocities greater than 78 mph no credit for braking is assumed. As velocity decreased, the effect of braking increased, e.g., a 40 mph velocity is reduced to 33 mph, whereas a 10 mph velocity is reduced to 7 mph.

The four cumulative distribution functions used for the velocity of highway accidents are presented in Table 5.1. They are estimated from historical accident data using the method of estimation described in Appendix G.

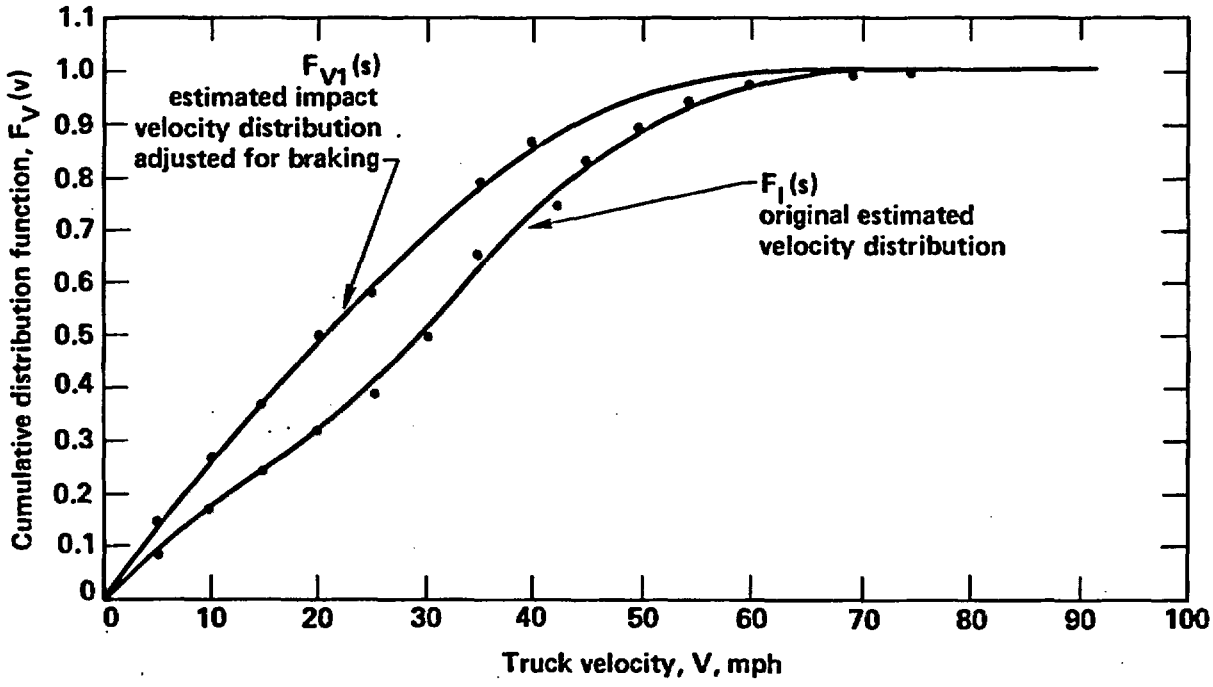

Figure 5-3 Distribution of vehicle velocities adjusted for braking.

Table 5.1
Cumulative Cask Velocity Distributions for Highway Analysis

Distributions							
V1		V2		V3		V4	
Cask Velocity,s (mph)	$F_S(s)$	Cask Velocity,s (mph)	$F_S(s)$	Cask Velocity,s (mph)	$F_S(s)$	Cask Velocity,s (mph)	$F_S(s)$
0.	0.	0.	0.	0.	0.	0.	0.
2.0	0.03834	7.74	0.00621	5.0	0.	2.0	0.06014
6.0	0.12916	10.94	0.01550	10.0	0.00141	6.0	0.17906
10.0	0.23508	15.48	0.04754	15.0	0.00821	10.0	0.29398
14.0	0.34886	18.95	0.1051	20.0	0.03387	14.0	0.40255
18.0	0.46237	21.89	0.1952	25.0	0.11129	18.0	0.50280
22.0	0.56877	24.47	0.3178	30.0	0.28292	22.0	0.59331
26.0	0.66345	26.81	0.4629	35.0	0.51279	26.0	0.67319
30.0	0.74353	28.95	0.6124	40.0	0.70110	30.0	0.74210
34.0	0.80877	30.95	0.7464	45.0	0.81951	34.0	0.80022
38.0	0.86020	32.83	0.8508	50.0	0.89168	38.0	0.84814
42.0	0.89961	34.61	0.9217	55.0	0.93543	42.0	0.88676
46.0	0.92881	36.29	0.9635	60.0	0.96178	46.0	0.91718
50.0	0.95009	37.91	0.9849	65.0	0.97751	50.0	0.94062
54.0	0.96547	39.46	0.9945	70.0	0.98680	54.0	0.95826
58.0	0.97634	41.67	0.9991	75.0	0.99227	58.0	0.97125
62.0	0.98383	43.08	0.9998	80.0	0.99547	62.0	0.98060
66.0	0.98908	44.45	0.9999	85.0	0.99766	66.0	0.98717
70.0	0.99261	56.86	1.0	90.0	0.99901	70.0	0.99169
74.0	0.99503			95.0	0.99961	74.0	0.99473
78.0	0.99670			100.0	0.99985	78.0	0.99672
82.0	0.99825			105.0	0.99995	82.0	0.99800
86.0	0.99910			110.0	0.99998	86.0	0.99881
90.0	0.99956			115.0	0.99999	90.0	0.99930
94.0	0.99979			150.0	1.0	94.0	0.99960
98.0	0.99990					98.0	0.99977
102.0	0.99995					102.0	0.99987
106.0	0.99998					106.0	0.99993
110.0	0.99999					110.0	0.99996
150.0	1.0					114.0	0.99998
						118.0	0.99999
						150.0	1.0

$F_S(s)$ = Probability that cask velocity is less than or equal to cask velocity listed.
V1: The truck velocity, adjusted for braking, prior to an accident
V2: The velocity due to bridge heights
V3: The vector sum of truck velocity adjusted for braking and velocity due to bridge heights
V4: The train velocities at grade crossing accidents

The following distributions of cask velocities are considered applicable to railway accidents:

TV1: The train velocities in collision accidents without braking
TV2: The train velocities in derailment accidents without braking
TV3: The velocities due to bridge heights
TV4: The vector sum of train velocities in derailment accidents and velocities due to bridge heights.

The cumulative distribution functions are presented in Table 5.2.

5.2.1.2.2 Impact Angle

The damage resulting from an accident is not controlled solely by the cask velocity at impact. A head-on impact is more severe then a sideswiping accident, even though both accidents can involve similar velocities. The reason is that accident severity is most directly related to the impact velocity, the component of the cask velocity vector perpendicular to the object impacted. The orientation of the cask motion, relative to the surface of the object impacted is called the impact angle, α. A 90^0 impact angle defines a head-on impact, i.e., the impact velocity and cask velocity at impact are the same. An impact angle close to 0^0 defines a sideswiping impact. In this case the impact velocity is a small fraction of the cask velocity. Mathematically, the impact velocity is the cask velocity times sine α.

As for cask velocities, the distribution of impact angle can depend on the accident scenario. For example, if the accident involves a collision with another vehicle on the highway, any impact angle is likely. Three impact angle distributions are used:

VV1: Uniform (0^0,90^0) - any impact angle is equally likely

$$F(x) = x/90 \qquad 0^0 \leq x \leq 90^0 \qquad (5.5)$$

Table 5.2
Cumulative Cask Velocity Distributions for Railway Analysis

Distributions							
TV1		TV2		TV3		TV4	
Cask Velocity,s (mph)	$F_S(s)$	Cask Velocity,s (mph)	$F_S(s)$	Cask Velocity,s (mph)	$F_S(s)$	Cask Velocity,s (mph)	$F_S(s)$
0.	0.	0.	0.	0.	0.	0.	0.
2.0	0.09385	2.0	0.07543	7.74	0.00621	5.0	0.
6.0	0.26286	6.0	0.22036	10.94	0.01550	10.0	0.00232
10.0	0.40788	10.0	0.35480	15.48	0.04754	15.0	0.01244
14.0	0.53042	14.0	0.47634	18.95	0.1051	20.0	0.04814
18.0	0.63240	18.0	0.58341	21.89	0.1952	25.0	0.14919
22.0	0.71598	22.0	0.67534	24.47	0.3178	30.0	0.35837
26.0	0.78345	26.0	0.75225	26.81	0.4629	35.0	0.60624
30.0	0.83709	30.0	0.81495	28.95	0.6124	40.0	0.77834
34.0	0.87908	34.0	0.86477	30.95	0.7464	45.0	0.87230
38.0	0.91147	38.0	0.90385	32.83	0.8508	50.0	0.92649
42.0	0.93606	42.0	0.93246	34.61	0.9217	55.0	0.95855
46.0	0.95446	46.0	0.95386	36.29	0.9635	60.0	0.97727
50.0	0.96801	50.0	0.96920	37.91	0.9849	65.0	0.98792
54.0	0.97784	54.0	0.97991	39.46	0.9945	70.0	0.99379
58.0	0.98486	58.0	0.98720	41.67	0.9991	75.0	0.99692
62.0	0.98980	62.0	0.99204	43.08	0.9998	80.0	0.99852
66.0	0.99323	66.0	0.99516	44.45	0.9999	85.0	0.99932
70.0	0.99557	70.0	0.99713	56.86	1.0	90.0	0.99970
74.0	0.99714	74.0	0.99834			95.0	0.99987
78.0	0.99818	78.0	0.99906			100.0	0.99995
82.0	0.99886	82.0	0.99948			105.0	0.99998
86.0	0.99929	86.0	0.99972			110.0	0.99999
90.0	0.99957	90.0	0.99985			150.0	1.0
94.0	0.99974	94.0	0.99992				
98.0	0.99985	98.0	0.99996				
102.0	0.99991	102.0	0.99998				
106.0	0.99995	106.0	0.99999				
110.0	0.99997	150.0	1.0				
114.0	0.99998						
118.0	0.99999						
150.0	1.0						

$F_S(s)$ = Probability that cask velocity is less than or equal to cask velocity listed.
TV1: The train velocities in collision accidents without braking
TV2: The train velocities in derailment accidents without braking
TV3: The velocities due to bridge heights
TV4: The vector sum of train velocities in derailment accidents and velocities due to bridge heights

VV2: Degenerate (90^{o}) - impact is head-on only

$$F(x) = \begin{cases} 0 & x < 90^{o} \\ 1 & x = 90^{o} \end{cases} \qquad (5.6)$$

VV3: Triangular (0^{o},90^{o}) - head-on impact is most likely

$$F(x) = x^{2}/90^{2} \qquad 0^{o} \leq x \leq 90^{o} \qquad (5.7)$$

The cumulative distribution functions are presented in Table 5.3.

5.2.1.3 Cask Orientation Distributions

The orientation of the cask with respect to the object impacted is called the orientation angle, β. It affects the severity of the cask response to mechanical loads. As described in Subsection 2.5.1.3 for impacts on surfaces, a 0^{o} cask orientation defines a sidewise impact while a 90^{o} cask orientation indicates impact of the cask on its end. Alternatively for impacts by train sills, a 0^{o} cask orientation defines a head-on impact to the cask side while a 90^{o} cask orientation indicates a near miss. Again, the cask orientation distribution can depend on the accident scenario, thus three distributions are used:

CT1: Uniform (0^{o},90^{o}) - all cask orientation angles equally likely

$$F(x) = x/90 \qquad 0^{o} \leq x \leq 90^{o} \qquad (5.8)$$

CT2: Triangular (0^{o},90^{o}) - end orientation impact on surfaces or head-on impact to side of cask by train is most likely

$$F(x) = x^{2}/90^{2} \qquad 0^{o} \leq x \leq 90^{o} \qquad (5.9)$$

Table 5.3
Cumulative Impact Angle Distributions

Impact Angle, α (^{o})	Distributions		
	VV1 $F_A(\alpha)$	VV2 $F_A(\alpha)$	VV3 $F_A(\alpha)$
0.	0.	0.	0.
5.0	0.05556	0.	0.00309
10.0	0.11111	0.	0.01235
15.0	0.16667	0.	0.02778
20.0	0.22222	0.	0.04938
25.0	0.27778	0.	0.07716
30.0	0.33333	0.	0.11111
35.0	0.38889	0.	0.15123
40.0	0.44444	0.	0.19753
45.0	0.50000	0.	0.25000
50.0	0.55556	0.	0.30864
55.0	0.61111	0.	0.37346
60.0	0.66667	0.	0.44444
65.0	0.72222	0.	0.52160
70.0	0.77778	0.	0.60494
75.0	0.83333	0.	0.69444
80.0	0.88889	0.	0.79012
85.0	0.94444	0.	0.89198
90.0	1.0	1.0	1.0

$F_A(\alpha)$ = Probability that impact angle is less than or equal to impact angle stated in left-hand column.
VV1: Uniform (0^o,90^o) - any impact angle is equally likely
VV2: Degenerate (90^o) - impact is head-on only
VV3: Triangular (0^o,90^o) - head-on impact is most likely

CT3: Triangular (0^o,90^o) - 45^o orientation impact on surface or 45^o impact on side of cask by train is most likely

$$F(x) = \begin{cases} x^2/2(45)^2 & 0^o \le x \le 45^o \\ 1-[(90-x)^2/2(45)^2] & 45^o \le x \le 90^o \end{cases} \qquad (5.10)$$

The cumulative distribution functions are presented in Table 5.4.

5.2.2 Thermal Loading Parameter Distributions

The thermal response of a cask, represented by the temperature reached at the middle of the lead shield thickness, is determined by three major thermal loading parameters: fire duration, flame temperature, and fire location with respect to the cask.

5.2.2.1 Fire Duration Distributions

The duration of a fire occurring during a transportation accident depends on a number of factors including

- the amount and type of fuel, combustibles, and other volatile materials available
- the availability and feasibility of fire fighting support.

The first factor is influenced by the type of accident. For example, a single truck accident is likely to involve a different fire environment than a truck-truck or truck-auto collision. Similarly, a truck hitting a bridge abutment is likely to cause a different type of fire than a truck jackknifing or overturning along the roadbed. To accommodate these possibilities, several fire duration distributions are considered in the analysis of both highway and railway accident fires. These distributions are generated using the simulation code developed at Sandia[2].

Table 5.4
Cumulative Cask Orientation Angle Distributions

Cask Orientation Angle, β (°)	Distributions CT1 $F_B(\beta)$	CT2 $F_B(\beta)$	CT3 $F_B(\beta)$
0.	0.	0.	0.
5.0	0.05556	0.00309	0.00617
10.0	0.11111	0.01235	0.02469
15.0	0.16667	0.02778	0.05556
20.0	0.22222	0.04938	0.09877
25.0	0.27778	0.07716	0.15432
30.0	0.33333	0.11111	0.22222
35.0	0.38889	0.15123	0.30246
40.0	0.44444	0.19753	0.39506
45.0	0.50000	0.25000	0.50000
50.0	0.55556	0.30864	0.60494
55.0	0.61111	0.37346	0.69753
60.0	0.66667	0.44444	0.77778
65.0	0.72222	0.52160	0.84568
70.0	0.77778	0.60494	0.90123
75.0	0.83333	0.69444	0.94444
80.0	0.88889	0.79012	0.97531
85.0	0.94444	0.89198	0.99383
90.0	1.0	1.0	1.0

$F_B(\beta)$ = = Probability that cask orientation angle is less than or equal to cask orientation angle stated in left-hand column.
CT1: Uniform (0^o,90^o) - all cask orientation angles equally likely
CT2: Triangular (0^o,90^o) - end orientation impact is most likely
CT3: Triangular (0^o,90^o) - 45^o orientation impact is most likely

The following fire duration distributions are used in the analysis of highway accident fires:

F1: Non-collision accident fires
F2: Off-road (or collision with fixed objects) accident fires
F3: Truck/truck collision accident fires
F4: Truck/automobile collision accident fires
F5: Truck/train collision accident fires.

These distributions are presented in Table 5.5. The distributions for accidents involving a truck colliding with a fixed object and a truck running off the highway are simulated separately but result in the same output.

The following train fire duration distributions are presented in Table 5.6 for analyzing railway accident fires:

TF1: Collision accident fires
TF2: Derailment accident fires
TF3: Other accident fires.

5.2.2.2 Flame Temperature Distributions

Flame temperature and fire duration are often correlated. Highly volatile and chemically reactive substances exhibit high reaction rates and high intensity (temperature), while substances with low reaction rates are consumed slowly and exhibit low intensity. However, information about the joint probability distribution of temperature and duration is not available. Also, the distribution of flame temperature can vary between accident scenarios due to several factors, including the likely amount of fuel available. This information is also not available, thus a simple flame temperature distribution is used in the probability analyses. This distribution, T_1, is based on a Weibull function for flame temperatures between $1400^{o}F$ and $2400^{o}F$:

T1: Weibull ($1400^{o}F$,$2400^{o}F$)

Table 5.5
Cumulative Fire Duration Distributions for Truck Cask Analysis

Fire Duration, d (hours)	Distributions F1 $G_D(d)$	F2 $G_D(d)$	F3 $G_D(d)$	F4 $G_D(d)$	F5 $G_D(d)$
0.	0.	0.	0.	0.	0.
0.083	0.3311	0.0321	0.0035	0.0131	0.00238
0.167	0.6596	0.2821	0.0451	0.1653	0.07222
0.250	0.8551	0.5860	0.1572	0.4179	0.16427
0.333	0.9625	0.7754	0.3488	0.6516	0.31099
0.417	0.9801	0.8769	0.5001	0.7878	0.43757
0.500	0.9897	0.9358	0.6034	0.8725	0.54957
0.583	0.9944	0.9643	0.6771	0.9161	0.64690
0.667	0.9970	0.9800	0.7322	0.9456	0.73075
0.750	0.9985	0.9902	0.7750	0.9662	0.80265
0.833	0.9992	0.9949	0.7960	0.9761	0.86416
0.917	0.9996	0.9973	0.8123	0.9838	0.87612
1.0	0.9998	0.9989	0.8257	0.9898	0.88589
1.083	0.99991	0.9995	0.8367	0.9936	
1.167	0.99996	0.9998	0.8459	0.9964	0.89828
1.250	0.99999	0.99995	0.8535	0.9984	
1.333	1.0	0.99998	0.8596	0.9993	0.90934
1.417		0.99999	0.8652	0.9997	
1.500		1.0	0.8696	0.9999	0.91874
1.583			0.8737	0.99996	
1.667			0.8779	0.99997	0.92730
1.750			0.8812	0.99999	
1.833			0.8847	1.0	0.93452
1.917			0.8882		
2.0			0.8917		0.94126
3.0			0.9287		0.96792
4.0			0.9503		0.98247
5.0			0.9641		0.99056
6.0			0.9773		0.99643
7.0			0.9905		1.0
8.0			1.0		

$G_D(d)$ = Probability that fire duration is less than or equal to fire duration stated in left-hand column.
F1: Non-collision accident fires
F2: Off-road (or collision with fixed objects) accident fires
F3: Truck/truck collision accident fires
F4: Truck/automobile collision accident fires
F5: Train collision accident fires

Table 5.6
Cumulative Fire Duration Distributions for Rail Cask Analysis

Fire Duration, d (hours)	Distributions TF1 $G_D(d)$	TF2 $G_D(d)$	TF3 $G_D(d)$
0.	0.	0.	0.
0.083	0.00238	0.01009	0.00943
0.167	0.07222	0.09213	0.09180
0.250	0.16427	0.17603	0.17574
0.330	0.31099	0.29164	0.29183
0.417	0.43757	0.39717	0.39789
0.500	0.54957	0.49517	0.49648
0.583	0.64690	0.58120	0.58291
0.667	0.73075	0.65917	0.66075
0.750	0.80265	0.72958	0.73139
0.833	0.86416	0.79154	0.79373
0.917	0.87612	0.80544	0.80765
1.0	0.88589	0.81870	0.82036
1.167	0.89828	0.83308	0.83454
1.333	0.90934	0.84752	0.91874
1.500	0.91874	0.86071	0.86292
1.667	0.92730	0.87388	0.87564
1.833	0.93452	0.88537	0.88704
2.0	0.94126	0.89665	0.89792
3.0	0.96792	0.94290	0.94342
4.0	0.98247	0.96790	0.96821
5.0	0.99056	0.98166	0.98239
6.0	0.99643	0.98868	0.98941
7.0	1.0	0.99380	0.99403
8.0		0.99702	0.99754
9.0		0.99910	0.99928
10.0		0.99978	0.99985
11.0		1.0	1.0

$G_D(d)$ = Probability that fire duration is less than or equal to fire duration stated in left-hand column.
TF1: Collision accident fires
TF2: Derailment accident fires
TF3: Other accident fires

$$F(x) = \left[1-e^{-\left(\frac{x-1400}{550}\right)^{1.83}}\right] / \left[1-e^{-\left(\frac{1000}{550}\right)^{1.83}}\right] \quad 1400^{o}F \leq x \leq 2400^{o}F \quad (5.11)$$

This distribution covers the range of flame temperature achievable in typical hydrocarbon fires.[2] These types of fires constitute the majority of fires which occur in transportation accidents. The cumulative distribution function is presented in Table 5.7.

5.2.2.3 Fire Location Distributions

The location of a fire has a significant affect on the heat flux to which a cask is exposed and hence on the temperature attained at the middle of the lead shield thickness. An engulfing fire typically produces a greater heat flux exposure to the cask and results in higher cask temperatures than a fire of the same temperature, size, and duration that is adjacent to the cask. The greater the distance of the fire from the cask, the less the thermal interaction and effective exposure.

As with the other fire parameters, no historical data is available for developing a distribution of fire location with respect to the cask. In lieu of such information, a uniform distribution of cask to fire location is assumed. The fire locations are varied between the truck and rail casks in proportion to the size differences between the two casks. The fire location distributions, L_1, used are:

Truck fires - Uniform (0 ft, 30.75 ft)

$$F(x) = x/30.75 \qquad 0 \text{ ft} \leq x \leq 30.75 \text{ ft} \qquad (5.12)$$

Train fires - Uniform (0 ft, 43 ft)

$$F(x) = x/43 \qquad 0 \text{ ft} \leq x \leq 43 \text{ ft} \qquad (5.13)$$

Table 5.7
Cumulative Flame Temperature Distribution

Flame Temperature, t (^{o}F)	$G_T(t)$
1400	0.
1500	0.04551
1600	0.15306
1700	0.29588
1800	0.45059
1900	0.59847
2000	0.72714
2100	0.83069
2200	0.90849
2300	0.96342
2400	1.0

$G_T(t)$ = Probability that flame temperature is less than or equal to temperature stated in left-hand column.

The cumulative distribution functions are presented in Table 5.8. A fire is considered engulfing if it is within 1/4 foot of the center of a truck cask or within one foot of the center of a rail cask.

5.3 Probability Calculation

The purpose of the probability calculation is to estimate the likelihood that specified sets of cask responses will be realized if an accident occurs. The calculation is based on combining the probabilistic information about the accident parameters with the probabilities of the various accident scenarios. The probability estimate is then combined with an estimate of the expected accident rate/truck or train-mile to estimate the expected frequency/mile of cask response in specified response regions. Once the radiological hazards for each cask response region are characterized, the risk, i.e., probability times hazard, associated with transporting spent fuel is estimated.

As described in Section 4.0, the potential cask response represented by the containment vessel strain and the lead mid-thickness temperature due to a transportation accident are partitioned into 20 response regions R(i,j), i=1,...,4, j=1,...,5, consisting of the combination of 4 structural response regions and 5 thermal response regions:

Structural Response Region	Condition
i=1	Less than 0.2% strain ($<S_1$)
2	Between 0.2% (S_1) and 2% (S_2) strain
3	Between 2% (S_2) and 30% (S_3) strain
4	Greater than 30% strain ($>S_3$)

Table 5.8
Cumulative Fire Location Distributions

Fire Location, ℓ (feet)	Distributions	
	Truck $G_L(\ell)$	Train $G_L(\ell)$
0.	0.	0.
1.0	0.03175	0.02326
2.0	0.06349	0.04651
6.0	0.19048	0.13953
10.0	0.31746	0.23256
14.0	0.44444	0.32558
18.0	0.57143	0.41860
22.0	0.69841	0.51163
26.0	0.8455	0.60465
30.00	0.9756	0.69767
30.75	1.0	
34.0		0.79070
38.0		0.88372
42.0		0.97674
43.0		1.0

$G_L(\ell)$ = Probability that fire location is less than or equal to fire location stated in left-hand column.

Thermal Response Region	Condition
j=1	Less than 500°F lead mid-thickness temperature ($<T_1$)
2	Between 500°F (T_1) and 600°F (T_2) lead mid-thickness temperature
3	Between 600°F (T_2) and 650°F (T_3) lead mid-thickness temperature
4	Between 650°F (T_3) and 1050°F (T_4) lead mid-thickness temperature
5	Greater than 1050°F lead mid-thickness temperature ($>T_4$)

The probabilities estimated in the probability analysis are the likelihood of the cask response being in each one of the response regions.

The initial step in modeling the probability calculations is to relate the containment vessel strain to impact velocity and the lead mid-thickness temperature to effective fire duration. The first part is done by developing strain-impact velocity curves for several object hardnesses. Similarly, the lead mid-thickness temperature-fire duration models are developed for several fire locations and a 1700°F flame temperature.

Given a fixed impact angle and cask orientation, the probability that containment vessel strain is within a given region is derived from the distribution of the impact velocity via the strain-impact velocity curves. For example, given a truck cask, using Fig. 7-3 and assuming an unyielding object and an end-on cask orientation, a strain between 0.2% (S_1) and 2% (S_2) corresponds to an impact velocity between 38 mph and 46 mph. Thus, assuming a head-on impact, i.e., 90° impact angle, the probability of the containment vessel strain being between 0.2% (S_1) and 2% (S_2), denoted $P(0.2 \leq S_t \leq 2)$, is equal to the probability that the cask velocity is between 38 mph and 46 mph. Recognizing the fact that the relationships between strain and cask velocity are conditional on the impact angle, cask orientation, and object hardness, the identity involving the strain and cask velocity probabilities can be written mathematically as:

$$P(0.2<S_t\leq 2 \mid \text{head-on, end-on impact with unyielding object}) = F_S(46) - F_S(38) \quad (5.14)$$

where $F_S(.)$ denotes the appropriate cumulative distribution function of cask velocity.

Taking into consideration the fact that the impact angle and cask orientation are variable, and recognizing that the hardness of the object impacted is identified by an accident scenario, the probability of the containment vessel strain given a specific accident scenario is obtained by averaging the probability in Equation 5.14 with respect to the appropriate distributions for impact angle and cask orientation. Mathematically,

$$P(0.2<S_t<2|A_k) = \int_{\alpha}\int_{\beta} \{F_S[s_2(\alpha,\beta,A_k)|A_k] - F_S[s_{0.2}(\alpha,\beta,A_k)|A_k]\} \times dF_A(\alpha|A_k)dF_B(\beta|A_k) \quad (5.15)$$

where A_k identifies an accident scenario and $F_S(.)$, $F_A(.)$ and $F_B(.)$ are the cumulative distribution functions for cask velocity, impact angle, and cask orientation, respectively. Equation 5.15 recognizes that the cask accident velocity corresponding to 0.2% (S_1) and 2% (S_2) strain depends on the impact angle, cask orientation, and hardness of the object impacted, i.e., the accident scenario.

As illustrated in Fig. 5.1, changing the cask orientation corresponds to varying the strain-impact velocity curve. This change is included in the probability analysis by developing strain-impact velocity curves for 0^o, 45^o, and 90^o cask orientation for each level of hardness of the impacted object. It is assumed, given a fixed impact angle, that the impact velocities for intermediate angles can be approximated by:

$$v_{\%}(\beta) = \begin{cases} v_{\%}(0^o) + \frac{\beta}{45}[v_{\%}(45^o) - v_{\%}(0^o)] & 0^o < \beta \leq 45^o \\ v_{\%}(45^o) + \frac{(\beta-45)}{45}[v_{\%}(90^o) - v_{\%}(45^o)] & 45^o \leq \beta < 90^o \end{cases} \quad (5.16)$$

That is, a linear interpolation is assumed between the 0^0 and 45^0 curves and between the 45^0 and 90^0 curves. Notationally, $v_{\%}(\beta)$ denotes the impact velocity corresponding to strain percent, %, for cask orientation angle, β. The corresponding strain-impact velocity curves for several β's are illustrated in Fig. 5-1.

The impact angle α relates the cask impact velocity to the cask accident velocity. If the impact is head-on, i.e., $\alpha=90^0$, then the impact velocity equals the accident velocity. On the other hand, if α is less than 90^0, then the impact velocity is less than the accident velocity. Since the velocity distributions V1 through V4 and TV1 through TV4 are distributions for accident velocities, it is necessary to transform the impact velocity corresponding to a strain level to an accident velocity. This transformation, for a fixed cask orientation angle, β, is given by

$$s_{\%}(\beta,\alpha) = v_{\%}(\beta)/\sin\alpha \qquad (5.17)$$

where $v_{\%}(\beta)$ represents impact velocity and $s_{\%}(\beta,\alpha)$ is the corresponding accident velocity for the given impact angle.

To illustrate how cask orientation and impact angle are handled in the calculations, we consider structural response region i=2, i.e., between 0.2% (S_1) and 2% (S_2) strain, being attained when a cask hits a concrete object at a 45^0 orientation angle and a 35^0 impact angle. From Table 5.9 for accident scenario No. 8 the impact velocities for 0.2% (S_1) and 2% (S_2) strain are $v_{0.2\%}(45^0)$ = 35 mph and $v_{2\%}(45^0)$ = 49 mph. (Note: for other orientation angles β, Equation 5.16 would be used to evaluate $v_{\%}(\beta)$.) Using Equation 5.17, the vehicle velocities necessary to result in impact velocities of 35 mph and 49 mph, if the angle of impact is 35^0, are (since $\sin 35^0$ = 0.57378):

$$s_{0.2\%}(45^0,35^0) = v_{0.2\%}(45^0) \;/\; 0.57378$$
$$= 61 \text{ mph}$$

Table 5.9
Probability Inputs for Highway Analysis

Accident index	Probability $\times 10^{-3}$	P(fire)	Fire duration	Temperature	Location	Distributions: Cask orientation	Impact angle	Speed	Strain-impact velocity curve	Damage state upper boundaries: <0.2% 0°	<0.2% 45°	<0.2% 90°	<2% 0°	<2% 45°	<2% 90°	<30% 0°	<30% 45°	<30% 90°
1	34.002	0.004	F1	T1	L1	CT1	VV1	V1		150	150	150	150	150	150	150	150	150
2	8.093	↓	F2	↓	↓	↓	↓	↓		↓	↓	↓	↓	↓	↓	↓	↓	↓
3	431.517	↓	F4	↓	↓	↓	↓	↓		↓	↓	↓	↓	↓	↓	↓	↓	↓
4	133.201	0.008	F3	↓	↓	↓	↓	↓		↓	↓	↓	↓	↓	↓	↓	↓	↓
5	7.701	0.011	F5	↓	↓	CT3	VV2	V4	5	9	14	150	20	27	↓	↓	↓	↓
6	38.113	0.009	F2	↓	↓	CT1	VV1	V1		150	150	150	150	150	↓	↓	↓	↓
7	1.039	0.004	↓	↓	↓	CT3	VV2	V2	4	42	150	38	59	150	64	↓	↓	↓
8	3.986	↓	↓	↓	↓	↓	↓	↓	2	32	35	38	51	49	46	↓	↓	↓
9	0.079	↓	↓	↓	↓	↓	↓	↓	3	↓	58	84	↓	101	150	↓	↓	↓
10	0.006	↓	↓	↓	↓	↓	↓	↓	2	↓	35	38	↓	49	46	↓	↓	↓
11	0.001	↓	↓	↓	↓	↓	↓	↓	1	↓	↓	↓	↓	↓	↓	↓	113	76
12	0.299	↓	↓	↓	↓	CT2	VV3	V1	2	↓	↓	↓	↓	↓	↓	↓	150	150
13	0.062	↓	↓	↓	↓	↓	↓	↓	↓	↓	↓	↓	↓	↓	↓	↓	↓	↓
14	0.011	↓	↓	↓	↓	↓	↓	↓		↓	↓	↓	↓	↓	↓	↓	↓	↓
15	0.850	↓	↓	↓	↓	CT1	VV1	↓		150	150	150	150	150	150	↓	↓	↓
16	40.079	↓	↓	↓	↓	↓	↓	↓		↓	↓	↓	↓	↓	↓	↓	↓	↓
17	5.111	↓	↓	↓	↓	↓	↓	↓		↓	↓	↓	↓	↓	↓	↓	↓	↓
18	37.050	↓	↓	↓	↓	↓	↓	↓		↓	↓	↓	↓	↓	↓	↓	↓	↓
19	23.063	0.011	F1	↓	↓	↓	↓	↓	3	32	58	84	51	101	↓	↓	↓	↓
20	1.981	↓	↓	↓	↓	↓	↓	↓	2	↓	35	38	↓	49	46	↓	↓	↓
21	0.297	↓	↓	↓	↓	↓	↓	↓	1	↓	↓	↓	↓	↓	↓	↓	113	76
22	13.192	↓	↓	↓	↓	CT2	VV3	V3	3	32	58	84	↓	101	150	↓	150	150
23	1.076	↓	↓	↓	↓	↓	↓	↓	2	↓	35	38	↓	49	46	↓	↓	↓
24	0.170	↓	↓	↓	↓	↓	↓	↓	1	↓	↓	↓	↓	↓	↓	↓	113	76
25	8.894	↓	↓	↓	↓	CT1	VV1	V1		150	150	150	150	150	150	↓	150	150
26	9.412	↓	↓	↓	↓	↓	↓	↓		↓	↓	↓	↓	↓	↓	↓	↓	↓
27	32.517	↓	↓	↓	↓	↓	↓	↓		↓	↓	↓	↓	↓	↓	↓	↓	↓
28	83.493	0.012	↓	↓	↓	↓	↓	↓		↓	↓	↓	↓	↓	↓	↓	↓	↓
29	54.603	↓	↓	↓	↓	↓	↓	↓		↓	↓	↓	↓	↓	↓	↓	↓	↓
30	20.497	0.130	↓	↓	↓	↓	↓	↓		↓	↓	↓	↓	↓	↓	↓	↓	↓
31	9.705	1.0	↓	↓	↓	↓	↓	↓		↓	↓	↓	↓	↓	↓	↓	↓	↓

$$s_{2\%}(45^{o},35^{o}) = v_{2\%}(45^{o}) \;/\; 0.57378$$
$$= 85.40 \text{ mph}$$

Given a fire, the thermal response of the cask, represented by the lead mid-thickness temperature is related to the duration of the fire. This relationship, illustrated in Fig. 5-2, depends on both flame temperature and fire location. Using an argument analogous to the development of the probability corresponding to a structural response region, the probability that the cask thermal response is in a specific region, for example, between $600^{o}F$ (T_2) and $650^{o}F$ (T_3) or thermal response region j=3, is given by

$$P(600<T<650|A_k \text{ with a Fire}) = \iint_{t\ell} [G_D[d_{650}(t,\ell)|A_k] - G_D[d_{600}(t,\ell)|A_k]] \times dG_T(t)dG_L(\ell) \quad (5.18)$$

where $G_D(.)$, $G_T(.)$, $G_L(.)$ denote the fire duration, flame temperature, and fire location cumulative distribution functions, respectively. Again, the fire duration, $d_{o_F}(t,\ell)$, corresponding to a lead mid-thickness temperature, ^{o}F, depends on the flame temperature and fire location. This is denoted in the argument of the fire duration distribution function. Also, the fire duration distribution varies with the accident scenario.

The basic mid-thickness temperature of the lead shield-fire duration curve is based on a $1700^{o}F$ real engulfing fire. The effects of the other fire parameters are included in the analyses by adjusting this basic curve. For fires that deviate from a $1700^{o}F$ fire, the same temperature is reached within the shield, but the time to reach this temperature is shorter or longer depending on the flame temperature. If the flame temperature is greater than $1700^{o}F$, the same lead mid-thickness temperature is reached in a shorter time; whereas if the flame temperature is below $1700^{o}F$, it takes longer to produce the same temperature in the middle of the lead shield thickness. Thus, for a given lead mid-thickness temperature, the effects of different flame temperatures for an engulfing fire are modeled by the identity

$$d_{0_F}(t,0) = \delta(t)\, d_{0_F}(1700^0,0 \text{ ft}) \tag{5.19}$$

A list of the factors $\delta(t)$ is presented in Table 5.10.

For fire location, as the distance between the fire and the cask increases, heat exposure decreases, and a longer duration fire is needed to produce the same temperature in the middle of the lead shield thickness as an engulfing fire. Thus, the effect of fire location on the lead shield temperature-fire duration relationship is modeled by a multiplicative factor. The model used is

$$\begin{aligned} d_{0_F}(t,\ell) &= \delta(\ell)\, d_{0_F}(t^0,0 \text{ ft}) \\ &= \delta(\ell)\, \delta(t)\, d_{0_F}(1700^0,0 \text{ ft}) \end{aligned} \tag{5.20}$$

where the factor $\delta(\ell)$ is given by

$$\delta(\ell) = 0.78e^{(0.7732+0.06287\ell)} \qquad \ell > 1.5 \text{ ft} \tag{5.21}$$

for a truck cask and

$$\delta(\ell) = 0.78e^{(0.62874 + 0.08471\ell)} \qquad \ell > 4 \text{ ft} \tag{5.22}$$

for a rail cask. In both cases, location is measured from the center of the cask, which is mathematically assumed to represent the location of an engulfing fire. Development of the flame temperature and fire location models in Equations 5.19 through 5.22 is discussed in Subsections 2.5.2.3 and 2.5.2.4. The effect on the basic lead mid-thickness temperature-fire duration curve for a truck cask is shown in Fig. 5-2.

Equations 5.15 and 5.18 are expressions for estimating the probability that the containment vessel strain is within a given structural response region, e.g., between 0.2% (S_1) and 2% (S_2) strain, and the probability, given a fire, that the lead mid-thickness temperature is within a given thermal response region, e.g., between 600°F (T_2) and 650°F (T_3), respectively. Both expressions are conditional on a given accident scenario. A cask response

Table 5.10
Heat Flux Factors for Flame Temperatures
(Engulfing Fire)

Flame Temperature,t (^{0})	$\delta(t)$
1400	1.72
1500	1.43
1600	1.21
1700	1.0
1800	0.86
1900	0.73
2000	0.64
2100	0.56
2200	0.49
2300	0.44
2400	0.39

expressions are conditional on a given accident scenario. A cask response region involves a combination of structural responses and thermal responses. Assuming that strain is <u>independent</u> of the lead shield temperature, these probabilities can be multiplied to estimate the probability associated with a response region. For example, for response region R(2,3), i.e., strain between 0.2% (S_1) and 2% (S_2) and lead mid-thickness temperature between 600°F (T_2) and 650°F (T_3), the probability, given accident scenario A_k is:

$$P[R(2,3)|A_k]=P(\text{Fire}|A_k)\Big[\int_{\alpha}\int_{\beta}\{F_S[s_2(\alpha,\beta,A_k)|A_k]-F_S[s_{0.2}(\alpha,\beta,A_k)|A_k]\}$$

$$\times\, dF_A(\alpha|A_k)dF_B(\beta|A_k)\Big]\Big[\int_t\int_{\ell}\{G_D[d_{650}(t,\ell)|A_k]-G_D[d_{600}(t,\ell)|A_k]\}$$

$$\times\, dG_T(t)dG_L(\ell)\Big] \quad (5.23)$$

where the probability of a fire is included in the expression. Similar expressions hold for each of the response regions R(i,j).

Two response regions correspond to accidents involving either no fire or fire only. In these cases, it is assumed that there is no cask thermal response and no cask structural response. For no fire, the response regions are denoted R(i,0), and the probabilities are

$$P[R(i,0)|A_k]=[1-P(\text{Fire}|A_k)]\;P[s_{\ell,i}\le S\le s_{u,i}|A_k] \quad (5.24)$$

where $s_{\ell,i}$ and $s_{u,i}$ denote the lower and upper strain limit for the ith region, respectively. For fire only, the response regions are denoted R(0,j), and the probabilities are

$$P[R(0,j)|\text{Fire only}]=P[d_{\ell,j}\le T\le d_{u,j}|\text{Fire only}] \quad (5.25)$$

where $d_{\ell,j}$ and $d_{u,j}$ denote the lower and upper shield temperature for the jth region, respectively.

The final step in the probability calculation is to combine the probabilities over all accident scenarios. Thus, for response region R(i,j),

$$P[R(i,j)] = \sum_{A_k} P(A_k)\ P[R(i,j)|A_k)] \qquad (5.26)$$

where $P(A_k)$ is the likelihood of accident scenario A_k given an accident. Tables 5.9 and 5.11 summarize the value of $P(A_k)$; $P(Fire|A_k)$; choice of distributions for each accident scenario; and the structural response region limits for 0^0, 45^o, and 90^o cask orientation for a truck cask and rail cask, respectively.

The actual probability calculations described in Equations 5.23 and 5.26 are done by a computer code, called TASP (Transportation Accident Scenario Probabilities). The inputs into the code are appropriate distributions for the accident parameters. These are combined for each accident scenario using Equation 5.23 and averaged over accident scenarios using Equation 5.26. The integration in Equation 5.23 is based on approximating the integrals by sums. Details of the integration are discussed in Appendix G. A flow chart of TASP is given in Fig. 5-4.

The results of the probability calculations are presented and discussed in Section 9.0.

Table 5.11
Probability Inputs for Railway Analysis

Accident index	Probability ×10⁻²	P(fire)	Fire duration	Temperature	Location	Distributions: Cask orientation	Impact angle	Speed	Strain-impact velocity curve	Damage state upper boundaries: <0.2% 0°	<0.2% 45°	<0.2% 90°	<2% 0°	<2% 45°	<2% 90°	<30% 0°	<30% 45°	<30% 90°
1	3.0400	0.01	TF1	T1	L1	CT1	VV1	TV1		150	150	150	150	150	150	150	150	150
2	8.5878		TF1															
3	0.1615		TF2			CT3	VV2	TV3	4	55	150	38	72	150	60			
4	0.0122								3		47	40		69	66			
5	0.0010								2			38		60	48	150	128	105
6	0.0002								1									
7	0.6192								2									
8	0.3433					CT1	VV1	TV1		150	150	150	150	150	150	150	150	150
9	0.5092					CT2	VV3	TV4	3	55	47	40	72	69	66	150	150	150
10	0.0415								2			38	56	60	48	150	128	105
11	0.0066								1							150	128	105
12	1.4437					CT1	VV1	TV2	3			40	60	69	66	150	150	150
13	0.1178								2			38	56	60	48	150	128	105
14	0.0186								1									
15	0.0465					CT2	VV3		2									
16	0.0096																	
17	0.0017																	
18	16.4477					CT1	VV1	TV1		150	150	150	150	150	150	150	150	150
19	3.2517																	
20	10.0148																	
21	0.8408						VV2	TV2	6	11	16	150	27	49	150			
22	15.9981						VV1	TV1		150	150	150	150	150	150			
23	31.9865																	
24	6.5000	0.90	TF3															

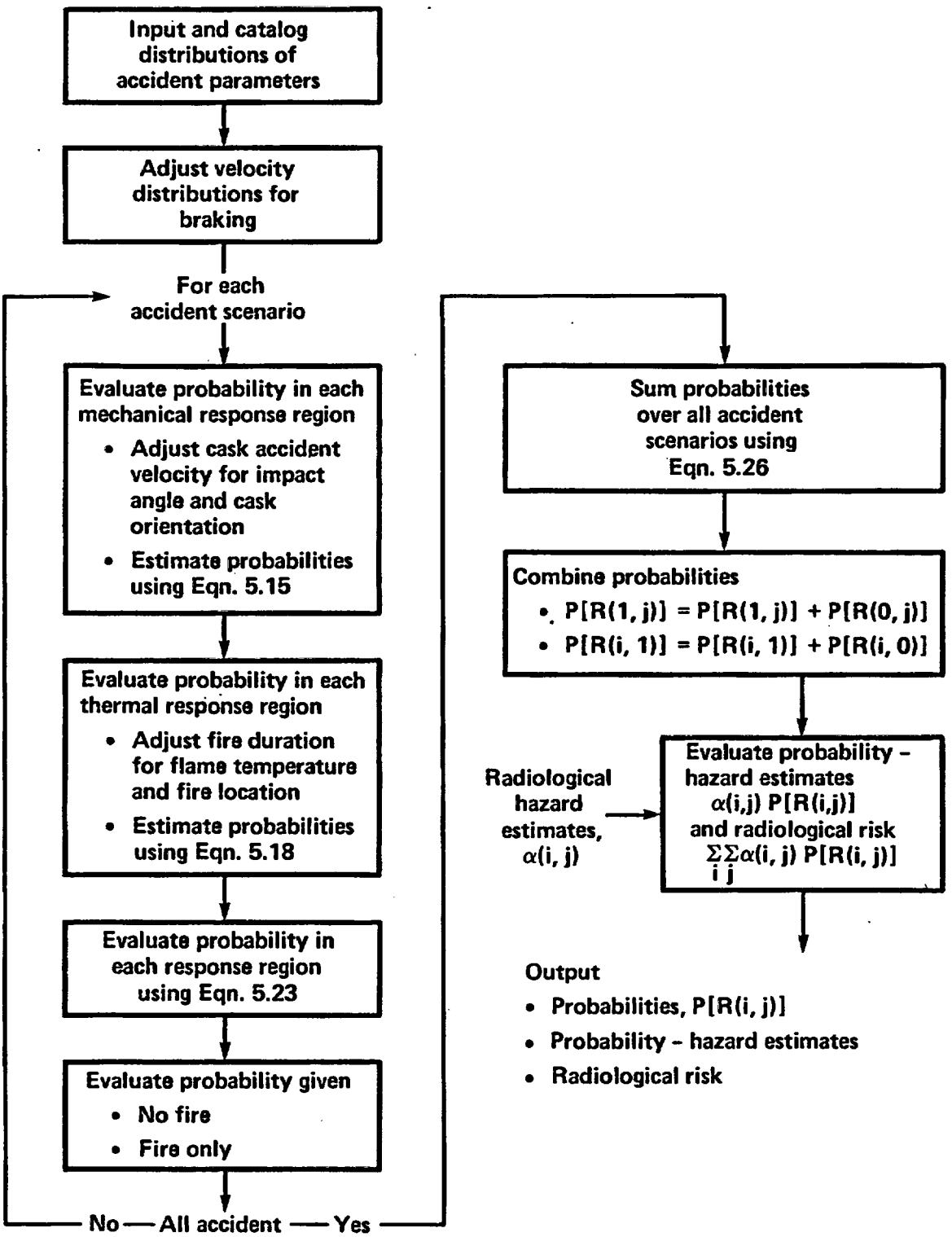

Figure 5-4 Flow chart of TASP computer code.

6.0 FIRST-STAGE SCREENING ANALYSIS

6.1 Introduction

A two-stage screening process is used to evaluate the level of protection provided by licensed fuel casks against real accident loading conditions. Response regions are developed on the basis of cask performance and are described in terms of damage. The response regions are used to sort or screen accident events in terms of the analytically predicted performance of the representative casks. Figure 6-1 shows the 20 response regions defined in Section 4.0. In the first-stage screening, the intent is to determine by analysis which accident-caused loading conditions can result in cask responses that will fall within the first response region R(1,1). Cask responses in this region are less than or equal to responses implied by the 10 CFR 71 accident test conditions.[1] The second-stage screening analysis identifies accidents which produce loading conditions that can cause cask responses outside the R(1,1) region. The first-stage screening analysis is discussed in this section; the second-stage screening analysis is discussed in Section 7.0.

Within the R(1,1) region, the cask structural response does not exceed a strain level of 0.2% (S_1) on the inner shell of the cask. The cask thermal response does not exceed a temperature level of 500°F (T_1) at the middle of the lead shield thickness. Within the R(1,1) region, all the major cask components important to safety during transportation accidents are expected to remain fully functional, and the cask meets regulatory requirements. The cask responses within the R(1,1) region do not exceed the responses that would be expected if the cask were subjected to the accident test conditions of 10 CFR 71. Since cask responses within the R(1,1) region do not result in any significant damage to the cask, no radiological release beyond the regulatory limit is expected from the accident causing this level of damage. In fact, in most cases, releases, if any, would be much less than regulatory limits.

The first-stage screening analysis follows this procedure:

- For each representative cask, dynamic structural and transient thermal analyses are performed to calculate responses to a range of loading

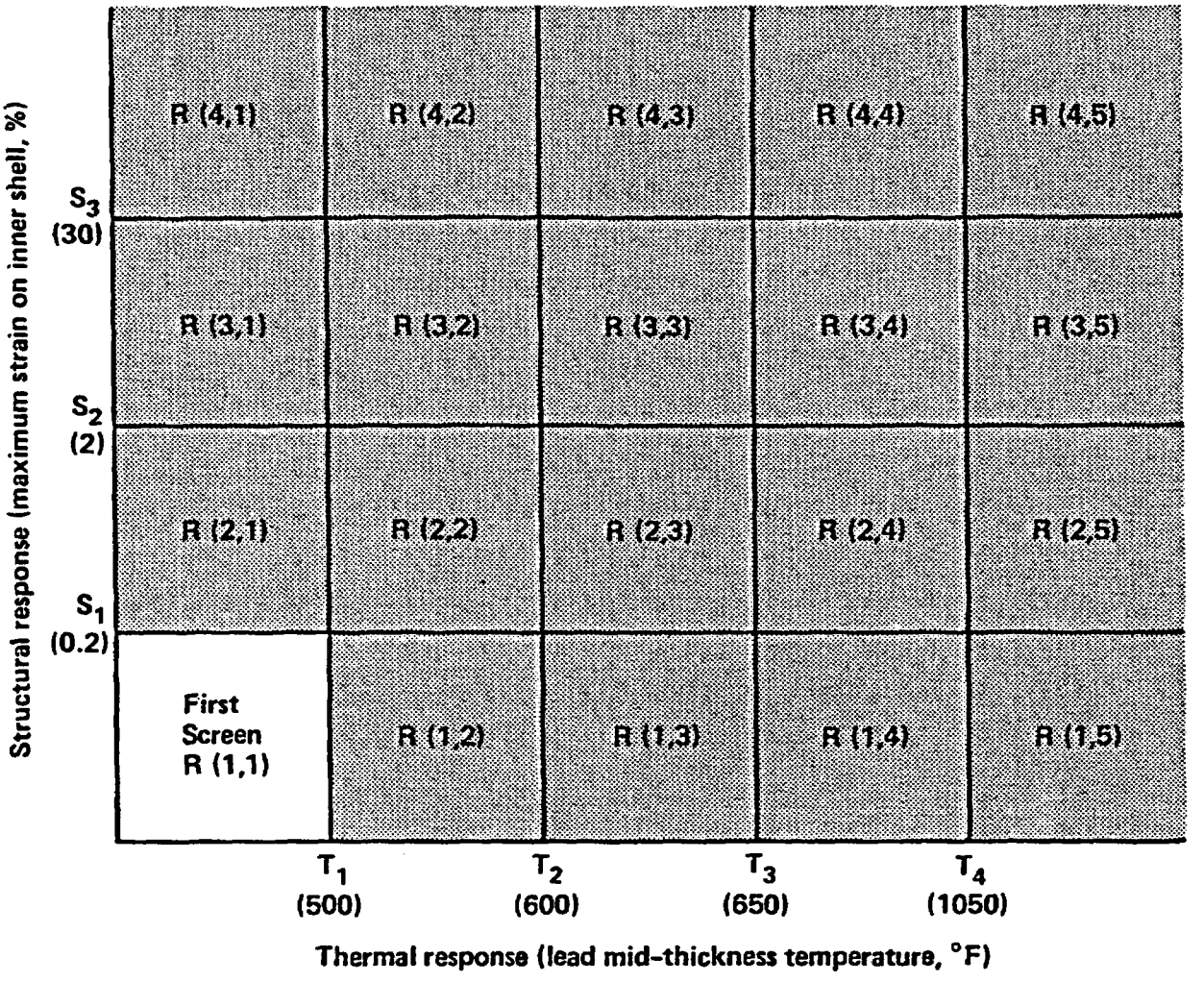

Note:
- The radiological hazard of cask responses falling in region R(1,1) are negligible and less than limits specified in existing regulations (10 CFR 71).
- The radiological hazard of cask responses falling outside region R(1,1) can exceed the limits specified in existing regulations (10 CFR 71).

Figure 6-1 Identification of first-stage screening.

conditions for the accident scenarios identified in Section 2.0. The loading conditions for the accident scenarios are defined by three mechanical loading parameters and three thermal loading parameters. The mechanical loading parameters are impact velocity, object hardness, and cask orientation. The thermal loading parameters are fire duration, flame temperature, and fire location with respect to the cask.

- The structural response is calculated for various impact velocities. The impact velocity is equal to the component of the accident velocity perpendicular to the surface impacted. It is arrived at by multiplying the accident velocity by the sine of the impact angle. Since the impact angle is not precisely known, it is assumed to follow selected probability distributions depending on the accident scenario under study.

- For each accident scenario, the loading conditions that result in cask responses within the R(1,1) region are determined by comparing the cask response with the response levels of 0.2% strain (S_1) on the inner shell for mechanical loads and $500^{o}F$ (T_1) at the mid-thickness of the lead for thermal loads.

- For each accident scenario, the probability of occurrence of the specific loading conditions that could result in cask responses within the R(1,1) region is estimated as described in Section 5.0, using the data bases identified in Section 2.0.

- The fraction of accidents with loading conditions that could result in cask responses within the R(1,1) region is calculated by summing the individual occurrence probabilities associated with each accident scenario.

The major differences between the first-stage and second-stage screening analyses involve the methods used in the structural and thermal analyses. For

the first-stage screening analysis, less sophisticated methods of analysis can be reliably used. For structural responses below the 0.2% strain (S_1) level, dynamic linear elastic analysis can be used with high confidence to evaluate mechanically induced structural responses. For responses beyond the 0.2% strain (S_1) level, 2% strain (S_2) and 30% strain (S_3), dynamic nonlinear analysis is required. For thermal responses below the 600°F temperature (T_2) level, standard transient heat transfer analysis methods can be used. These methods include transient heat transfer by conduction, radiation, and convection. Responses beyond the 600°F temperature (T_2) level include melting of the lead shield, which requires that the transient analysis method include the consideration of phase changes of materials. Figure 6-2 is a schematic diagram showing the general methods of analysis used in the cask response calculations for each of the response regions. Analyses are not performed to calculate responses beyond the 30% strain (S_3) and 1050°F temperature (T_4) levels since the uncertainties in calculational results would be large. However, in Section 8.0, the potential radiological significance is estimated for responses beyond these levels.

In order to consolidate the many variables and analyses required to cover the wide range of potential accident situations, the following approaches and assumptions are used in this study.

(1) Casks used for spent fuel shipments are assumed to be properly designed, fabricated, maintained, and operated in accordance with regulations. The intent of this evaluation is not to assess the probability and potential effects of cask defects or deficient or misapplied operational procedures.

(2) The accident loading parameter distributions in Section 5.0 are generated from the accident data identified in Section 2.0 and are assumed to represent loadings which could be experienced by a spent fuel cask. These accident data are derived from several broad data bases and are independent of any specific transportation route. The frequency of occurrence of certain accident scenarios and their loading conditions can

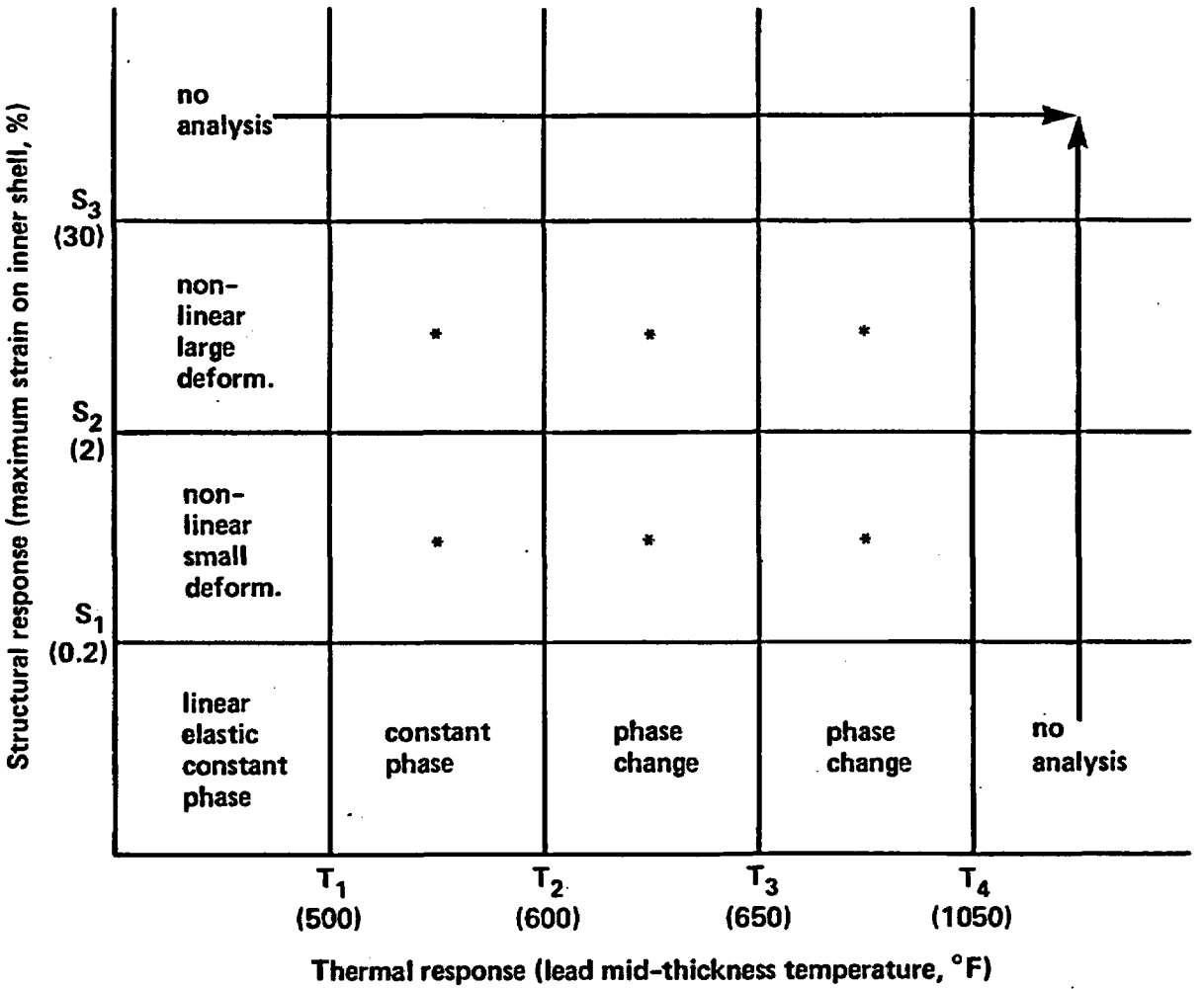

*Combined analysis

Figure 6-2 Methods of analysis used in cask response determinations.

experience some variations depending on the specific routing selected. These variations are considered minor for purposes of this study.

(3) In evaluating highway and railway accidents involving impacts, any damage done to the cask is assumed to result from striking a single object. Real accidents can involve impact with multiple objects; however, for impacts into the harder objects of interest, almost all of the energy involved in the accident is associated with the initial impact. In certain cases, such as accident scenarios involving impacts with bridge railings, conservative assumptions are made. In this scenario, it is assumed that the bridge railing does not cause the transport vehicle to stop but instead allows the cask to fall off the bridge and onto the surface below. The cask response is calculated for falling off the bridge and striking the surface below. Damage to the cask caused by hitting the bridge railing is not significant to the overall evaluation. Conservatism is further introduced in the probability portion of the evaluation because a cask is assumed to fall off a bridge whenever the truck hits the bridge railing.

(4) The representative truck and rail casks selected for this study and described in Section 3.0 are defined to meet regulatory requirements and generally reflect the designs of casks on the roads and railways today. In actual shipments there will be a variety of cask designs. For all of the accident conditions analyzed, most, if not all, would be expected to exhibit degrees of damage equal to or less than those calculated for the representative casks. Ideally the screening analyses would have used a variety of cask designs with their commensurate variety of potential responses. The results of using a representative cask design for the screening process undoubtedly results in an underestimate of the fraction of accidents leading to cask responses in the R(1,1) region. Conversely, the fraction of accidents leading to cask responses in the other regions is most likely overstated.

(5) If there is a lack of data or any unknown factors involved in the structural and thermal analyses or in the accident definition, one of two approaches is followed. Either reasonable assumptions are made from sensitivity study results, or conservative assumptions are made. This approach reduces the need to significantly expand the current data base or unnecessarily complicate the analysis.

Section 6.2 discusses the structural response analysis for impact loads on the representative truck casks. The response analysis determines which accident loading conditions can result in responses that are less than the 0.2% strain (S_1) level within the inner shell of the cask. Section 6.3 discusses the thermal response analysis for thermal loads on the cask that result in responses within the 500°F temperature (T_1) level at the mid-thickness of the lead shield. In Section 6.4 the probabilities of occurrence are estimated for highway and railway accident loading conditions that could result in cask responses falling in the R(1,1) region.

6.2 Structural Response Analysis

Impact loads dominate the structural evaluation. Other loads such as crushing and projectile loads are determined to have little effect on the structural screening analysis. The significance of these loads is discussed in Appendix E. Many accident loads are easily screened out. Minor accidents involving low impact loads, like a rollover or impact with low-resistance objects such as a cask hitting a tree, motorcycle, or automobile, are screened out because the maximum forces generated in these impacts cannot cause significant damage to the cask.

The structural response of a cask to loads generated by potentially significant accidents involving impacts with harder objects at high velocities are calculated. There are three parameters that are considered in estimating structural response. These are shown in Figure 6-3 for impacts on surfaces as impact velocity, cask orientation angle, β, and object hardness. Response calculations are made for various impact velocities and cask orientation angles. The impact velocity is the component of the cask velocity vector

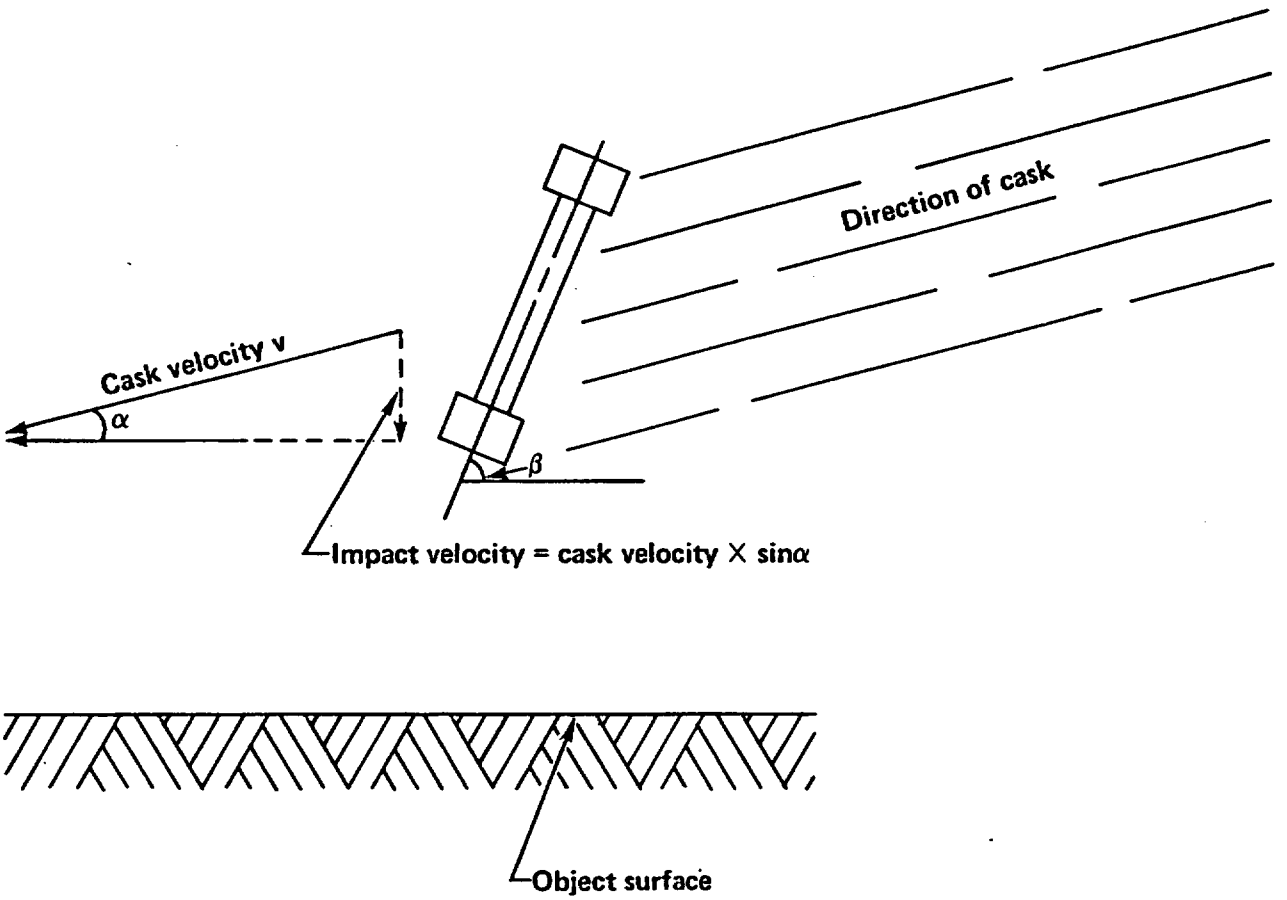

- o Object surface hardness
- o Impact velocity: Cask velocity component perpendicular to the object surface is defined as impact velocity.
- o Cask orientation is defined by angle β, the angle between the cask longitudinal axis and the surface of the object struck

Figure 6-3 Three impact loading parameters considered in the response analysis for impacts on surfaces.

perpendicular to the surface impacted. The angle of impact, α, represents the angle between the cask velocity direction and the surface of the impacted object. When an accident occurs, the cask velocity vector can be in any direction. However, it can always be decomposed into two components: one perpendicular to the impacted object surface and one parallel to it. In the cask response calculation, only the velocity component perpendicular to the object surface is considered. The velocity component parallel to the object surface introduces a sliding-friction effect to the cask structure. The sliding-friction effect will not produce any significant structural deformation to the cask; therefore, it is ignored. The angle defining the cask orientation is the angle between the cask longitudinal axis and the surface of the object struck. Object hardness needs to be considered because casks can strike objects such as concrete abutments, roadbeds, hard rock, soft rock, hard soil, and water. The hardness of the objects and their responses to impact vary over a wide range.

In some accidents, such as rail grade crossing accidents, the impact limiters on the cask can be bypassed and the side of the cask can be struck directly. Once again the mechanical loads depend on the impact velocity, the orientation of the cask and the hardness of the object struck. Figure 6-4 defines these three loading parameters for this type of accident. The impact velocity is the component of the relative velocity of the cask and object that is perpendicular to the cask axis. The angle of impact, α, represents the angle between the relative velocity direction and the cask axis. For the purposes of this study, the impact angle is conservatively assumed to be 90^{o}, that is perpendicular to the cask axis in all cases. Also, it is assumed that the impact occurs at the mid-plane of the cask to cause the most damage. The cask orientation angle, β, is the angle at which the impact occurs on the cask surface. In the worst case the cask is hit at 0^{o} or head-on. For orientation angles near 90^{o}, the cask is essentially not struck. The object hardness depends on the object hitting the cask, such as a train sill or a small bridge column.

Two methods of analysis are used in performing the first-stage screening: quasi-static and linear elastic dynamic. The quasi-static method is used to screen out minor accidents involving low-resistance objects such as poles and

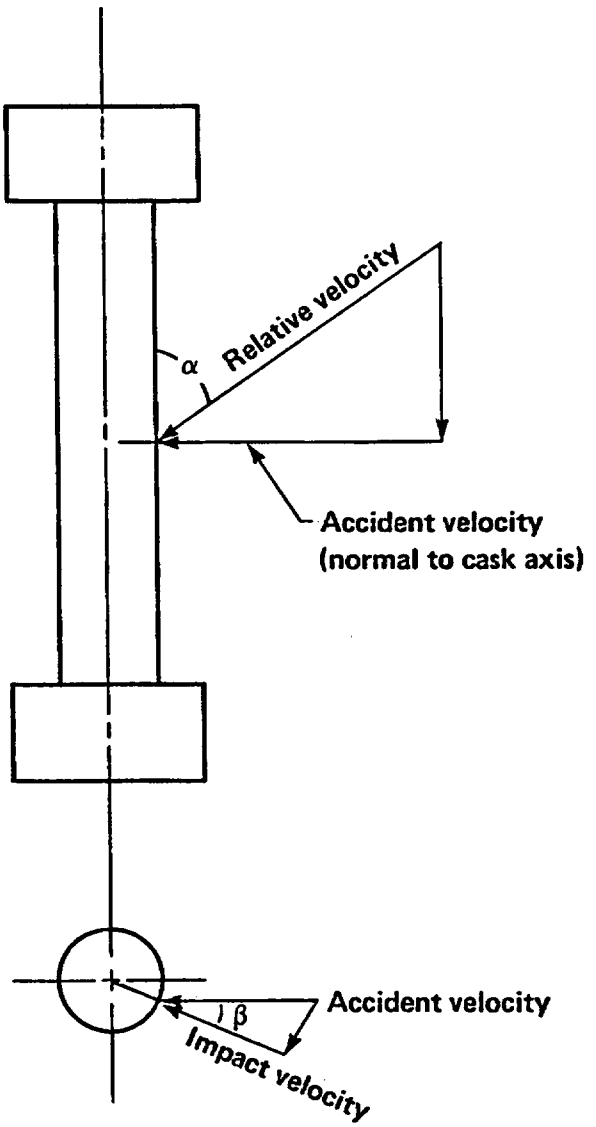

- Object hardness
- Impact velocity: Relative velocity component perpendicular to cask surface.
- Cask orientation angle, β: the angle between the accident velocity and impact velocity.

Figure 6-4 Three impact loading parameters considered in the response analysis for impacts with objects such as train sills.

automobiles. A variety of tools are used to accomplish the quasi-static evaluation, including engineering formulas, impact test data, and a computer code called NIKE 2-D, the 2-D designation indicating the two-dimensional modeling option.[2] The linear elastic method is used to perform a dynamic response analysis of the cask structure for accidents involving impacts with hard, massive objects in which cask damage cannot be ruled out by the quasi-static evaluations.

The IMPASC code is a linear elastic dynamic code within the SCANS computer program that can be operated on a personal computer.[3] IMPASC is developed specifically for analyzing dynamic impacts of shipping casks when the casks are subjected to loadings generated as a result of imposition of 10 CFR 71 accident test conditions. The code which is inexpensive to run can be used to analyze oblique impacts and to analyze non-linear behavior of an impact limiter. The deficiency is that IMPASC can model only collisions with unyielding surfaces and cannot handle real surfaces, such as soil or concrete. Also, IMPASC cannot assess lead slump.

In order to perform the dynamic response calculations, the IMPASC code is used in conjunction with two other codes called NIKE 2-D/3-D and DYNA 2-D/3-D; the 2D/3-D designation indicating that either two- or three-dimensional modeling can be performed.[2,4] The NIKE 2-D/3-D and DYNA 2-D/3-D codes are powerful finite element codes suitable for dynamic impact analysis. IMPASC is used to evaluate cask responses for impacts on an unyielding surface for various cask orientations. DYNA and NIKE are used to evaluate cask responses for endwise and sidewise impacts on unyielding and real surfaces. IMPASC is benchmarked against NIKE as discussed in Appendix E.

A cost-effective equivalent damage technique is used to estimate the response of the representative casks impacting real surfaces. The basic assumption in the equivalent damage technique involves conservation of energy; that is, the total energy of the falling cask is absorbed by deformation of the cask and the surface that it hits. In order to estimate the energy absorbed by the surface, the cask is first modeled as a rigid body and the impact surface as deformable and energy-absorbent. This model is used to

establish the force on a rigid cask generated by a real surface and the deformation of the real surface for several impact velocities. Next, calculations are made with the representative cask impacting an unyielding surface at different impact velocities. This establishes the impact forces on the cask and the corresponding cask deformations.

In order to account for the energy absorbed by an actual surface, the force determined from the first analysis, i.e., a rigid cask hitting a deformable surface, is applied to the representative cask to determine a corresponding cask deflection and an associated velocity. By summing both the cask and surface deflections and again considering the defined force level, an equivalent impact velocity on an unyielding surface can be estimated for a representative cask impacting a real surface. Figure 6-5 illustrates this analysis process for the case of a vertical end-drop of a cask without impact limiters. The process is discussed in detail, including the benchmark calculation, in Appendix E.

Three surfaces are used to represent the range of credible impact surfaces. These surfaces simulate hard rock, soft rock/hard soil, and tillable soil. Soft rock and hard soils are similar for impact and are represented as a single surface. Real surfaces exhibit complex response characteristics but can be considered to deform elastically during the early part of an impact, with a subsequent energy dissipation phase. The exact nature of the energy dissipation mechanism is not well known; therefore, for simplicity, an elastic-plastic formulation is used. The parameters used in this formulation, namely, the initial elastic modulus, the poisson ratio, and the yield stress are calibrated to approximate an equivalent energy-absorbent medium. To provide the calibration, penetration data[5] are used as discussed in Appendix E. Reasonable predictions of penetration are possible using the approximate elastic-plastic formulation. The resulting calibrated parameters are listed in Table 6.1 for each surface.

Subsection 6.2.1 describes the structural response analysis for highway accidents. The 31 accident scenarios identified in Section 2.0 are individually analyzed to determine the loading conditions that could cause

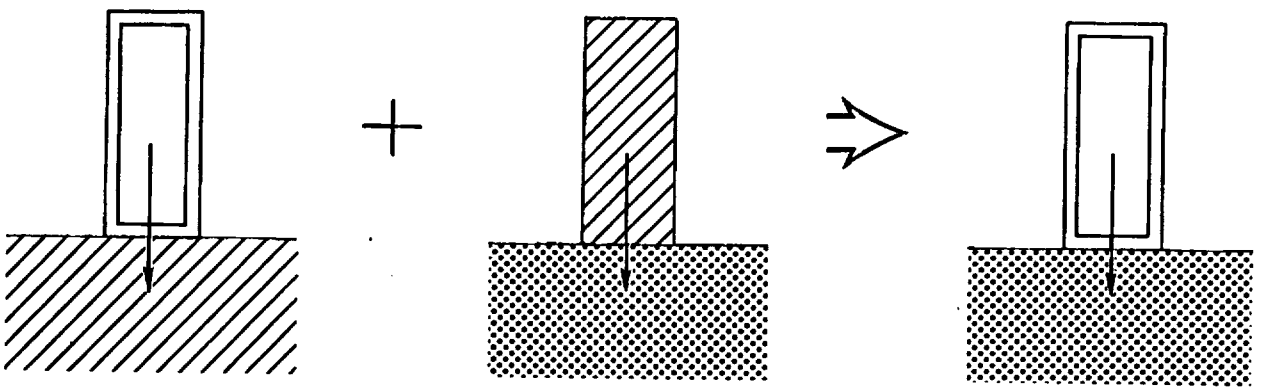

(a) Rigid cask impacts real surface

$$\left(\frac{F}{W}\right) g = \frac{V_1^2}{2d_{c1}}$$

(b) Representative cask impacts unyielding surface

$$\left(\frac{F}{W}\right) g = \frac{V_2^2}{2d_{s1}}$$

(c) Representative cask impacts real surface

$$\left(\frac{F}{W}\right) g = \frac{V_3^2}{2(d_{s1} + d_{c1})}$$

Figure 6-5 Equivalent damage technique.

Table 6.1
Material Parameters Selected for Real Surfaces

Surface type	Young's Modulus (psi)	Poisson Ratio	Yield Stress (psi)
Hard Rock	7,000,000	0.28	25,000
Soft Rock/Hard Soil	3,640,000	0.2	4,000
Tillable Soil	6,000	0.4	1,000

cask responses of 0.2% strain (S_1) or less. Subsection 6.2.2 describes a similar response analysis performed for 24 railway accident scenarios. Subsection 6.2.3 discusses the structural response results.

6.2.1 Cask Response Analysis for Highway Accidents

The representative truck cask described in Section 3.5 is used to perform the highway accident response analysis. Appendix E discusses the computer models of the cask and the detailed structural calculations used in the analysis. The structural evaluations use the highway accident scenarios presented in Figs. 2-3 and 2-4. The results of the response evaluations are described in Subsection 6.2.1.1 for accidents involving minor forces and in Subsection 6.2.1.2 for accidents in which the forces are potentially significant.

6.2.1.1 Response to Minor Accidents

Accident scenarios which result in minor forces are determined with an evaluation of cask performance under static loads. A static crushing force of 1.6 million pounds is applied to the cask side. The resulting strain calculated at the inner shell is less than 0.2% (S_1). When crushing the cask from the end, 3.2 million pounds of force generates a strain of less than 0.2% (S_1). Assuming that the sidewise impact force is linearly applied, the force/unit length that could cause local deformation can be estimated. The representative cask can resist a linear force of 100,000 pounds/foot, generating a strain of less than 0.2% (S_1). The linear force required to crush objects in many accidents is much less than 100,000 pounds/foot, and thus these accidents are screened out (placed in the R(1,1) response region).

The maximum force that an object generates during a high velocity impact can be estimated using quasi-static methods. By substituting equivalent static forces for inertial forces due to deceleration, calculations indicate that objects such as automobiles or truck trailers cannot generate forces greater than 100,000 pounds/foot-of-contact, even at high impact velocities. The automobile, as this calculation indicates, is a relatively soft object

when compared with the massive steel cask and is severely damaged. The energy generated by the high-velocity impact of the automobile is almost totally absorbed in the destruction of the automobile, and no impact force greater than 10,000 pounds/foot is applied to the shipping cask. Also, for such a relatively light object (<5,000 pounds), the massive cask (50,000 pounds) will accelerate the object, hence reducing the impact forces to values significantly less than the 10,000 pounds/foot.

Many other low-resistance objects, such as trees, road signs, utility poles, motorcycles, trailers, and trucks, are also in this relatively soft object category. All these objects pose no threat to the cask and require no further analysis. Table 6.2 identifies all objects that can generate a maximum quasi-static force less than 100,000 pounds/foot at any velocity. The percentage of accidents involving these objects is 94.7%.

The remaining highway accidents involve stronger and more massive objects, such as trains, bridge columns, abutments, and certain real surfaces such as roadbeds. The analysis of these accidents is described in the next subsection.

6.2.1.2. Response to Other Accidents

Truck accident scenarios involving impacts with trains, running off bridges or over embankments, and running into slopes or massive concrete structures require dynamic structural analysis. The cask dynamic response is analyzed for impacts with the principal objects involved in these accidents.

Figure 6-3 shows the variables considered in the dynamic response analysis: cask orientation, object hardness, and impact velocity. The IMPASC code is used only for unyielding targets. Different methods of analysis are used for soft objects, depending on their hardness. Hard objects are considered unyielding surfaces. The impact analysis application for these objects is presented in Subsection 6.2.1.2.1. Cask responses for relatively soft objects are discussed in Subsection 6.2.1.2.2

Table 6.2
Evaluation of Quasi-Static Force for Minor Highway Accidents[a/]

	Accident Scenario	Frequency	Total Force (lb)	Linear Force (lb/ft)
1.	Soft objects (cones, animals, etc.)	0.034	<1,000	< 1,000
2.	Motorcycle	0.008	<20,000	<10,000
3.	Automobile	0.432	<50,000	<10,000
4.	Truck, bus	0.133	<400,000	<70,000
5.	Train	0.008		[b/]
6.	Other (rocks, furniture, etc.)	0.038	<50,000	<10,000
7-11	Bridge railing	0.005		[b/]
12-14	Columns, abutments	<0.001		[b/]
15.	Bridge bottom structure	<0.001	<100,000	<30,000
16.	Wall barrier, post	0.040	<50,000	<50,000
17.	Signs, cushions	0.005	<10,000	<10,000
18.	Curb, culvert	0.037	<10,000	<10,000
19-21	Into slope	0.025		[b/]
22-24	Over embankment	0.014		[b/]
25.	Over embankment (draining ditch)	0.009		[c/]
26.	Trees	0.009	<100,000	<70,000
27.	Other (fences, bushes, etc.)	0.033	<50,000	<10,000
28.	Overturn	0.083		[c/]
29.	Jackknife	0.055		[c/]
30.	Other (cargo shift, etc.)	0.020	<1,000	<1000
31.	Fire only	0.010		No load
		1.000		

[a/] Accident scenarios are screened out as minor except those designated for dynamic analysis.

[b/] Linear force may exceed 100,000 lb/ft. Dynamic analysis is required.

[c/] Fall impact distance is <15 ft.; therefore the linear force is <100,000 lb/ft.

6.2.1.2.1 Response for Impacts with Unyielding Surfaces

This subsection assesses cask response during impact with objects such as hard rock, which have a hardness close to the unyielding surface specified in regulations. The analysis considers variations in two parameters: cask orientation angle and impact velocity. IMPASC is used to calculate the cask response for cask orientation angles, β, of 0^{o}, 10^{o}, 30^{o}, 50^{o}, 70^{o}, and 90^{o} and impact velocities of 30 mph, 38 mph and 45 mph. The 0^{o} cask orientation angle represents an impact to the side of the cask, whereas the 90^{o} cask orientation angle is an impact to the end of the cask.

For the 90^{o} angle case, the effects of truck cab crushing and lead slump pressures are considered. The sensitivity study results are given in Fig. 6-6. The results indicate that, for the representative truck cask, a line connecting the endwise and sidewise strain responses conservatively bounds the strain responses for all other cask impact orientations. Therefore, for cask orientations from $0\text{-}90^{o}$, the structural strain responses can be linearly interpolated between the sidewise and endwise strain responses. The strain in the inner cask shell can reach 0.2% (S_1) at an impact velocity of 32 mph for sidewise impacts and an impact velocity of 38 mph for endwise impacts.

6.2.1.2.2 Response for Real Objects

The equivalent damage technique estimates the representative truck cask response for endwise impacts on real surfaces. A rigid body with the outer dimensions and weight of the truck cask is dropped onto various surfaces from heights up to 480 feet and with equivalent velocities up to 120 mph. Figure 6-7 plots the interface forces for endwise impacts of the rigid body on tillable soil, soft rock/hard soil, and hard rock.

The impact force exceeds 1000 g for hard rock and 200 g for soft rock/hard soil. By comparison, an impact force of 40 g is presumed to cause a 0.2% strain (S_1) at the inner shell of the representative truck cask. For impact forces up to 40 g, the kinetic energy of the representative cask will be almost entirely absorbed by the cask's impact limiter. Above this force level, cask deformation will begin. Because 40 g << 200 g, soft and hard rock

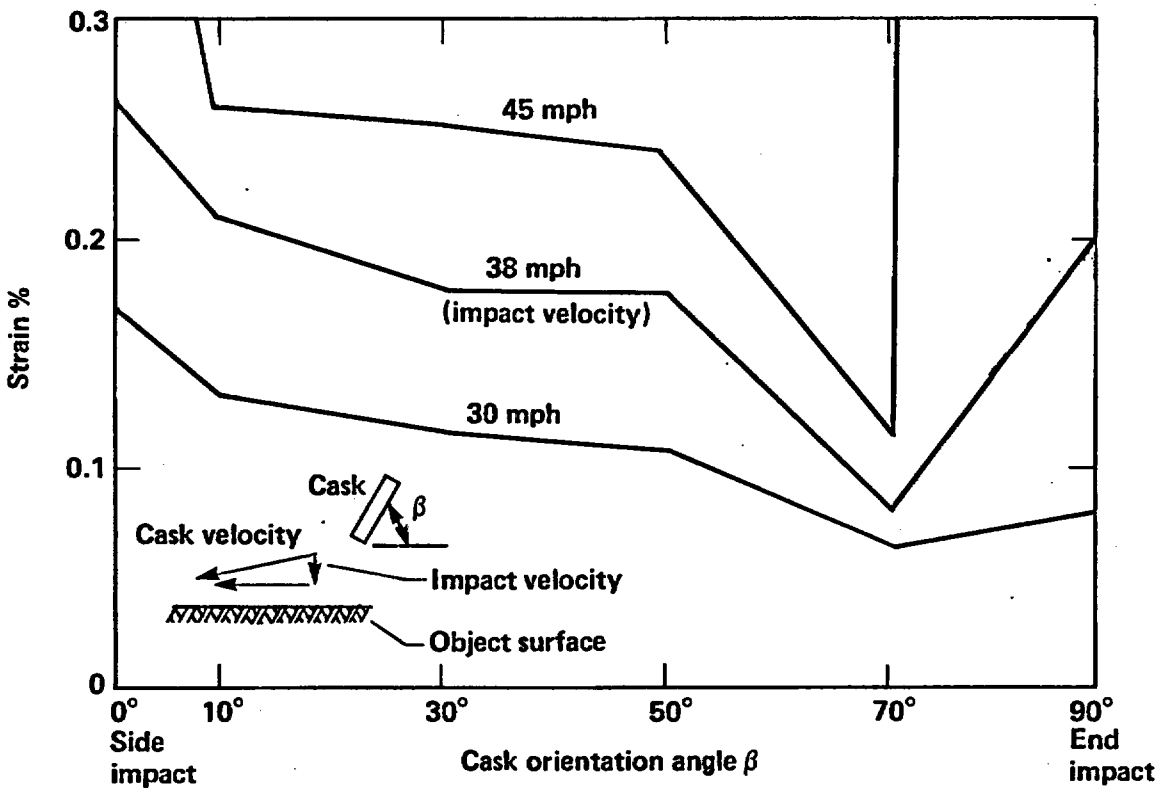

Figure 6-6 Strain versus impact velocity and cask orientation for the representative truck cask impacting an unyielding surface.

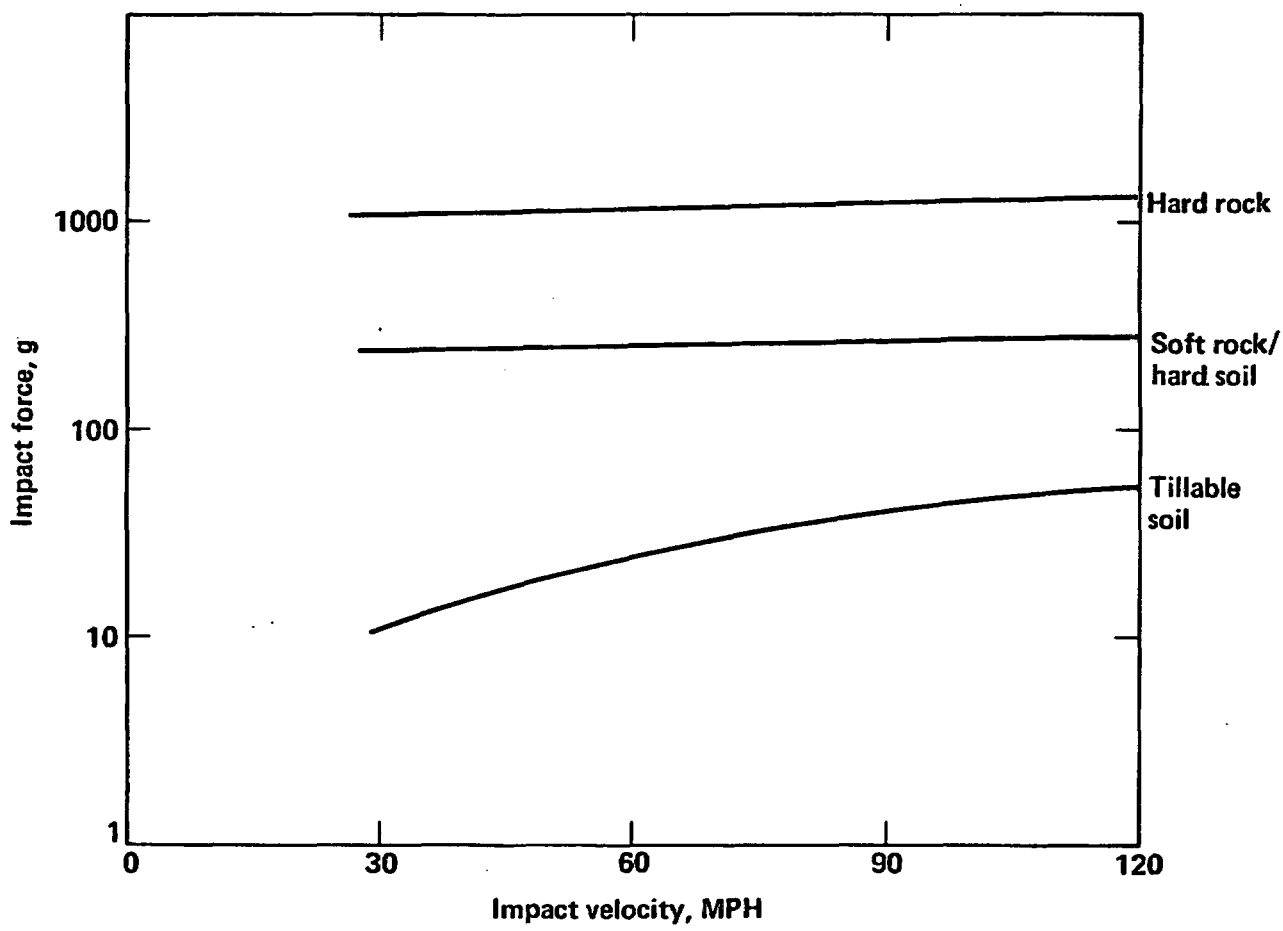

Figure 6-7 Impact force for a rigid truck cask dropped endwise onto real surfaces.

are treated as an unyielding surface. For impacts on tillable soils, the results shown in Fig. 6-7 indicate that significant energy can be absorbed by the soil at an impact force of 40 g. In this case, the representative cask can impact soil surfaces endwise at velocities up to 84 mph without exceeding the 0.2% strain (S_1) level.

A similar equivalent damage evaluation is performed for sidewise drops onto various surfaces. To evaluate grade-crossing accidents, sidewise impacts by train sills are also analyzed to determine conditions which could cause 0.2% strain (S_1) at the inner shell. Table 6.3 summarizes the impact velocities needed to attain the 0.2% strain (S_1) level for sidewise and endwise impacts on various surfaces, including water.

At the 0.2% strain (S_1) level and below, representative truck cask responses to impacts on hard or soft rocks are essentially equivalent to impacts on an unyielding surface for all orientation angles. Endwise and sidewise impact velocities of 38 mph and 32 mph respectively produce 0.2% strain (S_1) levels. For endwise impacts on soil, significant energy is absorbed by the soil, which allows the maximum impact velocity to increase to 84 mph.

For cask impacts on water at a 45^0 orientation, an impact velocity of 150 mph will not cause the strain to exceed the 0.2% (S_1) level. One-hundred-fifty mph is defined as the maximum credible impact velocity that can be attained based on review of the historical data base. This velocity corresponds to a drop height of 750 feet.

Head-on impact by locomotive sills at velocities greater than 9 mph can cause the 0.2% strain (S_1) level to be exceeded. The train sill goes between the impact limiters and strikes the side of the cask.

6.2.2 Cask Response Analysis for Railway Accidents

The representative rail cask described in Section 3.5 is used to perform the railway accident response analysis. The computer model of the cask and the detailed structural calculations used in the response analysis are discussed in Appendix E. The railway accident scenarios in Fig. 2-5 are used

Table 6.3
Impact Velocities Required to Reach the 0.2% Strain (S_1) Level
for Objects Impacted in Highway Accidents

Object Impacted	Impact Velocity at 0.2% Strain (mph)		
	Cask Orientation Angle (°)		
	0	45	90
Hard Rock	32	35[a/]	38
Soft Rock	32	35[a/]	38
Tillable Soil	32	58[a/]	84
Water	42	150	38
Train Sill	9	14	150

a/ Impact velocities at these orientation angles are linearly interpolated between the two bounding values.

as the basis for the structural evaluations. The results of the response evaluations are provided in Subsection 6.2.2.1 for minor accidents and in Subsection 6.2.2.2 for accidents in which the damage to a cask could be significant.

6.2.2.1 Response to Minor Accidents

Train accidents are primarily derailments or collisions with other trains. Collisions not involving derailment are usually minor. In non-derailment cases, the only events that must be considered are those in which the coupler of one rail car can override the impacted car and cause damage to a rail car or cask. Rail cars specially designed for casks place the cask in the center of the car. In general, collisions not involving derailment do not generate enough force for the coupler of an adjacent car to penetrate a rail cask because the coupler is too short, as shown in Fig. 6-8. In those cases where the force is great enough for the coupler to strike the cask, it is assumed that the cars derail and the coupler strikes the side of the cask. Impacts with small structures such as poles and retaining walls or impacts with the superstructure of locomotives or other cars cannot significantly damage a cask.

A rail cask is larger than a truck cask and requires greater forces to damage it. A 1.6-million-pound static crush (100,000 pounds/foot) is required on the side of the representative rail cask to cause a 0.2% strain (S_1) at the inner shell; whereas a 13.0-million-pound static force is required on the end of the cask to cause a similar level of strain. Based on the first-stage screening of the truck cask, dynamic impact analysis of the rail cask has to be considered only for derailment-caused impacts with massive objects or surfaces adjacent to railroad right-of-ways. Derailments that result in rollovers onto the adjacent railbed involve falls that are less than 15 feet and impact velocities less than 22 mph. These impact velocities can partially crush the rail cask impact limiters but cannot cause any significant damage to the cask.

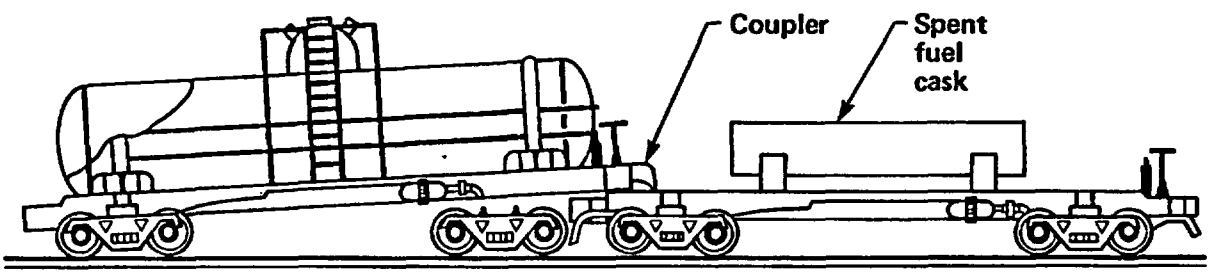

Figure 6-8 Rail car coupler override of spent fuel cask car.

Table 6.4 summarizes the 24 railway accident scenarios with their frequencies of occurrence. Those accident scenarios that can cause only minor cask damage are identified. The total fraction of minor accidents is calculated by summing the individual frequencies. The percentage of accidents screened out as minor is 96.1%. The remaining accidents involve derailments and impacts with massive objects such as train couplers, bridge columns, and abutments, and with surfaces such as rock. Subsection 6.2.2.2 discusses the analyses performed on the representative rail cask for these accidents.

6.2.2.2 Response to Other Accidents

Railway accident scenarios involving derailments and falls off bridges or run-offs over embankments or into slopes or massive concrete structures require dynamic analysis. These accidents may involve impacts with a variety of surfaces: hard rock, soft rock/hard soil, and tillable soil. The dynamic response of the cask for impacts with each of these objects is analyzed.

Three parameters are considered significant in the dynamic response analysis as shown in Figs. 6-3 and 6-4: cask orientation, object hardness, and impact velocity. Again, different methods of analysis are used to analyze objects of different hardness. Hard objects are considered unyielding surfaces and the impact analysis applicable for these objects is presented in Subsection 6.2.2.2.1 below. Cask responses for relatively soft objects are discussed in Subsection 6.2.2.2.2.

6.2.2.2.1 Response for Impacts with Unyielding Surfaces

This subsection assesses cask response during impact with objects such as rock that has a hardness close to the unyielding surface specified in regulations. The analysis considered variations in two parameters: cask orientation angle and impact velocity. IMPASC is used to calculate the cask response for cask orientation angles, β, of 0^{o}, 10^{o}, 30^{o}, 50^{o}, 70^{o}, and 90^{o} and impact velocities of 30 mph, 45 mph, and 60 mph. The 0^{o} cask orientation angle represents an impact to the side of the cask, whereas the 90^{o} cask orientation angle is an impact to the end of the cask.

Table 6.4
Evaluation Summary of Minor Railway Accidents[a/]

	Accident Scenario	Frequency	Total Force (lb)	Linear Force (lb/ft)
1.	Grade crossing	0.030	<400,000	<70,000
2.	Non-derailment	0.086	<500,000	<62,500
3-7	Over bridge	0.008		b/
8.	Over embankment - ditch	0.003		c/
9-11	Over embankment - other	0.006		b/
12-14	Into slope	0.016		b/
15-17	Columns, abutments	<0.001		b/
18.	Other structures	0.164	<500,000	<62,500
19.	Locomotive superstructure	0.033	<500,000	<62,500
20.	Rail car superstructure	0.100	<500,000	<62,500
21.	Coupler/sill	0.008		b/
22.	Roadbed	0.160		c/
23.	Earth	0.320		c/
24.	Other, fire cargo shift	0.065	<10,000	<10,000
	Total	1.000		

a/ Accident scenarios are screened out as minor except those designated as significant for dynamic analysis.

b/ Linear force may exceed 100,000 lb/ft. Dynamic Analysis is required.

c/ Fall impact distance is <15 ft; therefore the linear force is <100,000 lb/ft.

The sensitivity study results are given in Fig. 6-9. For the 90^{o} angle case, the effects of lead slump pressure and the crushing of the front end of the rail car are included. The results indicate that, for the representative rail cask, a line connecting the endwise and sidewise strain responses conservatively bounds the strain responses for all other cask orientations. Therefore, for cask orientations from $0\text{-}90^{o}$, the structural strain responses can be linearly interpolated between the sidewise and endwise strain responses. The strain in the inner cask shell can reach 0.2% (S_1) at an impact velocity of 55 mph for sidewise impacts and an impact velocity of 38 mph for endwise impacts.

6.2.2.2.2 Response for Real Objects

The equivalent damage technique estimates the representative rail cask response for endwise impacts on real surfaces. A rigid body with the outer dimensions and weight of the rail cask is dropped onto various surfaces from heights up to 480 feet and with equivalent velocities up to 120 mph. Figure 6-10 plots the interface forces for endwise impacts on tillable soil and soft rock/hard soil. Calculations are not performed for impacts on hard rock. It is apparent from the soft rock/hard soil cask results that a hard rock surface is essentially an unyielding surface with respect to the representative rail cask.

The impact force exceeds 400 g for soft rock/hard soil. The impact forces required for significant energy absorption by tillable soil exceed 40 g at velocities above 40 mph. Since the cask is designed to withstand an impact force of 40 g, it is presumed that such a force causes less than a 0.2% strain (S_1) at the inner shell of the representative rail cask. For impact forces up to 40 g on hard or soft rock surfaces, the kinetic energy of the representative cask will be almost entirely absorbed by the cask's impact limiter. For soil impacts, the kinetic energy will be absorbed by both the soil and the cask impact limiter.

A similar equivalent damage evaluation is performed for sidewise drops onto various surfaces. Table 6.5 summarizes the impact velocities needed to

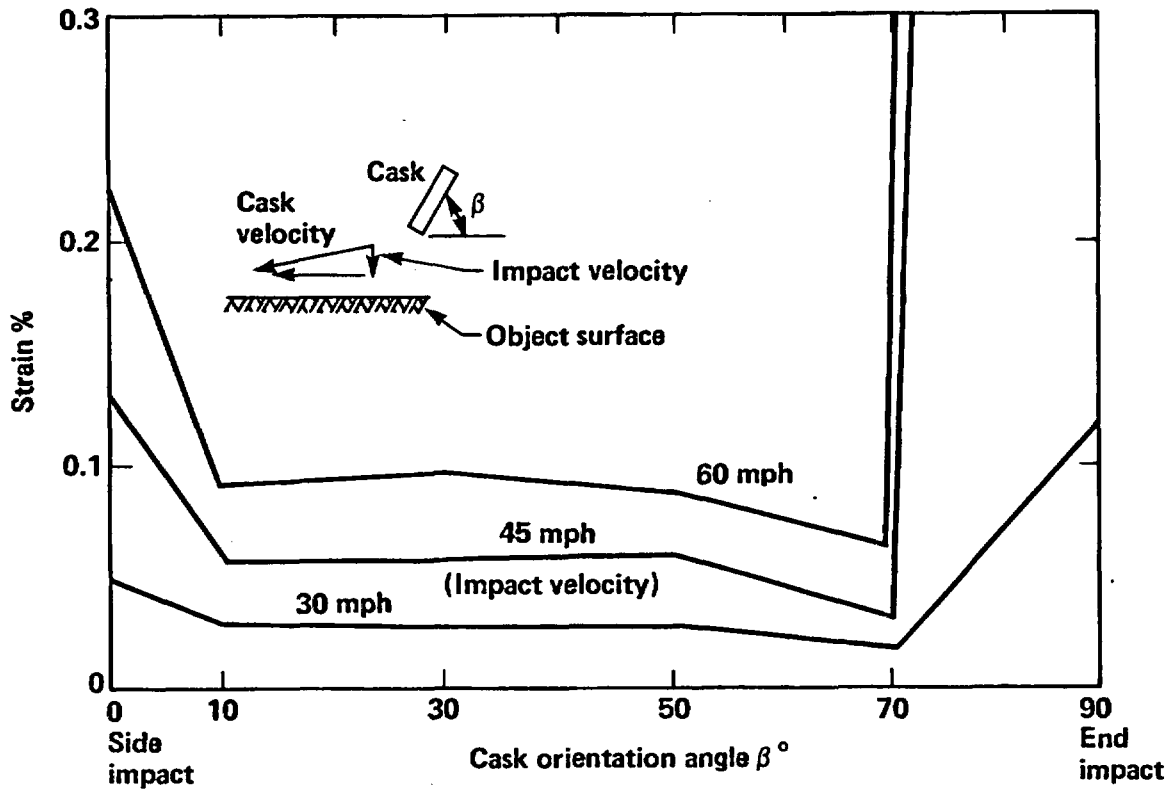

Figure 6-9 Strain versus impact velocity and cask orientation for the representative rail cask impacting an unyielding surface.

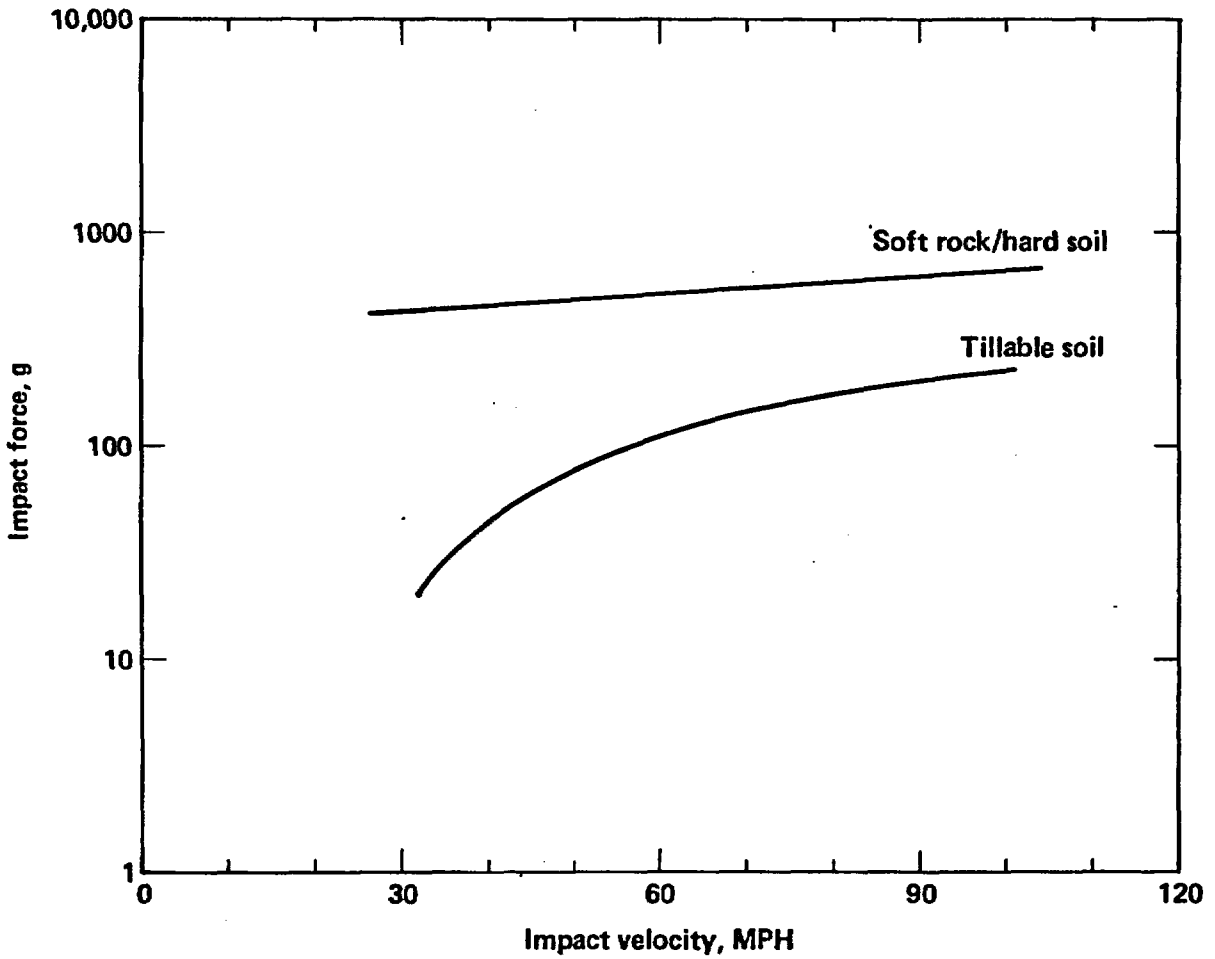

Figure 6-10 Impact force versus impact velocity for a rigid rail cask dropped endwise onto real surfaces.

Table 6.5
Impact Velocities Required to Reach the 0.2% Strain (S_1) Level for Objects Impacted in Railway Accidents

Object Impacted	Impact Velocity at 0.2% Strain (mph)		
	Cask Orientation Angle (°)		
	0	45	90
Hard Rock	55	47	38
Soft Rock	55	47	38
Tillable Soil	55	47	40
Water	55	150	38
Train Sill	11	16	150

a/ Impact velocities at these orientation angles are linearly interpolated between the two bounding values.

attain the 0.2% strain (S_1) level for sidewise and endwise impacts on various surfaces, including water.

At the 0.2% strain (S_1) level and below, the representative rail cask responses to impacts on hard rock, soft rock, or soil are essentially equivalent to impacts on an unyielding surface for all orientation angles. For cask impacts on water at a 45^0 orientation, an impact velocity of 150 mph can be reached without exceeding the 0.2% strain (S_1) level.

Head-on impacts by locomotive sills at velocities greater than 11 mph could cause the 0.2% strain (S_1) level to be exceeded. The train sill goes between the impact limiters and strikes the side of the cask.

6.2.3 Discussion of Structural Analysis Results

This section has thus far addressed highway and railway accidents that can generate structural cask responses less than the 0.2% strain (S_1) level. Cask structural responses within the 0.2% strain (S_1) level are in the elastic range and would not lead to any significant radiological releases. Cask response within these constraints will meet requirements imposed by existing regulations.

For those accidents requiring a dynamic structural calculation, the dynamic structural response of the cask is calculated using primarily elastic analysis methods. Dynamic elastic response methods are routinely used to analyze structures, and the results can be used with confidence.

Current and future cask designs are expected to be stronger than the selected representative cask designs and would be able to withstand higher mechanical loads before the 0.2% strain (S_1) level is reached. If a higher mechanical loading is required to cause the cask containment shell to reach the elastic limit, then a higher fraction of accidents will be screened out or shown to result in radiological hazards less than those in current regulations.

In July 1984, in Old Dalby, England, the United Kingdom Central Electricity Generating Board performed a train crash test with a steel spent

fuel cask.[6] The 100-mph train crash subjected the cask to a force greater than 8 million pounds but caused only minor deformation to the outside of the cask. The primary response of the cask structure was elastic. In fact, the force the train applied to the steel cask was less than 40% of the International Atomic Energy Agency test condition loads,[7] which are similar to the test conditions specified in 10 CFR 71. Therefore, the actual percentage of highway and railway accidents that are within the envelope of current accident test conditions and radiation hazard limits specified in regulations, are likely to be higher than the percentages indicated in Section 6.4.

6.3 Thermal Response Analysis

Thermal loads due to large fires dominate the thermal evaluation. Other thermal loads due to torch fires or cask burial in debris that result from self-heating are insignificant and are eliminated in the thermal screening analysis. Each type of accident is evaluated for its potential for causing damage to a spent fuel cask, such as melting of the lead shield or damage to the cask seal. Even accidents involving only impact of a spent fuel transport truck with small objects or the adjacent roadbed can result in a fire that could burn up to an hour because of the diesel fuel being carried by the truck. Other accidents involving impacts with tanker trucks, locomotives, and tank cars, each of which carry considerable amounts of fuel, can cause fires that could last for a few hours.

The intent of this section is to determine the fraction of accidents that will not cause a temperature exceeding 500°F (T_1) at the middle of the lead shield thickness of the representative casks. Heating the cask structure to 500°F (T_1) does not result in any significant deterioration of the cask components. This statement applies to cask seals, which are the component whose failure could signify the earliest onset of a potential radioactive release.

A finite element computer code called TACO 2-D is used to perform the thermal analysis of the cask.[8] Sensitivity studies indicate that a one-dimensional (1-D) heat transfer model can be used, which simplifies the

analysis, reduces computing time, and provides suitably conservative results. In all of the analyses, the representative casks neutron shield tank water is lost prior to the fire. The thin outer shell of the remaining neutron shield tank provides a thermal barrier to the fire. Loss of the shield water reduces heat transfer into the cask; it also removes a significant heat absorber, water.

Currently licensed cask designs are reviewed to relate the temperatures at the mid-plane of the cask to the temperatures at other locations, particularly the closure seals. Valve boxes located where they can be exposed to heat loads and temperatures approaching those in the middle portion of the cask are also considered. These sensitivity studies confirm the selection of the lead shield temperature as the most appropriate and conservative measure of cask thermal response.

Fire accidents have three loading parameters that can affect the response of a spent fuel cask: fire duration, flame temperature, and fire location. These loading parameters vary widely when considering all fire accidents. Longer fire durations and higher flame temperatures increase the thermal loads to the cask and affect temperature responses. The proximity of the cask to a fire is also important. The closer a cask is to a fire, the higher the thermal load; the worst case is a cask being engulfed by a fire.

In order to reduce the large amount of analysis otherwise required to cover a wide range of fire accidents, a simplified calculational method is developed. The method includes the following steps:

1. A reference fire condition is established to perform the thermal response analysis for the representative truck and rail casks. The first step in accomplishing this task is to relate the thermal condition specified in 10 CFR 71 to real fire conditions. As shown in Fig. 6-11, a cask is completely surrounded by fire in the accident test conditions used to guide design; whereas the cask would most likely be only partially surrounded by a fire in a real situation because of the shielding effects of the ground, transport vehicle, or other cask-supporting surfaces. For

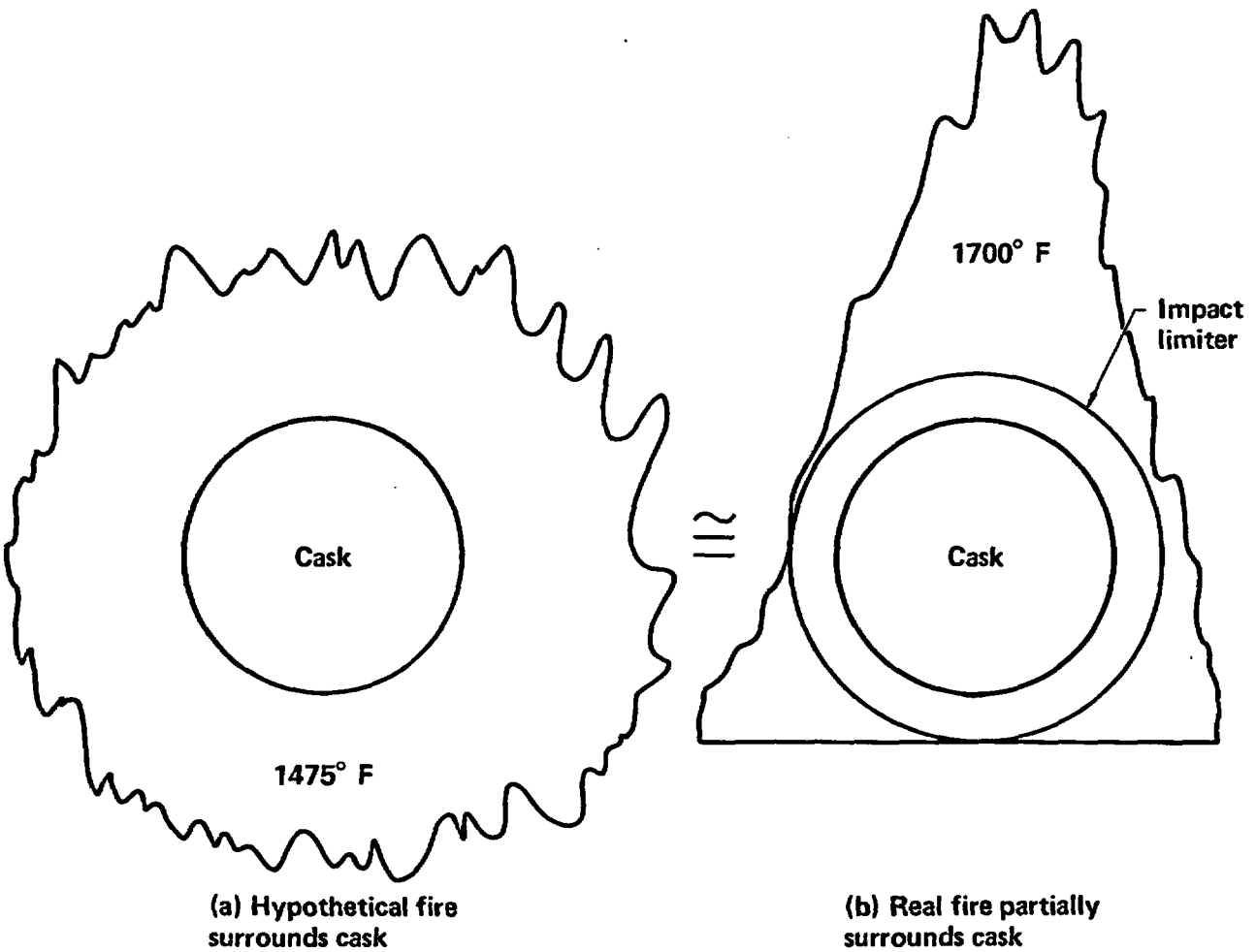

Figure 6-11 Comparison of an engulfing hypothetical fire and a real fire.

the same flame temperature, the average heat flux into the cask in a real engulfing fire is 0.78 of the heat flux on the cask in the hypothetical engulfing fire. A flame temperature of 1700°F is required for a real engulfing fire, including ground or transport vehicle shielding effects, to provide the same average heat flux and temperature response as the 1475°F hypothetical engulfing fire. The 1700°F real engulfing fire is the reference fire condition.

2. The heat fluxes and temperature responses of the truck and rail casks are calculated as a function of fire duration. These evaluations are performed using a 1-D model and the thermal parameters for the accident test conditions.

3. Based on sensitivity studies in Appendix F, the time to reach a specific temperature is approximately proportional to the incident heat flux on the cask caused by the fire. A fire that causes a heat flux twice that of the reference fire can heat a cask to a specified temperature in one-half the time. Conversely, a fire that causes a heat flux one-half the amount takes twice as long to heat the cask to a specified temperature. Using this correlation and the results from step 2, the fire durations required to reach the 500°F temperature (T_1) level are calculated for a range of heat fluxes that cover a wide range of real fire conditions.

4. The variation of heat loads on the representative casks is determined as a function of the flame temperature and location. The heat load variations are normalized to the engulfing real fire condition and defined as flux factors for flame temperature and load factors for fire location.

5. Using the fire duration results from step 3 and the heat flux factors from step 4, the fire duration required to reach the 500°F temperature (T_1) level is derived for a wide range of flame temperatures and locations.

The thermal response analysis of highway fire accidents is performed based on the above calculational method. The analysis appears in Subsection 6.3.1. The 31 highway accident scenarios are analyzed to determine the thermal loading conditions that can cause a temperature response of 500°F (T_1) or less at the mid-thickness of the lead shield of the representative truck cask. Subsection 6.3.2 describes a similar response analysis performed for 24 railway fire accident scenarios that could involve the representative rail cask. The thermal response results are discussed in Subsection 6.3.3.

6.3.1 Cask Response Analysis for Highway Fire Accidents

The representative truck cask described in Section 3.5 is used to perform the highway accident response analysis. Appendix F discusses the cask model and the detailed thermal calculations used in the response analysis.

The temperature response of the representative truck cask is calculated for a hypothetical engulfing fire with a 1475°F flame temperature. A flame emissivity of 0.9 is assumed. The temperature at the middle of the lead shield thickness is plotted in Fig. 6-12 as a function of fire duration. The lead mid-thickness temperature reaches 500°F (T_1) in 1.08 hours which is twice the regulatory fire duration. The total heat absorbed by the cask in reaching the 500°F temperature (T_1) is 5,000 Btu/ft^2 which results in an average thermal flux of approximately 4,630 Btu/hr-ft^2 compared with the initial rate of 17,000 Btu/hr-ft^2. The average thermal flux is lower because the thermal barrier formed by the water jacket rapidly reduces the heat flow into the cask during the first 10 minutes as shown in Fig. 6-13. These heat fluxes are equivalent to those on a cask in a real engulfing fire with a flame temperature of 1700°F.

For engulfing fires, the heat flux from the fire onto the surface of the truck cask depends on radiation heat transfer caused by the flame temperature. The average heat flux on the representative truck cask is calculated as a function of flame temperature for a hypothetical engulfing fire. The heat flux is then reduced by a factor of 0.78 to adjust the results

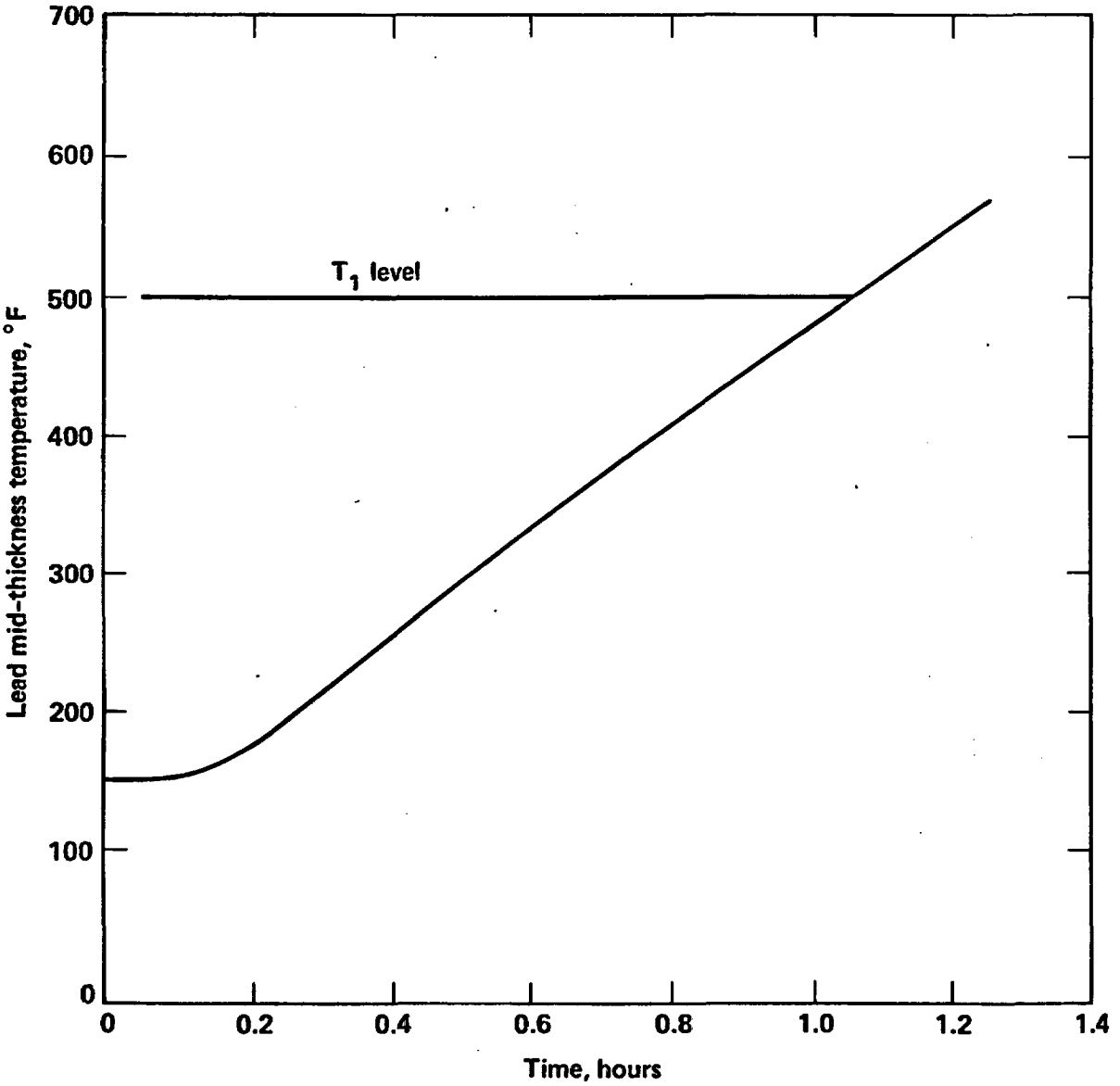

Figure 6-12 Representative truck cask temperature response to a hypothetical 1475°F (equivalent to a real 1700°F) fire versus fire duration.

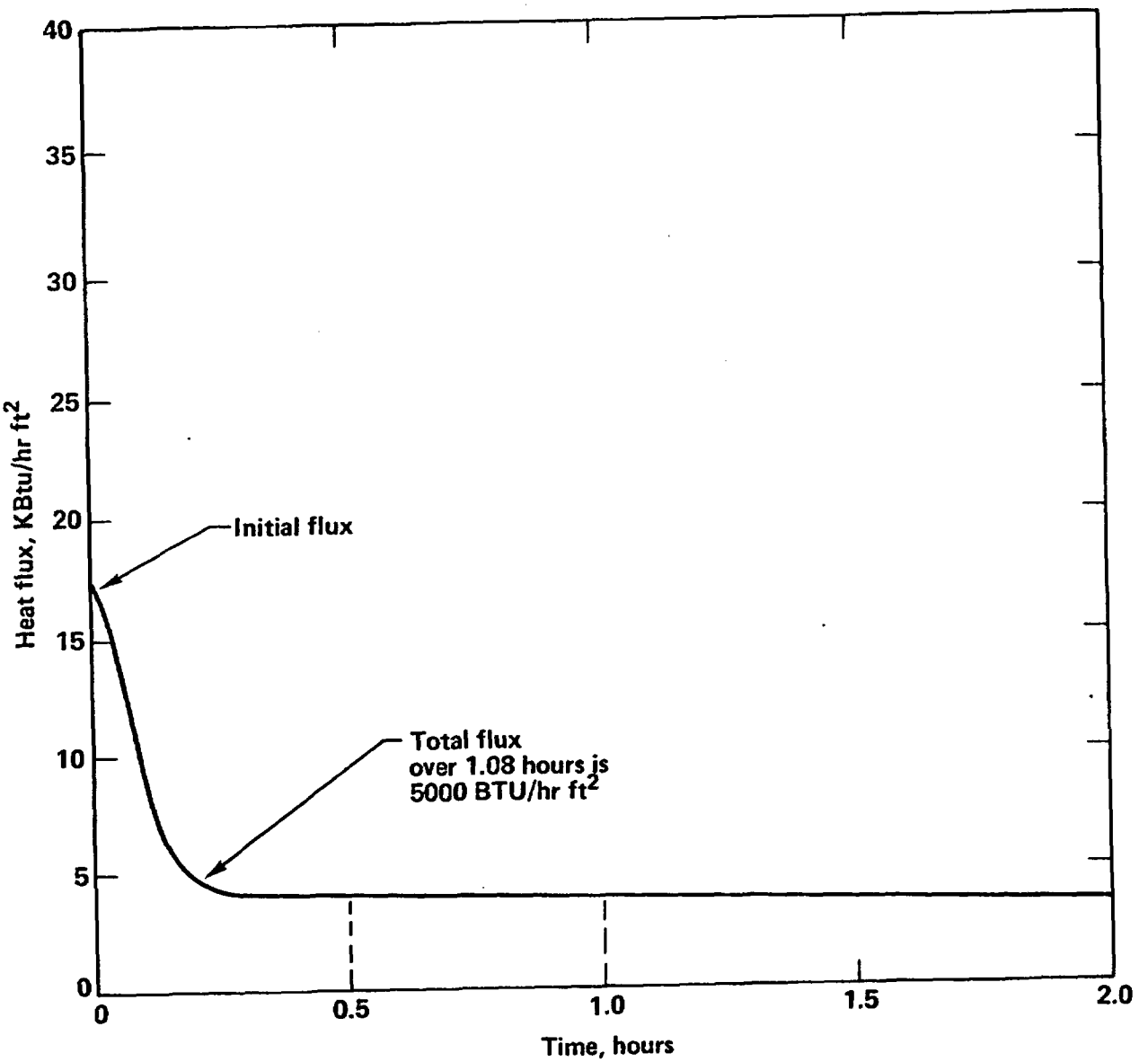

Figure 6-13 Heat flux versus fire duration for the representative truck cask exposed to the regulatory 1475°F fire.

for real fire conditions. This normalized heat flux factor is plotted in Fig. 6-14 as a function of flame temperature. For a 1700°F real fire, the average thermal flux on the representative cask is 4,630 Btu/hr-ft^2 and the heat flux factor is 1.0. As the flame temperature increases, the thermal flux increases, and the fire duration required to reach the 500°F temperature (T_1) level decreases.

The heat load to the truck cask also depends on the location of the fire with respect to the cask. In terms of location, an engulfing fire provides the maximum heat load to the cask. The heat load decreases rapidly as the distance between the fire and the cask increases. Figure 6-15 shows the effect of distance between cask and fire for the truck cask where the heat load factor is normalized with respect to a real engulfing fire.

The heat flux and load factors are used to calculate the change required in the 1.08 hour reference fire to reach the 500°F temperature (T_1) level for a variety of flame temperatures and durations. The fire durations for the wide range of fire conditions are calculated using the probabilistic code described in Section 5.0.

6.3.2 Cask Response Analysis for Railway Fire Accidents

The representative rail cask in Section 3.5 is used to perform the railway fire accident response analysis. The computer analysis of the cask and the detailed thermal calculations are provided in Appendix F.

The temperature response of the representative rail cask is calculated for a hypothetical engulfing fire with a flame temperature of 1475°F and flame emissivity of 0.9. The temperature at the middle of the lead shield thickness is plotted in Fig. 6-16. The lead mid-thickness temperature reaches 500°F (T_1) in 1.35 hours which is more than twice the regulatory fire duration. The total heat absorbed by the cask in reaching the 500°F (T_1) level is approximately 6,000 Btu/ft^2 which results in an average heat flux of approximately 4,445 Btu/hr-ft^2. These heat fluxes are equivalent to those on a cask in a real engulfing fire with a flame temperature of 1700°F.

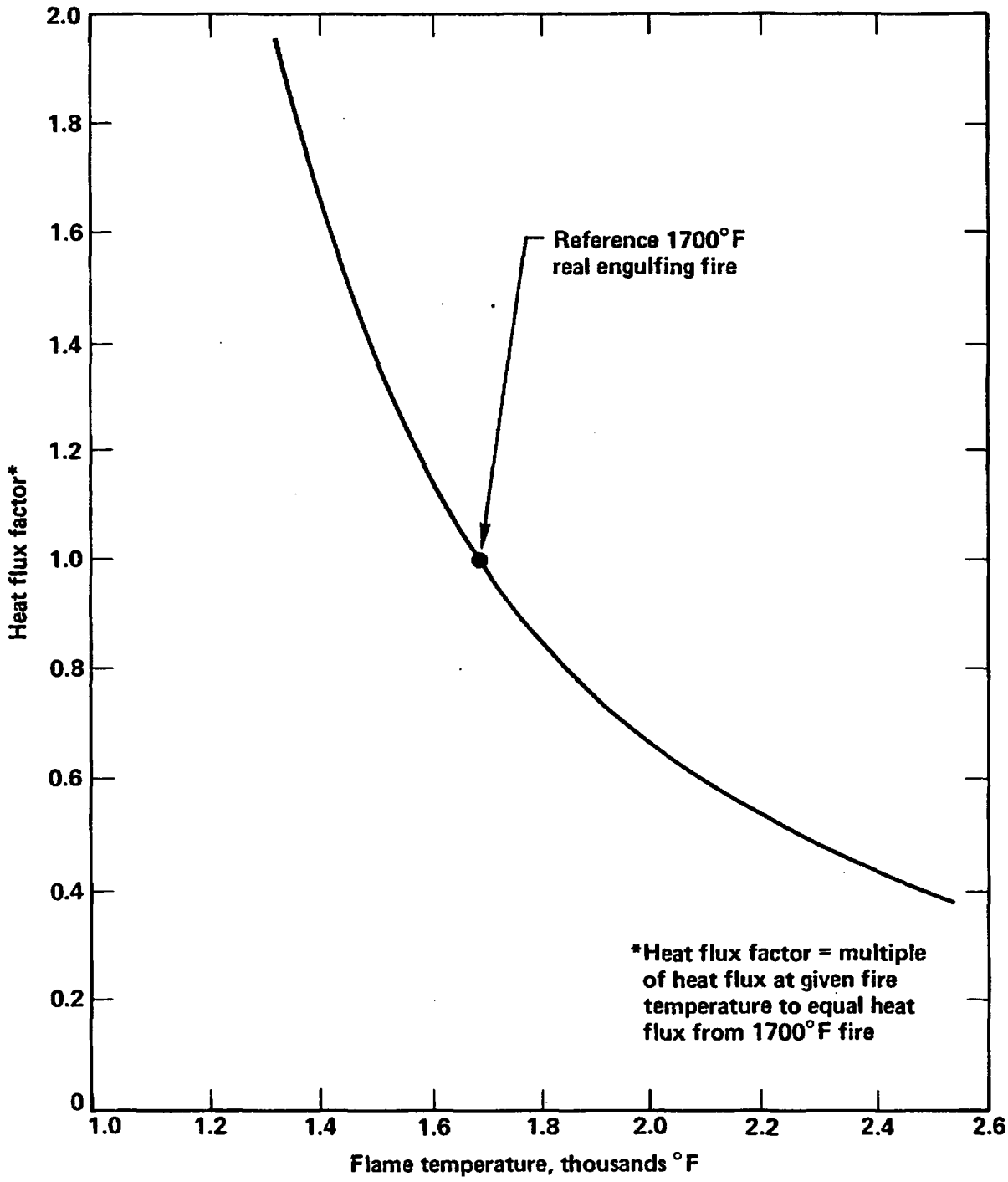

Figure 6-14 Average heat flux factor versus temperature for the representative truck cask.

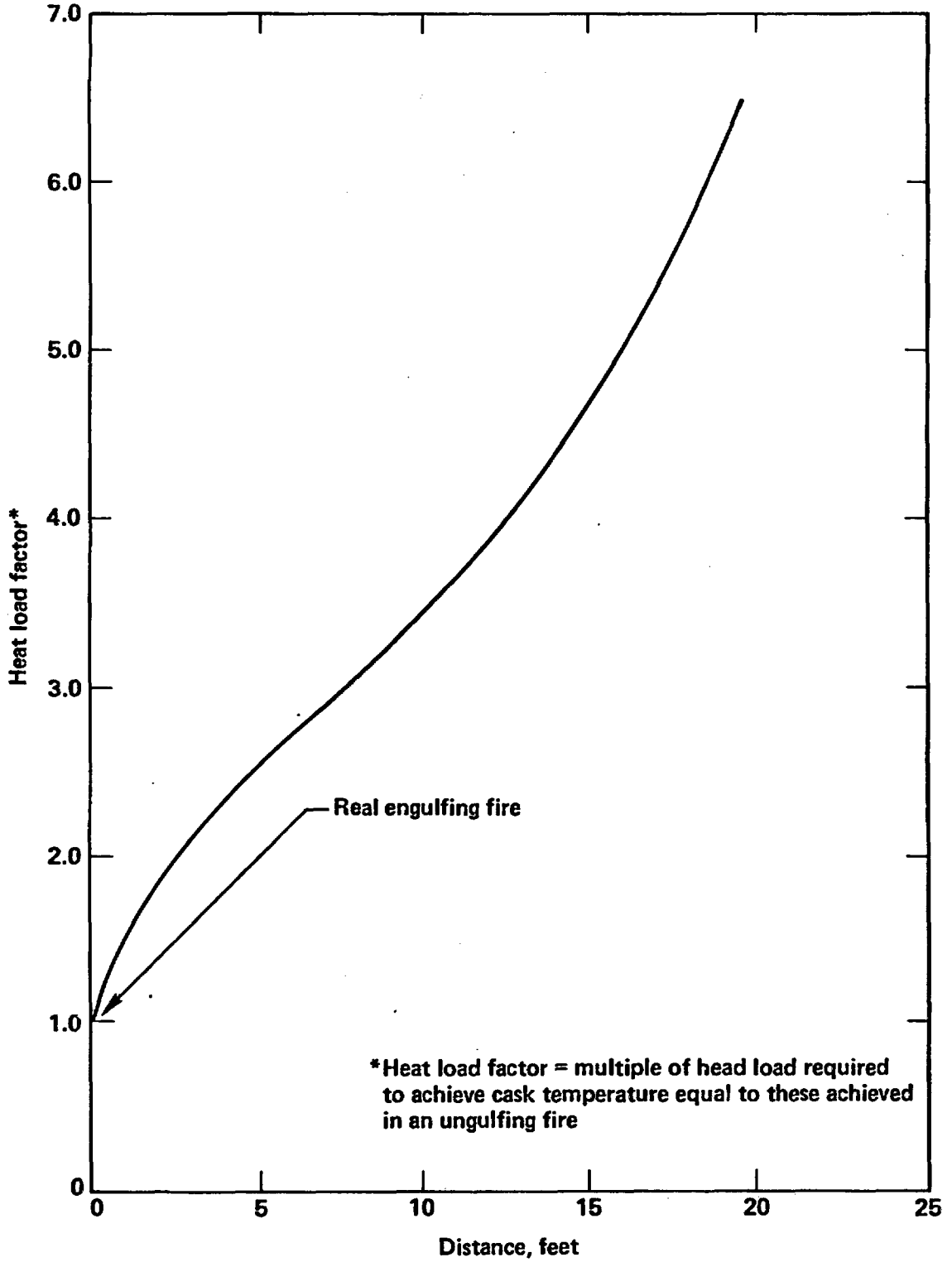

Figure 6-15 Heat load factor for real fire versus location of representative truck cask.

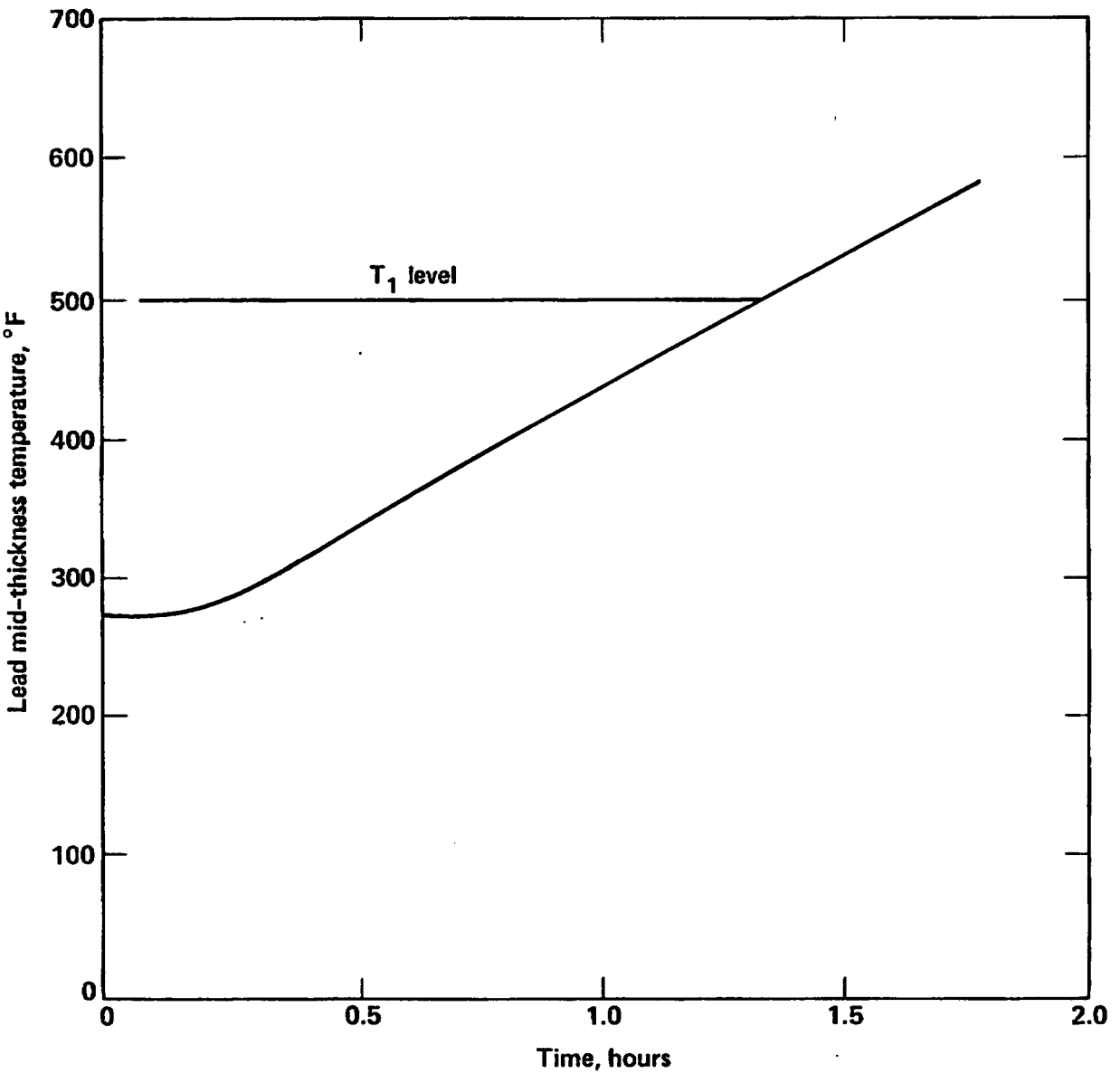

Figure 6-16 Representative rail cask temperature response to a hypothetical 1475°F (equivalent to a real 1700°F) fire versus fire duration.

For engulfing fires, the heat flux from a fire to the surface of the rail cask depends primarily on radiation heat transfer and is determined by the flame temperature. The heat flux dependency on the flame temperature is essentially the same as that for the truck cask discussed in Subsection 6.3.1. The average heat flux factors in Fig. 6-14 are used to adjust for flame temperature for the rail cask.

The heat load to the rail cask also depends on the location of the fire with respect to the cask. An engulfing fire provides the maximum heat load to the cask. The heat load decreases rapidly as the distance between the fire and the cask increases. Figure 6-17 shows the effect of distance between the cask and fire for the representative rail cask. The heat load factor is normalized with respect to an engulfing fire.

The heat flux and load factors are used to calculate the change required in the 1.35 hour reference fire to reach the 500°F temperature (T_1) level for a variety of flame temperatures and durations. The fire durations are calculated using the probabilistic code described in Section 5.0 for the wide range of fire conditions.

6.3.3 Discussion of Thermal Analysis Results

This section addresses highway and railway fire accidents which generate cask temperature responses less than or equal to the 500°F temperature (T_1) level. These accidents result in heating the cask structure to temperatures at which no significant deterioration of the cask components is expected. As a result, the radiological significance of such events is negligible.

The results indicate that the representative truck and rail casks can be exposed to a regulatory fire (1475°F, engulfing, etc.) for over 1 hour before the 500°F temperature (T_1) limit is reached. This fire duration is approximately twice as long as that specified in the regulations for the accident test conditions; hence, the representative cask designs have considerable margin with respect to the fire duration. This margin is due to the high heat capacity and thermal resistance inherent in the casks. The massiveness of spent fuel casks due to shielding and mechanical strength contributes significantly to the thermal response characteristics.

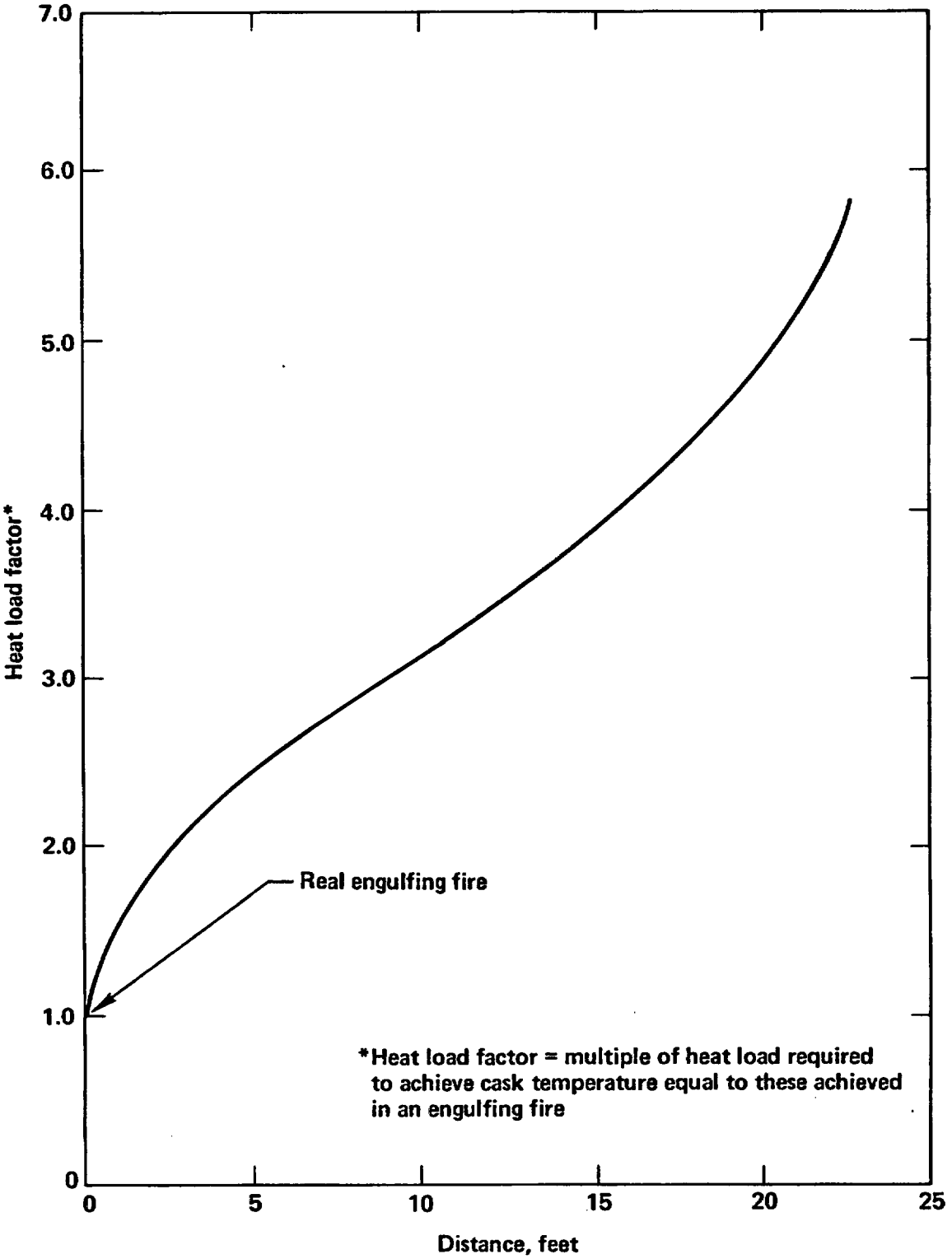

Figure 6-17 Heat load factor for real fire versus location of representative rail cask.

In reality, many currently licensed casks use components and seals that can reliably function at temperatures exceeding those associated with a 500°F (T_1) lead mid-thickness temperature for long periods of time without being damaged. Therefore, the actual percentage of highway and railway accidents that are within the thermal loading envelope of the accident test conditions is significantly higher than those documented in this study. The radiological hazards for these events are expected to be negligible.

6.4 Accident Screening Analysis

Section 5.0 provides the detailed probabilistic calculations performed in the accident screening analysis. From that analysis, approximately 99.4% of both highway and railway accidents leads to cask responses within the R(1,1) response region. At this level of damage, no radiological hazards of significance are expected; therefore, all are within the stated regulatory limits for radioactive releases and direct exposures. These results are discussed in detail in Subsection 9.2.1.

7.0 SECOND-STAGE SCREENING ANALYSIS

7.1 Introduction

The first-stage screening analyses identify classes of accidents in which the responses generated by the mechanical and thermal loadings are within the R(1,1) response region. At levels of response within the R(1,1) region, the accident event would not be expected to have any radiological significance. Approximately 99.4% of highway and railway accidents are expected to cause cask response states within the R(1,1) region.

The residual 0.6% of highway and railway accidents which could cause cask responses outside the R(1,1) region are addressed in this section. The intent of the second-stage screening is to determine what fractions of these residual accidents can be categorized into regions bounded by 30% strain (S_3) in the inner cask containment shell and by a lead mid-thickness temperature of 1050°F (T_4). These regions are shown in Fig. 7-1.

The light stippled area in Fig. 7-1, which covers regions R(1,2), R(2,1), and R(2,2), represents cask responses between the 0.2% (S_1) and 2% (S_2) strain levels and between the 500°F (T_1) and 600°F (T_2) temperature levels. These cask responses exceed the responses that would be generated if a shipping cask were subjected to the 10 CFR 71 accident test conditions.[1] Responses in this light stippled area can result in minor damage to the cask and could result in small radioactive releases or small increases in the direct radiation levels external to the cask. The radiological hazards associated with these cask responses could approach or slightly exceed the regulatory limits specified in 10 CFR 71 for transportation accidents.

The remaining eight regions, beyond the 2% strain (S_2) and 600°F temperature (T_2) levels, represent individual or combined cask responses between the 2% (S_2) and 30% (S_3) strain levels and between the 600°F (T_2) and 1050°F (T_4) temperature levels. For clarity, they are darkly shaded in Fig. 7-1. These responses are significantly greater than the responses expected after exposing the representative casks to the accident test conditions. Responses within the darkly shaded area in Fig. 7-1 can result in

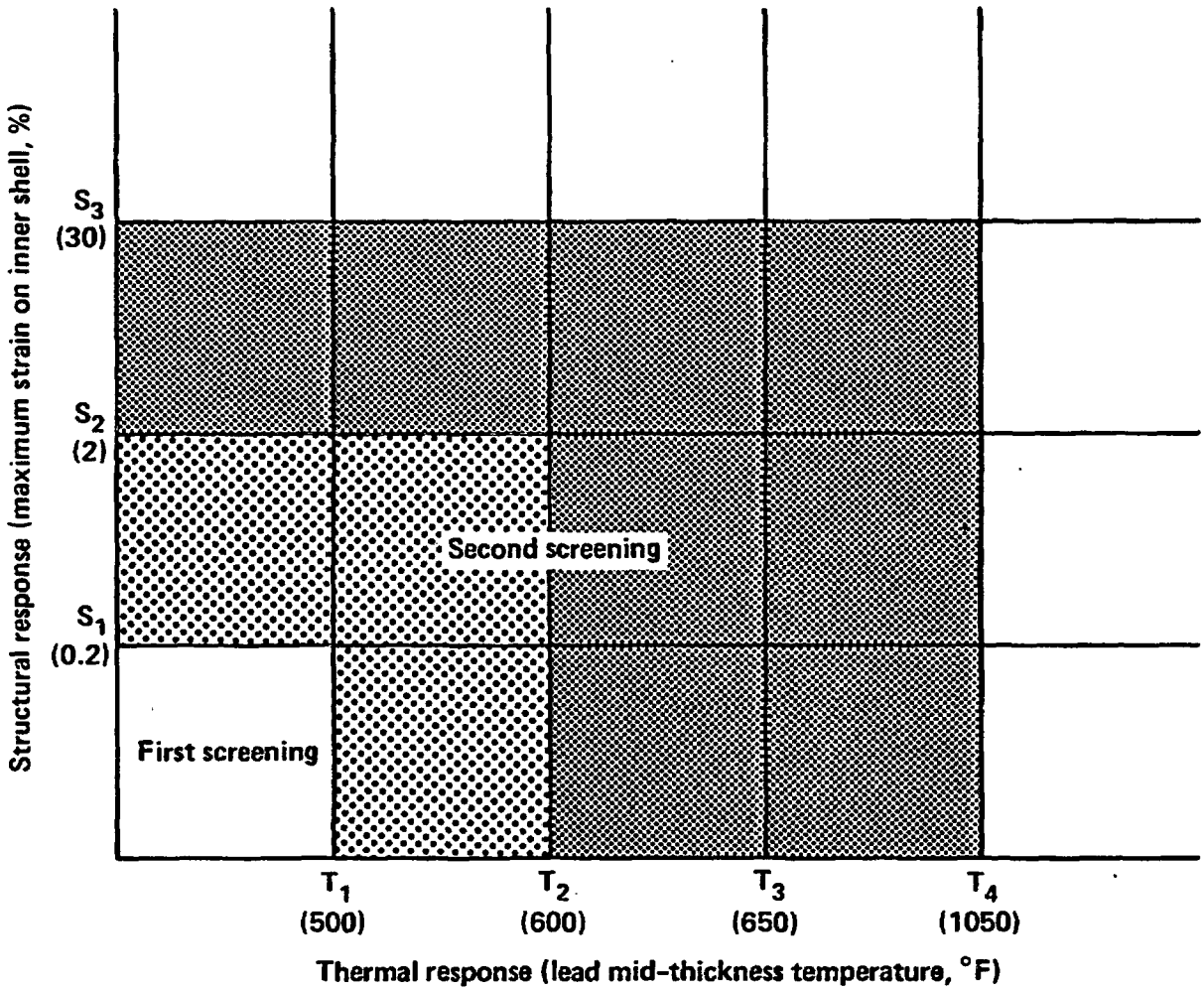

- First-stage screening analysis radiological hazards are negligible and less than 10 CFR 71 limits.
- Second-stage screening analysis radiological hazards can be less than, equal to, or greater than 10 CFR 71 limits.
  - Light stippled area - minor damage to cask, with consequent radiological hazards approaching or slightly exceeding 10 CFR 71 limits.
- - Dark shaded area - more substantial cask damage, with radiological hazards probably exceeding 10 CFR 71 limits.

Figure 7-1 Second-stage screening analysis relationship with response regions.

significant permanent deformation of the cask structure and melting of the lead shielding. Any radioactive material releases or increase in the direct radiation levels that could result from these cask responses are probably greater than the regulatory limits specified in 10 CFR 71 for transportation accidents.

The second-stage screening analysis involves calculations similar to those performed in the first-stage screening. The major difference between the two screening evaluations involves the calculational methods used. Nonlinear small-deformation analysis methods are needed to analyze the cask structure for deformations having strain levels within the 2% strain (S_2) limit. For strain levels beyond the 2% (S_2) limit, nonlinear, large deformation methods are needed. Thermal analysis methods account for the melting of the lead shield in the 600°F (T_2) to 1050°F (T_4) temperature range.

Section 7.2 discusses the structural response of the representative casks to mechanical loads; Section 7.3 addresses response to thermal loads. In Section 7.4, the results of both structural and thermal response are combined to estimate the fraction of accidents that fall within each of the response regions.

7.2 Structural Response Analysis

The classes of accidents requiring structural analysis in the second-stage screening typically involve impacts with massive objects or hard surfaces. In these accidents, dynamic forces greater than 400,000 pounds can be generated. The computer codes selected to perform the required analysis include two established codes called DYNA 2-D/3-D and NIKE 2-D/3-D; the 2-D/3-D designation indicating that either two- or three-dimensional modeling can be performed.[2,3] Two-dimensional calculations are much simpler and faster to run and are used whenever possible. The applicability of the 2-D modeling is verified through the performance of sensitivity studies which compared results of 2-D and 3-D modeling. The calculation methods and assumptions used in the 2-D modeling are discussed in further detail in Appendix E. The most significant aspects include the following:

1. For cask orientations between sidewise and endwise in the range of $0^{o} < \beta < 90^{o}$, the structural strain responses for the representative casks impacting solid surfaces are linearly interpolated from the results of sidewise, $\beta=0^{o}$, and endwise, $\beta=90^{o}$, impacts.

2. Two-dimensional plane strain analyses without impact limiters or end enclosures are performed for high velocity sidewise impacts, $\beta=0^{o}$, on hard rock, soft rock, and soil surfaces. This elimination of impact limiters overestimates strain responses of the representative casks, particularly for impact velocities less than 60 mph and for impacts on soft surfaces such as soil. The 2-D method is benchmarked with a 3-D impact analysis that modeled the representative truck cask with the inclusion of the impact limiters and end closures.

3. The strain responses of the representative casks impacting real surfaces are estimated using the equivalent damage technique discussed in Section 6.2 and in Appendix E.

The structural response analysis of highway accidents is in Subsection 7.2.1. Highway accident scenarios, in which the first-stage screening indicates the possibility of cask response outside the R(1,1) region, are evaluated. The fraction of these accidents causing responses within the 0.2% (S_1) to 2% (S_2) and 2% (S_3) to 30% (S_3) strain levels on the inner shell of the representative truck cask is determined. Subsection 7.2.2 describes a similar structural response analysis performed for the railway accidents. In Subsection 7.2.3 the overall structural analysis results are discussed.

7.2.1 Cask Response Analysis for Highway Accidents

The representative truck cask described in Section 3.5 is used in the second stage screening analysis for highway accidents. Appendix E discusses the computer models of the cask, material properties, and the detailed structural evaluations used in the response analysis.

The highway accident scenarios involve impacts by train sills and impacts occurring as a result of a truck running off a bridge, over an embankment, into a slope, or into a massive concrete structure.

In this evaluation, the maximum strain at the inner wall of the representative truck cask is calculated as a function of the impact velocity for both endwise and sidewise impacts with real surfaces.

7.2.1.1 Endwise Impacts

Since the representative truck cask is axi-symmetric along its length, a 2-D cask model with impact limiters is used to evaluate the response of the representative truck cask for endwise impacts on an unyielding surface. Figure 7-2 shows the strain response for the representative truck cask impacting an unyielding surface at 45 mph. The maximum strain of 3.63% occurs on the inner shell of the cask at the bottom junction with the end-cap, near the point of impact. The lead slumps to the impacted end of the cask, causing a 4-inch gap in the lead shield at the opposite end.

The cask impact calculations are performed, assuming impacts on an unyielding surface, over a range of velocities from 30 to 90 mph. As discussed in Appendix E, the energy absorption effects of crushing the transport truck cab are included in the analysis. The resultant impact force, maximum plastic strain at the inner shell of the cask, and the amount of lead slump are plotted as functions of impact velocity in Fig. 7-3. The 2% strain (S_2) level occurs when a cask impacts an unyielding surface at a velocity of 46 mph. At this velocity the impact force is 80 g, and the lead slump is about 3 inches. The 30% strain (S_3) level occurs when a cask impacts an unyielding surface at a velocity of 76 mph. The resultant impact force is 300 g and the lead slump is 16 inches. In both cases, the maximum strains occur because of lead slump at the bottom of the cask on the inner shell.

The equivalent damage technique, discussed in Section 6.2 and Appendix E, is used to estimate the cask response for endwise impacts on real surfaces. A rigid body with the outer dimensions and weight of the truck cask impacts varying surfaces at velocities up to 120 mph. The resultant interface forces

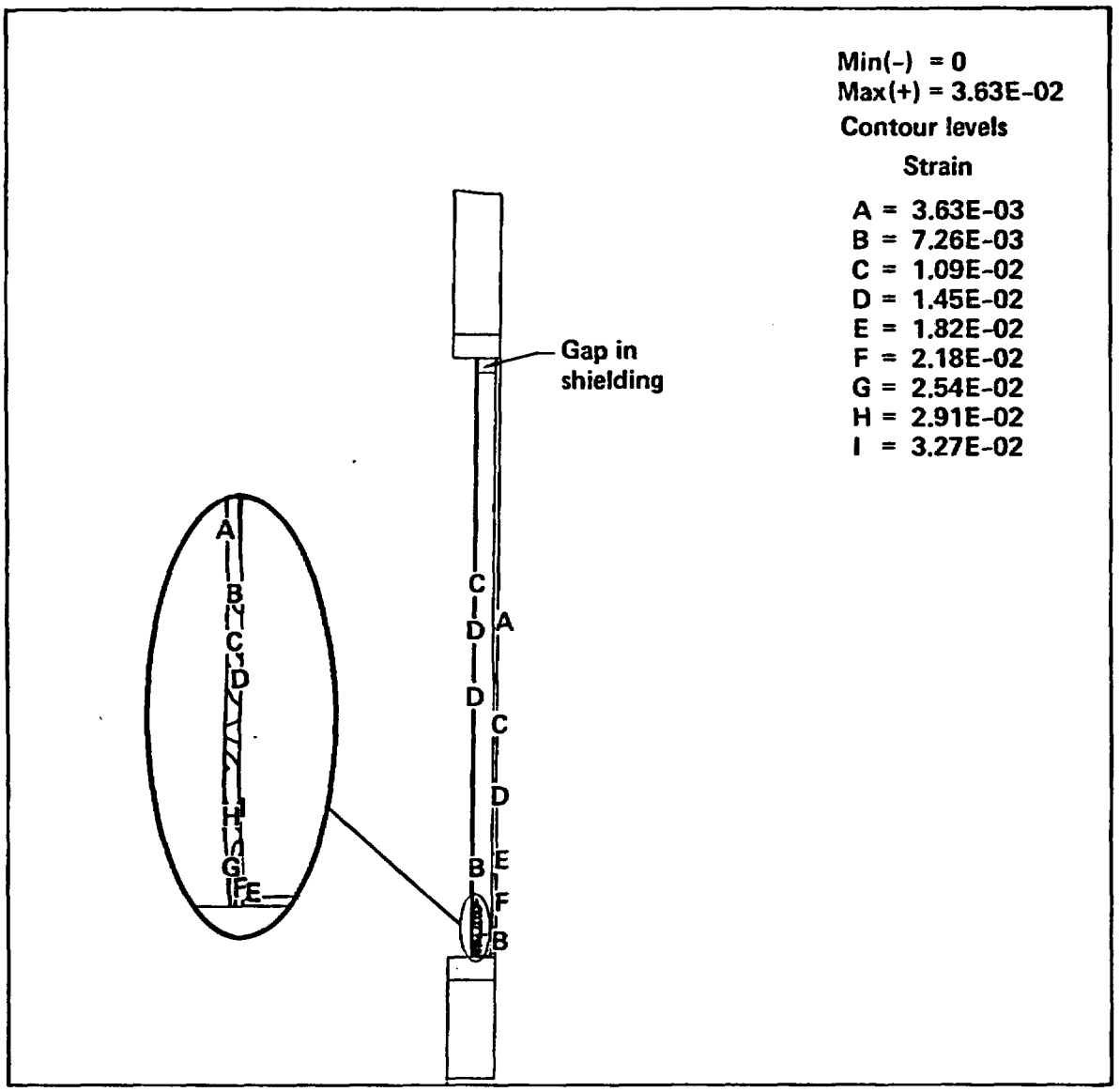

Figure 7-2 Example showing strain response of the representative truck cask for 45 mph endwise impact on an unyielding surface (2-D model with impact limiters) without any truck cab crushing included.

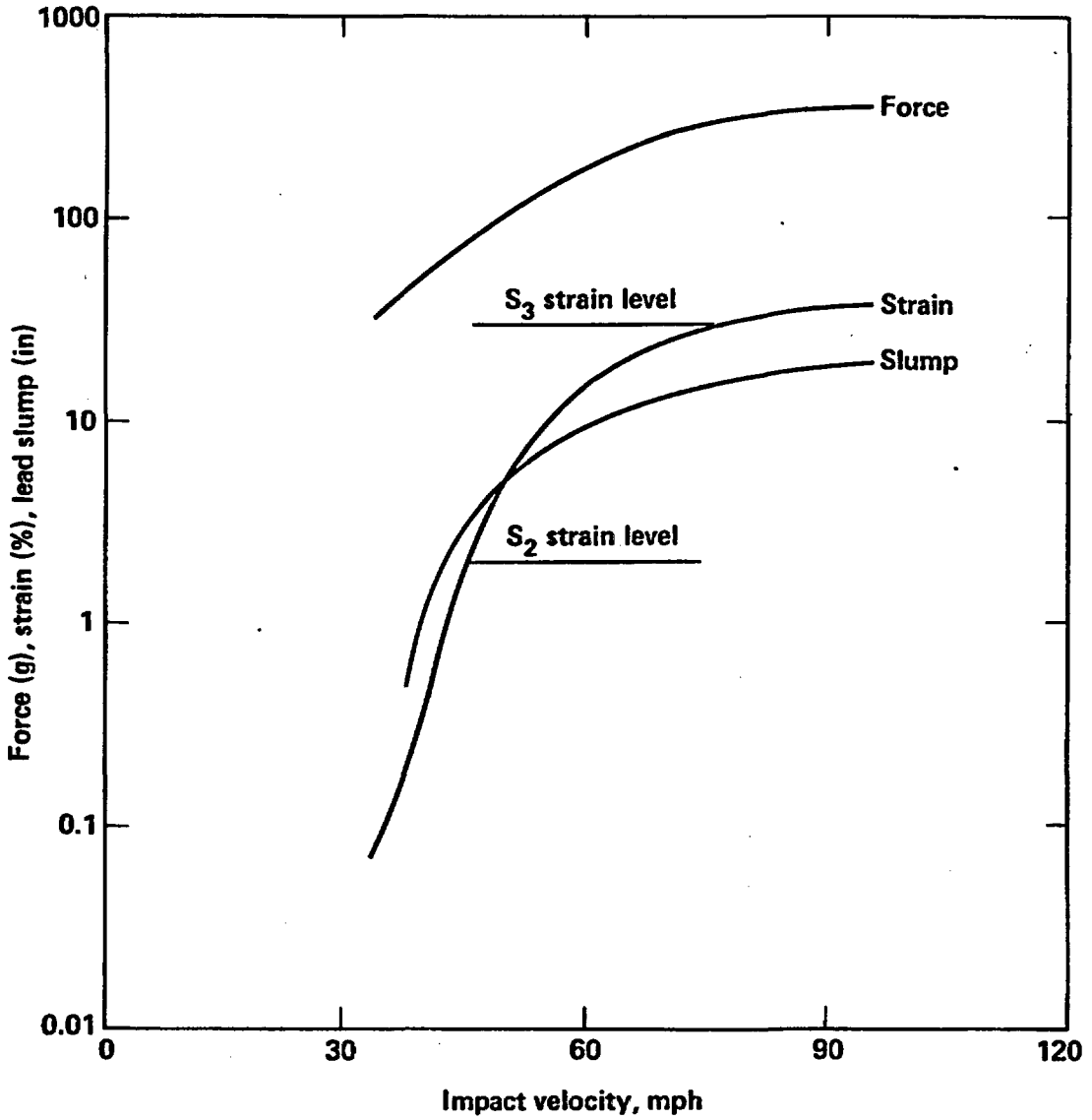

Figure 7-3 Response of the representative truck cask to endwise impacts on an unyielding surface (2-D model with impact limiters and cab crush).

were calculated in the first-stage screening and are plotted in Fig. 6-7. Using the equivalent damage technique, the 2% strain (S_2) level is reached at impact velocities of 46 mph for impacts on hard and soft rocks but is never reached for impacts on soil. The 30% strain (S_3) level is reached only for impacts on hard rocks at impact velocities exceeding 76 mph.

7.2.1.2 Sidewise Impacts

An approximate 2-D plane strain model is used to calculate the response for high-velocity sidewise impacts on soil, soft rock, and hard rock. Figure 7-4 shows the strain response for the representative truck cask without an impact limiter impacting tillable soil at 60 mph. The maximum strain of 8.47% occurs at the inner shell. During impact, the cask inner diameter decreases by 50% in the impact direction and collapses onto any spent fuel being transported.

In Fig. 7-5, the maximum plastic strain at the inner wall is plotted as a function of impact velocity for impacts on hard rock, soft rock, and tillable soil. In the approximate 2-D model, the strains calculated for a specific impact velocity are essentially the same for sidewise impacts regardless of the surface impacted. The 2% strain (S_2) level occurs at a velocity of 51 mph for impacts on all of the surfaces considered. The 30% strain (S_3) level does not occur because the representative cask walls collapse together or onto the spent fuel contents before the limit is reached.

7.2.1.3 Impact Response Summary

Table 7.1 summarizes the impact velocities at the 2% (S_2) and 30% (S_3) strain levels for sidewise, $\beta = 0^{\circ}$, and endwise, $\beta = 90^{\circ}$, impacts on hard rock, soft rock, and soil surfaces. Impacts of the cask on water and by a train sill are also included. In general, the endwise impacts result in higher strains to the cask than sidewise impacts for the same impact conditions on surfaces. The cask attains the 30% strain (S_3) level only at high-velocity endwise impacts on hard rock.

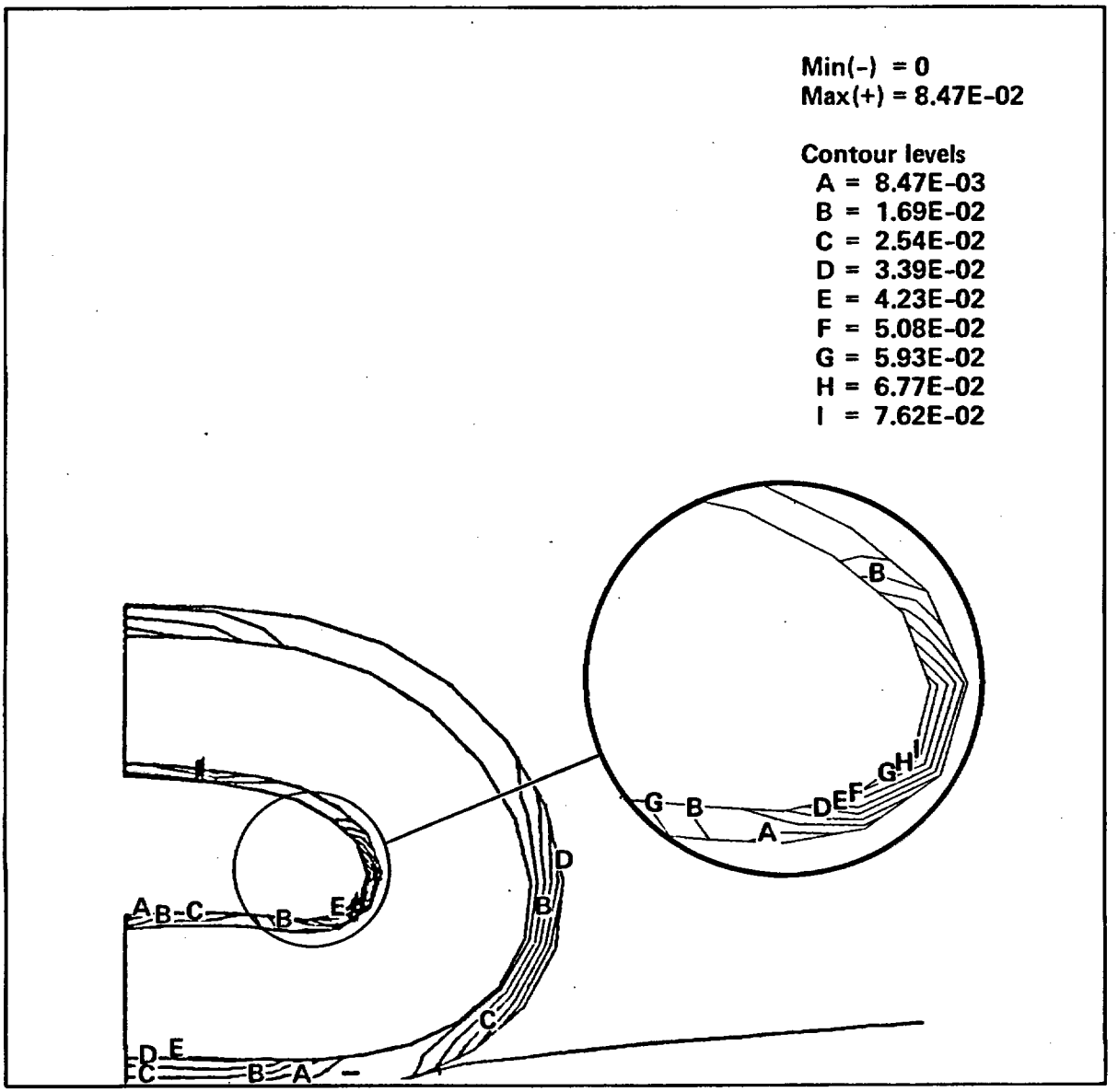

Figure 7-4 Example showing strain response of the representative truck cask for 60 mph sidewise impact on soil (2-D model without impact limiters) with strain exceeding the 2% (S_2) limit.

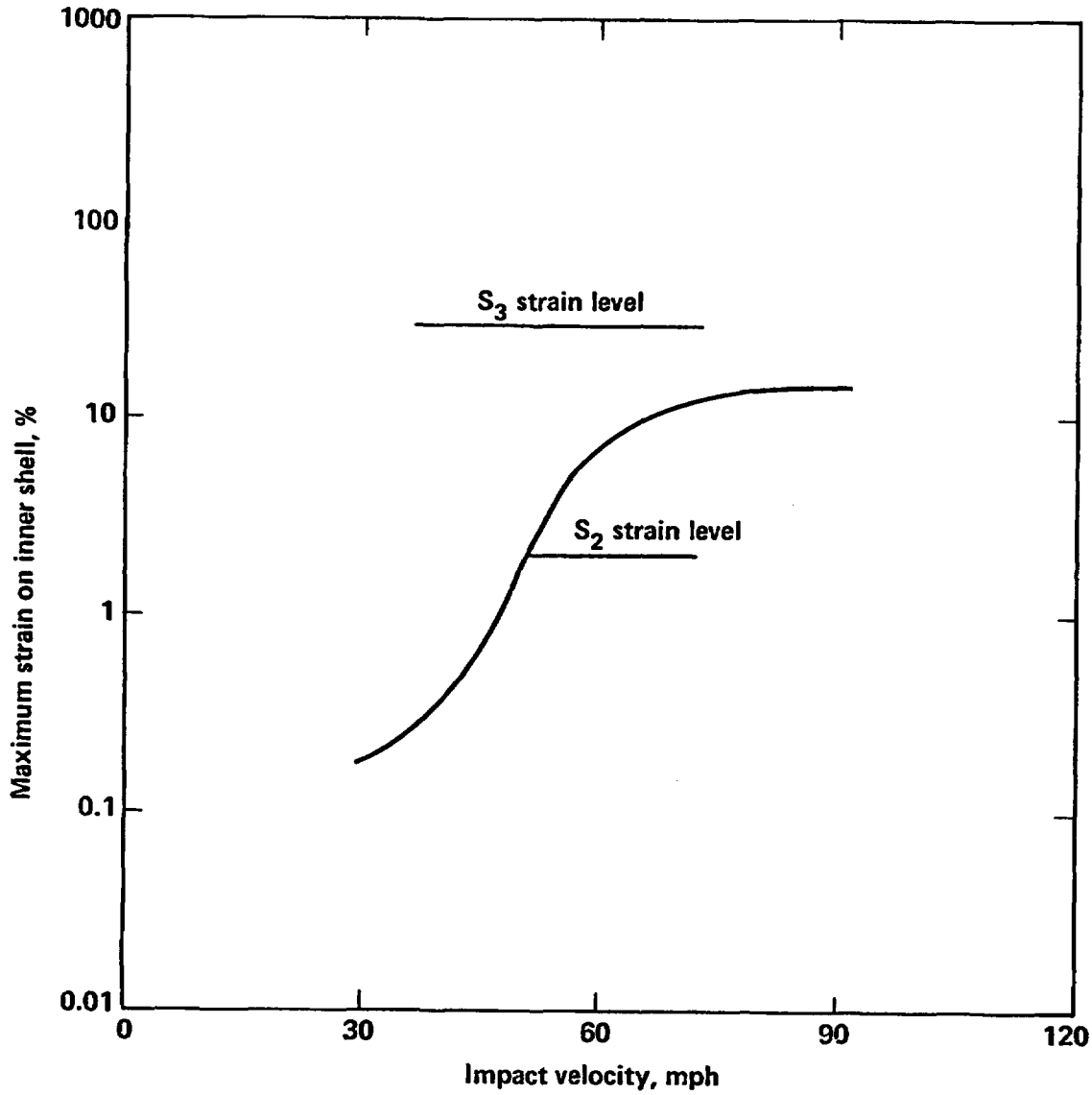

Figure 7-5 Response of the representative truck cask to sidewise impacts on various surfaces.

Table 7.1
Impact Velocities Required to Attain 2% (S_2) and 30% (S_3) Strain Levels for Objects Impacted in Highway Accidents

Object Impacted	Impact Velocity [a] at 2% Strain (S_2) (mph) — Cask Orientation Angle (°)			Impact Velocity [a] at 30% Strain (S_3) (mph) — Cask Orientation Angle (°)		
	0	45	90	0	45	90
Hard Rock	51	49 [b]	46	>150	113 [b]	76
Soft Rock	51	49 [b]	46	>150	>150 [b]	150
Tillable Soil	51	101 [b]	>150	>150	>150 [b]	>150
Water	59	>150	64	>150	>150	>150
Train Sill	20	27	>150	>150	>150	>150

[a] Impact velocity of >150 mph means that the strain level is not reached.

[b] Impact velocities at these orientation angles are linearly interpolated between the two bounding values.

7.2.2 Cask Response Analysis for Railway Accidents

The representative rail cask described in Section 3.5 is used in the railway accident response analysis. Appendix E discusses the computer models of the cask, the material properties, and the detailed structural evaluations use in the cask response analysis.

The railway accident scenarios of interest are those involving falls from bridges; drops over embankments; and impacts into slopes, train couplers, or massive concrete structures. Again, the maximum strain at the inner wall of the representative rail cask is calculated as a function of the impact velocity for both endwise and sidewise impacts with real surfaces.

7.2.2.1 Endwise Impacts

As was done in the truck cask analysis, a 2-D model is used to evaluate the response of the representative rail cask for endwise impacts on an unyielding surface. The cask impact calculations cover a range of velocities from 30 to 90 mph. Figure 7-6 shows the resultant impact force, maximum plastic strain at the inner shell of the cask, and the amount of lead slump as functions of impact velocity. The 2% strain (S_2) level occurs when a cask impacts an unyielding surface at a velocity of 48 mph. At this velocity the impact force is 102 g, and the lead slump is 6 inches. The 30% strain (S_3) level occurs when a cask impacts an unyielding surface at a velocity of 105 mph. The resultant impact force at this velocity is 500 g and the lead slump is 28 inches. In both cases the maximum strain occurs at the bottom of the cask on the inner shell.

The equivalent damage technique is used to estimate the cask response for endwise impacts on real surfaces. A rigid body with the outer dimensions and weight of the rail cask impacts various surfaces at velocities up to 120 mph. The resultant interface forces for these impacts are calculated in the first-stage screening and are plotted in Fig. 6-10. Using the equivalent damage technique, the 2% strain (S_2) level is reached at impact velocities of 48 mph for impacts on hard and soft rocks, and 65 mph for impacts on soil. The 30% strain (S_3) level is reached only for impacts on hard and soft rocks at an impact velocity of 105 mph.

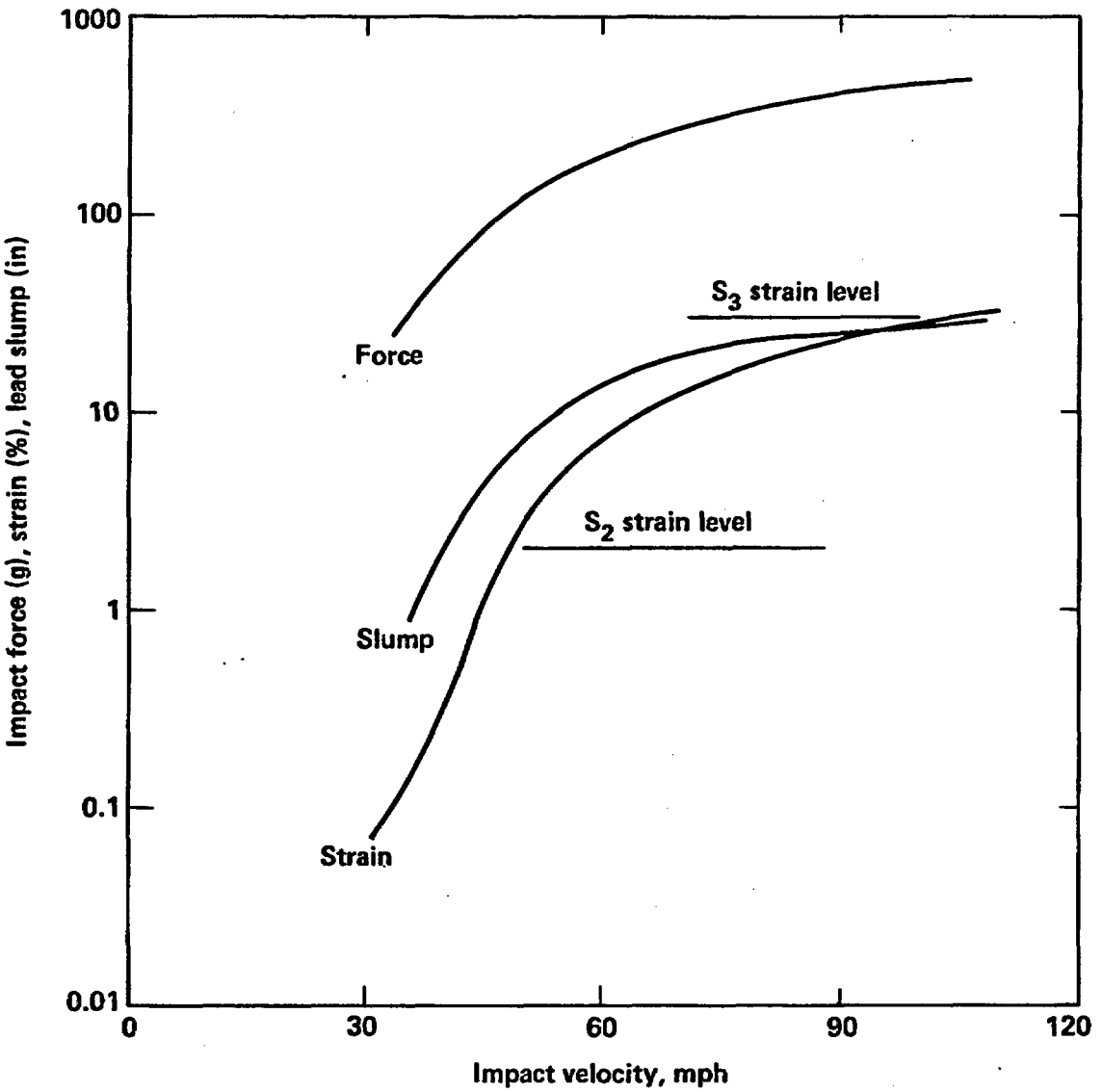

Figure 7-6 Response of the representative rail cask to endwise impacts on an unyielding surface (2-D model with impact limiters and railcar crush).

7.2.2.2 Sidewise Impacts

As done in the truck cask, a 2-D model of the rail cask is used to calculate the response for high-velocity sidewise impacts on soil, soft rock, and hard rock. In Fig. 7-7, the maximum plastic strain at the inner wall is plotted as a function of impact velocity. The 2% strain (S_2) level occurs at a velocity of 72 mph for impacts on hard and soft rock and on soil. The 30% strain (S_3) level can never occur because the representative cask walls collapse together or onto the spent fuel contents before the limit is reached.

7.2.2.3 Impact Response Summary

Table 7.2 summarizes the impact velocities at the 2% (S_2) and 30% (S_3) strain level for sidewise, $\beta = 0^{o}$, and endwise, $\beta = 90^{o}$, impacts on hard rock, soft rock, and soil surfaces. Impacts of the cask on water and by a train sill are also included. In general, the endwise impacts result in higher strains to the cask than sidewise impacts for the same impact conditions.

7.2.3 Discussion of Structural Analysis Results

This section has thus far addressed highway and railway accidents that can generate cask responses within the 2% (S_2) and 30% (S_3) strain levels. Cask structural responses at these levels result in permanent deformations to the cask and potential radioactive material releases or increases in direct radiation exposure levels which could approach or exceed the limits specified in 10 CFR 71.

The dynamic response of the cask is calculated using the DYNA and NIKE families of elastic-plastic finite element computer codes.[2,3] These codes were developed at the Lawrence Livermore National Laboratory (LLNL) around 1979, and their predicted results were extensively benchmarked. Appendix H, for example, discusses the capability of these computer codes to calculate the dynamic responses of a cylinder impacting a rail, a nose cone impacting a rigid wall, and a rod impacting a rigid wall obliquely.

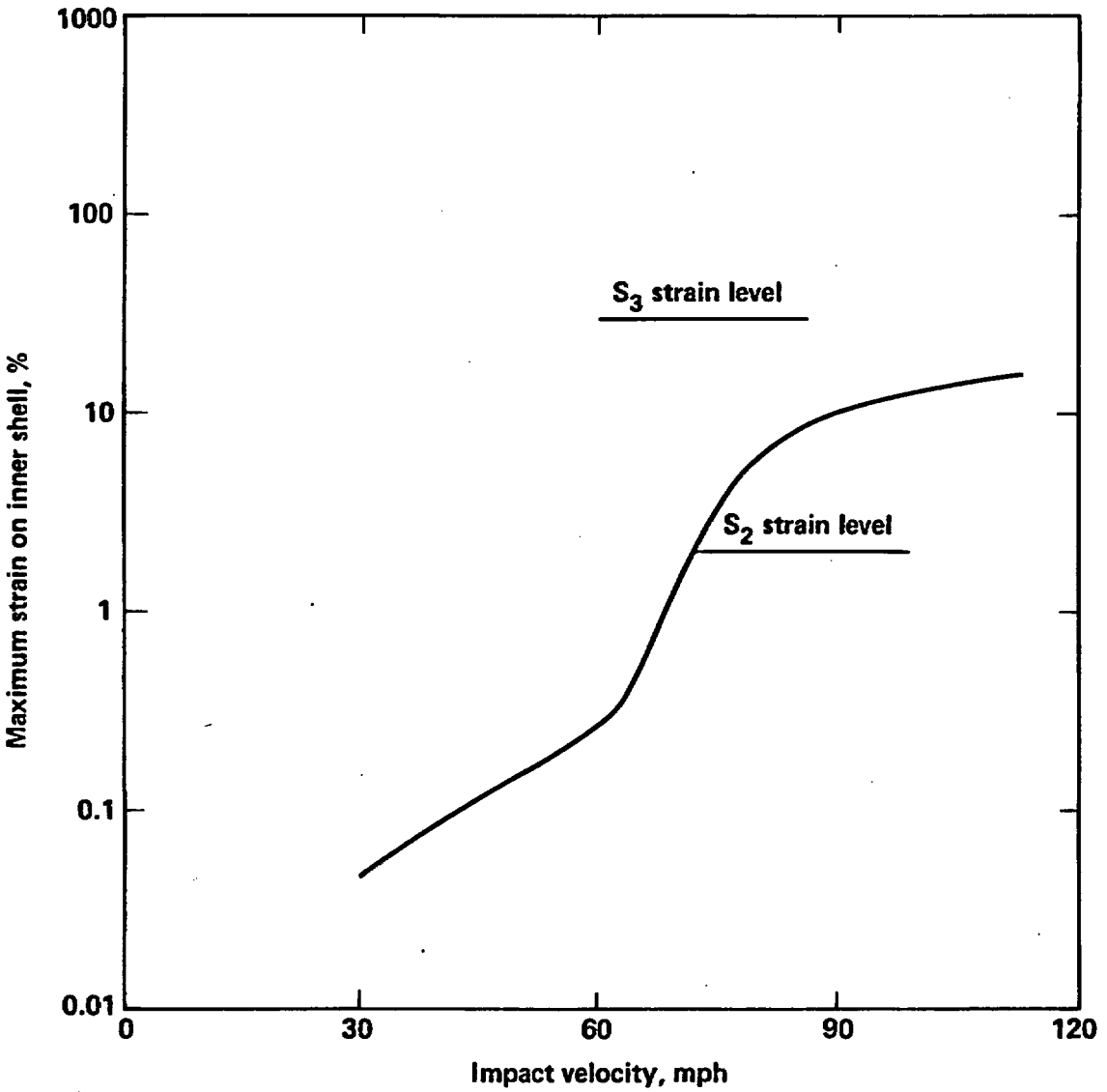

Figure 7-7 Response of the representative rail cask to sidewise impacts on various surfaces.

Table 7.2
Impact Velocities Required to Attain 2% (S_2) and 30% (S_3) Strain Levels for Objects Impacted in Railway Accidents

Object Impacted	Impact Velocity [a] for 2% Strain (mph) — Cask Orientation Angle (°)			Impact Velocity [a] for 30% Strain (mph) — Cask Orientation Angle (°)		
	0	45	90	0	45	90
Hard Rock	72	60 [b]	48	150	128 [b]	105
Soft Rock	72	60 [b]	48	150	128 [b]	105
Tillable Soil	72	69 [b]	65	150	150 [b]	150
Water	72	150	60	150	150	150
Train Sill	27	49	150	150	150	150

[a] Impact velocity of 150 mph means that the strain level is not reached.

[b] Impact velocities at these orientation angles are linearly interpolated between the two bounding values.

These benchmark cases demonstrate the capabilities of the codes to calculate the dynamic response of objects which, when subjected to impact, can experience large permanent deformations. In all three cases, the computer predictions were within a few percent of the deformations measured in the tests.

Benchmark tests of DYNA 3-D have also been performed in the United Kingdom. Excellent agreement was obtained in predicting the dynamic response of a missile impacting a pipe.[4] DYNA 3-D was also used to predict the high deformation characteristics and response of a metal fin on the MAGNOX spent fuel cask when subjected to a 30-foot drop onto an unyielding surface.[5] Again there was a good comparison between the test results and the computer predictions.

The Sandia National Laboratory (SNL) used scale model tests and a computer code similar to DYNA 2-D to predict the dynamic response and deformations of full-scale casks used in a series of crash tests. The full-scale tests included a 25-ton truck cask being struck by a 100-ton locomotive at 80 mph.[6] Following the high-velocity impact, the cask was dented at the points of impact on the side, was slightly bowed along the length, and had a small leak at the closure. In another test, a similar truck cask was carried at 80 mph on a truck which crashed into a huge unyielding concrete abutment.[7] The endwise impact resulted in some lead slump and a small leak at the closure. The results of both of these tests were in good agreement with the computer predictions.

These benchmark tests of the computer codes support their use in conservatively predicting the damage to a spent fuel cask which is subjected to severe accident conditions. In many cases in this study, conservative modeling assumptions are made to simplify the cask response evaluation over a wide range of accident conditions. Examples include the 2-D modeling of 3-D sidewise impacts, the use of elastic-plastic soil modeling, the use of the equivalent damage technique for estimating strain, and the assumption of no bonding between the lead shield and the inner shell of the cask. All these assumptions result in overpredicting the cask damage response to real accident

conditions. In addition, the representative cask is structurally weaker than current casks. Again, for the same impact conditions, damage to the representative casks will be greater than that which would be incurred by real casks.

7.3 Thermal Response Analysis

Many of the accident scenarios involving fire led to a cask response well within the R(1,1) region associated with the first-stage screening. This observation is true for both truck and rail casks, but more prevalent for truck casks.

The accidents of interest in this section involve fires of approximately 1-hour duration and longer. These fire accidents have three loading parameters that can affect the response of a spent fuel cask: fire duration, flame temperature, and fire location. Longer fire durations and higher flame temperatures increase the thermal loads to the cask and increase its temperature responses. Also, the closer the cask is to the fire, the better the thermal interaction and the higher the thermal load. In the worst case, the cask is submerged or engulfed by the fire.

The thermal screening analysis in this section compares the truck and rail cask responses to the three temperature response levels of 600°F (T_2), 650°F (T_3), and 1050°F (T_4) at the middle of the lead shield thickness. Since lead melts at 621°F, the calculation of the responses between 600°F (T_2) and 650°F (T_3) has to include the melting of the lead shield. The computer code TACO 2-D used in the first-stage screening has the capability of handling lead melt. TACO 2-D is used with the same one-dimensional (1-D) thermal models to perform the second-stage screening.[8] In other words, the thermal analysis is a continuation of the analysis performed for the first-stage screening, but includes consideration of lead melt.

The calculational method relies on the concept that the time to reach a specific cask temperature is approximately proportional to the incident heat flux on the cask caused by the fire. A fire that causes a heat flux twice the heat flux of a reference fire can heat a cask to a specified temperature in

one-half the time it takes the reference fire. Conversely, a fire that causes one-half the heat flux takes twice as long to heat the cask in comparison to a reference fire. For details on the calculational method, refer to Section 6.3.

The thermal response analysis of highway fire accidents is provided in Subsection 7.3.1. Subsection 7.3.2 describes a similar response analysis performed for the railway fire accidents. In Subsection 7.3.3, the overall thermal screening results are discussed.

7.3.1 Cask Response Analysis for Highway Fire Accidents

The representative truck cask described in Section 3.5 is used in the highway fire accident response analysis. Appendix F discusses the computer analysis model, the cask material properties, and the detailed thermal calculations. All highway accident scenarios are evaluated for cask responses to fire because in all scenarios, possibilities exist that a fire can occur and last longer than 1 hour.

The temperature response of the representative truck cask is calculated for a hypothetical engulfing fire with a flame temperature of 1475°F and flame emissivity of 0.9. This hypothetical fire approximates a real engulfing fire with a 1700°F flame temperature. The temperature at the middle of the lead shield thickness is plotted in Fig. 7-8 as a function of time. The lead mid-thickness temperature reaches 600°F (T_2) in 1.35 hours for the specified heat flux conditions. The total heat absorbed by the cask in reaching the 600°F temperature (T_2) level is approximately 6,000 Btu/ft^2 which results in an average thermal flux of approximately 4,450 Btu/hr-ft^2. As the lead mid-thickness temperature increases beyond the 600°F (T_2) level, the lead at the outer shell starts to melt. The lead melts at the inner shell in 2.1 hours as the mid-thickness temperature reaches 650°F (T_3). The 1050°F temperature (T_4) level is reached in 3.3 hours.

These temperature response and heat flux results from the hypothetical fire are used to evaluate real fires. For an engulfing fire, the heat flux from the fire onto the surface of the truck cask depends on radiation heat

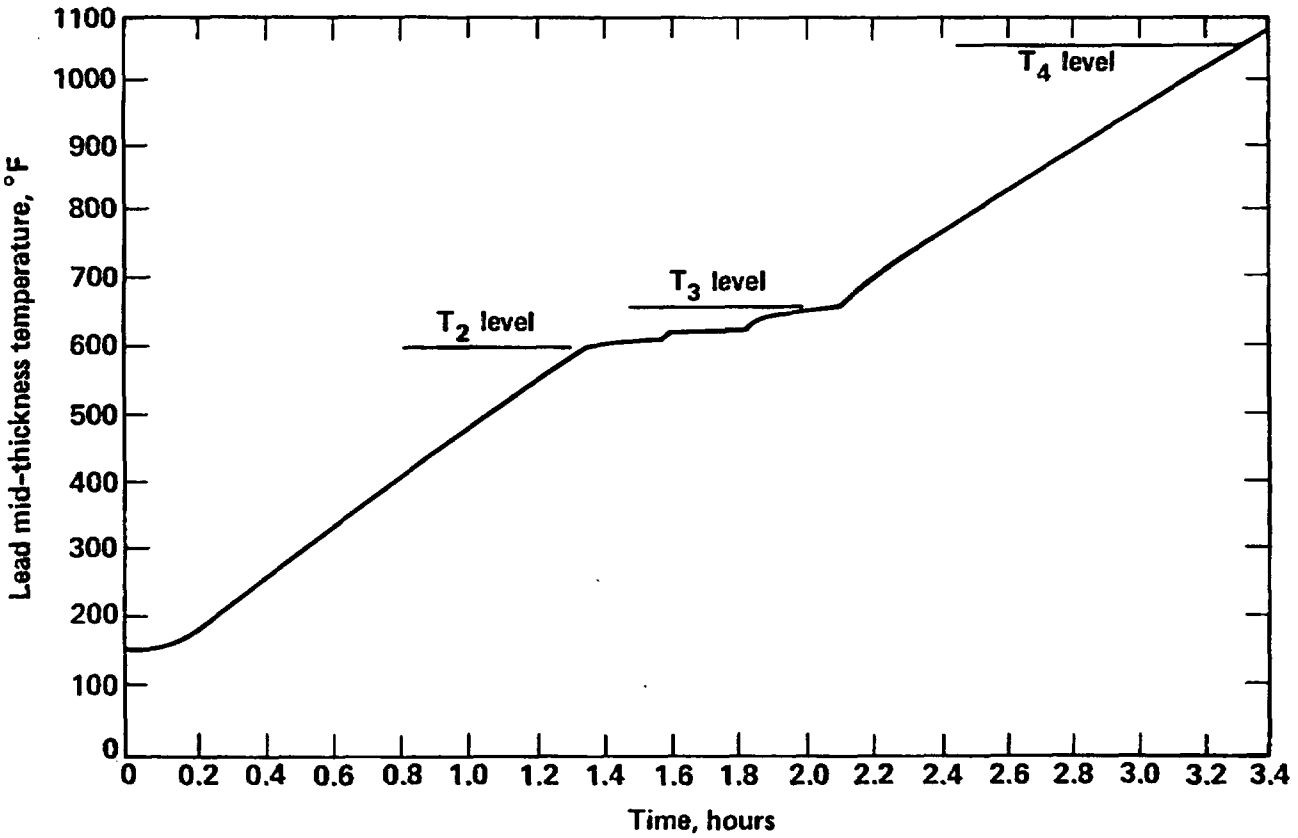

Figure 7-8 Representative truck cask temperature response to a hypothetical 1475°F (equivalent to a real 1700°F) fire versus fire duration.

transfer which is strongly dependent on the flame temperature. The average heat flux on the representative truck cask is calculated as a function of flame temperature for a hypothetical engulfing fire. The heat flux is then reduced by a factor of 0.78 to adjust the results to real engulfing fire conditions. The heat flux factors are derived in the first-stage screening evaluations, and the results are plotted in Fig. 6-14 as a function of flame temperature. For a 1700°F fire, the average thermal flux on the representative cask is 5,000 Btu/hr-ft^2 and the heat flux factor is 1.0.

The heat flux to the truck cask also depends on the location of the fire with respect to the cask. An engulfing fire provides the maximum heat flux to the cask. The heat flux decreases rapidly as the distance between the fire and the cask increases. As discussed in Subsection 6.3.2 and plotted in Fig. 6-15, the heat load factor is normalized with respect to a real engulfing fire.

As the flame temperature increases, the thermal flux to the cask increases, and the fire duration required to reach the 600°F (T_2), 650°F (T_3), and 1050°F (T_4) temperature levels decreases proportionally. On the other hand, as the cask distance from the fire increases, the thermal flux decreases and the duration time increases proportionally to reach the same temperature levels.

The heat flux and load factors are used to determine the amounts of increase or decrease required in each of the fire duration times to reach the 600°F (T_2), 650°F (T_3), and 1050°F (T_4) temperature levels for a variety of flame temperatures and fire locations.

7.3.2 Cask Response Analysis for Railway Fire Accidents

The representative rail cask described in Section 3.5 is used in the railway fire accident response analysis. Appendix F discusses the computer analysis model of the cask, the material properties, and the detailed thermal calculations used in the response analysis.

All railway accident scenarios are evaluated for cask responses to fire because in all scenarios, possibilities exist that a fire can occur and can last longer than 1 hour.

The temperature response of the representative rail cask is calculated for a hypothetical engulfing fire with a flame temperature of 1475°F and flame emissivity of 0.9. The temperature at the middle of the lead shield thickness is plotted in Fig. 7-9 as a function of fire duration. The lead mid-thickness temperature reaches 600°F temperature (T_2) in 1.8 hours for the specific thermal flux conditions. The total heat absorbed by the cask in reaching the 600°F temperature (T_2) level is approximately 7,900 Btu/ft^2 which results in an average thermal flux of approximately 4,400 Btu/hr-ft^2. As the lead mid-thickness temperature increases beyond the 600°F (T_2) level, the lead at the outer shell starts to melt. The lead melts at the inner shell in 2.6 hours as the lead mid-thickness temperature reaches 650°F (T_3). The 1050°F temperature (T_4) level is reached in 5.1 hours. These final temperature response and heat flux results are used to evaluate real fires.

As is done for the truck cask, heat flux and load factors are calculated for the rail cask, as plotted in Figs. 6-14 and 6-17. These factors are used to determine the amounts of increase or decrease in each of the fire duration times necessary to reach the 600°F (T_2), 650°F (T_3), and 1050°F (T_4) temperature levels for a variety of flame temperatures and fire locations.

7.3.3 Discussion of Thermal Analysis Results

Cask responses at the 600°F (T_2), 650°F (T_3), and 1050°F (T_4) temperature levels can involve deterioration of safety components and melting of the lead shield. Consequently, radioactive material releases and increases in direct radiation exposures are possible and could equal or exceed regulatory limits specified in 10 CFR 71 for transportation accidents.

The TACO 2-D code used to perform the thermal analysis was developed about 1978 at the LLNL and was benchmarked against proven engineering solutions for various thermal conditions.[8] The benchmark cases demonstrate the code's capability to calculate the temperature response for objects heated under steady state and transient conditions.[8] In all cases, TACO 2-D calculates temperature results, which are within a few percent of the exact solution.

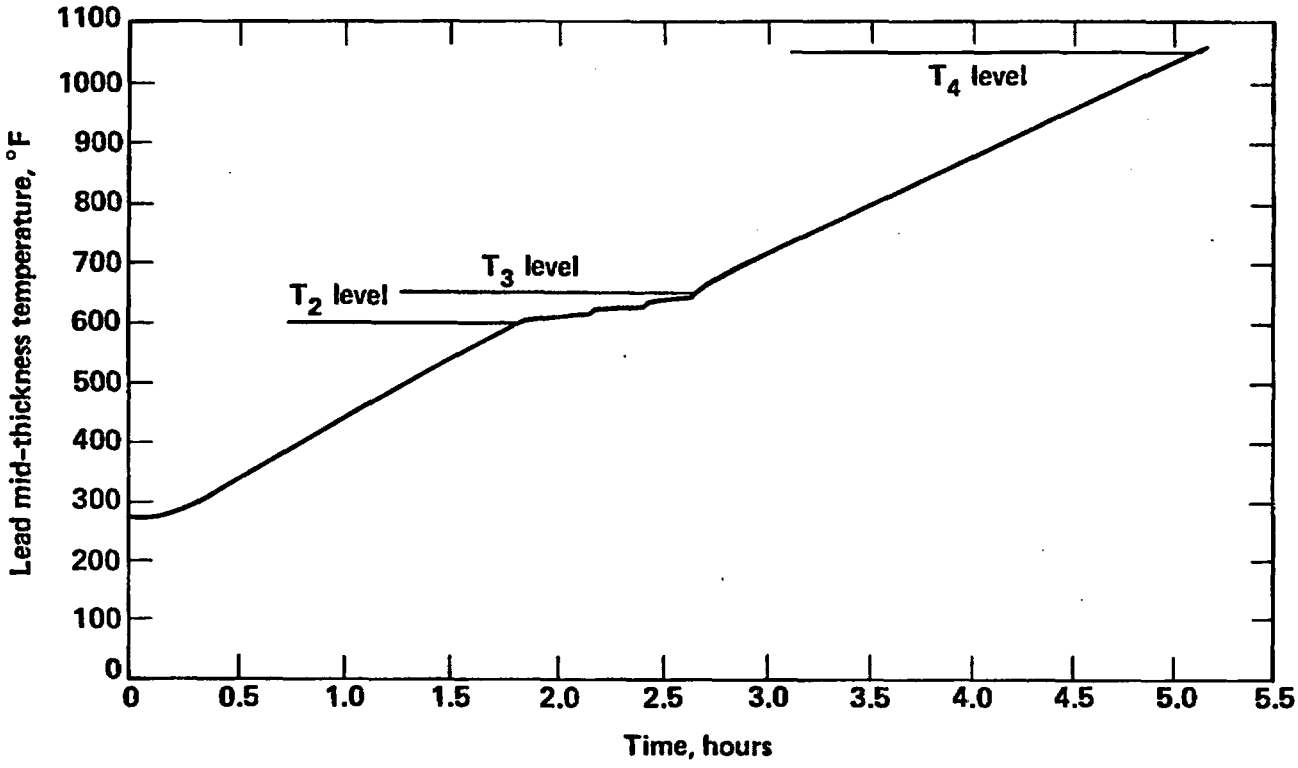

Figure 7-9 Representative rail cask temperature response to a hypothetical 1475°F (equivalent to a real 1700°F) fire versus fire duration.

In 1978, the SNL used similar computer codes to analyze temperatures from a test involving a spent fuel cask suspended over a pit filled with burning jet fuel.[9,10] Under these test conditions, the temperature measurement instruments and the code predictions showed that the environment in a real fire varies significantly along the length of the cask and as a function of time. The thermal flux varies with the wind and ventilation conditions surrounding the cask. Sandia concluded that the regulatory thermal test conditions (1475°F hypothetical engulfing fire) are equivalent to a real engulfing fire with much higher flame temperatures.

Both the benchmark computer code calculations and the Sandia fire test support the use of computer code modeling to evaluate the temperature response of a cask to a real fire accident. In this study, conservative modeling techniques are introduced to simplify the cask response evaluation over a wide range of fire accident conditions. A 1-D model of a hypothetical engulfing fire with a nominal flame temperature of 1475°F is used in lieu of a 2-D model with variable flame temperatures. In addition, no inclusion of heat loss with cask location is considered. These modeling assumptions overpredict the cask temperature response to fires. In addition, casks that use shielding material other than lead cannot incur damage due to melting.

7.4 Accident Screening Analysis

Section 5.0 discusses how the detailed probabilistic calculations are performed by the (Transportation Accident Scenario Probabilities) TASP code in the accident screening analysis. The fraction of accidents calculated by the TASP code is summarized in Figs. 7-10 and 7-11 respectively for the truck and train accidents for each response region. Assuming that an accident occurs, the percentage of both truck and train accidents within the 2% strain (S_2) and 600°F temperature (T_2) levels is about 99.8%. Fewer than 0.001% of truck accidents and 0.013% of rail accidents fall outside of the 30% strain (S_3) and 1050°F temperature (T_4) levels for which the cask structural and thermal analyses are performed.

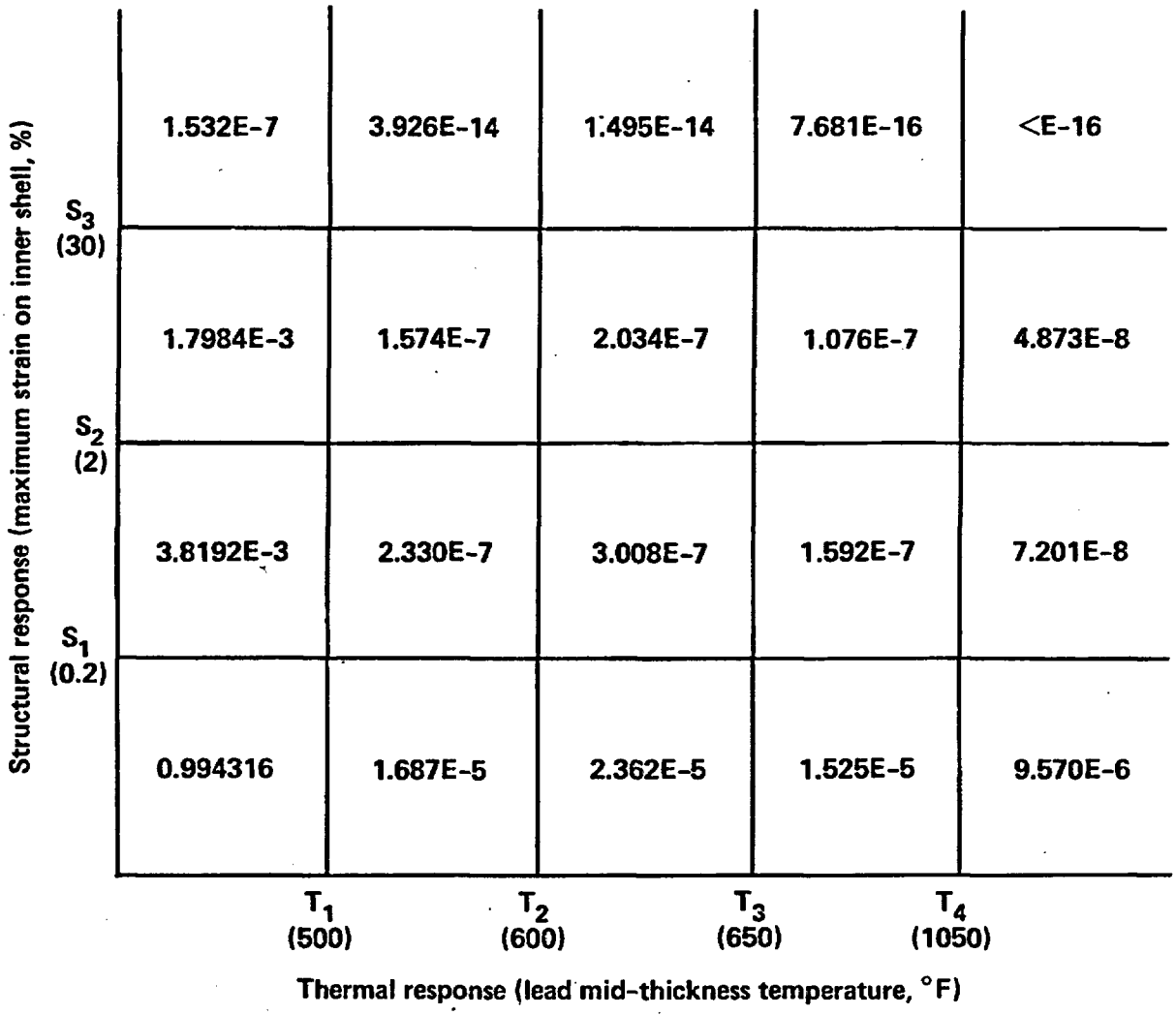

Note:
$E + x = 10^x$

Figure 7-10 Fraction of truck accidents that could result in responses within each response region, assuming an accident occurs.

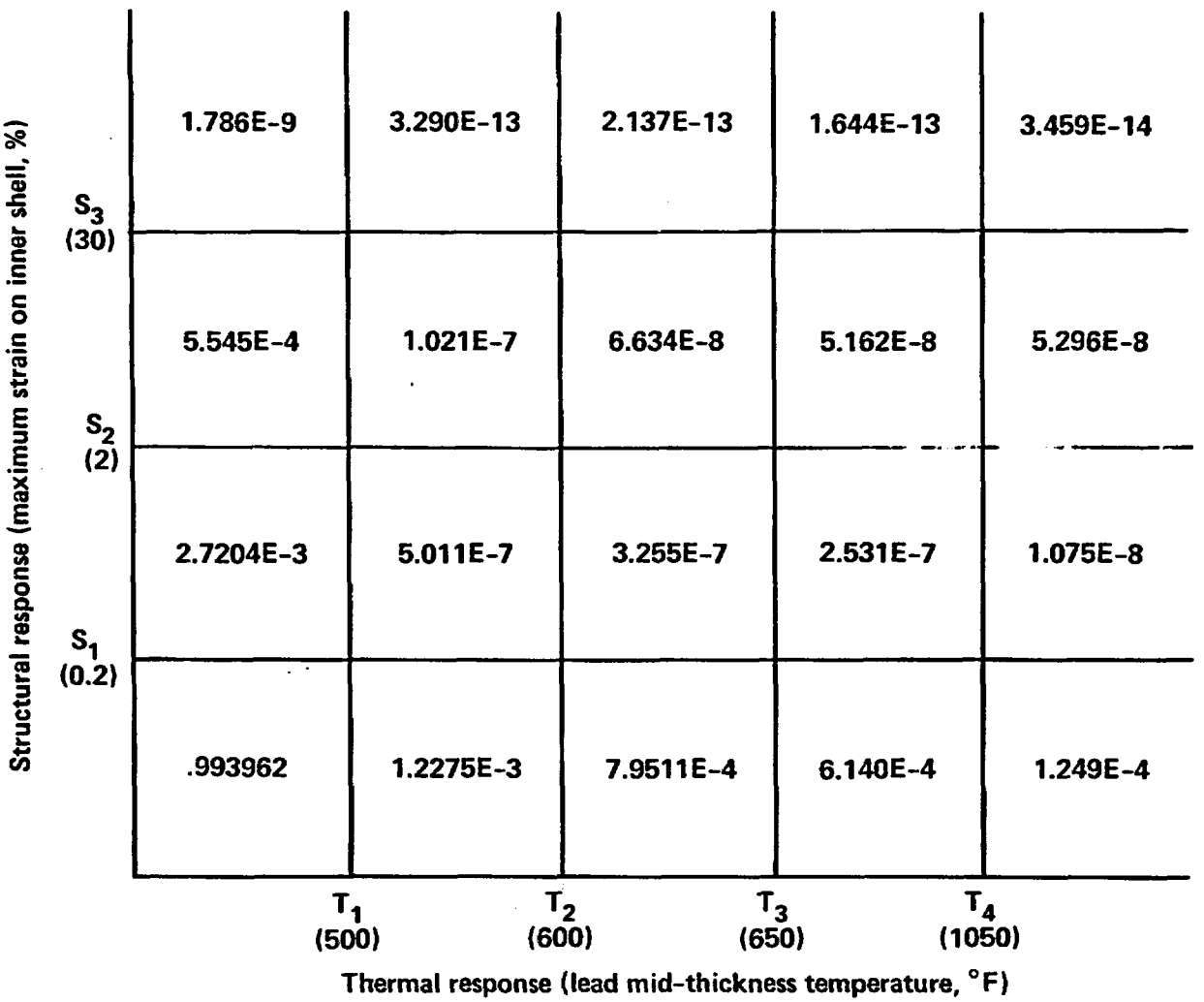

Note:
$E + x = 10^x$

Figure 7-11 Fraction of rail accidents that could result in responses within each response region, assuming an accident occurs.

The significance of these screening results is discussed in detail in Section 9.0 with respect to the existing regulatory requirements and the risk evaluations performed in NUREG-0170.[11]

8.0 POTENTIAL RADIOLOGICAL SIGNIFICANCE OF TRANSPORTATION ACCIDENTS

8.1 Introduction

The purpose of this section is to estimate the potential radiological hazards of various classes of transportation accidents involving a spent fuel shipment. Any significant radioactive material release or increase in the radiation levels from a cask following an accident will originate with the spent fuel. As the cask damage and response increase, the radiation hazard will also increase.

In the previous section, the specific levels of damage that a cask might experience in transportation accidents are categorized in terms of cask response regions. In this section, the potential radiological hazards from accident effects are estimated for each cask response region in terms of: (1) releases of spent fuel material, and (2) levels of radiation from the cask contents. Comparisons are then made in Section 9.0 with the release and radiation limits defined in 10 CFR 71[1] and the radiological risk estimates evaluated in the NUREG-0170, "Final Environmental Statement on the Transportation of Radioactive Material by Air and other Modes".[2]

8.2 Description of Spent Fuel

The characteristics of spent fuel strongly influences the potential radiological hazards of transportation accidents involving shipment. The level of radioactivity and the heat generated within the spent fuel depend on the amount of fission energy extracted from the fuel during its use in a power reactor. However, after the fuel is removed from the reactor, the total radioactivity decays or drops about 80 fold within 1 year and about 340 fold within 5 years. The radioactivity and thermal power in the spent fuel is produced, for the most part, by decay of radioactive isotopes residing within the solid fuel pellets. However, a small amount of gaseous and volatile radioactive material also migrates from the fuel pellets to the fuel rod gap. The radioactive inventory and thermal power of a typical spent fuel assembly is shown in Table 8.1 as a function of decay time.[3] The table

Table 8.1
PWR Fuel Assembly Decay Heat and Radioactivity[a/]

Radioisotopes	Radioactivity (Ci) Decay Time (years) 1	5	10
^{60}Co [b/]	3.57×10^{1}	2.11×10^{1}	1.09×10^{1}
^{85}Kr	3.99×10^{3}	3.08×10^{3}	2.23×10^{3}
^{90}Sr	3.42×10^{4}	3.10×10^{4}	2.75×10^{4}
^{90}Y	3.41×10^{4}	3.09×10^{4}	2.73×10^{4}
^{106}Ru	1.21×10^{5}	7.79×10^{3}	2.52×10^{2}
^{129}I	1.48×10^{-2}	1.48×10^{-2}	1.48×10^{-2}
^{134}Cs	1.00×10^{5}	2.60×10^{4}	4.85×10^{3}
^{137}Cs	4.73×10^{4}	4.32×10^{4}	3.85×10^{4}
^{137m}Ba	4.47×10^{4}	4.07×10^{4}	3.62×10^{4}
^{144}Ce	2.19×10^{5}	6.86×10^{3}	9.01×10^{1}
^{238}Pu	1.46×10^{3}	1.41×10^{3}	1.36×10^{3}
^{239}Pu	1.67×10^{2}	1.67×10^{2}	1.67×10^{2}
^{240}Pu	$2.06 \times 10^{2}2$	2.06×10^{2}	2.06×10^{2}
^{241}Pu	6.64×10^{4}	5.49×10^{4}	4.32×10^{4}
^{244}Cm	9.72×10^{2}	8.34×10^{2}	6.90×10^{2}
Total Activity[c/]	1.12×10^{6}	2.66×10^{5}	1.82×10^{5}
Decay Heat, KBtu[c/]	16.42	3.02	1.93

a/ Assumed burnup is 33,000 megawatt-days/metric ton of uranium[3].

b/ The ^{60}Co source is not a direct result of the fission process. It is produced from neutron activation of non-radioactive elements contained in structural materials and appears as crud on the fuel assembly surfaces[4].

c/ Includes all radioisotopes.

Note: Boxed column represents decay heat and radioactivity levels assumed for the fuel in this study.

identifies only the specific isotopes that are important in performing a radioactive release evaluation.

Different fuel assembly designs are used in nuclear power reactors. There are two major types of fuel assemblies used for the two principal reactor design concepts currently operating in this country--pressurized water reactors (PWRs) and boiling water reactors (BWRs). For purposes of this study, a typical PWR fuel assembly, shown in Fig. 8-1, is considered most representative for the following reasons. First, this assembly is most prevalent and typically contains the highest levels of radioactivity. Second, in terms of resistance to transportation accident loads, no significant difference can be identified in the gross structural response of the various fuel assembly designs. Finally, previous studies indicate that PWR fuel rods may be more susceptible to creep rupture than BWR fuel rods if subjected to high temperatures (1200^{o}F) for a long period of time (e.g., $\geq$ 11 hours).[5]

The radioactive inventory of the reference PWR fuel assembly is based on an assumed burnup of 33,000 megawatt-days/metric ton of uranium and a decay time of 5 years. This burnup level is typical of current PWR fuel. Variations in burnup occur and increases in burnup are expected in future reactor operations. The effect of burnup level on the potential radiological significance of transportation accidents will not be large, i.e., less than a factor of 2. The 5-year decay time is selected because the vast majority of all spent fuel shipments, namely those expected to be made to the Federal repository, will have experienced at least this period of decay.[6] Spent fuel with minimum decay times of 4 to 5 months can be shipped in licensed casks; however, such shipments are expected to be rare. The boxed column in Table 8.1 shows the general radioactive characteristics of the spent fuel assembly considered representative for this study.

8.3 Measures of Radiological Significance

The general description of the reference spent fuel assembly, shown in Table 8.1, identifies the radioactivity level in terms of curie content. The curie content is important to radiological significance from two

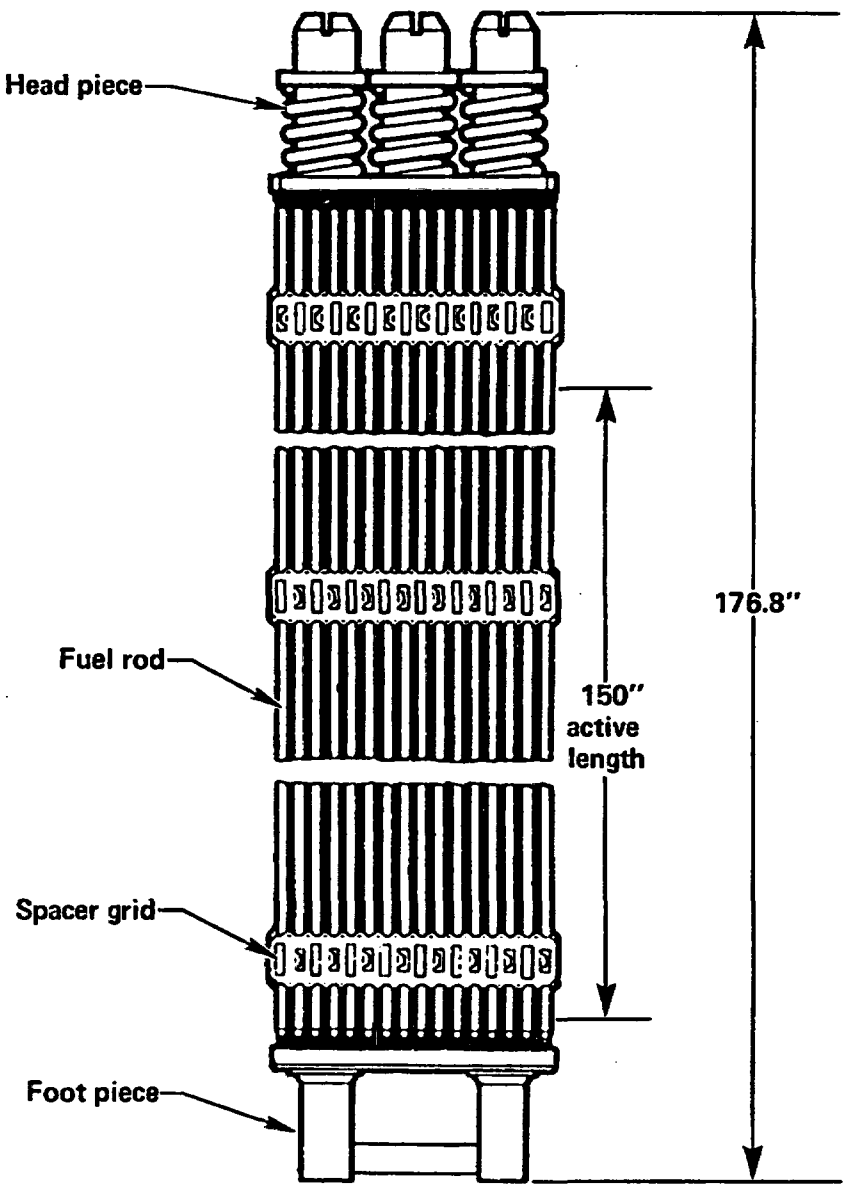

Figure 8-1 PWR fuel bundle.

standpoints. First, the curie content provides a starting point for establishing which isotopes should be evaluated for potential release from the containment barriers provided during the spent fuel shipment. These containment barriers include the fuel pellet itself, the fuel rod cladding, and the cask containment shell. Second, the curie content of each isotope indicates the magnitude of the radioactive source for determining the direct radiation level.

The potential for release of radioactive material from a cask depends heavily on the physical form of the radioactive material. Certain radioisotopes, such as ^{85}Kr, are in gaseous form. Elements such as cesium, ruthenium, iodine, and their compounds may be volatile at temperatures that can be achieved by the fuel during transportation accidents but will condense to solids at ambient temperatures. However, the vast majority of the radioactive material is in solid and relatively immobile form. The material release estimates made in the next section take into account the physical form of specific isotopes.

The radiological significance of any release is dependent not only on the total radioactivity or number of curies released but also on the hazard posed by a particular isotope. Krypton-85, for example, does not present a significant health hazard. On the other hand, particles of plutonium can be extremely hazardous. The potential radiological hazard of a particular radioisotope is implied by the release limits specified in 10 CFR 71. The 10 CFR 71 release limits for the radioisotopes of interest are listed in Table 8.2. The relative hazards of any two radioisotopes are roughly estimated by comparing their release limits. For example, the release limits for ^{85}Kr and ^{134}Cs are 10,000 and 10 curies, respectively; therefore, ^{134}Cs releases, on a radioactivity basis, are approximately 1,000 times as hazardous as ^{85}Kr. This report differs from other reports[2,7-10] in that it does not include detailed discussion of the radiological consequences or public health impacts created by the release of specific isotopes. Rather, the releases associated with each cask response region are compared to those releases estimated in NUREG-0170.[2] Each cask response region, therefore, requires a separate estimate of the release of gaseous, volatile, and solid radioactivity

Table 8.2
10 CFR 71 Release Limits for Radioisotopes

Radioisotope	Release Limit (Ci)
^{60}Co	7
^{85}Kr	10,000
^{90}Sr	0.4
^{90}Y	10
^{106}Ru	7
^{129}I	2
^{134}Cs	10
^{137}Cs	10
^{137m}Ba	40
^{144}Ce	7
^{238}Pu	0.003
^{237}Pu	0.002
^{240}Pu	0.002
^{241}Pu	0.1
^{244}Cm	0.01

from the shipping cask to the environment. Section 9.0 uses the results of NUREG-0170 to relate the release magnitudes to potential public health impacts which can be associated with these releases.[2]

The radiological significance of the direct radiation emanating from a cask as a result of shield degradation is typically controlled by those isotopes emitting high energy gamma rays. The potential for direct radiation exposure is presented for each cask response region in terms of an equivalent unshielded spent fuel radioactivity. This radioactivity represents the amount of material which, if no shielding were present, will lead to external radiation levels equal to those resulting from the calculated degradation in shielding associated with a specific cask response region.

8.4 Estimates of Radiological Hazards

8.4.1 Potential Radioactive Material Releases to the Environment

The potential for release of radioactive material to the environment from a spent fuel shipment requires consideration of three mechanisms for establishing a release path. These mechanisms are shown schematically in Fig. 8-2.

Under normal conditions, certain radioactive material contained in the ceramic fuel matrix migrates to the fuel rod gap. The migration involves radioactive gas and vapors formed during the fission process in the reactor. Since the claddings of most of the fuel rods are intact before the fuel is shipped, this cladding must be breached during transport before radioactive material is released into the cask cavity. A fuel rod's cladding can be breached by high impact forces or high thermal loads. The number of rods breached by mechanical forces is estimated by considering the rod responses over the range of impact forces that the cask might experience in a transportation accident. End-on impact is conservatively assumed since the almost 15-foot-long (0.4 inch diameter) rods are most susceptible to breaching by buckling. Figure 8-3 shows the percentage of fuel rods breached due to end-on impacts as a function of impact force on a cask.

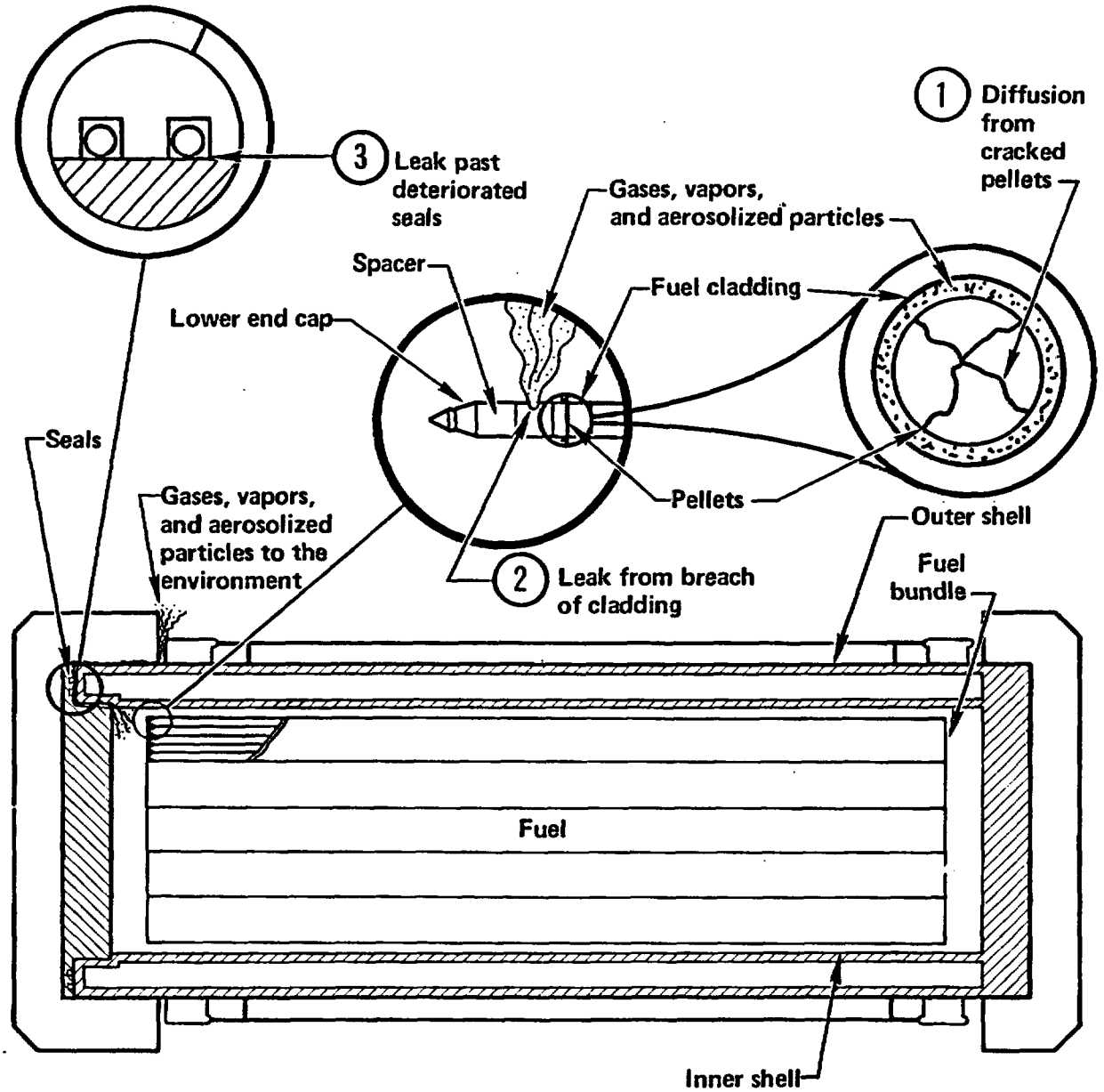

Figure 8-2 Three mechanisms required to establish a radioactive material release path.

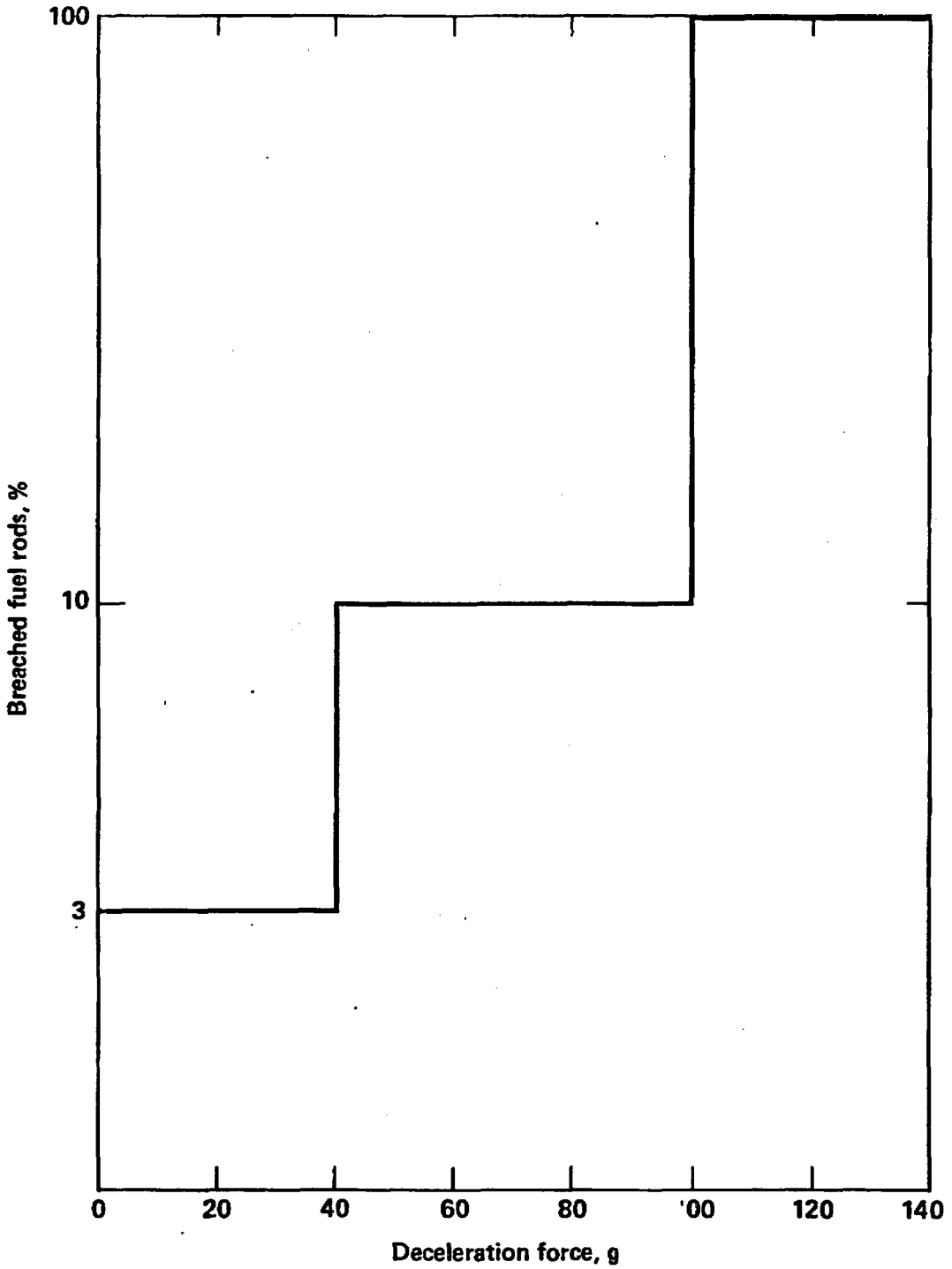

Figure 8-3 Percentage of fuel rods breached as a function of force for endwise impacts.

Cask impact forces are related to forces on the fuel rods necessary to achieve 0.2% (S_1), 2% (S_2), and 30% (S_3) maximum effective strain on the inner containment shell of the cask. Three percent of the rods are assumed to be breached if the cask containment shell experiences maximum effective strains equal to or less than 0.2% (S_1). Similarly, 10% of the rods are assumed to be breached for any transportation accident situation in which the containment shell experiences between 0.2% (S_1) and 2% (S_2) effective strain. Beyond 2% (S_2) effective strain, all rods are presumed to be breached. These results are shown in Fig. 8-4.

Fuel rod cladding response to thermal loads is also evaluated. In transportation accidents involving fires, heat may be absorbed by the cask and its spent fuel contents. The resulting temperature increase of the fuel rod cladding can cause an effect called thermal creep. This effect coupled with pressures generated within the rods can cause a breaching of the cladding. If the cask temperature level is 650°F (T_3) or less at the mid-thickness of the lead shield, no breaching is expected to occur because the fuel rod temperatures are too low to cause creep rupture. Beyond this thermal response level, temperatures at the center of the cask and at the center of the fuel assemblies are conservatively estimated to reach values which can breach up to 100% of the fuel rods for both the representative truck and rail casks. The results presented in Fig. 8-4 include response to both mechanical and thermal loads.

If a rod is breached, radioactive gases, volatiles, and solids can potentially escape from the fuel rods into the cask containment. Experimental information indicates that this escape involves three release mechanisms. The first mechanism is associated with the actual breaching of the rod and is referred to as the rod burst phenomenon. Pressure generated inside the fuel rods by both non-radioactive and radioactive gases and vapors cause an ejection of material to occur when the rod is breached. A temperature-controlled diffusion process is the second mechanism. Third, a chemical oxidation process involving the uranium fuel takes place if fuel temperatures exceed 400°F and air enters the cask cavity, thus replacing the normally inert containment vessel atmosphere. This process, which involves a change in the

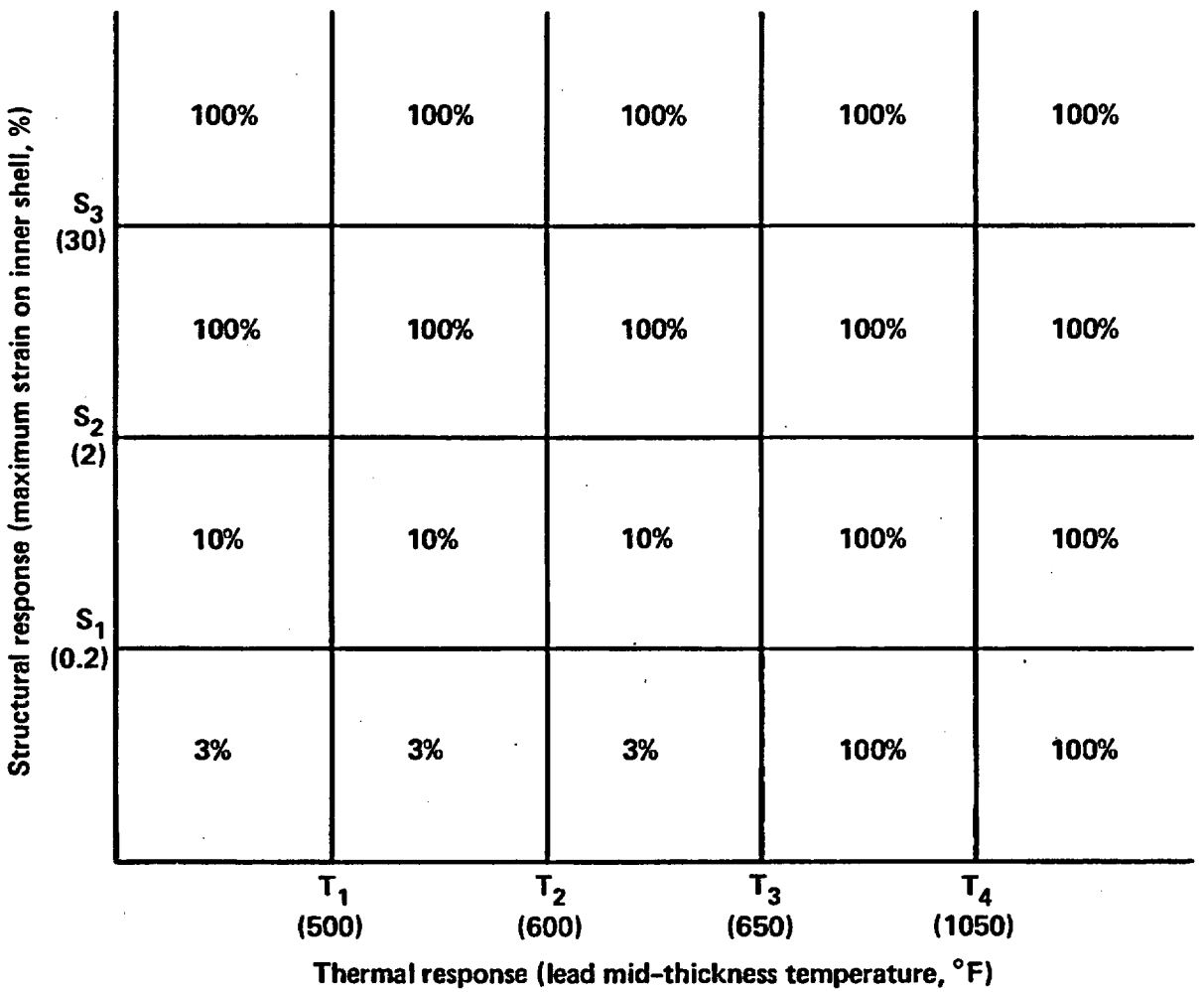

Figure 8-4 Percentage of fuel rods breached per fuel assembly in each cask response region.

chemical form or phase of the uranium oxide, causes further radioactive material releases.

Material release fractions for the significant radioisotopes are estimated using the results of experiments conducted at the Oak Ridge National Laboratories.[11] Table 8.3 summarizes these release fractions for the truck and rail cask response regions. The rod burst and oxidation mechanisms are the dominant mechanisms which control radioactive material release fractions. Thus, only the releases occurring as a result of these mechanisms are tabulated.

Once the radioactive material has entered the cask containment volume, a release to the environment can occur only through a leak or accident-caused breach of the cask containment boundary. Several processes, which are difficult to quantitatively analyze, will be expected to mitigate radioactive material releases. Particles released from the rods will tend to settle within containment without the presence of some driving force to promote their release. Even if such a force exists, particles can become lodged in leak passageways. Vapors released from the fuel rods will be cooled as they move to the cask walls in most accident events, and the vaporous material will tend to plate-out on all cask interior surfaces. These processes are expected to limit essentially all environmental releases to those materials existing in gaseous forms. In this study, however, because of the difficulty in quantifying these processes, any radioactive material released from the fuel rods is presumed to be released from the spent fuel cask if a leak path exists in the containment vessel. This leak path is presumed to exist for any transportation accident event resulting in (1) a maximum strain in the inner containment shell greater than 0.2% (S_1), or (2) lead mid-thickness temperatures exceeding 500^{o}F (T_1).

8.4.2 Potential Radiation Increases from Shielding Reduction

Under accident conditions, a reduction can occur in the radiation shielding provided by the shipping cask. Both neutron and gamma radiation shielding can be affected. Typical cask designs can lose the effectiveness of

Table 8.3
Material Release Fractions from Breached Fuel Rods
Occurring over 1 Week Following Rod Burst[a]

Cask Response Regions	Release Mechanism	Release Fraction to Cask Cavity				
		Gas	Vapors			Particles
		Kr	I	Cs	Ru	
R(1,1)-R(3,1)	Rod Burst	2.0×10^{-1}	3.0×10^{-4}	2×10^{-4}	2.0×10^{-5}	2×10^{-6}
R(1,2)-R(3,2)	Oxidation	1.3×10^{-1}	2.2×10^{-3}	1×10^{-6}	6.7×10^{-6}	0
R(1,3)-R(3,3)		3.3×10^{-1}	2.5×10^{-3}	2×10^{-4}	2.7×10^{-5}	2×10^{-6}
R(1,4)-R(3,4)	Rod Burst	2.0×10^{-1}	3.0×10^{-4}	2.0×10^{-4}	2.0×10^{-5}	2×10^{-6}
	Oxidation	1.7×10^{-1}	4.0×10^{-3}	8.0×10^{-6}	2.8×10^{-5}	0
		3.9×10^{-1}	4.3×10^{-3}	2.0×10^{-4}	4.8×10^{-5}	2×10^{-6}

[a] Approximately the same fractional release for truck and rail cask.

neutron shields and still meet existing standards for allowable external radiation levels. In this study, the neutron shielding is presumed lost in all transportation accidents. Of greater concern is the effectiveness of the gamma radiation shield. This type of shielding is provided by dense materials, with lead being the material of choice in the representative cask designs.

High-impact loads can cause the lead shielding to slump towards the impacting side of the cask, e.g., to the bottom of the cask for the impact orientation illustrated in Fig. 8-5. Shielding voids can be created and, in Fig. 8-5, this void is shown near the top of the cask.

The gamma dose versus lead slump is calculated for the rail cask for endwise impacts. The highest radiation increase occurs when the top of the rail cask impacts a surface and the lead slumps towards the cask closure region. In Table 8.4, the gamma dose is tabulated for various amounts of lead slump as a function of distance from the cask surface to the receptor. The dose from a truck cask with similar amounts of lead slump will be approximately 21 times lower than the rail cask, because the truck cask contains only 1 PWR assembly in comparison to 21 assemblies for the rail cask.

High thermal loads can cause the lead shield to melt and expand. The lead expansion can cause the inner wall of the cask to move inward. Upon cooling, the lead shrinks and creates a void along the length of the cask as illustrated in Fig. 8-6, causing the radiation level external to the cask to increase. As it turns out, thermal loads can cause only minor lead voids and increases in the local radiation.

To provide a consistent measure of radiological effects with cask damage, the radiological hazard created by a gamma shielding reduction is presented in terms of an equivalent inventory of unshielded spent fuel. This amount of spent fuel, if unshielded, will produce radiation levels equivalent to those emanating from the damaged cask. As an example of the calculation process, a transportation accident which leads to 2% maximum effective strain (S_2) in the cask shell is presumed. The measure of the resulting radiation level is calculated through the following steps: (1) the deceleration force necessary

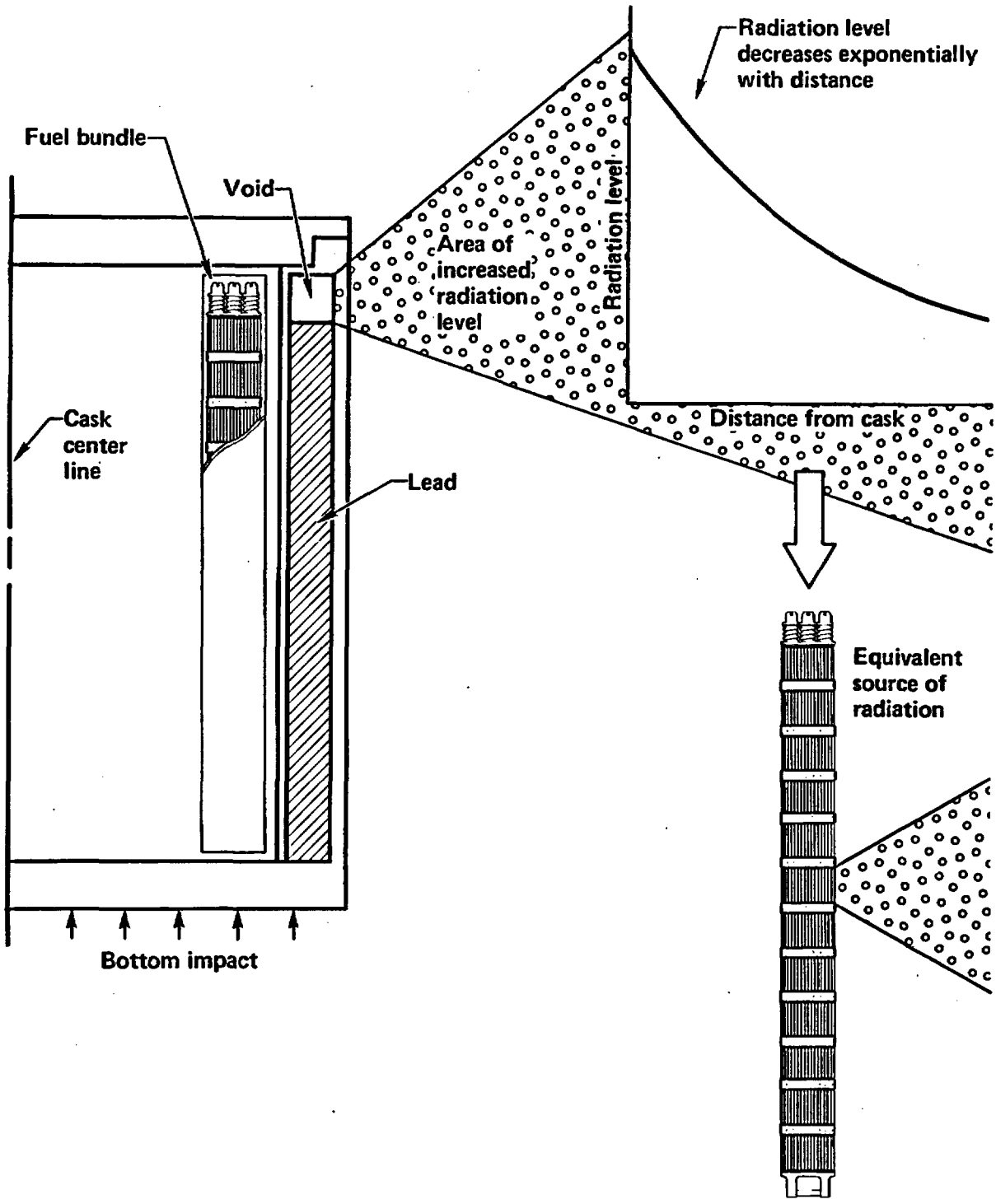

Figure 8-5 Lead voiding due to lead slump resulting from endwise impact of cask

Table 8.4
Gamma Dose Summary for Lead Slump in a Rail Cask[a/]
for Impacts on Closure Region

Gap at Cask Bottom Caused by Lead Slump (inches)	Dose Rate (mrem/hr) Distance from Cask Surface to Receptor (ft)				
	3	10	30	300	3000
5.0	1.02×10^{3}	1.93×10^{2}	2.38×10^{1}	1.65×10^{-1}	8.03×10^{-6}
10.0	8.64×10^{3}	1.30×10^{3}	1.53×10^{2}	9.13×10^{-1}	2.71×10^{-5}
15.0	1.65×10^{4}	2.80×10^{3}	2.88×10^{2}	1.70×10^{0}	4.72×10^{-5}

[a/] Truck cask dose is reduced by approximately the ratio of fuel assemblies or a factor of 21.

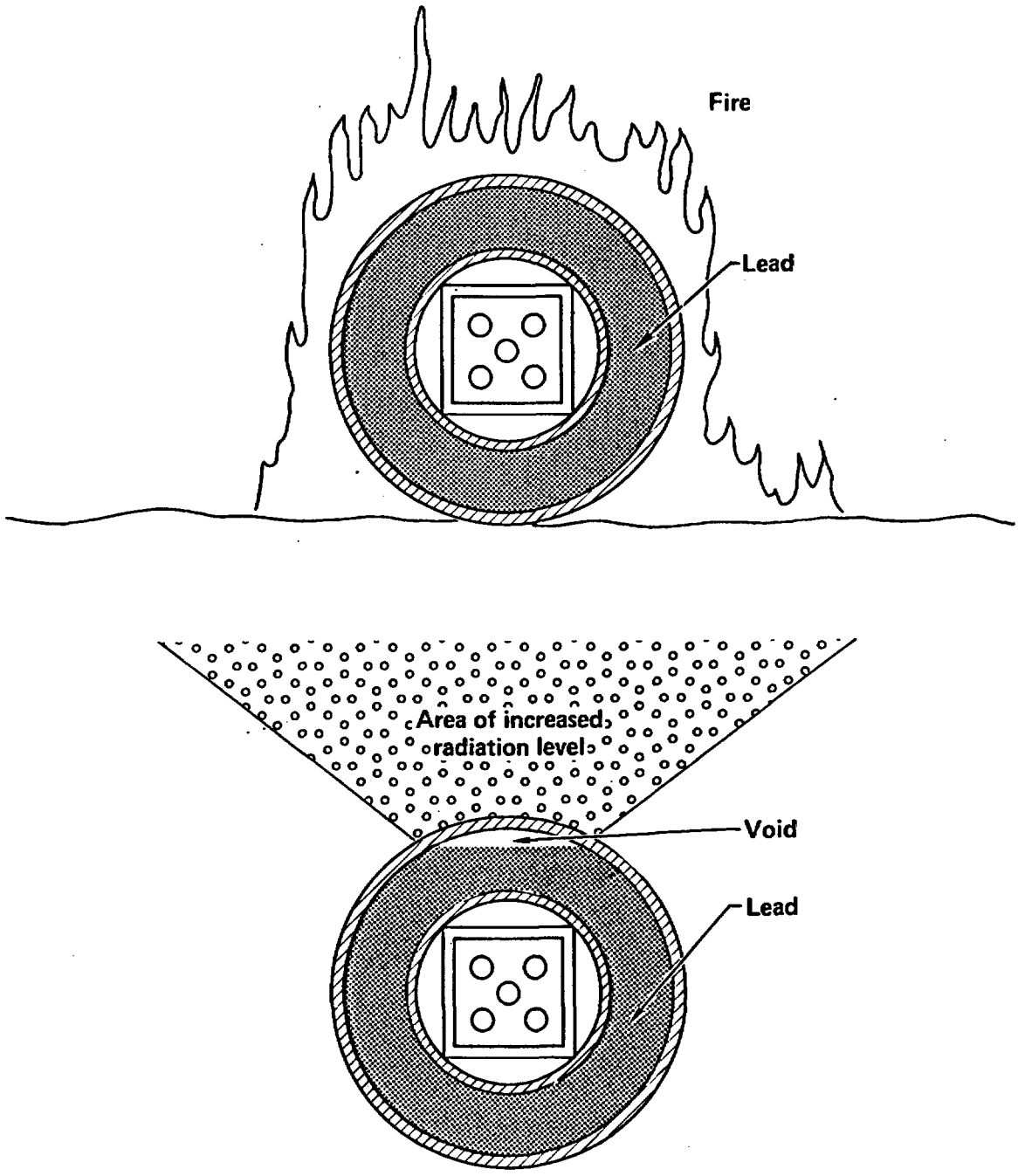

Figure 8-6 Lead voiding due to high thermal loads and lead melting.

to achieve the 2% maximum effective strain (S_2) level is determined, (2) the lead slump level caused by this deceleration force is evaluated, (3) the radiation level resulting from the lead slump is calculated, and (4) the amount of unshielded spent fuel contents which will result in equivalent radiation levels is determined.

8.5 Radiological Effect Estimates for Response Regions

The preceding evaluation provides the information necessary to estimate the radiological effects in each response region. The measures involve four parameters that can result in radiological hazards. The first three relate to potential releases of radioactive material from the cask to the environment, expressed in curies, and include: (1) the amount of radioactive gases, (2) the amount of volatiles (isotopes weighted for health hazards), and (3) the amount of solids (isotopes weighted for health hazards). The fourth measure relates to the potential for increased external cask radiation levels occurring as a result of losses or degradations in the cask shielding capabilities. This measure is the equivalent amount of the total spent fuel contents which, without shielding, will produce the calculated level of external cask radiation. These measures are shown in Figs. 8-7 and 8-8 and indicate the four types of radiological hazards estimated for the truck and rail cask response regions.

Radiological hazards beyond the 30% strain (S_3) and 1050°F temperature (T_4) levels are not calculated. They are assigned values 10 times those for region R(3,4) except for ^{85}Kr gas. The values assigned for ^{85}Kr gas are 1.62 times the region R(3,4) values because a high percentage of the gas is already released for states in the R(3,4) region.

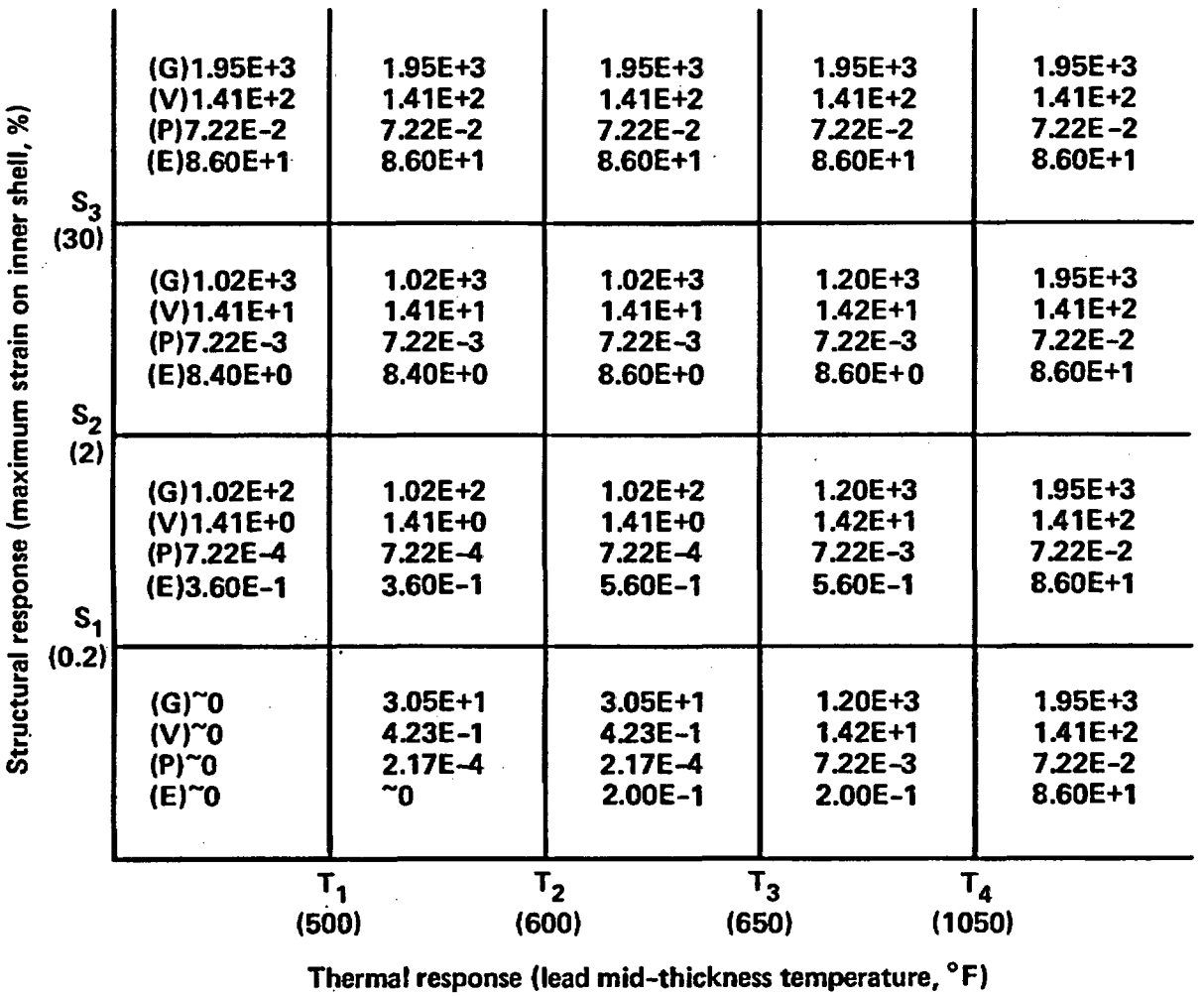

(G)=Noble gases, curies
(V)=Vapors, curies
(P)=Particles, curies
(E)=Exposure, curies

$E+x=10^x$

Figure 8-7 Radiological hazards estimated for response regions for a representative truck cask.

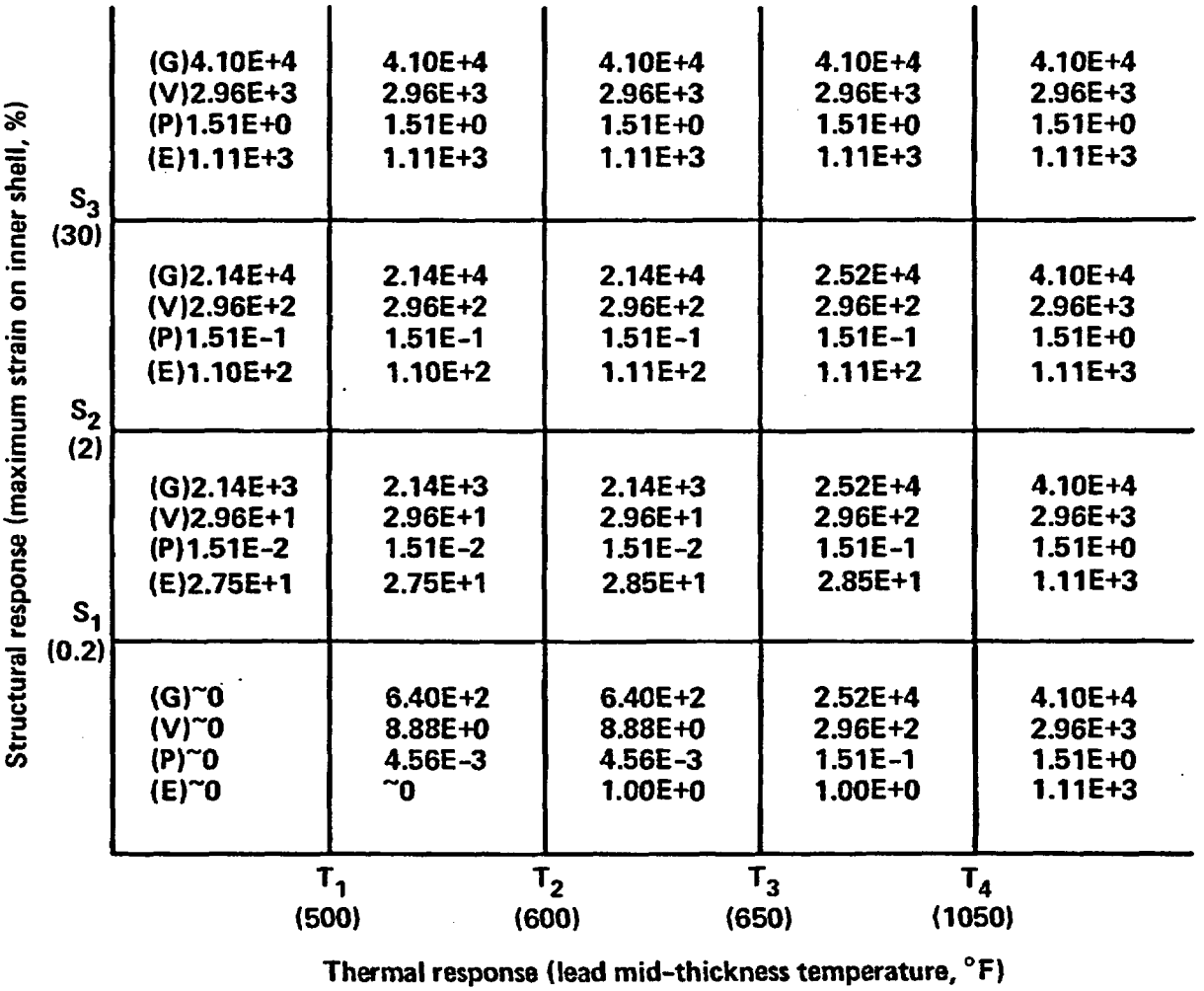

(G)=Noble gases, curies
(V)=Vapors, curies
(P)=Particles, curies
(E)=Exposure, curies
E+x=10^x

Figure 8-8 Radiological hazards estimated for response regions for a representative rail cask.

9.0 RESULTS AND CONCLUSIONS

9.1 Introduction

In previous sections, a detailed evaluation is made of how spent fuel casks designed to current regulations would respond in railway and highway accident environments. The loading conditions that could conceivably affect the response of a spent fuel cask are determined from surveys of accident records. The responses of the representative truck and rail casks to a wide variety of accident conditions are calculated and categorized into 20 cask response regions. These response regions define specific levels of damage that could be experienced by the cask during an accident. The boundaries of these regions are defined in terms of structural strain experienced by the cask containment shell and by material temperatures attained within the cask's lead shield. The potential for radioactive material releases or increased levels of external radiation are estimated for each of the 20 response regions for both the representative truck and rail casks.

The first response region is defined by structural and thermal response limits which would be within acceptable bounds implied by current regulations.[1] A major objective of this study is to determine the fraction of accidents causing responses within this region. This process is called the first-stage screening. For accidents which cause responses outside this region, a second-stage screening is conducted. This screening involves calculating cask responses to a wide variety of accident conditions and subsequently classifying the responses into the remaining 19 response regions. The expected fraction of transportation accidents resulting in responses in each region is then determined based on historical accident data using probabilistic analysis.

In Section 9.2 the results of both the first- and second-stage screenings are discussed. These results are compared with estimates made in the "Final Environmental Statement on the Transportation of Radioactive Material by Air or other Modes", NUREG-0170.[2] Several historical accidents are also categorized into response regions in order to provide a perspective on the

meaning of severe accidents as used in this study. Uncertainties in the study are discussed in Section 9.3. Conclusions and recommendations are provided in Section 9.4.

9.2 Results

9.2.1 First-Stage Screening

In the first-stage screening, accidents are characterized which will result in spent fuel cask responses that fall within the R(1,1) response region. Within the R(1,1) region, the cask structural response is elastic, and the strain on the inner shell of the cask does not exceed 0.2% (S_1). The cask thermal response does not exceed 500°F (T_1) at the middle of the lead shield thickness. Cask responses within the R(1,1) region are typically less than the response generated on real casks by the accident test conditions specified in 10 CFR 71.[1] Accidents which produce loading conditions that result in cask responses in the R(1,1) region do not result in significant damage to a spent fuel cask; therefore, no radiological significance is associated with these accident events.

Over 99.43% of all highway accidents result in a cask structural response falling within the 0.2% strain (S_1) level. Making up the largest algebraic segment are the 94.7% of highway accidents which involve minor mechanical loads resulting from rollovers of the transporting vehicle or impacts with low-resistance objects. The remaining 5.3% of highway accidents have the potential for generating significant loads, e.g., impacts with bridge columns, abutments, or trains. The cask response to these potentially significant accidents is dynamically evaluated. The calculations consider variations in the impact velocity, the cask orientation, and the hardness of the object struck. When all the factors for mechanical loads are considered, an additional 4.7% of all highway accidents cause responses within the 0.2% strain (S_1) level.

A similar evaluation is performed for railway accidents. The results indicate that over 99.67% of railway accidents cause structural responses not

exceeding 0.2% strain (S_1) on the inner shell of the cask. As with truck accidents, a large percentage (96.1%) of railway accidents are minor and would not cause any significant cask damage.

The thermal loadings from accidents involving fires are analyzed to determine the response of the truck and rail casks. The evaluations consider the effects of fire duration, flame temperature, and cask location relative to the fire. Given a fire accident, 99.97% of the truck and 99.04% of the train accidents will generate heat loads on the casks less than those that can occur for a half-hour regulatory 1475°F engulfing fire. However, as calculated in Section 6.3, a half-hour regulatory 1475°F engulfing fire can only heat the massive truck and rail casks to lead mid-thickness temperatures of 280°F and 320°F, respectively, which are well below the 500°F temperature (T_1) level where radiological hazards could be generated. Therefore, the fire must burn longer than one half-hour to reach the 500°F temperature (T_1) level and consequently, a higher percentage of accidents is included. For the truck cask, 99.99% or more of the accidents involving fire result in a lead mid-thickness temperature not exceeding 500°F (T1). For the rail cask, 99.72% or more of the accidents involving fire result in temperature responses falling within similar bounds.

The number of all accidents that included either mechanical or thermal loads or both is estimated. These estimates are used to determine the percentage of all highway and railway accidents causing cask responses within the R(1,1) region. For the representative truck and rail casks, 99.43% and 99.40%, respectively, of the highway and railway accidents are estimated to cause cask responses within the R(1,1) region as shown in Figs. 7-10 and 7-11. In those areas when the thermal load is expected not to exceed the regulatory 1475°F engulfing fire, the percentage of accident conditions within the 10 CFR 71 mechanical and thermal loading conditions is 99.41% for the truck cask and 98.70% for the rail cask.

The structural and thermal responses within the R(1,1) response region are evaluated with standard engineering methods of analysis. The structural response limit for this region is selected such that the inner shell of the representative cask will behave elastically and will experience no permanent deformations. The thermal response limit is selected such that no thermal

degradation will occur to the seals or other parts of the cask. Responses within these bounds will be within limits typically accepted when casks are subjected to the regulatory accident test conditions. At this level of cask damage, the radiological hazards are negligible and less than the 10 CFR 71 limits for radioactive material releases or for external radiation levels.

9.2.2 Second-Stage Screening

In the second-stage screening, accidents causing cask responses greater than the 0.2% strain (S_1) and 500°F temperature (T_1) levels are evaluated. At these higher levels of cask response, the potential exists for radioactive material releases and external radiation levels equal to or greater than the regulatory limits specified in 10 CFR 71. The highway and railway accident loading conditions not eliminated by the first-stage screening are included. A cask can be struck by a moving train or can fall off a bridge, plunge over an embankment, run into a slope, or strike a massive concrete structure. The thermal events include accidents involving high-temperature, long-duration, engulfing fires that can cause high ($\geq$ 500°F) temperature responses.

The second-stage screening considers response outside the R(1,1) region as shown in Fig. 9-1. The fraction of accidents having cask responses within each of these individual regions is summarized in Figs. 7-10 and 7-11 for the truck and rail casks, respectively.

In most cases, the radiological hazard associated with accidents in the response regions immediately adjacent to R(1,1) is limited and can be negligible. The rationale for this judgment is that 2% strain (S_2) will not cause extensive structural damage to the cask containment, and temperatures up to 600°F (T_2) will not significantly degrade shield or seal materials currently in use. For accidents causing cask responses within regions R(1,2), R(2,2), and R(2,1), the occurrence of even a limited radiological hazard will be dependent on the actual cask design, the amount of fuel being shipped, and the specifics of the accident--especially with respect to how mechanical and thermal loads are applied to the cask. In this study, the radiological hazards estimated for these three regions are based on the performance of the

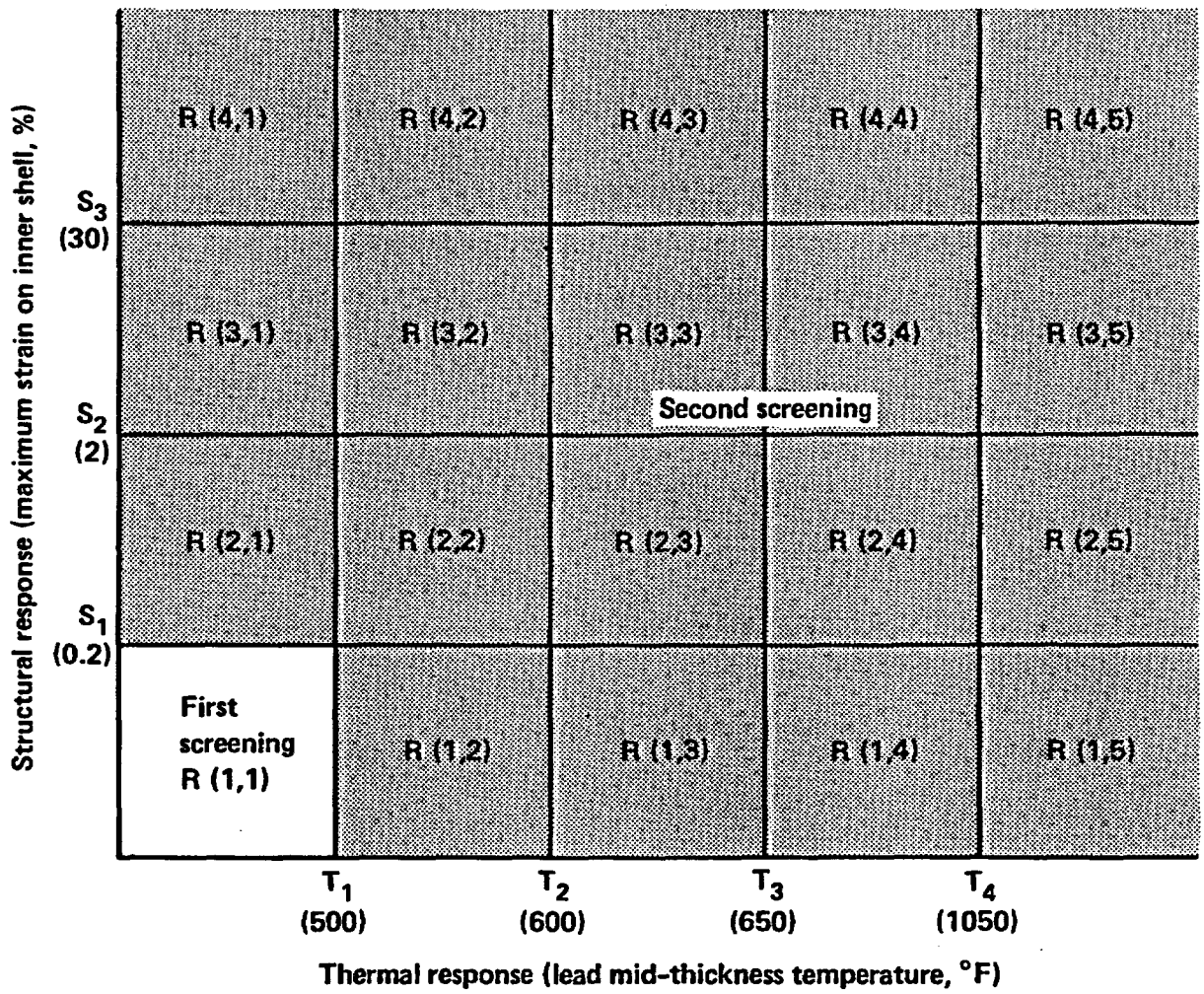

Note:
- First-stage screening radiological hazards are negligible and less than 10 CFR 71 limits.
- Second-stage screening radiological hazards can be equal to or greater than 10 CFR 71 limits.

Figure 9-1 · Two-stage screening process in the 20 response regions.

representative truck and rail casks. The estimated radioactive material releases and radiation levels are then compared with the regulatory limits applicable to casks which have been subjected to the accident test conditions.

The result of this comparison indicates that the estimated radioactive material releases and radiation levels are generally lower than the regulatory limits as specified in 10 CFR 71. Compared with the representative truck and rail cask designs, most existing cask designs can withstand higher mechanical and thermal loads without significant damage. Approximately 0.39% of highway and railway accidents that could involve spent fuel casks could result in radiological hazards approaching or slightly exceeding those implied by regulatory limits. The stated percentages of accidents are those which produce cask responses less than the 2% strain (S_2) and 600°F temperature (T_2) levels and represent the sum of the percentages determined by regions R(1,1), R(2,1), R(1,2) and R(2,2).

Cask responses between the 2% (S_2) and 30% (S_3) strain levels and between the 600°F (T_2) and 1050°F (T_4) temperature levels indicate both the possibility of significant, permanent deformation to the cask structure and melting of the lead shield. The radiological hazard associated with this degree of cask damage, will likely exceed the hazard implied by the regulatory limits as specified in 10 CFR 71. Less than 0.001% of the truck shipment accidents and 0.012% of the rail shipment accidents are estimated to cause strains beyond 30% (S_3) and temperatures beyond 1050°F (T_4) in the casks.

9.2.3 Comparison with Previous Risk Assessments: NUREG-0170

In the second-stage screening, accidents are identified in which the mechanical and thermal loading conditions on a cask can result in radioactive releases beyond the regulatory limits. To assess the radiological risk of these potential releases, a comparison is made between the probabilities of specific radiological hazards calculated in this study and similar estimates made in NUREG-0170.

The NUREG-0170 assessment indicates that the risk involved in spent fuel shipments is small. This conclusion provided part of the technical

justification necessary for the Nuclear Regulatory Commission (NRC) to make the judgment that the existing 10 CFR 71 regulations are adequate and not in need of immediate change.

The comparison with NUREG-0170 begins by establishing the probability of occurrence for accidents that can result in spent fuel cask responses in each of the 20 regions; that is, the probabilities presented in Figs. 7-10 and 7-11. The probabilities are multiplied by the radiological hazards applicable to each region, which are presented in Figs. 8-7 and 8-8. This product is called a probability-hazard estimate. These probability-hazard estimates are calculated for each of the three types of radioactive material releases assessed in Section 8.0 (gas, vapor, and particle) and the cask external radiation levels.

Figure 9-2 shows the truck cask probability-hazard estimates for each of the 20 response regions. Estimates are given for the releases of radioactive gases (^{85}Kr), radioactive vapors which include $^{134,137}Cs$ and ^{106}Ru, and radioactive solid particles which include $^{238,239,240,241}Pu$. The bottom estimate in each region applies to the external radiation level. This process provides numerical values which can be used for comparison. For instance, the maximum values calculated for these probability-hazard estimates occurs in region R(3,1). This region typically includes accidents involving high-velocity impacts which cause cask containment strain levels between 2% (S_2) and 30% (S_3) and a lead mid-thickness temperature of less than 500°F (T_1).

Figure 9-3 presents similar probability-hazard estimates for spent fuel shipments made by rail. For rail shipments, region R(1,5) has the maximum estimates with the single exception of radioactive gas release. Region R(1,5) includes accidents involving hot, long-duration fires resulting in lead mid-thickness temperatures beyond 1050°F (T_4). The region which has the highest radioactive gas release is R(1,4). The consequence of radioactive gas release, however, is extremely small in comparison to the significance implied by the other hazards.

The calculational methods and presentation of results in NUREG-0170 differ from those used in this study. In the NUREG-0170 evaluation, accident

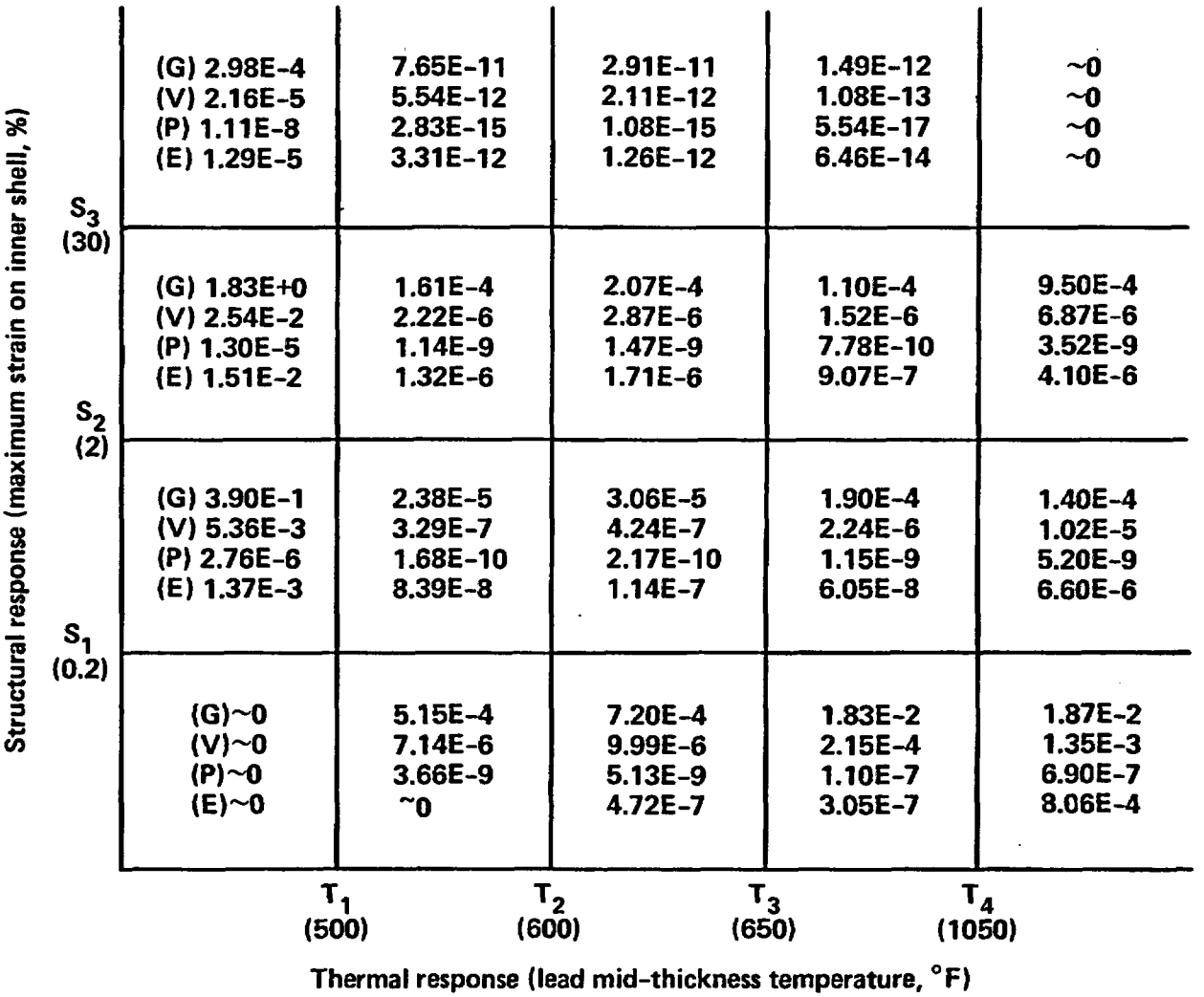

(G) = Noble gases, curies
(V) = Vapors, curies
(P) = Particles, curies
(E) = Exposure, curies

$E + x = 10^x$

Figure 9-2 Probability-hazard estimates in curies for the 20 truck cask response regions.

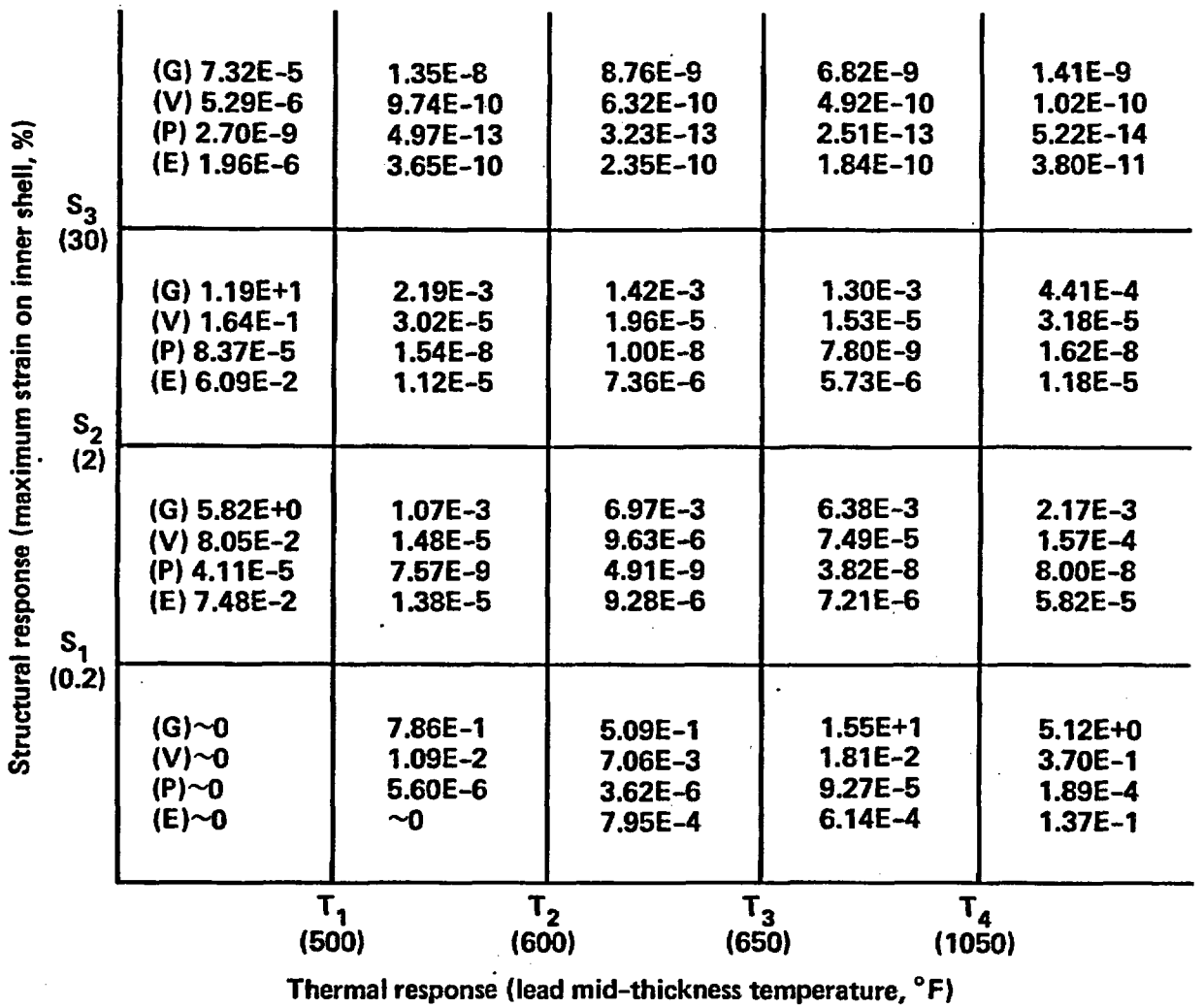

(G) = Noble gases, curies
(V) = Vapors, curies
(P) = Particles, curies
(E) = Exposure, curies (equivalent)

$E + x = 10^x$

Figure 9-3 Probability-hazard estimates in curies for the 20 rail cask response regions.

probability estimates, radioactive release fractions, and radiation levels were classified into eight categories of accident severity. The classification process was accomplished, in large part, through the use of conservative engineering judgments. The first two accident categories in NUREG-0170 were defined to include accidents with severities and radiological hazards less than the 10 CFR 71 hypothetical accident conditions and release limits. These two accident categories generally correspond to accidents causing responses within the R(1,1) region defined in this study. There is no direct correspondence between the other 6 NUREG-0170 categories and the remaining 19 response regions in this study. Therefore, only two direct comparisons can be made with NUREG-0170. The first involves a comparison of the fraction of transportation accidents which generate cask responses that cause no significant radiological hazards. The second point of comparison involves the average radiological risk calculated in this report and the average radiological risk estimate given in NUREG-0170.

In this study, the estimated percentage of accidents within region R(1,1) is 99.4% for both truck and rail shipments. The radiological significance of accidents involving R(1,1) cask responses is negligible. As a result, the estimated percentages of accidents that could create a radiological hazard to the public are 0.6% for both truck and rail shipments.

In contrast, the percentages of accidents estimated in NUREG-0170 to result in negligible radiological hazard is 91% for truck shipments and 80% for rail shipments. By subtraction, the estimated percentage of accidents that could result in radioactive releases is 9% for truck shipment and 20% for rail shipment. In comparing the estimated percentage of accidents that could have a radiological significance, the more detailed estimates in this study indicate that significantly fewer accidents are of radiological concern.

The second comparison between this study and NUREG-0170 essentially involves measures of radiological risk, given that an accident occurs. In this study, such a measure can be obtained by summing the probability-hazard values for all of the 20 response regions. The summation is performed for gas, vapor, and particle releases and for direct radiation level effects.

The components of the summation are shown for each type of release listed in Figs. 9-2 and 9-3. The same calculational method is used in summing the probability-hazard estimates for the eight accident categories in NUREG-0170. Since NUREG-0170 did not evaluate particle releases, a direct comparison is not possible. The comparative measures of radiological risk/accident from both studies are presented in Tables 9.1 and 9.2 for truck and rail shipments of spent fuel, respectively.

The expected gas, vapor, and direct radiation risks/accident in this study for truck shipment are at least 3 times lower than those documented in NUREG-0170. The estimated risk/accident for vapor releases (Cs) is at least 25 times lower in this study than in the NUREG-0170 evaluation. If radioactive particle releases are not considered, it is the vapor release that dominates the public health hazard.

In this study, the representative rail cask is designed to carry 21 fuel assemblies compared with 7 fuel assemblies for the rail cask assumed in NUREG-0170. When the differences in the carrying capacities are adjusted for comparison, the gas, vapor, and direct radiation risks/accident estimated in this study for rail shipment are at least 3 times lower than those documented in NUREG-0170. As with truck shipments, risk/accident from vapor releases (Cs) is at least 25 times lower in this study than that in NUREG-0170.

The release of aerosolized radioactive particles is considered in this study but not in NUREG-0170. The release of small quantities of aerosolized particles is important because the radiological hazard associated with particles containing transuranic isotopes such as ^{238}Pu can be 3,330 times higher on a curie-for-curie basis than the hazard from ^{134}Cs or ^{137}Cs. As Figs. 8-7 and 8-8 indicate, the estimated curie release of particles is about a factor of 1,950 less than the release of cesium vapors.

Further perspective on the significance of the particle releases predicted in this study can be gained by recalling that the cesium releases/accident in this study are at least a factor of 25 less than those that were predicted in NUREG-0170. As a result, the predictions of particle release made in this study produce an overall public health hazard less than one-tenth of the cesium hazard estimated in NUREG-0170.

Table 9.1
Comparative Measure of Risk/Accident for Spent Fuel
Shipment by Truck

	Twenty Response Regions (Ci)	NUREG-0170 (Ci)
Gas	2.26	10.7
Vapors	3.24×10^{-2}	1.26
Particles	$1.65E \times 10^{-5}$	--
Direct radiation	$1.73E \times 10^{-2}$	$6.93E \times 10^{-2}$

Table 9.2
Comparison of Release Risk/Accident for Spent Fuel
Shipment by Rail

	Twenty Response Regions (21 Fuel Assemblies) (Ci)	NUREG-0170 (7 Fuel Assemblies) (Ci)	NUREG-0170 (21 Fuel Assemblies) (Ci)
Gas	39.6	61.0	183.
Vapors	0.651	7.17	21.9
Particles	$4.16Ex10^{-4}$	--	--
Direct radiation	0.276	0.300	0.900

The radiological risk on a per accident basis can be expanded into risk/year estimates by considering highway and railway accident rates and by estimating the number of cask-miles traveled in a year. NUREG-0170 assumed that 3,000 metric tons of spent fuel would be transported annually in future shipments (1,530 truck, 652 rail). Spent fuel, when shipped by truck, was assumed to travel 1,525 miles/trip and, when shipped by rail, to travel 735 miles/trip. Based on current information, these assumptions on spent fuel shipments made in NUREG-0170 are reasonable and are used in this study, except that the rail mileage/trip is presumed to equal that for trucks, that is, 1,525 miles.

The estimated truck accident rate used in this study is 6.4×10^{-6} truck accidents/truck-mile compared to 1.7×10^{-6} truck accidents/truck-mile used in NUREG-0170. The truck accident risk/year associated with releases of radioactive material in gaseous, volatile, or particulate form or external radiation levels are estimated in this study as follows:

$$\text{Annual risk} = 6.4 \times 10^{-6} \ \frac{\text{truck accident}}{\text{truck-mile}} \times \frac{1525 \text{ truck-miles}}{\text{shipment}} \times 1530 \ \frac{\text{shipments}}{\text{year}} \times \frac{\text{release or external radiation level}}{\text{truck accident}}$$

Values for the last term (release or external radiation level/truck accident) appear in the first column (Twenty Response Regions) of Table 9.1.

The risk/year is calculated in a similar manner using values from NUREG-0170. Comparing the results of this study with NUREG-0170 values indicates that the estimated risks/year are smaller in this study, with the exception of particle releases which are not considered in NUREG-0170. If the risk/year for vapors and particles are combined after being weighted to account for their relative public health hazard, the total risk calculated in this study will be at least 3 times lower than the risk/year of vapor releases derived from the NUREG-0170 report. The risk/year from rail shipments can be compared in a manner similar to that used for truck transport.

The estimated train accident rate in this study is 1.19×10^{-5} train accidents/train-mile compared with the 1.05×10^{-5} train accidents/train-mile figure used in NUREG-0170. Assuming, as was done in NUREG-0170, that an average train length is 70 cars and an average of 10 cars are involved in each accident, the overall estimated accident rate in this study is 1.7×10^{-6} rail car accidents/rail car mile. Again, as with the truck shipments, the comparison indicates that the risks/year in this study are within those calculated for NUREG-0170, except for the particle release consideration. Combining the risk/year in this study for vapors and particles after appropriate weighting of the public health impacts results in a risk at least 4 times lower than the risk/year from vapor release calculated in NUREG-0170.

9.2.4 Estimated Responses for Sample Severe Accidents

In the previous section, emphasis is placed on compiling and analyzing a broad range of accident loading data. This data is used to estimate the probability of representative cask responses to accident loading conditions. In this section, estimates are made regarding representative cask responses to certain historic severe accidents.

From an extensive literature survey of historical accidents, approximately 400 truck and train accidents are selected as having high loading conditions. The selected accidents are summarized in Appendix A. For each accident, the following information is provided: report source, date of accident, type of accident, number of vehicles involved, velocity prior to the accident, height of any fall involved, object struck, and duration of any fire involved.

The loading conditions associated with four severe accidents are evaluated to identify the response region into which each accident would be categorized.

9.2.4.1 Caldecott Tunnel Fire[3]

A truck fire accident occurred in the Caldecott Tunnel near Oakland, California, on April 7, 1982. The fire was caused by collisions of a gasoline truck-trailer, a bus, and an automobile. The fire resulting from

approximately 8,800 gallons of gasoline had a peak flame temperature of 1900°F. Although it took 2 hours 42 minutes to completely extinguish the fire, the peak flame temperature and the burning of most of the gasoline occurred in less than 40 minutes, after which protected personnel entered the tunnel to search for survivors and to extinguish the fire.

The probable response of the representative truck cask to the mechanical and thermal loading conditions that occurred in the Caldecott Tunnel fire is estimated using the accident information and the cask response information in Section 6.0 and Appendix F.

The primary objects involved in the collisions were an automobile, a truck-trailer, and a bus. Accidents involving these relatively soft objects (i.e., when compared to a truck cask) are minor from a structural response standpoint. These objects cause low levels of force to be imposed on a truck cask regardless of the impact velocity and the cask orientation. Such impact forces cannot cause a strain at the inner cask shell to exceed 0.2% (S_1).

If the representative truck cask were exposed to an engulfing 1900°F fire such as the one in the Caldecott Tunnel, the fire duration required to reach 500°F (T_1) at the middle of the lead shield thickness is 45 minutes. The hot, engulfing fire lasted less than 40 minutes in the Caldecott Tunnel; therefore, a 500°F temperature (T_1) at the middle of the lead shield thickness would not be reached during this accident.

From this evaluation, the response of the representative truck cask to a Caldecott Tunnel fire accident environment is in region R(1,1) near the border with region R(1,2). The containment inner shell of the cask, the closure shell, and the lead shield would provide their safety functions without any significant degradation during and following the accident. No radioactive release or increase in radiation level is expected under these accident conditions.

9.2.4.2 I-80 Bridge Accident[4]

In March, 1981, a truck-tractor-trailer was struck by a pickup truck while on an overpass bridge on Interstate I-80 near San Francisco,

California. The truck-tractor-trailer veered into the bridge railing, broke through the railing and fell 64 feet to the soil surface below.

The probable response of the representative truck cask to the mechanical loading conditions that occurred with the drop onto the soil is estimated, assuming that the truck struck the ground at an orientation angle between 20^{0}-70^{0} and an impact angle of 90^{0} for free fall onto a flat surface.

In this accident, the cask impact velocity would be approximately 44 mph as determined by the fall of 64 feet. An impact velocity of at least 44 mph is required to reach a 0.2% strain (S_1) at the inner wall of the cask. Therefore, this accident is also just within the R(1,1) response region.

9.2.4.3 Livingston Train Fire[5]

On September 28, 1982, 43 railroad cars derailed near Livingston, Louisiana. Following the derailment, a fire started to burn various materials which included plastic pellets, vinyl chloride, and petroleum products. The fire which covered a wide area was allowed to burn for several days because of the toxic chemicals and explosions involved. A railroad car carrying motor fuel anti-knock compound (tetra-ethyl lead) exploded about 19 hours after the derailment. A second thermally induced explosion occurred on October 1, 82 hours after the derailment, involving a car carrying vinyl chloride. The fire cooled down sufficiently on the fifth day to permit fire-fighting operations. Six cars carrying vinyl chloride materials were purposely detonated on October 11 to dispose of the remaining unvented materials within them.

The probable response of the representative rail cask to the thermal loading conditions in the Livingston train fire accident is estimated by using the accident information and the cask response information in Subsections 6.3.2, 7.3.2, and Appendix F.

The representative rail cask could have been located anywhere in the derailed train wreckage and fire. The worst place for the cask would have been in the environment of the seven cars burning vinyl chloride, where one of the cars exploded and rocketed over 400 feet to the north of the derailment.

A maximum thermal loading condition on the cask can be calculated, assuming that the cask was in the position of the rocketing car. First, it is conservatively assumed that sufficient heat was absorbed by the vinyl chloride in the car to vaporize all of the compressed gas, thus causing the explosion. This would take no more than 3.5×10^7 Btu. It took approximately 82 hours to heat the vinyl chloride and cause the explosion. The cask area exposed to the fire is estimated to be no greater than 1370 ft.^{2} The average heat transfer to the car during the entire period is then

$$\dot{Q} = \frac{3.5 \times 10^7}{(1.3 \times 10^3)\ (8.2 \times 10^1)} = 3.1 \times 10^2 \ \frac{\text{Btu}}{\text{hr-ft}^2} .$$

This is the average heat flux to which the neutron shield or thermal barrier on the cask would have been exposed. The average heat transfer to the cask lead shield would have been approximately a factor of 3 lower due to the thermal shield. Assuming an average heat transfer rate of 103 Btu/hr-ft^2, the lead mid-thickness temperature would reach 500°F (T_1) in 62 hours. At 82 hours, when the railroad car carrying the vinyl chloride exploded, the lead mid-thickness temperature would have reached just over 600°F (T_2), with some lead melt occurring.

Assuming that the thermal conditions continued until the fifth day when cool down started, the lead mid-thickness temperature would have reached a temperature of 720°F, which is above 650°F (T_3), but lower than 1050°F (T_4). This assumption of thermal conditions is very conservative, particularly considering that the other six cars carrying vinyl chloride did not explode.

From this evaluation, the response of the representative rail cask to the environment of the Livingston derailment fire accident is in the R(1,1), R(1,2), R(1,3) or R(1,4) region depending on the location of the cask. Even using the worst assumptions, the lead mid-thickness temperature would not exceed 720°F. Any radioactive releases would be much less than those estimated in Section 8.0 for the R(1,4) region.

9.2.4.4 Derailment into the Alabama River[6]

On January 19, 1979, a train derailed off a bridge into the Alabama River near Hunter, Alabama.[6] One of the rail cars was carrying a pipe which struck the bridge and caused the derailment. Five rail cars fell into the mud of the river 75 feet below.

The probable response of the representative rail cask to the mechanical loading condition caused by impact on the water was estimated by assuming that the cask would strike the water at an orientation angle between 20^{o}-70^{o}.

In the accident, the rail cask impact velocity would be approximately 47 mph as determined by the fall of 75 feet onto the water surface. An impact velocity of at least 90 mph is required to reach a 0.2% strain (S_1) at the inner wall for the cask impact; therefore, this accident is placed well within the R(1,1) response region.

9.3 Uncertainties

This study evaluates the safety provided through current regulations for the transport of spent fuel. Structural and thermal responses of a representative shipping casks to a range of loading conditions which could occur in potential transportation accidents are evaluated. These evaluations are performed using realistic methods and assumptions. In many cases a range of values is possible for a specific parameter. However, when the realism of the assumption or method can be questioned or when an otherwise complex analysis can be simplified, elements of conservatism are introduced into the evaluations. These conservatisms, typically identified from sensitivity studies, are discussed individually in previous sections of this report. They are discussed collectively in this section, because an understanding of the collective uncertainties is crucial to any judgment made on the overall quality of study results.

Basically, the uncertainties can be classified under three headings: (1) cask response, (2) radiological significance of cask response, and (3) likelihood of accident events, cask response, and resulting radiological hazard.

9.3.1 Uncertainty in Cask Response

The calculated responses of a spent fuel cask subjected to mechanical and thermal loading conditions primarily depend on: (1) selection of the representative cask designs, (2) definition of accident loads, and (3) computer code applicabilities and modeling techniques used to estimate the cask response to accident loads.

9.3.1.1 Selection of Representative Cask Designs

The accident resistance of the representative cask determined the percentage of accidents causing specific cask response levels. The representative truck and rail casks are purposely defined to meet existing regulations. That is, the casks, if subjected to the accident test conditions in the regulations will respond in an acceptable manner. The representative truck cask is selected to have a capacity of 1 pressurized water reactor (PWR) fuel assembly while the rail cask capacity is 21 PWR fuel assemblies. Both cask designs use lead as a gamma shield material, and the fuel assemblies in both cases are presumed to have experienced a 5-year decay period prior to shipment.

The representative lead-shielded cask designs are selected by considering currently licensed cask designs and the purported design capabilities of future casks. Future casks are primarily being designed to transport existing spent fuel to the planned geologic waste repositories. These repositories are being designed to accept fuel which has experienced a decay time of 5 years or more. Because of this lengthy decay time, the gamma radiation emanating from the spent fuel is far less than the current casks are designed to accommodate. As a result, shielding for casks can be accomplished by all-steel containment shells, particularly for rail casks. Also, uranium-shielded casks may be used to transport spent fuel to the repositories. Any all-steel or uranium shielded cask design will be intrinsically more resistant to accident forces than either of the study's two representative cask designs. Therefore, the results of this study underpredict the performance of the total population of current and future cask designs.

The single element capacity chosen for the truck cask is typical for casks whose shipment does not require highway overweight permits. If capacity should be increased to two or, at most, three PWR assemblies, the minimum cask resistance to accident forces, assumed in this study, will not change significantly. Since the amount of radioactive material would be increased by, at most, a factor of 3, the radiological hazard associated with a specific accident sequence could conceivably increase by a similar factor. On the other hand, a larger capacity cask would require fewer shipments, by a factor of 3, hence the annual radiological risk would be unchanged.

An increase or decrease in the capacity of the rail cask would have a similar effect in increasing or decreasing the potential radiological hazard for a specific accident, but would not change the annual radiological risk.

9.3.1.2 Definition of Accident Loads

Real accidents can involve many different types of loading conditions such as impact, crush, torch fires, engulfing fires, and burial. In this study, the focus is on the response of representative casks to impact and large fire loadings. Three loading parameters are used to determine the impact loads: impact velocity, object hardness, and cask orientation. Three loading parameters are also used to determine the fire loads: fire duration, flame temperature, and fire location. Based on the reviews and sensitivity studies included in this study, the conclusion is that impact collisions and large fires impose loads which generally exceed those which can be achieved by other loading conditions. When the massiveness of the cask is considered, the loading magnitudes imposed by high-velocity impacts and large engulfing fires conservatively bound all values which can be achieved by other loading conditions.

9.3.1.3 Computer Code Applications and Modeling

The response of the representative casks to mechanical and thermal loads are calculated with computer codes. Where possible the computer models and results are benchmarked against existing test data. An elastic-plastic

material model is selected for performing response calculations for cask impacts on soil, soft rocks, and hard rocks. Although an elastic-plastic model oversimplifies real soil and rock characteristics, the shortcomings in the model are accommodated by benchmarking against penetration test data (see Appendix E).

The cask model is developed using, where possible, standard finite element model techniques, bounding conditions, and material properties. The modeling areas with the most uncertainty are the lead properties and the lead interfaces with the stainless steel shell of the cask. In the absence of reliable test data, the lead properties and boundary conditions are conservatively selected to estimate lead slump and resulting strain on the inner shell of the cask.

Ideally, three-dimensional (3-D) soil and cask models could be developed and benchmarked against test data on representative casks impacting well-characterized soil and rock surfaces. This benchmarking approach could reduce the uncertainties in the modeling and would improve the accuracy of calculating the structural response of the cask. However, the benefits derived from the improvement of modeling accuracy and the reduction of modeling uncertainty cannot be fully realized unless the soil distributions and soil uncertainties are better defined.

The thermal modeling of the cask and the fire are idealized. The modeling depend strongly on the use of structural engineering material properties, bounding conditions, and finite element techniques. A one-dimensional (1-D) fire and cask model is used to predict the cask response. The fire is represented by a homogeneous constant temperature and constant location. In reality, fires are a 3-D phenomenon in which the temperature and location can vary significantly in any given accident. Several conservative assumptions are made to accommodate the simplifications in modeling the fire and cask. For example, the mid-plane of the cask, which would be the hottest portion, is selected for the 1-D model. The temperature response levels representing thermal degradation are selected to exist at the mid-plane of the cask and over-predict the realistic response of the cooler

portions. For non-engulfing fires, heat absorption effects are included in the modeling, but heat loss effects, such as thermal radiation to the environment, are conservatively excluded.

Ideally, 3-D fire and cask models could be developed and benchmarked against test data on representative casks involved in well-characterized fires. This approach could reduce the uncertainties in the modeling and would improve the accuracy in calculating the thermal response of the cask. However, the benefits derived from the improvement of the thermal model cannot be fully realized unless the fire duration and flame temperature at fire locations are better defined.

9.3.2 Uncertainty in Estimating an Accident's Potential Radiological Hazard

A damaged spent fuel cask could potentially cause a radiological hazard with a magnitude dependent on (1) release of radioactive material from failed fuel rods, (2) release of radioactive material from the cask, (3) reduction in radiation shielding, and (4) reduction in subcriticality control.

9.3.2.1 Radioactive Releases from Fuel Rods

Endwise impact of the fuel rods is assumed to determine the fraction of rods which fail. This assumption is conservative in estimating the impact failure of fuel rods for all other cask orientations. The release of radioactive material from the fuel rods into the cask is estimated using Oak Ridge National Laboratory (ORNL) test data. The ORNL tests were performed by heating the rods to failure at high temperatures (greater than 1300^{o}F). The radioactive release is through a single leakage path caused by high internal pressure bursting the rod. Under accident conditions, rod failure is more likely during high impacts where multiple fractures to the rods can occur. In contrast to test conditions, the fuel rods will likely be at relatively low pressures and temperatures when impact occurs. Thus, the ORNL test data may or may not overestimate the actual releases under high-impact conditions. The radiological hazards could be better estimated with pertinent tests performed at high-impact conditions for the spent fuel rods.

9.3.2.2 Radioactive Releases from Casks

Radioactive releases from a cask depend on many factors which include failure of the fuel cladding, the temperature and pressure in the cask cavity, and a leakage path that could be through a closure seal. In this study, the assumption is made that all of the radioactive material released from failed fuel rods will be released from the cask. In reality, only a portion of the radioactive material from the failed fuel rods will be released from the cask cavity. Radioactive vaporous materials like cesium and its compounds will deposit on the cooler inner shell of the cask and the cooler flange areas. Radioactive particles will also be deposited on the walls and within the leakage paths. In some cases, the particles may plug the leakage path. Thus the estimates of the radioactive releases are higher than can be expected.

9.3.2.3 Reduction in Radiation Shielding

The external radiation from the representative cask is estimated by using lead slump calculations. These lead slump calculations assume boundary conditions that maximize the lead slump, hence the amount of external radiation. In reality, the lead slump will be less. Also, the use of depleted uranium or steel shielding will not allow shield slump and will exhibit lower external radiation for the same accident loading conditions.

9.3.2.4 Reduction in Subcriticality Control

For large casks containing more than three PWR bundles, the effectiveness of measures used to prevent a criticality event can be reduced under extreme loading conditions. Any reduction in criticality safety depends on both the cask and fuel basket design. However, since the margins used to prevent criticality are very high, and since careful evaluations of the criticality analysis and the design features are performed during cask licensing, the possibility of a criticality event is small even under extreme loading conditions. Using the probabilistic methods in Section 5.0, the probability of a rail cask's having a structural response greater than 2% strain (S_2) and

becoming submerged in water is estimated to be 0.00000078%, given an accident. Using the accident and rail shipment rates in this study, this type of accident is estimated to occur approximately once every ten million years.

9.3.3 Uncertainty in Probability Models

There is uncertainty associated with the probability distributions used in this study. However, two points should be emphasized. First, although direct experience with events involving the transport of casks would be the best source of information, very little, if any, such information is available. Thus, it is necessary to use data derived from similar types of experiences--results which can be considered to be a sample of what potentially will be experienced in the transport of spent fuel casks. Second, similar types of probabilistic analyses have been done based on sparse data similar to that used in this study. The important point for those other studies, and for this study as well, is the need to recognize that the uncertainty exists and to consider this uncertainty in the use of the results.

The estimated probabilities and probability distributions used in the probabilistic analyses are based on (1) accident statistics, (2) surveys of physical structures/features, (3) past analyses and models, and (4) engineering judgment, when no data is available.

9.3.3.1 Accident Statistics

The estimated accident rate for highway accidents is based on the number of accidents experienced by trucks transporting petroleum products during 1973-1981. The extent to which the past experience of trucks transporting petroleum products can be considered to be a random sample of the future experiences of trucks transporting fuel casks determines the quality of the estimate of the highway accident rate used in the analysis.

Similarly, the distributions of truck and train velocities in an accident are based on statistics compiled from actual accidents. The train velocities are derived from recorders in the locomotives, and are likely to represent a good sample. That velocity is directly attributed to the cask upon impact,

but does not include braking effects. Truck velocities are based on estimates by law enforcement officers in their investigation of accidents. The subset of accidents used in this study is based only on data accumulated in California. These accidents involved injury or fatality events that occur at higher velocities than non-injury accidents. It is assumed that the accident report data from 1973-1981 represent a sample of future incidents involving cask transports. Also, the experiences in North Carolina are used to empirically adjust for breaking. Overall, the distributions of train and truck velocities used in this study are conservative.

9.3.3.2 Surveys of Structures and Features

The hardness of earth surfaces adjacent to highways can vary over a wide range. This variability can have a significant effect on the loadings that could be imposed on a cask or any other impacting object. The water and land (hard rock, soft rock, and soil) distribution along proposed spent fuel shipment routes between the east coast and west coast is initially estimated using agricultural soil survey data and geological highway maps for the United States. The initial distribution indicates the types of surfaces which can be impacted along highways in the various regions of the United States. The initial distribution is adjusted to an expected highway distribution by performing highway surveys along representative portions of Federal Interstates 5 and 80 in California. Also, these highway surveys are used to estimate the distributions of bridge heights and column sizes along Federal Interstates.

Improved distribution estimates could be made if the highway surveys were actually performed along proposed spent fuel routes. However, for evaluating the risk for cross-country transportation of spent fuel, the representative distributions are reasonable.

9.3.3.3 Past Analysis and Models

Information on the occurrence of fires is very limited. Thus the thermal evaluations rely on the models developed in a previous analysis of severe

accidents[7]. As mathematical models, the flame temperature and fire duration distributions are only approximations of reality. Little or no information has been compiled which directly models the fire accident environment. The fire parameters, duration, temperature, and location, jointly affect the thermal loading on the cask and hence its response.

9.3.3.4 Engineering Judgment

Finally, engineering judgment is used to model the distributions of some accident parameters--impact angle and fire location. Distribution on these important parameters could not be found in actual data. For instance, a uniform distribution is assumed for impact angle and a linear model for fire location. In general, where judgment is used, conservative assumptions are made.

9.3.4 Overall Statement of Uncertainty

As discussed, there are numerous uncertainties associated with the analysis of the risks from transport of spent nuclear fuel. Related highway and railway accident data is limited, and what is reported is often insufficient or not applicable to developing the appropriate distributions and models necessary to estimate risk. Similarly, mathematical models of the fire environment in an accident and the structural and thermal responses of a cask given the corresponding accident loadings are limited in their ability to approximate the actual physical processes that occur during an accident. Thus, the estimated probabilities and risks have uncertainty associated with them.

However, recognizing the limited data and information on past accidents, the limitations of using mathematical models to model complex physical phenomena, and the limitations on the resources and time to do this analysis, it is felt that a reasonably conservative estimate of risk is provided.

9.4 Conclusions

The focus of this report is on the integrity of casks used for U.S. shipments of commercially generated spent fuel, specifically on the level

of safety provided in the event of a transportation accident. Since all shipping casks are designed to meet an existing set of regulatory standards, the report evaluates the level of safety being provided by current regulations.

The response of representative spent fuel casks are assessed under a range of transportation accident conditions. The accident conditions are derived from historical accident data applicable to truck and rail shipments. The responses of the casks are categorized by a two-stage screening process and compared with two benchmarks: 10 CFR 71 regulations, and NUREG-0170.

The first benchmark is chosen to evaluate cask responses to accident loading conditions which fall within the 10 CFR 71 accident test conditions. As discussed in Subsection 9.2.1, approximately 99.4% of the truck accidents and 98.7% of the rail accidents have both mechanical and thermal loading conditions less than those implied by 10 CFR 71 regulations. The 10 CFR 71 benchmark is also chosen to represent a level of radiological hazard currently reflected in existing regulations. This benchmark specifies limits for both radioactive material releases and the magnitude of the radiation level external to a cask. The limits are chosen to provide high assurance that public radiation exposures would be less than permissible annual limits established for workers in occupations involving the use of radioactive materials. When considering real cask capabilities to withstand thermal loading conditions beyond the regulatory ones, approximately 99.4% of the truck and rail accidents would result in negligible radiological hazards which are less than those implied by 10 CFR 71 regulations. As discussed in Subsection 9.2.2, an additional 0.4% of both highway accidents and railway accidents could result in radiological hazards near the regulatory limits.

The second benchmark value is chosen to provide a risk perspective; that is, a benchmark which includes probabilistic consideration of all possible levels of public radiological hazard. The probabilistic consideration was originally presented in NUREG-0170, an environmental impact statement which considered radiological risk from all shipments of radioactive material in the

U.S., including spent fuel. The significance of this particular document is that based, in part, on the overall assessment of risk which it provided, the NRC made a judgment on the adequacy of its transportation regulations. The judgment was made that the regulations were adequate and not in need of immediate change.

The benchmark taken from NUREG-0170 is the risk calculated specifically for spent fuel shipments. The evaluations in Subsection 9.2.3 indicate that the risks from spent fuel shipments derived in this study, are less than those previously estimated in the NUREG-0170 document. The evaluations in NUREG-0170 indicate that the expected radiological consequences from the shipment of 3000 metric tons of spent fuel per year is less than 1 latent cancer fatality every 2300 years.

The results of this study depend primarily on the quality of the cask response models, the radiation release models, and the probability models and distributions used in the analysis. Models for cask responses, radioactive releases, and distributions for the accident parameters are new developments based on current computer codes, limited test data on radioactive releases, and limited historical accident data. The results of this study apply to spent fuel casks which can be licensed by the NRC and are designed, manufactured, operated, and maintained in accordance with national codes and standards (or equivalent) which have adequate margins of safety embedded in them.

If the objective of this study is to precisely define spent fuel transportation risks, many improvements need to be made to these models to calculate the probability and radioactive release estimates and to quantify the uncertainties in the estimates. For example, tests could be performed to benchmark the DYNA/NIKE computer codes for predicting lead slump for a variety of realistic boundary conditions which would provide nominal values with uncertainty bounds. Similarly, more sophisticated modeling of rock surfaces, which includes cracking, could be developed and benchmarked for improving the prediction of cask responses to a variety of rock properties and impact conditions. Finally, the probability distributions for all the accident parameters, e.g., velocity, fire duration, impact angle, could be improved

with further research, data analysis and sensitivity studies. Human factors which affect the cask design, manufacture, operation, and maintenance could also be considered because they affect the cask response and contribute to the overall risk in transporting spent fuel.

None of these improvements are being considered at this point for two reasons: (1) the objective of this study is to estimate the level of safety provided to the shipment of spent fuel using casks licensed to current regulatory standards (a conservatively estimated measure of safety), and (2) the radiological risk in current and future commercial spent fuel shipments is a small component of the total risks applicable for all radioactive material shipments.

The attempt is made in this study to use realistic, yet conservative when appropriate, models and probabilistic distributions. Thus, the estimates derived from the analysis are usable to achieve the study's objective.

REFERENCES

All references are listed numerically by sections. Appendix references are at the end of each appendix.

Section 1.0

1. Office of the Federal Register, Title 10, Code of Federal Regulations, Part 71, Office of the Federal Register, Washington, DC, January 1984.

2. U.S. Nuclear Regulatory Commission, Final Environmental Statement on the Transportation of Radioactive Material by Air and Other Modes, U.S. Nuclear Regulatory Commission, Washington, DC, NUREG-0170, December 1977.

3. P. Eggers, Severe Rail and Truck Accidents: Toward a Definition of Bounding Environments for Transportation Packages, U.S. Nuclear Regulatory Commission, Washington, DC, NUREG/CR-3499, 1983.

Section 2.0

1. Accident Data on California State Highways, State of California Business, Transportation and Housing Agency, Department of Transportation, Division of Traffic Engineering, Sacramento, CA. Report prepared in cooperation with the U.S. Department of Transportation, Federal Highway Administration, 1983.

2. Office of the Federal Register, Title 49, Code of Federal Regulations, Part 177, Office of the Federal Register, Washington, DC, January 1983.

3. 1969 Accidents of Large Motor Carriers of Property, Bureau of Motor Carrier Safety, Federal Highway Administration, U.S. Department of Transportation, Washington, DC, December 1970.

4. 1970 Accidents of Large Motor Carriers of Property, Bureau of Motor Carrier Safety, Federal Highway Administration, U.S. Department of Transportation, Washington, DC, March 1972.

5. 1971-1972 Accidents of Large Motor Carriers of Property, Bureau of Motor Carrier Safety, Federal Highway Administration, U.S. Department of Transportation, Washington, DC, May 1974

6. Summary of Motor Vehicle Accidents in the Petroleum Industry for 1977, American Petroleum Institute, Washington, DC, May 1978.

7. Summary of Motor Vehicle Accidents in the Petroleum Industry for 1978, American Petroleum Institute, Washington, DC, August 1979.

8. Summary of Motor Vehicle Accidents in the Petroleum Industry for 1979, American Petroleum Institute, Washington, DC, June 1980.

9. Summary of Motor Vehicle Accidents in the Petroleum Industry for 1980, American Petroleum Institute, Washington, DC, September 1981.

10. Summary of Motor Vehicle Accidents in the Petroleum Industry for 1981, American Petroleum Institute, Washington, DC, August 1982.

11. Accident/Incident Bulletin No. 145, Calendar Year 1976, Office of Safety, Federal Railroad Administration, U.S. Department of Transportation, Washington, DC, December 1977.

12. Accident/Incident Bulletin No. 146, Calendar Year 1977, Office of Safety, Federal Railroad Administration, U.S. Department of Transportation, Washington, DC, August 1978.

13. Accident/Incident Bulletin No. 147, Calendar Year 1978, Office of Safety, Federal Railroad Administration, U.S. Department of Transportation, Washington, DC, October 1979.

14. Accident/Incident Bulletin No. 148, Calendar Year 1979, Office of Safety, Federal Railroad Administration, U.S. Department of Transportation, Washington, DC, July 1980.

15. Accident/Incident Bulletin No. 149, Calendar Year 1980, Office of Safety, Federal Railroad Administration, U.S. Department of Transportation, Washington, DC, June 1981.

16. Accident/Incident Bulletin No. 150, Calendar Year 1981, Office of Safety, Federal Railroad Administration, U.S. Department of Transportation, Washington, DC, June 1982.

17. Accident/Incident Bulletin No. 151, Calendar Year 1982, Office of Safety, Federal Railroad Administration, U.S. Department of Transportation, Washington, DC, June 1983.

18. 1973 Accidents of Motor Carriers of Property, Bureau of Motor Carrier Safety, Federal Highway Administration, U.S. Department of Transportation, Washington, DC, July 1975.

19. 1974 Accidents of Motor Carriers of Property, Bureau of Motor Carrier Safety, Federal Highway Administration, U.S. Department of Transportation, Washington, DC, 1975.

20. 1975 Accidents of Motor Carriers of Property, Bureau of Motor Carrier Safety, Federal Highway Administration, U.S. Department of Transportation, Washington, DC, 1976.

21. 1976 Accidents of Motor Carriers of Property, Bureau of Motor Carrier Safety, Federal Highway Administration, U.S. Department of Transportation, Washington, DC, October 1977.

22. 1977 Accidents of Motor Carriers of Property, Bureau of Motor Carrier Safety, Federal Highway Administration, U.S. Department of Transportation, Washington, DC, May 1980.

23. 1978 Accidents of Motor Carriers of Property, Bureau of Motor Carrier Safety, Federal Highway Administration, U.S. Department of Transportation, Washington, DC, May 1980.

24. 1979 Accidents of Motor Carriers of Property, Bureau of Motor Carrier Safety, Federal Highway Administration, U.S. Department of Transportation, Washington, DC, 1980.

25. 1980-1981 Accidents of Motor Carriers of Property, Bureau of Motor Carrier Safety, Federal Highway Administration, U.S. Department of Transportation, Washington, DC, August 1982.

26. 1982 Accidents of Motor Carriers of Property, Bureau of Motor Carrier Safety, Federal Highway Administration, U.S. Department of Transportation, Washington, DC, May 1983.

27. 1983 Accidents of Motor Carriers of Property, Bureau of Motor Carrier Safety, Federal Highway Administration, U.S. Department of Transportation, Washington, DC, October 1984.

28. TASAS Selective Record Retrieval Statewide Accident Summary for Year 1975, State of California Department of Transportation, Sacramento, CA, October 1979.

29. TASAS Selective Record Retrieval Statewide Accident Summary for Year 1976, State of California Department of Transportation, Sacramento, CA, October 1979.

30. TASAS Selective Record Retrieval Total Statewide Accidents for Year 1977, State of California Department of Transportation, Sacramento, CA, May 1978.

31. TASAS Selective Record Retrieval Statewide Accident Summary for Year 1978, State of California Department of Transportation, Sacramento, CA, April 1979.

32. TASAS Selective Record Retrieval, Summary Only, All Accidents for the Year 1978, State of California Department of Transportation, Sacramento, CA, August 1984.

33. TASAS Selective Record Retrieval, Summary Only, All Accidents for the Year 1979, State of California Department of Transportation, Sacramento, CA, August 1984

34. TASAS Selective Record Retrieval Statewide Accidents for Year 1981, State of California Department of Transportation, Sacramento, CA, April 1982.

35. TASAS Selective Record Retrieval Statewide Summary 1982, State of California Department of Transportation, Sacramento, CA, May 1983.

36. TASAS Selective Record Retrieval Statewide Summary 1983, State of California Department of Transportation, Sacramento, CA, April 1984.

37. Assessment of the Stiffness Characteristics of Bridge Substructure Components Encountered along a Section of Interstate 5, Engineering Computer Corporation, Sacramento, CA, February 1985. A contractor report to the Lawrence Livermore National Laboratory.

38. R. Imbsen, et al., Soil and Terrain Surveys, Engineering Computer Corporation, Sacramento, CA, January 1985. A contractor report to the Lawrence Livermore National Laboratory.

39. Soil Survey, United States Department of Agriculture, Bureau of Chemistry and Soils, Superintendent of Documents, Washington, DC.

40. Geological Highway Map, American Association of Petroleum Geologist, Tulsa, OK.

41. 1957 Annual Statistical Report, Department of California Highway Patrol, Sacramento, CA, May 1958.

42. 1958 Annual Statistical Report, Department of California Highway Patrol, Sacramento, CA, May 1959.

43. 1959 Annual Statistical Report, Department of California Highway Patrol, Sacramento, CA, May 1960.

44. 1960 Annual Statistical Report, Department of California Highway Patrol, Sacramento, CA, May 1961.

45. 1961 Annual Statistical Report, Department of California Highway Patrol, Sacramento, CA, May 1962.

46. 1962 Traffic Accident Statistics, Department of California Highway Patrol, Sacramento, CA, May 1963.

47. 1963 Traffic Accident Statistics, Department of California Highway Patrol, Sacramento, CA, May 1964.

48. 1964 Traffic Accident Statistics, Department of California Highway Patrol, Sacramento, CA, May 1965.

49. 1965 Traffic Accident Statistics, Department of California Highway Patrol, Sacramento, CA, April 1966.

50. 1966 Report of Fatal and Injury Motor Vehicle Traffic Accidents, Department of California Highway Patrol, Sacramento, CA, July 1967.

51. 1967 Report of Fatal and Injury Motor Vehicle Traffic Accidents, Department of California Highway Patrol, Sacramento, CA, July 1968.

52. E. G. Hamilton, Single, Variable Tabulations for 1979-1981 North Carolina Accidents, University of North Carolina Highway Safety Research Center, Chapel Hill, NC, September 1977.

53. R. K. Clarke, et al., Severities of Transportation Accidents, Sandia National Laboratories, Albuquerque, NM, SLA-74-0001, July 1976.

54. 1979 Virginia Traffic Crash Facts, Virginia Department of State Police, Richmond, VA, April 1980.

55. 1982 Virginia Traffic Crash Facts, Virginia Department of State Police, Richmond, VA, April 1983.

56. 1983 Virginia Traffic Crash Facts, Virginia Department of State Police, Richmond, VA, April 1984.

57. Rail-Highway Grade-Crossing Accidents/Incidents Bulletin for the Year Ended December 31, 1975, Office of Safety, Federal Railroad Administration, U.S. Department of Transportation, Washington, DC.

58. Rail-Highway Grade-Crossing Accidents/Incidents Bulletin for the Year Ended December 31, 1976, Office of Safety, Federal Railroad Administration, U.S. Department of Transportation, Washington, DC, December 1977.

59. Rail-Highway Grade Crossing Accident/Incident Bulletin No. 43, Calendar Year 1977, Office of Safety, Federal Railroad Administration, U.S. Department of Transportation, Washington, DC, July 1978.

60. Rail-Highway Crossing Accident/Incident and Inventory Bulletin No. 1, Calendar Year 1978, Office of Safety, Federal Railroad Administration, U.S. Department of Transportation, Washington, DC, October 1979.

61. Rail-Highway Crossing Accident/Incident and Inventory Bulletin No. 2, Calendar Year 1979, Office of Safety, Federal Railroad Administration, U.S. Department of Transportation, Washington, DC, September 1980.

62. Rail-Highway Crossing Accident/Incident and Inventory Bulletin No. 3, Calendar Year 1980, Office of Safety, Federal Railroad Administration, U.S. Department of Transportation, Washington, DC, June 1981.

63. Rail-Highway Crossing Accident/Incident and Inventory Bulletin No. 4, Calendar Year 1981, Office of Safety, Federal Railroad Administration, U.S. Department of Transportation, Washington, DC, June 1982.

64. Rail-Highway Crossing Accident/Incident and Inventory Bulletin No. 5, Calendar Year 1982, Office of Safety, Federal Railroad Administration, U.S. Department of Transportation, Washington, DC, June 1983.

65. 1969 Accidents of Large Motor Carriers of Property, Bureau of Motor Carrier Safety, Federal Highway Administration, U.S. Department of Transportation, Washington, DC, December 1970.

66. R. K. Clarke, et al., Severities of Transportation Accidents, Sandia National Laboratories, Albuquerque, NM, SLA-74-0001, July 1976.

67. P. Eggers, Severe Rail and Truck Accidents: Toward a Definition of Bounding Environments for Transportation Packages, U.S. Nuclear Regulatory Commission, Washington, DC, NUREG/CR-3499, 1983.

Section 3.0

1. Safety Analysis Report for NLI 1/1 Truck Cask, Docket No. 71-9010, National Lead Industries, Inc., Wilmington, DE, November 1972.

2. Safety Analysis Report for TN-8/TN9 Shipping Casks, Docket No. 71-9015/16, Transnuclear, Inc., White Plains, NY, October 1976.

3. Design and Analysis Report IF-300 Shipping Cask, Docket No. 70-1220, General Electric Company, San Jose, CA, January 1971.

4. Safety Analysis Report for the NLI-10-24 Shipping Cask, Docket No. 70-9023, National Lead Industries, Inc., Wilmington, DE, February 1976.

5. Office of the Federal Register, Title 10, Code of Federal Regulations, Part 71, Office of the Federal Register, Washington, DC, January 1984.

6. U.S. Nuclear Regulatory Commission, Regulatory Guide 7.6: Design Criteria for the Structural Analysis of Shipping Cask Containment Vessels, U.S. Nuclear Regulatory Commission, Washington, DC, March 1978.

7. U.S. Nuclear Regulatory Commission, Regulatory Guide 7.4: Leakage Tests on Packages for Shipment of Radioactive Materials, U.S. Nuclear Regulatory Commission, Washington DC, June 1975.

8. U.S. Nuclear Regulatory Commission Regulatory Guide 7.8: Load Combinations for the Structural Analysis of Shipping Casks, U.S. Nuclear Regulatory Commission, Washington, DC, May 1977.

9. U.S. Nuclear Regulatory Commission, Regulatory Guide 7.9: Standard Format and Content of Part 71 Applications for Approval of Packaging of Type B, Large Quantity, and Fissile Radioactive Material, U.S. Nuclear Regulatory Commission, Office of Standards Development, Washington, DC, January 1980, Rev-1.

10. U.S. Nuclear Regulatory Commission, Regulatory Guide 7.10: Establishing Quality Assurance Programs for Packaging Used in the Transport of Radioactive Material, U.S. Nuclear Regulatory Commission, Washington, DC, January 1983.

11. American Society of Mechanical Engineers, ASME Boiler and Pressure Vessel Code, the American Society of Mechanical Engineers, United Engineering Center, 345 East 47th Street, New York, NY 10017, July 1983.

12. U.S. Nuclear Regulatory Commission, (Draft) Regulatory Guide, Fracture Toughness Criteria for Ferritic Steel Shipping Cask Containment Vessels with a Maximum Wall Thickness of Four Inches (0.1m), U.S. Nuclear Regulatory Commission, Office of Nuclear Regulatory Research, Washington, DC, June 1986.

13. W. R. Holman, and R. T. Langland, Recommendations for Protecting Against Failure by Brittle Fracture in Ferritic Steel Shipping Containers Up to Four Inches Thick, Lawrence Livermore National Laboratory, Livermore, CA, UCRL-53013, NUREG/CR-1815, June 1981.

14. M. W. Schwartz, Recommendations for Protecting Against Brittle Fractures in Ferritic Steel Shipping Containers Greater Than Four Inches Thick, Lawrence Livermore National Laboratory, Livermore, CA, UCRL-53538, NUREG/CR-3826, April 1984.

15. L. E. Fischer, and W. Lai, Fabrication for Shipping Containers, Lawrence Livermore National Laboratory, Livermore, CA, UCRL-53544, NUREG/CR-3854, March 1985.

16. R. E. Monroe, H. H. Woo, and R. G. Sears, Recommended Welding Criteria for use in the Fabrication of Shipping Containers for Radioactive Materials, Lawrence Livermore National Laboratory, Livermore, CA, UCRL-53044, NUREG/CR-3019, March 1984.

Section 4.0

1. American Society of Mechanical Engineers, ASME Boiler and Pressure Vessel Code, Section III, Division 1, The American Society of Mechanical Engineers, United Engineering Center, 345 East 47th Street, New York, NY 10017, July 1983.

2. Manual of Steel Construction, 7th ed., American Institute of Steel Construction, Inc., 101 Park Avenue, New York, NY 10017, 1970.

3. M. G. Fontana and N. D. Greene, Corrosion Engineering, 2nd ed., McGraw-Hill Book Company, New York, NY, 1978.

4. A. J. Romano, et al., The Investigation of Container Materials for Bi and Pb Alloys, Part 1., Thermal Convection Loops, Brookhaven National Laboratory, Upton, NY, BNL 811(T313), July 1963.

5. G. M Tolson and A. Taboada, A Study of Lead and Lead-Salt Corrosion in Thermal Convection Loops, Oak Ridge National Laboratory, Oak Ridge, TN, 1966.

Section 5.0

1. E. G. Hamilton, Single, Variable Tabulations for 1979-1981 North Carolina Accidents, University of North Carolina Highway Safety Research Center, Chapel Hill, NC, September 1977.

2. R. K. Clarke, et al., Severities of Transportation Accidents, Sandia National Laboratories, Albuquerque, NM, SLA-74-0001, July 1976.

Section 6.0

1. Office of the Federal Register, Title 10, Code of Federal Regulation, Part 71, Office of the Federal Register, Washington, DC, January 1984.

2. J. O. Hallquist, NIKE-2D: An Implicit, Finite-Deformation, Finite Element Code for Analyzing the Static and Dynamic Response of Two-Dimensional Solids, Lawrence Livermore National Laboratory, Livermore, CA, UCRL-52678, 1979, and Revision 1, NIKE-2D: An Implicit, Finite-Deformation, Finite Element Code for Analyzing the Static and Dynamic Response of Two-Dimensional Solids, Lawrence Livermore National Laboratory, Livermore, CA, UCID-18822, 1981.

3. T. A. Nelson, et al., SCANS - Shipping Cask Analysis System, Vol. 1, Impact Analysis Code User's Manual, Lawrence Livermore National Laboratory, Livermore, CA, UCID-20674/Vol. 1, Draft Report to be published, U.S. Nuclear Regulatory Commission, Washington, DC, NUREG/CR-4554, 1986.

4. J. O. Hallquist, User's Manual for Dyna-2D--An Explicit Two-Dimensional Hydrodynamic Finite Element Code with Interactive Rezoning, Lawrence Livermore National Laboratory, Livermore, CA, UCID-18756, Rev. 2, 1984.

5. C. W. Young, "Depth Prediction for Earth-Penetrating Projectiles", Journal of the Soil Mechanics and Foundations Division, Proceedings of the American Society of Civil Engineers, Vol. 95, No. SM3, Proceedings Paper 6558, American Society of Civil Engineers, New York, NY, May 1969.

6. Institute of Mechanical Engineers, "The Resistance to Impact of Spent Magnox Fuel Transport Flasks", Power Industries Division of the Institute of Mechanical Engineers and the British Nuclear Energy Society, Seminar Paper, Mechanical Engineering Publications Ltd., London, England, April 30 and May 1, 1985.

7. International Atomic Energy Agency, Regulations for the Safe Transport of Radioactive Materials, Safety Series No. 6, International Atomic Energy Agency, Vienna, Austria, 1985.

8. P. J. Burns, TACO-2D-A Finite Element Heat Transfer Code, Lawrence Livermore National Laboratory, Livermore, CA, UCID-17980, Rev. 2, January 1982.

Section 7.0

1. Office of the Federal Register, Title 10, Code of Federal Regulations, Part 71, Office of the Federal Register, Washington, DC, January 1984.

2. J. O. Hallquist, User's Manual for Dyna-2D--An Explicit Two-Dimensional Hydrodynamic Finite Element Code with Interactive Rezoning, Lawrence Livermore National Laboratory, Livermore, CA, UCID-18756, Rev. 2, 1984.

3. J. O. Hallquist, NIKE-2D: An Implicit, Finite-Deformation, Finite Element Code for Analyzing the Static and Dynamic Response of Two-Dimensional Solids, Lawrence Livermore National Laboratory, Livermore, CA, UCRL-52678, 1979, and Revision 1, NIKE-2D: An Implicit, Finite-Deformation, Finite Element Code for Analyzing the Static and Dynamic Response of Two-Dimensional Solids, Lawrence Livermore National Laboratory, Livermore, CA, UCID-18822, 1981.

4. A. J. Neilson, A Dyna-3D Calculation for Impact on a Pipe Target, Safety and Engineering Science Division, Winfrith, AEEW-M2058, United Kingdom Atomic Energy Authority, Winfrith, England, 1981982, November 1983.

5. Institute of Mechanical Engineers, "The Resistance to Impact of Spent Magnox Fuel Transport Flasks", Power Industries Division of the Institute of Mechanical Engineers and the British Nuclear Energy Society, Seminar Paper, Mechanical Engineering Publications Ltd., London, England, April 30 and May 1, 1985.

6. M. Huerta and H. R. Yoshimura, A Study and Full-Scale Test of a High-Velocity Grade-Crossing Simulated Accident of a Locomotive and a

Nuclear-Spent-Fuel Shipping Cask, Sandia National Laboratories, Albuquerque, NM, SAND79-2291, TTC308, February 1983.

7. M. Huerta, Analysis, Scale Modeling, and Full-Scale Tests of a Truck Spent-Nuclear -Fuel Shipping System in High Velocity Impacts Against a Rigid Barrier, Sandia National Laboratories, Albuquerque, NM, SAND77-0270, 1978.

8. P. J. Burns, TACO-2D-A Finite Element Heat Transfer Code, Lawrence Livermore National Laboratory, Livermore, CA, UCID-17980, Rev. 2, January 1982.

9. H. J. Rack and H. R. Yoshimura, Postmortem Metallurgical Examination of a Fire-Exposed Spent Fuel Shipping Cask, Sandia National Laboratories, Albuquerque, NM, SAND-79-1424, UC-71, TTC-0018, April 1980.

10. R. B. Pope, et al., "An Assessment of Accident Thermal Testing and Analysis Procedures for Radioactive Materials Shipping Package," Paper Contributed by the American Society of Mechanical Engineers Heat Transfer Division to the Joint ASME/AIChE National Transfer Conference at Orlando, FL, April 8, 1980, American Society of Mechanical Engineers, New York, NY, April 1981.

11. U.S. Nuclear Regulatory Commission, Final Environmental Statement on the Transportation of Radioactive Material by Air and Other Modes, U.S. Nuclear Regulatory Commission, Washington, DC, NUREG-0170, December 1977.

Section 8.0

1. Office of the Federal Register, Title 10, Code of Federal Regulations, Part 71, Office of the Federal Register, Washington, DC, January 1984.

2. U.S. Nuclear Regulatory Commission, Final Environmental Statement on the Transportation of Radioactive Material by Air and Other Modes, U.S. Nuclear Regulatory Commission, Washington, DC, NUREG-0170, December 1977.

3. Generic Environmental Impact Statement on Handling and Storage of Spent Light Water Power Reactor Fuel, U.S. Nuclear Regulatory Commission, Washington, DC, NUREG-0575, August 1979.

4. N. C. Finley, et. al., Transportation of Radionuclides in Urban Environs, Draft Environmental Assessment, U.S. Nuclear Regulatory Commission, Washington, DC, NUREG/CR-0743, July 1970.

5. L. B. Shappert, et al., A Guide for the Design, Fabrication and Operation of Shipping Casks for Nuclear Applications, Oak Ridge National Laboratory, Oak Ridge, TN, ORNL-NSIC-68, February 1970.

6. U.S. Department of Energy, Mission Plan for the Civilian Radioactive Waste Program (Draft), U.S. Department of Energy, Washington, DC, DOE/RW-0005, April 1984.

7. L. Wilmot, Transportation Accident Scenarios for Commercial Spent Fuels, Sandia National Laboratory, Albuquerque, NM, SAND80-2124, February 1981.

8. H. K. Elder, et al., An Assessment of the Risk of Transporting Spent Nuclear Fuel by Truck, Pacific Northwest Laboratory, Richland, WA, PNL-2588, November 1978.

9. H. K. Elder, An Analysis of the Risk of Transporting Spent Nuclear Fuel by Train, Pacific Northwest Laboratory, Richland, WN, DE82-001048, September 1981.

10. W. H. Rhyne, et al., A Scoping Study of Spent Fuel Cask Transportation Accidents, U.S. Nuclear Regulatory Commission, Washington, DC, NUREG/CR-0811, SAI-OR-79-140-04, June 1979.

11. R. A. Lorenz, et al., Fission Product Release from Highly Irradiated LWR Fuel, U.S. Nuclear Regulatory Commission, Washington, DC, NUREG/CR-0722, February 1980.

Section 9.0

1. Office of the Federal Register, Title 10, Code of Federal Regulations, Part 71, Office of the Federal Register, Washington, DC, January 1984.

2. U.S. Nuclear Regulatory Commission, Final Environmental Statement on the Transportation of Radioactive Material by Air and Other Modes, U.S. Nuclear Regulatory Commission, Washington, DC, NUREG-0170, December 1977.

3. Highway Accident Report, Multiple Vehicle Collisions and Fire, Caldecott Tunnel, Near Oakland, CA, April 7, 1982, National Transportation Safety Board, Bureau of Accident Investigation, Washington, DC, PB83-916201, May 1983.

4. Newspaper Clipping, San Jose Mercury News, San Jose, CA, March 1981.

5. Railroad Accident Report, Derailment of Illinois Central Gulf Railroad Freight Train Extra 9629 East (GS-2-28) and Release of Hazardous Materials at Livingston, LA, September 28, 1982, National Transportation Safety Board, Bureau of Accident Investigation, Washington, DC, PB83-916305, NTSB/RAR-83/05, May 1983.

6. Railway Accident Report, National Transportation Safety Board, Bureau of Accident Investigation, Washington, DC, ATL 78 FR018.

7. P. Eggers, Severe Rail and Truck Accidents: Toward a Definition of Bounding Environments for Transportation Packages, U.S. Nuclear Regulatory Commission, NUREG/CR-3499, 1983.

NRC FORM 335 (2-84) NRCM 1102, 3201, 3202

U.S. NUCLEAR REGULATORY COMMISSION

BIBLIOGRAPHIC DATA SHEET

SEE INSTRUCTIONS ON THE REVERSE.

1. REPORT NUMBER (Assigned by TIDC, add Vol. No., if any)
NUREG/CR-4829, Vol. 1
UCID-20733

2. TITLE AND SUBTITLE
Shipping Container Response to Severe Highway and Railway Accident Conditions

Main Report

3. LEAVE BLANK

4. DATE REPORT COMPLETED
MONTH: April YEAR: 1986

5. AUTHOR(S)
L.E. Fischer, C.K. Chou, M.A. Gerhard, C.Y. Kimura, R.W. Martin, R.W. Mensing, M.E. Mount, M.C. Witte

6. DATE REPORT ISSUED
MONTH: February YEAR: 1987

7. PERFORMING ORGANIZATION NAME AND MAILING ADDRESS (Include Zip Code)
Lawrence Livermore National Laboratory
P. O. Box 808, L-197
Livermore, California 94550

8. PROJECT/TASK/WORK UNIT NUMBER

9. FIN OR GRANT NUMBER
A0397

10. SPONSORING ORGANIZATION NAME AND MAILING ADDRESS (Include Zip Code)
Division of Reactor System Safety
Office of Nuclear Regulatory Research
U.S. Nuclear Regulatory Commission
Washington, D.C. 20555

11a. TYPE OF REPORT
Technical

b. PERIOD COVERED (Inclusive dates)

12. SUPPLEMENTARY NOTES

13. ABSTRACT (200 words or less)

This report describes a study performed by the Lawrence Livermore National Laboratory to evaluate the level of safety provided under severe accident conditions during the shipment of spent fuel from nuclear power reactors. The evaluation is performed using data from real accident histories and using representative truck and rail cask models that likely meet 10 CFR 71 regulations. The responses of the representative casks are calculated for structural and thermal loads generated by severe highway and railway accident conditions. The cask responses are compared with those responses calculated for the 10 CFR 71 hypothetical accident conditions. By comparing the responses it is determined that most highway and railway accident conditions fall within the 10 CFR 71 hypothetical accident conditions. For those accidents that have higher responses, the probabilities and potential radiation exposures of the accidents are compared with those identified by the assessments made in the "Final Environmental Statement on the Transportation of Radioactive Material by Air and other Modes," NUREG-0170. Based on this comparison, it is concluded that the radiological risks from spent fuel under severe highway and railway accident conditions as derived in this study are less than risks previously estimated in the NUREG-0170 document.

14. DOCUMENT ANALYSIS – a. KEYWORDS/DESCRIPTORS
spent fuel casks
severe highway and railway accident conditions

b. IDENTIFIERS/OPEN-ENDED TERMS

15. AVAILABILITY STATEMENT
Unlimited

16. SECURITY CLASSIFICATION
(This page) Unclassified
(This report) Unclassified

17. NUMBER OF PAGES

18. PRICE

NUREG/CR-4829
UCID-20733
Vol. 2

Shipping Container Response to Severe Highway and Railway Accident Conditions

Appendices

Prepared by L. E. Fischer, C. K. Chou, M. A. Gerhard, C. Y. Kimura,
R. W. Martin, R. W. Mensing, M. E. Mount, M. C. Witte

Lawrence Livermore National Laboratory

**Prepared for
U.S. Nuclear Regulatory
Commission**

Reprinted October 1988

NUREG/CR-4829
UCID-20733
Vol. 2
RT

Shipping Container Response to Severe Highway and Railway Accident Conditions

Appendices

Manuscript Completed: April 1986
Date Published: February 1987

Prepared by
L. E. Fischer, C. K. Chou, M. A. Gerhard, C. Y. Kimura,
R. W. Martin, R. W. Mensing, M. E. Mount, M. C. Witte

Lawrence Livermore National Laboratory
7000 East Avenue
Livermore, CA 94550

Prepared for
Division of Reactor System Safety
Office of Nuclear Regulatory Research
U.S. Nuclear Regulatory Commission
Washington, DC 20555
NRC FIN A0397

ABSTRACT

This report describes a study performed by the Lawrence Livermore National Laboratory to evaluate the level of safety provided under severe accident conditions during the shipment of spent fuel from nuclear power reactors. The evaluation is performed using data from real accident histories and using representative truck and rail cask models that likely meet 10 CFR 71 regulations. The responses of the representative casks are calculated for structural and thermal loads generated by severe highway and railway accident conditions. The cask responses are compared with those responses calculated for the 10 CFR 71 hypothetical accident conditions. By comparing the responses it is determined that most highway and railway accident conditions fall within the 10 CFR 71 hypothetical accident conditions. For those accidents that have higher responses, the probabilities and potential radiation exposures of the accidents are compared with those identified by the assessments made in the "Final Environmental Statement on the Transportation of Radioactive Material by Air and other Modes," NUREG-0170. Based on this comparison, it is concluded that the radiological risks from spent fuel under severe highway and railway accident conditions as derived in this study are less than risks previously estimated in the NUREG-0170 document.

TABLE OF CONTENTS

TABLE OF CONTENTS (continued)

TABLE OF CONTENTS (continued)

TABLE OF CONTENTS (continued)

TABLE OF CONTENTS (continued)

TABLE OF CONTENTS (continued)

LIST OF FIGURES

LIST OF FIGURES (continued)

LIST OF FIGURES (continued)

LIST OF FIGURES (continued)

LIST OF FIGURES (continued)

LIST OF TABLES

LIST OF TABLES (continued)

PREFACE

This report describes a study conducted to estimate the responses of spent fuel casks to severe highway and railway accident conditions and to assess the level of safety provided to the public during the shipment of spent fuel. The study was performed by the Lawrence Livermore National Laboratory for the U.S. Nuclear Regulatory Commission (NRC), Office of Nuclear Regulatory Research.

This report is divided into two volumes: Volume I, the main report, describes the study, the technical approach, the study results, and conclusions; and Volume II, the Appendixes, provide supporting accident data and engineering calculations. This report has been reviewed by the Denver Research Institute at the University of Denver under a separate contract to the NRC as the peer review. A companion summary report entitled "Transporting Spent Fuel-Protection Provided Against Severe Highway and Railway Accidents" (NUREG/BR-0111) has been prepared by the NRC for wide distribution to federal agencies, local governments, and interested citizens.

Commercial spent fuel shipments are regulated by both the Department of Transportation (DOT) and the NRC. The NRC evaluates and certifies the design, manufacture, operation, and maintenance of spent fuel casks, whereas the DOT regulates the vehicles and drivers which transport the spent fuel.

Current NRC regulations require spent fuel casks to meet certain performance standards. The performance standards include normal and hypothetical accident conditions which a cask must be capable of withstanding without exceeding established acceptance criteria that

(1) limit the release of radioactive material from the cask,
(2) limit the radiation levels external to the cask, and
(3) assure that the spent fuel remains subcritical.

This study evaluates the possible mechanical and thermal loads generated by actual and potential truck and railroad transportation accidents. The magnitudes of the loads from accidents are compared with the loads implied from the hypothetical accident conditions. The frequency of the accidents that can produce defined levels of mechanical and thermal loads are developed from the accident data base. Using this information, it is determined that

for certain broad classes of accidents, spent fuel casks provide essentially complete protection against radiological hazards. For extremely severe accidents--those which could impose loads on the cask greater than those implied by the hypothetical accident conditions--the likelihood and magnitude of any radiological hazards are conservatively estimated. The radiological risk is then estimated and compared with risk estimates previously used by the NRC in judging the adequacy of its regulations.

The results of this study depend primarily on the quality of the cask response models, the radiation release models, and the probability models and distributions used in the analysis. Models for cask responses, radioactive releases, and distributions for the accident parameters are new developments based on current computer codes, limited test data on radioactive releases, and limited historical accident data. The results are derived using representative spent fuel casks which use design principles and materials that have been used in casks currently licensed by the NRC. The representative casks are assumed to have been designed, manufactured, operated, and maintained in accordance with national codes and standards (or equivalent) which have adequate margins of safety embedded in them. The results of this study are limited to spent fuel casks designed and fabricated under current technologies and operated under current regulations. New designs using alternative design principles and materials, or changes to regulations such as the imposition of a 75 mph national speed limit, could affect the results and conclusions of this study.

This study does not consider the effects which human factors can have on the cask design, manufacture, operation, and maintenance. If further study is conducted, human factors should be considered because they can contribute to the overall risk in each phase of transporting spent fuel.

L. E. Fischer

ACKNOWLEDGEMENTS

The authors wish to acknowledge the technical contributions made to this report by R. C. Chun, L. L. George, T. E. McKone, and M. W. Schwartz of Lawrence Livermore National Laboratory. The authors wish to thank G. E. Cummings of Lawrence Livermore National Laboratory for his report review and comments. The authors also wish to thank J. R. Cook, W. R. Lahs, and W. H. Lake of the U.S. Nuclear Regulatory Commission for their support and comments during the research and preparation of this report. Many thanks to N. J. Barnes and E. A. Sturmer for report preparation and D. Bowden for report editing.

In addition, the authors would particularly like to thank the following organizations for providing information and counsel which were used in preparing this report:

Anatech International Corporation
Association of American Railroads
Bureau of Motor Carrier Safety
California Department of Transportation
Central Electricity Generating Board, England
Denver Research Institute
Department of California Highway Patrol
Electric Power Research Institute
Engineering Computer Corporation
Federal Highway Administration
Federal Railroad Administration
Health and Safety Executive, England
Los Alamos National Laboratory
National Fire Protection Association
Oak Ridge National Laboratory
Ridihalgh, Eggers and Associates, Inc.
Sandia National Laboratories
Southern Pacific Transportation Company

APPENDIX A

List of Tables

APPENDIX A
Severe Accident Data

A.1 Introduction

Under the first phase of the Nuclear Regulatory Commission Transportation Model Study Program, Ridihalgh, Eggers and Associates (REA) reviewed hundreds of severe highway and railway accident reports for the period from 1961 to 1981.[A.1] Information on selected accidents was recorded onto a set of specially formatted data summary sheets. In this study, the severe accident data base was expanded to cover additional accidents in the 1980 - 1983 period. The accident data compiled by REA was reviewed to sort out the information related to structural and thermal loading conditions. This appendix describes the process used to select severe accidents and presents sample data summary sheets for four severe accidents. Also summarized are all of the selected severe accidents with some of their more important loading parameters.

A.2 Data Summary Sheets

A literature search reported over 100,000 truck and train accidents in the period from 1961 to 1983. Approximately 335 accidents were selected for the period 1961 to 1981,and 60 accidents were selected for the period 1981 to 1983. These accidents were judged to contain accident information that could be useful in assessing high physical loading conditions. All accidents had to involve either a truck or a train to be included in the selection process.

In general, the information contained in the accident reports was more related to public safety issues and the loss of life and property rather than to the physical loading conditions that occurred during an accident. For example, a severe accident typically reported could involve a truck and several cars resulting in a high loss of property and life, but could have occurred at moderate velocities (less than 45 mph) and loading conditions that could have been relatively high to the cars (40,000-150,000 pounds), but relatively low to the truck. On the other hand, a runaway truck could hit a bridge abutment at high speed (greater than 80 mph) which could result in high

loads (greater than 400,000 pounds), but never be included in a detailed national report because the loss of life and property would not be high, and the event would be so rare that it was not a public safety issue. All the compiled accident data were reviewed and the more important loading parameters that an accident can generate on a shipping container involved in such an accident are identified. Tables A.1 to A.4 present the data summary sheets for four typical severe accidents with high physical loading conditions.

The first data summary sheet, Table A.1, provides information on a truck-fire accident in the Caldecott Tunnel near Oakland, California, in April 1982. The accident involved a gasoline truck-trailer, an automobile, and a bus. A fire resulting from approximately 8,800 gallons of gasoline had a peak flame temperature of 1900°F. Although the fire lasted 2 hours and 42 minutes according to the records, the peak flame temperature was estimated to have occurred for at least 20 minutes but not for the entire fire duration.

Table A.2 summarizes a truck-bridge accident, where in March 1981, a truck-tractor-trailer was struck by a pickup while on an overpass bridge on Interstate I-80 near San Francisco, California. The truck-tractor-trailer veered into the bridge railing, broke through the railing and fell 64 feet to the soil surface below.

Table A.3 provides information on a train fire accident, where on September 28, 1982, 43 railroad cars derailed near Livingston, Louisiana. Following the derailment, a fire started to burn various materials which included plastic pellets, vinyl chloride, and petroleum products. The fire which covered a wide area was allowed to burn for several days because of the toxic chemicals and explosions involved. A railroad car carrying motor fuel anti-knock compound (tetra-ethyl lead) exploded about 19 hours after the derailment. A second thermally induced explosion occurred on October 1, 82 hours after the derailment, involving a car carring vinyl chloride. The fire cooled down sufficiently on the fifth day to permit fire-fighting operations. Six cars carring chloride materials were purposely detonated on October 11 to dispose of the remaining unvented materials within them.

Finally, Table A.4 summarizes a train-bridge accident, where on January 19, 1979, a train derailed off a bridge into the Alabama River near Hunter, Alabama. One of the rail cars was carrying a pipe which struck the bridge and caused the derailment. Five rail cars fell into the river 75 feet below.

A.3 Severe Accident Summary Tables

Using the severe accident data summary sheets as input, tables were prepared summarizing each of the selected severe accidents to highlight the information related to loading magnitudes. Three different tables were prepared: Truck-Train Grade Crossing Accidents, Table A.5; Truck Accidents, Table A.6; and Rail Accidents, Table A.7.

Each accident is identified by its location (name of state and city) and is listed by its location in alphabetical order. For each accident the following information is provided: report source, date of accident, type of accident, number of vehicles involved, the velocity prior to the accident, the height of any fall involved, any object struck, and the duration of any fire involved. In some cases, the information was not stated on the data summary sheets and an NS is entered in the corresponding column.

A.4 Reference

A.1 P. Eggers, Severe Rail and Truck Accidents: Toward a Definition of Bounding Environment for Transportation Packages, U.S. Nuclear Regulatory Commission, Washington, DC, NUREG/CR-3499, October 1983.

Table A.1
Caldecott Tunnel Fire Data Summary Sheet

1.0 ACCIDENT IDENTIFICATION

1.01 Date of Accident: April 7, 1982
1.02 Time of Accident: 0012
1.03 Rail, Highway or Both: Highway
1.04 Location: Caldecott Tunnel near Oakland, California
1.05 Railroad and/or Trucking Co. Involved: Armour Oil Company
1.06 Accident Report No.: NTSB/HAR-83/01, PB83-916201
1.07 Source: NTSB
1.08 Title: HIGHWAY ACCIDENT REPORT - Multiple Vehicle Collisions and Fire Caldecott Tunnel near Oakland, California April 7, 1982
1.09 Location of Document: REA
1.10 Location of Additional Information: NTSB
1.11 No. of Drawings/Photos: 16

2.0 ACCIDENT EVENT DATA

2.01 Initiating Event (derail, skid, overturn, explosion, collision, head to tail, head to head, tail to tail, head to side, fall): Head to tail collision
2.02 Cause: Intoxicated driver operating car, inattention of truck driver, excessive speed of bus
2.03 Number of Vehicles Involved: 1 truck and trailer, 1 car, 1 bus
2.04 Speed of Impact: Car stopped, truck 45 mph, bus 55 mph
2.05 Distance of Fall: Not applicable (N/A)
2.06 Weather Conditions: Clear
2.07 Ambient Temperature: $50^{o}F$
2.08 Distance Traveled from Impact Point: Truck about 536 ft., bus about 2,175 ft
2.09 Description of Vehicles Involved: Cargo tank truck with full trailer and 5,400 gallon aluminum cargo tank, Grumman Flexible 53-passenger bus, Honda Accord
2.10 Adjacent Structures or Natural Formations: Caldecott Tunnel
2.11 Description of Cargo Involved in Accident: 8,800 gallons of gasoline, bus had no passengers
2.12 Elevation of Vehicles at Time of Accident: Highway through tunnel
2.13 Description of Surface Impacted: Truck to car, bus to car, bus to truck trailer, bus to highway support pier, car to tunnel wall

3.0 SEQUENCE OF EVENTS

3.01 Description of First Event: Honda car struck curb and stopped at left edge of roadway one-third of way through tunnel
3.02 Description of Second Event: Left front tire of tank trailer struck right rear corner of Honda

3.03 Description of Third Event: Bus changed lanes and struck Honda and right front of the bus struck left side of the tank trailer

3.04 Description of Fourth Event: Trailer rolled over on right side and tank truck stops upright, gasoline spills

3.05 Description of Additional Events: Bus climbed left curb, traveled out of tunnel and impacted highway support pier. Gasoline spilled from trailer ignites.

3.06 Summary of Sequence of Events: N/A

4.0 POST ACCIDENT EVENT DATA

4.1 POST ACCIDENT EVENT DATA

4.1.01 Truck or Rail Car No. 1: Truck completely destroyed by fire, only remaining parts of cargo tank shell material included a 70 in by 96 in bottom sheet section from the rear compartment of the tank truck and a 40 in by 21 ft section from the right side of the trailer tank. Left safety cable broken, main leaf springs deformed and separated from spring shackle.

4.1.02 Truck or Rail Car No. 2: Bus center front components displaced 17 ft rearward, front axle beam bent 6 inches rearward with axle and suspension attachment devices displaced and destroyed. Forward entrance door separated, forward front door post and hinge bar displaced 17 feet rearward.

4.1.03 Truck or Rail Car No. 3: Honda destroyed by fire.

4.1.04 Truck or Rail Car No. 4: N/A

4.1.05 Additional Trucks or Rail Cars Damaged: Tractor and utility semitrailer (beer truck), Ford pickup, Toyota pickup and Pontiac Phoenix sedan in tunnel incurred extensive fire damage but were not involved in collision.

4.1.06 Evidence of Crushing: N/A

4.1.07 Evidence of Impact: Left front tire of tank trailer struck right rear corner of Honda, Honda impacted tunnel wall, left front bumper of bus struck rear bumper of Honda, right front of bus struck left side of tank trailer, bus impacted highway support pier

4.1.08 Evidence of Falling: N/A

4.1.09 Evidence of Puncture: N/A

4.1.10 Evidence of Bending/Deformation of Support Members: Front axle beam of bus bent 6 inches

4.1.11 Evidence of Tearing Structural Members: N/A

4.1.12 Evidence of Projectiles Distance Traveled, Size/Weight of Projectile: N/A

4.1.13 Other Evidence of Severe Structural Damage: Tank truck and trailer tank destroyed, Honda destroyed, bus heavily damaged

4.2 THERMAL/EXPLOSION DAMAGE DATA

4.2.01 Type of Fire(s) and Fuel(s) Involved and Amounts: 8,800 gallons of gasoline

4.2.02 Duration of Fire(s): 2 hours and 42 minutes
4.2.03 Evidence of Thermal Damage (e.g., melting, sagging or weakening): All low melting point and combustible material consumed by fire, only 2 sections of cargo tank shell material remained, examination of copper wires, aluminum casting, plastic parts, glass, glazed tile and concrete spalling provided a temperature determination in tunnel
4.2.04 Materials which Showed Evidence of Thermal Damage: Aluminum cargo tank
4.2.05 Evidence of Torch or Plume Fire: N/A
4.2.06 Evidence of Rocketing: N/A
4.2.07 Evidence of Explosions: Loud explosions were heard, lights went out, tiles fell from wall, final explosion shook building
4.2.08 No. of Vehicles Affected by Fires, Explosions: 1 cargo tank truck and tank trailer, 1 bus, 2 automobiles, 1 beer truck, 2 pickup trucks
4.2.09 Approximate Area Covered by Flames: 1,900 ft of tunnel
4.2.10 Evidence of Burial/Duration: N/A

4.3 LEAK OR SPILL DATA

4.3.01 Substance(s) Leaked or Spilled: Gasoline
4.3.02 Hazards/Damage Generated by Leakage/Spill: Fire
4.3.03 Amount Leaked or Spilled: 8,800 gallons
4.3.04 Area Contaminated by Spill: N/A

5.0 MISCELLANEOUS OTHER DATA

Fire produced temperature reaching 1900^{o}F and remained that high for at least 20 minutes. Photos of damaged vehicles included in report.

6.0 KEYWORD SUMMARY OF REPORT

Table A.2
I-80 Bridge Accident Data Summary Sheet

1.0 ACCIDENT IDENTIFICATION

1.01 Date of Accident: March 1981
1.03 Rail, Highway or Both: Highway
1.04 Location: I-80, San Francisco Bay
1.05 Railroad and/or Trucking Co. Involved: Thomas M. Bonnell Tractor/trailer
George A. Burris Pickup
1.07 Source: San Jose, California
1.08 Title: N/P Clipping
1.09 Location of Document: REA
1.10 Location of Additional Information: NTSB, BMCS, CHP
1.11 No. of Drawings/Photos: 1

2.0 ACCIDENT EVENT DATA

2.01 Initiating Event (derail, skid, overturn, explosion, collision, head to tail, head to head, tail to tail, head to side, fall): Collision and loss of control
2.02 Cause: Not applicable (N/A)
2.04 Speed of Impact: 55 mph
2.05 Distance of Fall: 64 feet
2.09 Description of Vehicles Involved: Commercial Tractor/trailer, pickup truck
2.10 Adjacent Structures of Natural Formations: East Bay overpass
2.11 Description of Cargo Involved in Accident: N/A
2.12 Elevation of Vehicles at Time of Accident: On bridge roadway
2.13 Description of Surface Impacted: Tractor/trailer to pickup, tractor/trailer to concrete barrier, tractor/trailer to gravel and earth

3.0 SEQUENCE OF EVENTS

3.01 Description of First Event: Pickup truck veered in front of the tractor/trailer
3.02 Description of Second Event: Tractor/trailer then struck the pickup and then itself. Tractor/trailer veered off the overpass, vaulted a concrete barrier and railing, and fell 64 feet.

4.0 POST ACCIDENT EVENT DATA

4.1 POST ACCIDENT EVENT DATA

4.1.01 Truck or Rail Car No. 1: Tractor/trailer was demolished
4.1.02 Truck or Rail Car No. 2: Pickup truck was damaged
4.1.05 Additional Trucks or Rail Cars Damaged: 73 feet of rail and 12 feet of concrete barrier was torn out of bridge

4.1.06 Evidence of Crushing: N/A
4.1.07 Evidence of Impact: Tractor/trailer collided first with pickup truck then with bridge barrier and finally with earth
4.1.08 Evidence of Falling: 64 feet from bridge to earth
4.1.09 Evidence of Puncture: N/A
4.1.10 Evidence of Bending/Deformation of Support Members: N/A
4.1.11 Evidence of Tearing Structural Members: N/A
4.1.12 Evidence of Projectiles Distance Traveled, Size/Weight of Projectile: None
4.1.13 Other Evidence of Severe Structural Damage: N/A

4.2 THERMAL/EXPLOSION DAMAGE DATA

4.2.01 Type of Fire(s) and Fuel(s) Involved and Amounts: None
4.2.05 Evidence of Torch or Plume Fire: None
4.2.06 Evidence of Rocketing: None
4.2.07 Evidence of Explosions: None

4.3 LEAK OR SPILL DATA

4.3.01 Substance(s) leaked or spilled: N/A

5.0 MISCELLANEOUS OTHER DATA

6.0 KEYWORD SUMMARY OF REPORT

6.01 Vehicle Class (R = rail, T = truck, C = rail & truck): T
6.02 Speed of Impact: 55 mph
6.03 Falling Distance: 64 feet
6.05 Impacting Object (I1 = locomotive, I2 = coupler, I3 = sill, I4 = axle, I5 = bar stock, I6 = plate stock, I7 = I-beam, I9 = rail, I10 = forging/casting, I11 = tractor, I12 = trailer, I13 = no evidence of impacted object, I14 = caboose, I15 = other): I11 I12
6.06 Object Impacted (01 = locomotive, 02 = nox car, 03 = tank car, 04 = coal car, 05 = tractor, 06 = trailer, 07 = cargo, 08 = cask, 09 = structural concrete, 010 = building, 011 = bridge, 012 = automobile, 013 = no evidence of impacted object, 014 = caboose, 015 = other): 011 015
6.08 Fire Duration: 0 minutes
6.09 Torch Duration: 0 minutes
6.10 Rocketing Distance: 0 feet
6.11 Weight of Rocketed Object: 0 pounds
6.12 Burial Event (B1 = evidence of burial larger than 24 hours, B2 = evidence of burial shorter than 24 hours, B3 = no evidence of burial): B3
6.13 Ambient Temperature: $0^{o}F$
6.16 Number of Fatalities: 0
6.17 Vehicle Type Involved in Accident (V1 = unit train, V2 = passenger train, V3 = mixed train cargo, V4 = tractor trailer, V5 = tandem trailer, V6 = unit truck, V7 = other): V4

6.18 Cargo Type Involved in Accident (Z1 = flammable, Z2 = explosive, Z3 = toxic, Z4 = ordnance, Z5 = radioactive, Z6 = other): Z6

Table A.3
Livingston Train Fire Data Summary Sheet

1.0 ACCIDENT INFORMATION

1.01 Date of Accident: September 28, 1982
1.02 Time of Accident: 0512
1.03 Rail, Highway or Both: Rail
1.04 Location: Livingston, Lousiana
1.05 Railroad and/or Trucking Co. Involved: Illinois Central Gulf Railroad
1.06 Accident Report No.: NTSB/RAR-83/05, PB83-916305
1.07 Source: NTSB
1.08 Title: RAILROAD ACCIDENT REPORT - Derailment of Illinois Central Gulf Railroad Freight Train Extra 9629 East (GS-2-28) and Release of Hazardous Materials at Livingston, Louisiana, September 28, 1982
1.09 Location of Document: REA
1.10 Location of Additional Information: NTSB
1.11 No. of Drawings/Photos: 11

2.0 ACCIDENT EVENT DATA

2.01 Initiating Event (derail, skid, overturn, explosion, collision, head to tail, head to head, tail to tail, head to side, fall): Derail
2.02 Cause: Disengagement of air hose coupling, excessive buff force, placement of empty cars in train profile
2.03 Number of Vehicles Involved: 1 train
2.04 Speed of Impact: 40 mph
2.05 Distance of Fall: Not applicable (N/A)
2.06 Weather Conditions: Clear
2.07 Ambient Temperature: 57°F
2.08 Distance Traveled from Impact Point: N/A
2.09 Description of Vehicles Involved: Extra 9629 East consisting of 3 locomotive units, 84 loaded cars, 16 empty cars and a caboose, 29 cars were tank cars loaded with hazardous materials and 5 tank cars with flammable petroleum products
2.10 Adjacent Structures or Natural Formations: Small community with buildings and pine groves surrounding tracks
2.11 Description of Cargo Involved in Accident: Plastic pellets, petroleum products, vinyl chloride, chemical products, styrene monomer, motor fuel anti-knock compound, toluene diisocyanate, phosphoric acid, hydrofluosilicic acid, sodium hydroxide, perchloroethylene, ethylene glycol
2.12 Elevation of Vehicles at Time of Accident: Railroad bed 47 foot above sea level
2.13 Description of Surface Impacted: Gondola car to gondola car, tank car to railroad bed

3.0 SEQUENCE OF EVENTS

3.01 Description of First Event: Train arrives Livingston and bottoms out at 2 crossings. Train went into emergency braking, automatic brake put into emergency position and throttle placed in ? position

3.02 Description of Second Event: 43 cars derail breaching 2 cars loaded with vinyl chloride

3.03 Description of Third Event: Leaking vinyl chloride gas ignites creating fireball exceeding 100 ft south and 150 ft north.

3.04 Description of Fourth Event: Explosion occurs and numerous fires break out

3.05 Description of Additional Events: Evacuation of area begun, hazardous materials unit notified and begin work. Next day tank car containing anti-knock compound explodes and rockets. September 30 fires intensify and vinyl chloride begins venting. October 1 vinyl chloride car explodes and rockets. October 4 styrene monomer re-ignites. October 5 styrene burns off and burning oil cars extinguished. October 10 and 11 vinyl chloride cars detonated. October 12 residents allowed to return. October 16 last derailed cars removed from accident site.

3.06 Summary of Sequence of Events: N/A

4.0 POST ACCIDENT EVENT DATA

4.1 POST ACCIDENT EVENT DATA

4.1.01 Truck or Rail Car No. 1: 19th and 20th cars detached from their trucks. 20th car had a vertical crease the full height

4.1.02 Truck or Rail Car No. 2: 3 tank cars loaded with petroleum products separated from their trucks and heavily damaged. 1 of these was breached.

4.1.03 Truck or Rail Car No. 3: Next 15 cars separated from their trucks and were damaged beyond economical repair

4.1.04 Truck or Rail Car No. 4: Next 18 cars were tank cars loaded with chemical products and were heavily damaged. 16 were punctured or breached.

4.1.05 Additional Trucks or Rail Cars Damaged: 5 cars had minor damage, 13 more cars separated from trucks, 15 tank cars had bottom outlet extensions sheared off

4.1.06 Evidence of Crushing: N/A

4.1.07 Evidence of Impact: Vertical crease full height of gondola car, tank cars overturned, several cars destroyed by impact

4.1.08 Evidence of Falling: N/A

4.1.09 Evidence of Puncture: 20 tank cars punctured or breached, shell punctures in car containing perchloroethylene

4.1.10 Evidence of Bending/Deformations of Support Members: 36 cars destroyed by crushing impacts during derailment or by post-accident fires

4.1.11 Evidence of Tearing Structural Members: 33 tank cars separated from trucks and many breached

4.1.12 Evidence of Projectiles Distance Traveled, Size/Weight of Projectile: Shell of tank car carrying anti-knock compound propelled about 80 ft north and its tank head about 25 ft south and most of its tub portion rocketed 425 ft north. Large section of steel outer insulating jacket found about 80 ft away. Other parts found 1,500 ft south

4.1.13 Other Evidence of Severe Structural Damage: 36 cars destroyed either by crushing impacts during the derailment or by post-accident fires, explosions, and demolition. Empty gondola car had vertical separation of bolster center plates.

4.2 THERMAL/EXPLOSION DAMAGE DATA

4.2.01 Type of Fire(s) and Fuel(s) Involved and Amounts: Vinyl chloride 163,043 gallons, styrene monomer 28,145 gallons, motor fuel anti-knock compound (tetra-Ethyl lead) 5,666 gallons, toluene diisocyanate 2,259 gallons. Fires also fed by plastic pellets

4.2.02 Duration of Fire(s): 8 days

4.2.03 Evidence of Thermal Damage (e.g., melting, sagging or weakening): 2 thermally induced explosions

4.2.04 Materials which Showed Evidence of Thermal Damage: N/A

4.2.05 Evidence of Torch or Plume Fire: Vinyl chloride gas vented and burned from domes

4.2.06 Evidence of Rocketing: Thermally-induced explosions of 2 tank cars that had not been punctured caused them to rocket violently.

4.2.07 Evidence of Explosions: First explosion blew in brick front of dwelling 250 ft north. 2 other thermally induced explosions.

4.2.08 No. of Vehicles Affected by Fires, Explosions: 13 train cars

4.2.09 Approximate Area Covered by Flames: 1,000 ft radius of derailment

4.2.10 Evidence of Burial/Duration: N/A

4.3 LEAK OR SPILL DATA

4.3.01 Substance(s) Leaked or Spilled: Phosphoric acid 148,552 gallons, hydrofluosilicic acid 19,780 gallons, sodium hydroxide 15,363 gallons, perchloroethylene 14,028 gallons, ethylene glycol 20,840 gallons, plastic pellets

4.3.02 Hazards/Damage Generated by Leakage/Spill: Acrid smoke and toxic gases as well as danger of fire and explosions

4.3.03 Amount Leaked or Spilled: More than 200,000 gallons of toxic chemical products

4.3.04 Area Contaminated by Spill: Several acres containing more than 60,000 cubic yards of soil to be expected

5.0 MISCELLANEOUS OTHER DATA

Photos of accident and information on chemical compounds included in report. 9999 in fields 6.8 and 6.9 indicates time frame longer

than 6 days. See 4.2.02. 3,000 people within 5-mile radius evacuated as long as 2 weeks

6.0 KEYWORD SUMMARY OF REPORT

6.01 Vehicle Class (R = rail, T = truck, C = rail & truck): R
6.02 Speed of Impact: 40 mph
6.03 Falling Distance: 0 feet
6.04 Crushing Events (C1 = locomotive, C2 = box car, C3 = coal car, C4 = flat car, C5 = tank car, C6 = tractor, C7 = trailer, C8 = unit truck, C9 = heavy cargo, C10 = tank truck, C11 = bridge, C12 = heavy support structure, C13 = no evidence of crushing, C14 = caboose, C15 = other): C5
6.05 Impacting Object (I1 = locomotive, I2 = coupler, I3 = sill, I4 = axle, I5 = bar stock, I6 = plate stock, I7 = I-beam, I9 = rail, I10 = forging/casting, I11 = tractor, I12 = trailer, I13 = no evidence of impacted object, I14 = caboose, I15 = other): I2 I15
6.06 Object Impacted (01 = locomotive, 02 = box car, 03 = tank car, 04 = coal car, 05 = tractor, 06 = trailer, 07 = cargo, 08 = cask, 09 = structural concrete, 010 = building, 011 = bridge, 012 = automobile, 013 = no evidence of impacted object, 014 = caboose, 015 = other): 03 02
6.07 Explosion Event (significant damage to: E1 = train or truck vehicles, E2 = surrounding structural members, E3 = cratering of ground, E4 = cargo, E5 = none): E1 E2 E4
6.08 Fire Duration (note: if 9,999 - see section 4.2.02): 9,999 minutes
6.09 Torch Duration (note: if 9,999 - see section 4.2.02): 9,999 minutes
6.10 Rocketing Distance: 425 feet
6.11 Weight of Rocketed Object: 10,000 pounds
6.12 Burial Event (B1 = evidence of burial larger than 24 hours, B2 = evidence of burial shorter than 24 hours, B3 = no evidence of burial): B3
6.13 Ambient Temperature: 57°F
6.14 Vehicle Damage (thousands of dollars): 1,500
6.15 Other Property Damage (thousands of dollars): 13,064
6.16 Number of Fatalities: 0
6.17 Vehicle Type Involved in Accident (V1 = unit train, V2 = passenger train, V3 = mixed train cargo, V4 = tractor trailer, V5 = tandem trailer, V6 = unit truck, V7 = other): V3
6.18 Cargo Type Involved in Accident (Z1 = flammable, Z2 = explosive, Z3 = toxic, Z4 = ordinance, Z5 = radioactive, Z6 = other): Z1 Z2 Z3 Z6
6.19 CAS Registry Numbers for Cargo Involved in Accident: None

Table A.4
Alabama River Derailment Data Summary Sheet

1.0 ACCIDENT IDENTIFICATION

1.01 Date of Accident: January 19, 1979
1.02 Time of Accident: 0740
1.03 Rail, Highway or Both: R
1.04 Location: Hunter, Alabama
1.05 Railroad and/or Trucking Co. Involved: Illinois Central Gulf Freight Train No. AM 118
1.06 Accident Report No.: ATL 78 F R018
1.07 Source: NTSB
1.08 Title: Accident File
1.09 Location of Document: REA
1.10 Location of Additional Information: NTSB
1.11 No. of Drawings/Photos: 2

2.0 ACCIDENT EVENT DATA

2.01 Initiating Event (derail, skid, overturn, explosion, collision, head to tail, head to head, tail to tail, head to side, fall): Collision with bridge
2.02 Cause: Improper lading
2.03 Number of Vehicles Involved: 72
2.04 Speed of Impact: 8 mph
2.05 Distance of Fall: 75 feet
2.06 Weather Conditions: Cloudy, dawn
2.07 Ambient Temperature: 45°F
2.09 Description of Vehicles Involved: 3 locomotive units, 1 caboose, 2 blkd flat cars, 1 tank car, 46 loads, 19 empties
2.10 Adjacent Structures or Natural Formations: RR bridge over the Alabama River
2.11 Description of Cargo Involved in Accident: Two 54 in. O.D.C.I. pipe cars, 1 tank car with fuel oil
2.12 Elevation of Vehicles at Time of Accident: RR bed on bridge deck
2.13 Description of Surface Impacted: Pipe to bridge, car to bridge, cars to river

3.0 SEQUENCE OF EVENTS

3.01 Description of First Event: Eight 54 in. pipes were strapped together in 2 groups of 4 each. The 2 groups laid in tandem
3.02 Description of Second Event: The pipes were then chained and blocked with wood sprags nailed to the car deck.
3.03 Description of Third Event: Sprags were not predrilled and later split loosening the load which was already unstable because of the "4-together" configuration. (Note: 3 pipes fastened in this fashion would have been stable).

3.04 Description of Fourth Event: One of the loose pipe snagged the bridge superstructure bringing down one span

3.06 Summary of Sequence of Events: 5 loaded cars dropped into the Alabama River

4.0 POST ACCIDENT EVENT DATA

4.1 POST ACCIDENT EVENT DATA

4.1.01 Truck or Rail Car No. 1: 5 cars in river were damaged
4.1.02 Truck or Rail Car No. 2: Bridge was seriously damaged
4.1.06 Evidence of Crushing: None
4.1.07 Evidence of Impact: One of the 54 inch pipes impacted against a bridge truss
4.1.08 Evidence of Falling: 5 cars fell into the river as the bridge collapsed
4.1.09 Evidence of Puncture: Not applicable (N/A)
4.1.10 Evidence of Bending/Deformation of Support Members: N/A
4.1.11 Evidence of Tearing Structural Members: N/A
4.1.12 Evidence of Projectiles Distance Traveled, Size/Weight of Projectile: None
4.1.13 Other Evidence of Severe Structural Damage: See above

4.2 THERMAL/EXPLOSION DAMAGE DATA

4.2.01 Type of Fire(s) and Fuel(s) Involved and Amounts: None
4.2.05 Evidence of Torch or Plume Fire: None
4.2.06 Evidence of Rocketing: None
4.2.07 Evidence of Explosions: None
4.2.10 Evidence of Burial/Duration: Cars were in the river and mud

4.3 LEAK OR SPILL DATA

4.3.01 Substance(s) Leaked or Spilled: The tank car filled with fuel oil was reported not to be leaking

6.0 KEYWORD SUMMARY OF REPORT

6.01 Vehicle Class (R = rail, T = truck, C = rail & truck): R
6.02 Speed of Impact: 8 mph
6.03 Falling Distance: 75 feet
6.04 Crushing Events (C1 = locomotive, C2 = box, C3 = coal car, C4 = flat car, C5 = tank car, C6 = tractor, C7 = trailer, C8 = unit truck, C9 = heavy cargo, C10 = tank truck, C11 = bridge, C12 = heavy support structure, C13 = no evidence of crushing, C14 = caboose, C15 = other): C13
6.05 Impacting Object (I1 = locomotive, I2 = coupler, I3 = sill, I4 = axle, I5 = bar stock, I6 = plate stock, I7 = I-beam, I9 = rail, I10 = forging/casting, I11 = tractor, I12 = trailer, I13 = no evidence of impacted object, I14 = caboose, I15 = other): I10

6.06 Object Impacted (01 = locomotive, 02 = box car, 03 = tank car, 04 = coal car, 05 = tractor, 06 = trailer, 07 = cargo, 08 = cask, 09 = structural concrete, 010 = building, 011 = bridge, 012 = automobile, 013 = no evidence of impacted object, 014 = caboose, 015 = other): 011

6.08 Fire Duration: 0 minutes

6.09 Torch Duration: 0 minutes

6.10 Rocketing Distance: 0 feet

6.11 Weight of Rocketed Object: 0 pounds

6.12 Burial Event (B1 = evidence of burial larger than 24 hours, B2 = evidence of burial shorter than 24 hours, B3 = no evidence of burial): B1

6.13 Ambient Temperature: $45^{o}F$

6.14 Vehicle Damage (thousands of dollars): 76

6.15 Other Property Damage (thousands of dollars): 2,000

6.16 Number of Fatalities: 0

6.17 Vehicle Type Involved in Accident (V1 = unit train, V2 = passenger train, V3 = mixed train cargo, V4 = tractor trailer, V5 = tandem trailer, V6 = unit truck, V7 = other): V3

6.18 Cargo Type Involved in Accident (Z1 = flammable, Z2 = explosive, Z3 = toxic, Z4 = ordnance, Z5 = radioactive, Z6 = other): Z1 Z6

Table A.5 Legend
Rail-Highway Grade-Crossing Accidents

Report Source

FRA	Federal Railroad Administration
NATL, year, report #	Department of Transportation, Federal Railroad Administration, Atlanta Office
NCHI, year, report #	Department of Transportation, Federal Railroad Administration, Chicago Office
N/HAB	National Transportation Safety Board, Highway Accident Brief
NOAK, year, report #	Department of Transportation, Federal Railroad Administration, Oakland Office
N/RHR	National Transportation Safety Board, Railroad Highway Report
NS	Not Stated
NTSB	National Transportation Safety Board

Accident Description

HtoS Col.	Head to Side Collision
Vhcl	Vehicle

Table A.5
Rail-Highway Grade-Crossing Accidents

Location	Report Source	Date of Accident	Accident Description	No. of Vhcl	Acc. vel. (mph)	Fall ht. (ft.)	Fire Y/N (dur)	Object Struck Description
Alabama								
Huntsville	NTSB 82-1	9/15/81	HtoS Col.	2	30	NS	Y(60M)	Cargo Tank
California								
Tracy	NTSB 76-1	3/9/75	HtoS Col.	2	50	NS	N	Gondola Car
Florida								
Plant City	N/RHR-78-2	10/2/77	Train-Truck	8	70	NS	Y(17M)	Pickup Truck
Georgia								
Aragon	N/RHR-75-1	10/23/74	Train-Bus	2	6	0	Y(NS)	Bus
Illinois								
Beckemeyer	N/RHR-76-3	2/7/76	Train-Truck	2	NS	0	N	Pickup Truck
Elwood	N/RHR-76-2	11/19/75	Truck-Train	2	82	0	N	Train
Loda	N/RHR-71-1	1/24/70	Train-Truck	2	79	0	Y(NS)	Tanker Truck

Continued on next page

Table A.5
Rail-Highway Grade-Crossing Accidents

Location	Report Source	Date of Accident	Accident Description	No. of Vhcl	Acc. vel. (mph)	Fall ht. (ft.)	Fire Y/N (dur)	Object Struck Description
Iowa								
Des Moines	N/RHR-77-2	7/1/76	Train-Car	2	30	0	N	Auto
Louisiana								
Goldonna	N/RHR-78-1	11/28/77	Train-Truck	2	56	0	Y(NS)	Truck/Trailer
Kenner	Modern Bulk Trans	11/25/80	Train-Truck	3	17	0	Y(NS)	Truck/Trailer
Kenner	NTSB 81-1	11/25/80	HtoS Col.	3	25	NS	Y(122M)	Cargo Tank
Missouri								
Gera	NCHI79FR019	1/11/79	Train-Truck	2	35	0	N	Truck/Trailer
Boutte	N/HAB-80-1	12/15/78	Train-Truck	2+	NS	0	N	Truck/Trailer
Nebraska								
Edgar	NTSB 76-201	8/31/76	Train-Truck	2	NS	0	N	Truck/Trailer
North Platte	NS	NS	Train-Truck	2	NS	0	Y(NS)	Truck/Trailer
Stratton	N/RHR-77-1	8/8/76	Train-Bus	2	57	0	N	Bus
Nevada								
Ocala	NOAK79FR023	12/18/78	Train-Truck	2	45	0	Y(NS)	Truck/Trailer

Continued on next page

Table A.5
Rail-Highway Grade-Crossing Accidents

Location	Report Source	Date of Accident	Accident Description	No. of Vhcl	Acc. vel. (mph)	Fall ht. (ft.)	Fire Y/N (dur)	Object Struck Description
New York								
Congers	N/RHR-73-1	3/24/72	Train-Bus	2	25	0	N	Bus
Mineola	NTSB 82-2	3/14/82	HtoS Col.	2	65	NS	Y(20M)	Van
North Carolina								
Sellers	NATL78FR011	NS	Train-Truck	2	79	0	NS	Truck/Trailer
Oklahoma								
Collinsville	NTSB 72-1	4/5/71	HtoS Col.	2	71	NS	N	Truck
Marland	N/RHR-77-3	12/15/76	Train-Truck	12	90	0	Y(NS)	Tanker Truck
Oregon								
Lafayette	NS	9/8/76	Train-Bus	2	50+	0	N	Bus
Pennsylvania								
Southampton	NTSB 82-3	1/2/82	Train-Truck	3	20	NS	Y(135)	Trailer
Yardley	N/RHR-76-4	6/5/75	Train-Truck	3	63	0	N	Truck/Trailer

Continued on next page

Table A.5
Rail-Highway Grade-Crossing Accidents

Location	Report Source	Date of Accident	Accident Description	No. of Vhcl	Acc. vel. (mph)	Fall ht. (ft.)	Fire Y/N (dur)	Object Struck Description
Virginia								
Tazewell	NTSB 76-135	NS	Train-Truck	2	31	0	Y(NS)	Trailer
West Virgina								
Woodland	FRA C-8-72	NS	Train-Vhcle	2	40	NS	NS	Earthmover

Table A.6 Legend
Truck Accidents

Report Source

BMCS	Bureau of Motor Carrier Safety
CONF	Conference
DOT	Department of Transportation
DOTHS	Department of Transportation
N/HAB	National Transportation Safety Board, Highway Accident Brief
N/HAR	National Transportation Safety Board, Highway Accident Report
NS	Not Stated
NUREG/CR	Nuclear Regulatory Commission Contractor Report
PATRAM	Conference on Packaging and Transportation of Radioactive Materials

Accident Description

Bldg Col.	Building Collision
Brdg Ovtrn	Bridge Overturn
HtoH Col.	Head to Head Collision
HtoS Col.	Head to Side Collision
HtoT Col.	Head to Tail Collision
Mltpl Col.	Multiple Collision
NS Trk. Fire	Not Stated Truck Fire
Ovtrn Col.	Overturn Collision
Trailer Sep.	Trailer Separation

Table A.6
Truck Accidents

Location	Report Source	Date of Accident	Accident Description	No. of Vhcl	Acc. vel. (mph)	Fall ht. (ft.)	Fire Y/N (dur)	Object Struck Description
Arizona								
Buckeye	N/HAB-80-1	11/15/78	HtoH Col.	2	NS	0	N	Tractor Truck
Gila Bend	BMCS 76-4	NS	HtoH Col.	6	80	0	Y(NS)	Car, Motorcycle
Arkansas								
Brisco	NS	4/27/76	Overturn	1	40	30	Y(NS)	Roadbed
Camden	N/HAB-80-2	4/13/78	HtoH Col.	2	NS	0	N	Pickup Truck
Jasper	N/HAR-81-1	6/5/80	Explosion	1	63	38	N	Hillside
Little Rock	N/HAB-80-1	1/27/78	HtoH Col.	3	NS	0	N	Truck/Trailer
California								
Coachella	N/HAR-80-6	4/23/80	HtoH Col.	2	60	NS	N	Bus
Coalinga	N/HAB-80-1	12/15/78	HtoH Col.	12	47	0	N	Mltpl Cars
Corona	N/HAR-75-7	2/28/75	Mltpl Col.	84	50	0	Y(NS)	Mltpl Cars, Trucks
El Centro 35 MI W	N/HAR-75-6	3/8/74	HtoH Col.	2	45	NS	N	Semi Trailer
Lemoore	N/HAR-83-02	10/8/82	HtoH Col.	3	55	NS	N	Van
Los Angeles	NS	NS	Explosion	6	0	0	Y(NS)	None

Continued on next page

Table A.6
Truck Accidents

Location	Report Source	Date of Accident	Accident Description	No. of Vhcl	Acc. vel. (mph)	Fall ht. (ft.)	Fire Y/N (dur)	Object Struck Description
Los Angeles	NS	NS	HtoH Col.	6	55	0	Y(NS)	Truck/Trailer
California (continued)								
Los Angeles	N/HAR-80-5	3/3/80	StoS Col.	3	45	NS	Y(55M)	Tank Truck
Martinez	N/HAR-77-2	5/21/76	Brdg Ovtrn	1	35	22	N	Ground
Oakland (near)	N/HAR-83-01	4/7/82	HtoH Col.	3	55	NS	Y(162M)	Car
Ontario	NS	11/4/74	Collision	1	50	0	Y(NS)	Tree, Sign, Steel, Concrete Wall
Sacramento	NS	NS	Overturn	4	NS	0	Y(4H)	Roadbed, Cars
Sacramento (near)	N/HAR-74-5	11/11/73	Collision	1	67	NS	N	Concrete
San Bernardino	N/HAR-81-2	11/10/80	HtoH Col.	24	55	NS	N	Semi Trailer
San Francisco Bay	San Jose News	3/81	Overpass Run Off	2	55	64	N	Pickup Truck, Ground
Ventura	N/HAR-72-4	8/18/71	HtoH Col.	13	60	0	Y(60M)	Car
Willow Creek	N/HAR-83-05	2/24/83	Skid	2	38	NS	N	Bus
Winterhaven	BMCS 79-2	4/4/79	Collision	2	NS	0	Y(NS)	Parked Car
Colorado								
Canon City	N/HAR-82-3	11/14/81	HtoS Col.	3	56	NS	Y(170M)	Tractor

Continued on next page

Table A.6
Truck Accidents

Location	Report Source	Date of Accident	Accident Description	No. of Vhcl	Acc. vel. (mph)	Fall ht. (ft.)	Fire Y/N (dur)	Object Struck Description
Fleming	NS	9/29/77	HtoH Col.	2	110	0	Y(NS)	Truck/Trailer
Colorado (continued)								
Golden	NS	6/10/74	Collision	1	35	0	Y(5H)	Rock Wall
Golden	BMCS 8-186	NS	Overturn	1	95	30	NS	Roadbed, Guardrail
Kit Carson	BMCS 8-097	NS	HtoH Col.	2	120	NS	Y(NS)	Truck/Trailer
Kit Carson	BMCS 8-089	NS	HtoH Col.	2	110	NS	Y(NS)	Truck/Trailer
Silverthorne	BMCS 8-028	NS	Collision	2	55	15	Y(NS)	Guardrail
District of Columbia								
Washington	BMCS 76-2	NS	Mltpl Col.	2	NS	NS	NS	Car
Florida								
Gretna	N/HAR-72-3	8/8/71	HtoH Col.	2	50	2	N	Car
Homestead	BMCS 7-178	NS	HtoS Col.	2	51	NS	Y(NS)	Truck/Trailer
Ocala	N/HAR-83-04	2/28/83	HtoT/HtoS	22	55+	NS	Y(120M)	Semi
Georgia								
Atlanta	N/HAR-78-5	6/20/77	HtoH Col.	7	45	0	N	Cars, Truck
Atlanta								

Continued on next page

Table A.6
Truck Accidents

Location	Report Source	Date of Accident	Accident Description	No. of Vhcl	Acc. vel. (mph)	Fall ht. (ft.)	Fire Y/N (dur)	Object Struck Description
W I-20	N/HAR-75-4	8/21/73	Skid, HtoS	2	45	NS	N	Car
Georgia (continued)								
Attapulgus	BMCS 4-206	12/15/73	HtoH Col.	2	90	0	Y(NS)	Truck/Trailer
Dalton	N/HAB-80-1	12/14/78	HtoH Col.	2	NS	0	N	Truck/Trailer
Doraville	N/HAB-80-2	7/21/78	Mltpl Col.	3	NS	0	N	Motorcycle, Dump Truck
Hamilton	H/HAR-76-5	6/6/75	HtoH Col.	7	50	0	N	Bus
Leslie	N/HAB-80-2	4/4/77	HtoH Col.	2	NS	0	N	Car
Lithonia	BMCS 80-2	1/8/80	HtoS Col.	2	35	0	N	Car
Loganville	N/HAB-80-1	6/20/78	HtoS Col.	2	NS	0	N	Car
Ludowici	N/HAB-80-1	5/2/78	HtoS Col.	3	NS	0	N	Car
Richmond Hill	N/HAB-80-1	6/19/78	HtoH Col.	3	NS	0	N	Car
Savannah	N/HAB-80-1	7/6/78	Jackknife	2	NS	0	N	Car
Waco	N/HAR-72-5	6/4/71	HtoH Col.	2	40	0	Y(+15M)	Car
Illinois								
Gibson City	5th PATRAM pg 804-806	NS	Jackknife	1	NS	NS	NS	Roadbed
Rosecrans	BMCS 5-030	4/29/76	Collision	1	55	0	Y(NS)	Bridge Barrier

Continued on next page

Table A.6
Truck Accidents

Location	Report Source	Date of Accident	Accident Description	No. of Vhcl	Acc. vel. (mph)	Fall ht. (ft.)	Fire Y/N (dur)	Object Struck Description
Indiana								
Chesterton	NS	NS	Jackknife	1	55	20	N	Guardrail
Indianapolis	BMCS 75-5	6/13/75	Overturn	1	50	18	NS	Roadbed
Iowa								
Winthrop	N/HAB-80-1	5/2/78	Overturn	1	NS	0	N	Roadbed
Kansas								
Kansas City	BMCS 7-064	8/6/76	Cargo Loss	1	NS	0	Y(NS)	Roadbed
Leon	N/HAB-80-2	5/15/78	HtoH Col.	3	NS	0	Y(NS)	Car
Mayetta	BMCS 80-1	1/6/80	HtoH Col.	2	50	0	Y(NS)	Pickup Truck
Wichita	NUREG/CR-0992	NS	Overturn	1	NS	NS	NS	Roadbed
Kentucky								
Beattyville	N/HAR-78-4	9/24/77	Runaway	17	36	0	Y(5H)	Roadbed
Carroll City	DOTHS602826	8/75	HtoH Col.	3	60	0	Y(105M)	Car/Trailer

Continued on next page

Table A.6
Truck Accidents

Location	Report Source	Date of Accident	Accident Description	No. of Vhcl	Acc. vel. (mph)	Fall ht. (ft.)	Fire Y/N (dur)	Object Struck Description
Louisiana								
Baton Rouge	NS	NS	Overturn	1	NS	0	Y(NS)	Roadbed
Lake Charles	N/HAR-82-4	8/27/81	Skid	26	30+	NS	N	Semi Trailer
Ramah	N/HAB-80-2	12/16/78	Mltpl Col.	4	NS	0	Y(NS)	Bridge Column
Maryland								
Bethesda	BMCS 78-2	3/14/78	Mltpl Col.	3	70	40	N	Car
Frostburg	N/HAR-81-3	2/18/81	HtoS Col.	17	50+	NS	N	Truck
Hagerstown	N/HAB-80-1	1/30/79	HtoH Col.	2	NS	0	N	Truck/Trailer
N. Carrollton	N/HAR-71-9	6/19/70	Skid, HtoT	2	NS	NS	N	Truck
Massachusetts								
Belcherstown	NS	NS	Collision	1	60	25	N	Utility Pole
Braintree	N/HAR-74-4	10/18/73	Overturn	1	55	0	Y(NS)	Roadbed
Michigan								
Detroit	NS	2/7/77	Collision	1	45	30	Y(NS)	Bridge Barrier
Flint	BMCS 5-076	8/19/76	Collision	1+	NS	20	Y(NS)	Bridge Rail, Roadbed

Continued on next page

Table A.6
Truck Accidents

Location	Report Source	Date of Accident	Accident Description	No. of Vhcl	Acc. vel. (mph)	Fall ht. (ft.)	Fire Y/N (dur)	Object Struck Description
Minnesota								
Floodwood	BMCS 5-169	NS	HtoH Col.	3	105	0	NS	Truck/Trailer
Mississippi								
Waynesboro	N/HAR-82-2	10/12/81	HtoH Col.	3	35	NS	N	Car/Pole
Missouri								
Fisk	BMCS 7-064	NS	Collision	1	55	45	NS	Bridge, River
Keytesville	NS	4/7/77	Collision	1	55	30	N	Bridge Barrier
Kansas City	N/HAB-80-2	7/13/77	Collision	1	55	0	N	Bridge Column
St. Louis	N/HAR-79-3	9/25/77	HtoH Col.	2	NS	0	N	Car
North Carolina								
Hertford	NS	1/10/78	Explosion	2	NS	0	Y(NS)	NS
Marion	N/HAR-78-6	1/25/78	HtoH Col.	2	70	0	N	Pickup Truck
Morganton	NS	4/27/78	HtoH Col.	2	75	0	N	Truck
North Dakota								
Freeman	BMCS 80-3	3/12/80	HtoH Col.	4	40	0	Y(NS)	Cars

Continued on next page

Table A.6
Truck Accidents

Location	Report Source	Date of Accident	Accident Description	No. of Vhcl	Acc. vel. (mph)	Fall ht. (ft.)	Fire Y/N (dur)	Object Struck Description
New Jersey								
Bordentown	N/HAR-75-3	10/19/73	Side Col.	4	55	50	Y(NS)	Car
Elizabethtown	NS	9/27/77	Explosion	1	0	0	Y(NS)	NS
Turnpike Exit 8	N/HAR-73-4	10/17/73	Side Col.	3	65+	0	Y(30M)	Guardrail
New York								
Alden	N/HAB-80-1	3/15/78	Collision	4	NS	0	N	Car
Brant	DOTHS801925	6/21/75	Collision	1	55	35	NS	Post, Roadbed
Brooklyn	N/HAR-71-6	5/30/70	Explosion	1	0	0	Y(NS)	NS
Buffalo	DOTHS600979	3/19/71	HtoH Col.	2	55	0	NS	Truck/Trailer
Buffalo	DOTHS600974	3/24/71	Overturn	1	60	NS	NS	Roadbed
Hamburg	DOTHS601762	4/10/72	Overturn	1	40	NS	NS	Roadbed
Locke	NS	NS	Jackknife	21	NS	0	Y(NS)	Building
Moreau	N/HAB-80-1	8/13/78	HtoH Col.	2	NS	0	N	Truck/Trailer
Ohio								
Ashtabula	Newscast	4/1/81	Overturn	1	NS	NS	NS	Roadbed
Valley View	N/HAR-77-3	8/20/76	Mltpl Col.	11	50	0	Y(NS)	Mltpl Cars

Continued on next page

Table A.6
Truck Accidents

Location	Report Source	Date of Accident	Accident Description	No. of Vhcl	Acc. vel. (mph)	Fall ht. (ft.)	Fire Y/N (dur)	Object Struck Description
Oklahoma								
El Reno	BMCS 6-606	NS	HtoH Col.	2	50	31	N	Truck/Trailer
Stroud	BMCS 6-046	NS	Collision	1	45	25	Y(NS)	Guardrail
Oregon								
Portland	DOT 72-5	11/18/72	Side Col.	1	NS	0	N	Concrete Wall
Pennsylvania								
Clarion	BMCS 69-5	NS	Collision	1	20	13	N	Bridge
Fulton County	N/HAB-80-1	2/22/79	Overturn	1	NS	0	N	Ground
Indiana	N/HAR-80-3	9/22/79	HtoH Col.	2	70	NS	N	Car
Lamar	N/HAB-80-1	2/7/79	Run Off Rd	2	NS	0	N	Guardrail
Lancaster Cnty	N/HAR-72-1	2/6/72	Collision	1	55	NS	N	Guardrail
Mt. Pleasant	N/HAB-80-1	2/14/79	Trailer Sep.	2	NS	0	N	Car
N. Cumberland	BMCS 3-208	NS	Overturn	2	55	0	N	Roadbed
Washington	NS	NS	Collision	1	50	0	Y(3H)	Guardrail
Washington	NS	NS	Overturn	7	50	0	N	Roadbed
Warfordsburg	N/HAB-80-1	5/5/79	Overturn	1	70	0	N	Roadbed

Continued on next page

Table A.6
Truck Accidents

Location	Report Source	Date of Accident	Accident Description	No. of Vhcl	Acc. vel. (mph)	Fall ht. (ft.)	Fire Y/N (dur)	Object Struck Description
Rhode Island								
West Greenwich	N/HAB-80-1	1/26/79	Bldg Col.	1	NS	0	N	Building
Tennessee								
Adams	BMCS 69-3	NS	HtoH Col.	3	110	0	N	Truck/Trailer
Carthage	BMCS 70-8	NS	Collision	1	55	50	N	Railing
Church Hill	NS	1/14/76	HtoH Col.	3	70	NS	Y(85M)	Truck/Tractor
Knoxville (east of)	Knoxville News	4/29/81	NS Trk. Fire	1	NS	0	Y(NS)	None
Koko	N/HAB-80-1	10/17/78	HtoS Col.	3	NS	0	N	Pickup Truck
Memphis	BMCS 73-8	NS	Mltpl Col.	4	100	0	N	Truck/Trailer
Nashville	N/HAR-74-2	7/27/73	Bridge Fall Off	1	55	65	N	Bridge Barrier, Ground
Oak Ridge	CONF 090174	NS	Overturn	1	55	7	NS	Ditch
Texas								
Cotulla	N/HAR-72-6	9/5/71	Ovtrn Col.	2	60	0	Y(NS)	Microbus
Eagle Pass	N/HAR-76-4	4/29/75	Overturn	51	55	0	N	Concrete Wall
Fairfield	BMCS 6-012	NS	Overturn	1	60	30	Y(NS)	Bridge Barrier
Fischer City	BMCS 78-3	12/8/78	HtoS Col.	2	55	0	NS	Bus

Continued on next page

Table A.6
Truck Accidents

Location	Report Source	Date of Accident	Accident Description	No. of Vhcl	Acc. vel. (mph)	Fall ht. (ft.)	Fire Y/N (dur)	Object Struck Description
Texas (continued)								
Fort Worth	BMCS 6-183	NS	Overturn	1	55	30	N	Roadbed
Fort Worth	NS	NS	Jackknife	1	55	55	N	Bridge Rail
Houston	N/HAR-77-1	5/11/76	Overturn	1+	54	15	N	Freeway Roadbed
Luling	N/HAR-81-4	11/16/80	Skid	1	55	NS	N	Ditch
Mesquite	BMCS 6-012	NS	HtoH Col.	2	105	0	N	Truck/Trailer
San Antonio	DOTHS800650	9/24/71	Overturn	1	60	0	N	Roadbed
Stratford	BMCS 6-026	NS	HtoH Col.	2	110	NS	NS	Truck/Trailer
Utah								
Bountiful	DOTHS801500	10/5/72	Collision	1	65	20	NS	Guardrail,Rdbed
Delta	N/HAR-80-2	9/12/79	HtoS Col.	2	55	NS	N	Van/Bridge
Farmington	DOTHS602309	1/23/73	Overturn	1	70	0	NS	Roadbed
Salt Lake City	DOTHS801499	10/16/72	Overturn	1	70	0	Y(3H)	Roadbed
Salt Lake City	DOTHS820160	NS	Collision	1	55	20	Y(NS)	Roadbed
Scipio	N/HAR-79-1	8/26/77	HtoH Col.	2	NS	0	N	Van

Continued on next page

Table A.6
Truck Accidents

Location	Report Source	Date of Accident	Accident Description	No. of Vhcl	Acc. vel. (mph)	Fall ht. (ft.)	Fire Y/N (dur)	Object Struck Description
Virginia								
Hanover City	N/HAB-80-1	12/17/79	HtoH Col.	2	NS	0	N	Car
Lynchburg	H/HAR-73-3	3/9/72	Overturn	1	25	0	Y(22H)	Rock
Quantico	Columbus, OH News	2/19/81	Bridge Run Off	1	55	80	N	Brdg Under Structure
Triangle	N/HAR-81-6	2/18/81	Collision	1	60	25	N	Guardrail
Washington								
Pasco	BMCS 10-058	NS	HtoH Col.	4	110	NS	NS	Truck/Trailer
Seattle	N/HAR-76-7	12/4/75	Jackknife	35	52	0	N	Support Column
Wyoming								
Baggs	NS	8/2/74	Side Col.	2	NS	0	Y(NS)	NS
Laramie	N/HAR-80-1	8/22/79	HtoH Col.	3	68	0	N	House, Vehicle

Table A.7 Legend
Train Accidents

Report Source

ASME	American Society of Mechanical Engineers
DOT	Department of Transportation
FRA	Federal Railroad Administration
ICC	Interstate Commerce Commission
NATL, year, report #	Department of Transportation, Federal Railroad Administration, Atlanta Office
NCHI, year, report #	Department of Transportation, Federal Railroad Administration, Chicago Office
NDCA, year, report #	Department of Transportation, Federal Railroad Administration, Washington D.C. Office
NDEN, year, report #	Department of Transportation, Federal Railroad Administration, Denver Office
NFTW, year, report #	Department of Transportation, Federal Railroad Administration, Fort Worth Office
N/HZM	National Transportation Safety Board, Hazardous Material Accident Report
NMKC, year, report #	Department of Transportation, Federal Railroad Administration, Kansas City Office
NNYC, year, report #	Department of Transportation, Federal Railroad Administration, New York City Office
NOAK, year, report #	Department of Transportation, Federal Railroad Administration, Oakland Office
N/RAR	National Transportation Safety Board,Railroad Accident Report
NS	Not Stated

Continued on next page

Table A.7 Legend Continued
Train Accidents

Report Number

NSEA, year	Department of Transportation, Federal Railroad Administration, Seattle Office

Accident Description

Brdg Col.	Bridge Collision
Brdg Fail	Bridge Failure
Drl Col.	Derail Collision
HtoH Col.	Head to Head Collision
HtoS Col.	Head to Side Collision
HtoT Col.	Head to Tail Collision
Int. Fire	Internal Fire

Continued on next page

Table A.7
Train Accidents

Location	Report Source	Date of Accident	Accident Description	No. of Vhcl	Acc. vel. (mph)	Fall ht. (ft.)	Fire Y/N (dur)	Object Struck Description
Alabama								
Florence	N/RAR-79-2	9/18/78	HtoH Col.	2 T	15	12	N	Train
Hunter	NATL78FR018	1/19/79	Brdg Col.	72	8	75	N	Bridge
Muscle Shoals	NATL79FR001	10/8/78	HtoH Col.	2 T	NS	0	N	Train
North Castle	N/RAR-77-9	1/16/77	Derail	22	43	21	N	RR Bed, RR Car
Alaska								
Hurricane	N/RAR-76-3	7/5/75	HtoH Col.	2 T	40	0	N	Train
Talkeetna	NSEA77FR005	12/1/76	Derail	71	NS	25	N	RR Bed, RR Car
Arizona								
Benson	N/RAR-75-2	5/24/73	Explosion	12	45	0	Y(8H)	NS
Benton	NFTW79FR018	12/25/78	Derail	137	45	23	Y(3H)	Bridge, RR Cars, River
Dequeen	NFTW79FR020	1/13/79	Derail	105	25	20	N	RR Bed, RR Car
Raso	NOAK79FR017	12/10/78	Derail	NS	40	0	N	RR Bed, RR Car
Rone	NFTW79FR014	12/4/78	Derail	125	15	14	N	RR Bed, RR Car

Continued on next page

Table A.7
Train Accidents

Location	Report Source	Date of Accident	Accident Description	No. of Vhcl	Acc. vel. (mph)	Fall ht. (ft.)	Fire Y/N (dur)	Object Struck Description
Arkansas								
Gilmore	NFTW79FR019	1/8/79	Derail	97	55	0	N	RR Bed, RR Car
Hartman	NFTW79FR008	2/27/77	Derail	109	40	0	Y(200M)	RR Bed, RR Car
Lewisville	N/RAR-78-8	3/29/78	Derail	47	35	0	Y(24H)	RR Bed, RR Car
Poping-Ozark	NFTW79FR012	11/9/78	Derail	131	38	NS	N	RR Bed, RR Car
Possum Grape (near)	N/RAR-83-06	10/3/82	HtoS Col.	2	50	30	Y(120)	Freight Car
California								
Andesite	NOAK79FR012	11/26/78	Derail	70	NS	0	N	RR Bed, RR Car
Bradley	NOAK79FR001	10/4/78	Derail	56	30	0	Y(5D)	RR Bed, RR Car
Hayward	N/RAR-80-10	4/9/80	Derail	1	52	30	Y(60M)	RR Bed, RR Car
Indio	N/RAR-74-1	6/25/73	HtoH Col.	2 T	60	0	Y(NS)	Train
Kelso	N/RAR-81-7	11/17/80	HtoH Col.	2	118	NS	N	Caboose
Oroville	NOAK79FR011	11/20/78	Derail	61	30	10	N	RR Bed, RR Car
Pinole	NOAK79FR013	12/1/78	Derail	73	40	0	N	RR Bed, RR Car
Roseville	DOT 4187	4/28/73	Explosion	289	0	0	Y(32H)	NS
San Francisco	N/RAR-79-5	1/17/79	Int. Fire	2	NS	0	Y(2H)	NS
Santa Margurita	NOAK79FR005	10/18/78	HtoH Col.	2 T	25	0	N	Train

Continued on next page

Table A.7
Train Accidents

Location	Report Source	Date of Accident	Accident Description	No. of Vhcl	Acc. vel. (mph)	Fall ht. (ft.)	Fire Y/N (dur)	Object Struck Description
California (continued)								
Surf	N/RAR-81-1	5/22/81	Derail	3	60	NS	N	RR Bed, RR Car
Therman	N/RAR-83-1	1/7/82	Derail	61	57	0	N	RR Bed, RR Car
Thousand Palms	N/RAR-80-1	7/24/79	HtoT Col.	2 T	20	0	Y(NS)	Train
Vidal	NOAK79FR025	2/5/79	Derail	78	45	15	N	RR Bed, RR Car
Colorado								
Lambert	NDEN76FR137	7/9/76	Derail	38	60	5	N	RR Bed, RR Car
Connecticut								
Darian	N/RAR-70-3	8/20/69	HtoH Col.	2 T	60	0	N	Train
North Canaan	N/RAR-77-4	7/13/76	HtoH Col.	2 T	20	0	N	Train
Sound View	N/RAR-72-1	10/8/70	Drl. Col.	2 T	60	0	Y(2.5H)	Train
Delaware								
Wilmington	N/RAR-76-7	10/17/75	HtoH Col.	3 T	25	0	N	Train

Continued on next page

Table A.7
Train Accidents

Location	Report Source	Date of Accident	Accident Description	No. of Vhcl	Acc. vel. (mph)	Fall ht. (ft.)	Fire Y/N (dur)	Object Struck Description
District of Columbia								
Washington	NDCA76FR151	7/18/76	Derail	84	36	25	Y(NS)	RR Bed, RR Car, Highway
Washington	N/RAR-82-6	1/13/82	Derail	1	10	NS	N	Wall
Florida								
Crestview	N/RAR-79-11	4/8/79	Derail	119	35	NS	Y(60H)	RR Bed, RR Car
Lochloosa	N/RAR-81-9	5/26/81	Derail	1	76	NS	N	RR Bed, RR Car
Pensacola	N/RAR-78-4	11/9/77	Derail	37	35	0	N	RR Bed, RR Car
Westlake Wales	FRA C71-72	NS	Derail	123	50	NS	NS	RR Bed, RR Car
Youngstown	N/RAR-78-8	2/26/78	Derail	145	45	0	N	RR Bed, RR Car
Georgia								
Covington	NATL79FR025	2/19/79	Derail	80	25	0	N	RR Bed, RR Car
Pembroke	NATL79FR021	2/7/79	Derail	134	31	5	N	RR Bed, RR Car
Rupert	NATL76FR219	9/11/76	Derail	108	50	0	N	RR Bed, RR Car
Vinings	NATL79FR016	1/15/79	Derail	60	35	0	N	RR Bed, RR Car

Continued on next page

Table A.7
Train Accidents

Location	Report Source	Date of Accident	Accident Description	No. of Vhcl	Acc. vel. (mph)	Fall ht. (ft.)	Fire Y/N (dur)	Object Struck Description
Illinois								
Bartonville	NCHI77FR016	NS	Derail	97	52	20	NS	RR Bed, RR Car
Chicago	N/RAR-77-10	2/4/77	HtoH Col.	2 T	9.5	NS	N	Train
Chicago	N/RAR-73-5	10/30/72	HtoH Col.	3 T	50	0	N	Train
Chicago	NCHI79FR004	10/29/78	HtoH Col.	2 T	20	0	N	Train
Chicago	N/RAR-76-9	1/9/76	HtoH Col.	2	35	NS	N	Rail Car
Cresent City	N/RAR-72-2	6/21/70	Derail	113	43	0	Y(56H)	RR Bed, RR Car
Decatur	N/RAR-75-4	7/19/74	Yard Col.	595	8.5	0	Y(NS)	RR Cars
Elburn	NCHI77FR025	2/21/77	Derail	105	53	0	N	RR Bed, RR Car
Flagg	NCHIRR76118	6/28/76	Derail	140	60	12	Y(NS)	RR Bed, RR Car, Bridge
Gorham	NCHI78FR030	NS	HtoH Col.	2 T	50	NS	Y(NS)	Train
Harvey	N/RAR-80-3	10/12/79	HtoH Col.	2 T	58	0	N	Train
Maquon	N/RAR-73-4	5/24/72	HtoH Col.	2 T	80	0	Y(NS)	Train
Morrison	NCHIRR76184	8/22/76	Derail	128	35	0	N	RR Bed, RR Car
Northbrook	NCHI77FR012	12/20/76	Derail	103	30	20	N	RR Bed, RR Car, Bridge
Salem	N/RAR-72-5	6/10/71	Derail	18	90	0	Y(NS)	RR Bed, RR Car
Stratford	NCHI79FR018	1/9/79	Derail	83	50	0	Y(10M)	RR Bed, RR Car
Springfield	N/RAR-81-5	10/30/80	Derail	1	63	NS	N	RR Bed, RR Car

Continued on next page

Table A.7
Train Accidents

Location	Report Source	Date of Accident	Accident Description	No. of Vhcl	Acc. vel. (mph)	Fall ht. (ft.)	Fire Y/N (dur)	Object Struck Description
Indiana								
North Haven	N/RAR-77-6	10/19/76	HtoH Col.	2 T	20	0	Y(NS)	Train
Sullivan	N/RAR-84-02	9/14/83	HtoH Col.	2	35	0	N	Caboose
Veedersburg	NCHI76FR112	6/25/76	Derail	47	44	NS	N	RR Bed, RR Car
Wheatfield	FRA B-8-72	NS	Derail	109	40	NS	Y(2H)	RR Bed, RR Car, Storage Tank
Iowa								
Cedar Rapids	NMKC79FR017	12/25/78	Derail	13	NS	22	N	River, Ice
Central Groove	NMKC79FR009	11/28/78	Derail	104	20	10	N	RR Bed, RR Car
Cudley	FRA B272BN1	NS	Derail	93	60	NS	Y(NS)	RR Bed, RR Car
Des Moines	N/RAR-76-8	9/1/75	Derail	63	25	0	Y(4D)	RR Bed, RR Car
Emerson	N/RAR-83-02	6/15/82	Derail	1	74	NS	N	RR Bed, RR Car
Gordons Ferry	NMKC79FR030	1/28/79	Derail	104	26	35	N	Miss. Rvr, RR
Cars								
Northwood	NMKC77FR010	1/23/77	Derail	104+	40	NS	N	RR Bed, RR Car
Pacific Jnctn	N/RAR-83-09	4/13/83	HtoH Col.	2	47	NS	N	Caboose
Woodburn	NMKC79FR023	1/12/79	Derail	106	50	0	N	RR Bed, RR Car

Continued on next page

Table A.7
Train Accidents

Location	Report Source	Date of Accident	Accident Description	No. of Vhcl	Acc. vel. (mph)	Fall ht. (ft.)	Fire Y/N (dur)	Object Struck Description
Kansas								
Atchison	NMKC79FR024	1/17/79	HtoH Col.	2 T	60	0	Y(100M)	Train
Fort Scott	NMKC79FR036	3/11/79	Derail	147	25	6	N	RR Bed, RR Car
Hecla	NMKC79FR001	10/5/78	HtoS Col.	2 T	32	0	N	Train
Lawrence	N/RAR-80-4	10/2/79	Derail	20	80	NS	N	RR Bed, RR Car
Lehigh	DOT B23-70	11/19/69	Derail	36	27	0	Y(NS)	RR Bed, RR Car
Malvern	N/RAR-75-1	7/5/74	Derail	21	77	NS	N	RR Bed, RR Car
Kansas/Missouri								
Fort Scott/ Liberal	NMKC79FR020	1/3/79	Derail	68	50	0	N	RR Bed, RR Car
Kentucky								
Fort Knox	N/RAR-83-07	3/22/83	Derail	1	28	NS	N	RR Bed, RR Car
Hanson	NDCA79FR020	1/7/79	Derail	115	42	0	N	RR Bed, RR Car
Mularaugh	N/RAR-81-1	7/26/80	Derail	1	35	NS	Y(5760M)	RR Bed, RR Car
Stepstone	NATL77FR007	11/8/76	Derail	54	38	20	N	RR Bed, RR Car

Continued on next page

Table A.7
Train Accidents

Location	Report Source	Date of Accident	Accident Description	No. of Vhcl	Acc. vel. (mph)	Fall ht. (ft.)	Fire Y/N (dur)	Object Struck Description
Louisiana								
Livingston	N/RAR-83-05	9/28/82	Derail	1	40	NS	Y (8D)	RR Bed, RR Car
Meeler	N/RAR-75-9	5/30/75	HtoH Col.	2 T	48	0	N	Train
Taft	N/RAR-73-6	2/21/73	HtoH Col.	2 T	43	0	Y(NS)	Train
West Monroe	NFTW79FR008	10/24/78	Derail	105	10	6	N	RR Bed, RR Car
Maryland								
Baltimore	N/RAR-78-1	6/12/77	HtoH Col.	2 T	30	0	Y(NS)	Train
Corsey	FRA C-17-72	NS	Derail	55	55	NS	NS	RR Bed, RR Car
Germantown	N/RAR-81-6	2/9/81	HtoH Col.	2	88	NS	NS	Train
Seabrook	N/RAR-79-3	6/9/78	HtoH Col.	2 T	35	NS	N	Train
Massachusetts								
Beverly	N/RAR-82-1	8/11/81	HtoH Col.	2	19	NS	N	Train
Somerville	N/HZM-81-1	4/3/80	HtoS Col.	2	4	NS	N	Tank Car

Continued on next page

Table A.7
Train Accidents

Location	Report Source	Date of Accident	Accident Description	No. of Vhcl	Acc. vel. (mph)	Fall ht. (ft.)	Fire Y/N (dur)	Object Struck Description
Michigan								
Kopje (Woodlnad)	NCHI78FR024	NS	Derail	38	34	8	NS	RR Bed, RR Car
Lansing	NCHI79FR015	12/28/78	Derail	74	40	0	N	RR Bed, RR Car
Minnesota								
DeGraff	NMKC76FR126	7/4/76	Derail	61	NS	0	Y(3M)	RR Bed, RR Car
Forbes	NMKC76FR059	NS	Derail	119	30	30	Y(2H)	RR Bed, RR Car
Hills	NMKC79FR012	NS	Derail	44	NS	NS	N	RR Bed, RR Car
Nashau	NMKC79FR011	1/30/78	Derail	55	40	9	N	RR Bed, RR Car
Mississippi								
Goodman	N/RAR-77-3	6/30/76	Derail	13	88	0	N	RR Bed, RR Car
Laurel	N/RAR-69-	1/25/69	Derail	144	30	0	Y(60H)	RR Bed, RR Car
Missouri								
Crystal City	N/RAR-84-01	7/18/83	Derail	94	52	25	N	RR Bed, RR Car
Dexter	NMKC79FR003	10/10/78	HtoH Col.	2 T	NS	0	N	Train
Dresden	NMKC79FR025	1/23/79	Derail	38	50	8	N	RR Bed, RR Car

Continued on next page

Table A.7
Train Accidents

Location	Report Source	Date of Accident	Accident Description	No. of Vhcl	Acc. vel. (mph)	Fall ht. (ft.)	Fire Y/N (dur)	Object Struck Description
Missouri (continued)								
Kansas City	NMKC79FR015	12/16/78	Derail	155	20	24	Y(20M)	RR Bridge, RR Bed, RR Car
Randles	NMKC79FR033	2/9/79	Drl. Col.	2 T	25	0	N	RR Bed, RR Car, Train
Springfield	NMKC79FR022	1/10/79	Derail	124	56	16	Y(NS)	RR Bed, RR Car
Montana								
Belt	N/RAR-77-7	11/26/76	Derail	126	38	NS	Y(12H)	RR Bed, RR Car
Browning	NSEA79FR003	10/23/78	Side Col.	2 T	25	30	N	Train
Butte	NSEA79FR013	12/18/78	Derail	81	26	0	NS	RR Bed, RR Car
Curry	FRA C-7-72	NS	Derail	84	50	NS	NS	RR Bed, RR Car
Essex	NSEA79FR001	10/3/78	Derail	35	59	0	N	RR Bed, RR Car
Glacier Park	N/RAR-80-6	3/14/80	Derail	10	37	12	N	RR Bed, RR Car
Greycliff	NSEA79FR006	11/3/78	Derail	74	55	12	Y(NS)	RR Bed, RR Car
Havre	NSEA79FR008	11/14/78	Derail	81	60	18	N	RR Bed, RR Car
Lohman	N/RAR-79-7	3/28/79	Derail	14	74	0	N	RR Bed, RR Car
Zurich	NSEA79FR009	12/8/78	HtoH Col.	2 T	35	0	N	Train

Continued on next page

Table A.7
Train Accidents

Location	Report Source	Date of Accident	Accident Description	No. of Vhcl	Acc. vel. (mph)	Fall ht. (ft.)	Fire Y/N (dur)	Object Struck Description
Nebraska								
Angora	N/RAR-80-7	2/16/80	HtoH Col.	2 T	49	0	N	Train
Arlington	NMKC79FR031	1/31/79	Derail	82	40	0	N	RR Bed, RR Car
Crete	N/RAR-71-2	2/18/69	Derail	169	52	0	N	RR Bed, RR Car
Glenville	NS	5/19/76	Derail	70	68	0	N	RR Bed, RR Car
Gothenburg	NMKC79FR035	3/12/79	Derail	109	60	0	N	RR Bed, RR Car
Hastings	N/RAR-77-1	8/2/76	Derail	119	45	0	N	RR Bed, RR Car
Josselyn	NMKC7FR006	NS	Derail	116	70	NS	NS	RR Bed, RR Car
Marsland	NMKC79FR026	1/25/79	Derail	110	45	40	N	RR Bed, RR Car
Potter	NMKC77FR004	11/13/76	Derail	90	NS	0	Y(1M)	RR Bed, RR Car
Ralston	N/RAR-77-8	12/16/76	Derail	12	53	40	N	RR Bed, RR Car
Nevada								
Elburz	NOAK76FR127	7/4/76	Derail	41	NS	10	N	RR Bed, RR Car
Hoya	NOAK79FR015	12/4/78	HtoH Col.	2 T	22	0	Y(2.5H)	RR Cars
New Jersey								
Edison	N/RAR-79-10	4/20/79	HtoH Col.	2 T	NS	0	Y(5M)	Truck, Machinery
Linden	N/RAR-80-12	7/9/80	Derail	2	30	NS	N	RR Bed, RR Car

Continued on next page

Table A.7
Train Accidents

Location	Report Source	Date of Accident	Accident Description	No. of Vhcl	Acc. vel. (mph)	Fall ht. (ft.)	Fire Y/N (dur)	Object Struck Description
New Mexico								
Des Moines	NDEN79FR001	10/25/78	Derail	62	23	NS	N	RR Bridge, RR Bed, RR Car
New York								
Brooklyn	N/RAR-82-2	7/3/81	HtoH Col.	2	12.7	NS	N	Subway Car
Dobbs Ferry	N/RAR-81-4	11/7/80	HtoH Col.	2	10	NS	Y(15M)	Power Car
New York City	N/RAR-75-8	1/2/75	HtoH Col.	2	35	NS	N	Rail Car
NY City Subway	N/RAR-79-8	12/12/78	Derail	8	NS	0	Y(NS)	RR Bed, RR Car, Concrete Wall
NY City Subway	N/RAR-79-8	1/15/79	Derail	10	NS	0	N	RR Bed, RR Car
NY City Subway	N/RAR-79-8	2/14/79	Derail	10	NS	NS	N	RR Bed
NY City Subway	N/RAR-79-8	3/21/79	Derail	8	NS	0	N	RR Bed
Oneonta	N/RAR-74-4	2/12/74	Derail	125	32	0	Y(7D)	RR Bed, RR Car
North Carolina								
Laleview	N/RAR-80-10	4/2/80	HtoH Col.	2 T	35	0	N	Train
Spencer	N/RAR-78-3	10/8/77	Side Col.	2 T	50	0	N	Train, RR Bed, RR Car

Continued on next page

Table A.7
Train Accidents

Location	Report Source	Date of Accident	Accident Description	No. of Vhcl	Acc. vel. (mph)	Fall ht. (ft.)	Fire Y/N (dur)	Object Struck Description
North Dakota								
Fairmont	NMKC79FR019	12/31/78	Derail	83	40	0	N	RR Bed, RR Car
Walcott	NMKC79FR034	2/17/79	Derail	64	48	15	N	RR Bed, RR Car
White Earth	NMKC79FR021	1/7/79	Derail	77	45	0	N	RR Bed, RR Car
Ohio								
Albany	FRA C-68-72	NS	Derail	93	30	NS	Y(NS)	RR Bed, RR Car, Creek Bed
Circleville	Columbus, OH News	2/17/81	Derail	490	NS	0	N	RR Bed, RR Car
Cleveland	N/RAR-75-3	5/8/74	Brdg Col.	96	33	25	N	Drawbridge
Columbus	ICC 4036	NS	Derail	29	43	0	Y(2H)	RR Bed, RR Car
Huntington	FRA B-3-72	NS	Derail	108	38	NS	Y(3H)	RR Bed, RR Car
Leetonia	N/RAR-76-2	6/6/75	HtoH Col.	2 T	29	0	N	Train
Leetonia	NCHI79FR005	11/1/78	HtoH Col.	5	32	0	N	Train
Lodi	NCHIRR76081	5/30/76	Derail	72	57	15	Y(2H)	RR Bed, RR Car
Pettisville	N/RAR-76-10	2/4/76	HtoH Col.	2 T	70	0	Y(NS)	Train
Pemberville	NCHI79FR012	12/3/78	Derail	185	35	0	N	RR Bed, RR Car
St. Louisville	Utica News	NS	Derail	83+	25	0	N	RR Bed, RR Car

Continued on next page

Table A.7
Train Accidents

Location	Report Source	Date of Accident	Accident Description	No. of Vhcl	Acc. vel. (mph)	Fall ht. (ft.)	Fire Y/N (dur)	Object Struck Description
Ohio (continued)								
Wooster	NCHI79FR008	11/18/78	HtoS Col.	2 T	23	0	N	Train, Tower
Wooster	NCHI77FR013	12/23/76	Derail	131	30	15	Y(10M)	RR Bed, RR Car
Oklahoma								
Alva	NFTW79FR028	3/21/79	Derail	83	42	5	N	RR Bed, RR Car
Leonard	ASME RAIL TRANSPORT PROCEEDINGS	NS	Derail	23	35	NS	NS	RR Bed, RR Car
Mustang	N/RAR-75-6	9/1/74	HtoH Col.	2 T	40	0	Y(NS)	Train
Sallisaw	NFTW79FR011	11/6/78	Derail	52	37	60	N	RR Bed, RR Car
Oregon								
Huntington	NSEA79FR012	12/18/78	Derail	97	60	20	N	RR Bed, RR Car

Continued on next page

Table A.7
Train Accidents

Location	Report Source	Date of Accident	Accident Description	No. of Vhcl	Acc. vel. (mph)	Fall ht. (ft.)	Fire Y/N (dur)	Object Struck Description
Pennsylvania								
Big Run	NNYC79FR031	2/13/79	Derail	74	34	0	N	RR Bed, RR Car
Bristol	N/RAR-82-5	3/29/82	HtoH Col.	2T	22	0	N	Train
Bryant	NNYC79FR021	NS	Derail	98	30	5	N	RR Bed, RR Car
Culmerville	NNYC79FR003	10/10/78	Derail	145	35	0	N	RR Bed, RR Car
Herndon	N/RAR-73-3	3/12/72	HtoH Col.	2 T	60	0	Y(NS)	Train
Munch	N/RAR-79-6	1/31/79	HtoH Col.	2 T	30	0	N	Train
North Wales	N/RAR-80-11	7/17/80	HtoH Col.	2	39	NS	N	Electric Car
Philadelphia	N/RAR-80-5	10/16/79	2HTOT CL.	3 T	28	0	N	Trains
Royersford	N/RAR-80-2	10/1/79	HtoH Col.	2 T	45	0	N	Train
Weatherby	NNYC78FA015	NS	Derail	145	NS	30	NS	RR Bed, RR Car
South Carolina								
Denmark	NATL79FR013	1/7/79	Derail	103	40	0	N	RR Bed, RR Car
Florence	N/RAR-78-6	2/24/78	Derail	20	20	0	Y(NS)	RR Bed, RR Car

Continued on next page

Table A.7
Train Accidents

Location	Report Source	Date of Accident	Accident Description	No. of Vhcl	Acc. vel. (mph)	Fall ht. (ft.)	Fire Y/N (dur)	Object Struck Description
Tennessee								
Brownsville	NATL77FR020	2/17/77	Derail	101	49	20	Y(4H)	RR Bed, RR Car
Fosterville	FRA C-5-72	NS	Derail	123	47	NS	NS	RR Bed, RR Car
N Johnsonville	N/RAR-82-4	12/28/81	HtoH Col.	2	25	45	N	Caboose
Pulaski	R/RAR-76-6	10/1/75	Derail	14	65	40	N	RR Bed, RR Car
Roddy	NATL79FR012	12/24/78	Derail	231	44	6	N	RR Bed, RR Car
Waverly	N/RAR-79-1	2/22/78	Derail	120	35	0	Y(6H)	RR Bed, RR Car
Texas								
Britton	NFTW79FR016	12/10/78	Derail	98	25	7	N	RR Bed, RR Car
Cotulla	N/RAR-74-3	12/1/73	HtoH Col.	2 T	40	0	Y(1.5H)	Train
Dallas	San Jose News	2/21/81	Derail	60	NS	50	Y(4H)	RR Bed, RR Car, Bridge
Garland	NFTW77FR007	3/20/77	Derail	44	NS	0	Y(NS)	RR Bed, RR Car
Houston	N/RAR-75-7	9/21/74	Yard Col.	503	20	0	Y(9H)	RR Cars
Houston	N/RAR-72-6	10/19/71	Derail	88	45	45	Y(5H)	RR Bed, RR Car
Marquez	NFTW79FR005	10/13/78	Derail	94	30	0	N	RR Bed, RR Car, Timber Brd?
Paxton	N/HZM-80-1	9/8/79	Derail	56	30	15	Y(NS)	RR Bed, RR Car

Continued on next page

Table A.7
Train Accidents

Location	Report Source	Date of Accident	Accident Description	No. of Vhcl	Acc. vel. (mph)	Fall ht. (ft.)	Fire Y/N (dur)	Object Struck Description
Texas (continued)								
Temple	N/RAR-83-08	3/17/83	HtoH Col.	8	35	NS	N	Freight Car
Tyler	NFTW79FR007	10/22/78	Derail	79	45	12	N	RR Bed, RR Car
Utah								
Lakeside	NDEN76FR111	6/25/76	Derail	52	NS	10	N	RR Bed, RR Car, Lake
Virginia								
Arlington	N/RAR-73-2	4/27/72	HtoH Col.	2 T	60	0	N	Train
Colonial Hghts	N/RAR-83-04	5/5/82	Derail	1	64	40	Y (8D)	RR Bed, RR Car
Crewe	N/RAR-82-3	11/28/81	HtoS Col.	3	27	NS	N	RR Car
Elma	N/RAR-79-4	12/3/78	Derail	12	79	NS	Y(NS)	RR Bed, RR Car
Franconia	N/RAR-71-1	1/27/70	Derail	1	65	NS	N	Embankment
Jarratt	N/RAR-76-11	5/5/76	Derail	58	72	0	N	RR Bed, RR Car
Rockfish	N/RAR-83-10	4/3/83	Derail	1	48	NS	N	Landslide

Continued on next page

Table A.7
Train Accidents

Location	Report Source	Date of Accident	Accident Description	No. of Vhcl	Acc. vel. (mph)	Fall ht. (ft.)	Fire Y/N (dur)	Object Struck Description
Washington								
Deer Park	NSEA79FR002	10/4/78	Derail	41	23	0	N	RR Bed, RR Car
Ephrata (Naylor)	NSEA79FR021	2/28/79	Derail	65	50	NS	N	RR Bed, RR Car
Kalama	NSEA76FR028	9/7/76	Derail	NS	52	35	N	RR Bed, RR Car, River
Kapowsin	NSEA79FR023	3/6/79	Brdg Fail	45	10	15	N	River, Bridge
Tacoma	NSEA79FR025	3/22/79	Derail	122	23	0	N	RR Bed, RR Car, RR Bridge
Tukailla	NS	10/8/77	HtoH Col.	2 T	50	NS	Y(NS)	Train
Wenatchee	N/RAR-76-1	8/6/74	Explosion	201	10	0	Y(NS)	NS
West Virginia								
Orleans Road	N/RAR-80-9	2/12/80	HtoH Col.	2 T	38	0	N	Train
South Ruffner	NDCA79FR028	2/4/79	Side Col.	2 T	78	5	N	Train
Welch	N/RAR-81-2	9/6/80	HtoS Col.	2	38	NS	NS	Freight Car

Continued on next page

Table A.7
Train Accidents

Location	Report Source	Date of Accident	Accident Description	No. of Vhcl	Acc. vel. (mph)	Fall ht. (ft.)	Fire Y/N (dur)	Object Struck Description
Wisconsin								
Columbus	NCHI79FR009	11/24/78	Derail	70	50	NS	N	RR Bed, RR Car
Cylon	FRA C-15-72	NS	Derail	95	45	NS	NS	RR Bed, RR Car
Franksville	NCHI79FR028	3/15/79	Derail	81	40	0	N	RR Bed, RR Car
Milawukee	NCHI79FR017	1/7/79	Derail	55	38	0	N	RR Bed, RR Car
Sturtevant	NCHI79FR024	2/12/79	Derail	84	40	NS	N	RR Bed, RR Car
Wyoming								
Dale Junction	NDEN79FR007	1/22/79	Derail	121	40	40	Y(56H)	RR Bed, RR Car
Granite	N/RAR-79-12	7/31/79	Derail	85	75	0	N	RR Bed, RR Car
Hermosa	N/RAR-81-3	10/16/80	HtoH Col.	2	40	NS	N	Caboose
Leroy	NDEN79FR002	11/3/78	Derail	92	60	0	N	RR Bed, RR Car
Ramsey	N/RAR-79-9	3/29/79	HtoH Col.	2 T	48	0	N	Train
Red Desert	NDEN77FR001	NS	Derail	66+	NS	NS	NS	RR Bed, RR Car
Sheridan	N/RAR-72-4	3/28/71	Yard COL.	14	15	0	N	RR Cars
Wamsutter	NDEN77FR007	2/23/77	Derail Side Col.	NS-T	67-54	0-0	N	RR Bed, RR Car, Train

APPENDIX B

List of Tables

APPENDIX B
Truck Accident Data

B.1 Introduction

This appendix summarizes both the highway accident data which form the basis for the distribution of accident scenarios and the estimates of the probability distributions used in the probabilistic analysis of future truck accidents involving the transport of spent nuclear fuel. The primary sources of data are the Bureau of Motor Carrier Safety (BMCS), American Petroleum Institute (API), California Highway Patrol (CHP), and the California Department of Transportation (CALTRANS) reports on highway accidents. In addition, a Sandia report on severe accidents was the source of fire duration distributions and estimates of the probability of a fire.

Section B.2 discusses the data used to estimate the truck accident rate. Section B.3 discusses the distributions of truck velocities. Section B.4 covers the distribution of train velocities used to analyze rail-highway grade crossing accidents. Section B.5 discusses the distribution of objects struck, and, finally, Sections B.6 and B.7 cover the fire accident data.

B.2 Truck Accident Rate

Information concerning truck accidents involving motor carriers of property that operate in interstate commerce is available in reports published by the BMCS of the U.S. Department of Transportation (DOT).[B.1-B.13] Truck accidents are defined by the BMCS as occurrences involving a motor vehicle operated by a motor carrier subject to the Federal Motor Carrier Safety Regulations (49 CFR 390-397) resulting in (1) the death of one or more human beings; (2) bodily injury to one or more persons who, as a result, receives medical treatment away from the scene of the accident; and/or (3) total damage to all property aggregating dollar damage at or above the dollar damage threshold limit based on actual cost or reliable estimates.

Prior to 1973, the BMCS tabulated only those truck accidents with damage of $250 or greater involving for-hire carriers, i.e., trucking firms that haul freight owned by another party. Since 1973, the BMCS has also tabulated

accidents involving private, i.e., firms using their own, or leased, vehicles as part of their commercial operation to transport their own goods, as well as accidents of for-hire carriers. However, since 1973, the total vehicle miles have not been included in the BMCS reports. The accident rate for the period 1960-1972, 2.48×10^{-6} accidents/vehicle-mile, is an estimate; however, (1) it is based on the experience some years ago, and (2) it is not clear what is defined as a truck. This definition is important because pickup trucks and vans, i.e., non tractor/semitrailer trucks, tend to have an accident rate closer to that of automobiles. Therefore, it was decided not to base the accident rate for this study on the BMCS data.

Another source of truck accident data is the database maintained by the API consisting of information supplied by petroleum industry companies. Accident data is available for the API for the period 1968 through 1981 for large trucks.[B.14-B.18] Although a precise definition of an accident is not included in the reports, an accident rate based on the API data was used in this study. The API accident rate data was judged to be more reliable because shipments involving hazardous materials are usually more tightly controlled than shipments involving non-hazardous materials. In addition, the API data was judged to be most applicable to spent fuel shipment because trucks that transport gasoline type products are of similar size and weight to trucks that transport spent fuel. The API data is expected to be conservative because the average trip length of a gasoline truck is less than 28 miles and involves all types of roads. This will result in a higher accident rate than an accident rate based on cross-country trips that involve primarily interstates.

To allow for the imposition of the national speed limit in 1973, only the data from 1973 through 1981 was used to estimate a truck accident rate. Table B.1 summarizes the API accident data for the years 1973 to 1981. The estimated accident rate, $5.94 \text{Ex} 10^{-6}$ accidents/truck-mile, is higher than the rate based on the BMCS data.

Table B.1
Petroleum Industry Accident Data Summary, 1973-1981[a/]

Year	No. of Compy.	No. of Trucks	No. of Accidents	Truck Miles x 1000	Accident Rate/ Truck-Mile
1973	73	20,046	3,804	508,783	$7.48\ 10^{-6}$
1974	73	20,147	3,151	469,804	$6.71\ 10^{-6}$
1975	69	29,071	4,089	779,260	$5.25\ 10^{-6}$
1976	70	22,748	3,528	585,609	$6.02\ 10^{-6}$
1977	69	21,508	2,784	519,446	$5.36\ 10^{-6}$
1978	68	19,113	2,562	404,748	$6.33\ 10^{-6}$
1979	63	21,414	2,889	467,939	$6.17\ 10^{-6}$
1980	62	21,970	2,391	455,324	$5.25\ 10^{-6}$
1981	81	21,158	2,445	465,571	$5.25\ 10^{-6}$
Total		197,175	27,643	4,656,484	$5.94\ 10^{-6}$
Avg/year		21,908	3,071	517,387	

a/ American Petroleum Institute.[B.14-B.18]

B.3 Distributions of Velocity for Truck Accidents

The velocity of the truck at the time of an accident is an important parameter in determining impact forces on cargos involved in highway accidents. This parameter, in combination with the angle of impact, is an estimate of the impact velocity of the cask at the time of the accident. The impact velocity, in combination with the cask orientation and the object struck or subsequent interaction of the truck with its environment after the accident begins, determines the forces and damage experienced by the cask. Thus, the distribution of truck velocities at the time of an accident is one of the necessary inputs into the probabilistic analysis of accidents involving spent fuel casks.

Considerable effort went into attempting to accumulate a database of accident data from past events which reasonably reflects what might be experienced by trucks transporting spent fuel casks in the future. To this end, annual reports on motor vehicle accidents, as accumulated by the CHP formed the basis for developing an appropriate collection of accident statistics.[B.19-B.29] Although data from several classifications of accidents have been reported, e.g., all injury accidents, injury truck accidents, and all fatal accidents, we chose to estimate the desired distribution of velocities on fatal and injury accidents involving truck/semitrailers.

The distribution of velocities covering the years 1958-1967 is given in Table B.2. An important question with regard to the use of the data in Table B.2 as a basis for estimating velocities for future truck accidents is whether the traffic conditions in the 1958-1967 time period is comparable to traffic conditions which can be expected to be experienced in the future. Prior to 1959 California highway speed limits were 55 mph for automobiles and 45 mph for trucks (defined as trucks with three or more axles and any truck or truck tractor pulling one or more trailers) and cars with trailers. In 1959 the motor vehicle code was changed to limit cars to 65 mph; however, trucks and cars with trailers were still limited to 45 mph except on highways with four or more lanes (at least two lanes in each direction), where the speed limit was 50 mph. In 1963, the motor vehicle code was changed to limit cars on

Table B.2
Distribution of Velocities for Truck/Semitrailers Involved in Fatal and Injury Accidents in California, 1958-1967[a/]

Velocity (mph)	Number of Accidents	Fractional Percent (%)	Cumulative Percent (%)
0	1,774	6.41	6.41
1-10	4,143	14.96	21.37
11-20	4,122	14.89	36.25
21-30	4,248	15.34	51.59
31-40	4,733	17.09	68.69
41-50	7,264	26.23	94.92
51-60	1,173	4.24	99.15
61-70	171	0.62	99.77
>70	63	0.23	100.00
Total	27,691	100.00	

a/ California Highway Patrol.[B.19-B.29]

freeways to 70 mph while trucks and cars with trailers were restricted to 50 mph on all highways.

The speed limits were again changed in 1967 to allow trucks and cars with trailers to travel up to 55 mph over all highways. These regulations remained in effect until superseded by the national speed limit in 1973. Because the speed limits during the 1958-1967 time period were lower than the present 55 mph limit for all vehicles, the velocities in Table B.2 may be biased towards lower velocities. However, by choosing fatal and injury accidents, rather than all accidents (including non injury accidents), this bias has been somewhat compensated for because injury and fatal accidents generally involve higher velocities.

Accident data from North Carolina[B.30] was used to estimate the effects of braking on impact velocity. Tables B.3 and B.4 summarize the distribution of velocities for accidents involving all types of vehicles resulting in fatalities, injuries, or property damage for the years 1979-1981. In Table B.3, the velocities are based on estimates of the original vehicle velocity while in Table B.4 the velocities are estimates of the velocity at impact. As discussed in Section 5.0, a comparison of these two distributions was used as a basis for adjusting the distribution of truck velocities for the effects of braking during the evolution of an accident prior to vehicle impact.

B.4 Distribution of Train Speeds at Rail-Highway Grade-Crossing Accidents

The U.S. DOT Federal Railroad Administration (FRA) defines rail-highway grade-crossing accidents as any impact between railroad on-track equipment and an automobile, bus, truck, motorcycle, bicycle, farm vehicle, or pedestrian at a highway-rail grade crossing in which the amount of damage done to railroad equipment is at least a specified damage threshold limit. If the impact causes damage to railroad equipment less than the dollar damage threshold limit, it is classified as an incident. Prior to 1975, the damage threshold limit was $750 and only rail-highway grade-crossing accidents were tabulated by the FRA.[B.34] In 1975, the threshold was increased to $1750 to account for

Table B.3
Distribution of Estimated Original Vehicle Velocities for All Types of Accidents, North Carolina, 1979-1981[a/]

Velocity (mph)	Year 1979	1980	1981	Total	Avg.	Fra. Pct. (%)	Cum. Pct. (%)
0	512	214	188	914	305	0.14	0.14
1-5	22,191	19,976	19,205	61,372	20,457	9.25	9.39
6-10	20,335	18,655	17,865	56,855	18,952	8.57	17.96
11-15	13,846	12,697	12,051	38,594	12,865	5.82	23.77
16-20	20,417	18,965	18,042	57,424	19,141	8.65	32.43
21-25	17,336	16,388	16,100	49,824	16,608	7.51	39.94
26-30	23,336	21,472	21,582	66,390	22,130	10.01	49.94
31-35	33,147	33,147	34,030	100,324	33,441	15.12	65.06
36-40	17,245	16,317	16,075	49,637	16,546	7.48	72.54
41-45	22,028	21,049	21,156	64,233	21,411	9.68	82.22
46-50	16,144	14,889	14,315	45,348	15,116	6.83	89.06
51-55	15,336	14,301	14,784	44,421	14,807	6.69	95.75
56-60	3,559	3,492	3,261	10,312	3,437	1.55	97.31
61-65	2,071	1,907	1,991	5,969	1,990	0.90	98.21
66-70	1,621	1,604	1,476	4,701	1,567	0.71	98.92
71-75	751	685	719	2,155	718	0.32	99.24
76-80	603	584	539	1,726	575	0.26	99.50
81-85	134	127	143	404	135	0.06	99.56
>85	1243	855	807	2,905	968	0.44	100.00
Not Stated[b/]	45,590	43,290	42,526	131,406	43,802	N/A	N/A

a/ University of North Carolina Highway Safety Research Center.[B.30]

b/ Excluded from percentage calculations.

Table B.4
Distribution of Estimated Vehicle Impact Velocities for All Types of Accidents, North Carolina, 1979-1981[a/]

Velocity (mph)	Year 1979	1980	1981	Total	Avg.	Fra. Pct. (%)	Cum. Pct. (%)
0	818	413	412	1643	548	0.26	0.26
1-5	30,831	29,125	29,181	89,137	29,712	14.08	14.34
6-10	29,236	28,273	28,026	85,535	28,512	13.51	27.85
11-15	20,279	19,905	19,811	59,995	19,998	9.48	37.33
16-20	26,955	26,958	26,423	80,336	26,779	12.69	50.02
21-25	18,904	18,386	18,619	55,909	18,636	8.83	58.85
26-30	23,914	23,301	23,023	70,238	23,413	11.09	69.94
31-35	19,368	19,123	18,706	57,197	19,066	9.03	78.98
36-40	15,991	15,091	14,589	45,671	15,224	7.21	86.19
41-45	11,589	10,866	10,554	33,009	11,003	5.21	91.41
46-50	9,754	9,249	8,726	27,729	9,243	4.38	95.79
51-55	4,936	4,945	4,730	14,611	4,870	2.31	98.10
56-60	2,056	2,028	1,861	5,945	1,982	0.94	99.03
61-65	818	678	691	2,187	729	0.35	99.38
66-70	697	687	673	2,057	686	0.32	99.71
71-75	250	241	239	730	243	0.12	99.82
76-80	262	251	205	718	239	0.11	99.93
81-85	58	55	52	165	55	0.03	99.96
>85	94	87	73	254	85	0.04	100.00
Not Stated[b/]	60,635	50,952	50,261	161,848	53,949	N/A	N/A

a/ University of North Carolina Highway Safety Research Center.[B.30]

b/ Excluded from percentage calculations.

the effects of inflation. Also, at this time, the FRA started to include rail-highway grade-crossing incidents in their grade crossing accident data.[B.31-B.38] This resulted in a substantial increase in the reported number of impacts between trains and other mobile objects in the grade-crossing accident data after 1975. Because of the difference in types of events recorded, only the rail-highway grade-crossing accident data after 1974 was used.

Table B.5 presents the distribution of train velocities at grade-crossing accidents/incidents involving motor vehicles. The reliability of the train accident/incident velocity at rail-highway grade-crossings can be considered good because railroad locomotives are equipped with accident recorders to record the train's velocity prior to, during, and after the accident, although on a very crude scale. The recorded train velocity while probably no more accurate than 5 to 10 mph, is certainly more reliable than after-the-fact velocity estimates made by investigating officers at highway accident sites.

B.5 Highway Accident Object Frequency

Data were collected from several sources to estimate the frequency of impact with particular objects. Two of the primary data sources were the CALTRANS for all vehicles and the BMCS for trucks.

Table B.6 presents the truck highway accident data obtained from the BMCS for the years 1973 through 1983.[B.4-B.13] The object struck (for collision accidents) or accident type (for noncollision accidents) are categories as given by the BMCS. These categories are divided into nonfixed-object collisions, fixed-object collisions (for collision accidents), ran-off-road accidents, impact-with-roadbed accidents, or other noncollision accidents (for noncollision accidents). The BMCS data were divided this way in order to provide subcategories that would correspond with those defined by the CALTRANS in their reports on objects struck during highway accidents.

Table B.7 presents the primary objects struck during highway accidents, as reported by the CALTRANS for all vehicles for 1975 through 1983.[B.39-B.47] All object struck subcategories are as defined by the CALTRANS and the object numbering system follows the CALTRANS convention.

Table B.5
Distribution of Train Velocities at Rail-Highway Grade-Crossing Accident/Incidents Involving Motor Vehicles, 1975-1982[a/]

Velocity (mph)	Year 1975	1976	1977	1978	1979	1980	1981	1982	Total	Fra. Pct (%)	Cum. Pct. (%)
0-9	3,887	3,793	3,923	4,098	3,788	3,224	2,715	2,125	27,553	33.79	33.79
10-19	2,221	2,428	2,339	2,431	2,303	1,950	1,724	1,364	16,765	20.56	54.35
20-29	1,919	2,098	2,152	2,097	2,042	1,589	1,459	1,257	14,611	17.92	72.27
30-39	1,365	1,511	1,600	1,582	1,457	1,277	1,061	935	10,788	13.23	85.50
40-49	960	1,026	1,086	1,106	985	887	825	742	7,617	9.34	94.84
50-59	391	433	419	382	351	330	279	294	2,879	3.53	98.37
60-69	109	127	119	95	87	96	94	97	824	1.01	99.38
70-79	61	59	68	62	51	49	55	56	461	0.56	99.94
80-89	4	6	8	2	2	2	4	1	29	0.04	99.98
>90	8	1	2	2	1	0	1	2	17	0.02	100.00
Total[b/]	10,925	11,482	11,716	11,857	11,067	9,402	8,222	6,873	81,544	100.00	

a/ U.S. Department of Transportation, Federal Railroad Administration, Office of Safety, Rail-Highway Grade-Crossing Accident/Incidents Bulletins.[B.34-B.41]

b/ Excludes accidents of unknown velocities.

Table B.6
Summary of Objects Struck and Type of Accident for Accidents Involving U.S. Private and For-Hire Motor Carriers, 1973-1983[a/]

Type of Accident	Total	Avg.[b/]	Fra. Pct. (%)	Remarks
I. Nonfixed Object Collision				
w/ Commercial Truck	42,848	3,895	12.88	
w/ Automobile	143,573	13,052	43.15	
w/ Pedestrian	4,493	408	1.35	
w/ Bus	1,477	134	0.44	
w/ Train	2,575	234	0.77	
w/ Bicyclist	1,259	114	0.38	
w/ Animal	2,111	192	0.63	
w/ Motorcycle	2,680	244	0.81	
w/ Other or Not Specified	16,157	1,469	4.86	Note 1
Subtotal	217,173	19,743	65.26	
II. Fixed Object Collision	29,476	2,680	8.86	Note 1
Collision Accidents Subtotal	246,649	22,423	74.12	
III. Ran Off Road	30,104	2,737	9.05	Note 1
IV. Impact with Roadbed				
Jackknife	18,184	1,653	5.46	
Overturn	27,792	2,527	8.35	
Subtotal	45,976	4,180	13.82	
V. Other Noncollision Accidents				
Separation of Units	1,033	93.9	0.31	
Fire	3,219	293	0.97	
Cargo Loss/Spillage	1,433	130	0.43	
Cargo Shift	1,139	104	0.34	
Other or Not Specified	3,213	292	0.97	
Subtotal	10,037	912	3.02	
Noncol. Accidents Subtotal	86,117	7,829	25.88	
Total Accidents	332,766	30,251	100.00	

a/ U.S. Department of Transportation, Bureau of Motor Carrier Safety. B.4-B.13

b/ Based on 11 year period.

Note 1: Object distribution from California TASAS accident survey, see Table B.8.

Table B.7
Objects Struck During California Accidents, 1975-1983[a/]

Object Struck		Total	Avg.[b/]	Fra. Pct. (%)
1.	Side of Bridge Railing	9,473	1,053	0.82
2.	End of Bridge Railing	1,689	188	0.15
3.	Pier, Column, Abutment	810	90	0.07
4.	Bottom of Structure (Overhead Bridge Structure)	639	71	0.06
5.	Bridge End Post in Gore (Older Bridge w/Protective Island)	275	30.6	0.02
10.	Light or Signal Pole	8,384	932	0.72
11.	Utility Pole	8,140	904	0.70
12.	Pole (Type Note Stated)	454	50	0.04
13.	Traffic Sign/Sign Post	9,687	1,076	0.83
14.	Other Signs Not Traffic	333	37	0.03
15.	Guardrail	25,354	2,817	2.18
16.	Barrier	41,432	4,604	3.57
17.	& 30. Wall (Concrete/Wood/Sound)	3,751	417	0.32
18.	Dike or Curb	69,134	7,682	5.96
19.	Traffic Island	2,590	288	0.22
20.	Raised Bars (Delineation Bars, as Traffic Islands w/o Curb)	67	7.4	0.01
21.	Concrete Object (Headwall, Drop Inlet)	921	102	0.08
22.	Guidepost, Culvert, Postmile Marker	9,020	1,002	0.78
23.	Cut Slope or Embankment	22,403	2,489	1.93
24.	Over Embankment	12,758	1,418	1.10
25.	In Water	45	5.0	0.004
26.	Drainage Ditch	7,850	872	0.68
27.	Fence	13,701	1,522	1.18
28.	Trees	8,392	932	0.72
29.	Plants	5,111	568	0.44
40.	Natural Material on Road	1,785	198	0.15
41.	Temporary Barricades, Cones	1,337	149	0.12
42.	Other Object on Road	10,517	1,169	0.91
43.	Other Object off Road	10,153	1,128	0.87
44.	Overturned	61,848	6,872	5.33
45.	Crash Cushion	1,199	133	0.10
98.	Unknown Object Struck	975	108	0.08
99.	No Object Involved	9,386	1,043	0.81
00.	Other Vehicle	801,256	89,028	69.02

Table B.7 Continued

Object Struck	Total	Avg.[b/]	Fra. Pct. (%)
Total Primary Object Struck	1,160,869	128,985	100.00
XX. Not Stated	180	20	N/A
YY. Not Applicable	239,655	26,628	N/A
ZZ. Invalid Code	164	18	N/A
Total Accidents	1,165,097	129,455	N/A

a/ TASAS Selective Record Retrieval.[B.39-B.47]

b/ Based on 9 year period.

N/A Not applicable.

The CALTRANS accident data were reordered according to the accident categories defined in Table B.6. The result is Table B.8. Certain objects in Table B.8 were combined because of the similarity of these objects when considered in structural analysis calculations. The BMCS and the CALTRANS data on the object frequencies were combined to derive the probability of occurrences of the different accident scenarios.

B.6 Truck Fire Duration Distributions

The thermal response of the cask during a truck fire depends on the temperature of the fire, location of the fire relative to the cask and the duration of the fire. The type and amount of combustible materials will significantly affect the duration of a fire. Thus, the fire duration distribution will vary for different accident scenarios. For example, a fire involving a collision with a tanker truck can be expected to last longer than a fire involving a collision with an automobile or a collision with a noncombustible fixed object. To assess the probabilities of a truck cask's experiencing different thermal response levels, five fire duration distributions were developed. These distributions were associated with automobile collisions, truck collisions, collisions with fixed objects, other collisions including overturns and jackknifing, and noncollision fires. The basis for these distributions was the fire duration program developed by Sandia.[B.48] These distributions are summarized in Table 5.5.

B.7 Probability of Fire

Not all truck accidents will involve a fire; thus it is necessary to estimate the probability of a fire given an accident. The likelihood of a fire can be expected to vary between accident scenarios. Several sources provided statistical information for several types of accidents.[B.1-B.13,B.48] The probabilities of a fire given each of the different accident scenarios used in this study and listed in Table 5.9, are based on the statistics presented in the Sandia report on severe accidents.[B.48]

Table B.8
Objects Struck During California Accidents
Reordered According to Type of Accident, 1975-1983[a/]

Type of Accident	Total	Avg.[b/]	Fra. Pct. (%)	Remarks
I. Nonfixed Object Collision				
40. Natural Material on Road	1,785	198	0.15	
41. Temporary Barricades, Cones	1,337	149	0.12	
42. Other Object on Road	10,517	1169	0.91	
98. Unknown Object Struck	975	108	0.08	
00. Other vehicle	801,256	8,9028	69.02	
Subtotal	815,870	9,0652	70.28	
II. Fixed Object Collision				
1-2. Side or End of Bridge Railing	11,162	1,240	0.96	Note 1
3. Pier, Column, Abutment	810	90	0.07	Note 2
4. Bottom of Structure	639	71	0.06	
5. Bridge End Post in Gore	275	30.6	0.02	
10-12. Light, Signal, Utility or Other Type Pole	16,978	1,886	1.46	
13-14. Traffic Sign/Sign Post or Other Signs	10,020	1,113	0.86	
15. Guardrail	25,354	2,817	2.18	
16. Barrier	41,432	4,604	3.57	
17&30. Wall (Concrete/Wood/Sound)	3,751	417	0.32	
18-20. Dike, Curb, Traffic Island or Raised Bars	71,791	7,977	6.18	
21. Concrete Object (Headwall, Drop Inlet)	921	102	0.08	
22. Guidepost, Culvert, Postmile Marker	9,020	1,002	0.78	
45. Crash Cushion	1,199	133	0.10	
Subtotal	193,352	21,484	16.66	
Collision Accidents Subtotal	1,009,222	112,136	86.94	
III. Ran Off Road				
23. Cut Slope or Embankment	22,403	2,489	1.93	Note 3
24. Over Embankment	12,758	1,418	1.10	Note 3
25. In Water	45	5.0	0.004	
26. Drainage Ditch	7,850	872	0.68	
27. Fence	13,701	1,522	1.18	
28. Trees	8,392	932	0.72	
29. Plants	5,111	568	0.44	
43. Other Object off Road	10,153	1,128	0.87	
Subtotal	80,413	8,935	6.93	

Table B.8 Continued

Type of Accident	Total	Avg.[b/]	Fra. Pct. (%)	Remarks
IV. Impact with Roadbed				
44. Overturned	61,848	6,872	5.33	
V. Other Noncollision Accidents				
99. No Object Involved	9,386	1,043	0.81	
Noncollision Accidents Subtotal	151, 647	16,850	13.06	
Total Accidents	1,160,869	128,985	100.00	

All LLNL calculations are based on static analysis. Static force is defined as ultimate static force at which complete collapse of object occurs.

a/ TASAS Selective Record Retrieval.[B.39-B.47]

b/ Based on 9 year period.

Note 1 Assume worst case that truck goes off bridge. Distributions of bridge heights and surfaces below bridges determined from Engineering Computer Corporation (ECC) survey in Appendix D.

Note 2 Distribution of bridge column size determined from ECC survey in Appendix D.

Note 3 Distribution of soil types and surfaces determined from ECC survey in Appendix D.

B.8 References

B.1 1969 Accidents of Large Motor Carriers of Property, Bureau of Motor Carrier Safety, Federal Highway Administration, U.S. Department of Transportation, Washington, DC, December 1970.

B.2 1970 Accidents of Large Motor Carriers of Property, Bureau of Motor Carrier Safety, Federal Highway Administration, U.S. Department of Transportation, Washington, DC, March 1972.

B.3 1971-1972 Accidents of Large Motor Carriers of Property, Bureau of Motor Carrier Safety, Federal Highway Administration, U.S. Department of Transportation, Washington, DC, May 1974

B.4 1973 Accidents of Motor Carriers of Property, Bureau of Motor Carrier Safety, Federal Highway Administration, U.S. Department of Transportation, Washington, DC, July 1975.

B.5 1974 Accidents of Motor Carriers of Property, Bureau of Motor Carrier Safety, Federal Highway Administration, U.S. Department of Transportation, Washington, DC, 1975.

B.6 1975 Accidents of Motor Carriers of Property, Bureau of Motor Carrier Safety, Federal Highway Administration, U.S. Department of Transportation, Washington, DC, 1976.

B.7 1976 Accidents of Motor Carriers of Property, Bureau of Motor Carrier Safety, Federal Highway Administration, U.S. Department of Transportation, Washington, DC, October 1977.

B.8 1977 Accidents of Motor Carriers of Property, Bureau of Motor Carrier Safety, Federal Highway Administration, U.S. Department of Transportation, Washington, DC, May 1980.

B.9 1978 Accidents of Motor Carriers of Property, Bureau of Motor Carrier Safety, Federal Highway Administration, U.S. Department of Transportation, Washington, DC, May 1980.

B.10 1979 Accidents of Motor Carriers of Property, Bureau of Motor Carrier Safety, Federal Highway Administration, U.S. Department of Transportation, Washington, DC, 1980.

B.11 1980-1981 Accidents of Motor Carriers of Property, Bureau of Motor Carrier Safety, Federal Highway Administration, U.S. Department of Transportation, Washington, DC, August 1982.

B.12 1982 Accidents of Motor Carriers of Property, Bureau of Motor Carrier Safety, Federal Highway Administration, U.S. Department of Transportation, Washington, DC, May 1983.

B.13 1983 Accidents of Motor Carriers of Property, Bureau of Motor Carrier Safety, Federal Highway Administration, U.S. Department of Transportation, Washington, DC, October 1984.

B.14 Summary of Motor Vehicle Accidents in the Petroleum Industry for 1977, American Petroleum Institute, Washington, DC, May 1978.

B.15 Summary of Motor Vehicle Accidents in the Petroleum Industry for 1978, American Petroleum Institute, Washington, DC, August 1979.

B.16 Summary of Motor Vehicle Accidents in the Petroleum Industry for 1979, American Petroleum Institute, Washington, DC, June 1980.

B.17 Summary of Motor Vehicle Accidents in the Petroleum Industry for 1980, American Petroleum Institute, Washington, DC, September 1981.

B.18 Summary of Motor Vehicle Accidents in the Petroleum Industry for 1981, American Petroleum Institute, Washington, DC, August 1982.

B.19 1957 Annual Statistical Report, Department of California Highway Patrol, Sacramento, CA, May 1958.

B.20 1958 Annual Statistical Report, Department of California Highway Patrol, Sacramento, CA, May 1959.

B.21 1959 Annual Statistical Report, Department of California Highway Patrol, Sacramento, CA, May 1960.

B.22 1960 Annual Statistical Report, Department of California Highway Patrol, Sacramento, CA, May 1961.

B.23 1961 Annual Statistical Report, Department of California Highway Patrol, Sacramento, CA, May 1962.

B.24 1962 Traffic Accident Statistics, Department of California Highway Patrol, Sacramento, CA, May 1963.

B.25 1963 Traffic Accident Statistics, Department of California Highway Patrol, Sacramento, CA, May 1964.

B.26 1964 Traffic Accident Statistics, Department of California Highway Patrol, Sacramento, CA, May 1965

B.27 1965 Traffic Accident Statistics, Department of California Highway Patrol, Sacramento, CA, April 1966.

B.28 1966 Report of Fatal and Injury Motor Vehicle Traffic Accidents, Department of California Highway Patrol, Sacramento, CA, July 1967.

B.29 1967 Report of Fatal and Injury Motor Vehicle Traffic Accidents, Department of California Highway Patrol, Sacramento, CA, July 1968.

B.30 E. G. Hamilton, Single, Variable Tabulations for 1979-1981 North Carolina Accidents, University of North Carolina Highway Safety Research Center, Chapel Hill, NC, September 1977.

B.31 Rail-Highway Grade-Crossing Accidents/Incidents Bulletin for the Year Ended December 31, 1975, Office of Safety, Federal Railroad Administration, U.S. Department of Transportation, Washington, DC.

B.32 Rail-Highway Grade-Crossing Accidents/Incidents Bulletin for the Year Ended December 31, 1976, Office of Safety, Federal Railroad Administration, U.S. Department of Transportation, Washington, DC, December 1977.

B.33 Rail-Highway Grade Crossing Accident/Incident Bulletin No. 43, Calendar Year 1977, Office of Safety, Federal Railroad Administration, U.S. Department of Transportation, Washington, DC, July 1978.

B.34 Rail-Highway Crossing Accident/Incident and Inventory Bulletin No. 1, Calendar Year 1978, Office of Safety, Federal Railroad Administration, U.S. Department of Transportation, Washington, DC, October 1979.

B.35 Rail-Highway Crossing Accident/Incident and Inventory Bulletin No. 2, Calendar Year 1979, Office of Safety, Federal Railroad Administration, U.S. Department of Transportation, Washington, DC, September 1980.

B.36 Rail-Highway Crossing Accident/Incident and Inventory Bulletin No. 3, Calendar Year 1980, Office of Safety, Federal Railroad Administration, U.S. Department of Transportation, Washington, DC, June 1981.

B.37 Rail-Highway Crossing Accident/Incident and Inventory Bulletin No. 4, Calendar Year 1981, Office of Safety, Federal Railroad Administration, U.S. Department of Transportation, Washington, DC, June 1982.

B.38 Rail-Highway Crossing Accident/Incident and Inventory Bulletin No. 5, Calendar Year 1982, Office of Safety, Federal Railroad Administration, U.S. Department of Transportation, Washington, DC, June 1983.

B.39 TASAS Selective Record Retrieval Statewide Accident Summary for Year 1975, State of California Department of Transportation, Sacramento, CA, October 1979.

B.40 TASAS Selective Record Retrieval Statewide Accident Summary for Year 1976, State of California Department of Transportation, Sacramento, CA, October 1979.

B.41 TASAS Selective Record Retrieval Total Statewide Accidents for Year 1977, State of California Department of Transportation, Sacramento, CA, May 1978.

B.42 TASAS Selective Record Retrieval Statewide Accident Summary for Year 1978, State of California Department of Transportation, Sacramento, CA, April 1979.

B.43 TASAS Selective Record Retrieval, Summary Only, All Accidents for the Year 1978, State of California Department of Transportation, Sacramento, CA, August 1984.

B.44 TASAS Selective Record Retrieval, Summary Only, All Accidents for the Year 1979, State of California Department of Transportation, Sacramento, CA, August 1984.

B.45 TASAS Selective Record Retrieval Statewide Accidents for Year 1981, State of California Department of Transportation, Sacramento, CA, April 1982.

B.46 TASAS Selective Record Retrieval Statewide Summary 1982, State of California Department of Transportation, Sacramento, CA, May 1983.

B.47 TASAS Selective Record Retrieval Statewide Summary 1983, State of California Department of Transportation, Sacramento, CA, April 1984.

B.48 R. K. Clarke, et al., Severities of Transportation Accidents, Sandia National Laboratory, Albuquerque, NM, SAND77-0001, 1977.

APPENDIX C

List of Tables

APPENDIX C
Railroad Accident Data

C.1 Introduction

This appendix summarizes both the railroad accident data which form the basis for the estimates of accident scenarios and the probability distributions used in the probabilistic analysis of future train accidents involving the transport of spent nuclear fuel. The primary sources of data were the statistical reports of railroad accidents produced by the Office of Safety, Federal Railroad Administration (FRA) of the U. S. Department of Transportation (DOT).[C.1-C.7] A Sandia report on severe accidents was the source of estimates of the probability of fire duration distributions.[C.8] Section C.2 discusses the data used to estimate the railroad accident rate and distribution of types of accidents. Section C.3 discusses the distributions of train velocity at the time of an accident; Section C.4 discusses the fire duration distribution.

C.2 Railroad Accident Rate

Federal law (49 CFR 225) requires all railroads to file monthly accident/incident reports with the Office of Safety, FRA of the U. S. DOT. A railroad is defined, by regulation, as any system of surface transportation of persons or property over rails. It includes line-haul freight and passenger railroads; switching and terminal railroads; and passenger-carrying railroads including rapid transit, commuter, scenic, street, subway, elevated cable, and cog railways.

Train accidents are defined by the FRA Office of Safety as any event involving on-track railroad equipment that results in damage to railroad on-track equipment, signals, track or track structure, and roadbed at or exceeding the dollar damage threshold. Prior to 1975, the threshold was $750. Since 1975 this limit has been adjusted, to account for inflation, from $1750 in 1975 to $4100 in 1982, the last year available for use in this study. Although initially adjusted biennially (i.e., every two years), since 1977 the adjustment has been annual. The yearly threshold limits are included in Table C.1.

Table C.1
Railroad Accident Rate, 1975-1982[a/]

Year	Train Miles X 1000	Number of Accidents	Accident Rate	Damage Threshold
1975	755,033	8,041	$1.06E\ 10^{-5}$	$1,750.00
1976	774,764	10,248	$1.32E\ 10^{-5}$	$1,750.00
1977	750,042	10,362	$1.38E\ 10^{-5}$	$2,300.00
1978	751,964	11,277	$1.50E\ 10^{-5}$	$2,600.00
1979	763,429	9,740	$1.28E\ 10^{-5}$	$2,900.00
1980	717,662	8,451	$1.18E\ 10^{-5}$	$3,200.00
1981	676,216	5,781	$8.55E\ 10^{-6}$	$3,700.00
1982	573,369	4,589	$8.00E\ 10^{-6}$	$4,100.00
Total	5,762,479	68,489	$1.19E\ 10^{-5}$	

a/ U.S. Department of Transportation, Federal Railroad Administration, Accident/Incident Bulletins[C.1-C.7]

In addition to train accidents, the FRA Office of Safety compiles and reports statistics on two related events: train incidents, and non-train incidents. Train incidents are defined as events involving on-track railroad equipment that result in the reportable death and/or injury or illness of one or more persons, but do not result in damage at or beyond the damage threshold, as defined in the previous paragraph. Non-train incidents are defined as events which result in a reportable death, injury, or illness arising from the operation of a railroad but not from the movement of railroad on-track equipment.

Damage to casks containing spent nuclear fuel will necessarily involve severe accidents (hence significant damage); thus, for this project, train accidents formed the basis for estimating railroad accident rates. Because of the effect of the damage threshold levels on the reported accidents, data from the period 1975 to 1982 were used to estimate the accident rate used in this study. The estimated railroad accident rate, 1.19×10^{-5} accidents/train-mile/year, is the ratio of the number of reported accidents to the total miles for the 1975 to 1982 period.

Table C.1 presents the train mileage and number of accidents, as well as rate and damage threshold for each year during 1975 to 1982. Train-miles, for this report, is defined as the sum of the locomotive miles, yard switching miles, and motor train miles as tabulated for each year by the FRA. The FRA defines a locomotive mile as the movement under its own power of a locomotive the distance of one mile whether coupled or without cars. This item covers miles run by locomotives in road services and in train and yard switching service. Switching miles are computed at the rate of 6 miles/hour for the time actually engaged in such service. A motor train-mile is a movement under its own power of a motor train a distance of one mile.

Accident severity varies between accidents, thus the level of damage that a cask might experience during an accident depends on the type of accident. Therefore, train accidents were subdivided into four types--collisions, derailments, rail-highway grade-crossing accidents, and other types of accidents. Data relevant to this distribution, derived from the FRA reports,

is given in Table C.2. Again, the distribution of accident types is based on the accidents during the 1975-1982 period. The important statistics are the percentages, for each type of accident, of all accidents presented in the bottom row of the table. For example, 13.41% of the train accidents were collisions.

Approximately 36% of the collisions involved derailment of at least one car.[C.8] These were grouped with the original derailment accidents. Derailment accidents were further partitioned into accident scenarios based on the events following the derailment. Accident scenarios considered included the car(s) falling over a bridge or embankment, hitting a slope or a structure, or rolling over. Categorization of derailment accidents into scenarios was not found in the literature. Thus, a distribution was developed based on similar statistics for truck accidents. This distribution is included in Fig. 2-5. To distinguish between the severity of accident scenarios, some of the accident scenarios were further subdivided, e.g., derailments involving a car's hitting a structure were subdivided into hitting small and large columns, abutments, and other accidents. Categorization of accidents into these types of scenarios was based on the Eggers study.[C.9]

C.3 Impact Velocity Distribution

The forces imposed on the cask at the moment of impact during an accident depend on the impact velocity of the cask or impacting object. Since impact velocity is a function of velocity and angle of impact, it is necessary to estimate the distributions of train velocities. Information on the train velocity at the time of an accident was derived, again, from the FRA data. Reliability of these statistics can be considered good since railroad locomotives are equipped with recorders to record the train's velocity prior to, during, and after the accident. The scale, although crude, is more reliable than the velocity estimates made by investigating officers at highway accident sites.

Distributions of train velocities based on accidents occurring on main lines during 1979 to 1982 are summarized in Tables C.3 through C.6 for

Table C.2
Distribution of Types of Railroad Accidents, 1975-1982[a/]

Year	Train Collisions	Train Derailments	Rail-Highway Grade-Xing Accidents	Other Accidents	Total Accidents	Accident Damage Threshold
1975	1,002	6,328	248	463	8,041	$1,750.00
1976	1,370	7,934	352	592	10,248	$1,750.00
1977	1,362	8,073	323	604	10,362	$2,300.00
1978	1,476	8,763	286	752	11,277	$2,600.00
1979	1,425	7,482	248	585	9,740	$2,900.00
1980	1,201	6,442	246	562	8,451	$3,200.00
1981	776	4,366	199	440	5,781	$3,700.00
1982	572	3,383	178	456	4,589	$4,100.00
Total	9,184	52,771	2,080	4,454	68,489	
Fra. Pct.(%)	13.41	77.05	3.04	6.50		

a/ U.S. Department of Transportation, Federal Railroad Administration, Accident/Incident Bulletins[C.1-C.7]

Table C.3
Distribution of Train Velocities, Collisions, Main Line, 1979-1982[a/]

Velocity (mph)	Year 1979	1980	1981	1982	Total	Fra. Pct. (%)	Cum. Pct. (%)
1-10	136	112	85	59	392	46.12	46.12
11-20	70	46	32	34	182	21.41	67.53
21-30	44	31	17	25	117	13.76	81.29
31-40	23	26	24	19	92	10.82	92.12
41-50	9	19	10	9	47	5.53	96.65
51-60	4	6	4	0	14	1.65	99.29
61-70	2	1	0	0	3	0.35	99.65
71-80	1	1	0	0	2	0.24	99.88
81-90	0	0	0	0	0	0.00	99.88
91	0	1	0	0	1	0.12	100.00
Total[b/]	289	243	172	146	850	100.00	

a/ U.S. Department of Transportation, Federal Railroad Administration, Accident/Incident Bulletins[C.1-C.7]

b/ Excludes accidents of unknown velocities

Table C.4
Distribution of Train Velocities, Derailments, Main Line, 1979-1982[a/]

Velocity (mph)	Year 1979	1980	1981	1982	Total	Fra. Pct. (%)	Cum. Pct. (%)
1-10	1,736	1,278	793	587	4,394	40.42	40.42
11-20	841	634	416	359	2,250	20.70	61.12
21-30	783	616	444	340	2,183	20.08	81.20
31-40	325	333	238	195	1,091	10.04	91.24
41-50	202	191	137	129	659	6.06	97.30
51-60	64	60	54	61	239	2.20	99.50
61-70	19	6	10	6	41	0.38	99.88
71-80	6	1	2	1	10	0.09	99.97
81-90	1	1	0	1	3	0.03	100.00
91	0	0	0	0	0	0.00	100.00
Total[b/]	3,977	3,120	2,094	1,679	10,870	100.00	

a/ U.S. Department of Transportation, Federal Railroad Administration, Accident/Incident Bulletins[C.1-C.7]

b/ Excludes accidents of unknown velocities

Table C.5
Distribution of Train Velocities for Rail-Highway Grade-Crossing Accidents/Incidents Involving Motor Vehicles, 1975-1982[a/]

Velocity (mph)	Year 1975	1976	1977	1978	1979	1980	1981	1982	Total	Fra. Pct. (%)	Cum. Pct. (%)
0-9	3,887	3,793	3,923	4,098	3,788	3,224	2,715	2,125	27,553	33.79	33.79
10-19	2,221	2,428	2,339	2,431	2,303	1,950	1,729	1,364	16,765	20.56	54.35
20-29	1,919	2,098	2,152	2,097	2,042	1,587	1,459	1,257	14,611	17.92	72.27
30-39	1,365	1,511	1,600	1,582	1,457	1,277	1,061	935	10,788	13.23	85.50
40-49	960	1,026	1,086	1,106	985	887	825	742	7,617	9.34	94.84
50-59	391	433	419	382	351	330	279	294	2,879	3.53	98.37
60-69	109	127	119	95	87	96	94	97	824	1.01	99.38
70-79	61	59	68	62	51	49	55	56	461	0.56	99.94
80-89	4	6	8	2	2	2	4	1	29	0.04	99.98
>90	8	1	2	2	1	0	1	2	17	0.02	100.00
Total[b/]	10,925	11,482	11,716	11,857	11,067	9,402	8,222	6,873	81,544	100.00	

a/ U.S. Department of Transportation, Federal Railroad Administration, Office of Safety, Rail-Highway Grade-Crossing Accident/Incidents Bulletins[B.34-B.41]

b/ Excludes accidents of unknown velocities

Table C.6
Distribution of Train Velocities, Other Accidents, Main Line, 1979-1982[a/]

Velocity (mph)	Year 1979	1980	1981	1982	Total	Fra. Pct. (%)	Cum. Pct. (%)
1-10	83	83	60	59	285	17.59	17.59
11-20	73	46	53	56	228	14.07	31.67
21-30	104	93	59	59	315	19.44	51.11
31-40	89	104	58	63	314	19.38	70.49
41-50	72	65	64	61	262	16.17	86.67
51-60	35	38	26	23	122	7.53	94.20
61-70	13	16	7	13	49	3.02	97.27
71-80	7	9	14	7	37	2.28	99.51
81-90	0	1	3	2	6	0.37	99.88
91	0	0	0	2	2	0.12	100.00
Total[b/]	476	455	344	345	1,620	100.00	

a/ U.S. Department of Transportation, Federal Railroad Administration, Accident/Incident Bulletins[C.1-C.7]

b/ Excludes accidents of unknown velocities

collisions, derailments, highway grade-crossing accidents, and other accidents respectively. The percentages and cumulative percentages shown in the bottom two rows of each table were used to estimate probability distributions for train velocities. The estimation procedure is discussed in Appendix G.

C.4 Probabilities of Fire and Fire Duration Distributions for Train Accidents

There is very little useful data regarding the occurrence of fires and the properties of the fire, such as duration, given a train accident. Table C.7 presents the results of surveys of train fires, compiled by the National Fire Protection Association for the years 1976-78 and 1982-83.[C.10,C.11] Over this time, for the railroads surveyed, approximately 1.24% of all railroad fires occur as a result of a collision or derailment. This is interpreted probabilistically as the (conditional) probability, given a fire, that the cause of the fire is either a collision or derailment. On the other hand, the probability of interest for this study is the (conditional) probability, given a collision (or a derailment), that a fire also occurs. To derive the latter probability from the former, it is necessary to have some estimate of the probability of a fire given an accident. The necessary data to estimate this probability was not found. Therefore, the Sandia study estimate of the probabilities of a fire's occurring, given an accident scenario was used.[C.8]

No information was found regarding the duration of fires resulting from train accidents. Therefore, the simulated estimates for fire duration as developed in the Sandia study were used.[C.8]

Table C.7
Railroad Fires Survey Results[a/]

Category	Year 1976	1977	1978	1982	1983	Total	Avg.	Pct.of Total(%)
Class I Railroads Surveyed:	22	16	16	NA	22	76	19.0	N/A
Trackage Surveyed (miles):	129,382	116,405	94,509	NA	NA	340,296	113,432	N/A
Total Class I Trackage (miles):	240,250	236,351	233,956	NA	NA	710,557	236,852	N/A
Percentage of Total (%):	53.85	49.25	40.40	N/A	N/A	N/A	47.89	N/A
Number of Fires due to Operations and Transportation								
Collisions and Derailments	18	24	14	19	12	87	17.4	1.24
Brake Shoe Sparks	198	157	115	188	63	721	144.2	10.30
Electrical Components	34	35	136	53	42	300	60.0	4.28
Engine Exhaust Sparks	354	23	17	120	195	709	141.8	10.12
Car and Van Heaters	34	10	12	3	17	76	15.2	1.09
Fuses	13	10	7	7	5	42	8.4	0.60
Hot Journal Boxes	20	33	19	11	11	94	18.8	1.34
Materials in Transit	19	64	22	5	8	118	23.6	1.68
I. C. Engines	23	10	14	25	8	80	16.0	1.14
Other	63	22	58	82	78	303	60.6	4.33
Subtotal	776	388	414	513	439	2,530	506.0	36.13
Number of Fires due to Maintenances and Services								
Smoking	23	20	13	11	19	86	17.2	1.23
Electrical	28	26	26	22	22	124	24.8	1.77
Flammable Liquids	3	10	3	6	7	29	5.8	0.41
Heaters and Appliances	72	69	78	69	29	317	63.4	4.55
Burning on Right-of-Way	11	12	1	117	8	149	29.8	2.13
Spontaneous Ignition	18	27	9	20	15	89	17.8	1.27
Welding, Cutting, Brazing	74	55	64	59	63	315	63.0	4.50
Other	41	43	26	29	24	163	32.6	2.33
Subtotal	270	262	220	333	187	1,272	254.4	18.16
Number of Fires due to Outside or Undetermined Causes								
Exposure Fires	56	50	25	27	16	174	34.8	2.48
Lightning and Storms	7	9	33	6	8	63	12.6	0.90
Trespassing (including Arson)	272	170	193	269	202	1,106	221.2	15.79
Other	29	51	16	27	13	136	27.2	1.94
Undetermined Causes	346	318	92	359	607	1,722	344.4	24.59
Subtotal	710	598	359	688	846	3,201	640.2	45.71
Grand Total	1,756	1,248	993	1,534	1,472	7,003	1,400.6	100.00

a/ National Fire Protection Association[C.8,C.9]
NA Information not available at time of table preparation
N/A Not applicable

C.5 References

C.1 Accident/Incident Bulletin No. 145, Calendar Year 1976, Office of Safety, Federal Railroad Administration, U.S. Department of Transportation, Washington, DC, December 1977.

C.2 Accident/Incident Bulletin No. 146, Calendar Year 1977, Office of Safety, Federal Railroad Administration, U.S. Department of Transportation, Washington, DC, August 1978.

C.3 Accident/Incident Bulletin No. 147, Calendar Year 1978, Office of Safety, Federal Railroad Administration, U.S. Department of Transportation, Washington, DC, October 1979.

C.4 Accident/Incident Bulletin No. 148, Calendar Year 1979, Office of Safety, Federal Railroad Administration, U.S. Department of Transportation, Washington, DC, July 1980.

C.5 Accident/Incident Bulletin No. 149, Calendar Year 1980, Office of Safety, Federal Railroad Administration, U.S. Department of Transportation, Washington, DC, June 1981.

C.6 Accident/Incident Bulletin No. 150, Calendar Year 1981, Office of Safety, Federal Railroad Administration, U.S. Department of Transportation, Washington, DC, June 1982.

C.7 Accident/Incident Bulletin No. 151, Calendar Year 1982, Office of Safety, Federal Railroad Administration, U.S. Department of Transportation, Washington, DC, June 1983.

C.8 R. K. Clarke, et al., Severities of Transportation Accidents, Sandia National Laboratory, Albuquerque, NM, SAND77-0001, 1977.

C.9 P. Eggers, Severe Rail and Truck Accidents: Toward a Definition of Brounding Environments for Transportation Packages, U.S. Nuclear Regulatory Commission, Washington, DC, NUREG/CR-3499, 1983.

C.10 Fire Protection Handbook, 15th Edition, G. P. McKinnon, Ed., National Fire Protection Association, Quincy, MA, 1981.

C.11 R. L. Best, National Fire Protection Association, Railroad Section, Quincy, MA, private communication, 1985.

APPENDIX D

List of Figures

List of Tables

APPENDIX D

Highway Survey Data and Bridge Column Properties[a/]

D.1 Introduction

One important element in calculating shipping cask responses to accident loads is object hardness. When a shipping cask strikes a soft surface such as sand, the response of the cask is much less than when striking a hard object such as a concrete column. This appendix presents the data and evaluation results on two major subjects related to hard objects:

1) Statistical data on the total number of bridges, bridge heights, and surface conditions adjacent to highways, and below bridges,

2) The characteristics of bridge columns.

D.2 Survey

D.2.1 Surface Conditions Adjacent to Highways and below Bridges

The hardness of earth surfaces adjacent to highways can vary over a wide range. This variability can have a significant effect on the loadings that could be imposed on a cask or any other impacting object. The water and land (hard rock, soft rock/hard soil, and tillable soil) distribution along proposed spent fuel shipment routes between the east coast and west coast was initially estimated using agricultural soil survey data and geological highway maps for the United States.[D.3,D.4] The initial distributions estimated from these sources were considered to be indicative of the types of surfaces which could be impacted along highways in the various regions of the United States. However, since highway construction and landscaping can greatly affect the adjacent surroundings, the initial distributions were used to select representative portions of Interstates 5 and 80 in California to

---

a/ The Engineering Computer Corporation (ECC) was the subcontractor that performed the highway surveys and bridge column analyses.[D.1,D.2]

perform detailed highway surveys and to establish final distributions along highways.

A 133-mile portion of Interstate 5 was selected for the study. This portion of highway starts from the borderline between San Diego County and Orange County and ends at the borderline between Kern County and Los Angeles County. This portion of highway contains 20 miles of suburban, 50 miles of city, and 63 miles of rural area. The terrain which this portion of the highway crosses is essentially flat for 70 miles, rolling hills for 41 miles, and mountains for 22 miles. The types of earth adjacent to the highway were classified into three groups: tillable soil, non-tillable soil, and hard rock. The survey was performed by viewing the California Department of Transportation (CALTRANS) photo log. The result of the survey is summarized in Table D.1. Although the highway crossed the Santa Susana Mountains, no hard rock, such as granite, was identified in the survey.

A similar highway survey of earth types adjacent to 122 miles of the roadway along a section of Interstate 80 from Davis, California, to the Nevada border was then performed. This section of Interstate 80 crosses the Sierra where numerous outcroppings of granite rock occur. The result of the soil survey is summarized in Table D.2. The survey also included the types and frequencies of surfaces that could be impacted below a bridge. These surfaces were classified into four categories: roadbeds, railbeds, water, and earth. The result of the survey is summarized in Table D.3.

D.2.2 Highway Bridges

The same portion of Interstate 5 was used to compile statistical data on the number of bridges, bridge heights, and the size of columns. A two-step procedure was used in compiling data.

Step 1: View the California Department of Transportation (CALTRANS) photo log (a motion picture of the roadway as viewed by a motorist). Estimate the bridge column sizes and the number of bridges.

Table D.1
Type of Soil Adjacent to Interstate 5 from San Diego County/Orange County Line to Los Angeles County/Kern County Line

County	Adjacent Soil Type (miles)			
	Tillable	Nontillable	Hard Rock	Total
Orange	44.27	0.12	0	44.39
Los Angeles	62.65	5.80	0	68.45
	16.39	3.60	0	19.99
Total	123.31	9.52	0	132.83

Table D.2
Type of Soil Adjacent to Interstate 80 from Davis, California to Nevada Border[a]

County	Adjacent Soil Type (miles)			
	Tillable	Nontillable	Hard Rock	Total
Yolo	2	0	0	2
Sacramento	18	0	0	18
Placer	60	2	3	65
Nevada	29	6	0	35
Sierra	1	1	0	2
Total	110	9	3	122

[a] 122-mile highway through mountainous terrain from Davis, California, to the California-Nevada borderline.

Table D.3
Type of Surface below Bridges on Interstate 80 from Davis, California to Nevada Border[a/]

County	Surface below Each Bridge (bridge totals)				
	Road	River	Earth	Railroad	Total
Yolo	1	1	0	1	3
Sacramento	7	0	0	1	8
Placer	22	5	1	1	29
Nevada	12	6	0	1	19
Sierra	0	0	0	0	0
Total	42	12	1	4	59

a/ 122-mile highway through mountainous terrain from Davis, California, to the California-Nevada border line.

Step 2: Review the general plans for several of the bridges to confirm the column sizes identified by visual inspection through the photo log and to obtain bridge heights.

Table D.4 presents the result of the survey for the total number of bridges tabulated according to the bridge heights. Along the 133-mile roadway, 121 bridges were counted. Only 3 bridges exceed 50 feet in height. The rate is approximately 0.91 bridges/mile.

While collecting data about the bridge rate, information was also collected on all of California state and interstate highways. The total number of bridges in California is 12,574 and the miles of state and interstate highways is 15,183. This is very close to the detailed survey results of Interstate Highway 5.

D.3 Bridge Column Structural Characteristics

In order to estimate the response of a cask when impacting a bridge column, it is necessary to determine the level of hardness for that particular column. The level of hardness is normally represented by the force-displacement curve.

This subsection describes the approach used to develop the force-displacement curves for various column designs and the results of the detailed sensitivity study.

From the survey of Interstate 5, two typical bridge constructions are commonly seen along interstate highways: single-column bent bridge and multi-column bent bridge, as shown in Figs. D-1 and D-2 respectively. Most of the bridge columns are either square or rectangular. Bridge span lengths and column bent widths vary from bridge to bridge. Since more than 12,000 bridges exist on state and interstate highways in California, estimating the column force-displacement curve for each bridge is a very complex task. In order to control the task, 13 different sizes of column cross-sections from 1 ft x 1 ft to 4 ft x 64 ft were selected. In combination with the number of bents, a total of 24 column configurations were selected for sensitivity study in

Table D.4
Bridges Along Interstate 5 from San Diego County/Orange County Line to Los Angeles County/Kern County Line Classified by Height[a/]

	Bridge Height (ft)								
County	0-10	11-20	21-30	31-40	41-50	51-60	61-70	71-80	81-90
Orange	3	4	16	4					
	1	3	7						
Los Angeles	1	3	17	6			1		
		7	16	2	2				
		5	18	1	1	1			1
Total	5	22	74	14	3	1	1		1

Total Mileage = 133 miles[a/]
Total Bridges = 121

a/ Each set (left/right pair, on/off ramps, etc.) counts only once. Special truck lanes in northern Los Angeles County are not counted.

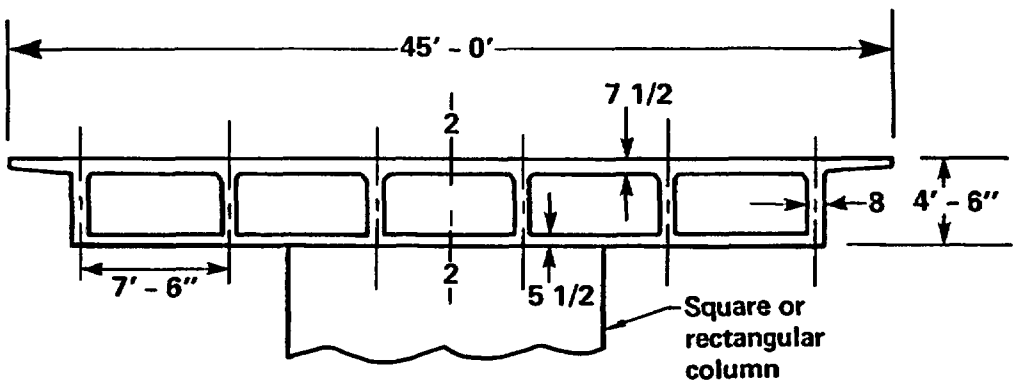

Section

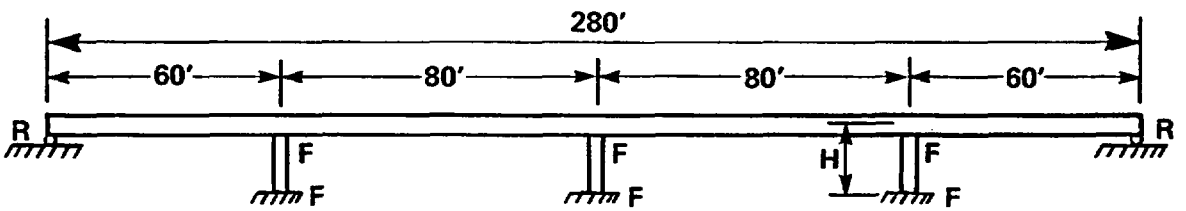

Elevation

Figure D-1 Single column bent bridge structure configuration.

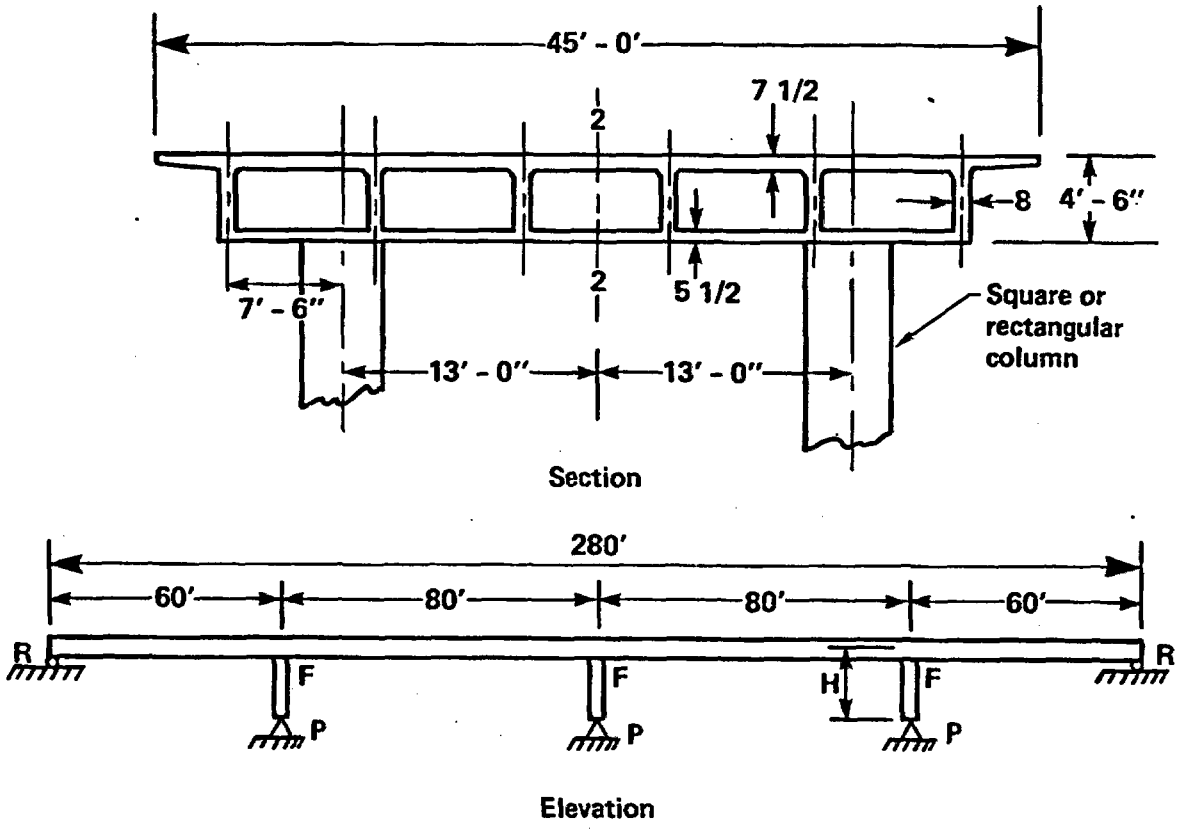

Figure D-2 Multi-column bent bridge structure configuration.

developing force-displacement curves. Table D.5 lists all column configurations selected for the sensitivity study. Some of the column dimensions, such as 32 ft x 32 ft, 16 ft x 16 ft, are not real structures. The inclusion of these dimensions in the analytical study is to help develop a set of continuous curves.

All 24 different configurations were categorized into four groups according to the shape of columns, i.e., square or rectangular, and number of bents, i.e., single-bent or multi-bent. These four groups formed the four basic cases for the sensitivity study as listed below and indicated in Table D.5.

Case A: Bridges with square columns and single-column bents.

Case B: Bridges with rectangular columns and single-column bents.

Case C: Bridges with square columns and multi-column bents.

Case D: Bridges with rectangular columns and multi-column bents.

D.4 Column Stiffness Sensitivity Study

The sensitivity study assumed that a shipping cask would strike the bridge column 4 feet above the rough surface, or 6 feet above the bottom of the column (bottom of pier). The study includes column heights of 20 feet and 30 feet.

For a single-bent column, the assumption is that the bottom of the column is pinned and the top of the column is fixed. A normalized static force of 1,000 kips is applied at 6 feet above the bottom of the column to represent the impact force of the shipping cask. Deformation at the point of impact is calculated for all column sizes of both cases A and B. The stiffness of the column is determined from the applied force and calculated deformation.

For the multi-bent configuration, the bridge is assumed to be a four-span bridge, which is most commonly seen along interstate highways. A beam-element

Table D.5
Twenty-Four Representative Column Configurations for Calculating Force-Displacement Curves

Class	Number of Bents	Shape of Column	Column Size (cross-section)
A	Single	Square	1 ft x 1 ft 2 ft x 2 ft 4 ft x 4 ft 8 ft x 8 ft 16 ft x 16 ft 32 ft x 32 ft
B	Single	Rectangular	4 ft x 1 ft 4 ft x 2 ft 4 ft x 8 ft 4 ft x 16 ft 4 ft x 32 ft
C	Multi	Square	1 ft x 1 ft 2 ft x 2 ft 4 ft x 4 ft 8 ft x 8 ft 16 ft x 16 ft 32 ft x 32 ft
D	Multi	Rectangular	4 ft x 1 ft 4 ft x 2 ft 4 ft x 8 ft 4 ft x 16 ft 4 ft x 32 ft 4 ft x 64 ft

model along the bridge roadway was developed to represent the bridge superstructure. The bridge is assumed to be pinned at both ends. At each pier location, the multiple-bent column configuration is modeled by a space frame pinned at the bottom of the frame structure. The combined bridge superstructure and column space frames formed the total bridge design. A normalized static force of 1,000 kips is applied 6 feet above the bottom of the column. The deformation at the point of impact is calculated by the Structural Analysis Program 6 (SAP6) program. The force-deformation relationship is used to determine the stiffness of the columns for each pier. This process is performed on all the column sizes for cases C and D.

Figure D-3 presents the results of this sensitivity study.

D.5 Force-Displacement Curve

The force-displacement curve was developed by following similar procedures to those described in the stiffness calculation. The same four groups (Cases A through D) were used. All the column sizes given in Table D.5 were included in the sensitivity study. During this exercise, column capacity was considered in resisting axial force, shear force, and bending moment. The angle of impact to the column was also considered. The impact was analyzed for every 15^{o} angle. The smallest column capacity for resisting impact at the various impact angles is selected to represent the column capacity. In estimating column capacity, the following assumptions were made to simplify the problem:

1. Vertical reinforcement is 2%

2. $fc' = 3,250$ psi

3. Tensile stress capacity of concrete $= 0.1\ fc' = 325$ psi

4. Ties are determined by the following formula

$$A_{sh} = 0.30\ S_t\ h_c\ \frac{fc'}{f_y}\ \left(\frac{Ag}{Ac} - 1\right) \qquad (D.1)$$

Case A : Square column, single-bent, column size D' x D'

Case B: Rectangular column, single-bent, column size 4' x D'

Case C: Square column, multi-bent, column size D' x D'

Case D: Rectangular column, multi-bent, column size 4' x D'

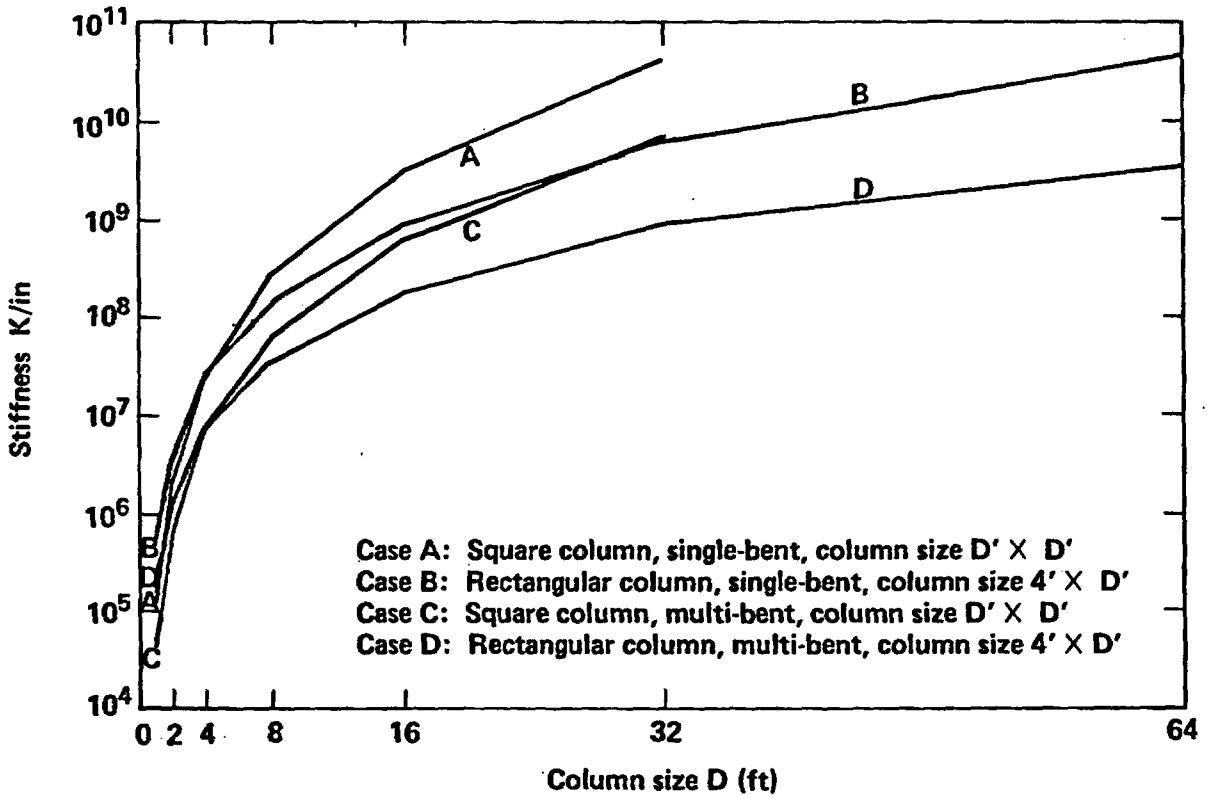

Figure D-3 Column stiffness for four bridge types.

or

$$A_{sh} = 0.12\ S_t\ h_c\ \frac{fc'}{f_y}\ (0.5 + 1.25\ \frac{Pe}{fc'Ag}) \qquad (D.2)$$

where

A_{sh} = area of transverse hoop bar, ft^2
fc' = specified compressive strength of concrete, psi
h_c = total depth of shear head cross-section, ft
S_t = vertical spacing of ties, ft
Pe = maximum design axial load, lbs
Ag = gross area of section, ft^2
Ac = area of concrete enclosed by tie, ft^2
f_y = specified yield strength of re-bar, psi

5. Height of column is 20 feet.

6. Distance from the face of concrete to the center of vertical re-bars is 3 inches.

7. Moment magnification due to slenderness is ignored.

8. P - Δ effect is ignored.

From assumption number 3, an axial force capacity was calculated for each different column size (cross section). For the flexural capacity, the Reinforced Column (RECOL) computer code was used to estimate column strength at yield point. These axial and flexural capacities of a column are combined with the results from the stiffness calculation as generated in the bridge model by using the SAP6 computer code to correlate the force-displacement relationship for each different column size.

These force-displacement relation curves used to relate the column yield force and displacement at the location of impact are listed in

Figs. D-4 through D-7 for all the column sizes listed in Table D.5. The possible dominant failure modes are identified in each curve. For example, for each column size, we identify whether a plastic hinge or a sudden shear failure occurs first. The shear capacity for a column is based on the equation

$$V_u = 2 (fc')^{1/2} bd + \frac{A_{sh} f_y d}{s} \qquad (D.3)$$

where

b = width of compression face, ft
d = distance from extreme compression fiber to centroid of tension reinforcement, ft
s = tie spacing, ft.

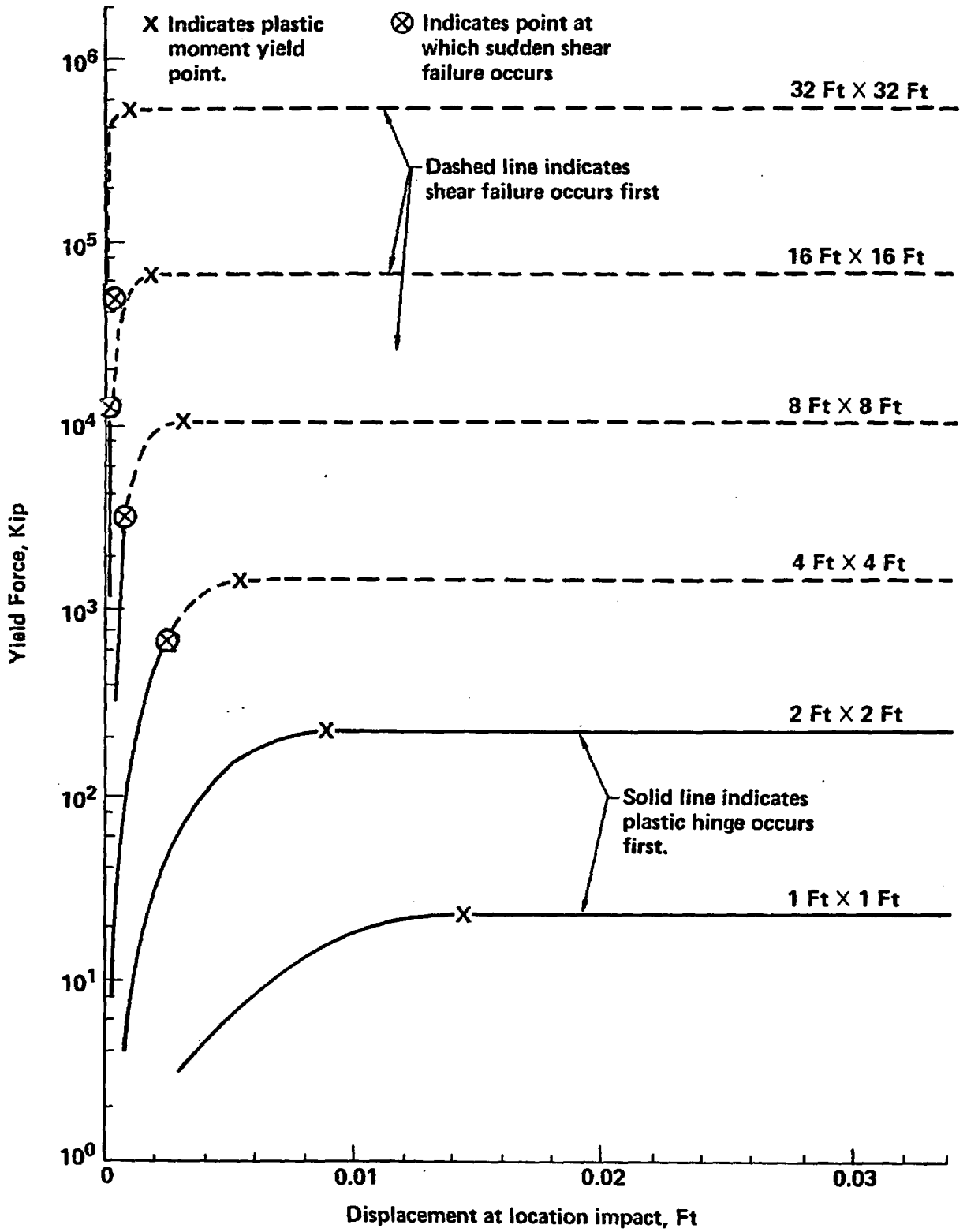

Figure D-4 Force-displacement curves for single, square bridge columns.

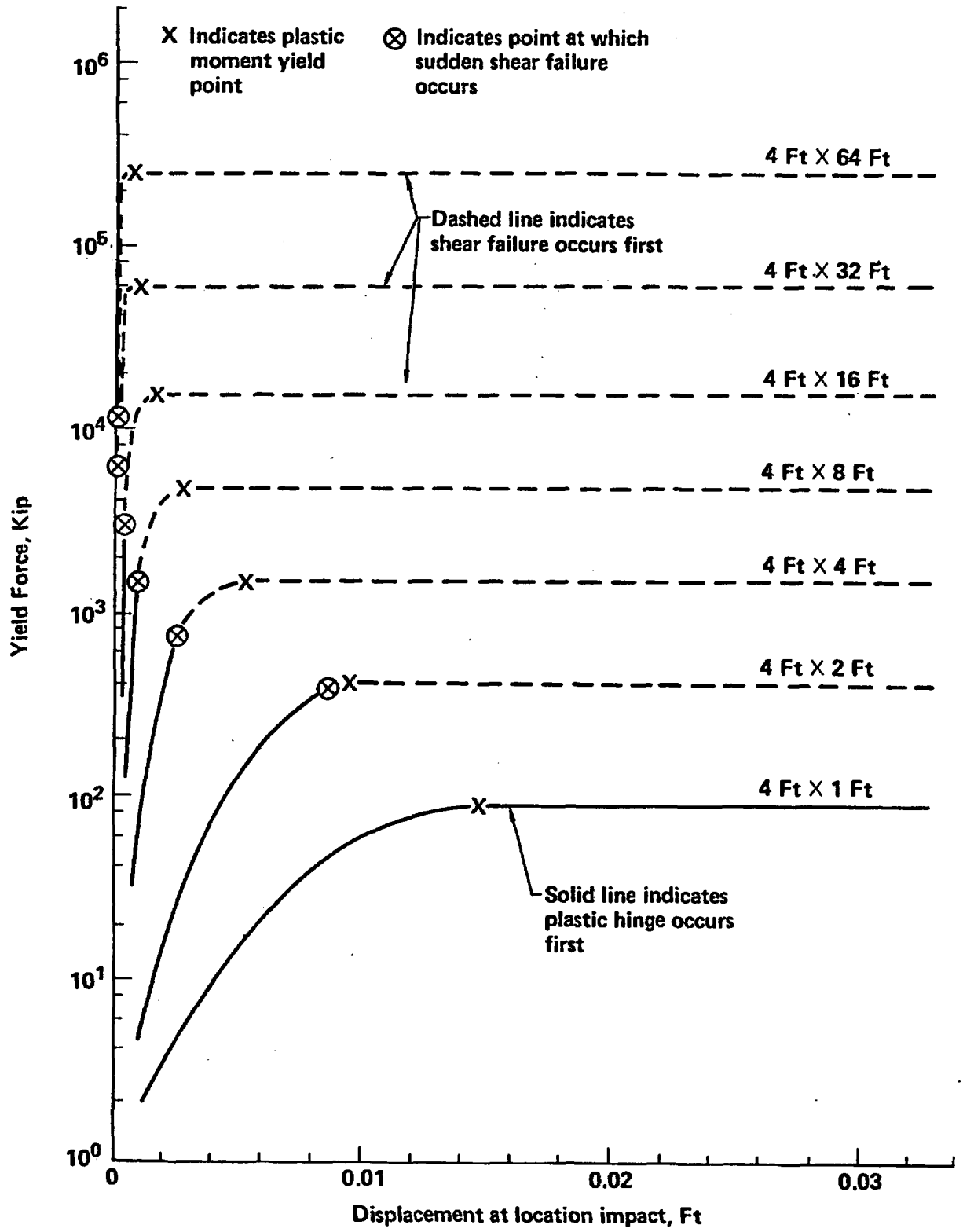

Figure D-5 Force-displacement curves for single, rectangular bridge columns.

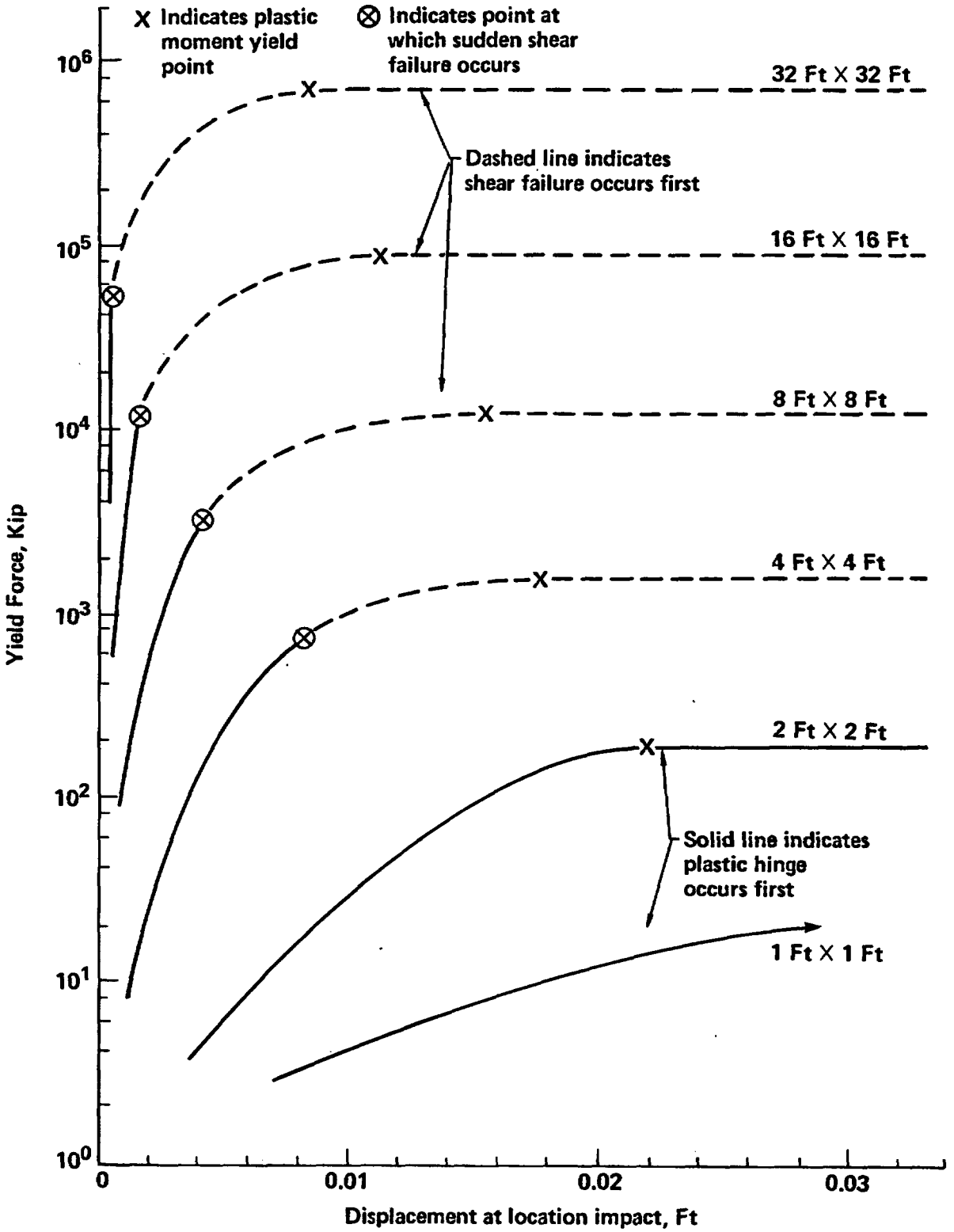

Figure D-6 Force-displacement curves for multi, square bridge columns.

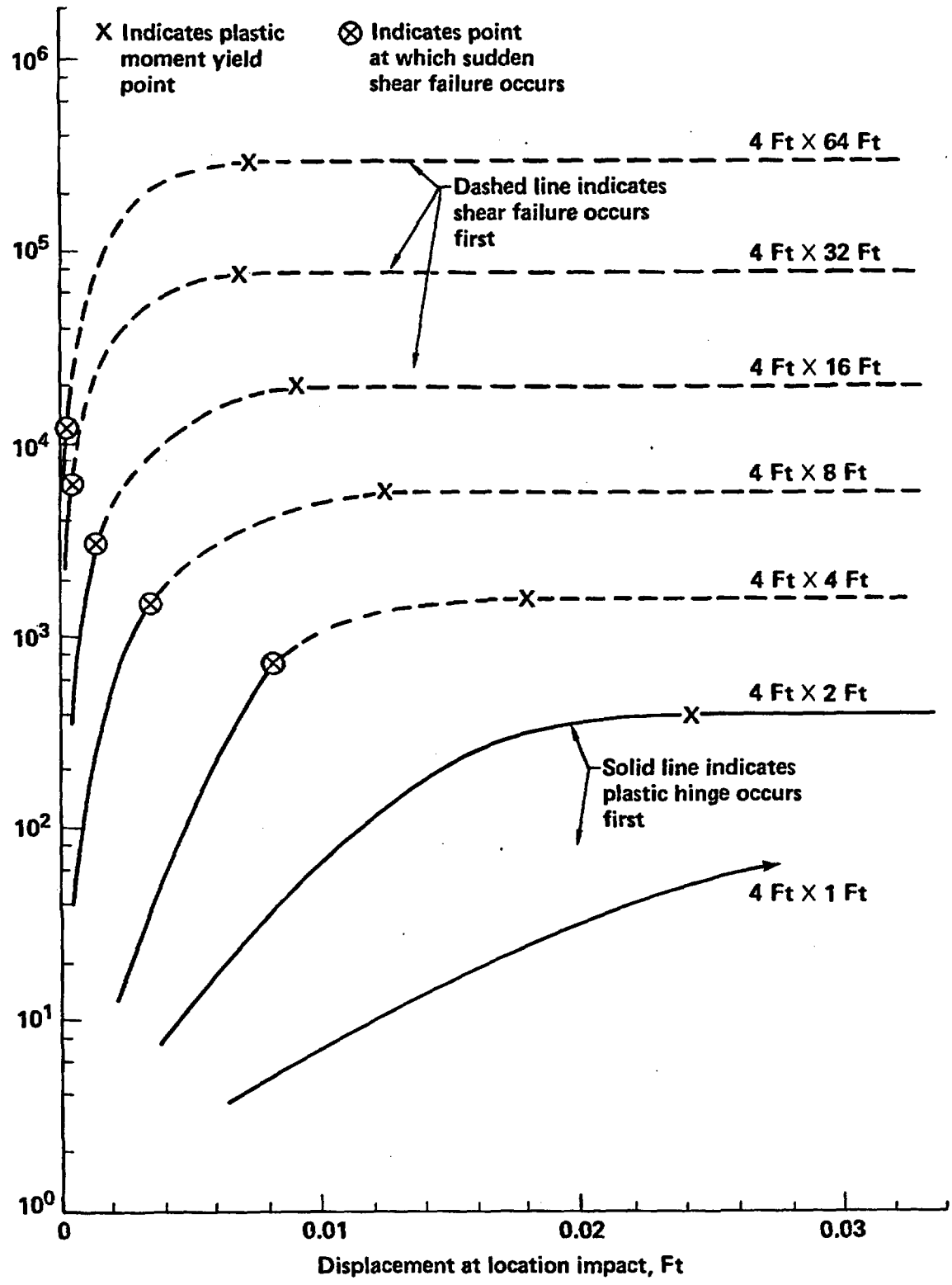

Figure D-7 Force-displacement curves for multi, rectangular bridge columns.

D.6 References

D.1 Assessment of the Stiffness Characteristics of Bridge Substructure Components Encountered along a Section of Interstate 5, Engineering Computer Corporation, Sacramento, CA, February 1985. A contractor report to the Lawrence Livermore National Laboratory.

D.2 R. Imbsen, et al., Soil and Terrain Surveys, Engineering Computer Corporation, Sacramento, CA, January 1985. A contractor report to the Lawrence Livermore National Laboratory.

D.3 Soil Survey, United States Department of Agriculture, Bureau of Chemistry and Soils, Superintendent of Documents, Washington, DC.

D.4 Geological Highway Map, American Association of Petroleum Geologist, Tulsa, OK.

D.5 University of Southern California, Structural Analysis Program 6 (SAP6), University of Southern California, Los Angeles, CA, 1980.

D.6 Engineering Computer Corporation, Reinforced Column (RECOL), Engineering Computer Corporation, Sacramento, CA, 1983.

APPENDIX E

List of Figures

APPENDIX E

List of Tables

APPENDIX E
Structural Analysis

E.1 Introduction

This appendix provides the structural models developed and the analyses performed to determine the responses of the representative truck and rail casks to a wide range of impact loads. The family of DYNA and NIKE computer codes were used extensively to calculate the responses of the casks.[E.1,E.2]

In Section E.2, the material properties used in the process for selecting the representative casks and evaluating the responses of the representative casks are presented. In Section E.3, the static analyses evaluations of different cask designs used to select the representative cask are presented.

In Section E.4, the types of mechanical loading conditions that can affect the strain response of a cask in an accident are discussed. In Section E.5, the quasi-static load evaluation performed for minor accidents are presented. In Section E.6, the structural model and strain response of the two representative casks to impacts on an unyielding surface are discussed. In Section E.7, the response of the two representative casks to impacts on real objects is estimated.

E.2 Materials Properties

Spent fuel casks must be designed and fabricated to national codes and standards or equivalent requirements. Although there is no specific section in the American Society of Mechanical Engineers (ASME) pressure vessel code applicable to spent fuel casks, the industry has used the ASME code extensively for designing and fabricating spent fuel casks. In this study, to the extent possible, properties of materials were taken from the ASME code.[E.3]

Although it is preferred to use probability distributions for material properties that are based on actual fabrication data, discrete bounding values from the ASME code were used in this study. This approach was taken to simplify the modeling and analysis. If distribution had been used, the modeling and analysis would have been unnecessarily complex and unwarranted for the scope of this study. Consequently, conservative material properties

based on the ASME code were used with loading calculations to estimate seal and weld damage to the representative casks.

Using ASME code properties, limiting plastic strain criteria were used in estimating the response and damage to the representative casks. In this case, the maximum strains would be associated with end-on impact caused by lead slump. Large local strains would be generated at the junctions of the inner containment shell and outer shell with the end closure. Ideally, weld joints would not be present in these areas where high local strains could occur. However, even if welds were present in these areas, most strains would be highly concentrated and could cause only local cracking. Since the extent of lead slump deformation would be limited, it would not be likely that the inner containment would completely rupture. Furthermore, the primary membrane strain on the inner containment cylinder would be compressive and a small fraction of the selected strain levels. The large strains developed at the discontinuities would be highly localized and oriented axially. On the outer shell, the primary membrane strains would be tensile. Even if complete separation from the end plate is postulated, the deformation of the lead would also limit the primary membrane strain to a small fraction of 30% strain. Consequently, the outer shell would remain intact and continue to maintain the integrity of the lead shielding. In conclusion, the postulated local strains on the order of 30% would not result in breaching of the cask but may result in local cracking.

Instead of evaluating specific closure and penetration designs, it was assumed for comparative purposes that closure and penetration seals fail when the strain level in the inner shell exceeds 0.2% (S_1). This approach was based on a review of current cask designs and their ability to withstand impact forces with large strains. Temperature effects on the material properties were included in the analysis performed. Strain-rate effects were not included for most material properties for the following reasons:

(1) There is no standard set of strain-rate properties in the ASME code or adopted by industry.

(2) Strain-rate effects generally improve material yield and ultimate strength by 0-30%, but reduce ductility. When strain-rate effects are included for the cask structural materials, then they should be included for surface materials such as rock and concrete. In general, the improvement of material strength properties is greater for ductile type metallic materials than for ceramic type materials. For the purpose of evaluating representative casks impacting representative surfaces, the inclusion of strain-rate effects is not warranted and their exclusion is reasonably conservative.

(3) The strain effect in reducing the structural material ductility was accounted for by using conservative static ultimate strain values for the structural materials.

E.2.1 304 Stainless Steel

Material properties were obtained for 304 stainless steel from the ASME code.[E.3] The properties are tabulated in Table E.1. The elastic-plastic material model used a bilinear fit representation with isotropic hardening. No strain-rate effects were included. The material model used was Material Type 3 in the NIKE 2-D/DYNA 2-D family of finite element codes; the 2-D designation indicating that two-dimensional modeling was performed.[E.1,E.2] These codes use an updated geometry to calculate strains. Therefore, it was necessary to use true stress and true strain data, rather than the engineering stress and strain data provided in the ASME code. In order to approximate a value for ultimate true stress, based on ultimate engineering stress, data from Conway, et al., was used.[E.4] The stress/strain data of Conway, et al., was not for SA-240, but for another 304 stainless. This, however, provided a means to interpolate a value of true stress for a given engineering stress from the ASME code.

$$\frac{75{,}000 - 71{,}300}{76{,}390 - 71{,}300} = \frac{\sigma_{u_{true}} - 85{,}730}{97{,}760 - 85{,}730} \qquad \text{(E.1)}$$

$$\sigma_{u_{true}} = 94{,}475 \text{ psi} .$$

Table E.1
304 Stainless Steel Structural Properties

Elastic modulus	E	=	27.6×10^6 psi
Hardening modulus	E_n	=	2×10^5 psi
Poisson's ratio	ν	=	0.29
Engineering ultimate stress	$\sigma_{u_{eng}}$	=	75×10^3 psi
True ultimate stress	$\sigma_{u_{true}}$	=	94.5×10^3 psi
Engineering ultimate strain	$\epsilon_{u_{eng}}$	=	0.40
True ultimate strain	$\epsilon_{u_{true}}$	=	0.34
Yield stress	σ_y	=	25×10^3 psi
Density	ρ	=	7.44×10^{-4} lb-sec^2/in^4

The ultimate engineering strain value provided by the ASME code of 40% is equivalent to a true strain value:

$$\varepsilon_{u_{true}} = \ln (1 + \varepsilon_{u_{eng}}) \qquad (E.2)$$

$$= \ln (1 + 0.4)$$

$$= 0.34.$$

The ultimate strain percentage used in this study is 30% (S_3) to accommodate for the effects of strain rate on the reduction of ductility. The hardening modulus was calculated as follows:

$$E_n = \frac{94,475 - 25,000}{0.34 - .00091} = 2 \times 10^5 \text{psi}. \qquad (E.3)$$

E.2.2 Lead

The material properties used for lead in this study are presented in Table E.2.[E.5] A bilinear fit was used to represent the elastic-plastic material. Strain hardening was used, with isotropic hardening in all calculations. It is considered to be unnecessarily conservative to exclude the strain-rate effect for the lead. The hardening modulus is more significant than the elastic modulus for lead because the lead shield yields relatively easily on impact. The hardening modulus used in this study compares well with the test results reported by Counts and Payne.[E.6] Additional benchmarking testing is required to define the lead properties and bonding effects at the cask inner shell with high confidence.

E.2.3 Uranium

The material properties used for uranium are summarized in Table E.3.[E.7] A bilinear fit was used to model its elastic-plastic characteristics for stress/strain.

Table E.2
Lead Structural Properties

Elastic modulus	E =	2.22×10^6 psi
Hardening modulus	E_n =	4.5×10^4 psi
Poisson's ratio	ν =	0.43
Yield stress	σ_y =	500 psi
Density	ρ =	1.06×10^{-3} lb sec^2/in^4

Table E.3
Uranium Structural Properties

Elastic modulus	E =	26×10^6 psi
Hardening modulus	E_n =	1×10^6 psi
Poisson's ratio	ν =	0.21
Yield stress	σ_y =	4.6×10^4 psi
Density	ρ =	1.74×10^{-3} lb-sec^2/in^4

E.2.4 Balsa Wood

An elastic-plastic model was selected for modeling the balsa wood.[E.8] The material properties used are tabulated in Table E.4.[E.8] Material Type 10, from DYNA 2-D, was used for the wood material model.

E.3 Preliminary Cask Designs and Cask Selection

Six preliminary cask designs were developed to perform screening analyses to assess their responses to high-loading conditions. The designs included the use of three types of gamma shielding materials: lead, depleted uranium, and steel. Three truck and three rail casks were developed using each type of shielding. The pertinent materials and dimensions for the six preliminary cask designs are provided in Figs. E-1 and E-2 for the truck and rail casks, respectively.

Static force evaluations were performed using the NIKE 2-D finite element computer code for the six casks. The loading conditions applied on each of the casks are illustrated in Table E.5. In case (a), a pressure load was applied on one end over the entire closure region of the cask in increments of 200 psi with the other end of the cask resting on an unyielding surface. In case (b), a circular cross-section of the cask was loaded in increments of 200 psi over the top area of the cask with the bottom resting on an unyielding surface. In case (b), the model had a unit or one inch thickness. The yield force results of the two loading calculations for each of the six casks are summarized in Table E.5. The lead cask yielded at significantly lower loading conditions in all cases. Based on these results, the lead shielded cask was selected for developing a representative cask design for impact analysis.

E.4 Mechanical Loading Conditions Caused by Accidents

Mechanical loading conditions on a cask caused by an accident can result in damage to the inner shell of the cask. Mechanical loading conditions include impact, puncture (including missiles), and crush. Two representative cask designs were developed as shown in Fig. E-3: one for truck shipments and one for rail shipments of spent fuel. The representative truck cask

Table E.4
Balsa Wood Structural Properties

Elastic modulus	E =	5.9×10^5 psi
Poisson's ratio	ν =	0.0
Yield stress	σ_y =	1.7×10^3 psi
Sheer modulus	G =	2.95×10^5 psi
Density	ρ =	1.35×10^{-5} lb-sec^2/in^4

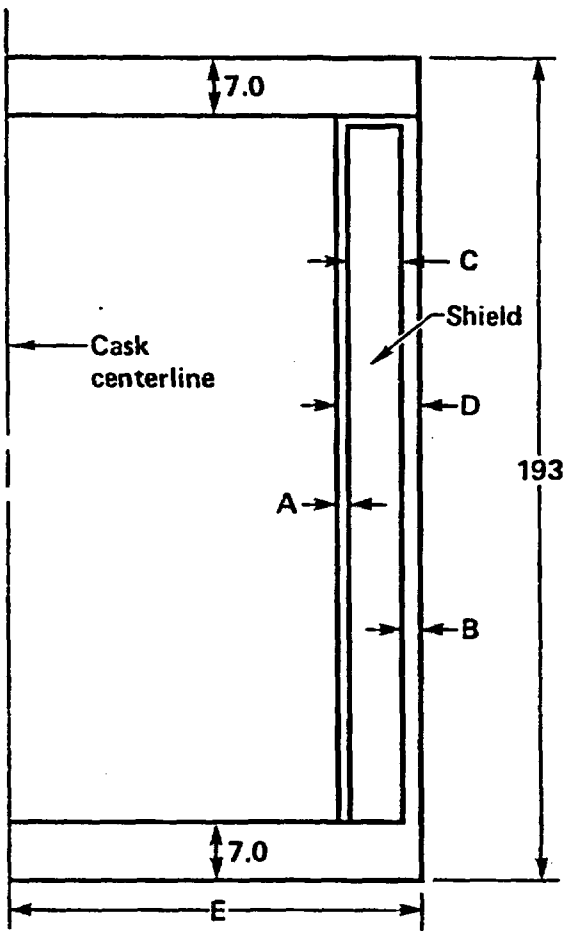

Dim	Thickness (in.)	Material
	Truck Cask 1	
A	0.5	304SS
B	1.25	304SS
C	5.25	Lead
E	13.75	304SS
	Truck Cask 2	
A	0.5	304SS
B	1.25	304SS
C	4.25	Depleted uranium
E	12.75	304SS
	Truck Cask 3	
D	12.25	Steel
E	19.00	Steel

Figure E-1 Preliminary truck casks with three types of shielding, used for static load analysis.

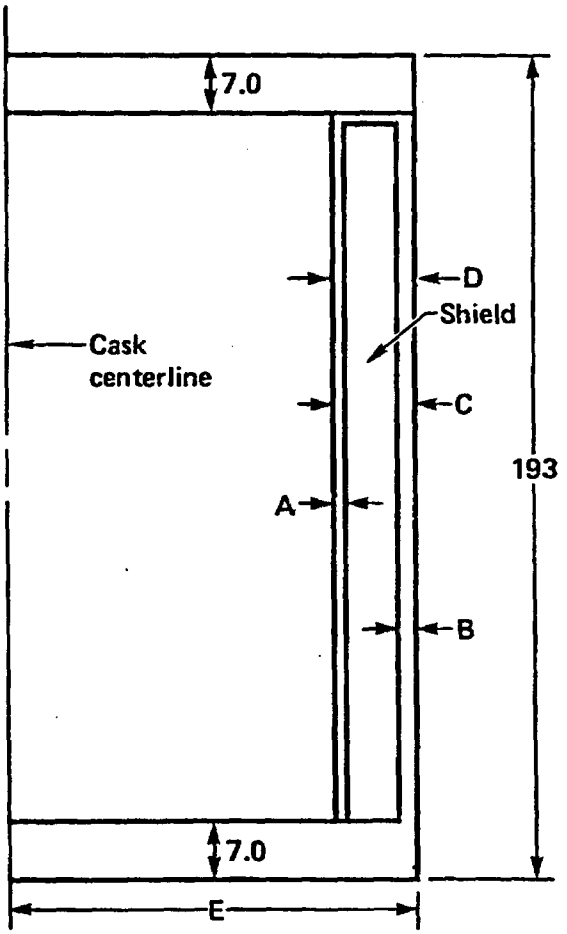

Dim	Thickness (in.)	Material
	Rail Cask 1	
A	0.5	304SS
B	1.5	304SS
C	5.25	Lead
E	26.0	304SS
	Rail Cask 2	
A	0.5	304SS
B	1.5	304SS
C	4.0	Depleted uranium
E	24.8	304SS
	Rail Cask 3	
D	12.25	Steel
E	30.75	Steel

Figure E-2 Preliminary rail casks with three types of shielding, used for static load analysis.

Table E.5
Summary of Static Loading Calculations for Six Preliminary Cask Designs

Loading Configuration	Cask Type	Yield Force (lbs)
	ENDWISE LOADING	
Case (a), endwise 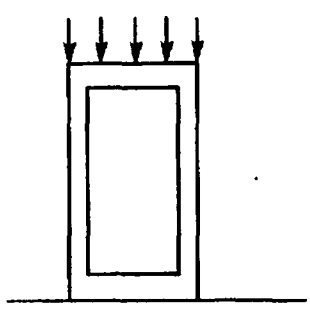	Truck	
	Lead	3,300,000
	Depleted uranium	8,000,000
	Steel	11,000,000
	Rail	
	Lead	8,000,000
	Depleted uranium	17,000,000
	Steel	40,000,000
	SIDEWISE LOADING	
Case (b), sidewise 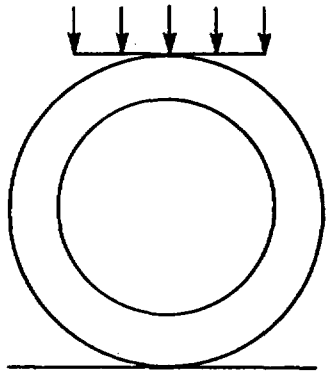	Truck	
	Lead	1,600,000
	Depleted uranium	11,000,000
	Steel	26,000,000
	Rail	
	Lead	260,000
	Depleted uranium	3,700,000
	Steel	11,500,000

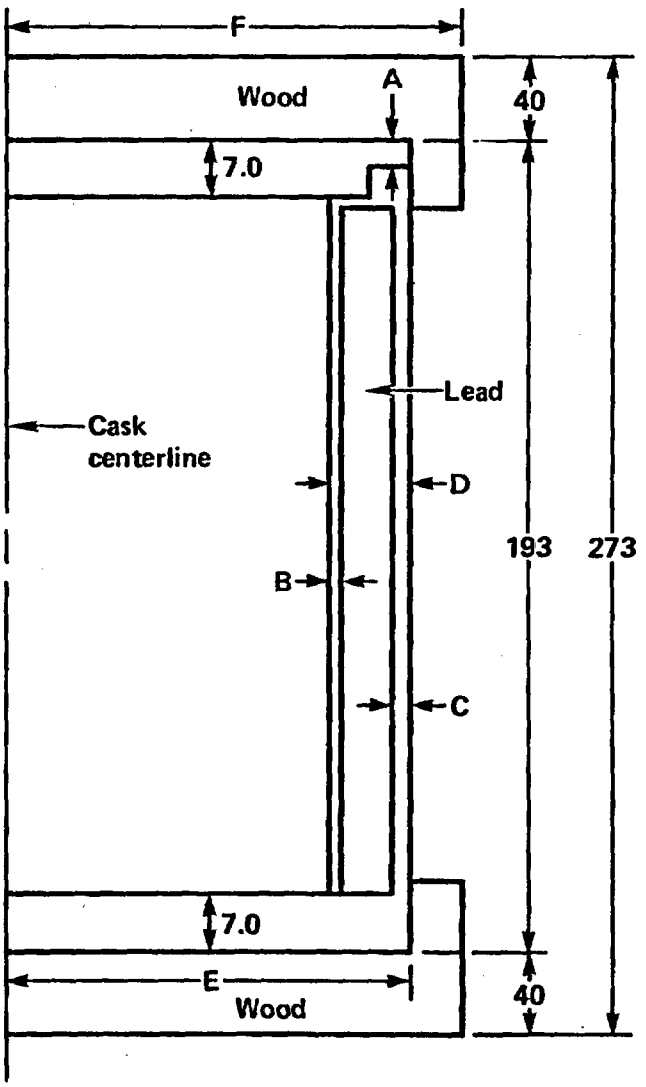

Dim	Truck inches	Rail inches
A	1.5	3.0
B	0.5	1.5
C	1.25	2.5
D	7.0	8.0
E	13.75	38.0
F	38.25	58.0

All material is 304SS except that noted otherwise

Figure E-3 Representative cask models used for truck and rail cask analysis.

(Fig. E-3) design uses the same dimensions as the preliminary lead truck cask design (Fig. E-1). The truck cask design allows transport of a single PWR fuel assembly. The representative rail cask design (Fig. E-3) dimensions differ from the preliminary lead rail cask design (Fig. E-2). The capacity of the rail cask is 21 PWR fuel assemblies which reflects the greater capacities of anticipated cask designs. Each design uses helium in the cask cavity.

Typically, as discussed in Sections E.6 and E.7, the dynamic force caused by impact on a hard surface can be in the range of 1-10 million pounds on the representative truck cask depending on the impact velocity (velocity component perpendicular to the surface impacted), the cask orientation, and the hardness of the surface. The strain at the inner wall of the cask can exceed 30% (S_3) at impact velocities greater than 75 mph. The dynamic forces generated by impacts on a hard surface are even higher for the rail cask compared to the truck cask because of the larger size and weight of the rail cask.

The possibility of puncture of the cask by a high energy-density object was evaluated. It was concluded that a high velocity I-beam would have the highest energy density of probable missiles generated in an accident and that the I-beam represented the bounding case for the puncture of a cask wall.[E.9] Assuming that the I-beam is the bounding case, the representative truck cask was analyzed with DYNA 3-D (the 3-D designation indicating that three-dimensional modeling was performed) for impact by a high energy I-beam.

The representative truck cask and I-beam were modeled using two planes of symmetry. The truck cask model included the inner and outer steel walls and the lead shielding but did not have end closures or impact limiters. The back side of the cask was supported by an unyielding surface. The 40 foot WF-21/96 I-beam was modeled as 1/4 of the length unit with an equivalent weight.

The impact velocity was 60 mph, resulting in an impact force of 40,000 pounds by the I-beam. The deformations due to the impact are shown in Fig. E-4. The impact caused the cask wall to flatten locally and the I-beam to yield significantly at the point of impact. A maximum plastic strain of 5% developed in the outer wall of the cask as shown in Fig. E-5. The maximum

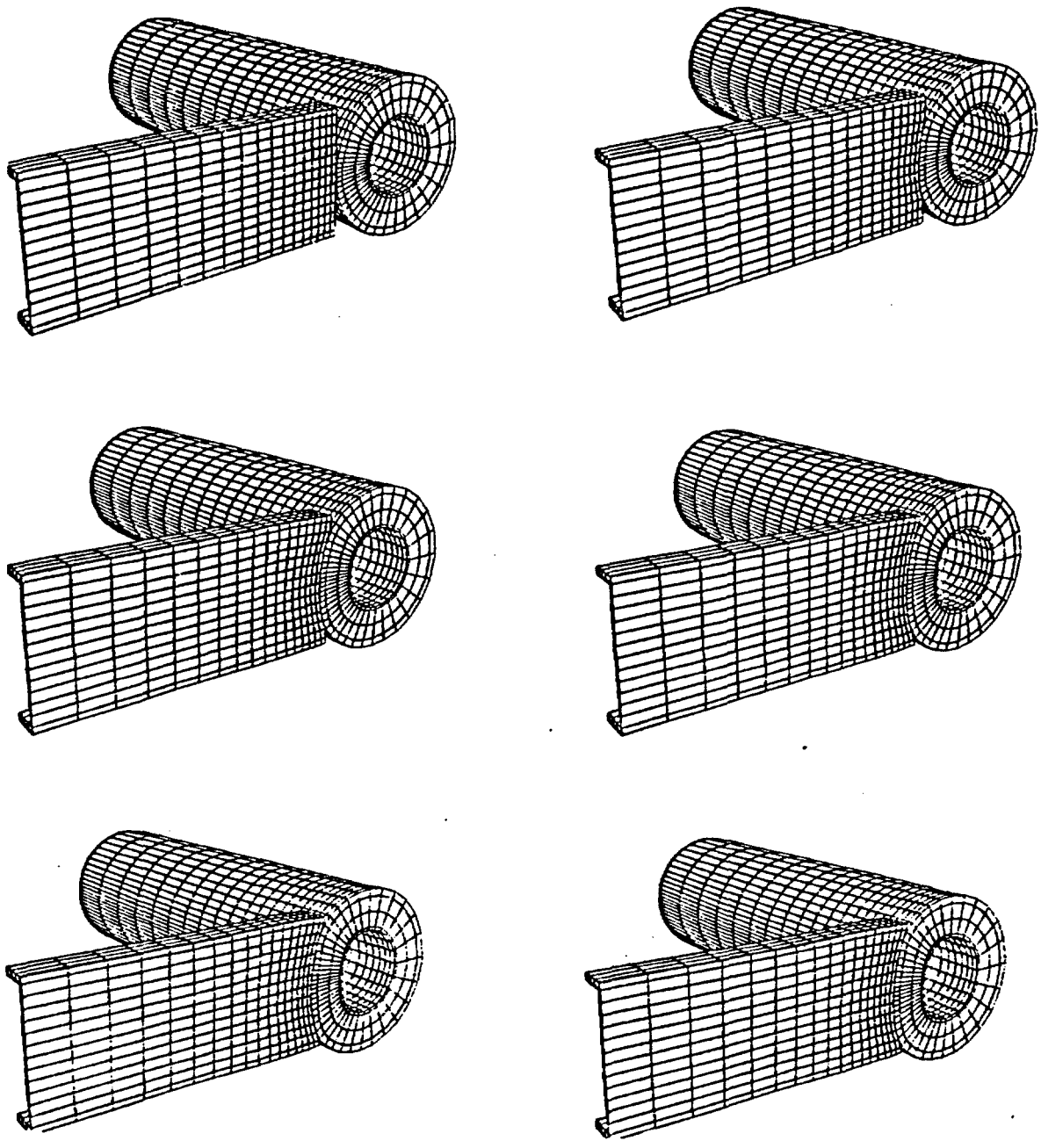

Figure E-4 Deformations of truck cask during 60 mph impact by a 21-inch I-beam.

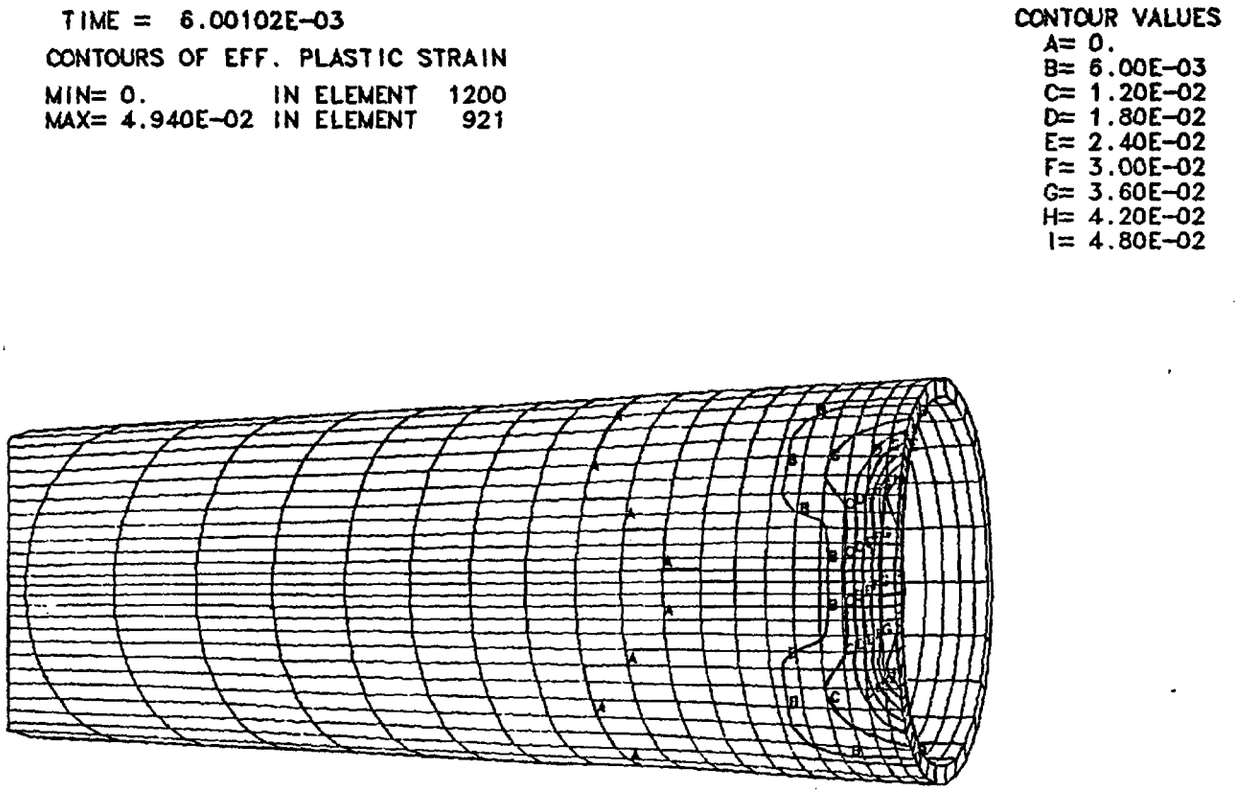

Figure E-5 Distribution of plastic strain in outer shell due to I-beam impact.

stress and shear in the outer wall were 34,950 psi and 19,500 psi, respectively. The I-beam did not penetrate the cask wall.

In comparison with the I-beam impact, the train sill impact discussed in Section 7.4 on the truck cask is more severe. The impact force exceeded 9 million pounds and the strain was 20% for a 60 mph impact. Therefore, it was concluded that the impact by a train sill is a more severe accident that may cause high local strains and stress to the cask walls. Due to the larger size and weight of the rail cask, it was also concluded that the impact of a train sill on the rail cask is more severe than the impact by an I-beam.

The possibility of crush of the representative casks by a heavy object was evaluated. Static force evaluations of the representative casks shown in Fig. E-3 were performed using the NIKE 2-D finite element computer code. As discussed in Section E.3, the loading conditions applied on each of the representative casks are the same as those used for the preliminary cask designs in Table E.5. The force deflection characteristics for each of the representative casks are shown in Figs. E-6 through E-9. The force where general yielding of the cask body occurs was selected for comparing their loading capabilities with the bounding crush loads from NUREG/CR-3498.[E.9]

In Table E.6, typical crush loads that could occur in real accidents are compared with the crush loading capabilities of the representative casks. The bounding crush load is a 200-ton locomotive that would rest on the rail cask by its sill. Both the truck and rail cask can support the weight of the locomotive without yielding.

Based on severe accident data, the frequency of occurrence of impact loads is at least a factor of 10 times higher than for puncture or crush loads. Therefore, since impact can generate higher loads and can occur more frequently, it is concluded that impact loads dominate the potential mechanical loading environment and only impact loads will be considered further.

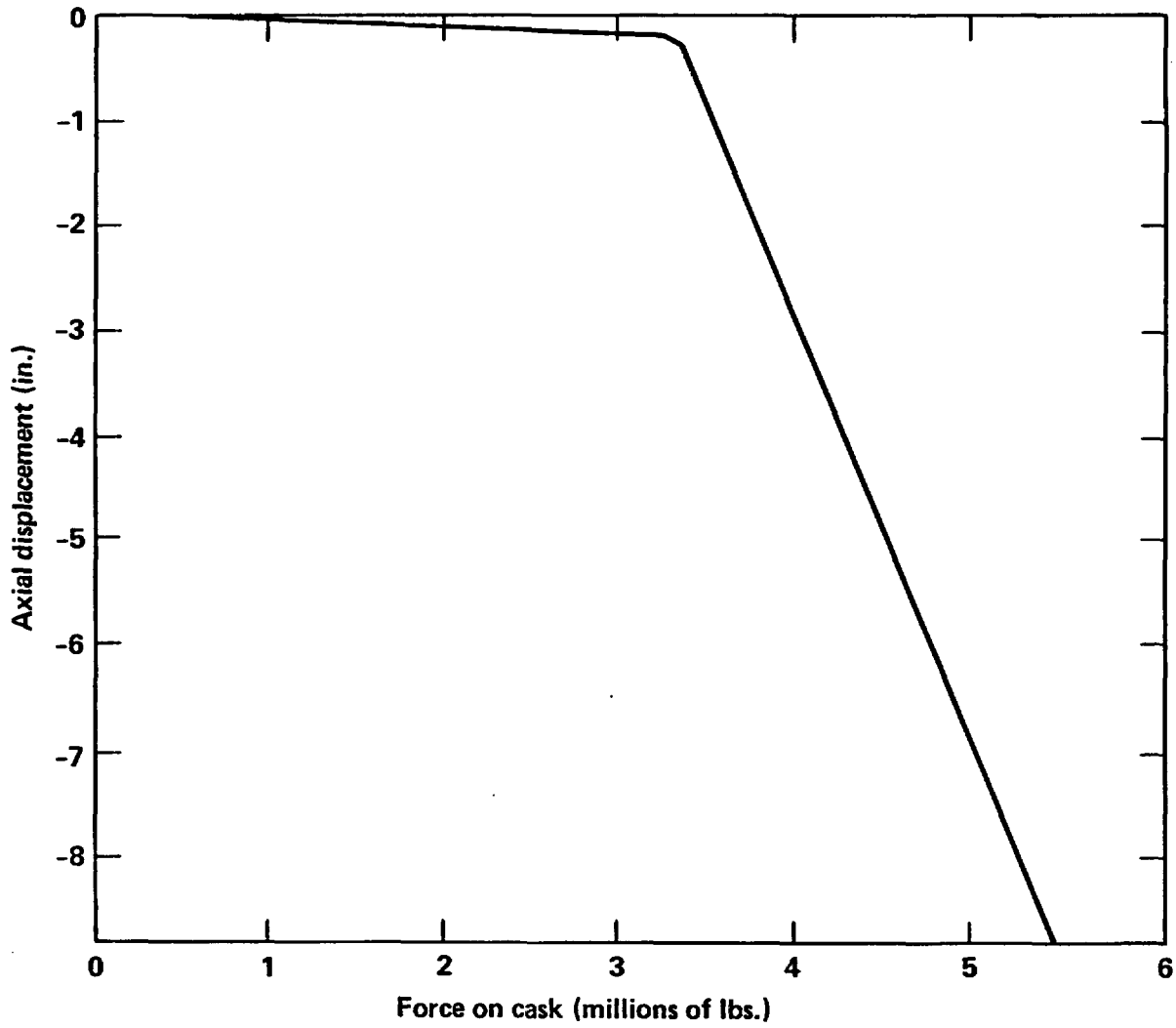

Figure E-6 Static force versus deflection for endwise loading of truck cask.

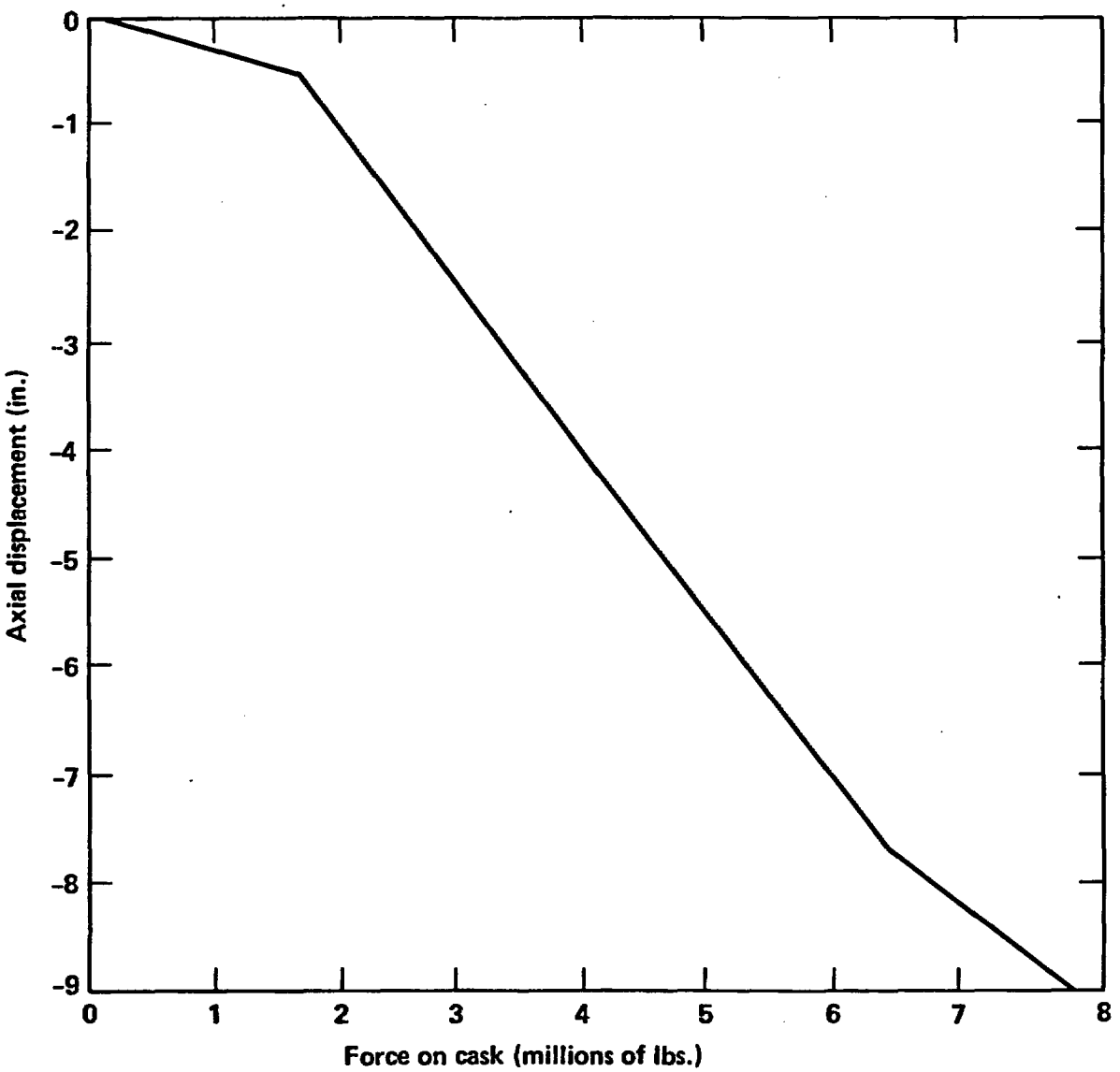

Figure E-7 Static force versus deflection for sidewise loading of truck cask.

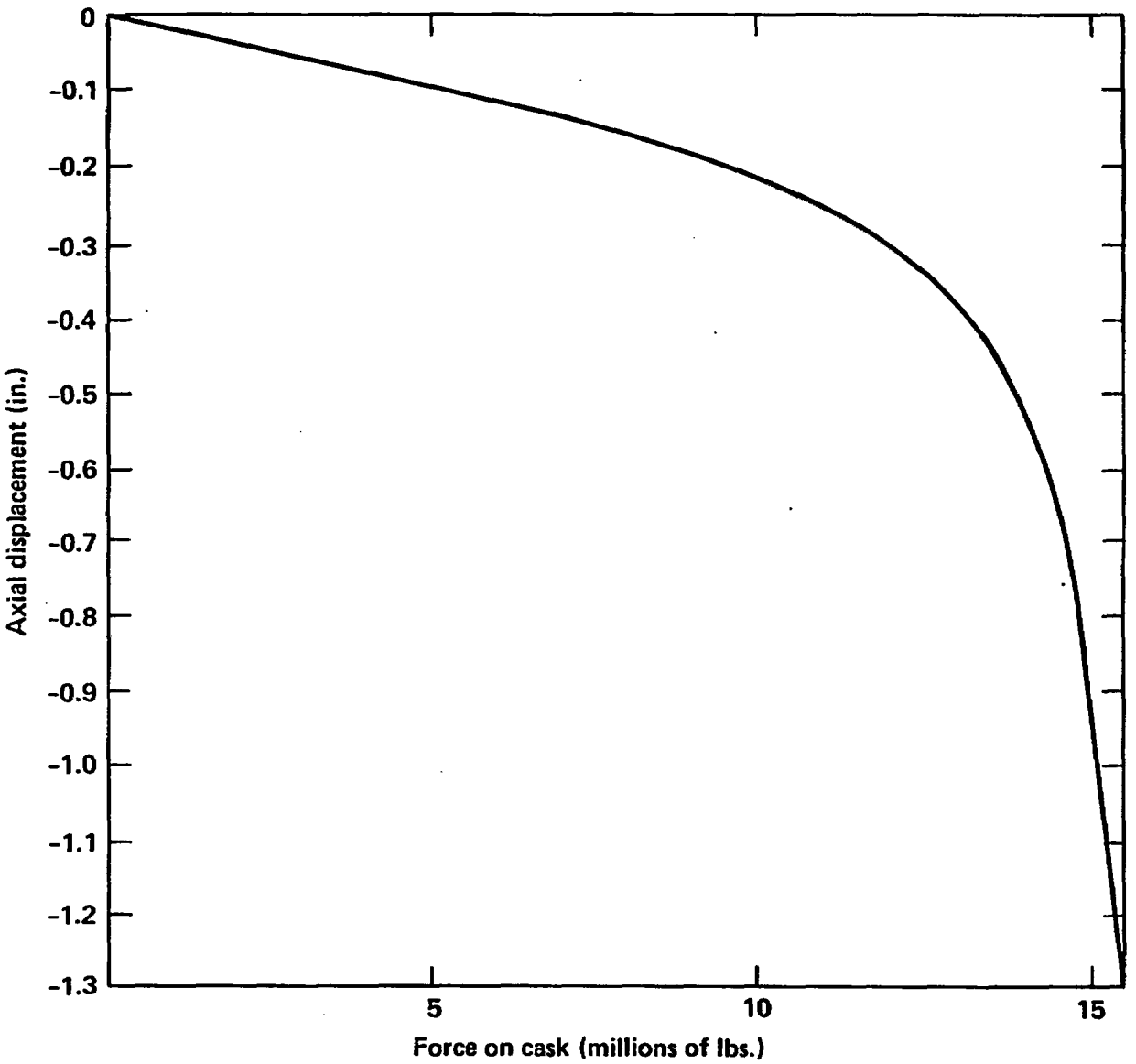

Figure E-8 Static force versus deflection for endwise loading of rail cask.

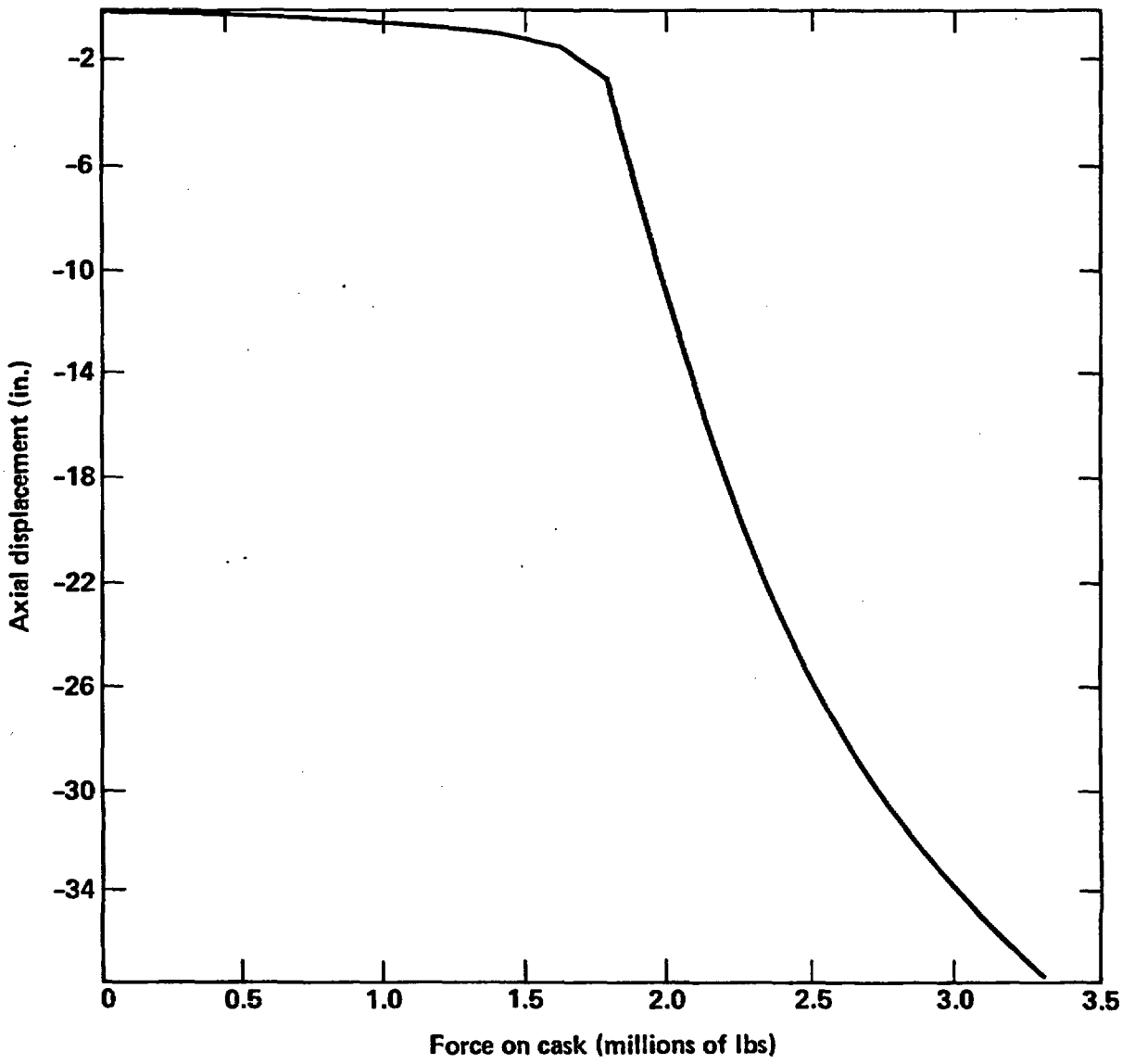

Figure E-9 Static force versus deflection for sidewise loading of rail cask.

Table E.6
Bounding Crush Loads Comparison with Crush Loading Capabilities of the Truck and Rail Casks

Bounding Crush Force Description	Resultant Force (lbs)	Truck Cask Capability (lbs)	Rail Cask Capability (lbs)
For highway accidents the weight of a 60,000 pound truck with its contents. Weight is carried across truck frame width.	60 thousand	1.6 million	1.6 million
For railway accidents the weight of a 200 ton locomotive. Weight is distributed across the train sill.	400 thousand	1.6 million	1.6 million

E.5 Quasi-Static Loads Due to Minor Accidents

In Section E.4, the minimum static force required to yield either the representative truck or rail cask was determined to be 1.6 million pounds. The static force required to yield the impacted object completely is in most cases significantly less than 1.6 million pounds. The static force required to yield either the representative truck or rail cask was compared with the force required to collapse potential objects to screen out low resistance objects from further analysis.

The maximum force that an object can generate during a high velocity impact was estimated using quasi-static methods. D'Alembert's principle was used to establish static force equivalent to the inertial force caused by deceleration. It was concluded that objects such as automobiles or truck trailers cannot generate forces greater than 400,000 pounds even at high velocities.

The static force required to collapse an automobile is less than 50,000 pounds.[E.10] The maximum impact forces for rail cars and truck tractor-trailers are estimated from the static forces reported for the crash tests of spent fuel casks.[E.11,E.12] The quasi-static forces for concrete structures such as walls, columns, and abutments were estimated from the mechanical loading analyses of the roadside structures given in Appendix D.

The method used to determine the maximum impact force trees and posts could resist was a one-dimensional (1-D) beam hand calculation to determine the limit moment. The loading condition we assumed is shown on Fig. E-10a. A plastic hinge forms when the entire tree/pole cross section yields at the location of maximum moment as shown in Fig. E-10b. A yield stress of 8,400 psi is assumed, based on three times the allowable for Douglas fir.[E.13] The bounding force (force to produce plastic hinge) for a solid circular Douglas fir cross section is $P = 233.38R^3$ lbs, where R is the radius of the tree in inches.

The bounding force for a pole, assuming a yield strength of 36 ksi, is

$$P = 1000\, R_o(R_o^2 - R_i^2)\left(\frac{1}{2 - \frac{t}{R_o}} + 1 - \frac{t}{R_o}\right) \qquad \text{(E.4)}$$

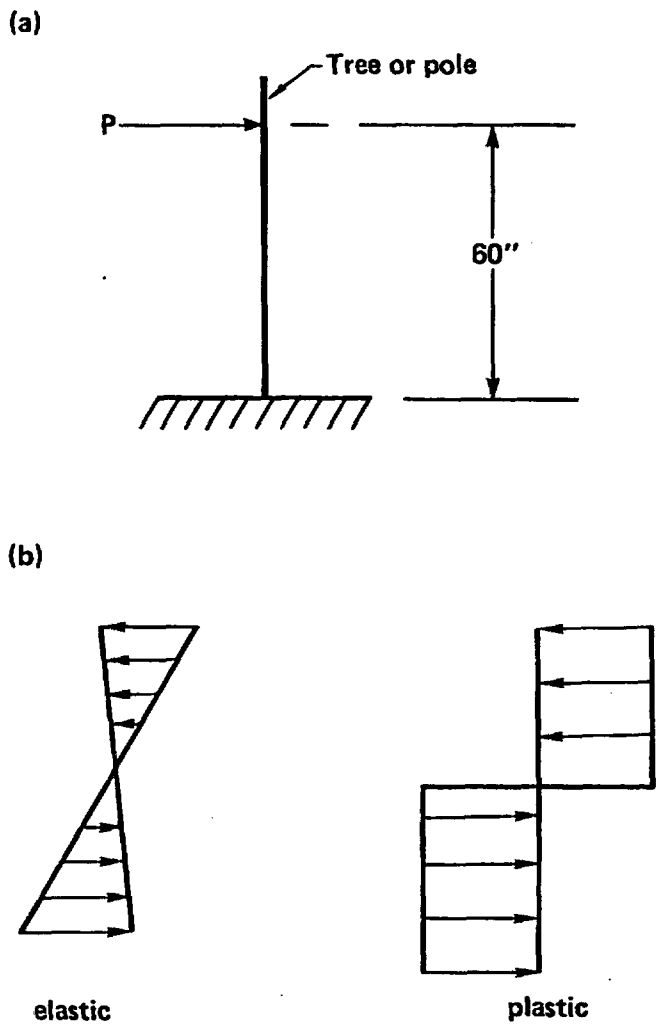

Plastic hinge forms when the entire cross section yields

Figure E-10 Loading conditions on trees and poles.

where

R_o = the pole outside diameter, inches,

R_i = the pole inside diameter, inches,

t = the pole wall thickness, inches.

Two examples of minor target bounding forces follow: a 1.5-foot-diameter Douglas fir tree has a bounding force of 1.7×10^5 lbs, and a 10-inch-diameter standard schedule pole has a bounding force of 2.95×10^4 lbs.

Low-resistance objects such as trees, road signs, electricity poles, motorcycles, passenger cars, trailers, and trucks can be screened out based on static analysis. Assuming that the impact force is linearly applied, the force/unit length that could cause local deformation can be estimated. The representative cask can resist a linear force of 100,000 pounds/foot to generate a strain of less than 0.2% (S_1) at the inner shell. The linear force to crush objects in many accidents is much less than 100,000 pounds/foot. Table E.7 lists objects that are typically impacted in an accident, many of which do not generate a maximum total force greater than 400,000 pounds or a linear force greater than 100,000 pounds/foot.

Stronger and more massive objects, such as trains, bridge columns, abutments, and real surfaces such as roadbeds are analyzed in Section E.7.

E.6 Impacts on Unyielding Surfaces

Impact calculation for the representative casks onto unyielding surfaces were divided into two categories: those where the cask structural response is essentially elastic and those where the cask structural response is elastic-plastic. The elastic response evaluations discussed in Subsection E.6.1 were performed primarily using the 1-D beam element code IMPASC.[E.14] The elastic-plastic response evaluations discussed in Subsection E.6.2 were performed using the DYNA and NIKE family of computer codes.

Table E.7
Quasi-Static Force Evaluation for Objects Potentially Impacted

Object	Total Force (lbs)	Linear Force (lbs/ft)
Truck Cask		
Endwise	3,300,000	
Sidewise	1,600,000	100,000
Rail Cask		
Endwise	13,000,000	
Sidewise	1,600,000	100,000
Auto	50,000	<10,000
Truck Tractor	100,000	<17,000
Truck Trailer	450,000	<70,000
Train	2,000,000	>250,000
Motorcycle	20,000	<10,000
Bus	300,000	<50,000
Sound Wall	50,000	<50,000
4 x 4 Column	900,000	>225,000

E.6.1 Elastic Response of the Cask

In order to perform the response calculation, it is essential that a proper computer code be selected. This computer code(s) must have the following special capacities or features:

1. Can provide dynamic impact analysis

2. Can analyze oblique impact

3. Can analyze impact limiter nonlinear behavior

4. Can analyze lead slump effect

5. Can be run inexpensively.

Three computer codes were selected, NIKE 2-D/3-D,[E.1] DYNA 2-D/3-D,[E.2] and IMPASC.[E.13] Each code has its special features, but also has weaknesses in meeting all the requirements. NIKE 2-D/3-D and DYNA 2-D/3-D are two of the most powerful finite element codes for dynamic impact analysis. They meet all the requirements listed above except that they are expensive to run. Especially when dealing with oblique impact and nonlinear impact limiters, the required 3-D modeling can result in costly calculations.

In order to manage the large amount of analysis required for this study, a code had to be found that could do analysis less expensively. The IMPASC code was selected. IMPASC was developed specifically for dynamic impact analysis of shipping casks to assess whether they meet the 10 CFR 71 design requirements. It has a special feature for handling oblique impact. This code can also analyze nonlinear behavior of the impact limiter, and is inexpensive to run. The deficiency is that IMPASC cannot assess the lead-slump effect.

The approach benchmarked the IMPASC results with DYNA/NIKE results to assess the lead slump, and then used the IMPASC code to run production calculations for impacts on an unyielding surface. From the sensitivity study

performed with the DYNA/NIKE codes in Subsection E.6.1.3, it was found that lead slump will not occur under any conditions as long as the axial force on the cask is smaller than 40 g. This is also the level at which it could be assured that the strain on the inner shell is less than 0.2% (S_1) and the closure seal is functional, since the impact limiter is designed to completely absorb the energy of this impact force level.

Sensitivity studies were performed to show that the inclusion of the cask contents does not significantly change the strain levels in the cask. The sensitivity studies included the following: lumping the weight of the contents at the bottom end of the cask, modeling the contents as elements with mass but no stiffness in the cask cavity, and modeling the contents with mass and an estimated stiffness to simulate fuel bundles and the fuel basket. Liquids such as water are not contained in the cask, because helium is the coolant. The resulting changes in stress-strains and g loads for the various models were not significant for the purposes of this study.

E.6.1.1 Truck Cask Impact

The IMPASC code was used to perform impact analysis on an unyielding surface for the truck cask. The analysis was done by varying the other two parameters: cask orientation angle and impact velocity. The cask response was calculated for the cask orientation angles of 0^o, 10^o, 30^o, 50^o, 70^o, and 90^o and impact velocities of 30 mph, 38 mph, and 45 mph. The impact velocity is defined as the velocity component in the direction perpendicular to the impact surface. The 0^o cask orientation angle represents impact to the side of the cask, whereas the 90^o cask orientation angle represents impact to the end of the cask.

For the 90^o angle case, the effects due to the truck cab crushing and lead slump pressure were included. The effects of lead pressure were calculated using NIKE and are discussed in Subsection E.6.1.3. The effects of the cab crush for front-wise impacts, which can be taken into account by increasing the impact velocity required to give equivalent strain, was estimated using an energy balance. The energy absorbed by the cab is estimated as

$$E_a = F_I \times d \tag{E.5}$$

where F_I is the impact or crush force of the truck cab in inches and d is the total distance the cab can be crushed in inches.[E.11] The kinetic energy required to cause the same response for the cask when the cab crush is included is estimated as

$$\left(\tfrac{1}{2} MV_2^2\right)_C = E_a + \left(\tfrac{1}{2} MV_1^2\right)_{WC} \tag{E.6}$$

where M is the mass of the truck and cask in lbs; V_2 is the impact velocity in ft/sec used to find the strain, taking into account cab crush energy absorption; and V_1 is the impact velocity in ft/sec without cab crush energy absorption as used in IMPASC code calculations. The mass of the truck was taken from SAND77-0270.[E.11] The velocity required to cause the same cask response when cab crush is considered is

$$V_2^2 = \frac{2E_a + MV_1^2}{M} \quad . \tag{E.7}$$

The effects of cab crush are included only for impact velocities up to 60 mph; at higher velocities the cask will break from its tie-downs and leave the truck without any velocity reduction caused by truck cab crush.[E.11] Table E.8 summarizes the velocities required to cause the same cask response when cab crush is included as compared to the velocities without cab crush. The effective impact velocity to take into account cab crush, V_2, is used to determine the strain for a given impact velocity as calculated by the IMPASC code. For instance, the strain at 30 mph as calculated by IMPASC for a truck cask is assumed to occur at 34.6 mph when cab crush is taken into account.

Table E.8
Impact Velocities Required to Include Cab and
Rail Car Crush Energy Absorption

Velocity without Crush (mph)	Velocity with Cab Crush (mph)	Velocity with Rail Car Crush (mph)
30	34.6	35
45	48.2	48.5
60	62.4	62.8

The strain variation with cask orientation angle for various impact velocities are given in Table E.9. From these results it was concluded that for the representative truck cask the endwise and sidewise strain responses bound the strain responses for all cask orientations. For cask orientations from $0\text{-}90^{0}$ the structural strain responses can be linearly interpolated between the sidewise and endwise strain responses. The strain is 0.2% (S_1) at the impact velocity of 32 mph for sidewise impacts and 38 mph for endwise impacts.

E.6.1.2 Rail Cask Impact

The IMPASC code was used to perform these analyses. The analysis was done by varying the other two parameters, i.e., cask orientation angle and impact velocity. The cask response was calculated for the cask orientation angles of 0^{0}, 10^{0}, 30^{0}, 50^{0}, 70^{0}, and 90^{0} and impact velocities of 30 mph, 45 mph, and 60 mph. The impact velocity is defined as the velocity component in the direction perpendicular to the object surface. The 0^{0} cask orientation angle represents the impact to the side of the cask, whereas the 90^{0} cask orientation angle is the impact to the end of the cask. The results of this sensitivity study are given in Table E.10. As done for the truck cask, for the 90^{0} angle case we included the effects of lead slump pressure and crushing the front end of the rail car transporting the cask. Table E.8 summarizes the velocities required to include the rail car crush effects. From the results it is concluded that for the representative rail cask, the endwise and sidewise strain responses bound the strain responses for all cask orientations. For cask orientations from $0\text{-}90^{0}$, the structural strain responses can be linearly interpolated between the sidewise and endwise strain responses. The strain at the inner wall is 0.2% (S_1) at the impact velocity of 55 mph for sidewise impacts and 38 mph for endwise impacts.

E.6.1.3 IMPASC and NIKE Comparison

The IMPASC code was benchmarked for endwise impacts at 30 mph on an unyielding surface against the NIKE computer code. Table E.11 summarizes the pertinent results for the representative truck and rail casks. For the truck

Table E.9
Truck Cask Strain Response to Impact on Unyielding Surface at Various Cask Orientations

Cask Orientation Angle (°)	Strain (%) Impact Velocity (mph) 30	38	45
0	0.175	0.270	0.650
10	0.133	0.210	0.260
30	0.115	0.180	0.255
50	0.107	0.180	0.244
70	0.064	0.081	0.115
90[a/]	0.060	0.200	2.00

[a/] Includes effects of cab crush and lead slump for 90° impact

Table E.10
Rail Cask Strain Response to Impact on Unyielding Surface at Various Cask Orientations

Cask Orientation Angle (°)	Strain (%) Impact Velocity (mph) 30	45	60
0	0.046	0.135	0.235
10	0.027	0.057	0.091
30	0.027	0.059	0.096
50	0.026	0.059	0.088
70	0.015	0.031	0.060
90[a/]	0.05	1.00	7.00

[a/] Includes effects of cab crush and lead slump for 90° impact

Table E.11
IMPASC Endwise Impact Benchmark Calculation
Against NIKE 2-D

	Truck at 30 mph		Rail at 30 mph		
	NIKE 2-D	IMPASC	Bonded Elastic NIKE 2-D	Unbonded Elastic-Plastic NIKE 2-D	IMPASC
Force (g)	37.5	45.0	36	36	28.6
σ axial (psi)	-9543.	-12200	-6732	-12035	-7100
Maximum deflection of limiter (inches)	25.8	26.5	25.3	25.8	26.5
Maximum plastic strain or effective strain if elastic (°)	0.00077	N/A	0.00038	0.0012	N/A

cask calculations, the material properties of Section E.2 and cask configuration of Fig. E-15 were used. In the NIKE calculation the lead was assumed to be unbonded from the stainless steel shells, whereas in the IMPASC calculation the lead was assumed to be bonded. The calculated impact force was approximately 38 g at 30 mph and the impact limiter deflection was approximately 26 inches in both calculations. Rail cask calculations were made with NIKE for bonded and unbonded lead. The results for the bonded lead are in good agreement with the IMPASC results which are also based on the assumption of bonded lead. The effect of assuming the lead unbonded is primarily an increase of the stress and strain on the inner shell of the cask caused by the lead pressure. From this benchmark comparison it was concluded that significant lead slump would not occur and the plastic strain is less than 0.2% (S_1) when the axial impact force on the cask is less than 40 g.

E.6.2 Elastic-Plastic Response by Cask

Elastic-plastic calculations were necessary when cask impact forces exceeded 40 g. Several of the capabilities of the DYNA and NIKE finite element codes that are critical to such calculations are (1) elastic-plastic material models, (2) sliding interfaces, (3) dynamic solutions, and (4) the ability to solve large deformation problems. The cask models include a 304 stainless steel inner wall, lead shielding and a 304 stainless steel outer wall. Each of the materials was modeled as a bilinear elastic-plastic material. The material properties used are summarized in Section E.2. The calculations were performed for endwise and sidewise impacts. The cask responses to impacts at other cask orientations are assumed to be bounded by the endwise and sidewise response results.

E.6.2.1 Endwise Impacts

Endwise impact calculations were performed for the representative truck and rail casks striking an unyielding surface. The casks were dropped from several heights onto an unyielding surface to obtain their responses over a range of impact conditions. The casks were modeled as 2-D axisymmetric composite cylinders with closures as shown in Fig. E-5. MAZE was used to

generate the finite element meshes. DYNA 2-D/NIKE 2-D were used to perform the impact calculations.[E.15]

E.6.2.1.1 Truck Cask Impact

The truck cask was modeled using two elements for the inner shell as shown in Fig. E-11. The results of the endwise impact calculations are summarized in Table E.12. The sudden deceleration of impact caused the lead shielding to slump and the cask length to decrease as shown in Fig. E-12 for the 60 mph impact. The maximum strain conditions occur at the inner wall at the flange joint as shown in Fig. E-13 for the 60 mph impact. The velocity changes with time, or decelerations, of the steel structure and the lead shielding were significantly different as shown in Fig. E-14 for the 60 mph impact. All impact calculations were terminated after rebound occurred. The lead slump is determined by finding the void between the cask steel body and lead shield. For example, consider a truck cask impacting at 60 mph. The time for the lead and the steel to reach zero velocity is extrapolated from Fig. E-14 as 19 msecs. Then the curves on Fig. E-12 are extrapolated to 19 msecs. This gives 16.5 inches of axial displacement at the top of the lead, and 4.2 inches in the steel at the top of the lead cavity. The relative displacement is the lead slump, and is (16.5 - 4.2) 12.3 inches.

An average interface deceleration force was calculated for the cask at each impact velocity by averaging the interface force over the time it took the steel structure to come essentially to a stop as shown in Fig. E-14. For example, consider the truck cask impacting at 60 mph. The time for the total steel mass to come nearly to a stop is 6 msecs as determined from Fig. E-14. The steel interface force acting for the first 6 msec of impact ranges from a high of 373 g to a low of 143 g, therefore the average interface force is the sum of the forces divided by 2 or 258 g. The average interface deceleration force was used to estimate the cask response to impacts on real surfaces as discussed in Section E.7.

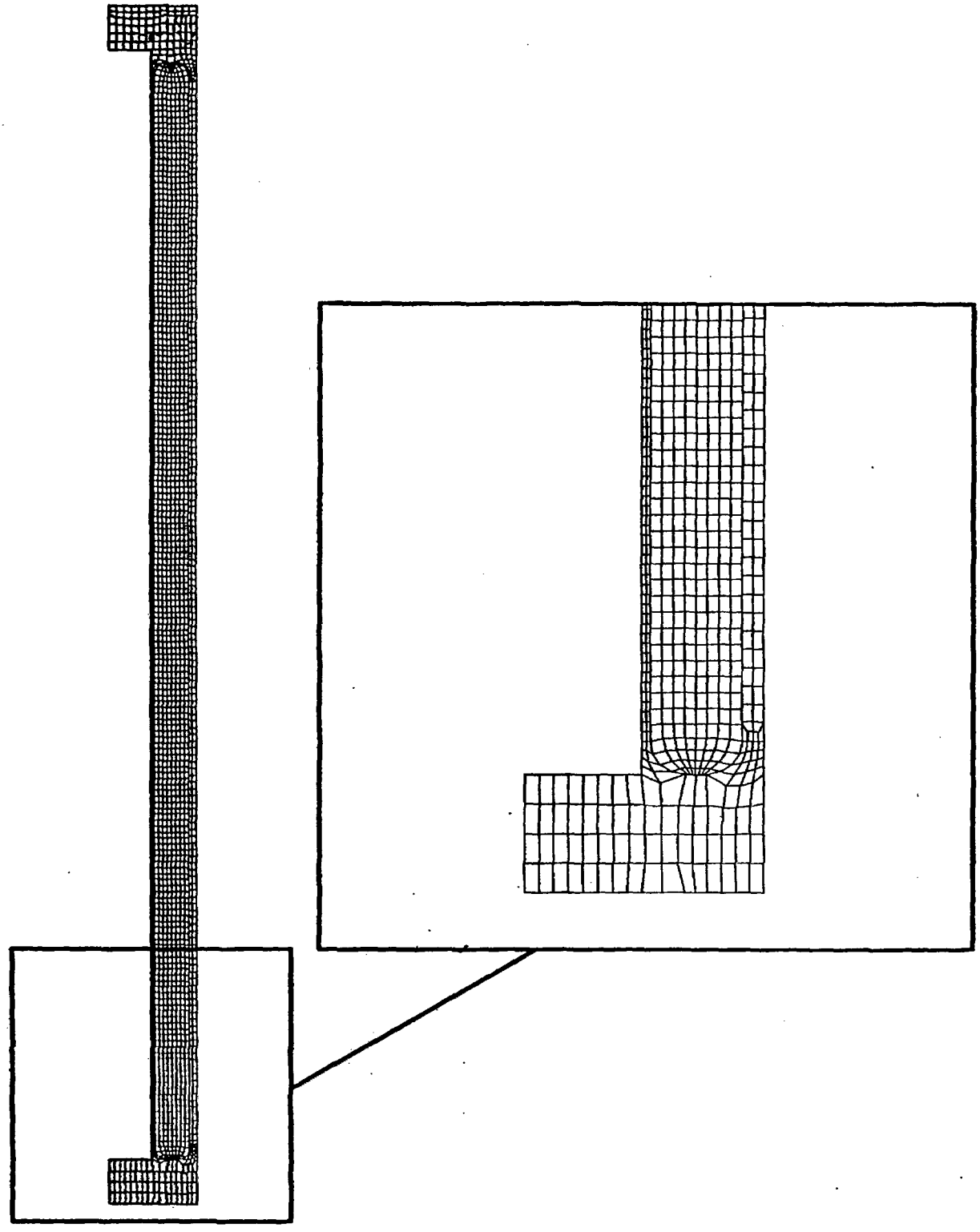

Figure E-11 Finite element mesh for two-element inner-wall model by truck cask.

Table E.12
Summary of Truck Cask Endwise Impact Results[a/]

Velocity (mph)	Interface Deceleration Force (g)	Strain Inner Shell (%)	Lead Slump (in)
30	38	0.077	0
45	90	3.60	4
60[b/]	258	23.3	12.3
90[b/]	353	36.2	24

[a/] Cab crush not included in analysis.

[b/] Impact limiter not included in analysis.

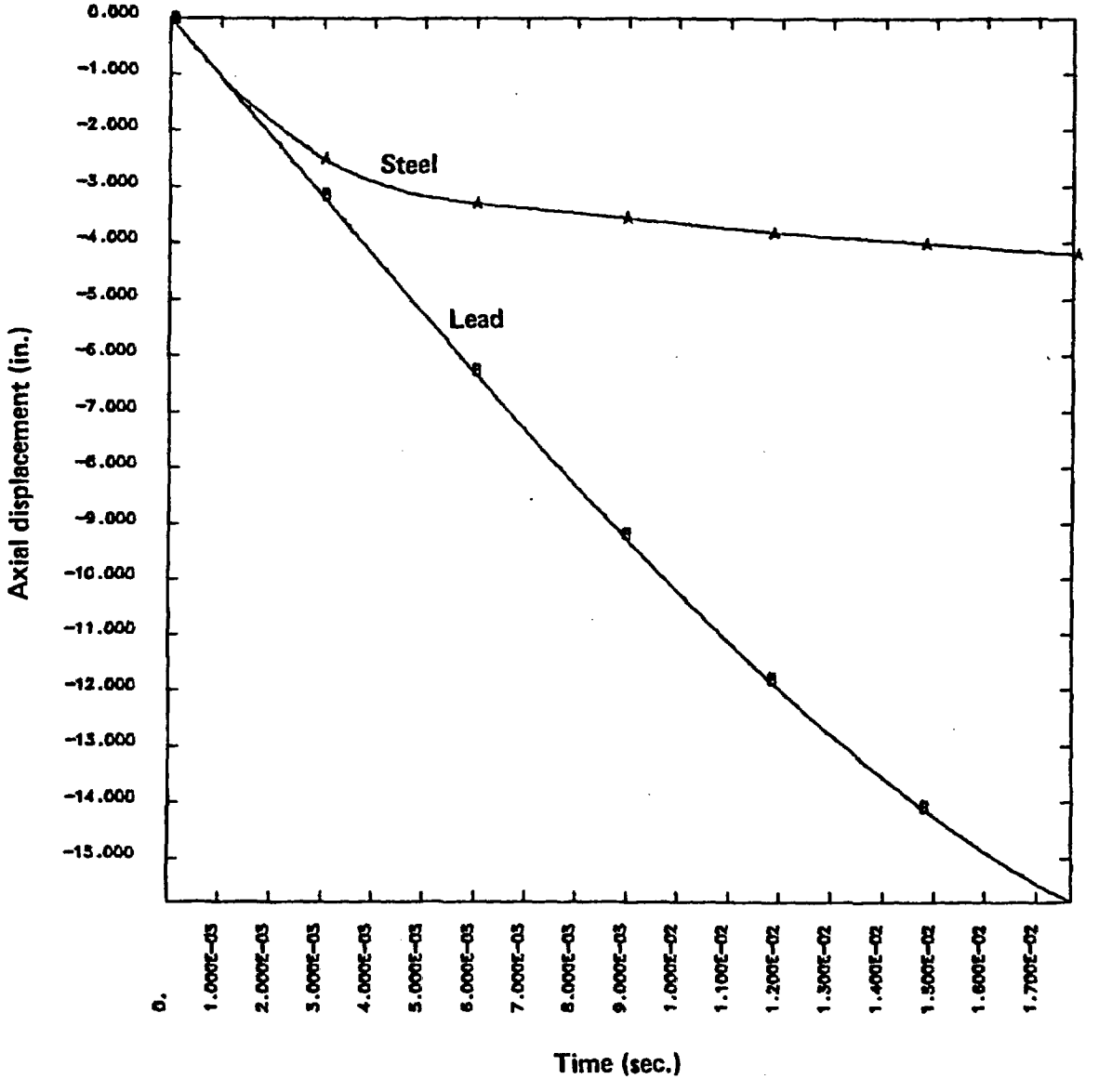

Figure E-12 Lead slump in truck cask at 60 mph impact.

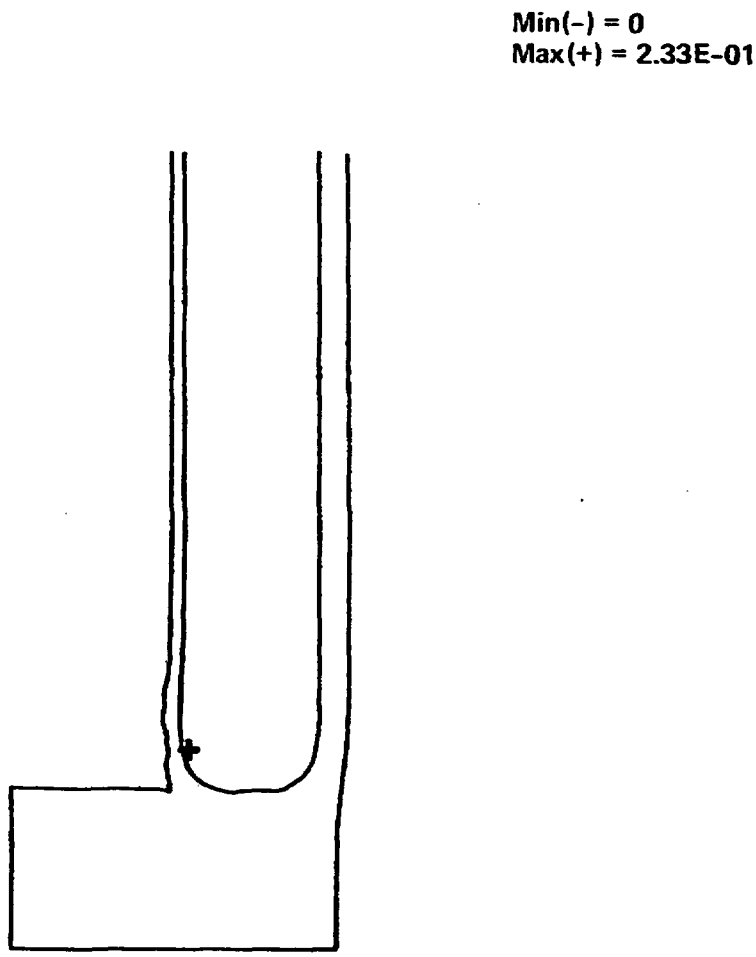

Figure E-13 Strain in lower steel structure for truck cask impact at 60 mph.

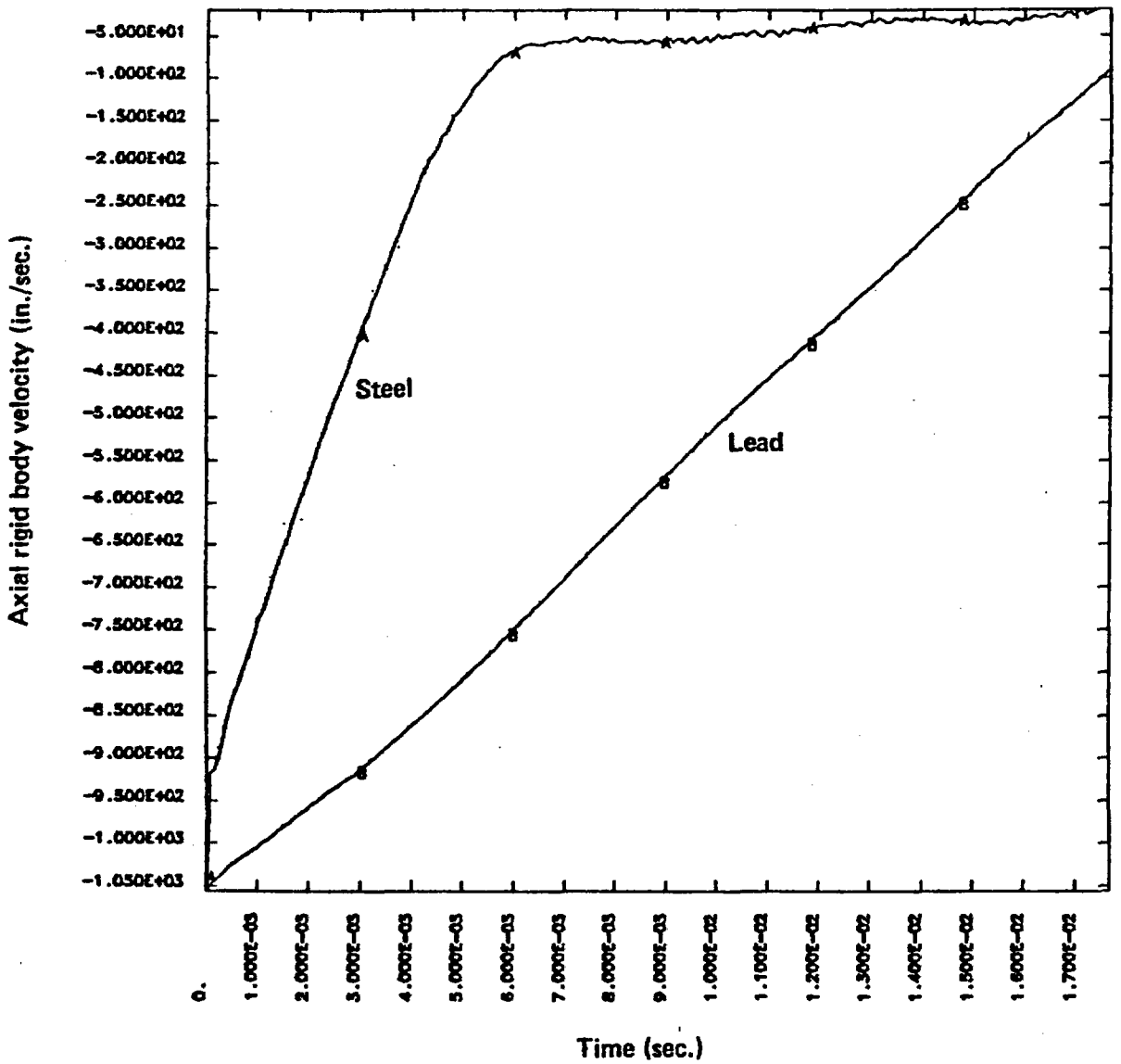

Figure E-14 Velocity versus time for truck cask impact at 60 mph.

E.6.2.1.2 Rail Cask Impact

The rail cask was modeled using two elements for the inner shell as shown in Fig. E-15. The results of the endwise impact calculations are summarized in Table E.13. The lead slump that occurred in the rail cask is shown in Fig. E-16 for the 90 mph impact. The strain condition in the steel structure at the end of impact is shown Fig. E-17 for the 90 mph impact. The velocity change for the steel structure and lead shielding is shown in Fig. E-18. The average interface deceleration force was calculated from Fig. E-18 for the 90 mph impact with the method discussed in Subsection E.6.2.1.1 for the truck cask.

E.6.2.2 Sidewise Impacts

Two-dimensional plane strain analyses without impact limiters or end enclosures were performed for sidewise impacts on an unyielding surface to estimate the 3-D responses for the casks. This approximate 2-D method overestimates strain responses of the representative casks, particularly for impact velocities less than 60 mph and for impacts on soft surfaces such as soil. The 2-D method was benchmarked in Subsection E.6.2.2.3 with a 3-D impact analysis that modeled the representative truck cask with impact limiters and end closures. This approximate method eliminates the need to perform a series of 3-D sidewise impact analyses.

The 2-D truck cask models were developed using the SLIC interactive mesh generator.[E.16] The dimensions in the SLIC command file were modified to generate the rail cask models. The cask models do not include contents. DYNA 2-D (2), an explicit 2-D hydrodynamic finite element program, was used to do the plane strain analysis.

E.6.2.2.1 Truck Cask Impact

For unyielding surface impacts, a vertical symmetry plane was used in the modeling as shown in Fig. E-19 to reduce the solution cost. The calculations were performed for three different truck cask initial velocities: 30 mph, 60 mph, and 90 mph. The calculations were terminated when the cask started to

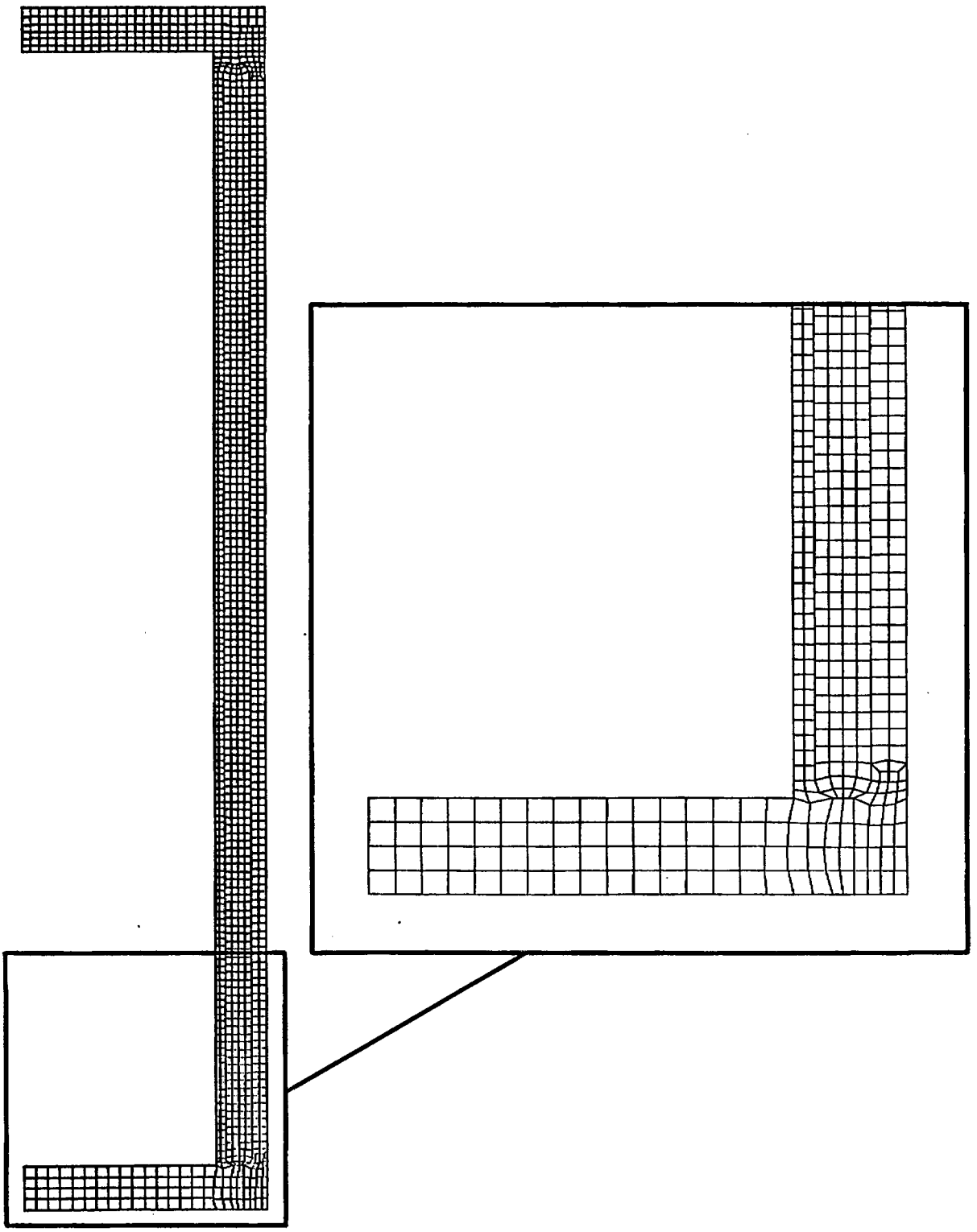

Figure E-15 Finite element mesh for rail cask.

Table E.13
Summary of Rail Cask Endwise Impact Results[a/]

Velocity (mph)	Interface Deceleration Force (g)	Strain Inner Wall (%)	Lead Slump (in)
30	36	0.12	0.5
45	103	1.9	6.0
90[b/]	425	24.3	24.8

[a/] Cab crush not included in analysis.

[b/] Impact limiter not included in analysis.

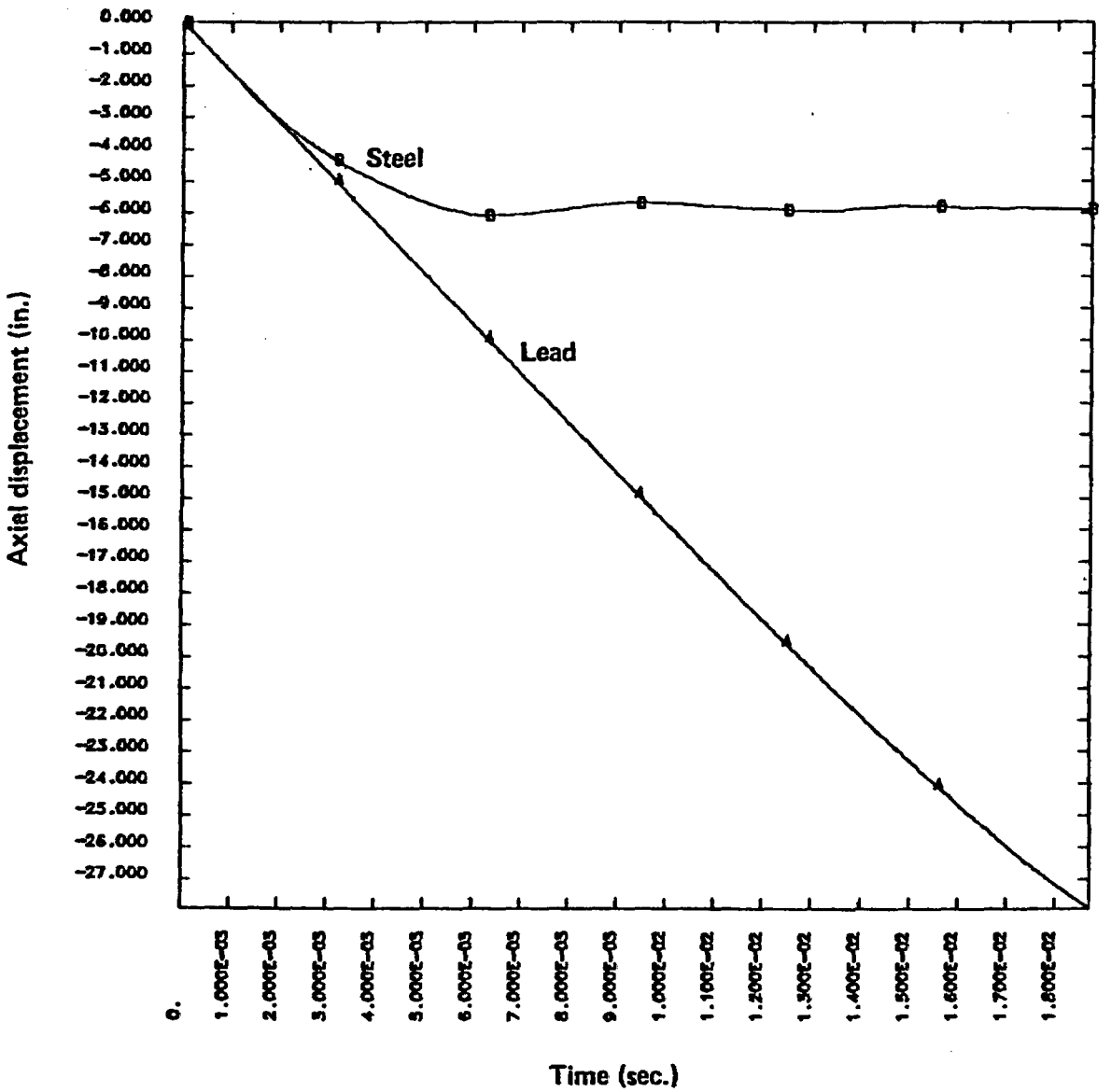

Figure E-16 Lead slump in rail cask at 90 mph impact.

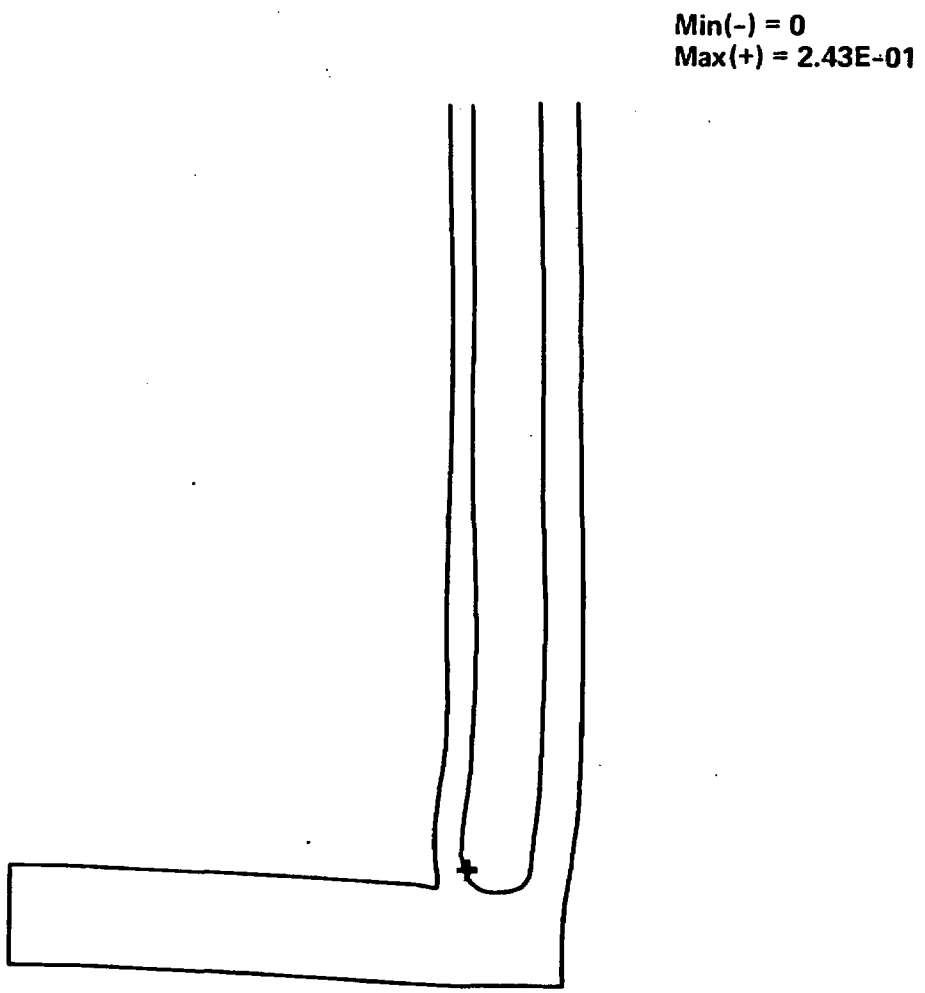

Figure E-17 Strain in lower steel structure for rail cask impact at 90 mph.

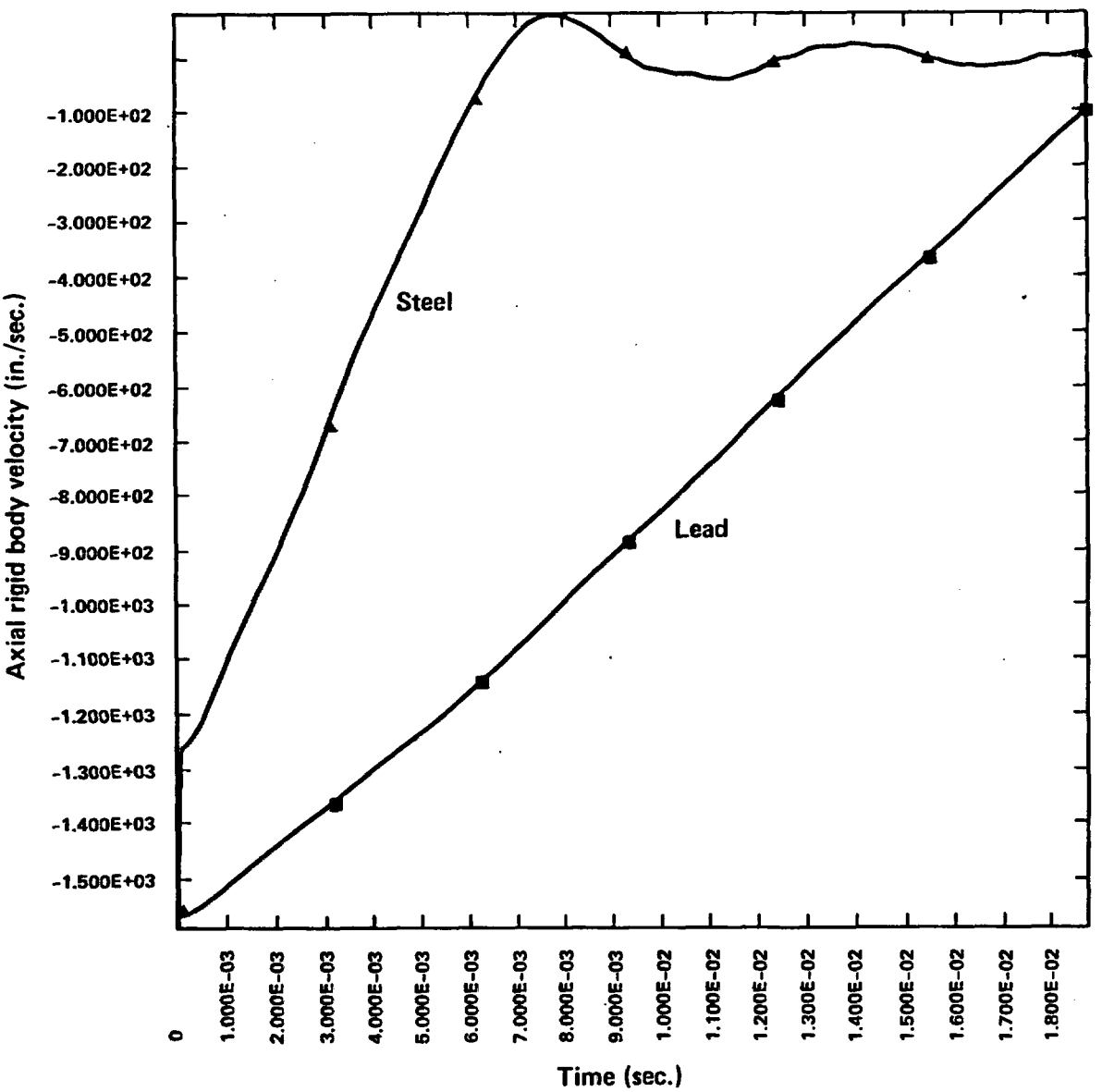

Figure E-18 Velocity versus time for rail cask impact at 90 mph.

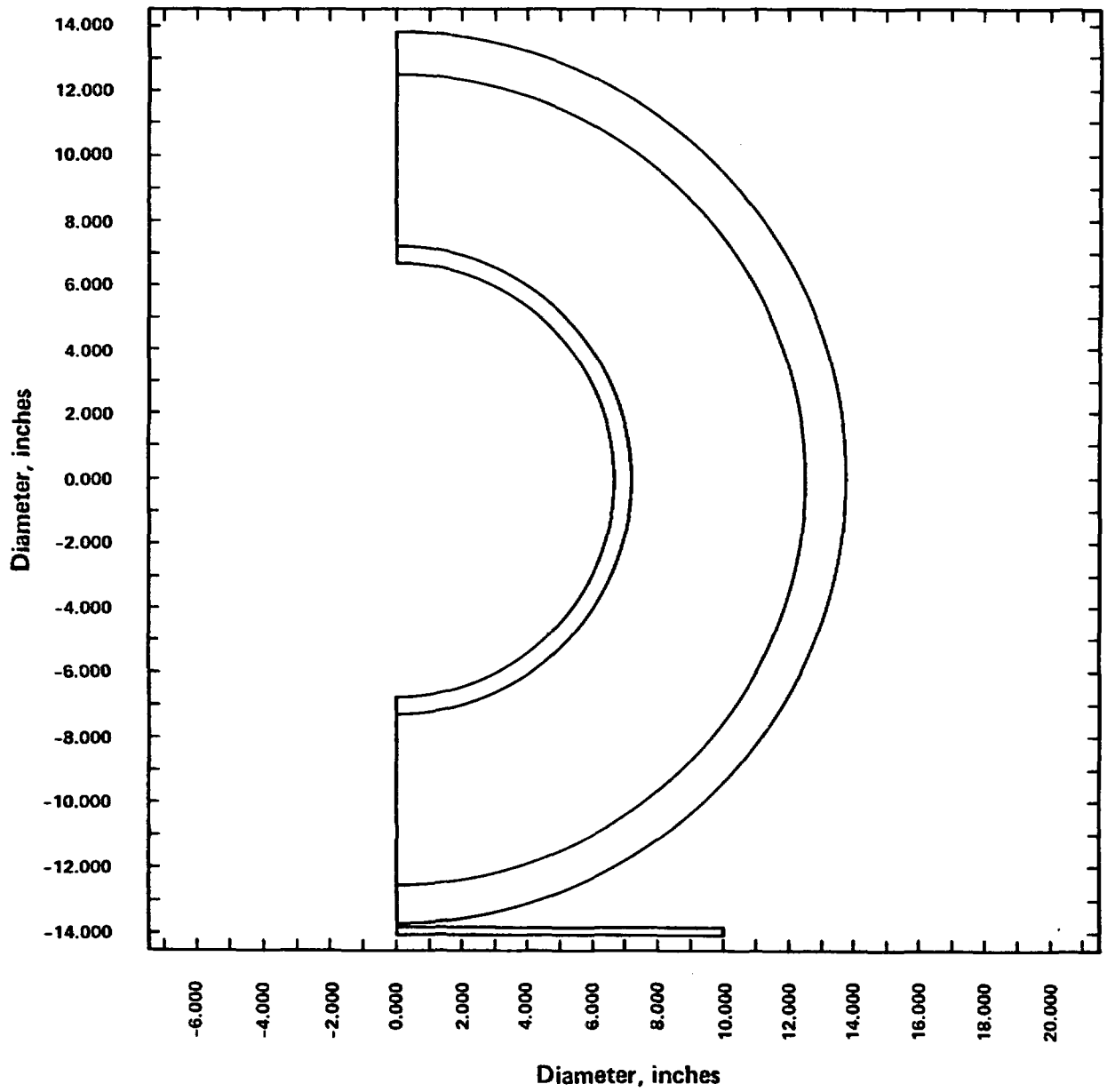

Figure E-19 Model of a truck cask impacting an unyielding surface.

rebound. The sudden deceleration caused the cask to flatten as shown in Fig. E-20.

For the 30 mph impact, the cask experienced 160 g's and sustained a maximum effective stress of 36,000 psi and maximum plastic strain of 5.9% in the steel shells. For 60 mph, the g's increased to 342, the maximum effective stress increased to 45,300 psi and the maximum plastic strain increased to 14%. These results are summarized in Table E.14. The location of the maximum plastic strain is shown in Fig. E-21 for the 60 mph impact.

E.6.2.2.2 Rail Cask Impact

Calculations were performed for the rail cask with initial velocities of 30 mph and 60 mph. The 30 mph calculation was terminated when the cask started to rebound. The 60 mph calculation was terminated when the cask started to fold on itself. The sudden deceleration caused the cask to flatten considerably and, in the 60 mph case, to develop a plastic hinge as shown in Fig. E-22. The cask contents would to some degree resist the formation of the plastic hinge. However, the cask contents were not modeled.

For the 30 mph impact, the cask experienced a force of 29 g's and sustained a maximum effective stress of 32,400 psi and maximum plastic strain of 4.1% in the steel shells. For 60 mph, the g's increased to 47, the maximum effective stress increased to 37,400 psi and the maximum plastic strain increased to 7.2%. These results are summarized in Table E.15. The location of the maximum plastic strain is shown in Fig. E-23 for the 60 mph impact.

E.6.2.2.3 Three-Dimensional Sidewise Impact

A 3-D truck shipping cask was modeled for the side-drop analysis with impact limiters. As shown in Fig. E-24, the model includes the inner and outer steel shells, the lead shielding, the steel end caps, and the balsa wood impact limiters. The finite element model was generated using SLIC, an interactive mesh generator. The impact limiters were not tied to the cask, conservatively allowing them to slide relative to the cask because any bolt retaining forces that could be present are unknown. Two planes of symmetry

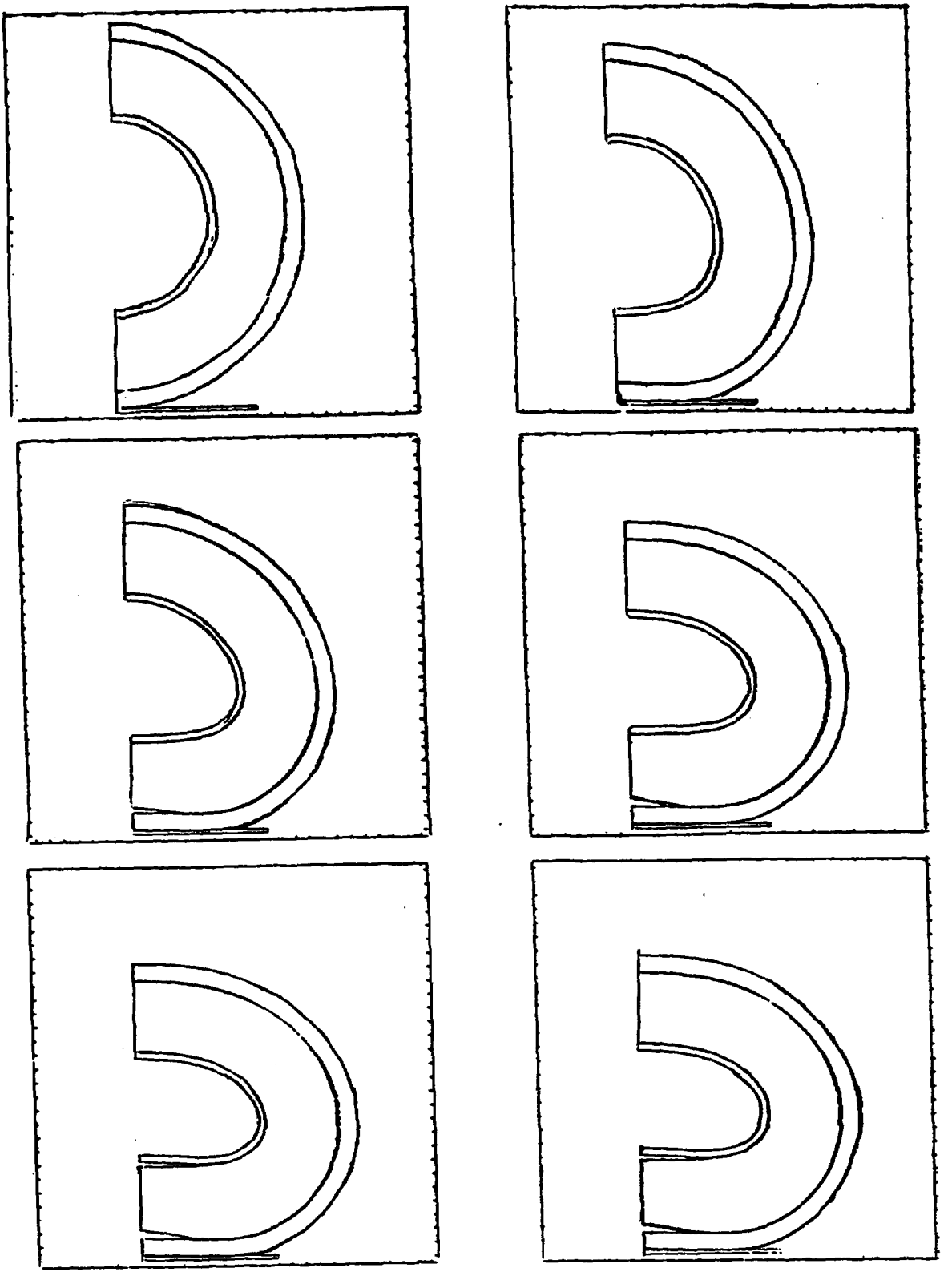

Figure E-20 Truck cask impact on unyielding surface at 60 mph.

Table E.14
Results of Truck Cask Sidewise Impact on an Unyielding Surface

Cask impact velocity (mph)	30	60	90
Time at which rebound starts (sec)	0.0085	0.008	0.0075
g load on cask (g)	160	342	547
Maximum effective stress (psi)	36,000	45,300	63,100
Maximum plastic strain (%)	5.9	14.	23.1

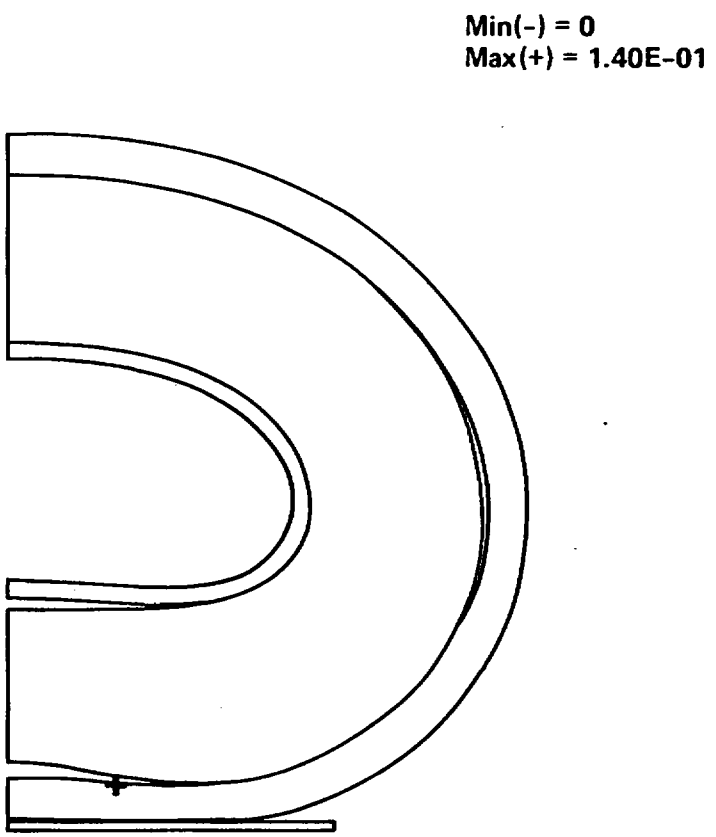

Figure E-21 Impact on unyielding surface at 60 mph - maximum plastic strain location.

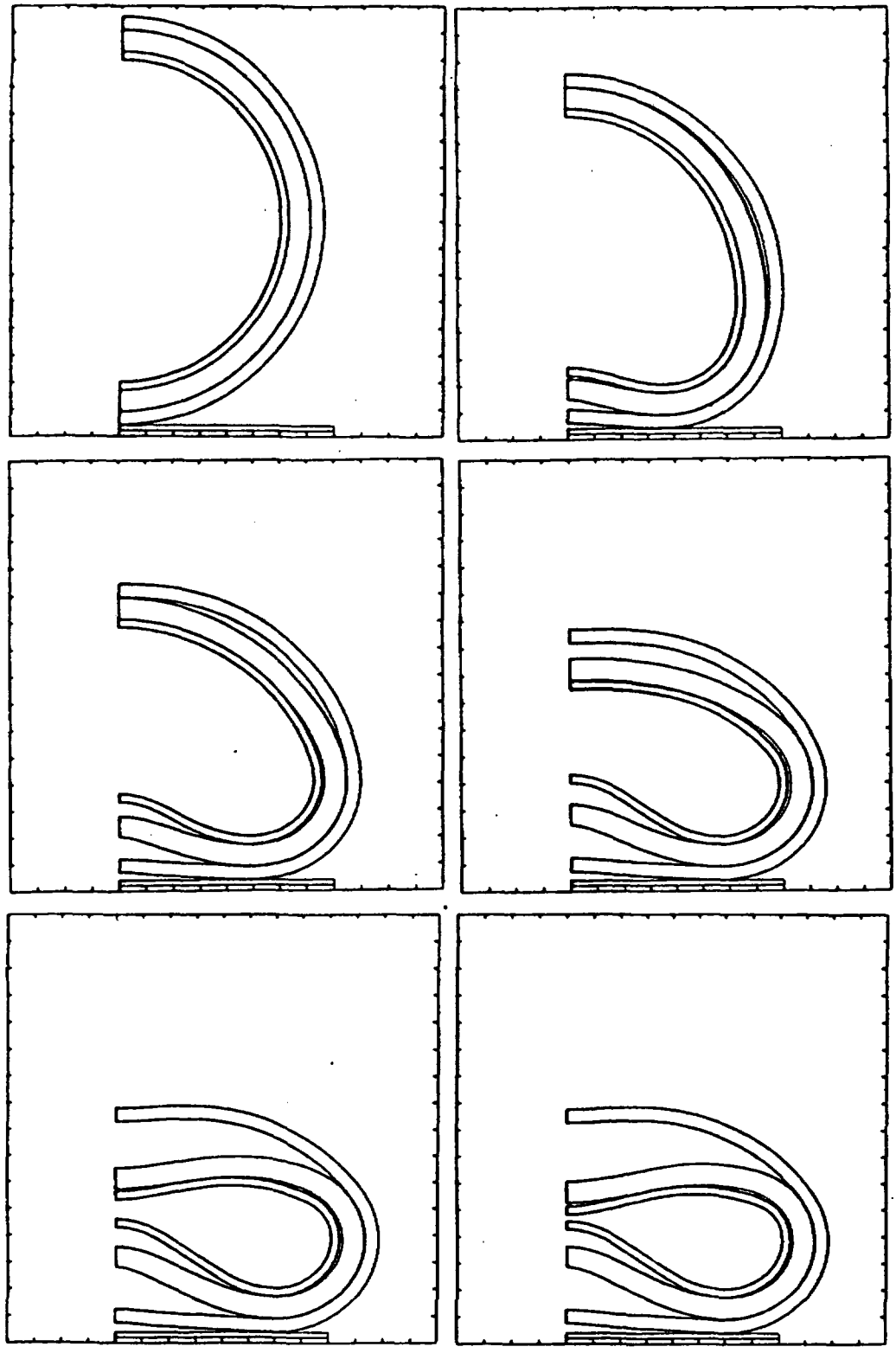

Figure E-22 Rail cask impact on unyielding surface at 60 mph.

Table E.15
Results of Rail Cask Sidewise Impact on an Unyielding Surface

Cask impact velocity (mph)	30	60
Time at which rebound starts (sec)	0.048	N/A
g load on cask (g)	29	47
Maximum effective stress (psi)	32,400	37,400
Maximum plastic strain (%)	4.1	7.2

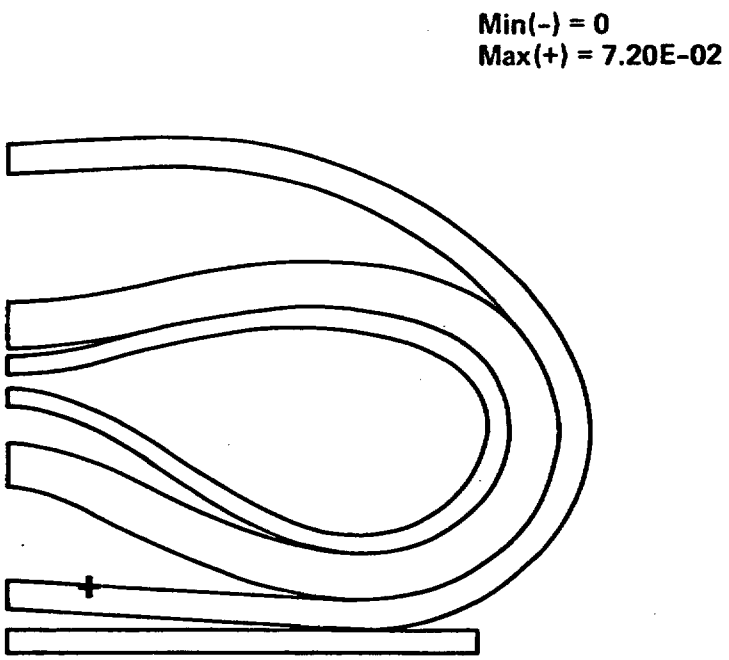

Figure E-23 Rail cask impact on unyielding surface at 60 mph - maximum plastic strain location.

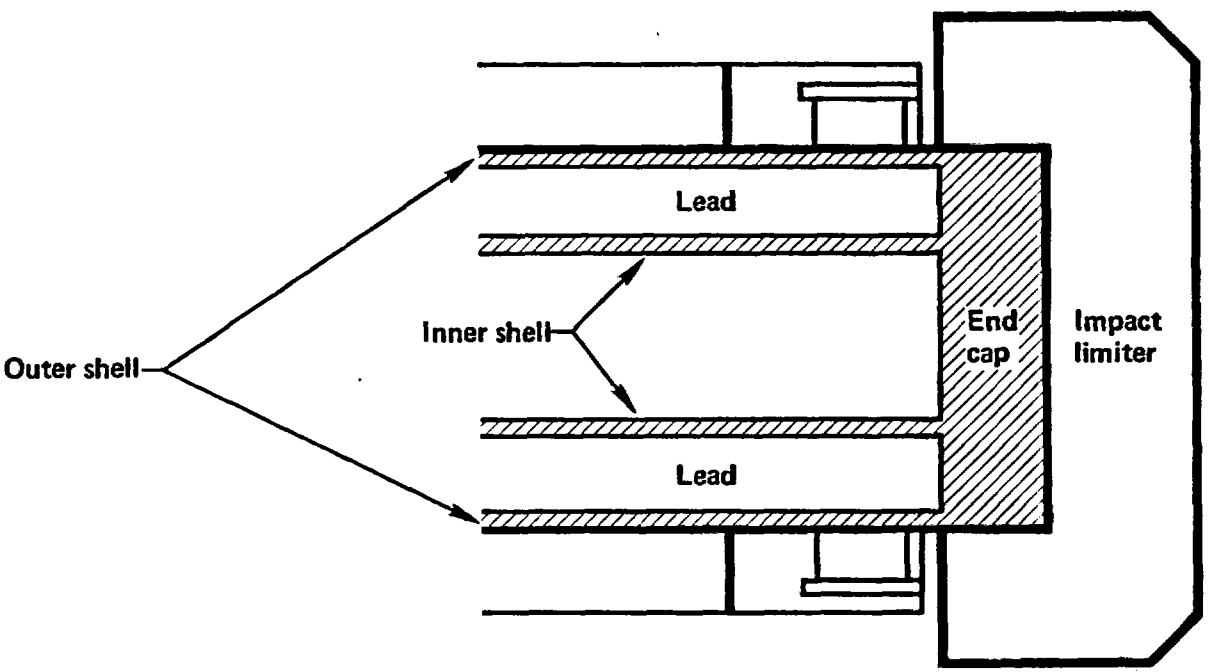

Figure E-24 Full side drop geometry including impact limiters.

were incorporated to reduce the model's complexity. The inner and outer steel shells were modeled using the thick shell option in DYNA 2-D.

The impact velocity was 60 mph, resulting in deceleration of 108 g's and the deformation shown in Fig. E-25. The cask bowed because it was supported by the impact limiters around the end caps. The center of the cask impacted the unyielding surface at almost 60 mph. The contact area increased to approximately half the length of the cask when impact was complete and rebound started to occur. The strain distribution shown in Fig. E-26 indicates that the maximums occur at the center of the cask. The maximum effective stress was 42,500 psi; the maximum plastic strain was 8.7%; and the maximum shear stress was 24,400 psi.

The calculation of the full side-drop with impact limiters showed several things. First, the cask bows when the ends impact first because of the impact limiters. Second, as the cask bows and the center of the cask impacts the unyielding surface, the center of the cask is still traveling at almost full speed. The bowing does not slow down the center of the cask.

A thin slice of the cask was isolated at the center and compared with a 2-D plane strain calculation with the same impact velocity of 60 mph. The deformations are virtually the same as shown in Fig. E-27. The stresses and strains also compared favorably. Since the deformed slopes compared so closely, it was concluded that 2-D calculations can be used to represent 3-D impacts on surfaces at 60 mph and greater.

E.7 Impacts on Real Objects

Ideally, it would be desirable to perform the response calculations assuming both representative casks and real impact surfaces. This can be done using either DYNA 2-D/3-D or NIKE 2-D/3-D computer codes. However, given that computer runs have to be performed to cover many variations in cask orientation angle, surface hardness, and impact velocities, expense precludes the use of DYNA or NIKE codes for each case.

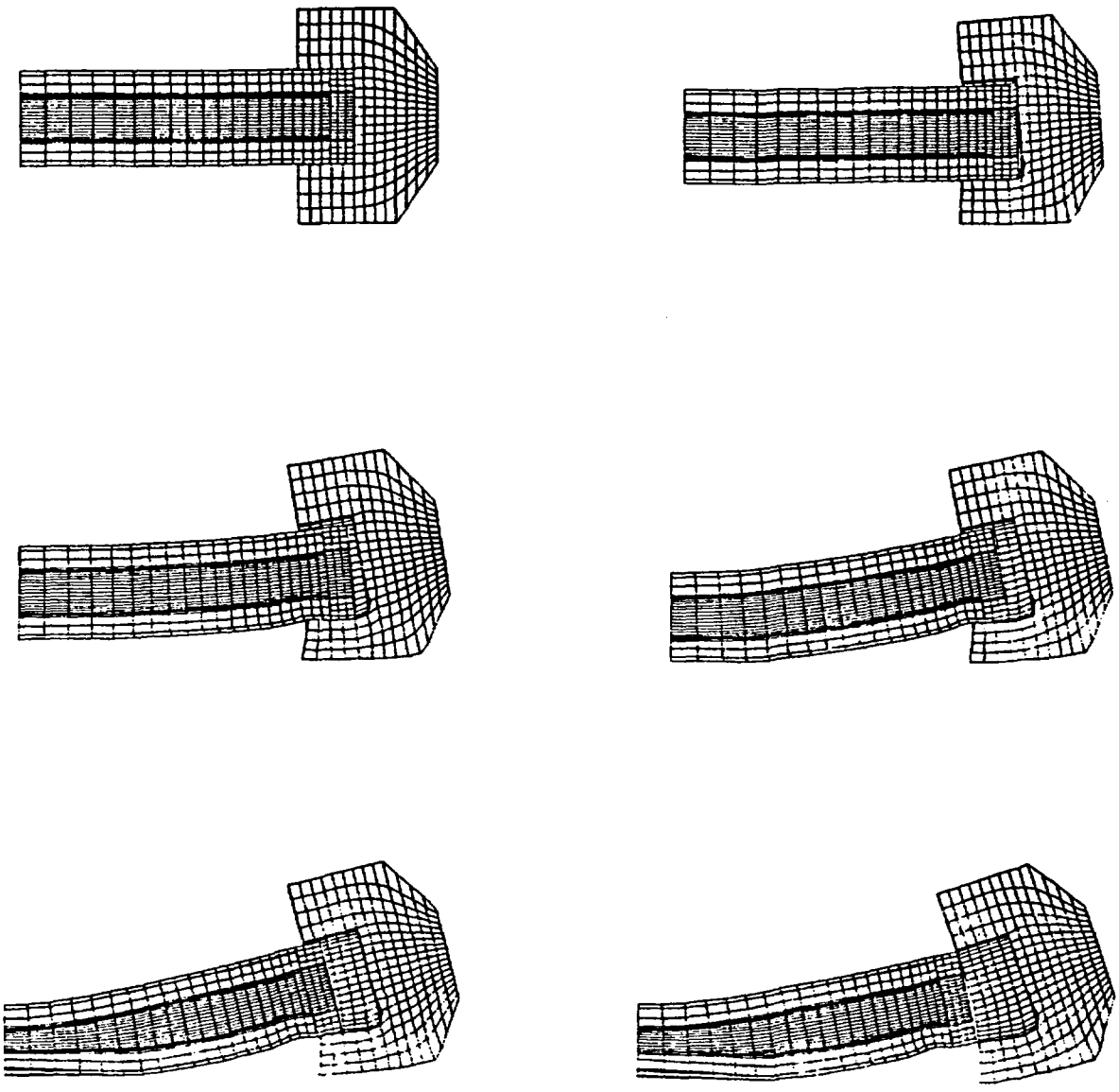

Figure E-25 Deformations of truck cask during 60 mph side drop (side view)

time · 2.99004e-02
contours of eff. plastic strain
min· 0. in element 3561
max· 8.686e-02 in element 3163

contour values
a· 8.69e-03
b· 1.74e-02
c· 2.61e-02
d· 3.47e-02
e· 4.34e-02
f· 5.21e-02
g· 6.08e-02
h· 6.95e-02
i· 7.82e-02

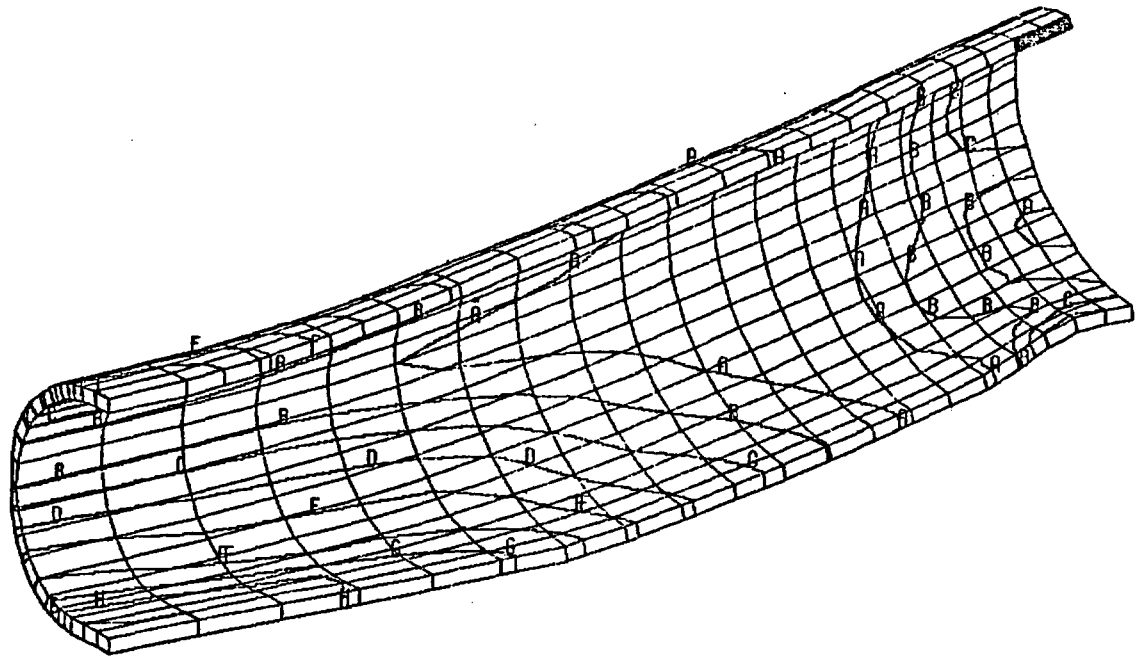

Figure E-26 Distribution of plastic strain at end of impact (outer shell).

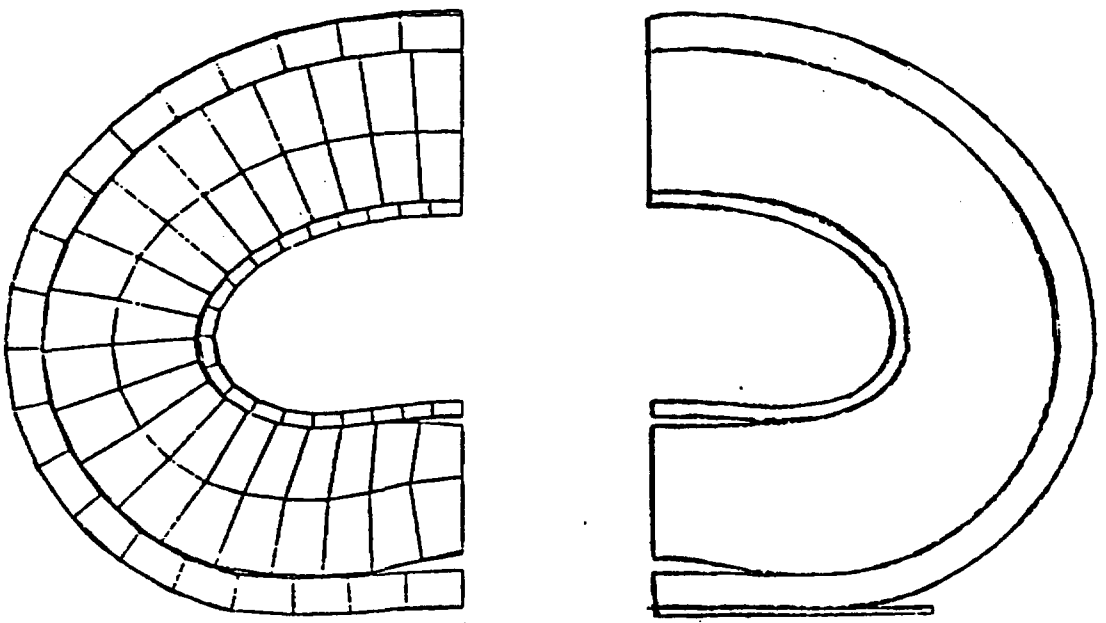

3-D Calculations

2-D Calculations

Figure E-27 Comparison of 2-D deformations with 3-D deformations at the center of the cask.

To simplify the otherwise massive finite element analyses necessary to analyze a representative, i.e., a deformable cask impacting a deformable surface, an equivalent damage technique was devised. Using the equivalent damage technique described in Subsection E.7.1, the cask response was estimated for impacts on real surfaces.

E.7.1 Equivalent Damage Technique

In the equivalent damage technique, the total deformation, and thus the total energy absorption caused by impact, is divided into two parts. The basic assumption is that the total energy of the falling cask is absorbed by deformation of the cask itself and the surface that it hits. In order to estimate how much of the energy is absorbed by the surface, the cask is modeled as a rigid body, and the surface is modeled as an energy-absorbing medium. Using this model, the impact force on the rigid cask can be determined for several velocities. In order to accomplish the necessary analyses, the characteristics of several real target surfaces must be determined.

The energy absorbed by the cask itself is estimated by modeling a deformable cask impacting an unyielding surface. Impact forces and corresponding cask deformations are determined for different impact velocities using this model. In a real situation both the cask and surface would deform. Taking the deformations from the two separate calculations and summing them gives a conservative estimate of the total deformation when a real cask hits a real surface. Since the force required to cause a 0.2% strain (S_1) in the cask is known, the product of this force and the sum of the separately calculated deformations, calculated for the same force, conservatively gives the total deformation energy. By equating this total deformation energy to the kinetic energy, an equivalent velocity can be calculated. This equivalent velocity is then used to modify the curves generated by use of the IMPASC code (in which only an unyielding surface can be modeled) to take into account the effect of the real surface. Figure E-28 shows the analysis for the case of vertical end-drop without limiters.

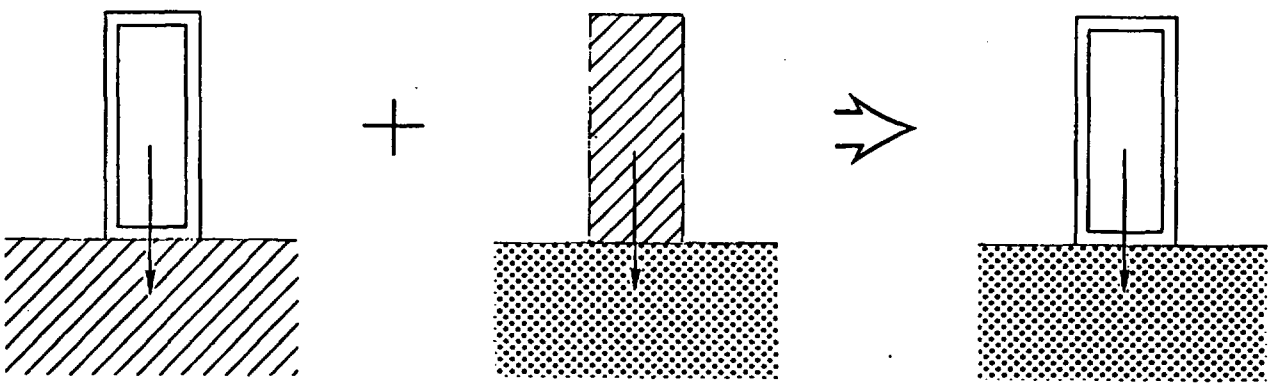

(a) Rigid cask impacts real surface

$$\left(\frac{F}{W}\right) g = \frac{V_1^2}{2d_{c1}}$$

(b) Representative cask impacts unyielding surface

$$\left(\frac{F}{W}\right) g = \frac{V_2^2}{2d_{s1}}$$

(c) Representative cask impacts real surface

$$\left(\frac{F}{W}\right) g = \frac{V_3^2}{2(d_{s1} + d_{c1})}$$

Figure E-28 Equivalent damage technique.

To illustrate the application of the equivalent damage technique, this discussion is restricted to the case of cask end-drop without limiters and a strain of 0.2% (S_1) even though this technique was used to calculate cask responses for other orientations, for casks with limiters, and higher strain levels.

In case (a), the representative truck or rail cask is impacted onto an unyielding surface so that all the kinetic energy is absorbed by the cask. The strain response of the cask is calculated as a function of impact velocity. Assuming constant deceleration during impact, the deceleration force can be estimated from an energy balance:

$$\left(\frac{F}{W}\right) g = \frac{V_1^2}{2d_{c1}} = \text{deceleration force in g for unyielding surface} \quad \text{(E.8)}$$

where F is the force of impact in pounds, W is the cask weight in pounds, g is the gravitational constant in ft/sec^2, V_1 is the impact velocity in ft/sec, and d_{c1} is the cask deformation in inches.

The cask deformation, d_{c1}, is related to the maximum strain on the inner wall where the 0.2% strain (S_1) level is defined. The deceleration force, cask deformation, and the maximum strain at the inner wall are calculated over a range of impact velocities. The deceleration force, (F/W)g, is identified where the 0.2% strain (S_1) level occurs.

In case (b), a rigid body with the same outer dimensions as the cask is impacted onto real surfaces such as hard rock, soft rock, and tillable soil. All the kinetic energy is then absorbed by the surface. The deceleration force can be estimated by

$$\left(\frac{F}{W}\right) g = \frac{V_2^2}{2d_{s1}} = \text{deceleration force in g of a rigid cask on a real surface} \quad \text{(E.9)}$$

where V_2 is the impact velocity in ft/sec and d_{s1} is the penetration into the surface in inches Again the deceleration force is calculated over a range of impact velocities. The impact velocity V_2 is determined for the same impact force identified in case (a) at the 0.2% strain (S_1) level.

In case (c), the representative cask is impacted onto real surfaces. The impact velocity and kinetic energy are absorbed by both the cask and the surface. The deceleration force can be estimated by

$$\left(\frac{F}{W}\right) g = \frac{V_3^2}{2(d_{s1} + d_{c1})} = \text{deceleration force in g of a representative cask on a real surface} \qquad (E.10)$$

where V_3 is the impact velocity corresponding to the 0.2% strain (S_1) level, and d_{s1} and d_{c1} are the penetration into the surface and cask deformation, respectively, as calculated separately for the same force. By equating Equations E.9 and E.10, the velocity V_3 is calculated:

$$V_3^2 = \frac{V_2^2(d_{s1} + d_{c1})}{(d_{s1})} \geq V_2^2 \quad . \qquad (E.11)$$

A higher impact velocity is required to give equivalent damage for the case where energy is absorbed by both the cask and the surface. The equivalent damage technique was conservatively applied by assuming that either the cask or the impacted surface absorb all of the impact energy. The resulting average force on the cask was then used to estimate the strain on the inner shell. Consequently, the strain is significantly overestimated in those cases when significant energy is absorbed by both the cask and the surface. As shown by the benchmark calculation, this approach over compensates for the simplifying assumptions made to develop the equivalent damage technique.

This equivalent damage technique was benchmarked by impacting the representative truck cask on soft rock and then comparing the calculated strain with the estimated strain from the equivalent damage technique for the same impact conditions.

To simplify the comparison, the impact limiter was not included in the benchmark analysis. The representative cask was impacted at 30 mph on the soft rock surface. The cask response to the impact is summarized in Table E.16. The cask response using the equivalent damage technique is also summarized. The percentage strain response for the actual case is 5.4% compared to 14.3% estimated using the equivalent damage technique. In this benchmark case, it was assumed that all of the energy is absorbed by the soft rock, because the resultant force is lower than that resulting from an equivalent drop onto an unyielding surface. From this benchmark calculation it was concluded that the equivalent damage technique as used in this study overestimates the cask response, yet provides reasonable results for estimating purposes.

E.7.2 Soil Impacts

A simple soil model was developed and benchmarked for evaluating impacts on soil with the representative casks as discussed in Subsections E.7.2.1 and E.7.2.2. The responses of the representative casks for endwise impacts on soil were estimated in Subsection E.7.2.3 using the equivalent damage technique. The responses of the casks were calculated with 2-D cask models in Subsection E.7.2.4 for sidewise impacts.

E.7.2.1 Soil Model

Three surfaces are considered to represent a range of credible impact scenarios. The surfaces considered simulate a hard rock, a soft rock including concrete, and tillable soil. Real surfaces exhibit complex characteristics but can be considered to deform elastically during the early part of the impact, followed by an energy dissipation phase. The exact nature of the energy dissipation mechanisms is not well known; therefore, a reasonable and simple elastic-perfectly plastic formulation was used. The two

Table E.16
Comparison of Equivalent Damage Technique Result
with Real Surface Impact Results

	Real Cask on Soft Rock Surface	Rigid Cask on Soft Rock Surface	Real Cask on Unyielding Surface	Equivalent Damage Technique
Cask Velocity (mph)	30	30	28.4	30.0
Duration of Impact (msecs)	17	7.5	17.0	17.0
Interface Force at Impact (g)	203	222	222.0	222.0
Maximum Plastic Strain (%)	5.4	N/A	14.3	14.3
Lead Slump (in)	6	N/A	6.12	6.12

parameters used in this formulation, namely the initial elastic modulus and the yield stress, can be calibrated to approximate an equivalent energy-absorbing medium. To provide the calibration, penetration data[E.19] were used as discussed in Subsection E.7.2.2. Reasonable predictions of penetration were possible using the equivalent elastic-plastic formulation.

The material parameters required by the bilinear computer model, an elastic-plastic model referred to as Material Type 3 in the NIKE/DYNA input manuals, are

E = Young's modulus, psi,

ν = Poisson's ratio, unitless,

σ_y = yield strength, psi,

ρ = density, lb-sec^2/in^4,

β = hardening parameter, unitless,

E_n = hardening modulus, psi,

σ_{1ult} and σ_{3ult} = principle stresses at ultimate stress state, psi.

A suitable range of yield stresses had to be determined for use within the elastic-perfectly plastic model. The standard method for predicting soil failure is the Mohr-Coulomb failure criterion, which states that soil will fail in shear at a value proportional to the applied confining pressure, which varies with soil depth. Even if it is assumed that yielding begins at a stress level equal to the failure stress (corresponding to the elastic-perfectly plastic response assumption), it is necessary to consider a range of failure stress levels.[E.17]

To calculate the failure stress, σ_{ult}, the data of J.M. Duncan, et al., were used to provide an extensive list of soil parameters.[E.18] Also, a

relationship between the deviatoric failure stress, $(\sigma_1 - \sigma_3)_f$, the friction angle, θ, and the cohesion intercept is given by Duncan with the formula

$$(\sigma_1 - \sigma_3)_f = \frac{2c \cos \theta + 2\sigma_3 \sin \theta}{1 - \sin \theta} \quad . \tag{E.12}$$

The deviatoric failure stress is related to the ultimate deviatoric stress as follows:[E.17]

$$(\sigma_1 - \sigma_3)_f = R_f(\sigma_1 - \sigma_3)_{ult} . \tag{E.13}$$

where R_f is the failure ratio. Because $(\sigma_1 - \sigma_3)_f$ is always less than $(\sigma_1 - \sigma_3)_{ult}$, the value of R_f is always less than 1, usually 0.5-0.9. Duncan lists soil parameters for about 150 soils. If, for a particular type of soil, e.g. sandy clay, the largest θ, c, and σ_3, and the lowest value for R_f are selected, a conservative value for the deviatoric failure stress can be calculated. Rearranging equation (E.13) gives:

$$\sigma_{ult} = \sigma_{1ult} = \frac{(\sigma_1 - \sigma_3)_f}{R_f} + \sigma_{3ult} \quad . \tag{E.14}$$

For an elastic-plastic model it is conservative to use the ultimate stress as the yield stress to estimate the maximum force on the cask.

From Duncan's data a summary of the conservative parameters found for 12 general categories of soils is given in Table E.17.

Table E.17
Soil Parameters

Soils	Max θ (°)	Max c (tons/ft^2)	Max σ_3 (psi)	Min R_f (unitless)	σ_y (psi)
Rockfill	53	0	728	0.51	12051
Sandy Gravel	58	10.01	728	0.57	15107
Clayey Gravel/Clayey Sand	34	2.6	504	0.55	2847
Silty Sand/Sandy Silt	53	0.54	219	0.57	3277
Sand	49	0	1104	0.63	11892
Silty Clay	33	3.3	222	0.58	1161
Lean Clay	3	1.10	93.33	0.52	118
Fat Clay	4	1.5	156	0.65	196
Silt	45	0	115	0.57	1090

E.7.2.2 Soil Model Benchmark Calculations

The soil model was benchmarked by comparing with test data. This was accomplished in two phases. The first was an analytical plate bearing test. This test is often used to evaluate soils, subgrades, and pavements, especially in road design, and uses the modulus of subgrade reaction, k, which is measured in situ with a plate bearing test. The test involves loading a circular disk, or stack of disks, usually 30 inches in diameter, at a specified deflection rate, and measuring the deflection at a predetermined load, usually 10 psi. The modulus k is calculated as follows:

$$k = \frac{p}{\Delta} \text{ , psi/in,} \qquad \text{(E.15)}$$

where

p = unit load on plate, psi

Δ = deflection of plate, inches.

The results obtained for the modulus of subgrade reaction, k, were compared with predicted values[E.18] and are summarized in Table E.18. The purpose of this check was to verify that the selected elastic plastic material model produced results that were not completely out of line. The results indicate that for elastic loads, the model significantly over-predicts the soil stiffness. The over-prediction is conservative for this study.

The second phase of the benchmark process was a review of work presented by C.W. Young,[E.20] and a comparison of his results with the soil model results. Young's method was developed to predict depth of earth-penetrating projectiles. Young uses a material parameter, which he calls S, in his formulation and has tabulated values of S for a large variety of soils. Typical values of S from Young[E.20] are listed in Table E.19 with the bilinear soil parameters.[E.17,E.19,E.21]

From Table E.18 it is concluded that the parameters used to model soils can vary over a wide range for different types of soil and rocks. Also the types of soils and rocks can vary significantly within a specific land region. To make the work manageable in analyzing impact with surfaces, the

Table E.18
Plate Bearing Test Simulation with NIKE 2-D

Soil	Calculated k (psi/in)	Predicted k[E.19] (psi/in)
Dense Sand $E = 10^4$ psi $\nu = 0.3$	1100	300 or more
Sandy Clay $E = 5 \times 10^3$ psi $\nu = 0.3$	750	200-300
Hard Sand $E = 5 \times 10^3$ psi $\nu = 0.48$	840	300-800

Table E.19
Summary of Soil Types and Range of Soil Parameters[E.17,E.19,E.21]

Soils	Range of Soil Parameters			
	Bilinear Model Parameter			Soil Constant,
	E (psi)	ν	σ_y (psi)	S ($sec^2/\sqrt{lb}$)
Clay	50-38,000	0.1-0.5	100-3,000	4-50
Silt	300-500	0.3-0.35	1,000-3,500	8-50
Sand	1,000-28,000	0.15-0.4	2,800-15,000	4-12
Soft Rock	20,000-2,000,000	0.1-0.4	10,000-16,000	0.8-5
Hard Rock	5,000,000-26,000,000	0.12-0.4	12,000-25,000	0.3-0.8
Concrete	3,000,000-5,000,000	0.1-0.2	3,000-8,000	0.8-3

surfaces were classified into three groups: hard rock, soft rock including concrete, and tillable soil. The material properties selected to represent each of these groups are tabulated in Table E.20. The range of values for the parameters and Young's[E.20] soil constant S are tabulated for each group.

In Fig. E-29, the impact forces calculated using the elastic plastic model are plotted for impact on each of the three surfaces by a rigid truck cask as a function of impact velocity. Impact force ranges calculated using experimental formulas[E.20] and a rigid truck cask are also plotted for general S soil constants for comparison. For each of the groups there is good agreement between the DYNA 2-D results and the experimental ones.

E.7.2.3 Endwise Impacts on Soil

In order to use the equivalent damage technique to estimate the response of the representative casks for endwise impacts on real surfaces, the impact forces had to be calculated. These analyses were 2-D axisymmetric dynamic finite element analyses, using the code DYNA 2-D. A typical mesh is shown in Fig. E-30. The model includes an unyielding cylindrical falling body which has the same weight and radius as the representative truck and rail casks. A slideline was included between the unyielding cask and the surface. Slideline type three, sliding with voids, was selected from the DYNA 2-D Users Manual. The other possibility, slideline type four, was rejected because the penalty formulation required some adjustment depending upon the stiffness of the soil and the impact velocity, which was not suitable for a parametric study. The impact forces were calculated at four velocities, 30, 60, 90, and 120 mph. The impact forces are summarized in Table E.21 for the representative truck and rail casks.

E.7.2.4 Sidewise Impacts on Soil

Two-dimensional plane strain analysis without impact limiters or end closures were performed for sidewise impacts on the three surfaces to estimate the 3-D responses of the two representative casks. The 2-D truck and rail cask models were developed using the MAZE interactive mesh generators. The cask models do not include contents. DYNA 2-D was used to calculate the responses.

Table E.20
Selected Soil Parameters for this Study

Represented Surface	Bilinear Model Parameter			Soil Constant, S Range
	E (psi)	ν	σ_y (psi)	($sec^2/in/lb$)
Soil	6,000	0.4	1,000	5-50
Soft Rock, Concrete	3,640,000	0.2	4,000	1-5
Hard Rock	7,000,000	0.28	25,000	0.3

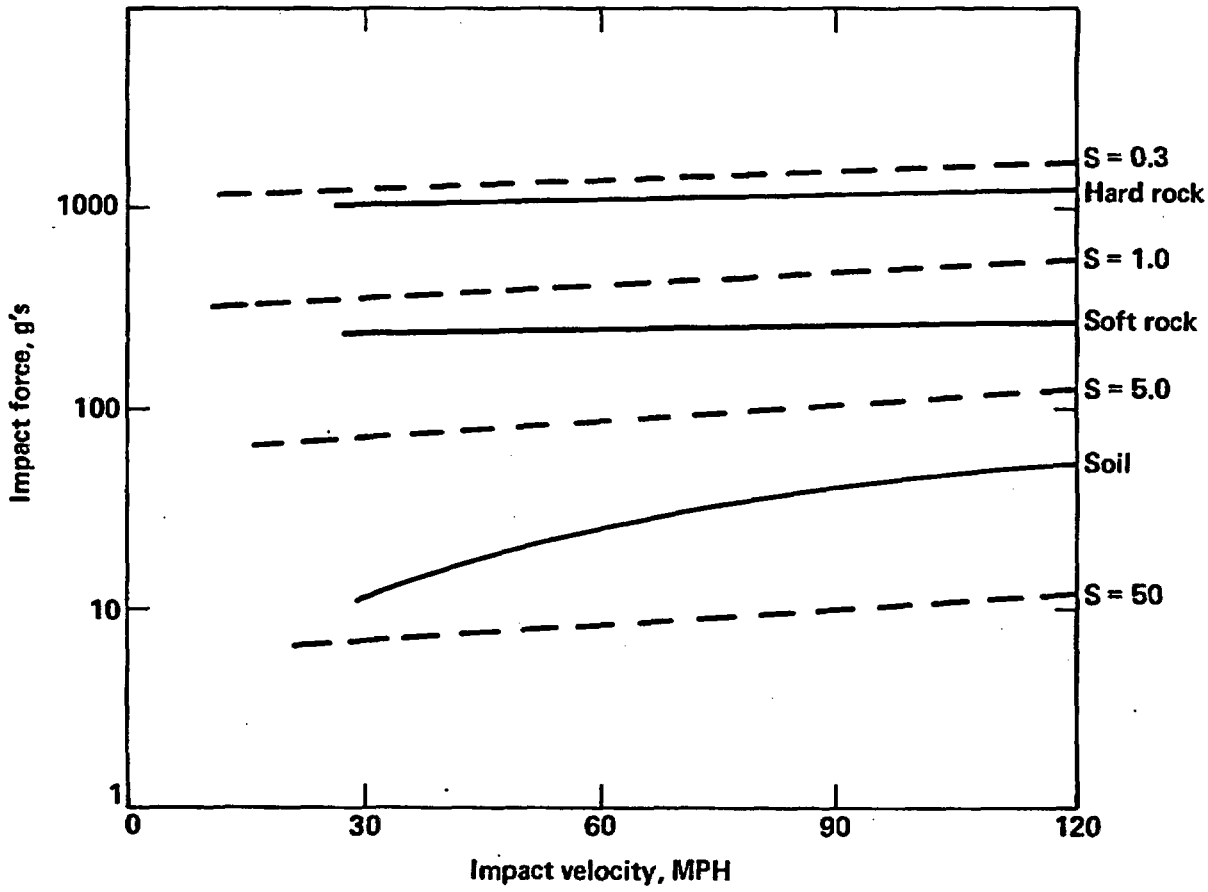

S = Soil constant

Figure E-29 Soil model comparison with penetration test data.

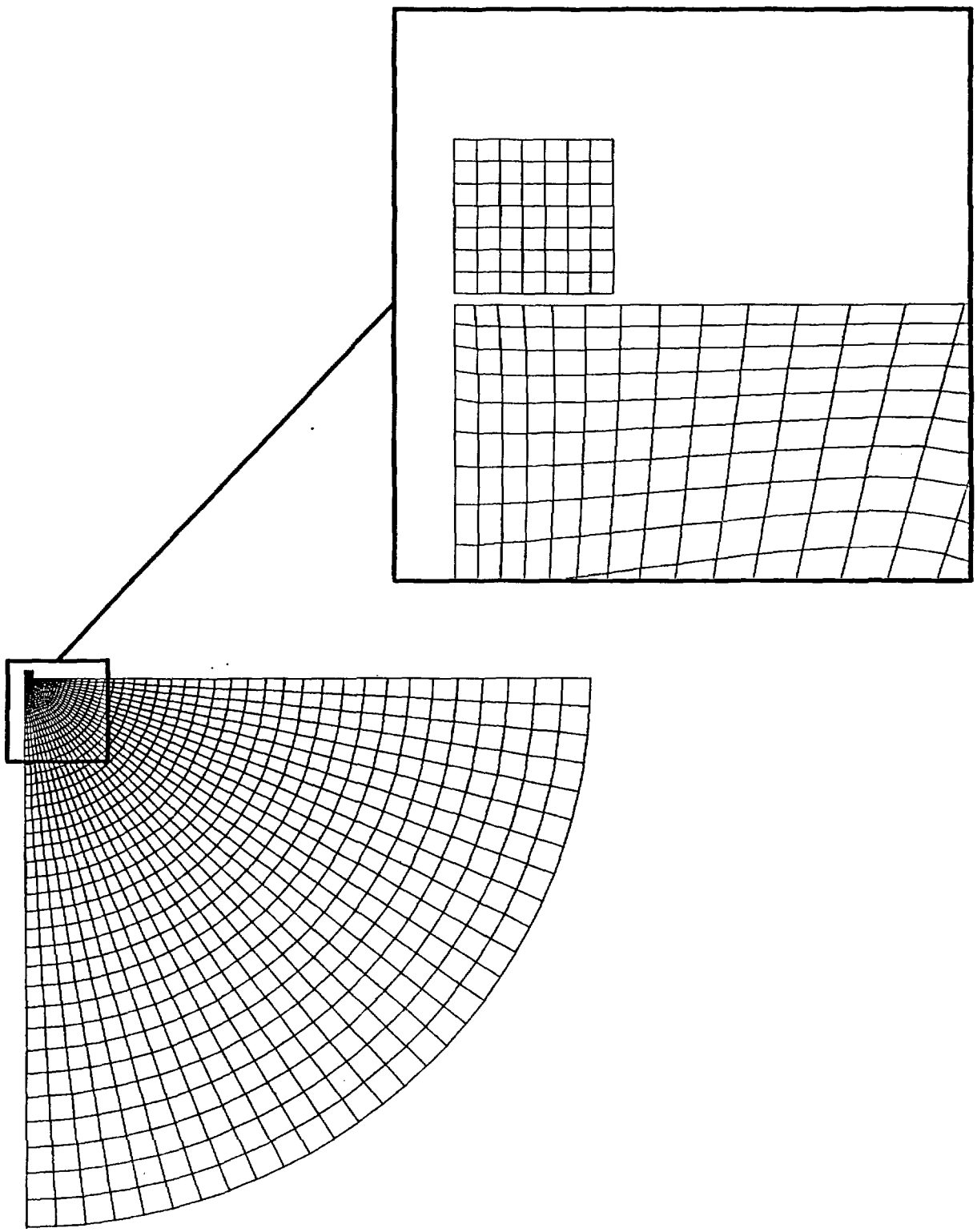

Figure E-30 Finite element mesh for drops on soils.

Table E.21
Summary of Cask Responses to Endwise Impacts on Real Surfaces

Velocity (mph)	Impact Force (g)					
	Truck Cask			Rail Cask		
	Surface Type			Surface Type		
	Hard Rock	Soft Rock	Soil	Hard Rock	Soft Rock	Soil
30	1050	250	12	--	420	16
60	1310	270	26	--	--	110
90	1340	--	40	--	600	200
120	1360	290	54	--	--	--

E.7.2.4.1 Truck Cask Impacts

The truck cask response to endwise impacts on hard rock surfaces was essentially the same as the response to impact on an unyielding surface. Since the cask stiffness is less for sidewise impacts, sidewise impact analyses were performed only for impacts on soil and soft rock. The calculations were performed for 30 mph and 60 mph impacts on soil and 30 mph and 90 mph impacts on soft rock. The effective plastic strain distribution at the time the maximum occurs is shown in Fig. E-31 for the 60 mph impact on soil. The results of the impact calculations are summarized in Table E.22. The maximum strain response of the cask was 2.45% and 7.62% at the inner shell for the 30 mph and 60 mph impacts on the soil. The strain response at the inner shell was 5.03% and 13.6% for the impacts on the concrete surface at 30 mph and 90 mph, respectively.

E.7.2.4.2 Rail Cask Impacts

As was done for the truck cask, sidewise impact analyses were performed for the rail cask for impacts on soil and soft rock. The calculations were performed for 30 mph and 60 mph impacts on soil and 30 mph and 90 mph impacts on soft rock. The effective plastic strain distribution at the time the maximum occurs is shown in Fig. E-32 for one of the cases studied. The results of the impact calculations are summarized in Table E.23. The maximum strain responses at the inner shell for impacts on soil were 2.17% and 3.37% at 30 mph and 60 mph, respectively. The maximum strain responses of the rail cask was lower than those of the truck cask because of its greater flexibility.

E.7.3 Water Impact

An analysis of water impact for wedge shaped bodies is provided in the literature for use in ship hull design.[E.22,E.23] A phenomenon, substantiated during an experimental investigation of flat bottom slamming at the Naval Ship Research and Development Center, is described wherein, during flat bottom slamming, air is trapped between the impact surface of the falling body and the water surface, thereby cushioning the impact.[E.23] Thus the impact angle

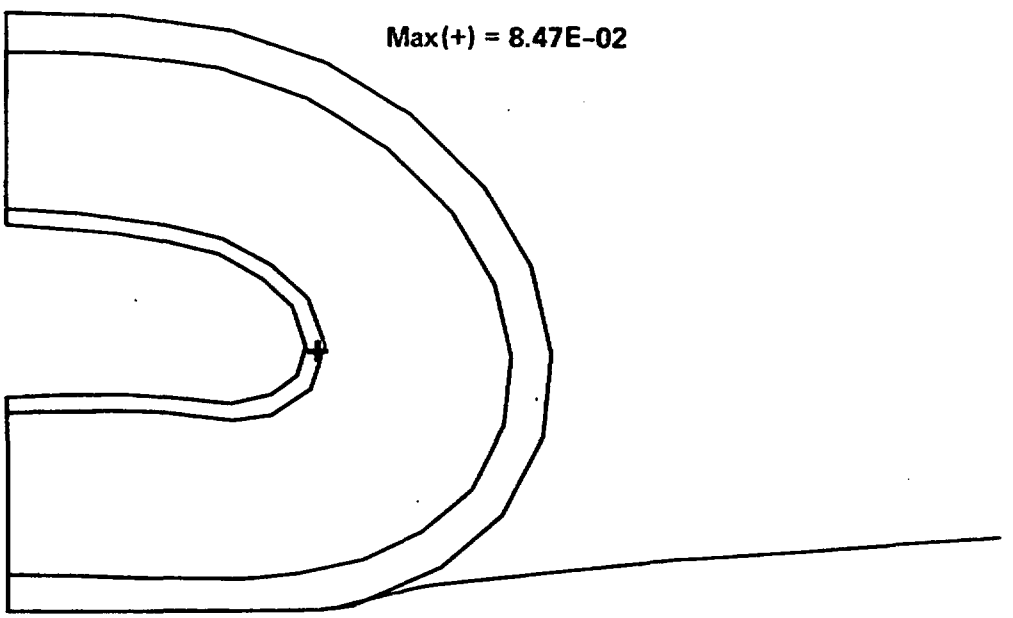

Figure E-31 Maximum plastic strain location on truck cask for impact at 60 mph on soft rock.

Table E.22
Results of Truck Cask Sidewise Impacts on Real Surfaces
(without Impact Limiter)

Velocity (mph)	Strain at Inner Wall (%)	
	Surface Type	
	Soil	Soft Rock
30	2.45	5.03
60	7.62	--
90	--	13.6

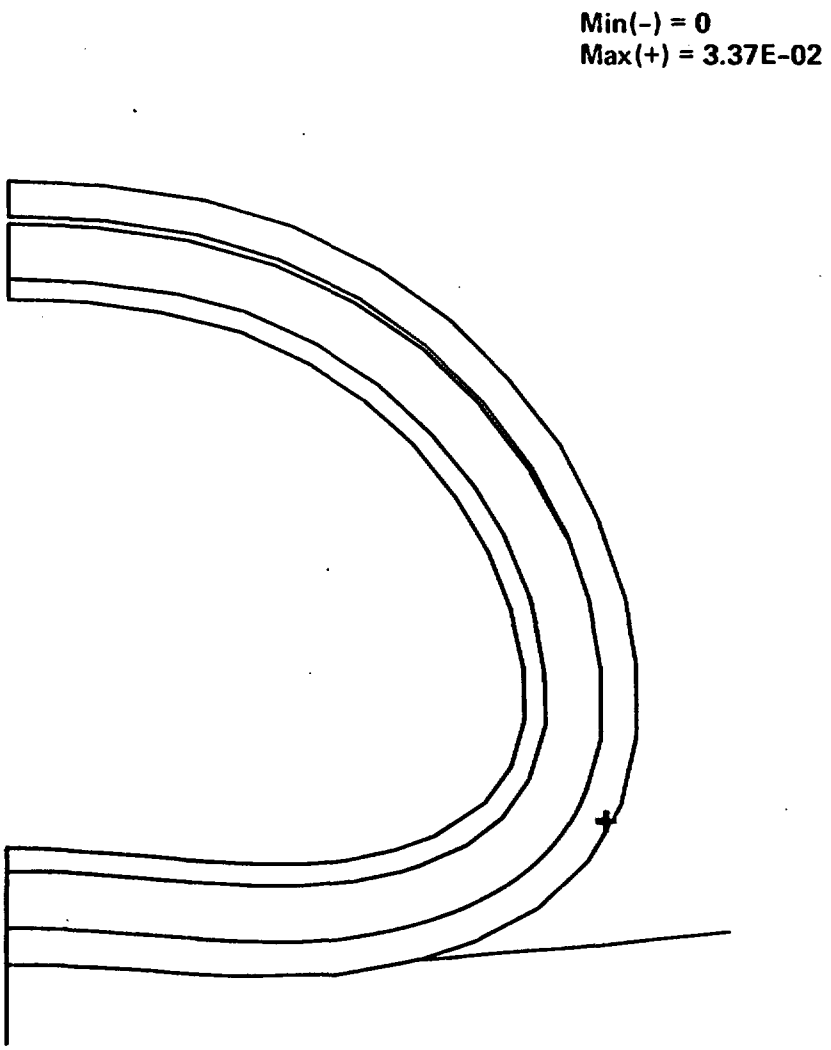

Figure E-32 Maximum plastic strain location on rail cask for impact at 60 mph on soft rock.

Table E.23
Results of Rail Cask Sidewise Impacts on Real Surfaces
(without Impact Limiter)

Velocity (mph)	Strain at Inner Wall (%)	
	Surface Type	
	Soil	Soft Rock
30	2.17	3.78
60	3.37	--
90	--	10.10

producing the highest impact force is not 90^{o}, but 87^{o}. An approximation of the impact force on a cask falling into a body of water is made by integrating the pressure, over an area equal to the cask end cross sectional area:[E.23]

$$p(x) = \frac{1}{2}\rho V^2\left[\frac{\pi}{(90-\beta)\left(1-\frac{x^2}{L^2}\right)^{1/2}} - \frac{\frac{x^2}{L^2}}{1-\frac{x^2}{L^2}} + \frac{2\bar{z}}{V^2}\left(L^2-x^2\right)^{1/2}\right] \qquad \text{(E.16)}$$

and

$$\text{Force} = \int_0^L q\, p(y)\,dy \qquad \text{(E.17)}$$

where

$y = Lx$, ft,

$q = 2L\left(x - x^2\right)^{1/2}$, ft,

β = compliment of deadrise angle, ^{o},

ρ = mass density of water, lb/ft^3,

L = cask diameter, ft,

V = cask impact velocity, ft/sec,

$\bar{z} = 0$ (i.e., assume that impact acceleration, = 1 g, is negligible).

Using Simpson's Rule for integration, the interface forces were calculated for the two unyielding casks with the same external dimensions as the representative casks for four impact velocities and three cask orientations. For the large diameter rail cask, the loads due to impact on water can be quite high for the 87^{o} impact angle. However these loads drop off rapidly for other impact angles. The results of the calculations are summarized in Table E.24. The equivalent damage technique is used to estimate the strain response of the casks to the calculated impact forces.

E.7.4 Train Sill Impacts

E.7.4.1 Impact on Truck Cask

Two scenarios were evaluated for a locomotive sill impacting a truck cask: the sill impacting the cask sidewise head-on; and the sill impacting the cask sidewise off-center. The cross-section of the model used to simulate a locomotive sill is shown in Fig. E-33 and consists of two plates connected with two large I-beams.[E.9] The sill was modeled as a solid object with modified properties. For the sidewise head-on impacts the sill was modeled as a plate 3.5 inches thick to approximate its axial strength. For the sidewise off-center impacts the sill was modeled as a plate 11.5 inches thick to approximate its bending strength. In both cases, the density of the sill was calculated for a locomotive weight of 200 tons.

The sill was first modeled as shown in Fig. E-34 to impact at a point at 45^{o} on the truck cask from the sidewise head-on position. Calculations were made with the locomotive sill impacting the cask at velocities of 30 mph and 60 mph. In both cases, the cask moved away from the sill at an angle and achieved a velocity lower than the initial sill velocity. Also, the sill underwent a slight rotation and remained undamaged. However, the cask sustained large deformations where the sill scraped across it. Also as illustrated in Fig. E-35, the sudden acceleration caused the cask to flatten.

For the 30 mph impact, the cask experienced a force of 110 g's and sustained a maximum effective stress of 40,100 psi and maximum plastic strain of 7.5% in the steel shells. For 60 mph, the force increased to 206 g's, the

Table E.24
Interface Force for Water Impact
(All Results Listed in Multiples of Cask Weight,
No Impact Limiters or Cab Crush Included)

Velocity (mph)	Unyielding Truck Cask Impact Orientation			Unyielding Rail Cask Impact Orientation		
	87^0	45^0	0^0	87^0	45^0	0^0
30	17.7	0.9	12.6	37.8	1.9	10
60	70.8	3.6	50.4	151.3	7.6	39
90	159.3	8.5	119	340.5	17.1	88
120	283.2	14.5	203	605.3	30.4	155

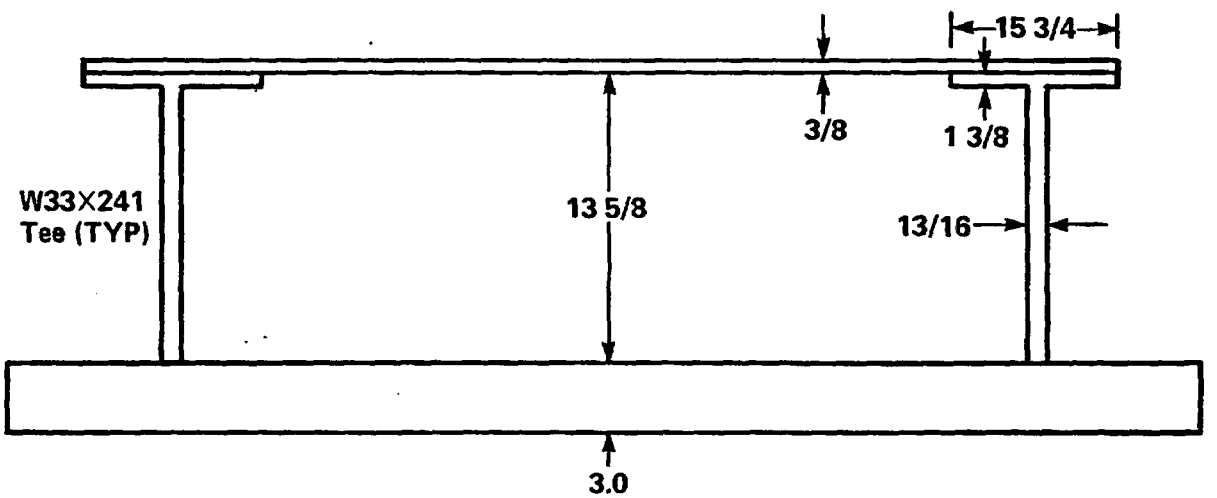

Figure E-33 Locomotive sill cross section.

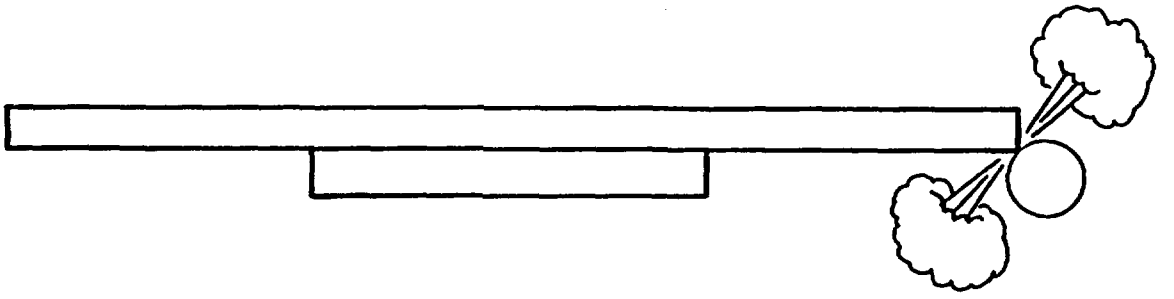

Figure E-34 Sidewise off-center locomotive sill impact.

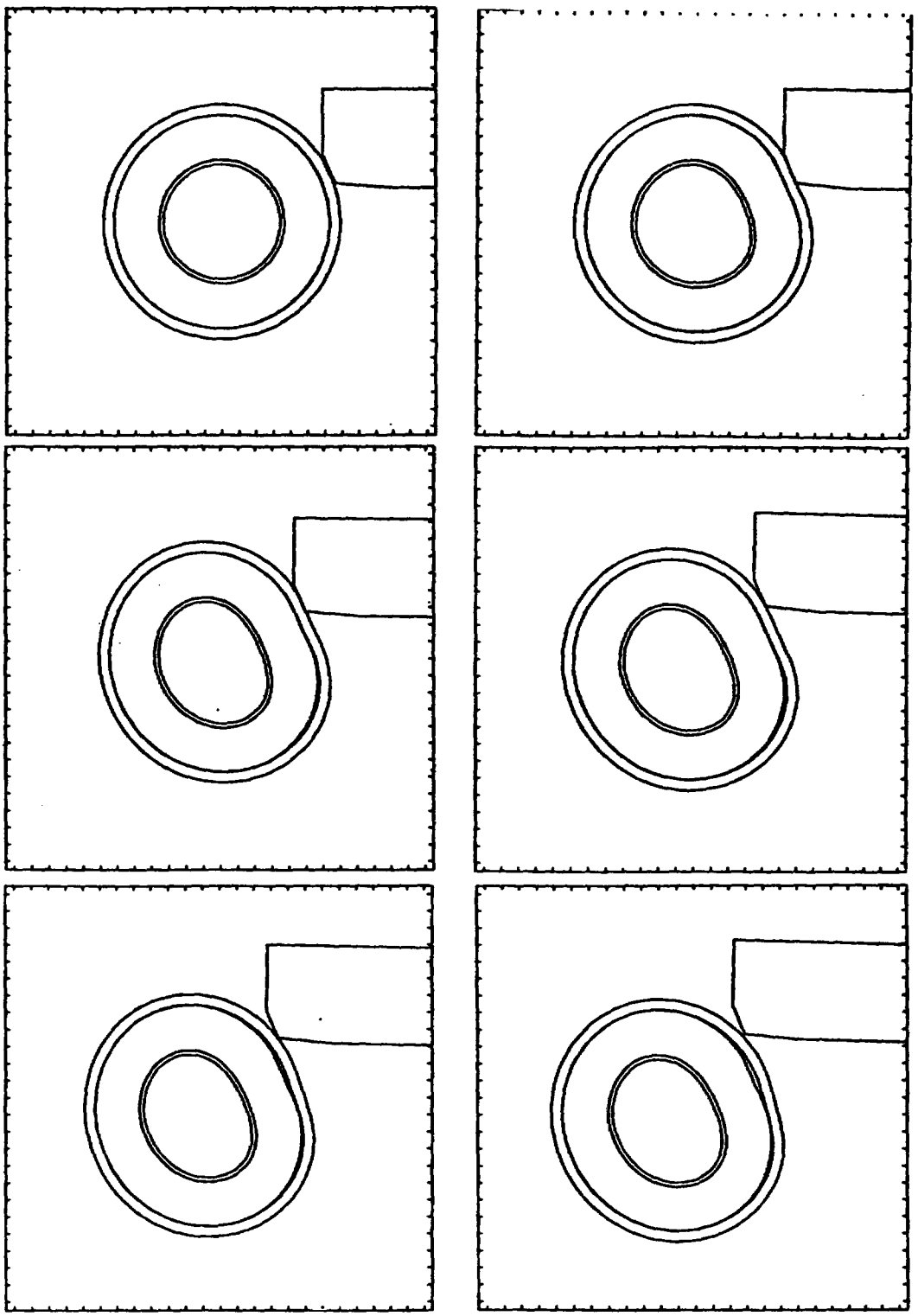

Figure E-35 Thirty mph sidewise off-center sill impact.

maximum effective stress increased to 50,000 psi, and the maximum plastic strain increased to 12.8%. These results are summarized in Table E.25. The location of the maximum plastic strain is shown in Fig. E-36.

For the sidewise head-on impact, the complete 2-D strain truck cask model was analyzed for impact with the locomotive sill. This model was used only for the impact at 30 mph; based on these results, symmetry was used for the 60 mph impact to reduce the solution cost. The modeling is shown in Fig. E-37. In both cases, the cask achieved a velocity higher than the sill velocity and the sill was undamaged. However, the cask sustained large deformations in the impact zone. Also, the sudden acceleration caused the cask to flatten as shown in Fig. E-38.

For the 30 mph impact, the cask experienced a force of 138 g's, a maximum effective stress of 50,000 psi, and a maximum plastic strain of 12.4% in the steel shells. For 60 mph, the force increased to 265 g's, the maximum effective stress increased to 65,000 psi, and the maximum plastic strain increased to 20%. These results are summarized in Table E.26. The location of the maximum plastic strain is shown in Fig. E-39.

None of our cask models included contents. For the truck cask, the mass of the contents is not large compared to the mass of the cask. The truck cask is very much like a thick-walled cylinder and under the severe impact conditions, it is able to support itself. For the rail cask, the mass of the contents is very large compared to the mass of the cask. Also, the rail cask is like a thin-walled cylinder. Under the severe impact conditions, it is unable to support itself. Thus, contents are very important to the rail cask calculations and should be modeled to provide more accurate impact forces and g loads and to support the cask as it collapses.

Our comparison of the maximum effective stresses and plastic strains sustained by the two casks for the different impact conditions shows that the sidewise sill head-on impact into the truck cask is the most severe. The off-center impact is less severe because the sill transfers less energy as it strikes a glancing blow to the cask. The truck cask impacting on the unyielding surface is less severe than the sidewise head-on impact. However, the maximum g loads occur in the impacts on an unyielding surface. The

Table E.25
Results Sidewise of Off-Center Sill Impact Against Truck Cask

Locomotive sill velocity (mph)	30	60
Locomotive sill velocity (in/sec)	528	1056
Duration of impact (sec)	0.012	0.011
Velocity at end of impact (in/sec)	425	637
Angle of departure of cask (°)	52	42
g load on cask (g)	110	206
Maximum effective stress (psi)	40,100	50,800
Maximum plastic strain (%)	7.5	12.8
Maximum plastic strain at inner shell(%)	2.3	3.8

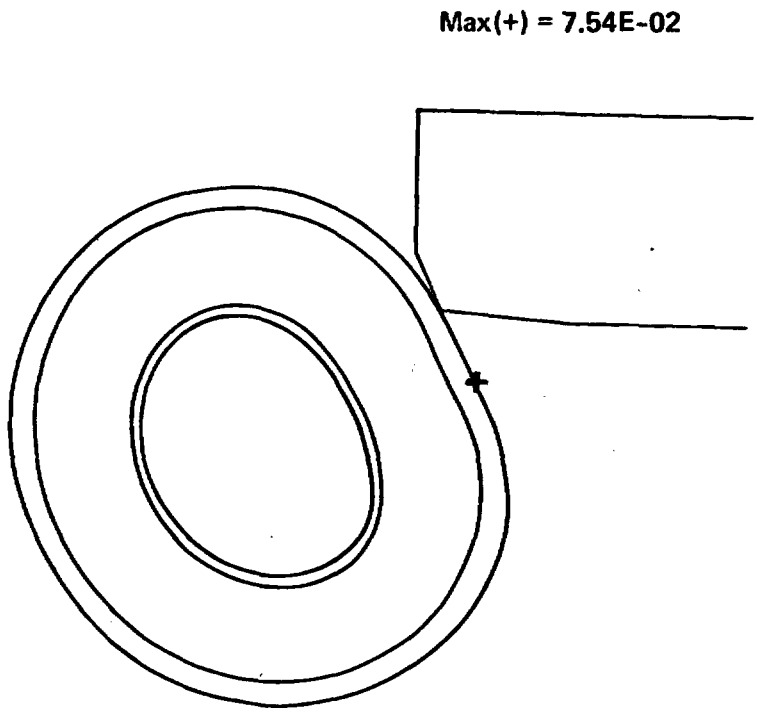

Figure E-36 Thirty mph sidewise off-center sill impact-maximum plastic strain location.

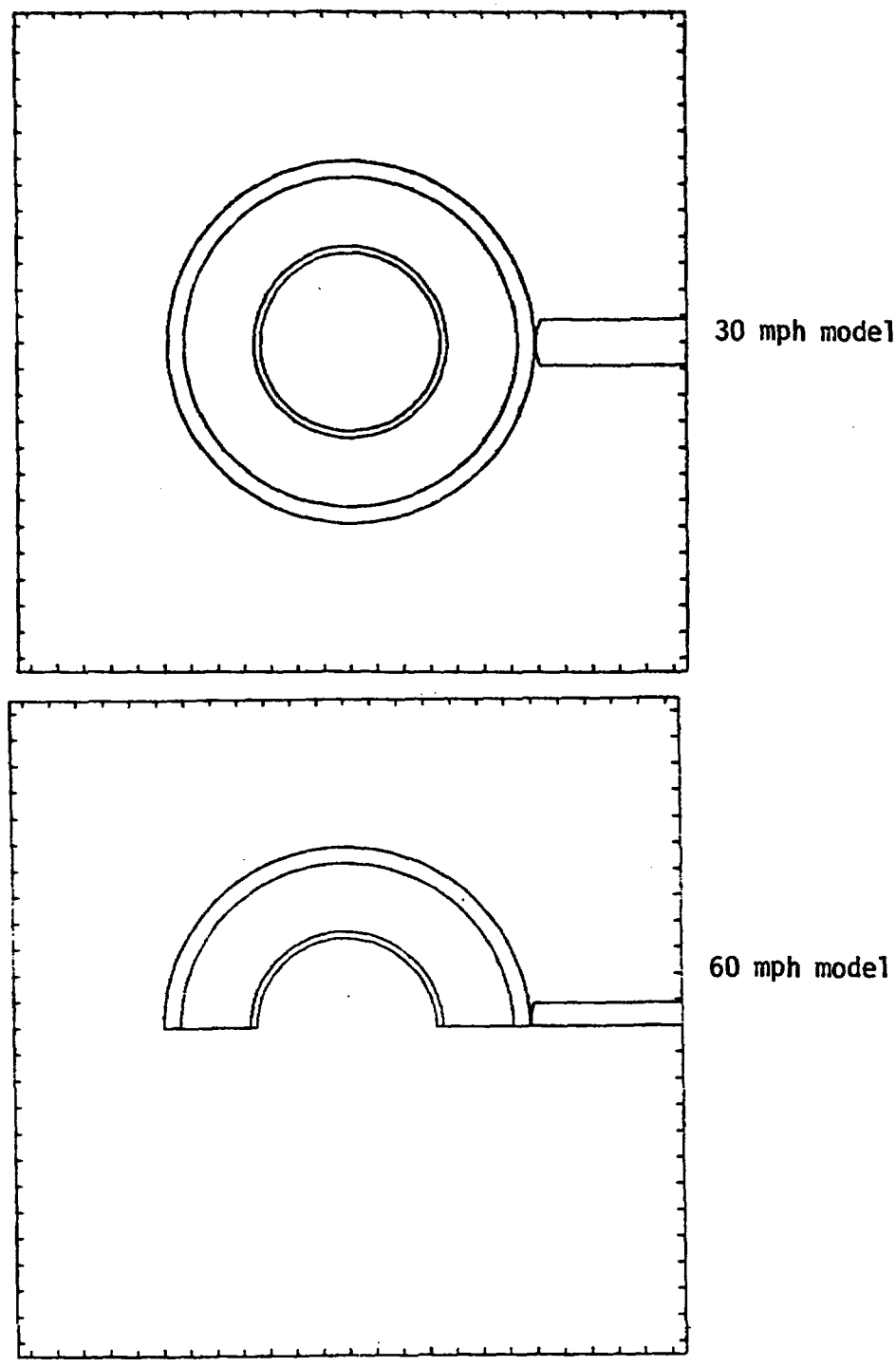

Figure E-37 Model configurations for sidewise head-on sill impact. Note use of symmetry for 60 mph case.

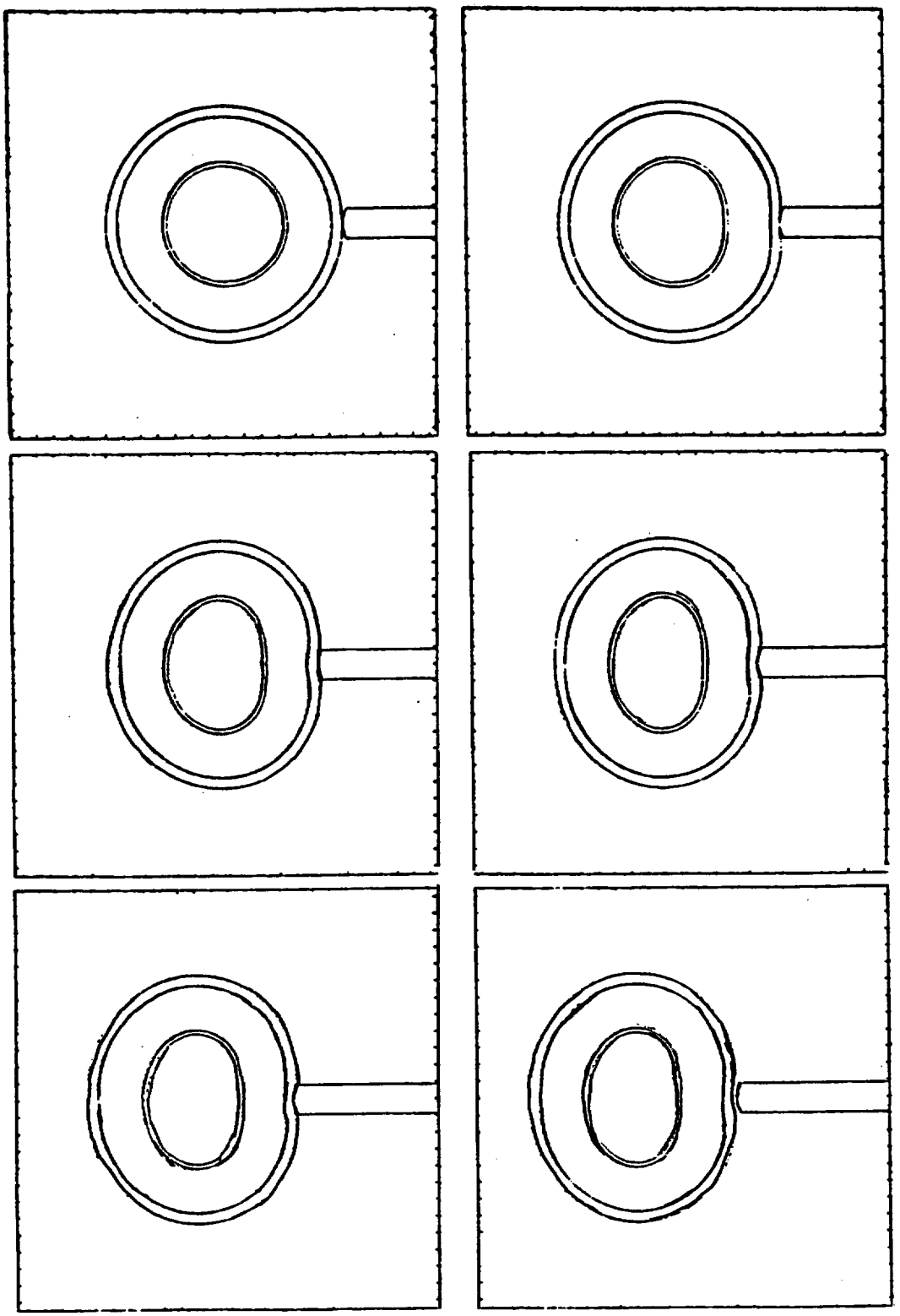

Figure E-38 Sidewise head-on sill impact at 30 mph.

Table E.26
Results of Sidewise Head-on Sill Impact Against Truck Cask

Locomotive sill velocity (mph)	30	60
Locomotive sill velocity (in/sec)	528	1056
Duration of impact (sec)	0.0125	0.0135
Velocity at end of impact (in/sec)	575	1130
g load on cask (g)	138	265
Maximum effective stress (psi)	50,000	65,000
Maximum plastic strain (%)	12.4	20
Maximum plastic strain at inner shell (%)	3.7	6.0

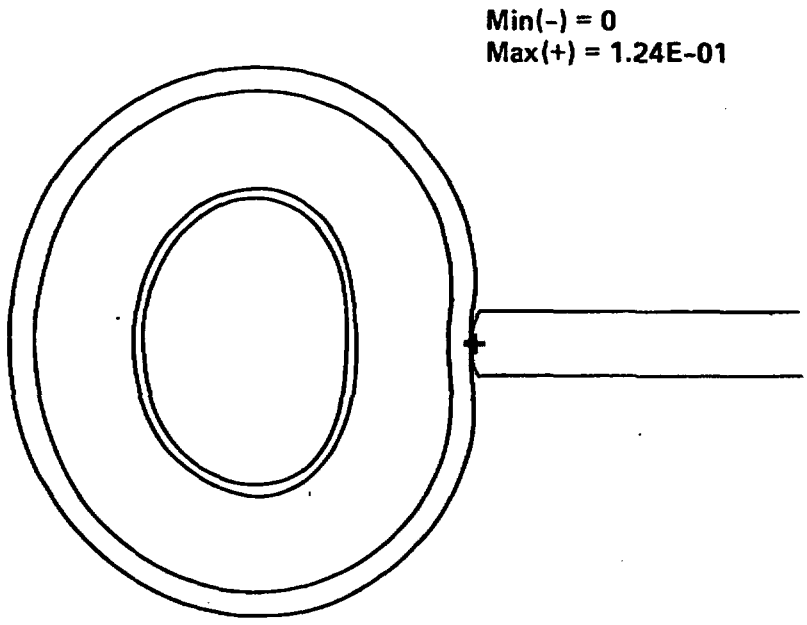

Figure E-39 Thirty mph sidewise head-on sill impact-maximum plastic strain location.

sidewise head-on impact causes severe local deformations before the cask is accelerated to its final speed. Also, the locomotive sill has some give to it. These combined effects soften the impact. The rail cask endures the least severe stresses, strains, and g loads, yet it sustains the most severe deformations. This is because the rail cask is more ductile than the truck cask, causing a very soft impact.

E.7.4.2 Impact on Rail Cask

The response of the representative rail cask was estimated for impacts with a train sill by using the truck cask results. The response was estimated by multiplying the truck cask results for the train sill impact times the rail cask results for the unyielding surface impact and dividing by the truck cask results for the unyielding surface impact. The estimated responses of the representative rail cask to impacts by a train sill are summarized in Table E.27. The estimated strains are conservatively high because of the greater size and weight of the rail cask compared to the truck cask.

Table E.27
Estimated Response of Rail Cask to Impact by Train Sill

Velocity (mph)	Strain Response (%) Impact Orientation	
	0^{o}	45^{o}
30	2.3	1.4
60	3.6	2.3

E.8 References

E.1 J. O. Hallquist, NIKE 2-D: An Implicit, Finite-Deformation, Finite Element Code for Analyzing the Static and Dynamic Response of Two-Dimensional Solids, Lawrence Livermore National Laboratory, Livermore, CA, UCRL-52678, 1979, and Revision 1, NIKE 2-D: An Implicit, Finite-Deformation, Finite Element Code for Analyzing the Static and Dynamic Response of Two-Dimensional Solids, Lawrence Livermore National Laboratory, Livermore, CA, UCID-18822, 1981.

E.2 J. O. Hallquist, User's Manual for Dyna 2-D--An Explicit Two-Dimensional Hydrodynamic Finite Element Code with Interactive Rezoning, Lawrence Livermore National Laboratory, Livermore, CA, UCID-18756, Rev. 2, 1984.

E.3 American Society of Mechanical Engineers, ASME Boiler and Pressure Vessel Code, Section III, Division 1, The American Society of Mechanical Engineers, United Engineering Center, 345 East 47th Street, New York, NY 10017, July 1983.

E.4 J. B. Conway, R. h. Stentz, and J. T. Berling, Fatigue, Tensile, and Relaxation Behavior of Stainless Steels, Technical Information Center, Office of Information Services, United States Atomic Energy Commission, Oak Ridge, TN, 1975.

E.5 Safety Analysis Report for the NLI-10-24 Shipping Cask, Docket No. 70-9023, National Lead Industries, Inc., Wilmington, DE, February 1976.

E.6 J. Counts and J. B. Payne, Evaluation of Analysis Methods for Type B Shipping Container Impact Problems, Los Alamos Scientific Laboratory, Los Alamos, NM, LA-6640-MS, 1979.

E.7 Consolidated Safety Analysis Report IF-300 Shipping Cask "Appendix I", Docket No. 70-1220, General Electric Company, San Jose, CA, January 1971.

E.8 C. R. Adams, et al, A Comparison of Analytical Techniques for Analyzing a Nuclear-Spent-Fuel Shipping Cask Subjected to an End-on Impact, U.S. Nuclear Regulatory Commission, Washington, DC, NUREG/CR-2018, 1981.

E.9 P. Eggers, Severe Rail and Truck Accidents: Toward a Definition of Bounding Environments for Transportation Packages, U.S. Nuclear Regulatory Commission, Washington, DC, NUREG/CR-3498, 1984.

E.10 N. E. Shoemaker, et al., Consumer Information Crash Test Program, U.S. Department of Transportation, Washington, DC, DOT HS-802011, September 1976.

E.11 M. Huerta, Analysis, Scale Modeling, and Full-Scale Tests of a Truck Spent-Nuclear-Fuel Shipping System in High Velocity Impacts Against a Rigid Barrier, Sandia National Laboratory, Albuquerque, NM, SAND77-0270, 1978.

E.12 M. Huerta, Analysis, Scale Modeling, and Full-Scale Tests of a Railcar and Spent-Nuclear-Fuel Shipping Cask in a High Velocity Impact Against a Rigid Barrier, Sandia National Laboratory, Albuquerque, NM, SAND78-0458, Febuary 1980.

E.13 Uniform Building Code, International Conference of Building Officials, Whittier, California, 1979.

E.14 T. A. Nelson, et. al., SCANS - Shipping Cask Analysis System, Vol. 1, Impact Analysis Code User's Manual, Lawrence Livermore National Laboratory, Livermore, CA, UCID-20674/Vol. 1, Draft Report to be published, U.S. Nuclear Regulatory Commission, Washington, DC, NUREG/CR-4554, 1986.

E.15 J. O. Hallquist, MAZE, An Input Generator for DYNA 2-D and NIKE 2-D, Lawrence Livermore National Laboratory, Livermore, CA, UCID-19029, June 1983.

E.16 M. A. Gerhard, SLIC, Interactive Graphic Mesh Generator, Lawrence Livermore National Laboratory, Livermore, CA, UCRL-52823, September 1979.

E.17 G. F. Sowers, Introductory Soil Mechanics and Foundations: Geotechnical Engineering, Fourth Edition, MacMillan Publishing Company, New York, NY, 1979.

E.18 J. M. Duncan, P. Byrne, K. S. Wong, and P. Mabry, Strength, Stress-Strain and Bulk Modulus Parameters for Finite Element Analyses of Stresses and Movements in Soil Masses, University of California at Berkeley, Berkeley, CA, UCB/GT/80-01, 1980.

E.19 W. Yoder, Principles of Pavement Design, Second Edition, J. Wiley and Sons, New York, NY, 1975.

E.20 C. W. Young, "Depth Prediction for Earth-Penetrating Projectiles", Journal of the Soil Mechanics and Foundations Division, Proceedings of the American Society of Civil Engineers Vol. 95, No. SM3, Proceedings Paper 6558, American Society of Civil Engineers, New York, NY, May 1969.

E.21 J. E. Bowles, Foundation Analysis and Design, Second Edition, McGraw-Hill, New York, NY, 1977

E.22 H. Wagner, Über Stoss und Gleitvorgänge an der Oberfläche von Flussigkeiten," Zeitschrift Für Angewandte Mathematik und Mechanik, August 1932.

E.23 S. L. Chuang, "Experiments on Slamming of Wedge-Shaped Bodies," Journal of Ship Research, September 1967.

APPENDIX F

List of Figures

List of Tables

APPENDIX F
Thermal Analysis

F.1 Introduction

This appendix provides the thermal models developed and the analyses performed to determine the responses of the representative truck and rail casks to a wide range of fire conditions. The computer code TACO-2D was used to perform the calculations.[F.1]

In Section F.2, the types of thermal loading conditions that can effect the temperature response of a cask in an accident are discussed. The highest loading condition is caused by large, long-duration fires and is selected for further evaluation. In Section F.3, the thermal loading conditions on a cask caused by real fire conditions are discussed. Referenced fire conditions and modeling are defined for evaluating real fire effects on casks.

In Section F.4, the thermal model and transient temperature response of the two representative casks to regulatory fire conditions are discussed. In Section F.5, the transient temperature response of the two representative casks is estimated for different heat loading conditions and a wide spectrum of real fire conditions defined by fire duration, temperature, and location.

F.2 Thermal Loading Conditions Caused by Accidents

Thermal loading conditions on a cask caused by an accident can result in cask temperature increases. The thermal loading conditions include fires, torch fires, and cask burial. Typically, as discussed in Section F.5, a fire can heat a cask at an average heat flux of 5,000 Btu/hr-ft^2 from several minutes to several hours. The total heat absorbed in a fire can be 1,000 to 50,000 BTU/ft^2 depending on the fire temperature, location, and duration.

Torch fires can heat a localized area of a cask at rates 1.5 to 2.5 times higher than a fire, but in comparison to fires, do not deposit large quantities of heat into the cask. As demonstrated in torch fire tests at Sandia,[F.2] no significant localized damage occurs to the cask even at the high heating fluxes because the heat is quickly dissipated to other portions of the cask thus limiting the rise in the local temperature.

Burial of the cask can cause the temperature of the cask and contents to rise because of the decay heat from the fuel. Burial of the cask can cause thermal isolation, where the decay heat from the fuel may have to be transferred through the surrounding material causing the burial. The decay heat flux from the fuel in a cask is typically 50-350 Btu/hr-ft^2 depending primarily on the number of fuel assemblies, their burnup, and their time out of a reactor. The decay heat flux from the fuel assemblies is 15-50 times lower than that which can be typically absorbed from a fire. The cask, which is relatively large and not easily buried, would have to be buried for several days before any significant damage to the cask could occur that could result in radioactive releases.

Based on severe accident data, the frequency of occurrence of fires is at least 10 times higher than for torch fires or complete burial of a cask. Therefore, since fires can generate higher heat loads and can occur more frequently, it is concluded that fires dominate the potential thermal environment and only fires require further evaluation.

F.3 Reference Fire Conditions and Modeling

In Fig. F-1(a), a three-dimensional (3-D) model of a cask engulfed in a real fire is given. The heat transfer from the fire to the cask can vary with time and position along the length and around the diameter of the cask. The effects of the fire can be significantly different on the various components located on the cask. To simplify the heating analysis of the cask and its components, currently licensed cask designs were reviewed to relate the temperatures at the middle portion of the cask to the temperatures of the other positions of the cask, particularly the closure seals. The location of valve boxes was also considered because they could be exposed to heat loads and temperatures approaching this middle portion of the cask. From this review, it was concluded that the temperature response and damage to the cask and its components could be conservatively bounded by analyzing the middle portion of the cask and using the four temperature response levels defined in Section 4.0 for the centerline of the lead shielding. Using this approach, the 3-D model in Fig. F-1(a) is reduced to the two-dimensional (2-D) model in Fig. F-1(b) for analysis.

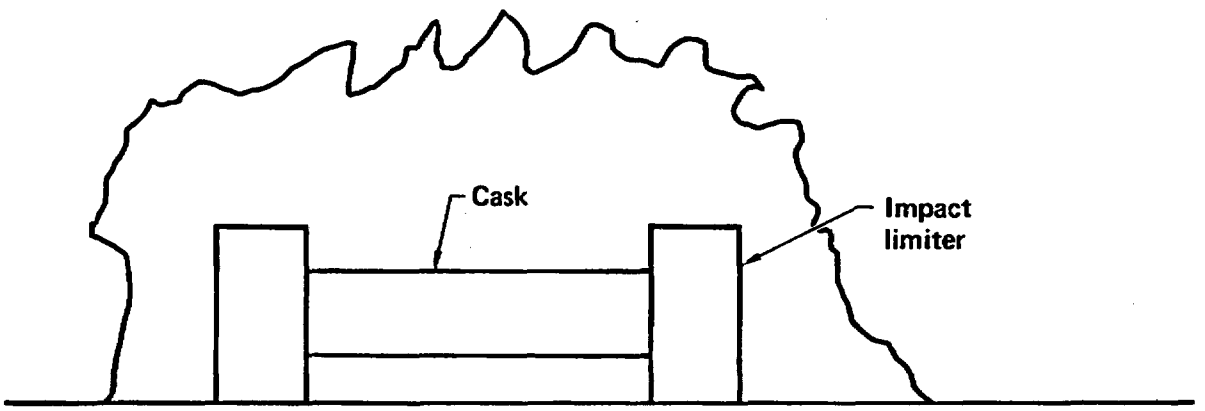

a) Three-dimensional cask fire model

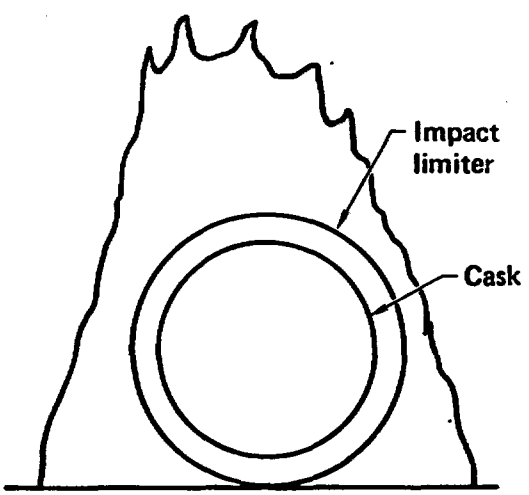

b) Two-dimensional cask fire model

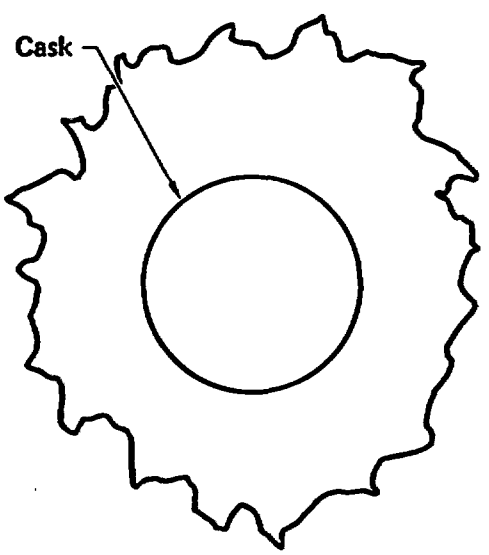

c) One-dimensional cask fire model

Figure F-1 Fire modeling of casks.

In a real engulfing fire, the spent fuel cask is partially shielded from the heat by either the transport vehicle or the ground. In real fires the amount of heat transferred to the cask differs significantly from that from a hypothetical totally engulfing fire, represented by the one-dimensional (1-D) model in Fig. F-1(c).

The role of convection from the flame may be significant for cases in which the cask is enclosed within or very near the flame while on either the ground or the vehicle. There does not appear to be sufficient experimental evidence to formulate any general rule to evaluate convection coefficients in this geometry. Also the flame temperature can vary significantly along the diameter of the cask. A common analytical approach is to consider the flame to be isothermal, with a single value for emissivity and a conservatively high temperature to attempt to account for the convective effects, since these are the most highly variable and difficult effects to measure and to model.

In the case of engulfing fires, the radiative heat load from an isothermal fire to the cask can be calculated as follows:[F.3]

$$\dot{Q}_r = \sigma A_s \, C_{s-f}(T_f^4 - T_{s,o}^4) \qquad \text{(F.1)}$$

where

$\dot{Q}_r$ = radiant heat load per unit length and time, Btu/ft-hr

σ = Stefan-Boltzman constant , Btu/hr-ft^2-°K^4

C_{s-f} = configuration factor, unitless

A_s = area of cask exposed to flame, ft^2/ft

T_f = flame temperature, absolute, °R

$T_{s,o}$ = initial cask surface temperature, absolute, °R

For a real fire the configuration factor for two gray, diffuse bodies exchanging heat is given by:

$$A_s C_{s-f} = \frac{1}{\frac{1-\varepsilon_f}{\varepsilon_f A_f} + \frac{1}{A_s F_{s-f}} + \frac{1-\varepsilon_s}{\varepsilon_s A_s}} , \text{ ft}^2/\text{ft} \qquad \text{(F.2)}$$

where

A_f = area of flame involved, ft^2/ft

F_{s-f} = geometric view factor from cask to fire, unitless

ε_f = flame emissivity = 0.9, unitless

ε_s = cask surface emissivity = 0.8, unitless

and all other terms are as previously defined.

If it is assumed as shown in Fig. F-1(b) that no significant fire exists below the horizontal centerline and within the diametral dimension of the cask, the geometric view factor from the cask to the fire below the centerline for one side of the lower portion of the cask is given by:

$$(A_s F_{s-f})_B = \frac{\pi r}{4} , \text{ ft}^2/\text{ft} \qquad \text{(F.3)}$$

where

r = radius of cask, ft

for a 2-D infinitely long cylinder. The area-configuration factor calculated using Equation F.2 is:

$$(A_s C_{s-f})_B = \frac{2\pi}{\frac{1-\varepsilon_f}{\varepsilon_f} + \frac{2}{\pi}\left(\frac{1+\varepsilon_s}{\varepsilon_s}\right)} \text{ , } ft^2/ft \qquad (F.4)$$

Assuming that the cask is completely engulfed by the fire above the centerline, the area-configuration factor above the centerline is given by:

$$(A_s C_{s-f})_A = \pi r \bar{\varepsilon} \text{ , } ft^2/ft \qquad (F.5)$$

where

$$\bar{\varepsilon} = \text{effective emissivity} = \frac{1}{1/\varepsilon_f + 1/\varepsilon_s - 1} \text{ .}$$

Adding the results of Equations F.4 and F.5 together, the total area-configuration factor for a real fire is:

$$(A_s C_{s-f})_T = \frac{2\pi}{\frac{1-\varepsilon_f}{\varepsilon_f} + \frac{2}{\pi}\left(\frac{1+\varepsilon_s}{\varepsilon_s}\right)} + \pi r \bar{\varepsilon} \text{ , } ft^2/ft \qquad (F.6)$$

A hypothetical regulatory engulfing fire is shown as a 1-D fire in Fig. F-1(c). The regulatory fire is defined as having a fire temperature of 1475°F, a flame emissivity of 0.9, and a fire duration of 0.5 hour. The area-configuration factor for the regulatory fire is:

$$(A_s C_{s-f})_T = 2\pi r\bar{\varepsilon} \quad , \ ft^2/ft \tag{F.7}$$

Then the ratio of the heat load of real fires to a hypothetical uniform fire is the ratio of Equations F.6 and F.7:

$$\frac{\dot{Q}_r}{\dot{Q}_h} = \frac{\left[\frac{1-\varepsilon_f}{\varepsilon_f} + \frac{2}{\pi}\left(\frac{1+\varepsilon_s}{\varepsilon_s}\right)\right]^{-1}}{r\bar{\varepsilon}} + 1/2 = 0.78 \tag{F.8}$$

for the same flame emissivity of 0.9, cask surface emissivity of 0.8, fire temperature, and cask surface temperature.

Based on Equation F.8, a higher flame temperature is required for the cask to absorb the same amount of heat for a real fire compared to a hypothetical fire. As derived in Section F.5, the hypothetical regulatory fire with a fire temperature of 1475°F generates the same heat load on a cask as a 1700°F real fire. The reference fire conditions are defined to be the 1700°F real fire that generates the same heat load as the regulatory fire. The 1-D model (Fig. F-1(c)) can be used to approximate the 2-D model (Fig. F-1(b)) provided that the heat loading conditions are appropriately accounted for.

F.4 Cask Temperature Response to Regulatory and Reference Fire Conditions

The transient thermal response of a representative truck and rail cask to an engulfing reference fire was analyzed using TAC0.[F.1] A 1-D model of the casks engulfed by the regulatory fire simplifies the calculation and predicts reasonably well the thermal response of the major volume of the casks. This model is used to estimate the cask response to the reference 1700°F real fire engulfing a cask. Figure F-2 shows the geometry of the modeled casks.

The initial temperature distribution within each cask from heat generated by the spent fuel was established before subjecting the cask to the modeled

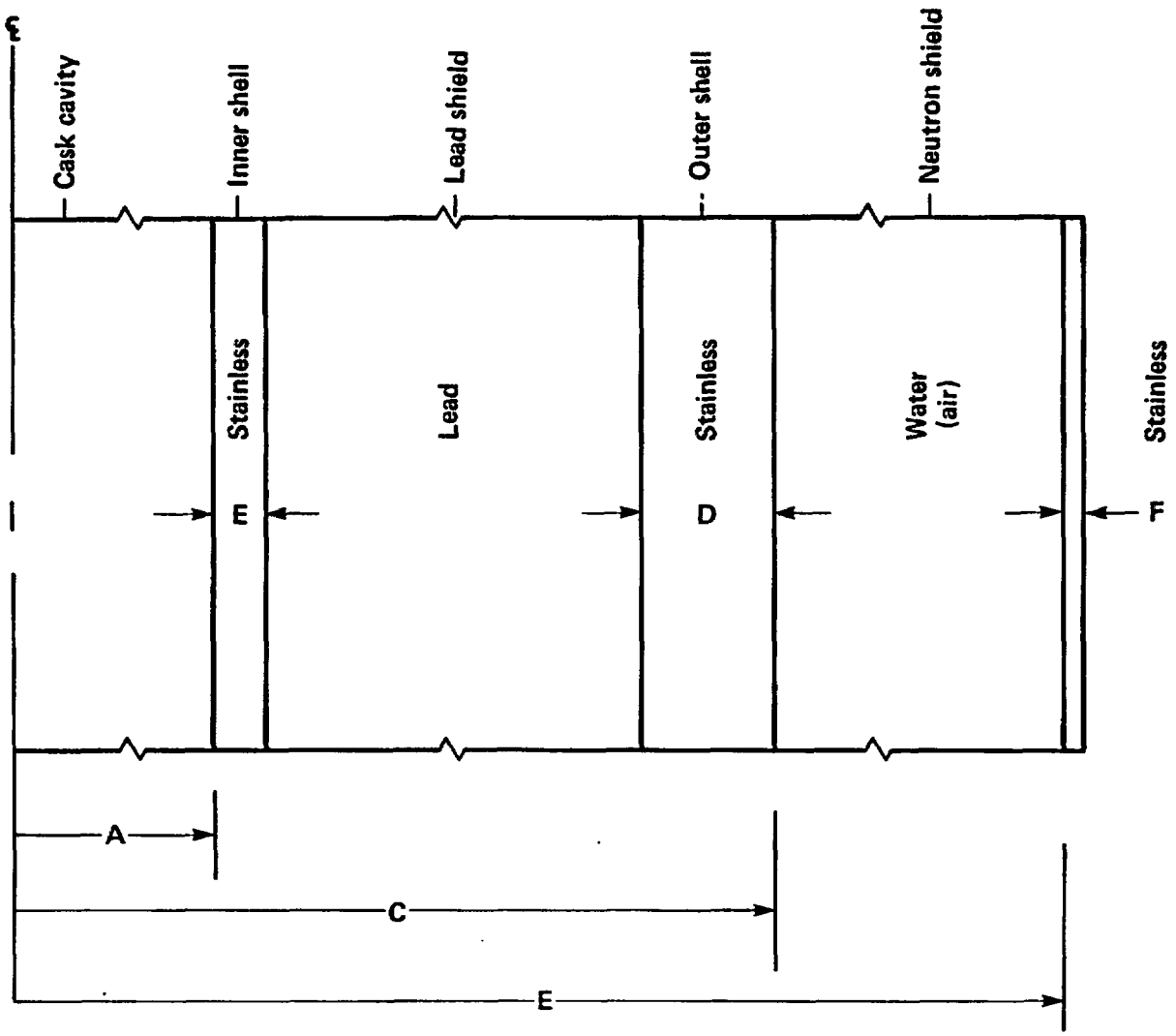

Dimension	Truck cask (in.)	Rail cask (in.)
A	6.75	30.00
B	0.50	1.50
C	13.75	38.00
D	1.25	2.50
E	18.25	42.50
F	0.25	0.25

Figure F-2 Modeled cask dimensions for TACO input.

fire environment. The steady-state evaluation was performed using TACO, with the assumption that the neutron shield tank is filled with water. The heat transfer through the water is by conduction and natural convection. A convenient way to model the natural convection is through the use of an effective conductivity for the water. Holman gives a relationship for effective conductivity of a fluid in a horizontal cylindrical annulus as:[F.4]

$$\frac{k_e}{k} = C(Gr_\delta \, Pr)^r, \text{ unitless} \qquad (F.9)$$

where

k_e = effective thermal conductivity, Btu/hr-ft-°F,

k = thermal conductivity, Btu/hr-ft-°F,

Gr_δ = Grashof Number = $\frac{g\rho^2\beta\delta^3\Delta T}{\mu^2}$, unitless

Pr = Prandtl Number, unitless

g = gravitational constant, ft/sec^2

β = volume coefficient of expansion, 1/°F

δ = annulus width, ft

ρ = density, lb/ft^3

μ = dynamic viscosity, lb/sec-ft

ΔT = temperature difference across annulus, °F

$$r = 0.29 \text{ for } 6 \times 10^3 \leq GrPr < 10^6$$

$$0.20 \qquad 10^6 \leq GrPr < 10^8$$

$$C = 0.11 \text{ for } 6 \times 10^3 \leq GrPr < 10^6$$

$$0.40 \qquad 10^6 \leq GrPr < 10^8.$$

This expression was evaluated over the expected temperature range, and an average value of effective conductivity of water as a function of bulk temperature was used.

Table F.1 tabulates the material thermal properties used in the analysis. Table F.2 lists the internal heat assumed for the fuel assemblies within the two casks. A uniform value of 1.0 Btu/hr-ft^2-°F was used to represent natural convective heat removal from the cask surface.

The results of the steady-state analysis for the casks show a surface temperature of 147°F for the truck and 242°F for the rail cask.

For the regulatory fire, only radiation heat transfer occurs. The heat flux from a hypothetical engulfing fire on the surface of the cask due to radiation heat transfer is given by:

$$q = \sigma\tilde{\varepsilon}(T_f^4 - T_s^4) \text{ , Btu/hr-ft}^2 \qquad \text{(F.10)}$$

where

T_s = cask (neutron shield) surface temperature, absolute, °R

and all other terms are as previously defined.

It is next assumed that before being engulfed by fire, the water leaks out of the neutron shield tank. Heat transfer in the annulus is now through the combined modes of radiation across the gap and convection and conduction

Table F.1
Material Thermal Properties

Stainless Steel
Density 494.2 lb/ft^3

Temperature (°F)	Thermal Conductivity (Btu/hr-ft-°F)	Specific Heat (Btu/lb)
50	7.92	0.107
250	8.64	0.11
500	9.72	0.120
750	10.86	0.133
1000	12.06	0.138
1250	13.5	0.144
1500	14.46	0.150
2372	16.92	0.170

Lead
Density 708.5 lb/ft^3
Melt Point 621.5°F
Latent Heat 10.25 Btu/lb

Temperature (°F)	Thermal Conductivity (Btu/hr-ft-°F)	Specific Heat (Btu/lb)
50	19.97	0.031
250	19.2	0.032
619	10.4	0.0332
1500	8.64	0.034
1832	8.64	0.0328

Water
Density 62.43 lb/ft^3
Specific Heat 1.0 Btu/lb°F

Temperature (°F)	Eff. Thermal Conductivity (Btu/hr-ft-°F)
104	2.76
140	3.01
176	3.25
212	3.46
284	4.34

Table F.2
Internal Heating from Fuel Assemblies

	Heat Load (KBtu/hr)
Truck Cask	6.82
Rail Cask	71.4

through the air. As in the case for water, the same relationship holds, but a single value of effective thermal conductivity of the air as a function of bulk temperature can lead to serious errors. The equation for total heat transfer in the annulus is:

$$q_{an} = \frac{\sigma(T_s^4 - T_i^4)}{\frac{1}{\varepsilon_i} + \frac{d_i}{d_o}\left(\frac{1}{\varepsilon_o} - 1\right)} + \frac{2K_e(T_s - T_i)}{d_i \ln(d_o/d_i)}, \text{ Btu/hr-ft}^2 \qquad \text{(F.11)}$$

where

d_i = neutron shield inner diameter, ft

d_o = neutron shield outer diameter, ft

K_e = effective air thermal conductivity, Btu/hr-ft-°F

T_i = neutron shield inner diameter temperature, absolute, °R

and all other terms are as previously defined.

Solving this equation over the entire expected temperature range for both surfaces of the annulus and then using an interval halving technique results in a constant value for the effective air thermal conductivity, with a maximum root-mean-square error in the total heat transferred of less than 2.5%, for equal surface emissivities between 0.3 and 0.5.

The temperature response of the representative truck cask was calculated for the regulatory fire with a flame temperature of 1475°F, a flame emissivity of 0.9, and a cask surface emissivity of 0.8. The temperature at the middle of the lead shield thickness is plotted in Fig. F-3. The cask temperature reaches 500°F (T_1) in 1.08 hours and 600°F (T_2) in 1.35 hours. As the lead mid-thickness temperature increases beyond the 600°F (T_2) level, the lead at

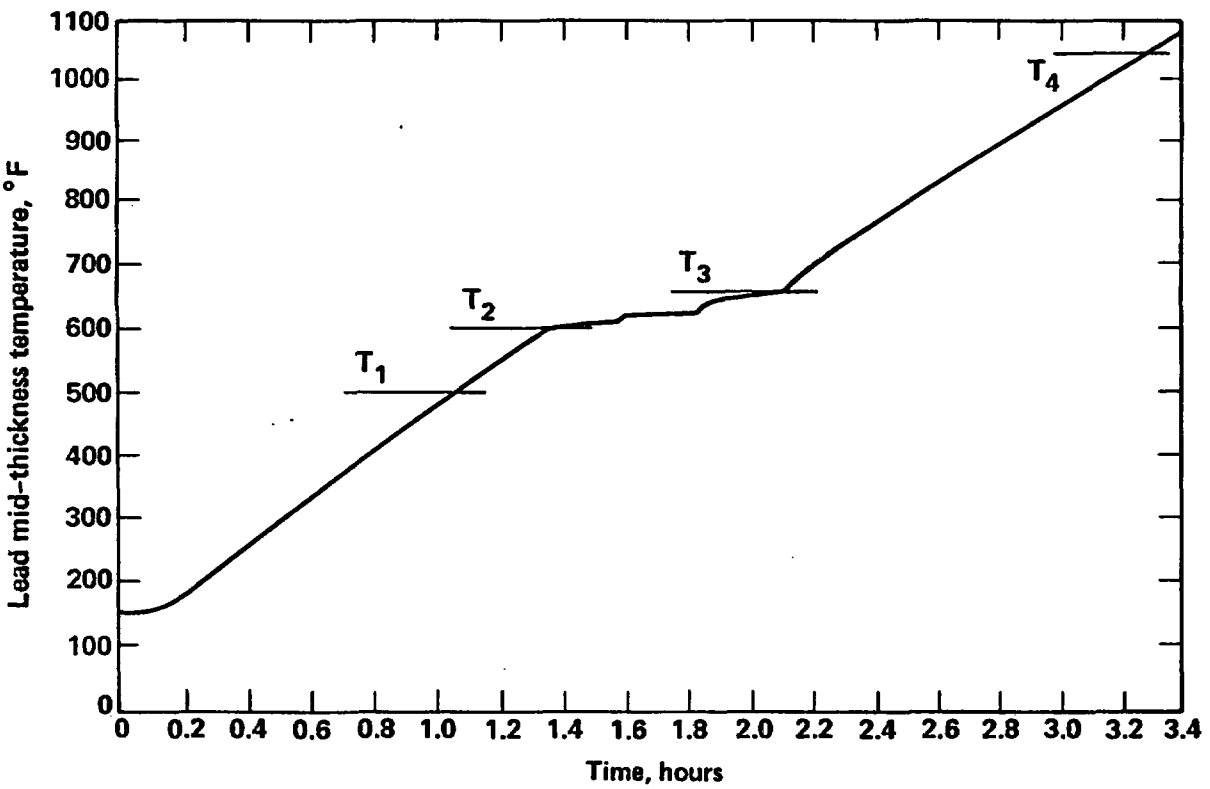

Figure F-3 Lead mid-thickness temperatures for truck cask versus duration of regulatory fire.

the outer shell starts to melt. The lead melts at the inner shell in 2.1 hours as the mid-thickness temperature reaches 650°F (T_3). The 1050° temperature (T_4) level is reached in 3.3 hours.

The temperature response of the representative rail cask was also calculated for the hypothetical engulfing fire. The temperature at the middle of the lead shield thickness is plotted in Fig. F-4. The cask temperature reaches 500°F (T_1) in 1.35 hours, and 600°F (T_2) in 1.8 hours. As the lead mid-thickness temperature of the lead increases beyond the 600°F (T_2) level, the lead at the outer shell starts to melt. The lead melts at the inner shell in 2.6 hours as the mid-thickness temperature reaches 650°F (T_3). The 1050°F temperature (T_4) level is reached in 5.1 hours.

These temperature response and heat flux results for the regulatory fire were used to evaluate real fires.

F.5 Cask Response to a Spectrum of Real Fire Conditions

In order to calculate the thermal response of a cask to a real engulfing fire, certain fire parameters are required. The principal parameters required are fire temperature, flame emissivity, convection velocities, and fire duration. These fire parameters depend upon variables that include type of fuel, amount of fuel, the fuel-air mixture, fire geometry, local temperatures, humidity, and wind conditions. Based on the information provided, the fire temperatures range from 1400 to 2400°F, flame emissivities range from 0.4 to 1.0, and convection velocities range from nearly 0 to 20 feet/second.[F.5-F.10]

The initial heat flux from a hypothetical engulfing fire on the surface of the cask is given by:

$$\dot{q} = \sigma\tilde{\varepsilon}(T_f^4 - T_{s,o}^4) + h\,(T_f - T_{s,o})\ ,\ \text{Btu/hr-ft}^2 \qquad \text{(F.12)}$$

where

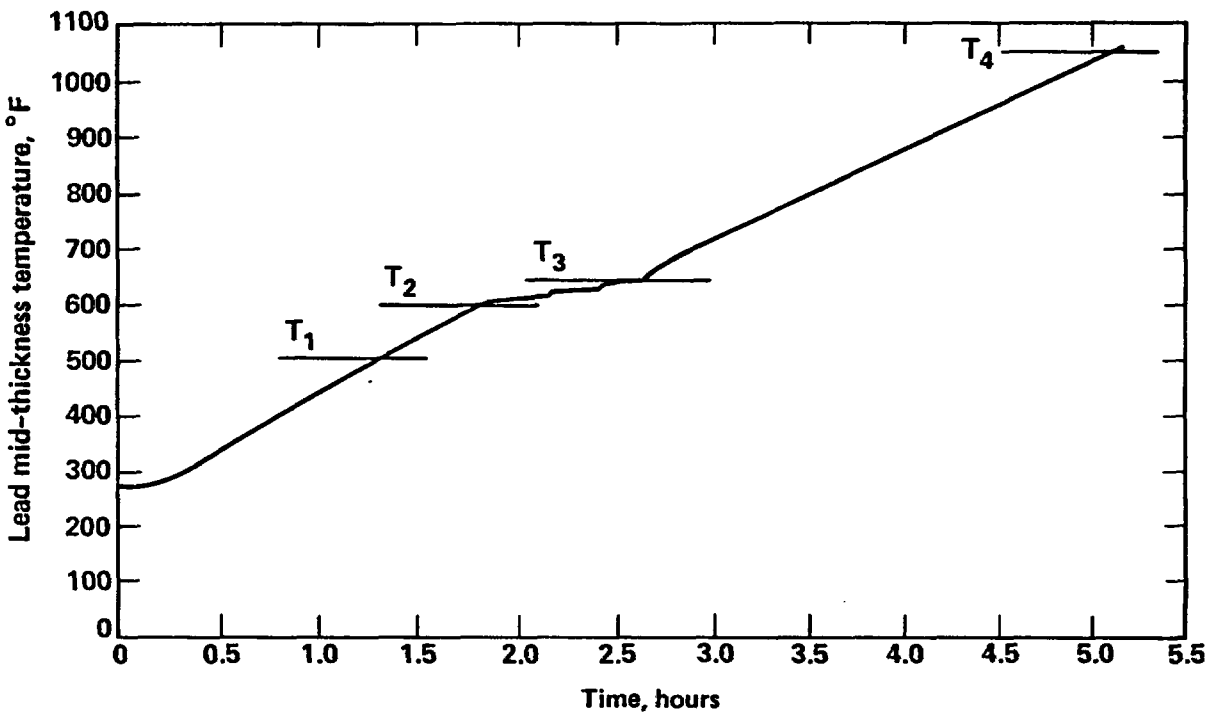

Figure F-4 Lead mid-thickness temperatures for rail cask versus duration of regulatory fire.

h = convective heat transfer coefficient, Btu/hr-ft^2-^{o}F

and all other terms are as previously defined.

Experimentally determined values for the convection heat transfer coefficient in an engulfing fire have been determined.[F.7] The values given for an 8.53 inch diameter cylinder range from 5.2 to 15.8 Btu/hr-ft^2-^{o}F as a perimeter mean. These values can be scaled within the scaled Reynolds Number by the following relationship:

$$h = h_{ref}\left(\frac{d_{ref}}{d}\right)^{0.195} \text{, BTU/hr-ft}^2\text{-}^o\text{F} \qquad \text{(F.13)}$$

where

h_{ref} = reference convection heat transfer coefficient, Btu/hr-ft^2-^{o}F

d_{ref} = reference diameter = 8.53 inches,

d = diameter, inches

as long as the scaled Reynolds Number is within the range of applicability. The scaled Reynolds Number is given by:

$$R_e = Re_{ref}\left(\frac{d}{d_{ref}}\right)^{0.805} \text{, unitless} \qquad \text{(F.14)}$$

where

R_e = scaled Reynolds Number, unitless

Re_{ref} = reference Reynolds Number = 73,725.

The scaled values of the convection heat transfer coefficient are found to be:

3.9 to 11.9 Btu/hr-ft^2-°F for the truck cask,

and

3.3 to 10.1 Btu/hr-ft^2-°F for the rail cask.

Figure F-5 gives the initial heat flux on the surface of the truck cask as a function of flame temperature, flame emissivity, cask emissivity, and convection heat transfer coefficient. This figure provides a wide spectrum of fire conditions which can be related to the regulatory fire conditions in terms of initial heat fluxes. For example, from Fig. F-5, it is determined that an engulfing fire with a flame temperature of 1300°F, a flame emissivity of 0.9, a cask emissivity of 0.8, and a convection heat transfer coefficient of 5 Btu/hr-ft^2-°F generates the same initial heat flux to a cask surface as a regulatory fire. For these specific conditions, the initial response of the cask would be essentially the same as its initial response to a regulatory fire. The initial heat fluxes for a rail cask are similar.

A sensitivity study was performed to compare the response of the representative cask for different fire conditions and initial heat fluxes to the responses calculated for the regulatory fire. The initial heat flux to the cask when engulfed by a regulatory fire is:

q = 17,646 Btu/hr-ft^2 for the truck cask and

q = 17,510 Btu/hr-ft^2 for the rail cask.

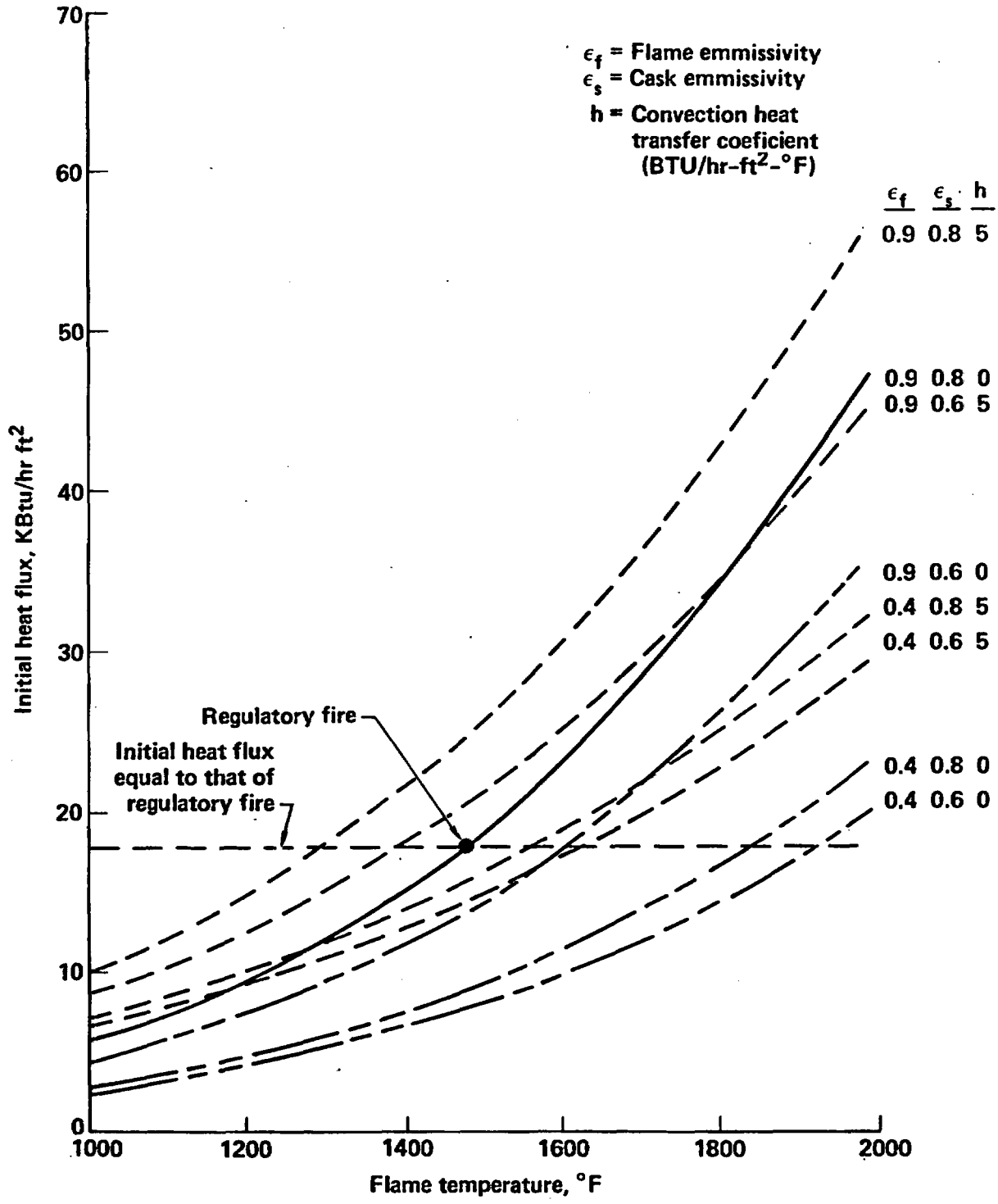

Figure F-5 Initial heat flux on truck cask for various fire conditions (1-D model).

The second fire for comparison was chosen arbitrarily, but within the limits of real fires. The flame temperature was chosen to be 1825°F, flame emissivity of 0.9, and a surface emissivity of 0.8. The initial heat flux to the cask is:

$q = 35{,}260$ Btu/hr-ft^2 for the truck cask and

$q = 34{,}650$ Btu/hr-ft^2 for the rail cask.

Thus the initial heat flux is about double that caused by the regulatory fire for each of the casks.

The variations of the heat flux for the regulatory and 1825°F fires are plotted in Fig. F-6 as a function of time for the truck cask. The heat flux drops rapidly and then decreases slowly because the water jacket acts as a thermal barrier. The heat fluxes after about 1 hour are reduced to 4,500 Btu/hr-ft^2 for the regulatory fire and 6,750 BTU/hr-ft^2 for the 1825°F fire. The integrated heat flux absorbed into the cask is plotted in Fig. F-7 for the regulatory and 1825°F fires. The integrated flux rises rapidly at first until the thermal barrier heats up and then limits the heat flux to the cask. The centerline temperatures for the lead shield are plotted in Figs. F-3 and F-8 for the regulatory and 1825°F fires, respectively. For the regulatory fire, lead melt starts after 1.35 hours and takes 0.75 hours to complete all the melting. As would be expected for the 1825°F fire with a heat flux 1.5 times higher than lead, melt starts at 0.9 hours and is completed after 0.5 hours or times which are 1.5 times shorter than the regulatory fire. The times to reach the melting temperatures and to melt the lead are actually determined when the total integrated heat flux values of approximately 6,000 Btu/ft^2 and 9,000 Btu/ft^2, respectively, are reached.

The cask heat-up rate and temperature are primarily determined by the heat flux from the fire because the heat from the fuel bundle is about 41 Btu/hr-ft^2. Therefore, it is concluded that the time it takes a specific fire to heat the cask to a specific temperature is approximately proportional to the average heat flux or heat load to the cask.

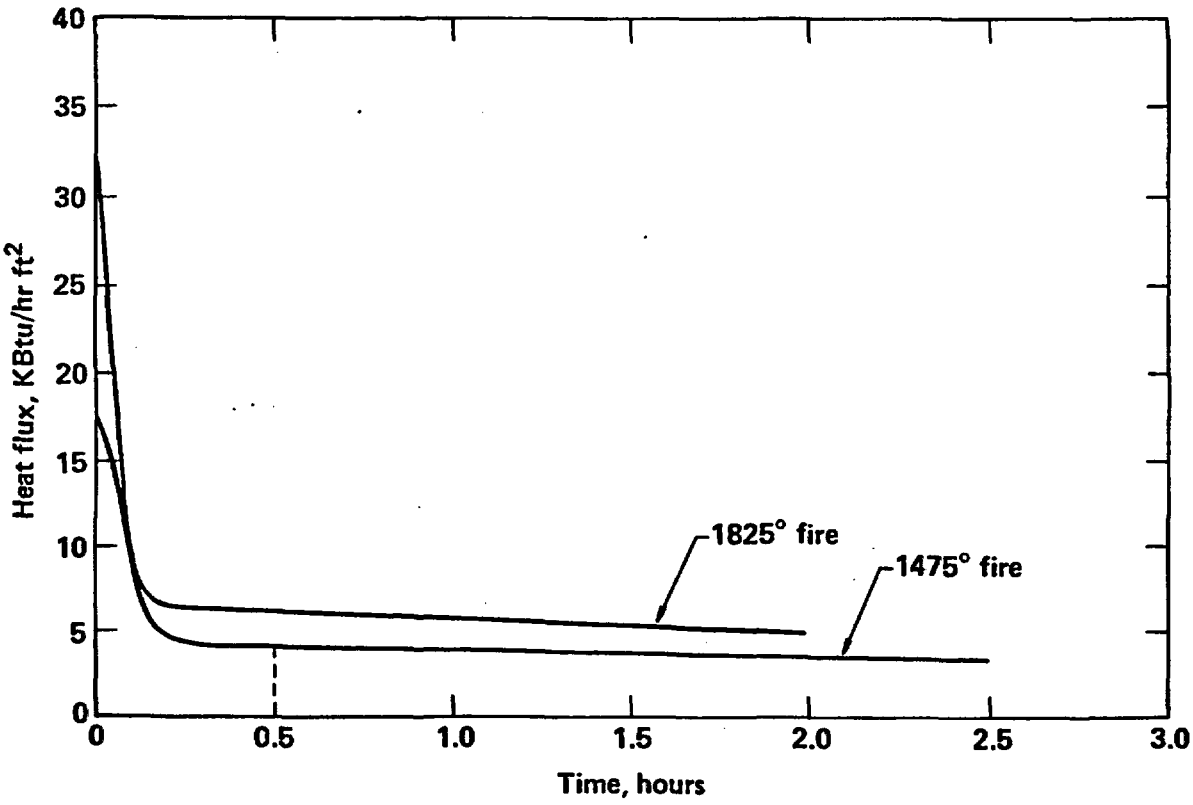

Figure F-6 Heat flux on truck cask versus duration of 1475°F and 1825°F fires.

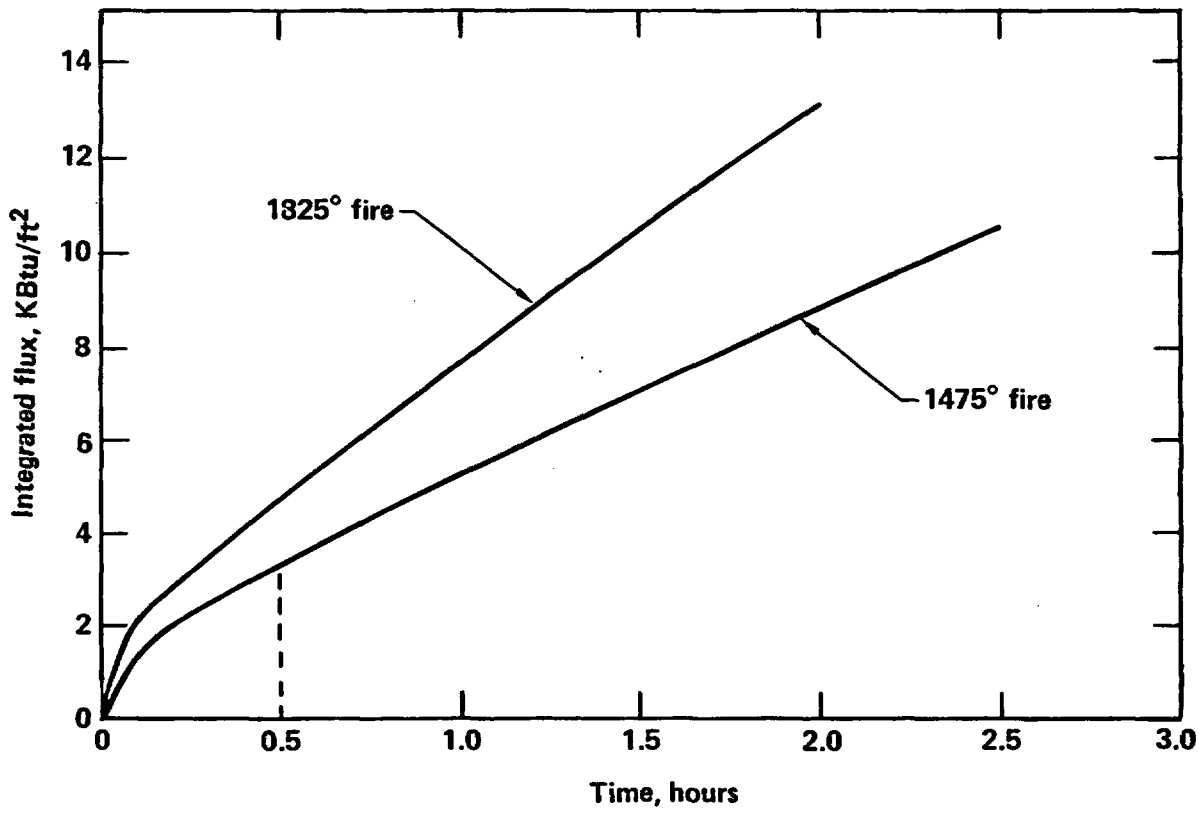

Figure F-7 Integrated heat flux on truck cask versus duration of 1475°F and 1825°F fires.

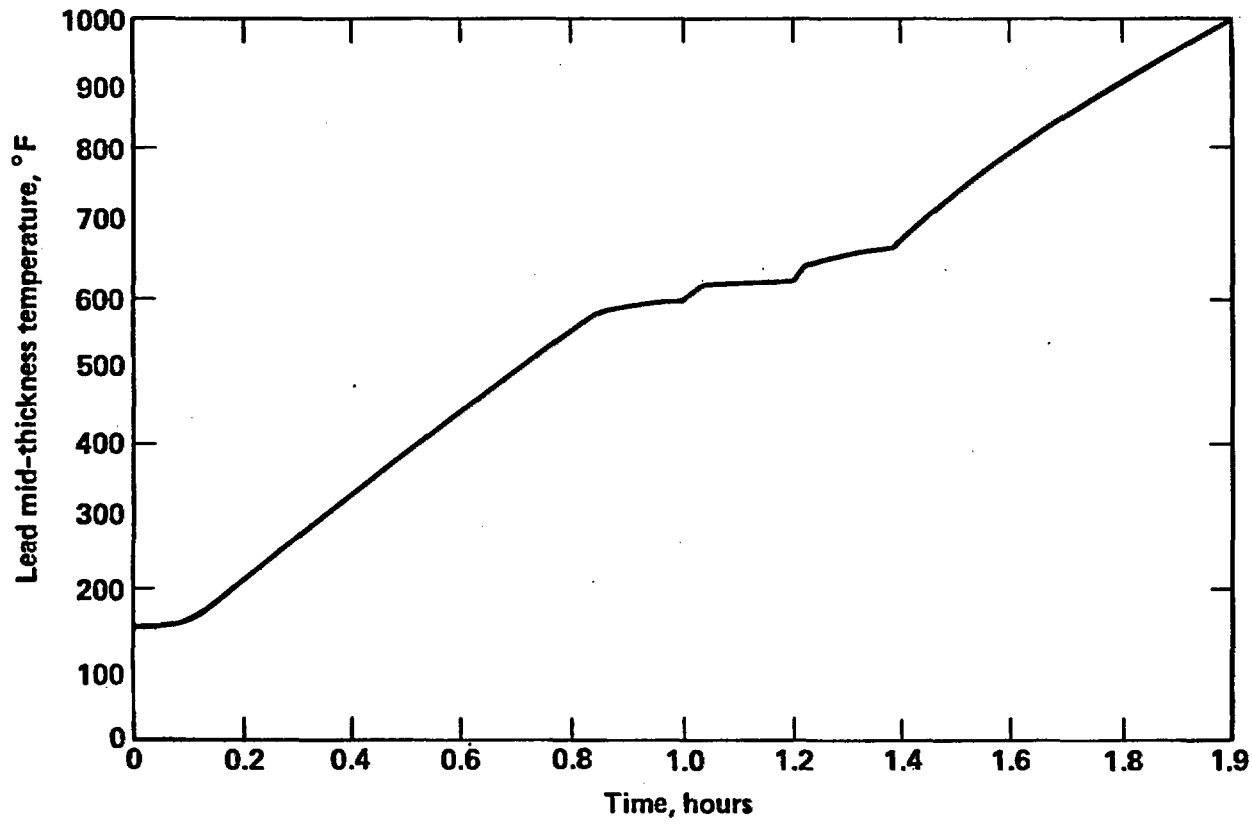

Figure F-8 Lead mid-thickness temperature for truck cask versus duration of 1825°F fire.

The transient thermal analysis for the rail cask was performed in a manner similar to that used for the truck cask. The variations of the heat fluxes for the regulatory and 1825°F fires are plotted in Fig. F-9 as functions of time. As with the truck cask case, the heat flux drops rapidly and levels off because the water jacket acts as a thermal barrier. The heat fluxes after about 1 hour are reduced to 4,500 Btu/hr-ft^2 for the regulatory fire and 7,000 BTU/hr-ft^2 for the 1825°F fire. These results are similar to those calculated for the truck and indicate that these heat flux values apply to a wide range of cask sizes. The cask will heat up at a rate determined by the heat flux from the fire. The time to reach a particular temperature for the cask is determined by the heat flux. The centerline temperatures for the lead shielding are plotted in Figs. F-4 and F-10 for the regulatory and 1825°F fires, respectively. For the regulatory fire, the lead melting begins about 1.8 hours after the fire initiation and is complete at about 2.6 hours. For the 1825°F fire, the lead melt begins at 1.2 hours and is complete within 1.8 hours. These melting times are nearly proportional to the fire heat fluxes or heat loads.

In Fig. F-11, the heat flux on the surfaces of the truck and rail cask is plotted as a function of flame temperature, flame emissivity of 0.9, and cask emissivity of 0.8. The initial heat flux is given. Also, the average heat flux values are given at 1 hour durations for the 1475°F and 1825°F fires.

As derived in Section F.3, the heat load ratio of a real fire to a hypothetical fire is 0.78 for the same flame temperature. To absorb the same heat load per unit time from a real engulfing fire compared to a hypothetical engulfing fire, the average heat flux on the cask has to be increased. The required heat flux is 1.28 times higher for a real fire. From Fig. F-11 it is determined that a flame temperature of 1700°F is required to provide an average flux of 6,400 Btu/hr-ft^2 which is 1.28 times higher than the heat flux derived from regulatory conditions. Therefore, it is concluded that a 1700°F real fire provides a heat load to the cask and results in temperature responses similar to those for a 1475°F regulatory fire.

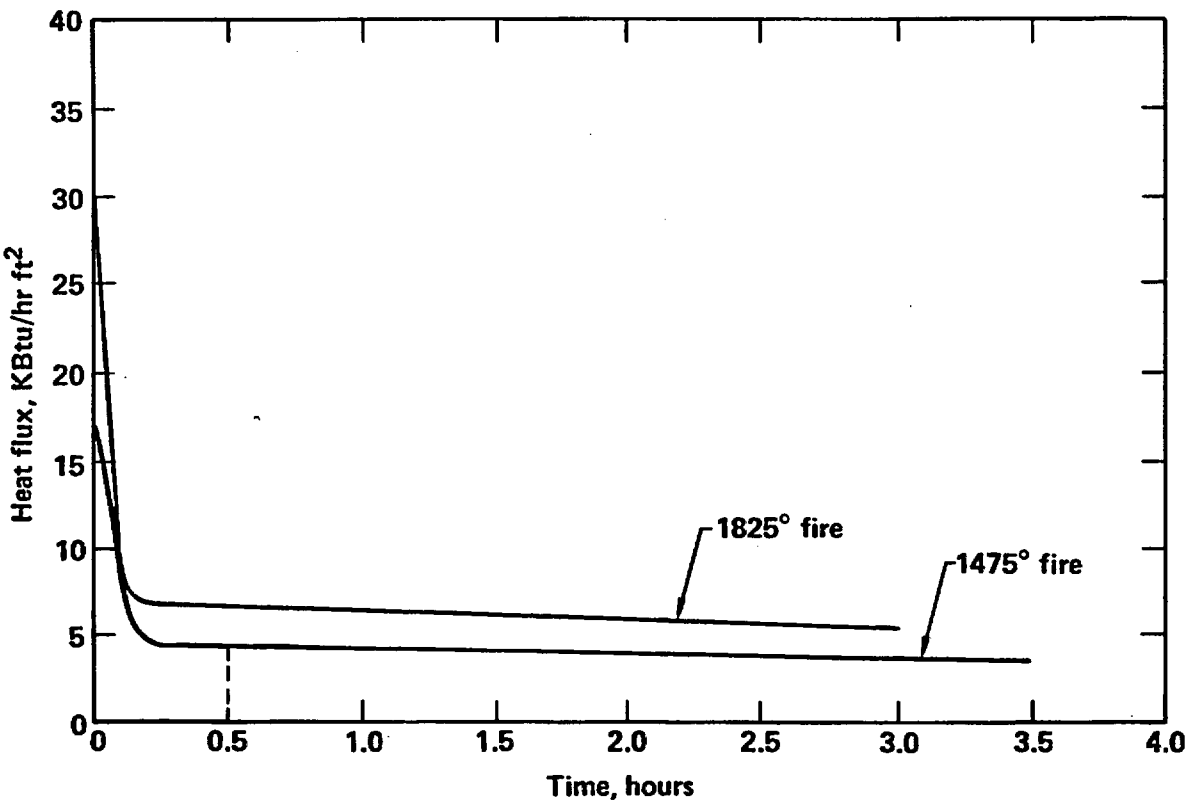

Figure F-9 Heat flux on rail cask versus duration of 1475°F and 1825°F fires.

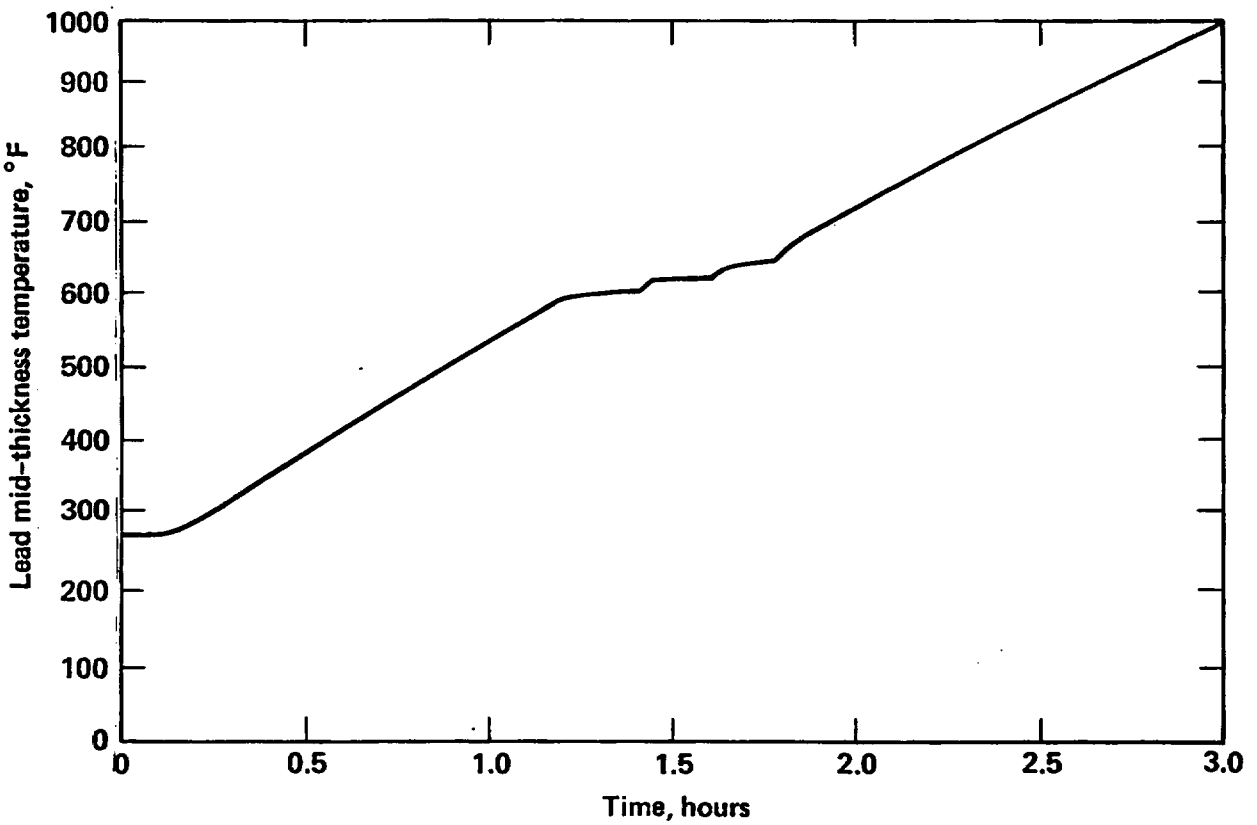

Figure F-10 Lead mid-thickness temperature for rail cask versus duration of 1825°F fire.

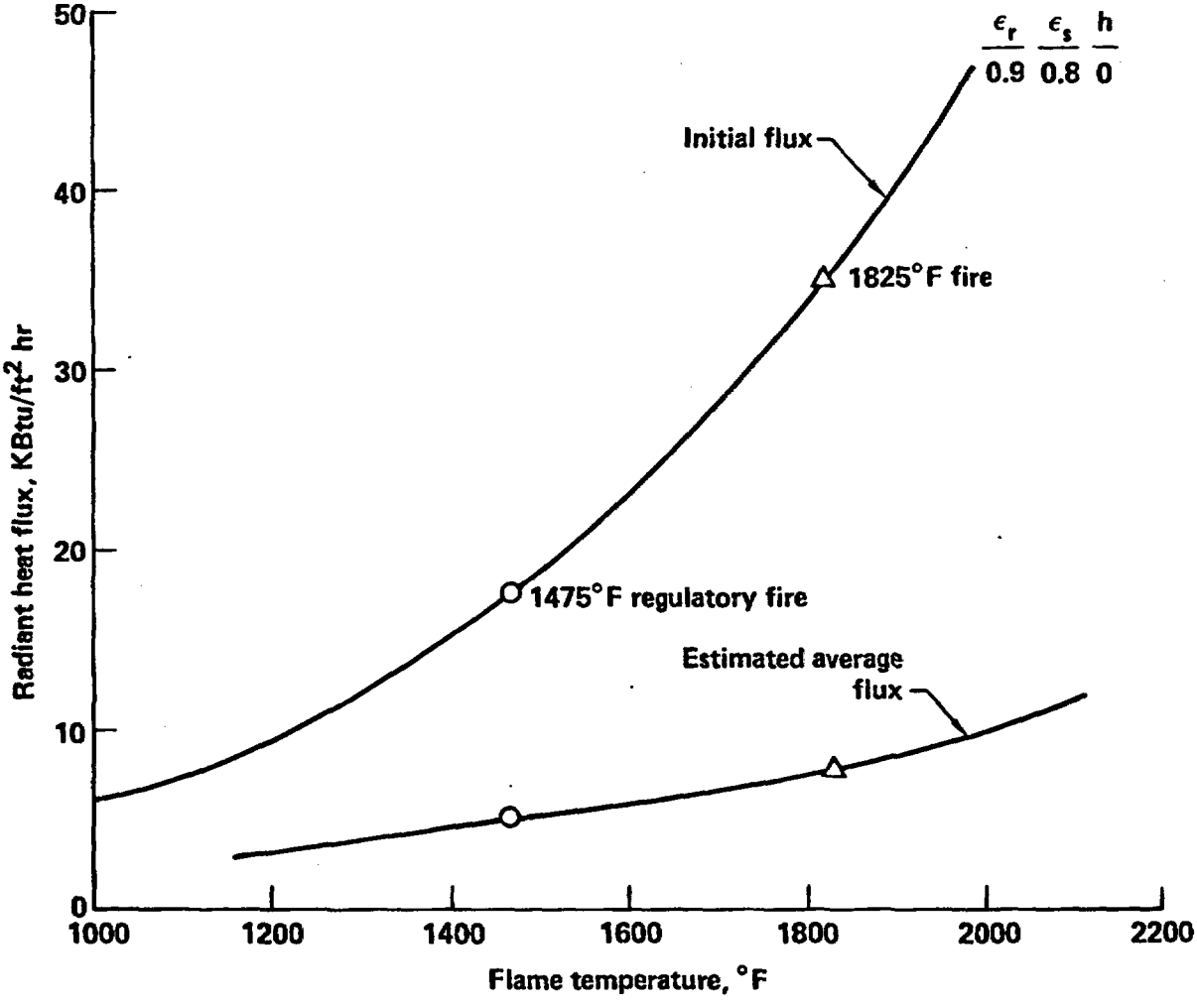

Figure F-11 Initial and average heat flux on truck and rail cask versus flame temperature.

The heat load to the cask also varies with the location of the fire with respect to the cask. For the case in which the flame front is just tangent to the cask, as shown in Fig. F-12, the geometric view factor to the part of the cask below the horizontal centerline is:[F.11]

$$A_s F_{s-f} = \frac{\pi r}{4} \text{ , } ft^2/ft \qquad (F.15)$$

The geometrical view factor to the upper portion of the cask is given by the relationship:

$$A_s F_{s-f} = \frac{r\delta}{2} \text{ , } ft^2/ft \qquad (F.16)$$

where

$\delta = \pi - 2 \tan^{-1}(\frac{r}{h-r})$, radians

h = flame height, ft

Finally, for the case in which the cask is removed a distance from the flame front as shown in Fig. F-13, the geometric view factor from the entire cask to the flame is given by:[F.11]

$$A_s F_{s-f} = r[\tan^{-1}(\frac{h-r}{x}) + \tan^{-1}(\frac{r}{x})] \text{ , } ft^2/ft \qquad (F.17)$$

where

x = separation distance, ft

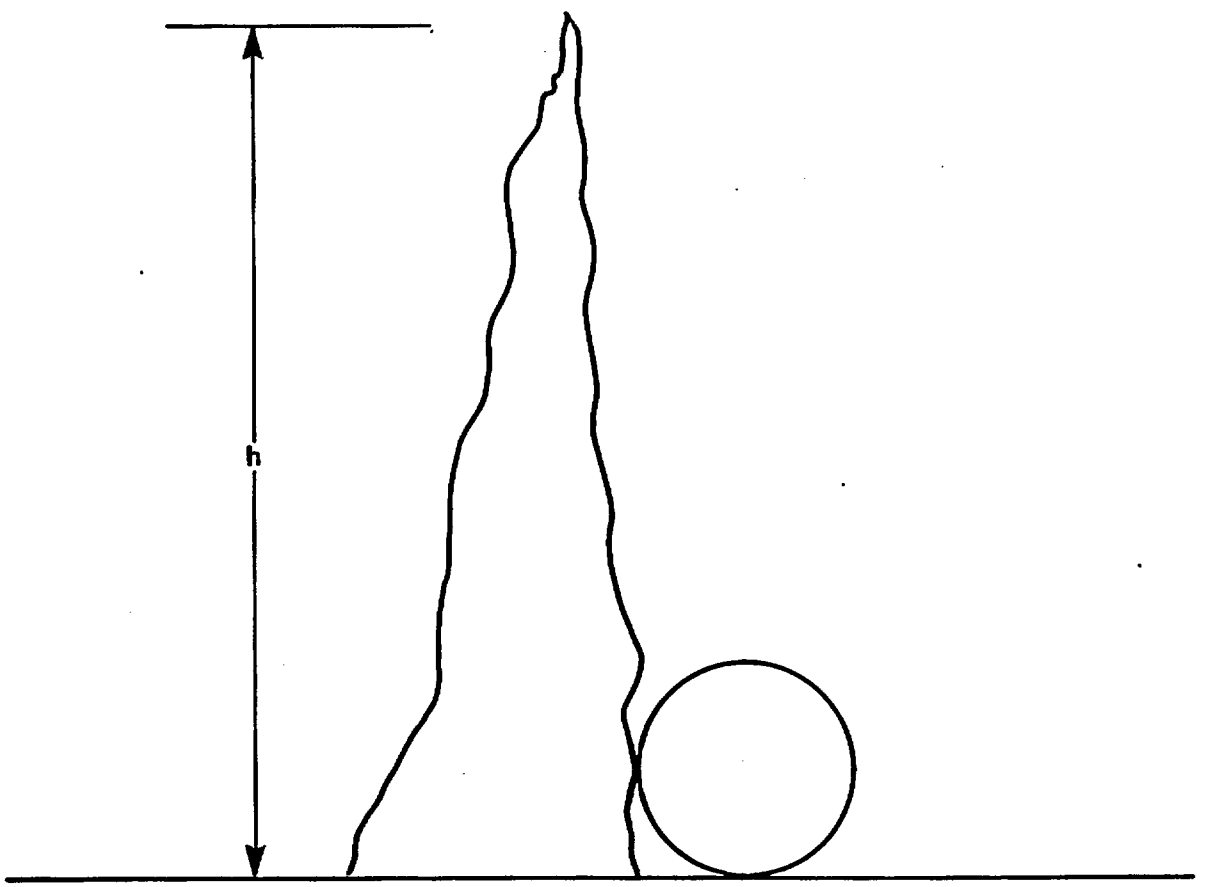

Figure F-12 Cask on ground with tangent flame front.

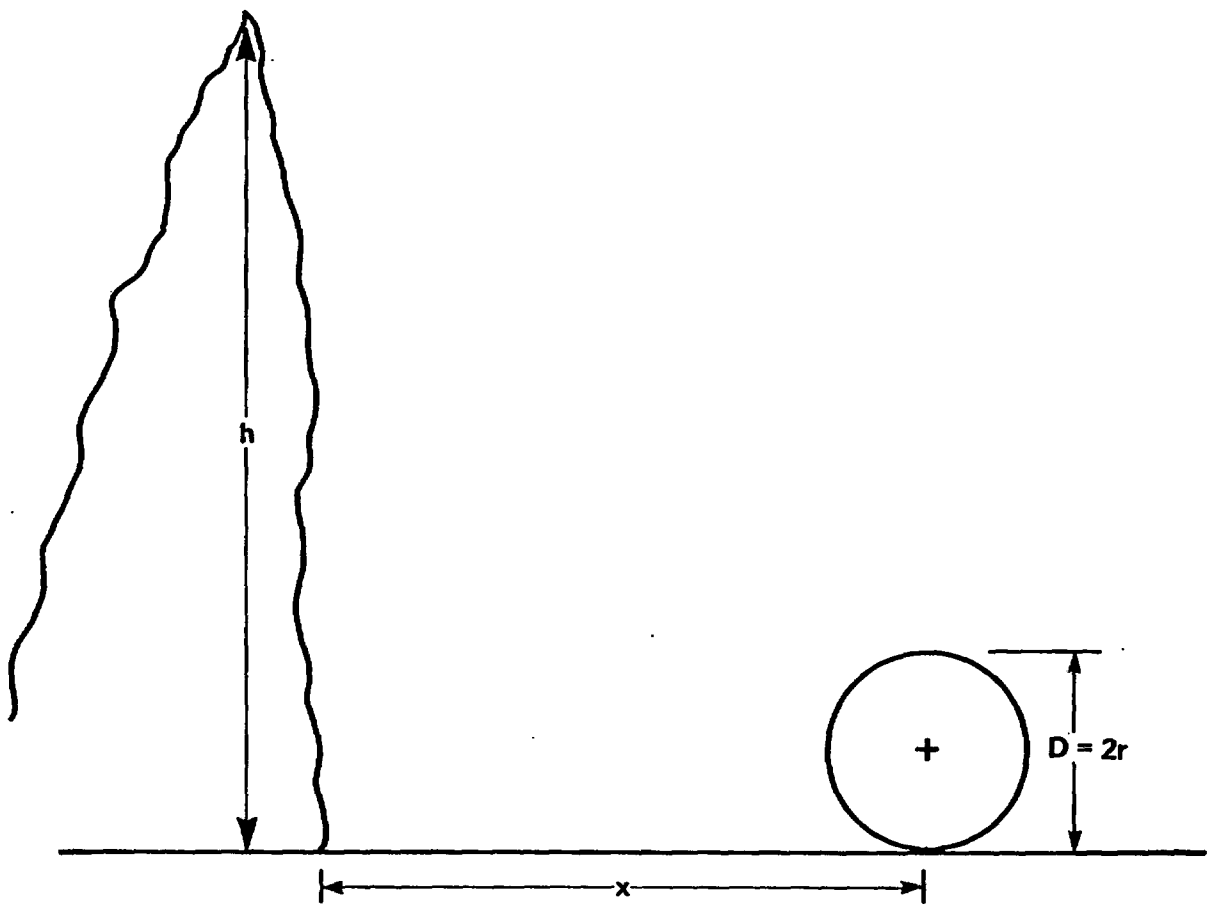

Figure F-13 Cask on ground--distant from flame front.

$$A_s = r(\pi + \psi) \text{ , } ft^2/ft$$

$$\psi = \tan^{-1}\left(\frac{h-4}{x}\right) - \tan^{-1}\left(\frac{r}{h^2 + x^2 - 2hr}\right) \text{ , radians}$$

and all other terms are as previously defined.

Evaluating these expressions over a range of distances relative to the cask diameter results in the family of curves for the heat load on the cask relative to the engulfing fire value versus the separation distance divided by the cask diameter as shown in Fig. F-14. The total heat load drops rapidly from the reference regulatory value as the distance from the fire increases. In addition at distances removed from the flame, a lower value of emissivity for the cask surface is likely since a blackening of the surface from soot in the flame is less probable, leading therefore to even lower heat loading. In addition to lower heat loading, the cask involved in a nonengulfing fire is able to reject heat by reradiation and natural convection to the environment.

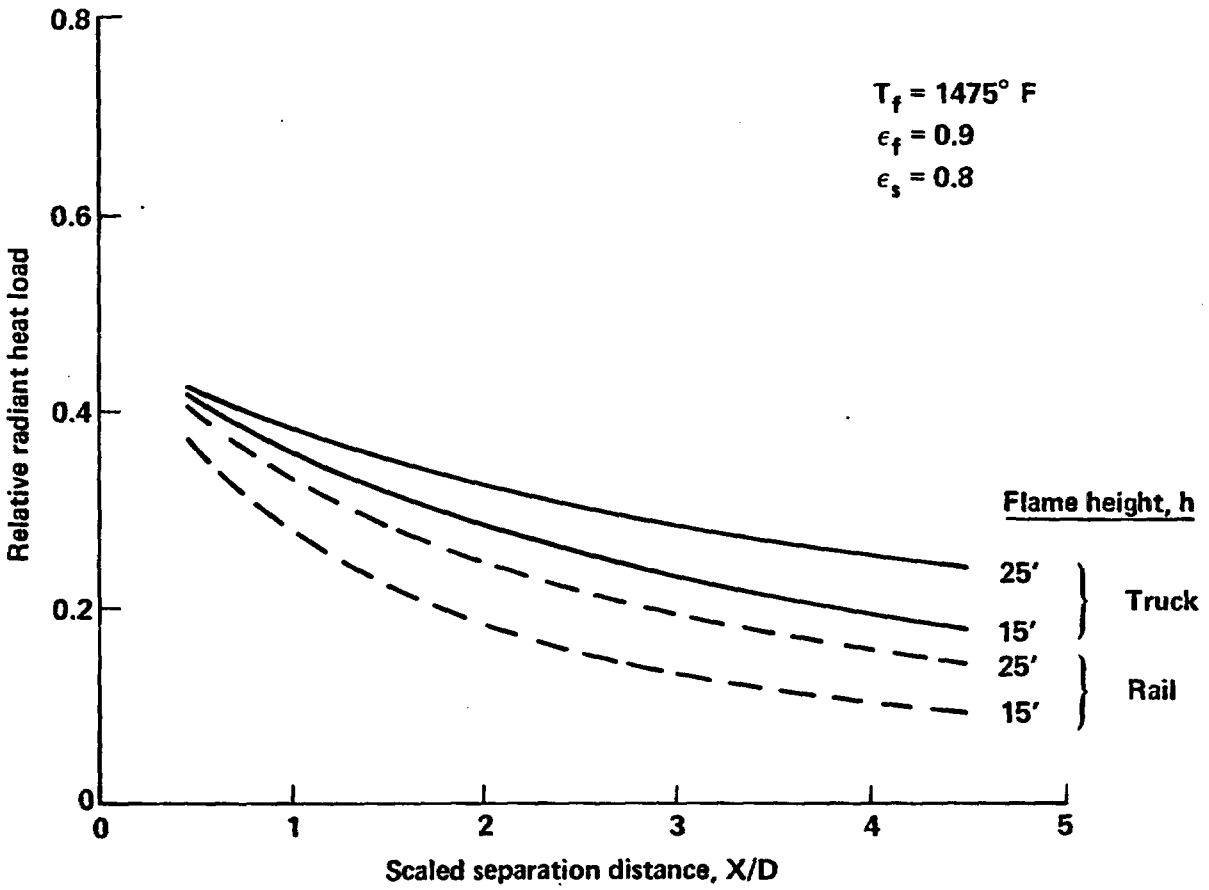

Figure F-14 Fraction of heat load from nonengulfing fires.

References

F.1 P. J. Burns, TACO-2D - A Finite Element Heat Transfer Code, Lawrence Livermore National Laboratory Report, Livermore, CA, UCID-17980, Rev. 2, January 1982.

F.2 M. G. Vigil, A. A. Trujillo, H. R. Yoshimura, HNPF Spent Fuel Cask Temperature Response; Torch Impinging on Water Filled Neutron Shield, Sandia National Laboratory, Albuquerque, NM, SAND82-0704, March 1982.

F.3 W. H. McAdams, Heat Transmission, McGraw-Hill, New York, NY, 1954.

F.4 J. P. Holman, Heat Transfer, McGraw-Hill, New York, NY, 1976.

F.5 R. K. Clarke, et. al., Severities of Transportation Accidents, Sandia National Laboratory, Albuquerque, NM, SLA-74-001, July 1976.

F.6 Final Report on Assessment of Rail Cask Performance in Railroad Accident Environments, Ridihalgh, Eggers and Associates, Columbus, OH, June 1977.

F.7 L. H. Russel, and J. A. Canfield, "Experimental Measurement of Heat Transfer to a Cylinder Immersed in a Large Aviation-Fuel Fire", Journal of Heat Transfer, August 1973.

F.8 B. E. Bader, "Heat Transfer in Liquid Hydrocarbon Fuel Fires", Proceedings-International Symposium for Packaging and Transportation of Radioactive Materials, January 1965.

F.9 B. Hagglund, and L. Persson, The Heat Radiation from Petroleum Fires, FOA Report C 20126-d6(A3), Forsvarets Forskningsanstalt, Huvudenhet 2, July 1976.

F.10 L. Orloff, and J. de Ris, Froude Modeling of Pool Fires, Technical Report FMRC J. I. OHON3.BU RC81-BT-9, Factory Mutual Research, October 1983.

F.11 R. Siegel, and J. R. Howell, Thermal Radiation Heat Transfer, McGraw-Hill, New York, NY, 1972.

APPENDIX G
Probability Estimation Techniques

G.1 Introduction

Assessment of the probability of the potential responses of a cask to various accident scenarios depends on (1) the description of the distributions of the accident parameters given an accident, and (2) integration of these probability distributions over the appropriate subranges of values of the accident parameters. An important accident parameter is the velocity of the transporting vehicle, either truck or train, at the time of the accident. The distribution of vehicle velocities at the point of an accident is unknown; however, there are data which can be used to estimate the distribution of velocities either subjectively, as in the case of trucks, or recorded, as for trains. In Section G.2, a method of estimation, called maximum entropy, is described for developing the distribution of vehicle velocities using observed velocities at past accidents. This method was applied to both trucks and trains to develop estimates of the appropriate probability distributions of velocity. Given descriptions of the distributions of vehicle velocities and other accident parameters, assessment of the probability of potential cask responses involves integrating several probability functions. The integration process is described in Section G.3. Specifically, Section G.3 describes an approximation, based on sums of discrete probabilities, to the integration of the continuous distributions.

G.2 Maximum Entropy Method of Estimation

Given the historical data on velocities of vehicles involved in accidents, there are several methods, such as least squares, maximum likelihood, and density estimation, which can be used to estimate the probability distribution of velocities. Most methods require some identification of the form (family) of the probability distributions. Several distributions and mixtures of distributions were fitted to the accident data but no one family consistently fit all the data.

Since a specific parametric family of distributions was not readily identifiable, a reasonable approach is to evaluate a nonparametric estimate of the probability distributions of velocity. Although not as powerful, i.e., it has a greater uncertainty, the nonparametric approach allows the data to determine the form of the distribution of velocities rather than forcing the distribution to be of some specific type, e.g., normal or lognormal. If a specific distribution is used and it is not correct, then estimates of probabilities derived from the incorrect distribution can be biased significantly. Thus, we chose to estimate the distributions of velocity nonparametrically.

To determine a nonparametric estimate of the distributions of velocity, we based the estimates on the maximum entropy method of estimation. This approach is based on information theory and provides a procedure for estimating a probability distribution, with maximum entropy, consistent with the information available about a random variable. Subject to certain conditions and the appropriate interpretation of probability,[G.1] it can be shown that the entropy function

$$H(p_1, \ldots, p_K) = - \sum_{k=1}^{K} p_i \log p_i \qquad (G.1)$$

measures the amount of "uncertainty" represented by a probability distribution $(p_1, \ldots, p_K)$ for a variable X (where it is assumed that X is discrete and has range $x_1, \ldots, x_K$). Given some information about the distribution of X, such as its expected value and variation or uncertainty, a reasonable criterion for estimating the probability distribution $p_1, \ldots, p_K$ is to maximize the entropy function, (G.1), consistent with the information available, i.e., if μ_o, σ_o^2 are the expected value and variance, to estimate $p_1, \ldots, p_k$ such that

$$\sum_{k=1}^{K} x_k p_k = \mu_o$$

$$\sum_{k=1}^{K} (x_k - \mu_o)^2 \, p_k = \sigma_o^2 \tag{G.2}$$

That is, an estimate of the probability distribution $p_1, \ldots, p_K$ is the set of values $\tilde{p}_1, \ldots, \tilde{p}_k$ such that

$$H(\tilde{p}_1, \ldots, \tilde{p}_k) = \max_{(p_1, \ldots)} H \; (p_1, \ldots, p_K) \tag{G.3}$$

subject to the constraints

$$\sum_{k=1}^{K} p_k = 1$$

$$\sum_{k=1}^{K} x_k \, p_k = \mu_o$$

$$\sum_{k=1}^{K} (x_k - \mu_o)^2 \, p_k = \sigma_o^2 \; .$$

Introducing Lagrangian multipliers $\lambda_0, \lambda_1, \lambda_2$ associated with the three constraints, the estimated probabilities are

$$\tilde{p}_i = e^{-[\lambda_0 + \lambda_1 x_i + \lambda_2 (x_i - \mu_o)^2]} \tag{G.4}$$

where

$$\lambda_0 = \log \sum_{k=1}^{K} e^{-[\lambda_1 x_k + \lambda_2 (x_k - \mu_o)^2]} \tag{G.5}$$

and λ_1, λ_2 are solutions to the equations

$$\eta^{-1} \sum_{k=1}^{K} x_k \, e^{-[\lambda_1 x_k + \lambda_2 (x_k - \mu_o)^2]} = \mu_o \tag{G.6}$$

$$\eta^{-1} \sum_{k=1}^{K} (x_k - \mu_o)^2 \, e^{-[\lambda_1 x_k + \lambda_2 (x_k - \mu_o)^2]} = \sigma_o^2 \tag{G.7}$$

where

$$\eta = \sum_{k=1}^{K} e^{-[\lambda_1 x_k + \lambda_2 (x_k - \mu_o)^2]} \tag{G.8}$$

Thus, a discrete probability distribution can be constructed which maximizes entropy and which equals the specified mean and variance. In our application of the methodology, we used the mean and the variance of the historical data on velocities as the available information.

If the variable X is considered to be a continuous variable, i.e., its probability distribution has a density function, the estimated density function f(x) can be approximated, based on maximizing entropy, using the identity

$$dp = f(x)dx \quad . \tag{G.9}$$

Approximating the density function by a discrete relative histogram $[(\Delta p_k, \Delta x_k) : k=1, \ldots, K]$,

$$f(x_k) \simeq \frac{\Delta p_k}{\Delta x_k} . \tag{G.10}$$

However, in our notation $\Delta p_k = p_k$ and, assuming a partition of the (finite) range R_x of X into N equal subintervals of length Δx,

$$\Delta x = R_x/N \tag{G.11}$$

the maximum entropy estimate of $f(x_k)$ is

$$\tilde{f}(x_k) = \lim_{\Delta \to 0} \frac{e^{-[\Delta\lambda_0 + \Delta\lambda_1 x_k + \Delta\lambda_2 (x_k - \mu_o)^2]}}{R_x/N} \tag{G.12}$$

$$\simeq \frac{e^{-[\lambda_0 + \lambda_1 x_k + \lambda_2 (x_k - \mu_o)^2]}}{R_x/N}$$

for sufficiently small Δ.

The estimated probability distribution, as described by the estimated cumulative distribution function, is based on cumulative sums of the $\tilde{f}(x_k)$'s, interpolating for $x = x_k$. This is the method used to estimate the probability distributions for vehicle velocities prior to and at the point of an accident. The uncertainty of using the sample information for specifying μ_o and σ_o^2 was not quantified, nor was the sensitivity investigated for the predicted probabilities of the various response states. Some parametric

estimates of the distributions of velocities were analyzed, and these would provide some basis for an investigation of sensitivity.

G.3 Discretized Probability Integration

Estimation of the probability that the response of a cask to an accident is a specific response state, e.g., R(2,3), between 0.2% (S_1) and 2% (S_2) strain and between 600°F (T_2) and 650°F (T_3) lead mid-thickness temperature, is based on evaluating a pair of double integrals of probability distribution and density functions (see Equation 5.23). Some of the probability distribution and density functions are known analytically, but some, for example the distributions of velocities estimated by the method of maximum entropy, are only known numerically. In either case, the integration is complex and cannot be done analytically. Instead, evaluation of the estimated probabilities is based on the identity, given the appropriate conditions,

$$\int_a^b H(t)dt = \lim_{\Delta \to 0} \sum_{k=1}^{K(\Delta)} [H(t_k + \Delta_u) - H(t_k - \Delta_\ell)]\Delta t_k \qquad (G.13)$$

$$= \sum_{k=1}^{K(\Delta)} [H(t_k + \Delta_u) - H(t_k - \Delta_\ell)]\Delta t_k$$

for sufficiently small Δ . In this application, the function H(t) itself involves the integral of probability distributions and density functions.

The computer code TASP was developed to perform the necessary summations to approximate the probability integrals (in addition, the code contains all the appropriate probabilities). In each case the code partitions the range of integration into an appropriate number of subintervals to integrate over a probability distribution. When appropriate, the code conservatively evaluates a function at the upper (lower) limit of a subinterval to assure that the estimated probability is conservative. However, the estimate is not overly

conservative because a reasonable number of subintervals are used for the approximation. Thus, in the context of the inputs, the estimated probabilities are considered good estimates.

G.4 References

G.1 E. T. Jaynes, "Information Theory and Statistical Mechanisms", Physical Review, Vol. 106, No. 4, May, 1957, pp. 620-630.

APPENDIX H

List of Figures

APPENDIX H

Benchmarking for Computer Codes Used in Impact Analyses

H.1 Introduction

Several computer codes were used in the structural impact analyses to estimate cask responses for the various accidental impact loading conditions in this study. Impact is a governing loading condition in the cask structural evaluation. The results and conclusions stated in this report rely on the adequacy of these codes to estimate structural response. Impact is a loading condition which can generate large amounts of energy during a very short duration of impact. During the impact, energy changes form from potential into kinetic, and into strain energy. After the initial impact, the cask has a potential for bouncing back into the air depending on the target hardness and the property of impact limiters. Rigid body motion is involved during this process. In order to estimate the structural damage due to the second impact, i.e., the other end of the cask hitting the target after bouncing around in the air, the computer code needs to have a special capability of handling rigid body motion. Most of the finite element computer codes available today cannot handle the rigid body motion and, therefore, were not selected for this study. To assess cask response to the impact orientation, i.e., the angle between the cask longitudinal axis and the target surface, the selected computer codes need to have the capability of handling impact at an angle. Impact limiters play an important role in cask response. During impact, the limiter will enter a nonlinear region. The selected computer codes need to be capable of handling nonlinear impact-limiter responses.

The representative casks selected in this study use a lead layer for shielding. In order to model the lead behavior inside the inner and outer steel shells, the computer codes need to be capable of handling sliding between two surfaces of different materials. Not every computer code can satisfy all these specified requirements. Certain computer codes may be capable of meeting partial requirements. It is necessary that the user understands the limitations of the codes selected.

Three computer codes were selected to perform various types of impact analysis in this study. They are DYNA 2-D/3-D, NIKE 2-D/3-D (the 2D/3D designation indicating that either two-dimensional or three-dimensional modeling can be performed), and IMPASC (part of the SCAN system). All three codes were developed and maintained at Lawrence Livermore National Laboratory through other programs in the Laboratory. The limitations of each code are understood. During the course of calculating cask response, the analytical group worked very closely with the code development group. In many cases, the codes were modified to suit the specific needs of this study. There is high confidence that these codes were properly used within code capability in calculating cask response when subjected to impact loads. The qualifications of users is only part of the concerns in assuring adequate analytical solutions.

The next question is how can the selected computer codes simulate the impact conditions and the structural response. To answer this question, computer codes are generally benchmarked by comparing their results against one or more of the following: (1) results from closed form engineering solutions, (2) test data, and (3) other computer codes which have been benchmarked. This appendix presents benchmark codes for DYNA 3-D. The other codes, DYNA 2-D, NIKE 2D/3-D, and IMPASC have been benchmarked against DYNA 3-D, hence this benchmark test also generally applies to the other codes.

To date, these codes have not been benchmarked for predicting lead slump. Although at least one foreign country has performed impact tests with lead casks and used DYNA 2-D for benchmarking, these results are proprietary and cannot be disclosed. Therefore all of the calculations done in this study with DYNA and NIKE were performed assuming conservative lead properties and boundary conditions that over predict lead slump and the strain on the inner wall of the representative cask models.

H.2 Benchmark Calibrations for DYNA 3-D

H.2.1 Impact of Cylinder into Rail

The steel cylinder shown in Fig. H-1 is impacted into a long rigid rail at 1676 cm/sec. Attached to the ends of this cylinder are weights of 62.3 M dyne. An experimental test was conducted and the final configuration was measured.

One quarter of the cylinder was modeled by using DYNA 3-D with two planes of symmetry using the mesh illustrated in Fig. H-2. This mesh contains 3432 elements. Elastic-perfectly plastic behavior was assumed for the steel with a yield strength of 0.0131 Mbar.

Deformed shapes at approximately millisecond increments are shown in Fig. H-3. At 6.4 ms the cylinder can be seen to have completely rebounded with its final deformed shape. A maximum residual dent of 1.53 inches was calculated. A maximum dent of 1.44 inches was measured at the same location in an experimental test.

H.2.2 Nose Cone Analysis

Figure H-4 shows the DYNA 3-D mesh (6074 nodes, 4356 elements) used to model a steel (yield strength = 0.0048 Mbar, E_t = 0.0138 Mbar) nose cone that, on impact, has been designed by Sandia Laboratories in Livermore to limit the resultant force transmitted to the aft section.[H.1] The mass of the aft section is mocked with a high-density material, 131,477 gm/cm^3, in the top rows of elements.

This problem is interesting from a code development viewpoint because it exercises the sliding interface logic. Five interfaces are defined of which two are tied. The locations of these interfaces are depicted in Fig. H-5.

Deformed shapes at 3,000 μs intervals are shown in Fig. H-6. At 15,000 μs the peak deformation is reached and the nose cone begins to rebound.

Comparisons with experimental data from a static test showed excellent agreement with the calculation.[H.1] The final shape obtaining in the experiment was very close to the final computed shape. In Fig. H-7, the computed force deflection curve from DYNAP is compared to the experiment. Only minor discrepancies exist.

H.2.3 Oblique Impact of Rod

An aluminum rod 30.5 cm long and 0.638 cm in diameter impacts a rigid wall oriented at 10^{o} at a velocity of 20,170 cm/sec. The material behavior is simulated with material model 11 using the properties defined in UCRL-80465.[H.2] Fig. H-8 shows the DYNA 3-D calculational mesh.

The computed results showed good agreement with the experimental profiles up to 600 μs. At later times the experiments showed more curvature in the rod. Four factors probably contributed to these late time discrepancies.

- coarse zoning,
- inaccurate material properties,
- rigid wall approximation to armor plate,
- lack of interface friction.

Figure H-9 shows a sequence of deformed configurations. Figure. H-10 shows a view of 300 μs to illustrate the cross-sectional zoning. Figure H-11 shows the residual experimental profile for comparison to the computed result at 3,000 μs.

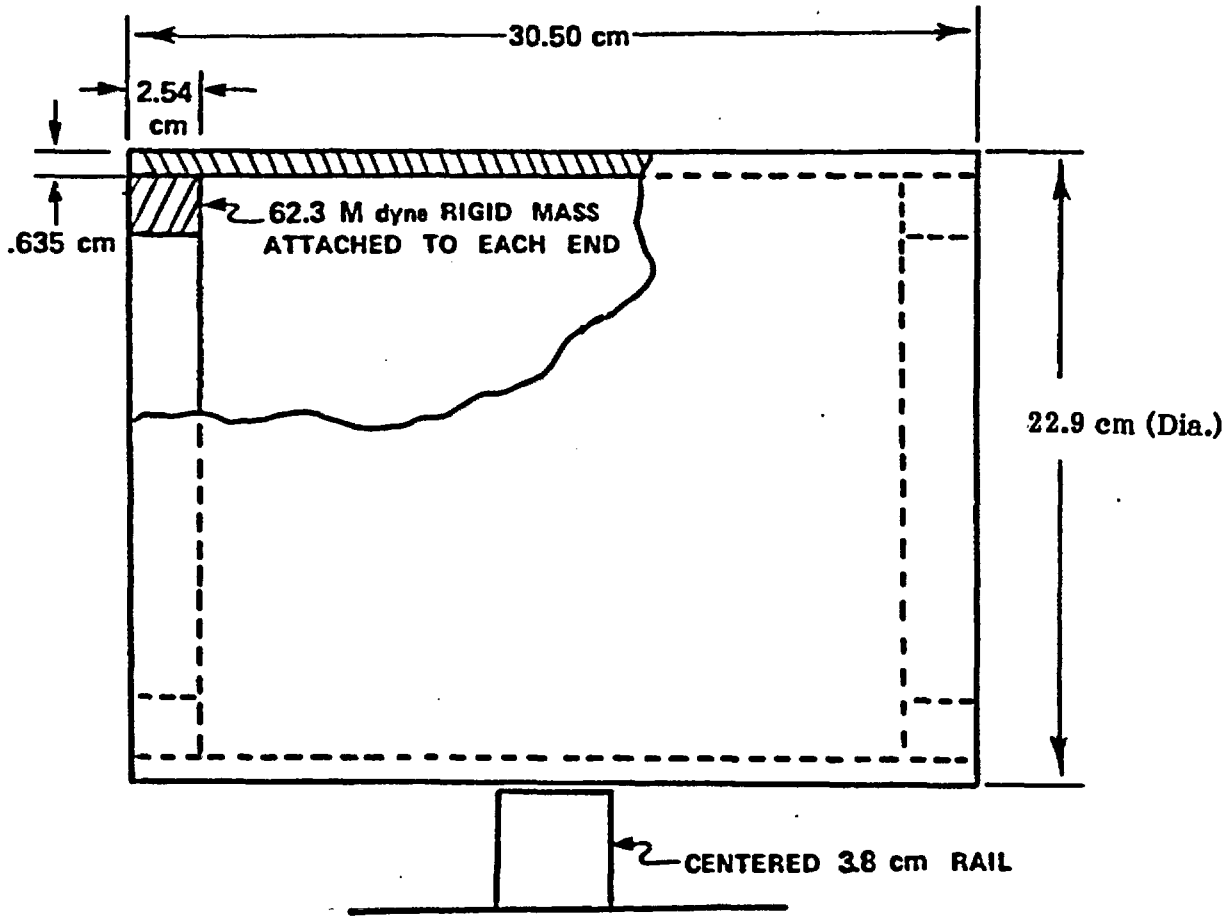

Figure H-1 Impact of weighted steel cylinder into a rigid rail.

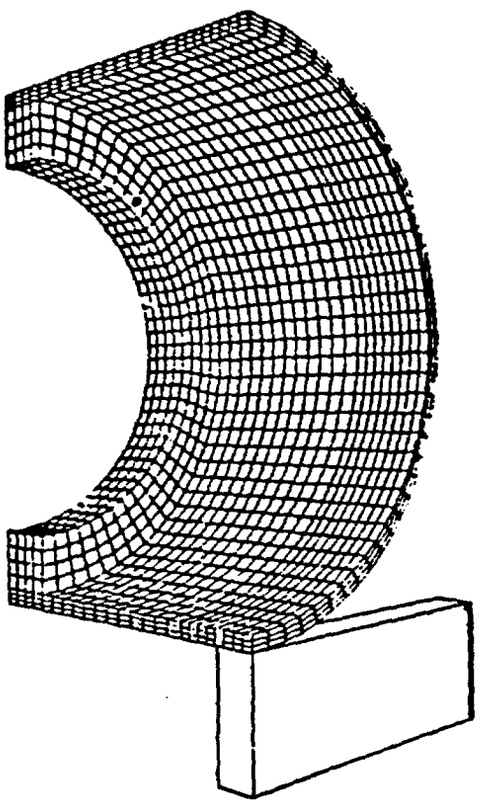

Figure H-2 Finite element mesh for one-quarter of the cylinders.

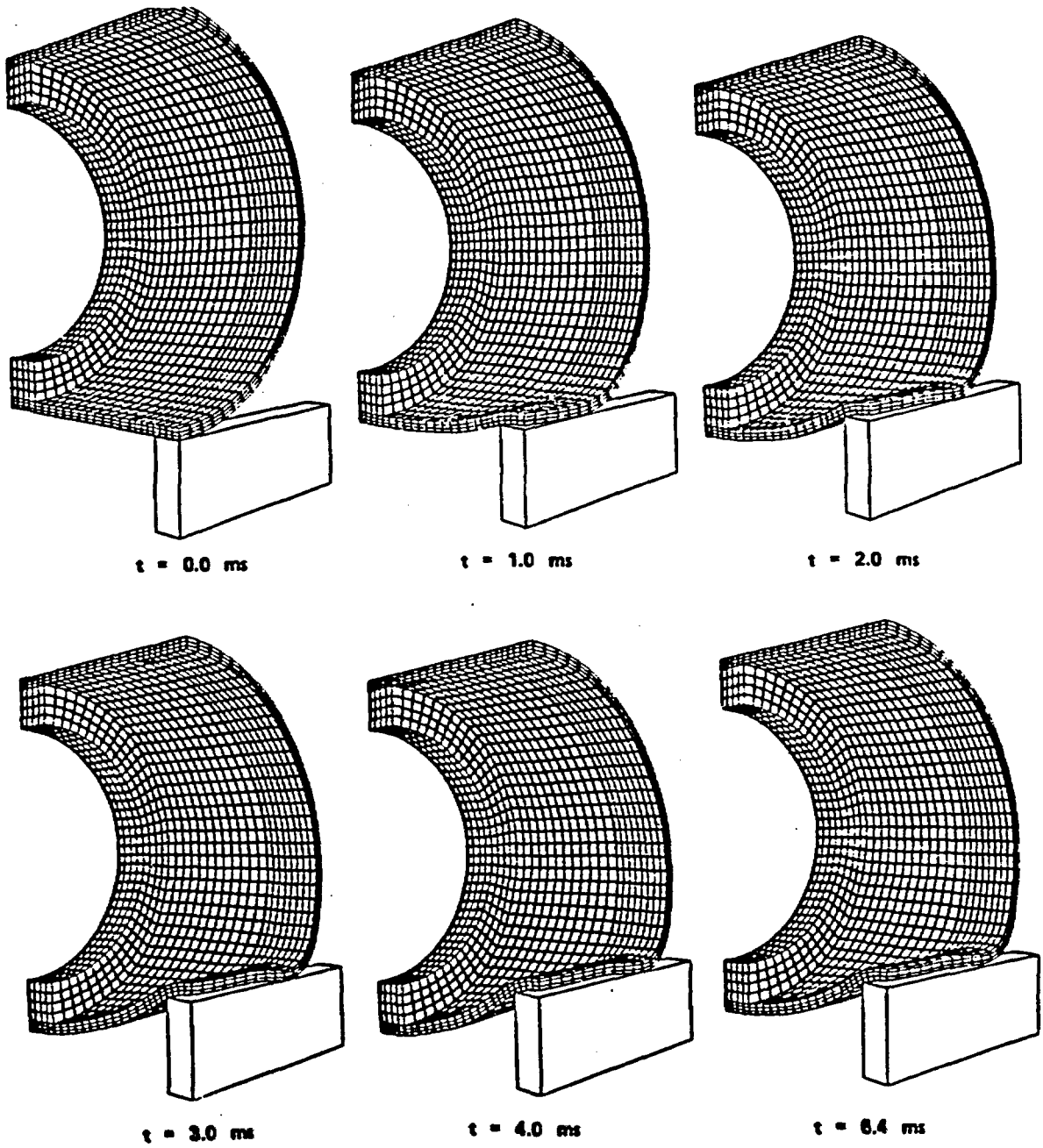

Figure H-3 Deformed shapes of the cylinder impacting a rail (DYNA 3-D analytical solutions).

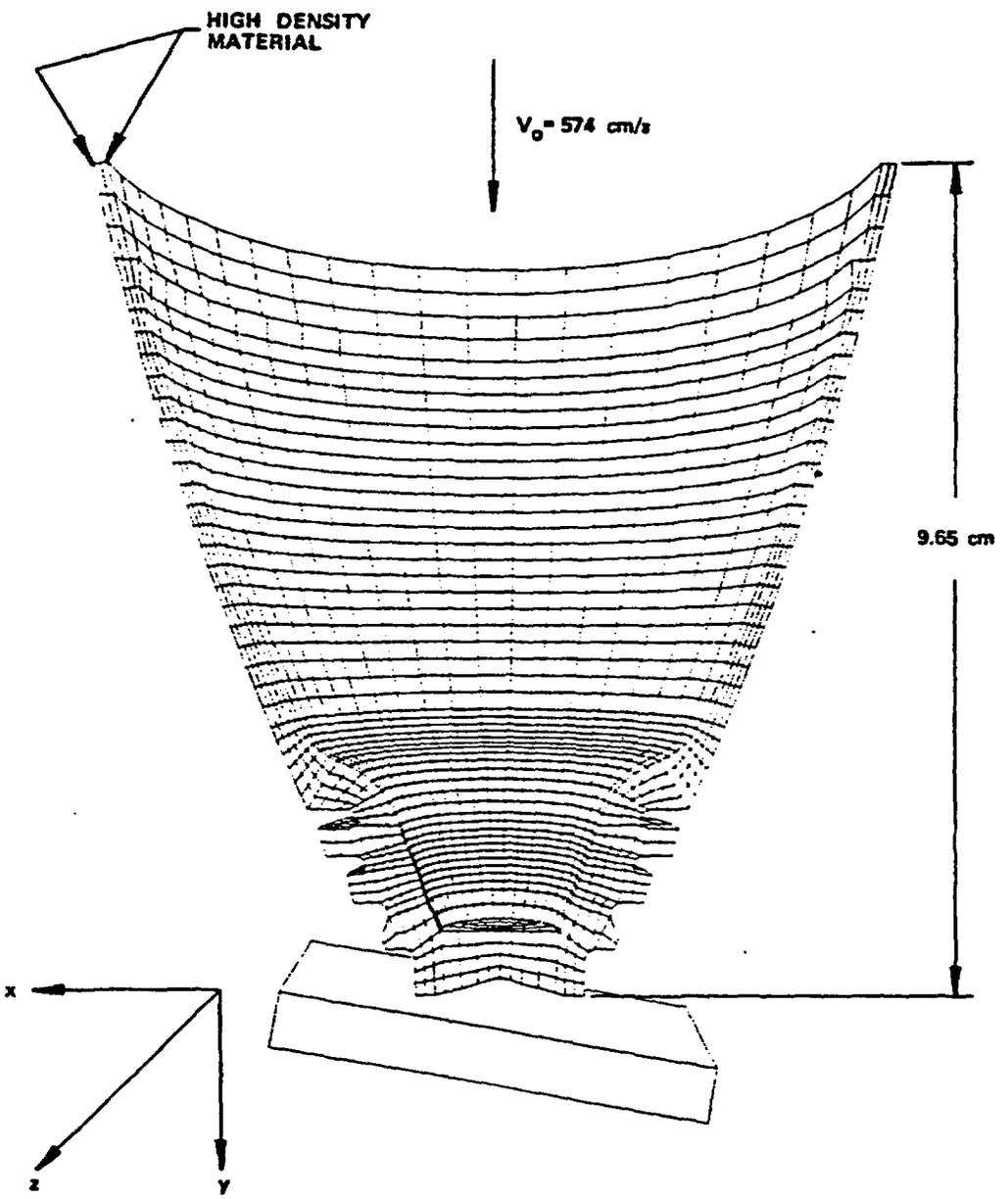

Figure H-4 Mesh of steel nose cone.

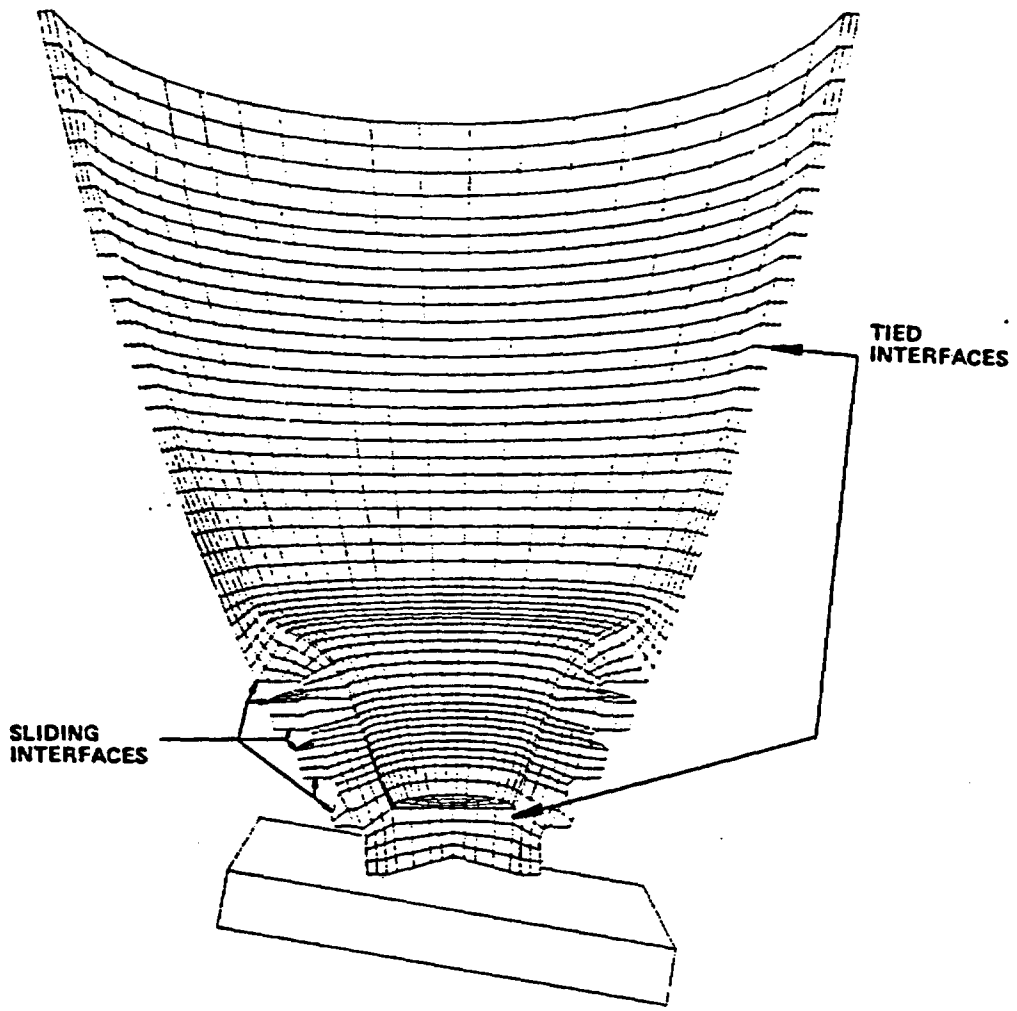

Figure H-5 Location of tied and sliding interfaces.

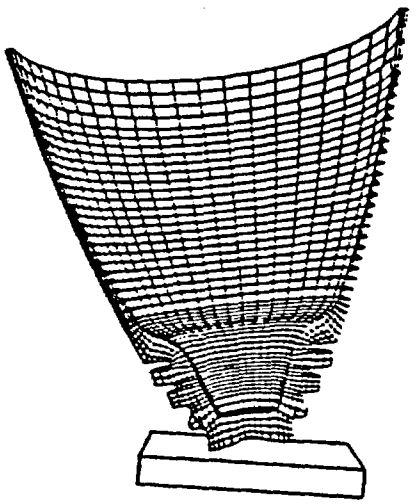

t = 0.0

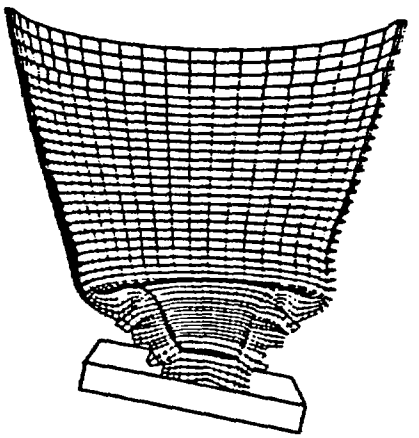

t = 3000 μs

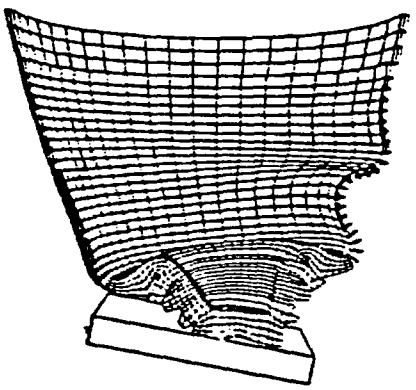

t = 6000 μs

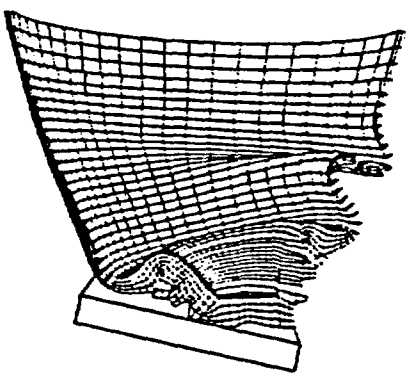

t = 9000 μs

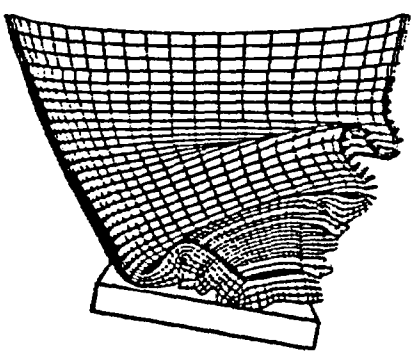

t = 12000 μs

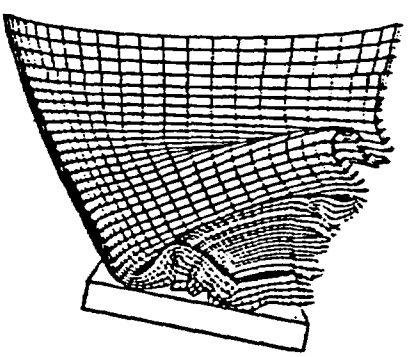

t = 15000 μs

Figure H-6 Sequence of deformed configurations.

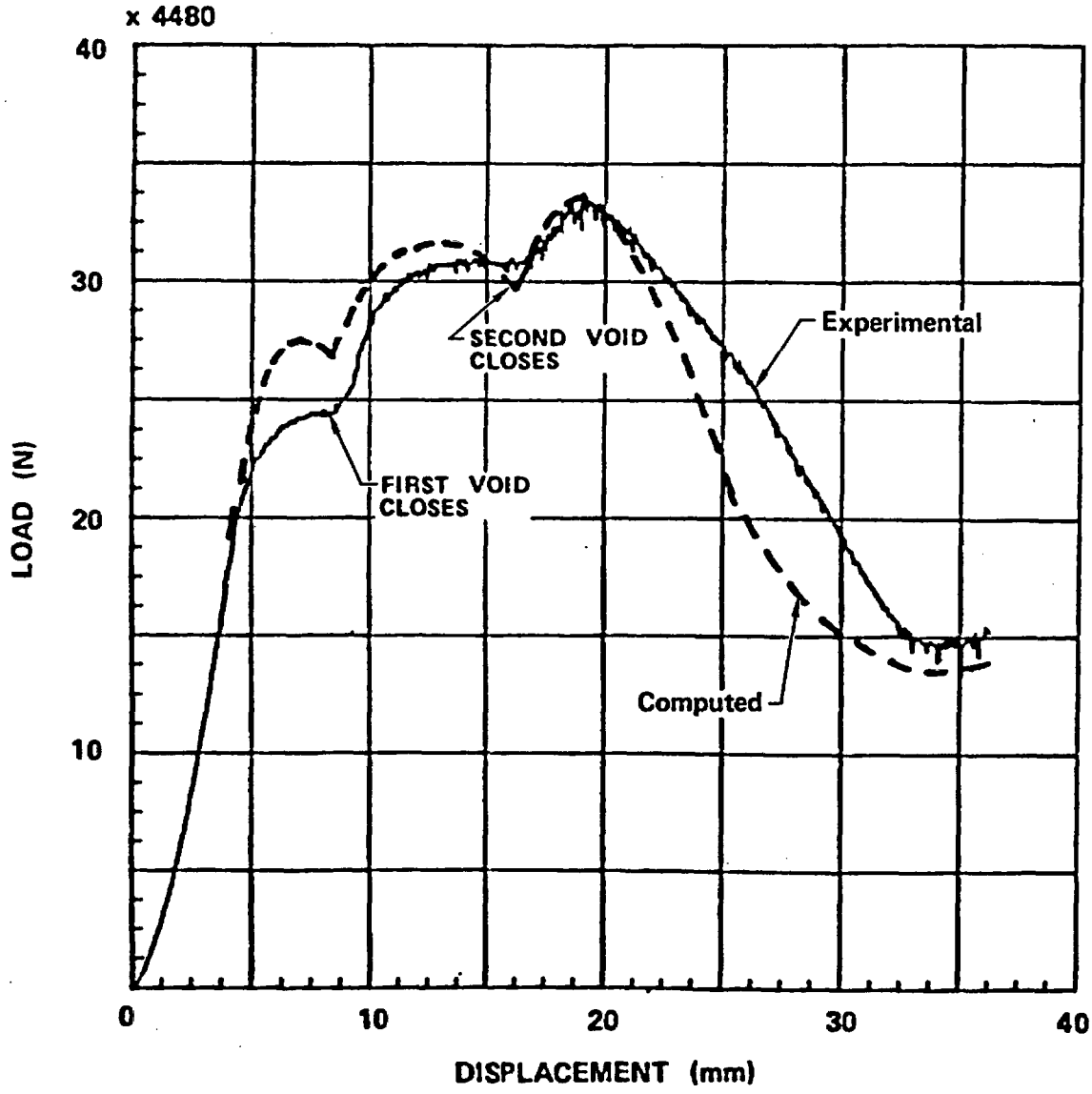

Figure H-7 Computed and experimental force-displacement curve. The steps in the curves correspond to void closures.

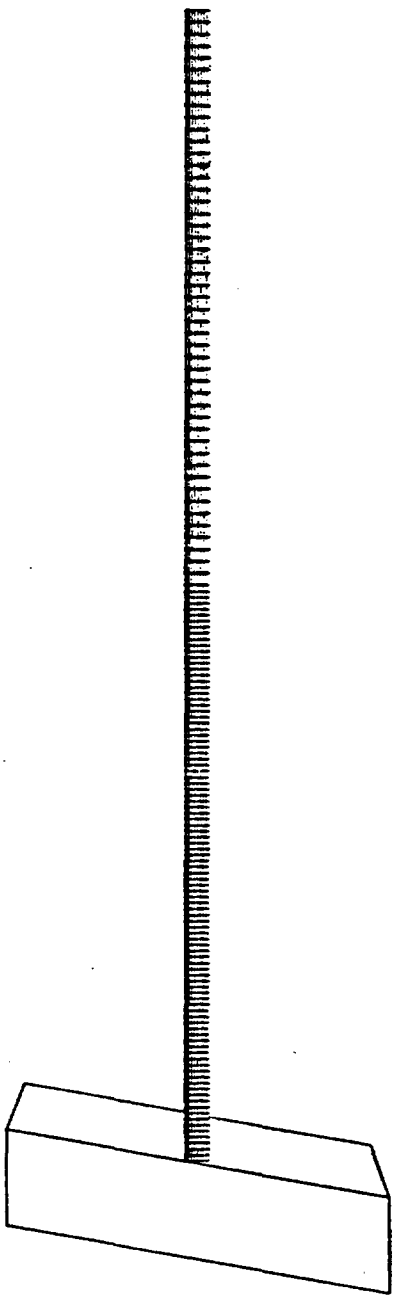

Figure H-8 Calculational mesh for the oblique rod impact problem.

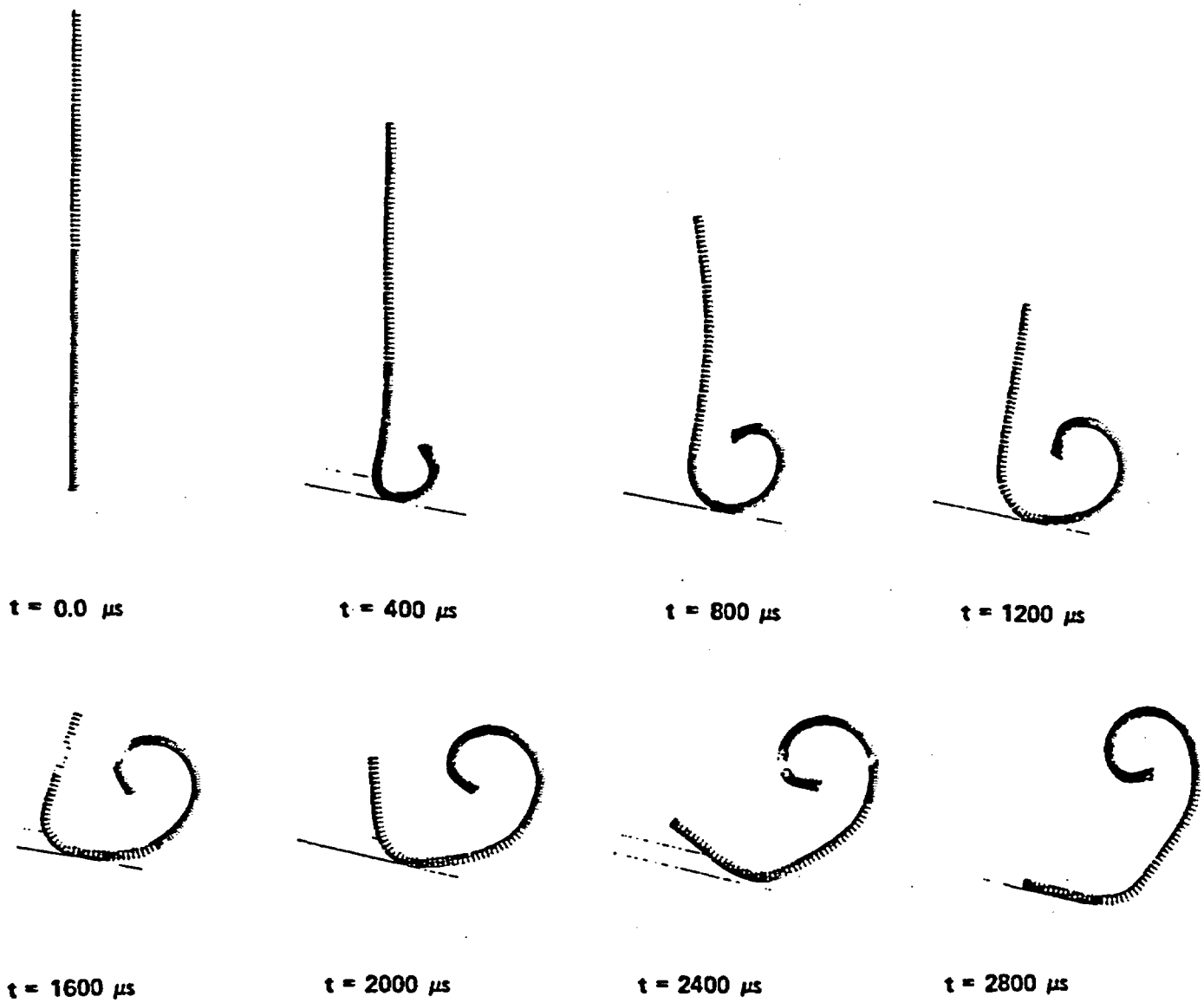

Figure H-9 Deformed shapes of a rod impacting an oblique rigid wall.

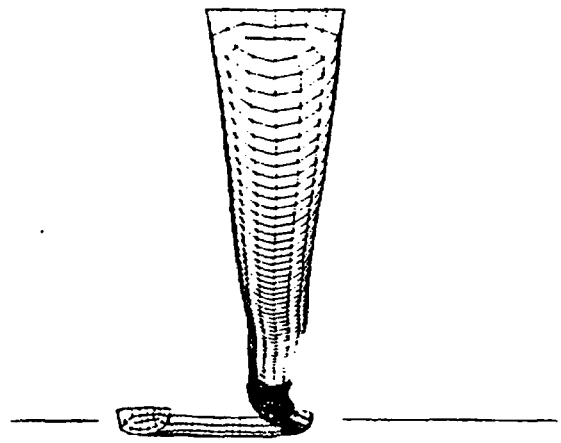

Figure H-10 Another view of a rod at 300 μs.

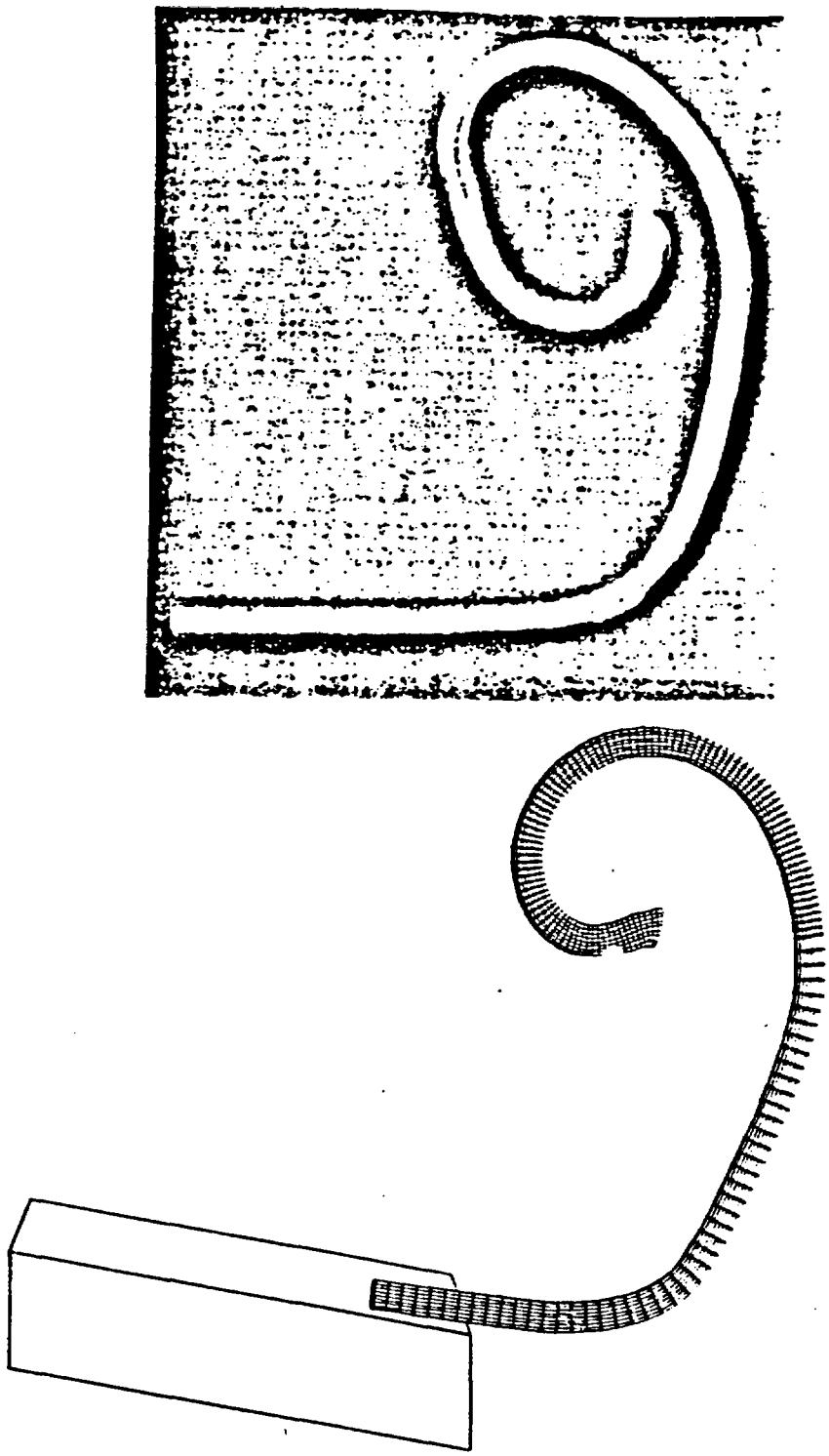

Figure H-11 Final profiles at 3000 μs (a) experiment and (b) computed.

References

H.1 M. Chiesa and M. Callabresi, "Nonlinear Analysis of a Mitigating Steel Nose Cone," Computers and Structures, Vol. 13, Sandia National Laboratories, Livermore, CA, 1981, p. 295.

H.2 D. J. Steinberg and M. W. Guinan, A High-Strain Constitutive Model for Metals, Lawrence Livermore National Laboratory, Livermore, CA, UCRL-80465, 1978.

NRC FORM 336 (2-84) NRCM 1102, 3201, 3202

U.S. NUCLEAR REGULATORY COMMISSION

BIBLIOGRAPHIC DATA SHEET

SEE INSTRUCTIONS ON THE REVERSE

1. REPORT NUMBER (Assigned by TIDC, add Vol. No., if any)
NUREG/CR-4829, Vol. 2
UCID-20733

2. TITLE AND SUBTITLE
Shipping Container Response to Severe Highway and Railway Accident Conditions

Appendices

3. LEAVE BLANK

4. DATE REPORT COMPLETED
MONTH: April YEAR: 1986

5. AUTHOR(S)
L.E. Fischer, C.K. Chou, M.A. Gerhard, C.Y. Kimura, R.W. Martin, R.W. Mensing, M.E. Mount, M.C. Witte

6. DATE REPORT ISSUED
MONTH: February YEAR: 1987

7. PERFORMING ORGANIZATION NAME AND MAILING ADDRESS (Include Zip Code)
Lawrence Livermore National Laboratory
P. O. Box 808, L-197
Livermore, California 94550

8. PROJECT/TASK/WORK UNIT NUMBER

9. FIN OR GRANT NUMBER
A0397

10. SPONSORING ORGANIZATION NAME AND MAILING ADDRESS (Include Zip Code)
Division of Reactor System Safety
Office of Nuclear Regulatory Research
U.S. Nuclear Regulatory Commission
Washington, D.C. 20555

11a. TYPE OF REPORT
Technical

b. PERIOD COVERED (Inclusive dates)

12. SUPPLEMENTARY NOTES

13. ABSTRACT (200 words or less)

This report describes a study performed by the Lawrence Livermore National Laboratory to evaluate the level of safety provided under severe accident conditions during the shipment of spent fuel from nuclear power reactors. The evaluation is performed using data from real accident histories and using representative truck and rail cask models that likely meet 10 CFR 71 regulations. The responses of the representative casks are calculated for structural and thermal loads generated by severe highway and railway accident conditions. The cask responses are compared with those responses calculated for the 10 CFR 71 hypothetical accident conditions. By comparing the responses it is determined that most highway and railway accident conditions fall within the 10 CFR 71 hypothetical accident conditions. For those accidents that have higher responses, the probabilities and potential radiation exposures of the accidents are compared with those identified by the assessments made in the "Final Environmental Statement on the Transportation of Radioactive Material by Air and other Modes," NUREG-0170. Based on this comparison, it is concluded that the radiological risks from spent fuel under severe highway and railway accident conditions as derived in this study are less than risks previously estimated in the NUREG-0170 document.

14. DOCUMENT ANALYSIS – a. KEYWORDS/DESCRIPTORS
spent fuel casks
Severe highway and railway accident conditions

b. IDENTIFIERS/OPEN-ENDED TERMS

15. AVAILABILITY STATEMENT
Unlimited

16. SECURITY CLASSIFICATION
(This page) Unclassified
(This report) Unclassified

17. NUMBER OF PAGES

18 PRICE

UNITED STATES
NUCLEAR REGULATORY COMMISSION
WASHINGTON, D.C. 20555